



IMPACTS OF CO₂ PERTURBATION ON THE ECOLOGY AND BIOGEOCHEMISTRY OF PLANKTON COMMUNITIES DURING A SIMULATED UPWELLING EVENT: A MESOCOSM EXPERIMENT IN OLIGOTROPHIC SUBTROPICAL WATERS

EDITED BY: Eric 'Pieter Achterberg, Jan Taucher, Ulf Riebesell and
Lennart Thomas Bach

PUBLISHED IN: Frontiers in Marine Science



frontiers

Frontiers eBook Copyright Statement

The copyright in the text of individual articles in this eBook is the property of their respective authors or their respective institutions or funders. The copyright in graphics and images within each article may be subject to copyright of other parties. In both cases this is subject to a license granted to Frontiers.

The compilation of articles constituting this eBook is the property of Frontiers.

Each article within this eBook, and the eBook itself, are published under the most recent version of the Creative Commons CC-BY licence.

The version current at the date of publication of this eBook is CC-BY 4.0. If the CC-BY licence is updated, the licence granted by Frontiers is automatically updated to the new version.

When exercising any right under the CC-BY licence, Frontiers must be attributed as the original publisher of the article or eBook, as applicable.

Authors have the responsibility of ensuring that any graphics or other materials which are the property of others may be included in the CC-BY licence, but this should be checked before relying on the CC-BY licence to reproduce those materials. Any copyright notices relating to those materials must be complied with.

Copyright and source acknowledgement notices may not be removed and must be displayed in any copy, derivative work or partial copy which includes the elements in question.

All copyright, and all rights therein, are protected by national and international copyright laws. The above represents a summary only. For further information please read Frontiers' Conditions for Website Use and Copyright Statement, and the applicable CC-BY licence.

ISSN 1664-8714

ISBN 978-2-88966-031-5

DOI 10.3389/978-2-88966-031-5

About Frontiers

Frontiers is more than just an open-access publisher of scholarly articles: it is a pioneering approach to the world of academia, radically improving the way scholarly research is managed. The grand vision of Frontiers is a world where all people have an equal opportunity to seek, share and generate knowledge. Frontiers provides immediate and permanent online open access to all its publications, but this alone is not enough to realize our grand goals.

Frontiers Journal Series

The Frontiers Journal Series is a multi-tier and interdisciplinary set of open-access, online journals, promising a paradigm shift from the current review, selection and dissemination processes in academic publishing. All Frontiers journals are driven by researchers for researchers; therefore, they constitute a service to the scholarly community. At the same time, the Frontiers Journal Series operates on a revolutionary invention, the tiered publishing system, initially addressing specific communities of scholars, and gradually climbing up to broader public understanding, thus serving the interests of the lay society, too.

Dedication to Quality

Each Frontiers article is a landmark of the highest quality, thanks to genuinely collaborative interactions between authors and review editors, who include some of the world's best academicians. Research must be certified by peers before entering a stream of knowledge that may eventually reach the public - and shape society; therefore, Frontiers only applies the most rigorous and unbiased reviews.

Frontiers revolutionizes research publishing by freely delivering the most outstanding research, evaluated with no bias from both the academic and social point of view. By applying the most advanced information technologies, Frontiers is catapulting scholarly publishing into a new generation.

What are Frontiers Research Topics?

Frontiers Research Topics are very popular trademarks of the Frontiers Journals Series: they are collections of at least ten articles, all centered on a particular subject. With their unique mix of varied contributions from Original Research to Review Articles, Frontiers Research Topics unify the most influential researchers, the latest key findings and historical advances in a hot research area! Find out more on how to host your own Frontiers Research Topic or contribute to one as an author by contacting the Frontiers Editorial Office: researchtopics@frontiersin.org

IMPACTS OF CO₂ PERTURBATION ON THE ECOLOGY AND BIOGEOCHEMISTRY OF PLANKTON COMMUNITIES DURING A SIMULATED UPWELLING EVENT: A MESOCOSM EXPERIMENT IN OLIGOTROPHIC SUBTROPICAL WATERS

Topic Editors:

Eric 'Pieter Achterberg, GEOMAR Helmholtz Center for Ocean Research Kiel, Germany

Jan Taucher, GEOMAR Helmholtz Center for Ocean Research Kiel, Germany

Ulf Riebesell, GEOMAR Helmholtz Center for Ocean Research Kiel, Germany

Lennart Thomas Bach, University of Tasmania, Australia

Citation: Achterberg, E. P., Taucher, J., Riebesell, U., Bach, L. T., eds. (2020). Impacts of CO₂ Perturbation on the Ecology and Biogeochemistry of Plankton Communities During a Simulated Upwelling Event: A Mesocosm Experiment in Oligotrophic Subtropical Waters. Lausanne: Frontiers Media SA.
doi: 10.3389/978-2-88966-031-5

Table of Contents

- 05** *Influence of Ocean Acidification and Deep Water Upwelling on Oligotrophic Plankton Communities in the Subtropical North Atlantic: Insights From an In situ Mesocosm Study*
Jan Taucher, Lennart T. Bach, Tim Boxhammer, Alice Nauendorf, The Gran Canaria KOSMOS Consortium, Eric P. Achterberg, María Algueró-Muñiz, Javier Arístegui, Jan Czerny, Mario Esposito, Wanchun Guan, Mathias Haunost, Henriette G. Horn, Andrea Ludwig, Jana Meyer, Carsten Spisla, Michael Sswat, Paul Stange and Ulf Riebesell
- 23** *Ocean Acidification Experiments in Large-Scale Mesocosms Reveal Similar Dynamics of Dissolved Organic Matter Production and Biotransformation*
Maren Zark, Nadine K. Broda, Thomas Hornick, Hans-Peter Grossart, Ulf Riebesell and Thorsten Dittmar
- 34** *Photochemical vs. Bacterial Control of H_2O_2 Concentration Across a pCO_2 Gradient Mesocosm Experiment in the Subtropical North Atlantic*
Mark J. Hopwood, Ulf Riebesell, Javier Arístegui, Andrea Ludwig, Eric P. Achterberg and Nauzet Hernández
- 45** *Ocean Acidification-Induced Restructuring of the Plankton Food Web Can Influence the Degradation of Sinking Particles*
Paul Stange, Jan Taucher, Lennart T. Bach, María Algueró-Muñiz, Henriette G. Horn, Luana Krebs, Tim Boxhammer, Alice K. Nauendorf and Ulf Riebesell
- 58** *High CO_2 Under Nutrient Fertilization Increases Primary Production and Biomass in Subtropical Phytoplankton Communities: A Mesocosm Approach*
Nauzet Hernández-Hernández, Lennart T. Bach, María F. Montero, Jan Taucher, Isabel Baños, Wanchun Guan, Mario Espósito, Andrea Ludwig, Eric P. Achterberg, Ulf Riebesell and Javier Arístegui
- 72** *Processes That Contribute to Decreased Dimethyl Sulfide Production in Response to Ocean Acidification in Subtropical Waters*
Stephen D. Archer, Kerstin Suffrian, Kevin M. Posman, Lennart T. Bach, Patricia A. Matrai, Peter D. Countway, Andrea Ludwig and Ulf Riebesell
- 91** *Plankton Community Respiration and ETS Activity Under Variable CO_2 and Nutrient Fertilization During a Mesocosm Study in the Subtropical North Atlantic*
Alba Filella, Isabel Baños, María F. Montero, Nauzet Hernández-Hernández, Adriana Rodríguez-Santos, Andrea Ludwig, Ulf Riebesell and Javier Arístegui
- 102** *Response of Subtropical Phytoplankton Communities to Ocean Acidification Under Oligotrophic Conditions and During Nutrient Fertilization*
Jan Taucher, Javier Arístegui, Lennart T. Bach, Wanchun Guan, María F. Montero, Alice Nauendorf, Eric P. Achterberg and Ulf Riebesell

- 116** *Response of Pelagic Calcifiers (Foraminifera, Thecosomata) to Ocean Acidification During Oligotrophic and Simulated Up-Welling Conditions in the Subtropical North Atlantic Off Gran Canaria*
Silke Lischka, Paul Stange and Ulf Riebesell
- 127** *Analyzing the Impacts of Elevated- CO_2 Levels on the Development of a Subtropical Zooplankton Community During Oligotrophic Conditions and Simulated Upwelling*
María Algueró-Muñiz, Henriette G. Horn, Santiago Alvarez-Fernandez, Carsten Spisla, Nicole Aberle, Lennart T. Bach, Wanchun Guan, Eric P. Achterberg, Ulf Riebesell and Maarten Boersma
- 145** *Effects of Elevated CO_2 on a Natural Diatom Community in the Subtropical NE Atlantic*
Lennart T. Bach, Nauzet Hernández-Hernández, Jan Taucher, Carsten Spisla, Claudia Sforna, Ulf Riebesell and Javier Aristegui
- 161** *Application of Stable Carbon Isotopes in a Subtropical North Atlantic Mesocosm Study: A New Approach to Assess CO_2 Effects on the Marine Carbon Cycle*
Mario Esposito, Eric P. Achterberg, Lennart T. Bach, Douglas P. Connelly, Ulf Riebesell and Jan Taucher



Influence of Ocean Acidification and Deep Water Upwelling on Oligotrophic Plankton Communities in the Subtropical North Atlantic: Insights from an *In situ* Mesocosm Study

OPEN ACCESS

Edited by:

Hongbin Liu,
Hong Kong University of Science and
Technology, China

Reviewed by:

Elvira Pulido-Villena,
Mediterranean Institute of
Oceanography, France
Antonio Bode,
Spanish Institute of Oceanography,
Spain

*Correspondence:

Jan Taucher
jtaucher@geomar.de

[†]Membership in the Gran Canaria
KOSMOS Consortium is given in the
acknowledgments.

Specialty section:

This article was submitted to
Marine Biogeochemistry,
a section of the journal
Frontiers in Marine Science

Received: 23 December 2016

Accepted: 13 March 2017

Published: 04 April 2017

Citation:

Taucher J, Bach LT, Boxhammer T,
Nauendorf A, The Gran Canaria
KOSMOS Consortium, Achterberg EP,
Algueró-Muñiz M, Aristegui J, Czerny
J, Esposito M, Guan W, Haunost M,
Horn HG, Ludwig A, Meyer J, Spisla
C, Sswat M, Stange P and Riebesell U
(2017) Influence of Ocean Acidification
and Deep Water Upwelling on
Oligotrophic Plankton Communities in
the Subtropical North Atlantic: Insights
from an *In situ* Mesocosm Study.
Front. Mar. Sci. 4:85.
doi: 10.3389/fmars.2017.00085

Jan Taucher^{1*}, Lennart T. Bach¹, Tim Boxhammer¹, Alice Nauendorf¹,
The Gran Canaria KOSMOS Consortium[†], Eric P. Achterberg¹, María Algueró-Muñiz²,
Javier Aristegui³, Jan Czerny¹, Mario Esposito^{1,4}, Wanchun Guan^{1,5}, Mathias Haunost¹,
Henriette G. Horn², Andrea Ludwig¹, Jana Meyer¹, Carsten Spisla^{1,2}, Michael Sswat¹,
Paul Stange¹ and Ulf Riebesell¹

¹ Marine Biogeochemistry, Biological Oceanography, GEOMAR Helmholtz Centre for Ocean Research Kiel, Kiel, Germany,

² Alfred-Wegener-Institut, Helmholtz-Zentrum for Polar and Marine Research, Biological Institute Helgoland, Helgoland,

Germany, ³ Oceanografía Biológica, Instituto de Oceanografía y Cambio Global, Universidad de Las Palmas de Gran Canaria, Las Palmas de Gran Canaria, Spain, ⁴ School of Ocean and Earth Sciences, University of Southampton, Southampton, UK,

⁵ Department of Marine Biotechnology, Wenzhou Medical University, Zhejiang, China

Oceanic uptake of anthropogenic carbon dioxide (CO₂) causes pronounced shifts in marine carbonate chemistry and a decrease in seawater pH. Increasing evidence indicates that these changes—summarized by the term ocean acidification (OA)—can significantly affect marine food webs and biogeochemical cycles. However, current scientific knowledge is largely based on laboratory experiments with single species and artificial boundary conditions, whereas studies of natural plankton communities are still relatively rare. Moreover, the few existing community-level studies were mostly conducted in rather eutrophic environments, while less attention has been paid to oligotrophic systems such as the subtropical ocean gyres. Here we report from a recent *in situ* mesocosm experiment off the coast of Gran Canaria in the eastern subtropical North Atlantic, where we investigated the influence of OA on the ecology and biogeochemistry of plankton communities in oligotrophic waters under close-to-natural conditions. This paper is the first in this Research Topic of *Frontiers in Marine Biogeochemistry* and provides (1) a detailed overview of the experimental design and important events during our mesocosm campaign, and (2) first insights into the ecological responses of plankton communities to simulated OA over the course of the 62-day experiment. One particular scientific objective of our mesocosm experiment was to investigate how OA impacts might differ between oligotrophic conditions and phases of high biological productivity, which regularly occur in response to upwelling of nutrient-rich deep water in the study region. Therefore, we specifically developed a deep water collection system that allowed us to obtain ~85 m³ of seawater from ~650 m depth. Thereby, we replaced ~20%

of each mesocosm's volume with deep water and successfully simulated a deep water upwelling event that induced a pronounced plankton bloom. Our study revealed significant effects of OA on the entire food web, leading to a restructuring of plankton communities that emerged during the oligotrophic phase, and was further amplified during the bloom that developed in response to deep water addition. Such CO₂-related shifts in plankton community composition could have consequences for ecosystem productivity, biomass transfer to higher trophic levels, and biogeochemical element cycling of oligotrophic ocean regions.

Keywords: ocean acidification, plankton community composition, mesocosm experiment, marine biogeochemistry, ecological effects of high CO₂

INTRODUCTION

Over the past few centuries, anthropogenic emissions of carbon dioxide (CO₂) have resulted in an increase of atmospheric concentrations from average pre-industrial levels of ~280 to more than 400 ppmv (parts per million volume) in the year 2014 (IPCC, 2014). About one third of this carbon is currently taken up by the world oceans (Sabine et al., 2004; Le Quéré et al., 2009), leading to a decrease in pH and pronounced shifts in seawater carbonate chemistry that occur at a pace unprecedented in recent geological history (Zeebe and Wolf-Gladrow, 2001; IPCC, 2014). This process, which is commonly referred to as “ocean acidification” (OA), is expected to have substantial consequences for marine ecosystems (Wolf-Gladrow and Riebesell, 1997; Caldeira and Wickett, 2003).

Research on potential OA effects on marine organisms has experienced a rapid development over the past decade. Some studies observed pronounced effects of elevated CO₂ on particular organism groups or species, leading to the designation of potential winners and losers in the future ocean (Kroeker et al., 2010, 2013; Wittmann and Pörtner, 2013). However, most experiments were conducted under rather artificial environmental conditions and with cultures of single species, thereby neglecting ecological interactions. It is therefore difficult to predict how OA effects observed in such studies translate into responses of natural ecosystems with multiple trophic levels and complex species interactions. In order to understand how entire communities and food webs respond to environmental changes such as ocean acidification, it is necessary to close our knowledge gap between physiological responses of single species to complex effects on the ecosystem level (Riebesell and Gattuso, 2015).

In situ mesocosm experiments with large incubation volumes have proven to be a valuable tool for this purpose. They allow the incubation of entire plankton communities from bacteria to fish larvae, and can be sustained on time scales sufficiently long to study the seasonal succession of organisms under close-to-natural conditions (Gamble and Davies, 1982; Riebesell et al., 2013a). Although, only few such “whole community” studies have been conducted so far, it already becomes apparent that the response to elevated CO₂ is highly variable among different ocean regions and plankton communities and often differs from effects on single species observed in the laboratory (Schulz et al., 2013;

Riebesell et al., 2013b; Paul et al., 2015; Bach et al., 2016; Gazeau et al., 2016).

The few reported community-level studies mostly focused on rather eutrophic environments at higher latitudes, such as the Arctic Ocean or temperate waters, since these regions are commonly assumed to be most vulnerable to ongoing changes in carbonate chemistry (Orr et al., 2005; Yamamoto-Kawai et al., 2009). However, recent evidence from the Baltic Sea, North Sea, and Mediterranean Sea indicated that OA effects might be most pronounced when inorganic nutrient concentrations are low (Paul et al., 2015; Sala et al., 2015; Bach et al., 2016; Hornick et al., 2016). How plankton communities in the vast oligotrophic regions of the subtropical gyres might respond to OA is presently unknown. While productivity in these waters is usually relatively low, their immense size—covering about 40% of the Earth's surface—makes their total contribution significant on a global scale (McClain et al., 2004; Signorini et al., 2015).

In the mesocosm study presented here, we investigated how OA might influence plankton communities in the oligotrophic regions of the subtropical North Atlantic. Therefore, we conducted a 9-week *in situ* mesocosm experiment in Gando Bay, Gran Canaria (Spain). A particular research objective was to investigate how the potential response to OA differs between oligotrophic conditions and bloom situations, which regularly develop through upwelling of deep water e.g., by mesoscale eddies in the Canary region (Aristegui et al., 1997; Sangra et al., 2009).

The research campaign was hosted and supported by the Plataforma Oceánica de Canarias (PLOCAN), which is situated near Melenara Bay (municipality of Telde) on the east coast of Gran Canaria. More than 50 scientists and technicians from different institutes and countries participated in this study in an international collaboration with the common aim to investigate the impact of ocean acidification on physiological, ecological, and biogeochemical processes in an oligotrophic plankton community.

The present paper is the first within this Research Topic of *Frontiers in Marine Biogeochemistry* and serves two primary purposes: Firstly, we will provide a detailed description of the study site, experimental setup, sampling, and measurement procedures, and key events during the study. This will provide a framework and reference for the other more specific papers in this Research Topic (see Table S1 for a summary of planned

publications). Secondly, we will investigate whether elevated pCO₂ levels affect plankton community composition, with a particular focus on possible differences between oligotrophic conditions and periods of high productivity in response to upwelling of deep water.

METHODS

Study Site

The *in situ* mesocosm experiment was conducted in the Gando Bay, which is located on the east coast of Gran Canaria (Figure 1A). Situated about 100 km off the West-African coast, the Canary Islands are primarily influenced by the subtropical North Atlantic gyre and to a lesser extent by the Canary current upwelling system (Barton et al., 1998; Arístegui et al., 2009). Accordingly, the waters surrounding Gran Canaria are usually characterized by warm surface temperatures and a pronounced thermal stratification of the water column, resulting in predominantly oligotrophic conditions with low nutrient concentrations and plankton biomass throughout the year (Arístegui et al., 2001). However, exceptions can occur due to mesoscale variability, e.g., island eddies that transport nutrients from the mesopelagic zone into the surface waters (Arístegui et al., 1997; Sangra et al., 2009) or upwelling filaments that carry nutrients from the West-African coast into waters surrounding the Canary Islands (Barton et al., 1998; Pelegri et al., 2005). Such

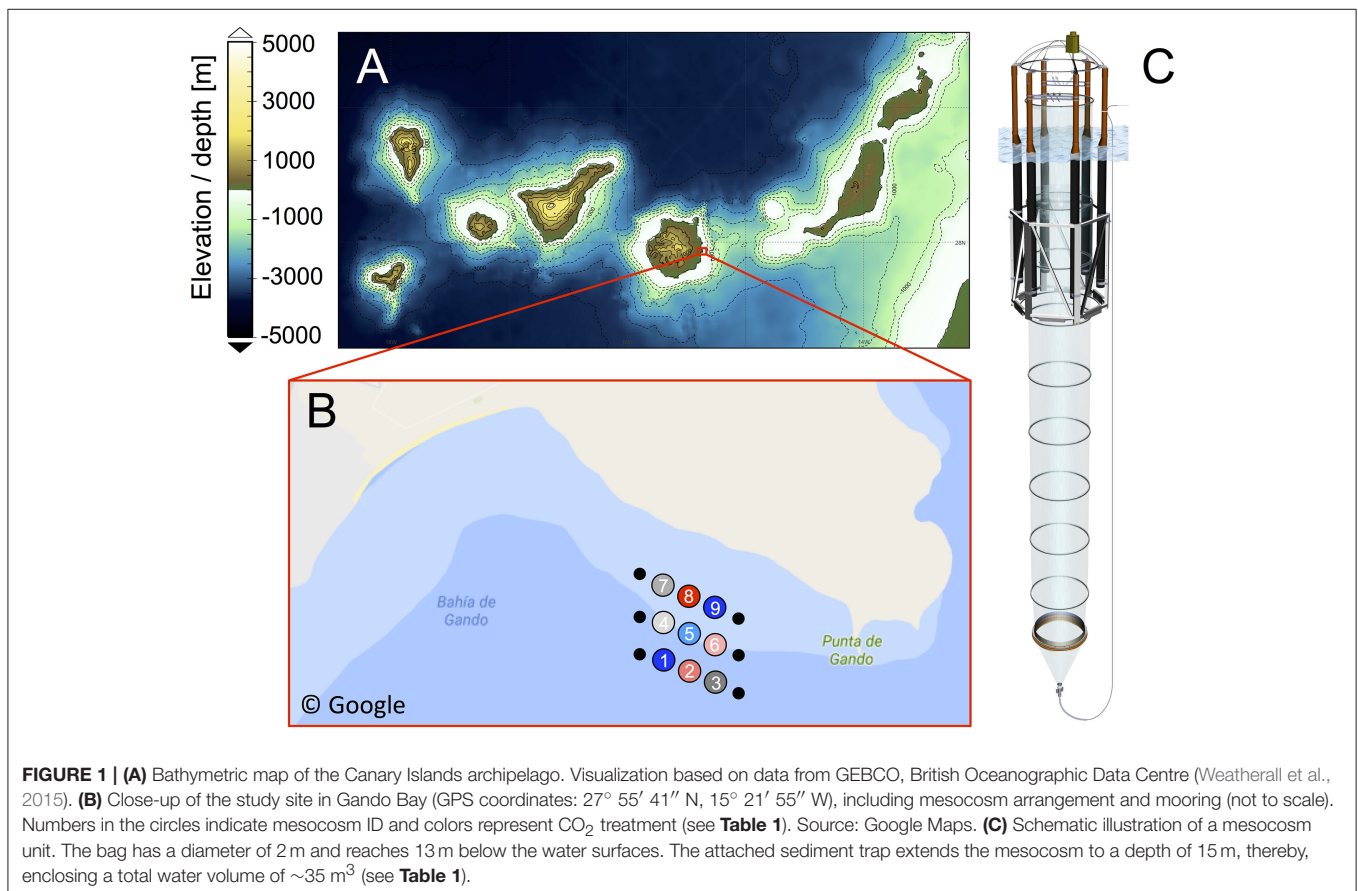
events can have a profound influence on productivity in the Canary region.

Mesocosm Setup, Deployment Procedure, and Maintenance

On September 23rd 2014, the research vessel *Hesperides* deployed nine “Kiel Off-Shore Mesocosms for Future Ocean Simulations” (KOSMOS, M1–M9; Riebesell et al., 2013a), which were moored in clusters of three in the northern part of Gando Bay (27° 55′ 41″ N, 15° 21′ 55″ W) at a depth of ~20–25 m (Figure 1).

Each mesocosm unit consisted of an 8 m high flotation frame, a cylindrical mesocosm bag (13 m length, 2 m diameter) made of transparent thermoplastic polyurethane foil (1 mm thick) that allows for penetration of light in the PAR spectrum, as well as a conical sediment trap (2 m long) that tightly seals the bottom of the mesocosm and allows for collection of sinking organic material with a vacuum pump system on a regular basis (Figure 1C).

The bags were folded and mounted onto the floatation frames prior to deployment. Once in the water, the bags were unfolded immediately and submerged below the water surface with the upper opening 1 m below sea surface. Both the upper and lower openings were covered with meshes (3 mm mesh size) to exclude patchily distributed nekton and large zooplankton like fish larvae or jellyfish from the enclosed water bodies. The mesocosm bags



were then left floating in the water column for 4 days to allow for rinsing of the bags' interior and free exchange of plankton (<3 mm) between the mesocosms and the surrounding water. On September 27th, divers replaced the mesh at the bottom of the mesocosm bags with the sediment traps, while a boat crew simultaneously pulled the upper part of the bags above the sea surface. This step separated the water bodies within the mesocosms from the surrounding water and thus marked the start of the experiment (day $-4 = t-4$, **Figure 2**). The entire procedure lasted for <2 h, thereby minimizing differences between the enclosed water masses among mesocosms.

The experiment lasted for 62 days in total, starting with the closing of the mesocosms on $t-4$ and finishing with the last sampling of the sediment trap on $t57$. Day $t0$ (October 1st) denotes the day of the first CO₂ manipulation, corresponding to the establishment of elevated pCO₂ as the experimental treatment (see Section CO₂ Manipulation). In the fourth week of the experiment ($t24$), we injected deep water into the mesocosms

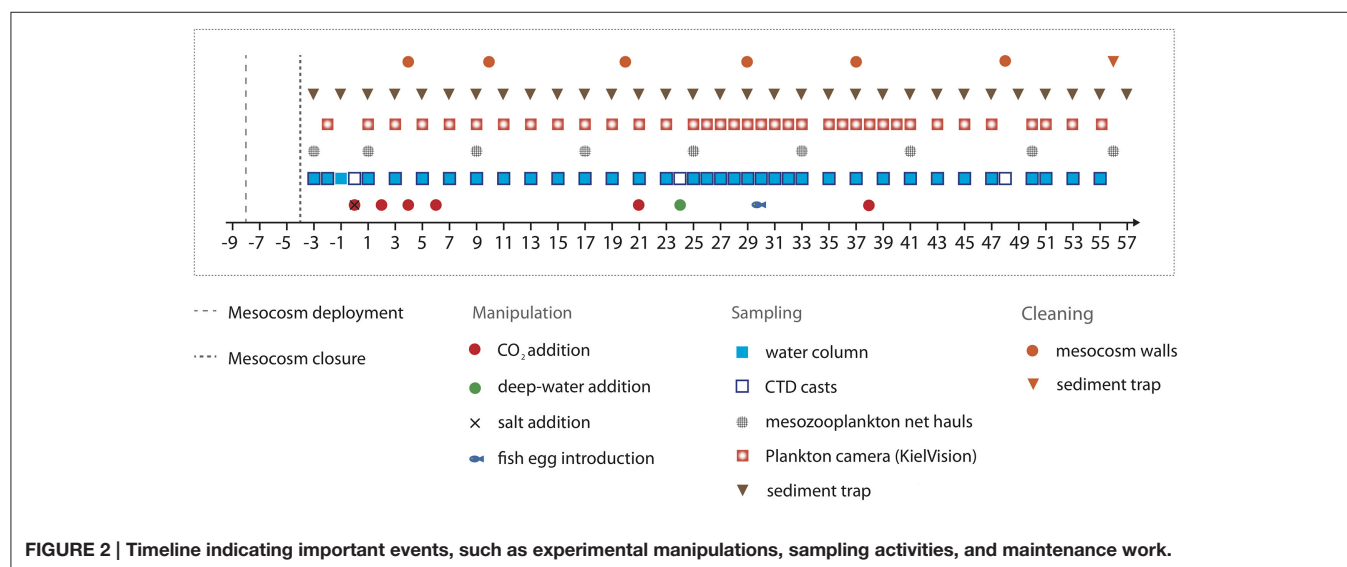
to simulate a natural upwelling event (Section Simulated Upwelling through Addition of Deep Water). Unfortunately, one mesocosm (M6) was lost on $t26$, when strong currents in Gando Bay pulled some of the moorings and mesocosms ~50 m seawards. The bag of M6 was irreparably damaged during the recovery procedure. Thus, M6 was excluded from sampling and analyses after $t26$.

Mesocosms were cleaned from the inside and outside to minimize wall growth by benthic organisms, which would consume nutrients and eventually lead to decreasing light intensities inside the mesocosms. Therefore, mesocosm wall cleaning was conducted in regular intervals throughout the experiment (**Figure 2**) using a specifically designed cleaning ring for the inner surface, and scrubbers for the outside of the mesocosm bags (Riebesell et al., 2013a; Bach et al., 2016). Unfortunately, however, the conical sediment trap and parts of the lowest mesocosm segment could not be cleaned from the inside due to the narrow tapered design. These

TABLE 1 | Mesocosm experimental setup, including symbols and color-code for other figures, mesocosm volumes right before deep water addition, amount of deep water (DW) added to each mesocosm, and average pCO₂ values during different phases of the experiment (see Section Oligotrophic Phase and Plankton Bloom in Response to Deep Water Addition for definition of phases).

Mesocosm	Symbol	Volume [m ³]	DW addition [m ³]	pCO ₂ [μatm]				Comment
				Phase I	Phase II	Phase III	Mean $t1-t55$	
M1	■	37.75	8.95	401	374	326	369	
M2	■	34.18	8.11	1,050	748	830	887	
M3	▲	31.57	7.50	636	493	546	563	
M4	●	36.93	8.66	800	620	710	716	hole on $t11$
M5	●	34.00	8.07	502	404	427	448	
M6	▲	34.03	8.08	976	–	–	–	lost on $t27$
M7	■	35.25	8.36	746	571	672	668	
M8	●	34.95	8.29	1,195	902	944	1,025	
M9	▲	35.21	8.36	406	343	297	352	hole on $t13$

Note that the control treatment (M1 and M9) did not receive CO₂ enrichment and followed ambient pCO₂ for the entire study.



parts corresponded to ~7% of the inner surface of the mesocosm, which experienced some degree of wall growth (see Section Plankton Community Structure and Influence of Ocean Acidification).

CO₂ Manipulation

To simulate ocean acidification in our experiment, we added different amounts of CO₂-saturated seawater to the mesocosms, following the method described in Riebesell et al. (2013a). For preparation of CO₂-saturated seawater, we collected about 1,500 L of natural seawater from Melenara Bay at ~10 m depth using a pipe and pre-filtration system connected to the PLOCAN facilities. The water was aerated with pure CO₂ gas for at least 1 h until reaching saturation and pH_{NBS} values of ~4.7. Afterwards, the water was filtered again (20 µm) and transferred into 20 L bottles, which were then transported by boat to the mesocosm study site.

For addition of the CO₂-saturated water to the mesocosms, we used a special distribution device (“spider”) with a large number of small tubes to distribute the water uniformly within a radius of ~1 m. By constantly pulling the spider up and down inside the mesocosms, we ensured homogenous CO₂ enrichment throughout the entire water columns. By adding different amounts of CO₂-saturated seawater to seven of the nine mesocosms, we set up an initial gradient in pCO₂ from ambient levels (~400 µatm) to concentrations of ~1,480 µatm in the highest CO₂ treatment. No CO₂ water was added to mesocosms M1 and M9, which served as a control (ambient pCO₂). To avoid an abrupt disturbance of the plankton community, this initial CO₂ manipulation was carried out incrementally in four steps over a period of 7 days between t0 and t6 (Figure 2). Two further CO₂ additions were conducted during the experiment in order to account for loss of CO₂ through air-sea gas exchange. The first time was on t21 during the oligotrophic phase to adjust pCO₂ before deep water addition, and the second time on t38 in the post-bloom phase (Figure 2).

Simulated Upwelling through Addition of Deep Water

One of the major goals of this study was to investigate whether potential effects of elevated CO₂ on natural plankton communities in the study region might differ between oligotrophic conditions and during bloom situations. Such plankton blooms regularly occur in response to upwelling of deep water, which is primarily driven by mesoscale variability (e.g., eddies) and results in transport of nutrient-rich water masses from several hundreds of meters depth to the (usually) nutrient-poor surface layer (Aristegui et al., 1997; Basterretxea and Aristegui, 2000). Besides inorganic nutrients, oceanic deep water masses usually exhibit distinct signatures of minor constituents such as dissolved organic matter and trace metals, elevated pCO₂, or seeding populations of plankton species (Pitcher, 1990; Hansell et al., 2009; Aparicio-Gonzalez et al., 2012; Tagliabue et al., 2014). All of these factors may have minor or major influences on the ecosystem in the surface layer, which go beyond the effects of the major nutrients N, P, and Si. Consequently, a “simple” addition of inorganic nutrients

would not be sufficient for a realistic simulation of a natural upwelling event.

To overcome this challenge, we specifically developed a deep water collection system that allowed us to obtain the large amounts of nutrient-rich deep water required for mimicking an upwelling event in our mesocosm experiment. The goal was to replace ~20% of the mesocosm volumes with deep water, thereby ensuring a sufficiently large input of inorganic nutrients comparable to those observed during natural upwelling events in the region (Aristegui et al., 1997; Neuer et al., 2007).

The flexible walls of the deep water collector consisted of fiber-reinforced food-grade polyvinyl chloride material (opaque), which was high-frequency welded into a pear-like shape with a volume of ~85 m³ (Figure 3A). The opening (diameter of ~25 cm) was equipped with a specifically-designed water intake device (based on a modified propeller drive) and a sealing disc as a closure mechanism for the deep water collector. Operation of both components was time-controlled (programmable), thereby allowing for remotely operated collection of water at a desired depth. A screen with 10 mm mesh size covered the opening to ensure that no large particles or organisms entered the deep water collector. Furthermore, a weight of ~300 kg was attached to the deflated deep water collector before deployment to submerge it in the ocean until the target depth was reached. An acoustic trigger was installed to release the weight after completion of the water intake, thereby allowing the rise of the filled deep water collector to the sea surface, only driven by the gentle buoyancy of 24 floats attached to the main frame (Figure 3B).

On October 23rd (t22), we transported the deep water collection system to a location about 4 nautical miles north-east from the study site, where water depth was ~1,000 m and thus sufficiently deep for deployment. Transport and operation of the deep water collector was carried out with the vessel “SAPCAN IV” (chartered from Amadores harbor service, Las Palmas). Upon arrival at the target location, the deep water collector was lowered to a depth of ~650 m, where ~85 m³ of water were collected (Figures 3C,D). After resurfacing of the collector, it was gently towed back to the study site, where it was anchored until addition to the mesocosms 2 days later on t24. In the meantime, defined amounts of water had to be removed from the mesocosms to create space for subsequent addition of deep water. To accomplish this, we used a submersible pump (Grundfos SP-17-5R) to remove known volumes of water from the mesocosms at ~5 m depth on October 24th (t23).

In order to reach the desired mixing ratio of deep water of about 20%, a total of ~75 m³ of deep water were distributed among the nine mesocosms. Before addition, we characterized the deep water biologically and chemically by the full set of variables also routinely sampled in the mesocosms (see Table 2). Since deep water addition had to be carried out for each mesocosm separately one after another, we anticipated that this procedure would last at least several hours. To minimize nutrient uptake and growth by phytoplankton during this time, we conducted the deep water addition during night time, thus ensuring identical starting conditions of all mesocosms for the following experimental phase. Accordingly, deep water was added in two steps during the night of October 25th–26th (t24–t25), lasting for ~9 h in total.

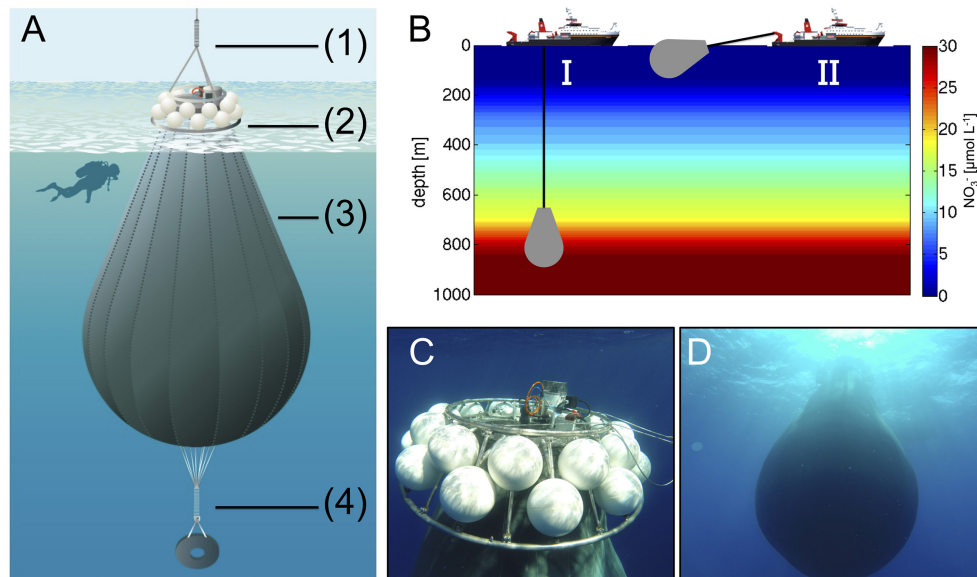


FIGURE 3 | (A) Schematic illustration of the deep water collector, including (1) an expander for compensation of ship movement, (2) remotely-controlled filling and closing mechanism, and floatation bodies (total buoyancy ~400 kg), (3) a flexible tank welded from fiber-reinforced food-grade PVC with a volume of ~85 m³, and (4) a weight system for submersion with acoustic release trigger. Illustration by R. Erven. **(B)** Ship-operated collection of nutrient-rich deep water with the custom-designed system (I) and towing of the bag to the study site (II). **(C,D)** Underwater photographs of the deep water collector after successful deployment (Pictures taken by the KOSMOS dive team).

The actual transfer of deep water to the mesocosms was conducted by submerging a pump (the same as for water removal described above) into the deep water collector and pumping the water into the mesocosms with an injection device similar to the “spider” used for CO₂ additions (see above), but with larger tube diameters and larger volume throughput. Continuous up and down movement of this enlarged spider during addition ensured homogenous vertical distribution of deep water inside the mesocosms. In the first step, we added ~80% of the calculated amount of deep water to each mesocosm. Since the salinity of the deep water was much lower than in the mesocosms (35.7 vs. 37.7), the mixing ratio of mesocosm water with deep water could be calculated from precisely measured changes in salinity. Based on CTD profiles and salinity calculations immediately after the first deep water addition, the second addition was then used for fine-tuning and adjustment of all mesocosms to identical deep water mixing ratios and concentrations of inorganic nutrients. Furthermore, by adding defined amounts of deep water with known salinity, and measuring the resultant salinity change in the mesocosms, we could accurately estimate the total volume of seawater in each mesocosm enclosure. The volumes determined by this method were ~35 m³ on average (±5%, see **Table 1**).

Addition of Fish Larvae

One of our study objectives was to investigate how effects of OA on plankton communities might propagate to higher trophic levels. Accordingly, we added ~330 eggs of greater amberjack (*Seriola dumerili*) to each mesocosm on October 31st (t30), which was during the time of peak biomass after deep water

addition on t24. The number of added eggs was determined as a trade-off between preventing potential top-down effects from becoming too strong on the one hand, and providing the presence of sufficient fish for sampling (based on expected survival) on the other hand. Eggs of greater amberjack were collected from existing broodstock, held by the Aquaculture research group (GIA) of the University of Las Palmas de Gran Canaria (ULPGC). All protocols within the breeding facilities were approved within the EU project “AQUAEXCELL” (ethics permit number: OEBA-ULPGC04/2016). The fish eggs were gently introduced by submerging the brood containers inside the mesocosms (~3 m depth) from day t30 until t32, with calculated time of hatching at 2 days after introduction.

Unfortunately, it was not possible to determine the abundance of fish larvae on a continual basis. No larvae of *S. dumerili* could be found in the net catches, possibly due to their escape from the towed net. Deployment of light traps was not successful either. Some dead fish larvae were found by screening the sediment trap material on the days after hatching. While this approach did not provide robust quantitative estimates, e.g., due to the fragility and rapid decay of dead organisms, it indicated substantial mortality of fish larvae within the first few days after hatching. Furthermore, no live individuals were found in the final sampling (t56) with a 1 mm net that covered the full diameter of the mesocosms, indicating that there was no survival of fish larvae until the end of the experiment. Nevertheless, it should be kept in mind that fish larvae might have had a top-down effect on the plankton communities in the mesocosms after ~t32, even though this possible influence is most likely negligible.

TABLE 2 | Overview of measured variables in the experiment, including the analytical method, sampling method, and frequency, as well as corresponding papers providing an in-depth analysis of respective variables.

Variable	Analytical method	Sampling method and frequency	Corresponding paper
Bacteria and virus abundances	Microscopy/Flow cytometry	Pump sampling, every 2nd day, daily t25–t33	Taucher et al. b/ Hornick et al.
Bacterial protein production	¹⁴ C-Leucine uptake	IWS, every 2nd day, daily t25–t33	Hornick et al.
Bacterial community composition	¹⁴ C-Leucine uptake	IWS, every 2nd day, daily t25–t33	Hornick et al.
Biogenic silica	Spectrophotometry	Pump sampling, every 2nd day, daily t25–t33	Taucher et al. b
Carbon cycling: stable isotopes	Mass spectrometry	IWS, every 2nd day, daily t25–t33	Esposito et al.
Chlorophyll <i>a</i>	HPLC	Pump sampling, every 2nd day, daily t25–t33	This paper
Copepod condition	Stereomicroscopy	Apstein net, every 8 days	Algueró-Muñoz et al.
Dimethylsulfide (DMS) and precursor compounds	Gas chromatography	IWS, every 2nd day, daily t25–t33	Archer et al./ Suffrian et al.
Dissolved inorganic carbon (DIC)	IR absorption	IWS, every 2nd day, daily t25–t33	This paper
Dissolved organic carbon and nitrogen (DOC, DON)	High-temperature catalytic combustion	IWS, every 2nd day, daily t25–t33	Zark et al.
Dissolved organic phosphorus (DOP)	microwave digestion, spectrophotometry	IWS, every 2nd day, daily t25–t33	Taucher et al. b
Dissolved organic matter: molecular composition	ultra-high resolution mass spectrometry (FT-ICR-MS)	IWS, every 8 days	Zark et al.
Inorganic nutrient concentrations	Colorimetry (NO ₃ , PO ₄ , Si(OH) ₄), fluorometry (NH ₄)	IWS, every 2nd day, daily t23–t33	This paper
Light intensity (PAR)	CTD sensor	CTD profiles, every 2nd day, daily t25–t33	This paper
Mesozooplankton abundances	Stereomicroscopy, Image-based approach (ZooScan)	Apstein net, every 8 days	Algueró-Muñoz et al.
Mesozooplankton size distribution and biomass	Image-based approach (ZooScan)	Apstein net, every 8 days	Taucher et al. b
Mesozoopl. Metabolism (ETS, IDH, and GDH)	Spectrophotometry and fluorometry (kinetic assay)	Apstein net, every 8 days	Osma, N et al.
Microzooplankton abundances	Microscopy	IWS, every 8th day	Algueró-Muñoz et al.
N ₂ -fixation rates (light and dark)	¹⁵ N incorporation, EA-IRMS	IWS, every 4th day	Singh et al./ Wannicke et al.
Particle size distribution and characterization (<i>in situ</i>)	Underwater camera system (“KielVision”)	Imaging profiles, every 2nd day, daily t25–t43	Taucher et al. c
pH	Spectrophotometry and CTD sensor	IWS and CTD profiles, every 2nd day, daily t23–t33	This paper
Phytoplankton abundances and taxonomic identification	Microscopy	IWS, every 4th day	Taucher et al. b
Phytoplankton group abundances	Flow Cytometry	Pump sampling, every 2nd day, daily t25–t33	Taucher et al. b
Phytoplankton pigments	High-performance liquid chromatography (HPLC)	Pump sampling, every 2nd day, daily t25–t33	This paper/ Taucher et al. b
Plankton community metabolism (ETS, IDH)	Spectrophotometry (kinetic assay)	IWS, every 4th day, every 2nd day t25–t33	Tames-Espinosa et al.
Primary production (size-fractionated)	¹⁴ C and ¹³ C incorporation	IWS, every 4th day, every 2nd day t25–t33	Aristegui et al./ Singh et al.
Protein content of biomass	Spectrophotometry	IWS and sediment trap sampling in 2–4 day intervals	Tames-Espinosa et al.
Pteropods and foraminifera abundance	Stereomicroscopy	Apstein net, every 8 days, sediment trap sampling, every 2nd day	Lischka et al.
Salinity, temperature	CTD sensor	CTD profiles, every 2nd day, daily t25–t33	This paper
Sinking material—flux and elemental composition	Elemental analyzer, spectrophotometry	Sediment trap sampling, every 2nd day	Stange et al. a
Sinking material—sinking speed and respiration rates	Optical measurement (FlowCam), O ₂ consumption	Sediment trap sampling, every 2nd day	Stange et al. b
Sinking material—metabolism (ETS, IDH)	Spectrophotometry (kinetic assay)	Sediment trap sampling, every 4th day	Tames-Espinosa et al.
Transparent exopolymer particles (TEP)	Spectrophotometry	IWS, every 4th day, every 2nd day from t25 to t33	Taucher et al. c
Total alkalinity	Potentiometric titration	IWS, every 2nd day, daily t23–t33	This paper
Total particulate carbon and nitrogen (TPC, TPN)	Elemental analyzer	Pump sampling, every 2nd day, daily t25–t33	This paper/ Stange et al. a
Total particulate phosphorus (TPP)	Spectrophotometry	Pump sampling, every 2nd day, daily t25–t33	Stange et al. a

Sampling Procedures and CTD Operations

We conducted out a comprehensive sampling effort for a wide range of physical, ecological, and biogeochemical variables in the mesocosms and the surrounding waters on every second day, usually lasting from 9 a.m. until noon. An exception was the period right after deep water addition (t25–t33), when a rapid response of the plankton community was observed, and most variables were sampled on a daily basis.

Our preferred method of sample collection in mesocosm studies involves use of depth-integrating water samplers (IWS, HYDRO-BIOS, Kiel), which gently take in a total volume of 5 L uniformly distributed over the desired depth. However, this method is rather time-consuming, with one IWS haul usually lasting 3–4 min. Because the sample volume of oligotrophic water required for filtrations, incubations, etc., usually amounted to at least 60–70 L per mesocosm per day, we decided to adjust our sampling strategy and applied two methods of water collection in parallel, depending on the requirements of the various measurement variables (Table 2).

For variables that are sensitive to gas exchange or contamination, we collected integrated water samples using the IWS over 0–13 m water depth and directly filled subsamples into separate containers on the sampling boats following the specific requirements and protocol for the respective variable (see Section Data Analysis and Statistics). These sensitive variables were dissolved inorganic carbon (DIC), pH, dimethyl sulfide (DMS), inorganic nutrients [nitrate (NO₃⁻), nitrite (NO₂⁻), dissolved silicate (Si(OH)₄), ammonium (NH₄⁺), phosphate (PO₄³⁻)], dissolved organic carbon, nitrogen, and phosphorus (DOC, DON, DOP), and water for all *in vitro* incubation experiments such as primary production (¹³C and ¹⁴C), N₂-fixation, bacterial degradation of sinking organic matter, or bacterial protein production assays.

Samples for other variables (e.g., particulate organic matter) were obtained with a custom-built pump system that allowed for a much faster collection of large sampling volumes. The system consisted of a manually operated pump, a 20 L carboy, a valve with integrated pressure gauge that connected to a 20 m long plastic tube (25 mm diameter), and a special inlet with several water intakes mounted to the open end of the tube. By applying the pump, a gentle vacuum was created (<150 mbar) in order to suck in water from the mesocosms into the tube and carboy. By moving the tube and attached inlet up and down during pumping (0–13 m), integrated water samples similar to the ones obtained by the IWS could be collected. To achieve this, pumping rate and vertical movement were synchronized with the holding capacity of the sampling carboy in order to avoid overflow of water before the sample could be considered integrated, i.e., before the vertical profile was completed. The 20 L sample carboys were then stored protected from direct sunlight on deck of the boats until sampling was completed. Once on shore, the samples were stored in a dark and temperature-controlled room (set to 16°C) where subsamples were taken for a variety of ecological and biogeochemical measurements (Table 2).

Sinking particulate matter was collected in the sediment traps at the bottom of the mesocosms. Sampling of the sediment traps was carried out every second day throughout the entire

study, using a vacuum system connected to the tubes, which were attached to the collection cups following Boxhammer et al. (2016).

Mesozooplankton samples were acquired with an Apstein net (55 μm mesh size, 0.17 m diameter opening) in 8-day intervals. The maximum sampling depth of net tows was 13 m to avoid contact of the Apstein net with the sediment trap material, thus resulting in an overall sampling volume of ~295 L per net tow. Mesozooplankton samples were kept dark and cool until transport to shore, where they were preserved with sodium tetraborate-buffered formalin (4% v/v) for counting and taxonomic analyses. The number of zooplankton net catches per sampling day was restricted to every 8 days to avoid “overfishing,” i.e., exerting a too strong influence on top-down control of the system by removing zooplankton biomass.

CTD casts were carried out with a hand-held self-logging CTD probe (CTD60M, Sea and Sun Technologies) in each mesocosm and in the surrounding water on every sampling day. Thereby we obtained vertical profiles of temperature, salinity, pH, dissolved oxygen, chlorophyll *a*, and photosynthetically active radiation (PAR). Technical details on the sensors and data analysis procedures are described by Schulz and Riebesell (2013). Potentiometric measurements of pH_{NBS} (NBS scale) from the CTD were corrected to pH_T (total scale) by daily linear correlations of mean water column potentiometric pH_{NBS} to pH_T as determined from carbonate chemistry.

Sample Processing, Measurements, and Analysis

Carbonate Chemistry

Samples for dissolved inorganic carbon (DIC) and total alkalinity (TA) were gently sterile-filtered (0.2 μm pore size) using a peristaltic pump and stored at room temperature until measurement on the same day.

DIC concentrations were determined by infrared absorption using a LI-COR LI-7000 on an AIRICA system (MARIANDA, Kiel). Measurements were made on three replicates, with overall precision typically being better than 5 μmol kg⁻¹. TA was analyzed by potentiometric titration using a Metrohm 862 Compact Titrator and a 907 Titrando unit following the open-cell method described in Dickson et al. (2003). The accuracy of both DIC and TA measurements was determined by calibration against certified reference materials (CRM batch 126), supplied by A. Dickson, Scripps Institution of Oceanography (USA).

Other carbonate chemistry variables such as *p*CO₂, pH (on the total scale: pH_T), and aragonite saturation state (Ω_{aragonite}), were calculated from the combination of TA and DIC using CO2SYS (Pierrot et al., 2006) with the carbonate dissociation constants (K₁ and K₂) of Lueker et al. (2000).

Inorganic Nutrients

Samples for inorganic nutrients were collected in acid-cleaned (10% HCl) plastic bottles (Series 310 PETG), filtered (0.45 μm cellulose acetate filters, Whatman) directly after arrival of water samples in the laboratory, and analyzed on the same day to minimize potential changes due to biological activity. NO₃⁻

+ NO₂[−] (=NO₃[−]/NO₂[−]), Si(OH)₄, and PO₄^{3−} concentrations were measured with a SEAL Analytical QuAAtro AutoAnalyzer connected to JASCO Model FP-2020 Intelligent Fluorescence Detector and a SEAL Analytical XY2 autosampler. AACE v.6.04 software was used to control the system. The measurement approach is based on spectrophotometric techniques developed by Murphy and Riley (1962) and Hansen and Grasshoff (1983). Ammonium concentrations were determined fluorometrically following Holmes et al. (1999). Refractive index blank reagents were used (Coverly et al., 2012) in order to quantify and correct for the contribution of refraction, color, and turbidity on the optical reading of the samples. Instrument precision was calculated from the average standard deviation of triplicate samples [$\pm 0.007 \mu\text{M}$ for NO₃[−]/NO₂[−], $\pm 0.003 \mu\text{M}$ for PO₄^{3−}, $\pm 0.011 \mu\text{M}$ for Si(OH)₄, and $\pm 0.005 \mu\text{M}$ for NH₄⁺]. Detection limits for the different nutrients were 0.03 (NO₃[−]/NO₂[−]), 0.008 (PO₄^{3−}), 0.05 (Si(OH)₄), and 0.01 (NH₄⁺) $\mu\text{mol L}^{-1}$. Analyzer performance was controlled by monitoring baseline, calibration coefficients, and slopes of the nutrient species over time. The variations observed throughout the experiment were within the analytical error of the methods.

Chlorophyll *a* and Phytoplankton Pigments

Samples for chlorophyll *a* (chl-*a*) and other phytoplankton pigments were analyzed by reverse-phase high-performance liquid chromatography (HPLC, Barlow et al., 1997) following collection by gentle vacuum filtration (<200 mbar) onto glass fiber filters (GF/F Whatman, nominal pore size of 0.7 μm) with care taken to minimize exposure to light during filtration. Samples were retained in cryovials at -80°C prior to analysis in the laboratory. For the HPLC analyses, samples were extracted in acetone (100%) in plastic vials by homogenization of the filters using glass beads in a cell mill. After centrifugation (10 min, 5,200 rpm, 4°C) the supernatant was filtered through 0.2 μm PTFE filters (VWR International). From this, phytoplankton pigment concentrations were determined by a Thermo Scientific HPLC Ultimate 3,000 with an Eclipse XDB-C8 3.5 μm 4.6 \times 150 column. Contributions of individual phytoplankton groups to total Chl-*a* were then estimated using the CHEMTAX software, which classifies phytoplankton based on taxon-specific pigment ratios (Mackey et al., 1996). Furthermore, phytoplankton samples for microscopy were obtained every 4 days, fixed with acidic Lugol solution and analyzed using the Utermöhl technique (Utermöhl, 1931), with classification until the lowest possible taxonomical level.

Particulate Matter

Samples for particulate carbon and nitrogen (TPC/TPN) were filtered (<200 mbar) onto pre-combusted GF/F glass fiber filters (450°C for 6 h; Whatman 0.7 μm nominal pore size). Afterwards, sample filters were dried (60°C) overnight and wrapped in tin foil until analysis. Concentrations of carbon and nitrogen were measured on an elemental CN analyzer (EuroEA) following Sharp (1974). Note that for particulate carbon, one out of three replicate TPC filters per sample was fumed with hydrochloric acid (37%) for 2 h before measurement in order to remove particulate inorganic carbon (PIC) and thereby allowing us to

distinguish between inorganic and organic forms of particulate carbon (Bach et al., 2011). Comparison of TPC and POC (particulate organic carbon) indicated that PIC was virtually absent in the seawater during our study, i.e., TPC was constituted almost entirely of POC.

Zooplankton Community Composition

Microzooplankton samples were obtained every 8 days, immediately fixed after sub-sampling with acidic Lugol solution and stored in 250 mL brown glass bottles until analysis using the Utermöhl technique (Utermöhl, 1931). In the scope of this study we distinguished between ciliates and heterotrophic dinoflagellates.

Abundances of mesozooplankton (mostly copepods and appendicularia) from net haul samples (>55 μm , every 8 days) were counted using a stereomicroscope (Olympus SZX9) and classified until the lowest possible taxonomical level.

Data Analysis and Statistics

To identify potential ecological effects of CO₂ on the composition of the plankton community, we carried out multivariate analysis for abundance data of the different plankton groups. Therefore, we calculated the average abundances of different plankton groups during three experimental phases: (I) the oligotrophic phase until t23, (II) the phytoplankton bloom between t25 and t35, and (III) the post-bloom phase from t37 until the end of the study. All phytoplankton data used are from HPLC and CHEMTAX analysis, whereas numbers for micro- and meso-zooplankton were obtained by microscopy. In total, we distinguished 13 plankton functional groups that we used for analysis in the present study.

To account for the different scales of abundance of the various plankton groups, ranging from picophytoplankton (<2 μm) to mesozooplankton larger than 1 mm, all abundance data were normalized by their range as:

$$N_{\text{norm}} = N / (N_{\text{max}} - N_{\text{min}}) \quad (1)$$

where *N* is the abundance of each individual group, and *N*_{min} and *N*_{max} refer to the highest and lowest values found in the nine mesocosms. Thereby, all data are scaled to a range between 0 and 1, while maintaining the overall sample variance, as well as the relative differences between mesocosms.

After normalization of raw data, we generated ecological distance matrices using Bray–Curtis dissimilarity, which were then used for all multivariate analyses conducted here. In a first step, we performed non-metric multidimensional scaling (NMDS) to visualize ordination of the plankton communities in the mesocosms in response to CO₂ in the different experimental phases.

For a more quantitative assessment of how CO₂ might have influenced plankton community structure, we investigated the relationship between ecological distance (Bray–Curtis dissimilarity) and environmental distance, in this case pCO₂ (using Euclidian distance). Therefore, we applied a linear regression model to environmental and ecological distance data, using the same data matrices and phases as described above for

the NMDS approach. Thus, every data point in the regression analyses corresponds to a pair-wise comparison of mesocosms with respective environmental distance (differences in pCO₂) and ecological distance (Bray–Curtis dissimilarity). The latter was calculated using the same (normalized) abundance data from plankton groups as for the NMDS analysis. This method allowed us to detect whether differences in plankton community composition were related to pCO₂. A statistically significant relationship between CO₂ and plankton community composition was assumed for $p < 0.05$ in the linear regression. The Mantel Test serves to ensure that these patterns did not arise by chance (when $p < 0.05$). All multivariate statistical analysis were conducted with the Fathom Toolbox for MATLAB (Jones, 2015).

RESULTS AND DISCUSSION

Environmental Boundary Conditions

Environmental conditions in Gando Bay during the mesocosm experiment were typical for late summer/early fall in the study region. Average temperatures in the mesocosms slightly decreased from ~24.4 to 22.3°C over the course of the study, corresponding to decreasing air temperatures during early autumn (Figure 4, Supplementary Material). Vertical profiles of temperature and salinity from the CTD showed a uniform distribution of both variables, indicating that there was no stratification and that the water columns in the mesocosms

were well-mixed throughout the entire study period (Figure 4). Temperature profiles of the surrounding waters in Gando Bay were very similar to those in the mesocosms.

Average salinity in the mesocosms steadily increased from ~36.95 to 38.05 during the experimental period, interrupted only by a decrease due to addition of (less saline) deep water on t24 (Figure 4). The salinity increase was driven by evaporation, which was substantial due to relatively high temperatures and usually windy conditions (see Supplementary Material). In contrast, salinity in the surrounding waters remained almost constant throughout the experimental period. Because of this salinity difference, we could easily detect the presence of holes due to damaged mesocosm walls based on daily changes in salinity: When lower salinity water from the surrounding water entered the mesocosms, the daily increase in salinity of a particular mesocosm was lower than in the other mesocosms. Based on these observations, we could observe that M4 and M9 had holes around t11 (M4) and t13 (M9). Divers sealed the holes immediately after detection, by gluing small rubber patches onto the outside of the mesocosm bags.

To what extent these water intrusions might have affected the composition of the plankton communities in the mesocosms is difficult to assess, especially since they occurred during the oligotrophic phase when plankton abundances were low and measurement variability was comparably high. However, we did not observe anomalies in any of the measured variables

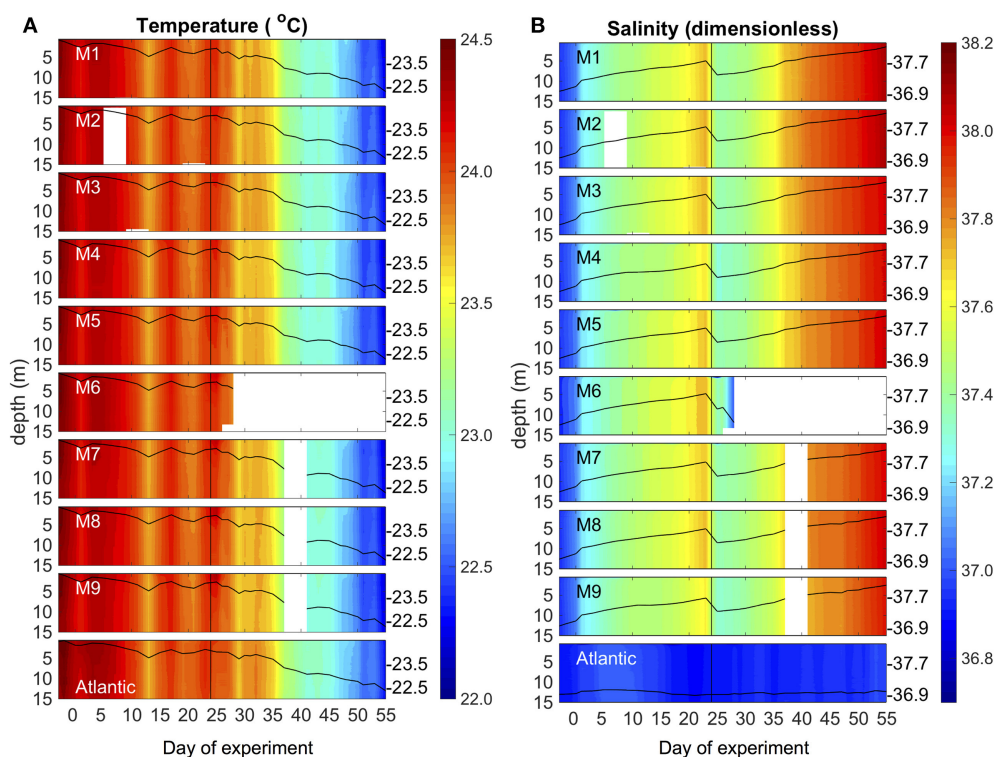


FIGURE 4 | Vertical profiles of temperature (A) and salinity (B) in the mesocosms (M1–M9) and the surrounding Atlantic over the course of the study. Average values over the entire water column are represented by the black lines on top of the colored contours, including the corresponding additional y-axes on the right side of the boxes. The vertical black line on t24 denotes deep water addition into the mesocosms.

during or after these damages. Furthermore, neither M4 nor M9 displayed any fundamental differences in plankton community composition or succession patterns throughout the rest of the study. Thus, we are confident that the temporal water intrusions through the holes only had a minor influence on the results presented here.

Carbonate Chemistry and Simulated Ocean Acidification

The injection of different amounts of CO₂-enriched seawater into the mesocosms in the period between t0 and t6 elevated DIC concentrations from initial values of ~2,079 up to 2,342 $\mu\text{mol kg}^{-1}$ in the highest CO₂ treatment (M8). The corresponding increase in pCO₂ resulted in a treatment gradient ranging from 410 to 1414 μatm after the initial CO₂ enrichment (t7, **Figure 5**).

Afterwards, pCO₂ in the mesocosms decreased quite rapidly due to gas exchange at the air-sea interface. Although, we did not carry out direct measurements of gas exchange, the rapid decreases in pCO₂ and DIC until t20 were not reflected in build-up of total particulate carbon (TPC, **Figure 7C**), suggesting that the loss of inorganic carbon can be attributed predominantly to outgassing of CO₂. This is consistent with theoretical considerations, which suggest that rates of gas exchange should be high under the environmental conditions during our study, i.e., relatively high water temperatures, high wind speeds, and constant convective mixing of the entire water column in the mesocosms (Smith, 1985; Jähne et al., 1987). During the plankton bloom between t25 and

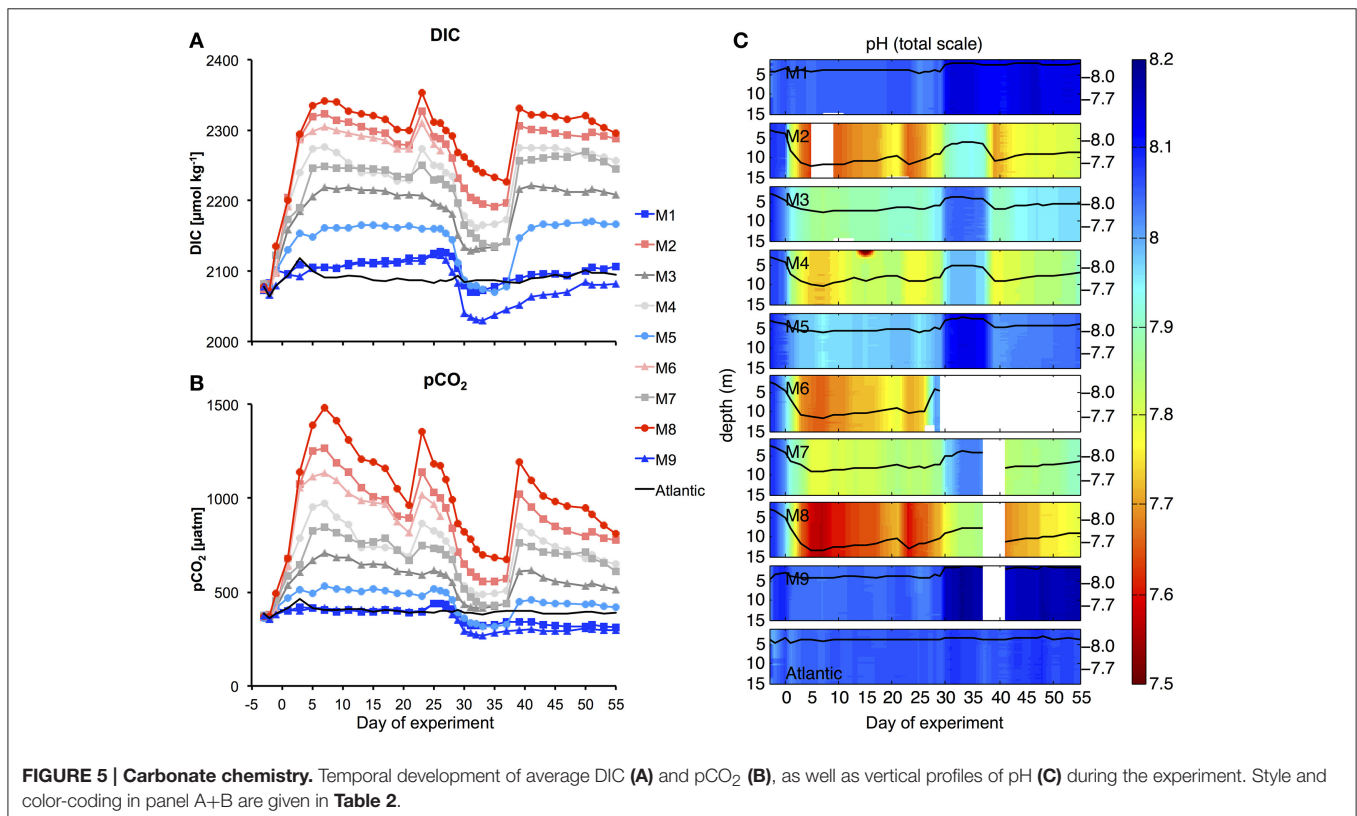
t35 (see Section Oligotrophic Phase and Plankton Bloom in Response to Deep Water Addition), the decline in DIC concentrations was further enhanced by photosynthetic CO₂ fixation.

To compensate for the loss of CO₂ and readjust the treatment gradient, we conducted two more CO₂ enrichments on t21 and t38 (**Figure 5**). Altogether, the CO₂ gradient could be maintained reasonably well throughout the entire study. Furthermore, vertical profiles of pH show that carbonate chemistry conditions were distributed equally over the depth of the mesocosms, ensuring that all organisms in the water column experienced similar CO₂ conditions (**Figure 5C**).

Oligotrophic Phase and Plankton Bloom in Response to Deep Water Addition

Oligotrophic Phase

During the first few weeks of the experiment, we observed typical oligotrophic conditions in the mesocosms. Concentrations of all inorganic nutrients were very low and relatively constant. Average concentrations of NO₃⁻+NO₂⁻, PO₄³⁻, and Si(OH)₄ until t23 were 0.06 ± 0.01, 0.026 ± 0.004, and 0.26 ± 0.04 $\mu\text{mol L}^{-1}$, respectively (**Figure 6**). These values are within the range of observations for oligotrophic conditions in this region (Neuer et al., 2007). Correspondingly, chlorophyll *a* concentrations were very low, amounting to ~0.1 $\mu\text{g L}^{-1}$ on average until t23 (**Figure 7A**). Despite these low nutrient concentrations, chl-*a* slightly increased from ~0.05 to 0.13 $\mu\text{g L}^{-1}$ between t1 and t11 (**Figure 7B**).



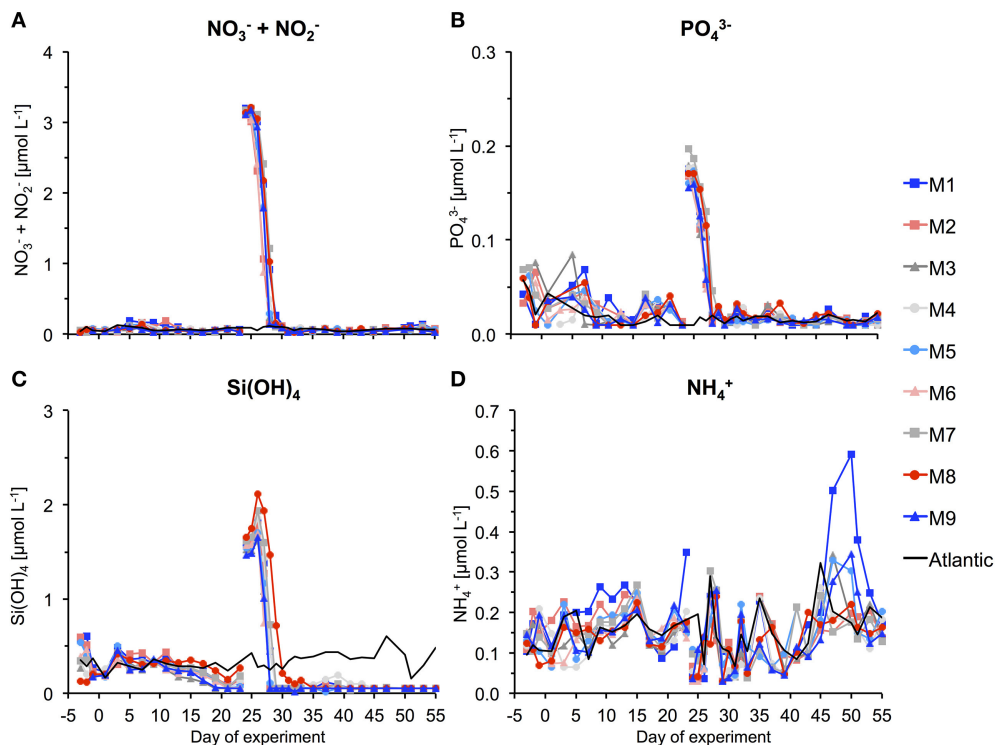


FIGURE 6 | Inorganic nutrient concentrations over the course of the study. The gap and associated change in concentrations between t23 and t25 denotes addition of nutrient-rich deep water to the mesocosms. (A) Nitrate and nitrite, (B) phosphate, (C) silicate, and (D) ammonium.

Between t16 and t22, easterly winds transported dust from the Sahara desert to the Canary Islands and the experiment site. Such dust events regularly occur in the study area and can sometimes constitute a considerable source for input of trace nutrients, such as iron (Gelado-Caballero et al., 2012). The total dry deposition flux from t16 to t22 was estimated at $\sim 230 \text{ mg m}^{-2}$, which is comparable to other weak dust events in the region (Gelado-Caballero, Personal Communication). It is noteworthy that some nutrients displayed changes that coincided with the period of dust deposition. Si(OH)_4 concentrations began to decrease slightly until t23, and NH_4^+ also decreased between t15 and t19. While it is possible that this was at least partly driven by stimulation of phytoplankton growth in response to dust deposition, a closer look at the temporal development of chl-*a* indicates that growth began in fact much earlier (from t1 onwards, Figure 7B). Thus, we conclude that dust deposition did most likely not have a major effect on the phytoplankton communities in our experiment.

Deep Water Addition and Phytoplankton Bloom

On day t22, we collected $\sim 85 \text{ m}^3$ of oceanic deep water with inorganic nutrient concentrations of 16.7, 1.05, and $7.46 \mu\text{mol L}^{-1}$ for $\text{NO}_3^- + \text{NO}_2^-$, PO_4^{3-} , and Si(OH)_4 , respectively. After injection of known volumes of deep water into the mesocosms in the night from day t24 to t25, inorganic nutrients were elevated to concentrations of ~ 3.15 , 0.17 , and $1.60 \mu\text{mol L}^{-1}$

for $\text{NO}_3^- + \text{NO}_2^-$, PO_4^{3-} , and Si(OH)_4 , respectively (Figure 6, Table 3).

Chl-*a* concentrations increased rapidly in response to supply of inorganic nutrients from the deep water addition. Maximum values were reached on t28 in all mesocosms, being elevated by more than 25-fold compared to oligotrophic conditions before the bloom (Figures 7A,B). Correspondingly, inorganic nutrients were depleted quickly, reaching values close to detection limit between t28 and t30 (Figure 6).

After the bloom peak, chl-*a* declined rapidly until t35, when it even started to increase again slightly in some of the mesocosms (M2, M8). Afterwards, chl-*a* levels displayed some fluctuations with an overall decreasing tendency until the end of the study. Yet, concentrations remained clearly elevated compared to oligotrophic conditions before the bloom.

Particulate Carbon

The proportional increase of TPC concentrations after deep water addition was similar to that of chlorophyll *a* during the phytoplankton bloom (Figure 7C). However, the decline of TPC after the bloom peak was much slower and concentrations remained at levels much higher than before the bloom, suggesting that a large portion of biomass generated by phytoplankton was retained in the water column, e.g., by being transferred into heterotrophic biomass or by accumulating as detritus with close to neutral buoyancy (mucus-rich aggregates/marine snow).

Definition of Experimental Phases

Based on the timing of deep water addition and the temporal development of chlorophyll *a* concentrations described above, we define three major experimental phases (**Figure 7A**): The oligotrophic phase (I) from t1 until t23 covers the entire period of low chl-*a* concentrations before addition of deep water on t24. Phase II lasts from t25 to t35 and encompasses the entire bloom event that occurred in response to deep water addition.

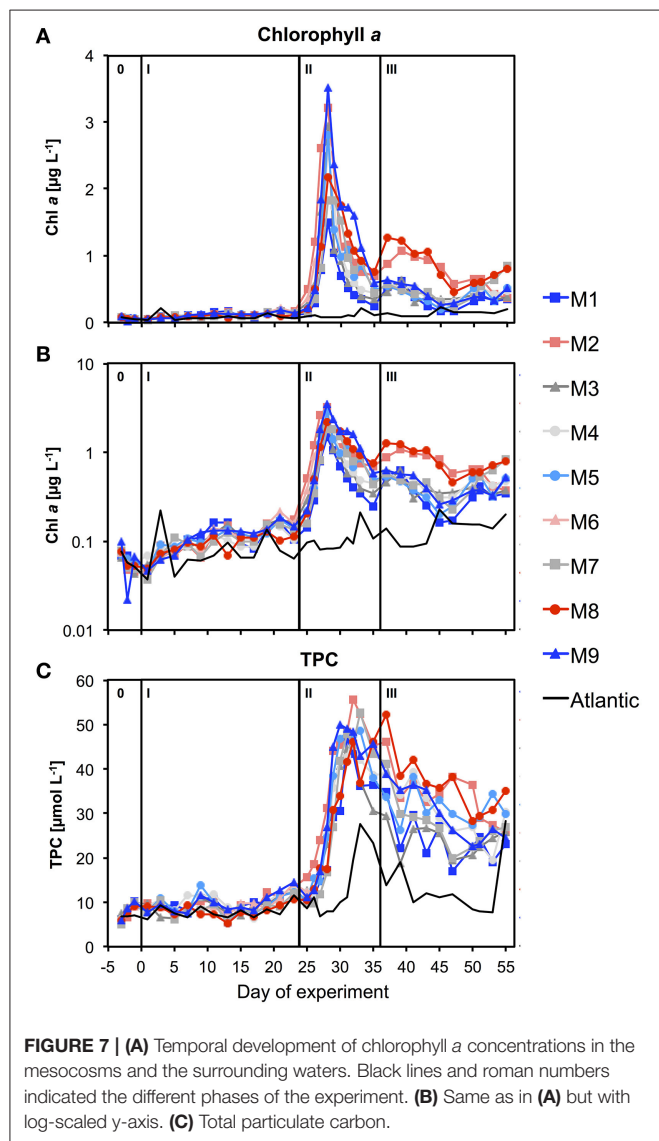


TABLE 3 | Inorganic nutrient concentrations in the mesocosms after deep water addition (t25).

	M1	M2	M3	M4	M5	M7	M8	M9	Mean ± SD
NO ₃ ⁻ +NO ₂ ⁻	3.17	3.01	3.11	3.18	3.16	3.19	3.21	3.18	3.15 ± 0.06
PO ₄ ³⁻	0.17	0.17	0.16	0.18	0.17	0.19	0.17	0.16	0.17 ± 0.01
Si(OH) ₄	1.57	1.63	1.52	1.66	1.55	1.65	1.74	1.49	1.60 ± 0.09
NH ₄ ⁺	0.04	0.04	0.04	0.09	0.09	0.08	0.04	0.10	0.07 ± 0.03

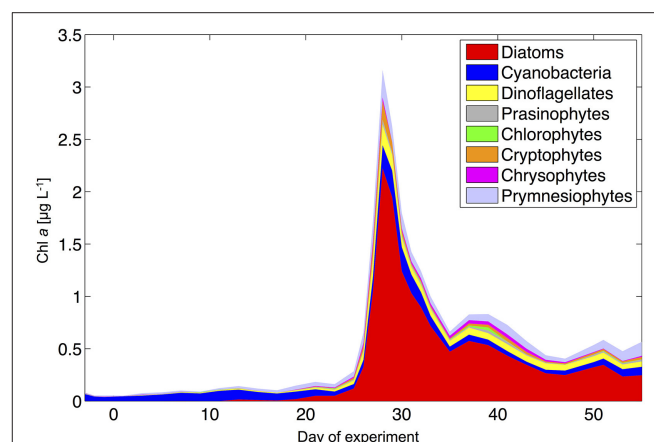
This includes both the major chl-*a* build-up until t28 as well as the subsequent bloom decline until t35, when the decrease in chl-*a* stopped. The post-bloom phase (III) covers the entire remaining period from t37 until the end of the experiment on t57. Note that phase 0 includes baseline data from the time before the first CO₂ manipulation (t-3 and t-1) and was thus excluded from statistical analysis of CO₂ effects.

Plankton Community Structure and Influence of Ocean Acidification

During the oligotrophic phase, the phytoplankton community was dominated by small phytoplankton, mostly consisting of cyanobacteria (*Synechococcus*), which constituted 70–80% of chlorophyll *a* (**Figure 8**). This picture changed in phase II, when deep water addition resulted in a pronounced phytoplankton bloom that was dominated by diatoms, accounting for >70% of total chlorophyll *a*. Microscopic analysis revealed that the dominant species were relatively large chain-forming diatoms such as *Leptocylindrus* sp., *Guinardia* sp., and *Bacteriastrum* sp., but also detected other species such as *Nitzschia* sp. at lower abundances. The remaining phytoplankton consisted mainly of dinoflagellates, Dictyocha-like flagellates (belonging to chrysophytes) in some mesocosms, and prymnesiophytes (mostly *Phaeocystis* sp.) throughout the experiment (**Figure 8**).

Microzooplankton communities in the mesocosms were mainly composed of ciliates and heterotrophic dinoflagellates, whereas mesozooplankton was dominated by different copepod species and nauplii, but also included other functional groups such as appendicularia (Algueró-Muñiz et al., in preparation).

It should be noted that underwater video footage indicated the formation of some patchy benthic growth on parts of the inner mesocosm surfaces, which could not be cleaned (i.e., the conical sediment trap and parts of the lowest mesocosm segment, see Section Mesocosm Setup, Deployment Procedure, and Maintenance). Pigment analysis of this organic material suggested that it consisted to a large part of *Phaeocystis* colonies. In fact, adhesion to surfaces and subsequent rapid colony



formation is characteristic for *Phaeocystis* (Rousseau et al., 2007). However, since the affected area was rather small compared to the mesocosm volume (~10 m² uncleaned mesocosm wall surface vs. 35 m³ mesocosm volume), we are confident that this wall growth did not significantly affect the results for phytoplankton community composition and biogeochemistry presented in this study.

Altogether, the phytoplankton succession pattern observed in our mesocosms—switching from prevalence of picoeukaryotes and picocyanobacteria (*Synechococcus*) toward a system dominated by large diatoms and dinoflagellates—is typical for the transition from open ocean gyres to coastal upwelling regions, as well as for the species succession in mesoscale eddies (Aristegui et al., 2004; Brown et al., 2008).

The main objectives of our mesocosm campaign were to investigate (a) how ocean acidification could change plankton community composition and food-web structure in oligotrophic environments, and (b) if such potential changes might amplify or weaken during periodic upwelling events of nutrient-rich deep water. In the present paper we assess how increasing CO₂ could affect the structure of plankton community as a whole. Therefore, we included and analyzed data from different functional groups of plankton, but did not investigate patterns within these groups at more taxonomic detail, e.g., on the species level. Such questions will be investigated in more targeted studies presented within the framework of this Research Topic (Table S1).

Our analysis at the level of functional groups revealed a significant effect of CO₂ on plankton community structure, both under oligotrophic conditions (phase I) and throughout the bloom induced by simulated upwelling of deep water (phases II and III). NMDS spaces (Figure 9) show the ordination of the mesocosms according to differences in their plankton community composition. The NMDS analysis of the different phases suggests the emergence of clear differences in plankton community structure, resulting in ordination of mesocosms according to the CO₂ treatment. Notably, these differences are not attributable to the response of only one or two dominant species, but emerged from overall shifts across the entire plankton community, including various groups of phytoplankton, micro- and meso-zooplankton (Figure 9). Particularly during the bloom (phase II) and post-bloom (phase III), the two highest CO₂ mesocosms (M2, M8) appear strongly separated from the others (Figures 9B,C).

More detailed analyses of the multivariate ecological datasets reveal a significant correlation between environmental distance (i.e., differences in pCO₂) and dissimilarity among plankton communities in the mesocosms throughout the entire study (Figure 10). During the initial oligotrophic phase (A), the plankton communities in the mesocosms were generally very similar to each other (low ecological distance between 0.1 and 0.2). However, the significant positive correlation between pCO₂ (distance) and ecological distance indicates that differences between plankton communities were larger at increasing differences in pCO₂ (Figure 10A, Table 4). In other words, differences in community composition were significantly related to differences in pCO₂ already during oligotrophic condition. These findings suggest that restructuring of

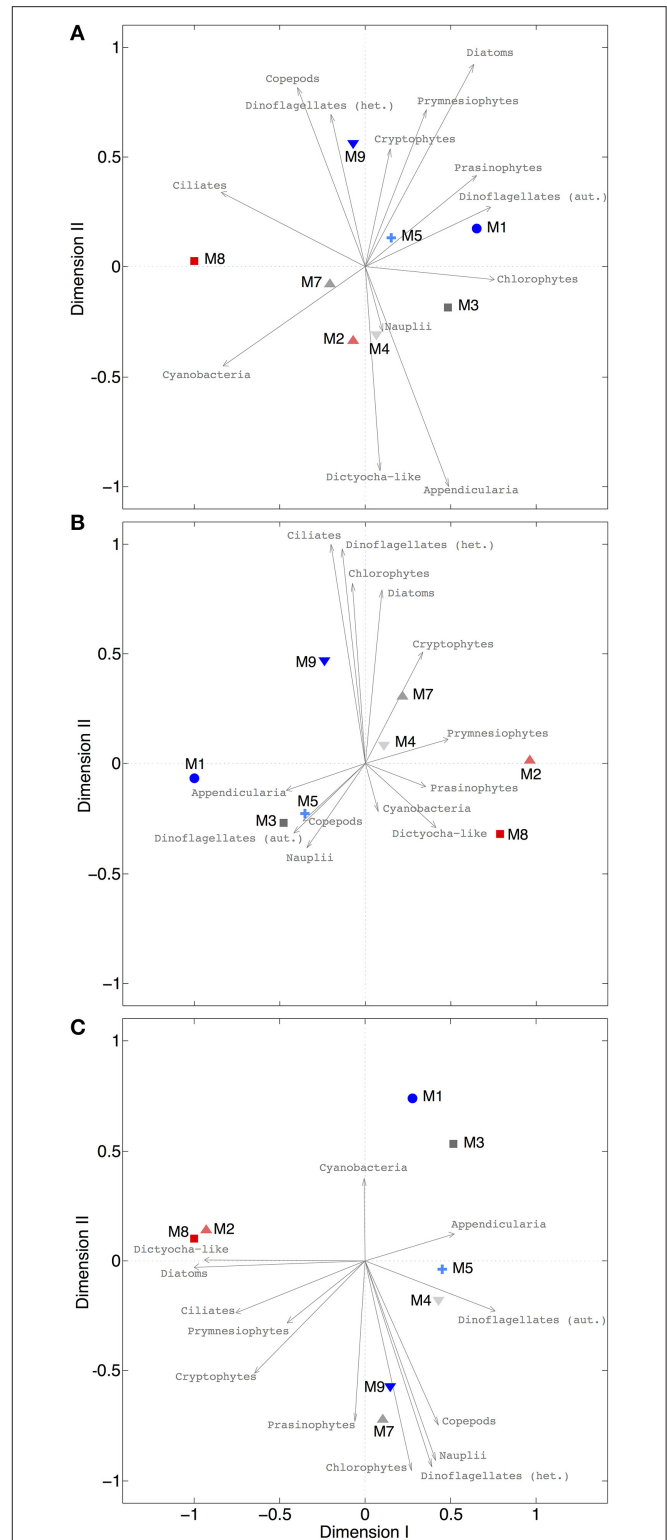


FIGURE 9 | NMDS plots for different phases. (A) Oligotrophic phase (final stress = 0.0079), **(B)** plankton bloom (final stress = 0.0004), **(C)** post-bloom phase (final stress = 0.0221). Since all stress values are <0.1, it can be assumed that all configurations show actual dissimilarities among plankton communities in the mesocosms. Arrows indicate the role of the various plankton groups in ordination of the mesocosms.

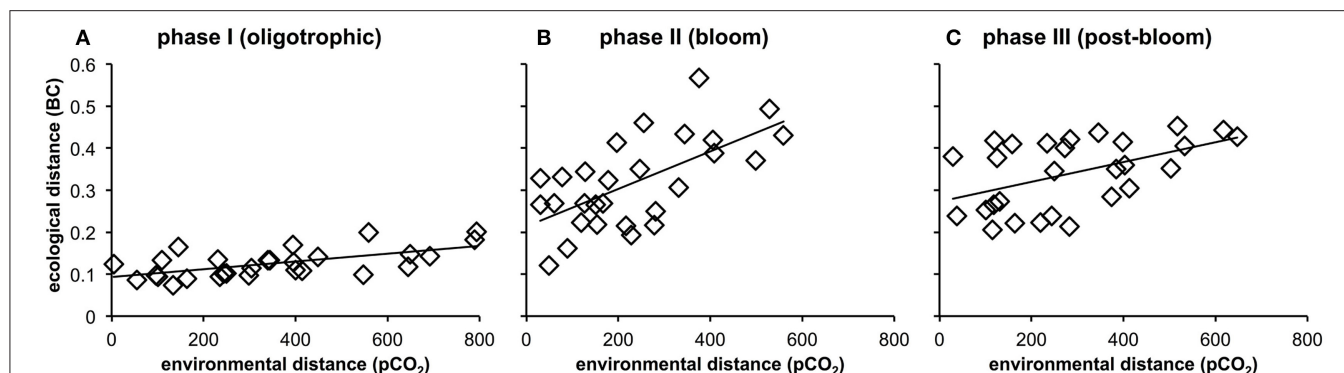


FIGURE 10 | Relationship between environmental distance (difference in pCO₂) and ecological distance (difference in plankton community composition) in the mesocosms during the oligotrophic phase (A), the deep water induced phytoplankton bloom (B), and the post-bloom phase (C). Correlations were significant for all experimental phases ($p < 0.05$, $n = 56$, **Table 4**). See Methods (Data Analysis and Statistics) for more detailed information on the statistical analysis.

TABLE 4 | Linear regression of ecological vs. environmental distance.

Linear regression: Ecological distance vs. environmental distance (pCO ₂)					Mantel test	
Equation	R ²	F	p		r	p
Phase I $y = 9 \cdot 10^{-5}x + 0.0932$	0.38	32.432	<0.001		0.61	0.0044
Phase II $y = 0.0004x + 0.2136$	0.40	36.648	<0.001		0.64	0.0040
Phase III $y = 0.0002x + 0.2727$	0.24	17.259	<0.001		0.49	0.0126

Results from linear regression and Mantel test with $p < 0.05$ denoting that dissimilarities among plankton communities in the mesocosms became significantly (linearly) stronger with increasing CO₂.

Significant values ($p < 0.05$) are marked in bold.

plankton communities can occur under prolonged low-nutrient conditions, where observed variability in biomass is generally low. This conclusion is in line with recent studies in different oceanic regions, which reported most prominent effects of OA when inorganic nutrients were depleted (Paul et al., 2015; Sala et al., 2015; Bach et al., 2016). However, our study is the first to demonstrate this for oligotrophic waters of the subtropical North Atlantic.

Interestingly, the magnitude of the pCO₂ effect on community structure became even larger during the bloom, displaying a much more distinct influence of pCO₂ on plankton community structure as visible by a much steeper slope of the correlation in **Figure 10B** (also see **Table 4**). This finding suggests that rather subtle changes in community composition arising under oligotrophic conditions can be amplified during productive phases in response to upwelling events, resulting in pronounced differences in succession patterns and food-web structure under high CO₂ conditions. The correlation between environmental distance (pCO₂) and ecological dissimilarity (community structure) was still visible, but weaker, during the post-bloom phase (**Figure 10C**). This might be explainable by the overall increase in variability among mesocosms, which is indicated by the generally higher ecological distance of ~0.3–0.4 even at low pCO₂ differences. Although, the correlation between

environmental distance (pCO₂) and ecological dissimilarity (community structure) weakened during the post-bloom phase (**Figure 10C**), the CO₂ effect became visible in bulk variables such as chl-*a* or particulate carbon during this period (**Figure 7**). These effects are mostly driven by the two mesocosms with highest CO₂ concentrations (M2, M8), which also appear notably separated in the NMDS space during phase II and III (**Figures 9B,C**).

Evaluation of Simulated Upwelling of Deep Water

The results presented in the previous sections indicated a successful deep water addition to the mesocosms that broadly resembled natural upwelling events and associated phytoplankton blooms in the study region. Compared to field observations of nutrient and chlorophyll during upwelling-induced blooms in the Canary Islands region, nutrient inputs as well as rate and magnitude of biomass accumulation in our experiment were slightly elevated (Aristegui et al., 1997; Garcia-Munoz et al., 2004; Neuer et al., 2007; Lathuiliere et al., 2008).

These differences likely arise from diverging modes of deep water input between our experiment and the real ocean. Eddy-induced upwelling of deep water around the Canary Islands occurs gradually over several days or weeks, thereby constantly mixing nutrient-rich deep water with nutrient-depleted surface water (Aristegui et al., 1997; Sangra et al., 2005, 2009). In our experiment, deep water was injected in a pulsed manner (i.e., within a few hours). This created a nutrient increase that was somewhat stronger than usually observed during natural eddy-driven upwelling events in the study region. In a broader sense, these different modes of deep water input between our mesocosm experiment and eddy-induced upwelling in the real ocean can be considered analogous to batch cultures and chemostat approaches in laboratory studies, respectively.

We cannot exclude the possibility that differences between pulsed and prolonged-diluted nutrient supply could alter the build-up rates and magnitude of biomass accumulation, and thereby possibly also community composition and

biogeochemical cycling. However, since plankton community structure and species succession during our study closely resembled those during natural bloom events in the Canary Islands region (Basterretxea and Aristegui, 2000; Aristegui et al., 2004), we are confident that our findings are broadly representative for natural marine ecosystems of the study area.

CONCLUSION AND OUTLOOK

Our study presents the first results from an *in situ* mesocosm experiment, in which we investigated how ocean acidification could affect plankton communities in the oligotrophic waters of the subtropical North Atlantic. One of our particular interests was to assess whether sensitivities to elevated CO₂ might differ between oligotrophic conditions and bloom situations, which regularly develop in response to periodic upwelling of nutrient-rich deep water in the study region. Using a specifically-designed deep water collector, we obtained 85 m³ of water from 650 m depth and successfully simulated a natural upwelling event in our mesocosm experiment.

Our analysis revealed a pronounced effect of increasing CO₂ concentrations on plankton community composition in the eastern subtropical North Atlantic. Moreover, our results suggest that a CO₂-driven restructuring of plankton communities under oligotrophic conditions might further amplify in bloom situations occurring in response to upwelling of deep water. These shifts in plankton community structure might profoundly influence food-web interactions and biogeochemical cycling of subtropical ecosystems. Since oligotrophic waters of the great ocean gyres cover more than half of the global ocean surface, we conclude that future research efforts in the field of ocean acidification should increasingly focus on the possible impacts in these vast oceanic regions.

AUTHOR CONTRIBUTIONS

Conceived and designed the experiment: UR, JT, LB, TB, JC, MS, and PS. Performed the experiment: All authors. Analyzed the data: JT, LB, TB, AN, MA, JA, ME, WG, HH, AL, JM, CS, and PS. Wrote the paper: JT with input from all co-authors.

ACKNOWLEDGMENTS

We would like to thank the Oceanic Platform of the Canary Islands (Plataforma Oceánica de Canarias, PLOCAN) for their hospitality, magnificent support and sharing their

research facilities with us. Another special thanks goes to the Marine Science and Technology Park (Parque Científico Tecnológico Marino, PCTM) and the Spanish Bank of Algae (Banco Español de Algas, BEA), both from the University of Las Palmas (ULPGC), who provided additional facilities to run experiments, measurements, and analyses.

Furthermore, we thank the captain and crew of RV *Hesperides* for deploying and recovering the mesocosms (cruise 29HE20140924), and RV *Poseidon* for transporting the mesocosms and support in testing the deep water collector during cruise POS463.

This project was funded by the German Federal Ministry of Education and Research (BMBF) in the framework of the coordinated project BIOACID—Biological Impacts of Ocean Acidification, phase 2 (FKZ 03F06550). UR received additional funding from the Leibniz Award 2012 by the German Research Foundation (DFG). Furthermore, the Natural Environment Research Council provided funding for EA and ME as part of the UK Ocean Acidification Programme (NE/H017348/1).

Members of the Gran Canaria KOSMOS Consortium

Nicole Aberle-Malzahn, Steve Archer, Maarten Boersma, Nadine Broda, Jan Büdenbender, Catriona Clemmesen, Mario Deckelnick, Thorsten Dittmar, Maria Dolores-Gelado, Isabel Dörner, Igor Fernández-Urruzola, Marika Fiedler, Matthias Fischer, Peter Fritsche, May Gomez, Hans-Peter Grossart, Giannina Hattich, Joaquin Hernández-Brito, Nauzet Hernández-Hernández, Santiago Hernández-León, Thomas Hornick, Regina Kolzenburg, Luana Krebs, Matthias Kreuzburg, Julia A. F. Lange, Silke Lischka, Stefanie Linsenbarth, Carolin Löscher, Ico Martínez, Tania Montoto, Kerstin Nachtigall, Natalia Osma-Prado, Theodore Packard, Christian Pansch, Kevin Posman, Besay Ramírez-Bordón, Vanesa Romero-Kutzner, Christoph Rummel, Maria Salta, Ico Martínez-Sánchez, Henning Schröder, Scarlett Sett, Arvind Singh, Kerstin Suffrian, Mayte Tames-Espinosa, Maren Voss, Elisabeth Walter, Nicola Wannicke, Juntian Xu, Maren Zark.

SUPPLEMENTARY MATERIAL

The Supplementary Material for this article can be found online at: <http://journal.frontiersin.org/article/10.3389/fmars.2017.00085/full#supplementary-material>

REFERENCES

- Aparicio-Gonzalez, A., Duarte, C. M., and Tovar-Sanchez, A. (2012). Trace metals in deep ocean waters: a review. *J. Mar. Syst.* 100, 26–33. doi: 10.1016/j.jmarsys.2012.03.008
- Aristegui, J., Barton, E. D., Alvarez-Salgado, X. A., Santos, A. M. P., Figueiras, F. G., Kifani, S., et al. (2009). Sub-regional ecosystem variability in the Canary Current upwelling. *Prog. Oceanogr.* 83, 33–48. doi: 10.1016/j.pocean.2009.07.031
- Aristegui, J., Barton, E. D., Tett, P., Montero, M. F., Garcia-Munoz, M., Basterretxea, G., et al. (2004). Variability in plankton community structure, metabolism, and vertical carbon fluxes along an upwelling filament (Cape Juby, NW Africa). *Prog. Oceanogr.* 62, 95–113. doi: 10.1016/j.pocean.2004.07.004
- Aristegui, J., Hernández-León, S., Montero, M. F., and Gomez, M. (2001). The seasonal planktonic cycle in coastal waters of the Canary Islands. *Sci. Mar.* 65, 51–58. doi: 10.3989/scimar.2001.65s151
- Aristegui, J., Tett, P., Hernandez-Guerra, A., Basterretxea, G., Montero, M. F., Wild, K., et al. (1997). The influence of island-generated eddies on chlorophyll

- distribution: a study of mesoscale variation around Gran Canaria. *Deep Sea Res. I Oceanogr. Res. Pap.* 44, 71–96. doi: 10.1016/S0967-0637(96)00093-3
- Bach, L. T., Riebesell, U., and Schulz, K. G. (2011). Distinguishing between the effects of ocean acidification and ocean carbonation in the coccolithophore *Emiliania huxleyi*. *Limnol. Oceanogr.* 56, 2040–2050. doi: 10.4319/lo.2011.56.6.2040
- Bach, L. T., Taucher, J., Boxhammer, T., Ludwig, A., Achterberg, E. P., Algueró-Muiz, M., et al. (2016). Influence of ocean acidification on a natural winter-to-summer plankton succession: first insights from a long-term mesocosm study draw attention to periods of low nutrient concentrations. *PLoS ONE* 11:e0159068. doi: 10.1371/journal.pone.0159068
- Barlow, R. G., Cummings, D. G., and Gibb, S. W. (1997). Improved resolution of mono- and divinyl chlorophylls a and b and zeaxanthin and lutein in phytoplankton extracts using reverse phase C-8 HPLC. *Mar. Ecol. Prog. Ser.* 161, 303–307. doi: 10.3354/meps161303
- Barton, E. D., Aristegui, J., Tett, P., Canton, M., García-Braun, J., Hernández-León, S., et al. (1998). The transition zone of the Canary Current upwelling region. *Prog. Oceanogr.* 41, 455–504. doi: 10.1016/S0079-6611(98)00023-8
- Basterretxea, G., and Aristegui, J. (2000). Mesoscale variability in phytoplankton biomass distribution and photosynthetic parameters in the Canary-NW African coastal transition zone. *Mar. Ecol. Prog. Ser.* 197, 27–40. doi: 10.3354/meps197027
- Boxhammer, T., Bach, L. T., Czerny, J., and Riebesell, U. (2016). Technical note: sampling and processing of mesocosm sediment trap material for quantitative biogeochemical analysis. *Biogeosciences* 13, 2849–2858. doi: 10.5194/bg-13-2849-2016
- Brown, S. L., Landry, M. R., Selph, K. E., Jin Yang, E., Rii, Y. M., and Bidigare, R. R. (2008). Diatoms in the desert: plankton community response to a mesoscale eddy in the subtropical North Pacific. *Deep Sea Res. II Top. Stud. Oceanogr.* 55, 1321–1333. doi: 10.1016/j.dsr2.2008.02.012
- Caldeira, K., and Wickett, M. E. (2003). Anthropogenic carbon and ocean pH. *Nature* 425, 365–365. doi: 10.1038/425365a
- Coverly, S., Kerouel, F., and Aminot, A. (2012). A re-examination of matrix effects in the segmented-flow analysis of nutrients in sea and estuarine water. *Anal. Chim. Acta* 712, 94–100. doi: 10.1016/j.aca.2011.11.008
- Dickson, A. G., Afghan, J. D., and Anderson, G. C. (2003). Reference materials for oceanic CO₂ analysis: a method for the certification of total alkalinity. *Mar. Chem.* 80, 185–197. doi: 10.1016/S0304-4203(02)00133-0
- Gamble, J. C., and Davies, J. M. (1982). “Application of enclosures to the study of marine pelagic systems,” in *Marine Mesocosms: Biological and Chemical Research in Experimental Ecosystems*, eds G. D. Grice and M. R. Reeve (New York, NY: Springer), 25–48.
- García-Munoz, M., Aristegui, J., Montero, M. F., and Barton, E. D. (2004). Distribution and transport of organic matter along a filament-eddy system in the Canaries – NW Africa coastal transition zone region. *Prog. Oceanogr.* 62, 115–129. doi: 10.1016/j.pocean.2004.07.005
- Gazeau, F., Sallon, A., Maugendre, L., Louis, J., Dellisanti, W., Gaubert, M., et al. (2016). First mesocosm experiments to study the impacts of ocean acidification on plankton communities in the NW Mediterranean Sea (MedSea project). *Estuar. Coast. Shelf Sci.* 186, 11–29. doi: 10.1016/j.ecss.2016.05.014
- Gelado-Caballero, M. D., López-García, P., Prieto, S., Patey, M. D., Collado, C., and Hernández-Brito, J. J. (2012). Long-term aerosol measurements in Gran Canaria, Canary Islands: particle concentration, sources and elemental composition. *J. Geophys. Res. Atmosp.* 117, D03304. doi: 10.1029/2011JD016646
- Hansell, D. A., Carlson, C. A., Repeta, D. J., and Schlitzer, R. (2009). Dissolved organic matter in the ocean: A controversy stimulates new insights. *Oceanography* 22, 202–211. doi: 10.5670/oceanog.2009.109
- Hansen, H. P., and Grasshoff, K. (1983). “Automated chemical analysis,” in *Methods of Seawater Analysis*, eds K. Grasshoff, M. Ehrhardt, and K. Kremling (Weinheim: Verlag Chemie), 347–379.
- Holmes, R. M., Aminot, A., Kerouel, R., Hooker, B. A., and Peterson, B. J. (1999). A simple and precise method for measuring ammonium in marine and freshwater ecosystems. *Can. J. Fish. Aquat. Sci.* 56, 1801–1808. doi: 10.1139/f99-128
- Hornick, T., Bach, L. T., Crawford, K. J., Spilling, K., Achterberg, E. P., Brussaard, C. P. D., et al. (2016). Ocean acidification indirectly alters trophic interaction of heterotrophic bacteria at low nutrient conditions. *Biogeosci. Discuss.* 2016, 1–37. doi: 10.5194/bg-2016-61
- IPCC (2014). *Climate Change 2014: Impacts, Adaptation, and Vulnerability. Part A: Global and Sectoral Aspects. Contribution of Working Group II to the Fifth Assessment Report of the Intergovernmental Panel on Climate Change*. Cambridge, UK; New York, NY: Cambridge University Press.
- Jähne, B., Heinz, G., and Dietrich, W. (1987). Measurement of the diffusion coefficients of sparingly soluble gases in water. *J. Geophys. Res.* 92, 10767–10776. doi: 10.1029/JC092iC10p10767
- Jones, D. L. (2015). *Fathom Toolbox for Matlab: Software for Multivariate Ecological and Oceanographic Data Analysis*. College of Marine Science, University of South Florida, St. Petersburg, FL.
- Kroeker, K. J., Kordas, R. L., Crim, R. N., Hendriks, I. E., Ramajo, L., Singh, G. S., et al. (2013). Impacts of ocean acidification on marine organisms: quantifying sensitivities and interaction with warming. *Glob. Chang. Biol.* 19, 1884–1896. doi: 10.1111/gcb.12179
- Kroeker, K. J., Kordas, R. L., Crim, R. N., and Singh, G. G. (2010). Meta-analysis reveals negative yet variable effects of ocean acidification on marine organisms. *Ecol. Lett.* 13, 1419–1434. doi: 10.1111/j.1461-0248.2010.01518.x
- Lathuilière, C., Echevin, V., and Levy, M. (2008). Seasonal and intraseasonal surface chlorophyll-a variability along the northwest African coast. *J. Geophys. Res.* 113, C5. doi: 10.1029/2007JC004433
- Le Quéré, C., Raupach, M. R., Canadell, J. G., Marland, G., Bopp, L., Ciais, P., et al. (2009). Trends in the sources and sinks of carbon dioxide. *Nat. Geosci.* 2, 831–836. doi: 10.1038/ngeo689
- Lueker, T. J., Dickson, A. G., and Keeling, C. D. (2000). Ocean pCO₂ calculated from dissolved inorganic carbon, alkalinity, and equations for K₁ and K₂: validation based on laboratory measurements of CO₂ in gas and seawater at equilibrium. *Mar. Chem.* 70, 105–119. doi: 10.1016/S0304-4203(00)00022-0
- Mackey, M. D., Mackey, D. J., Higgins, H. W., and Wright, S. W. (1996). CHEMTAX - a program for estimating class abundances from chemical markers: application to HPLC measurements of phytoplankton. *Mar. Ecol. Prog. Ser.* 144, 265–283. doi: 10.3354/meps144265
- McClain, C. R., Signorini, S. R., and Christian, J. R. (2004). Subtropical gyre variability observed by ocean-color satellites. *Deep Sea Res. II Top. Stud. Oceanogr.* 51, 281–301. doi: 10.1016/j.dsr2.2003.08.002
- Murphy, J., and Riley, J. P. (1962). A modified single solution method for the determination of phosphate in natural waters. *Anal. Chim. Acta* 27, 31–36. doi: 10.1016/S0003-2670(00)88444-5
- Neuer, S., Cianca, A., Helmke, P., Freudenthal, T., Davenport, R., Meggers, H., et al. (2007). Biogeochemistry and hydrography in the eastern subtropical North Atlantic gyre. Results from the European time-series station ESTOC. *Prog. Oceanogr.* 72, 1–29. doi: 10.1016/j.pocean.2006.08.001
- Orr, J. C., Fabry, V. J., Aumont, O., Bopp, L., Doney, S. C., Feely, R. A., et al. (2005). Anthropogenic ocean acidification over the twenty-first century and its impact on calcifying organisms. *Nature* 437, 681–686. doi: 10.1038/nature04095
- Paul, A. J., Bach, L. T., Schulz, K. G., Boxhammer, T., Czerny, J., Achterberg, E. P., et al. (2015). Effect of elevated CO₂ on organic matter pools and fluxes in a summer Baltic Sea plankton community. *Biogeosciences* 12, 6181–6203. doi: 10.5194/bg-12-6181-2015
- Pelegrí, J. L., Aristegui, J., Cana, L., Gonzalez-Davila, M., Hernandez-Guerra, A., Hernández-León, S., et al. (2005). Coupling between the open ocean and the coastal upwelling region off northwest Africa: water recirculation and offshore pumping of organic matter. *J. Mar. Syst.* 54, 3–37. doi: 10.1016/j.jmarsys.2004.07.003
- Pierrot, D. E., Lewis, E., and Wallace, D. W. R. (2006). *MS Excel Program Developed for CO₂ System Calculations. ORNL/CDIAC-105a*. Carbon Dioxide Information Analysis Center, Oak Ridge National Laboratory, U.S. Department of Energy, Oak Ridge, TN.
- Pitcher, G. C. (1990). Phytoplankton seed populations of the Cape Peninsula upwelling plume, with particular reference to resting spores of Chaetoceros (bacillariophyceae) and their role in seeding upwelling waters. *Estuar. Coast. Shelf Sci.* 31, 283–301. doi: 10.1016/0272-7714(90)90105-Z
- Riebesell, U., Czerny, J., von Brockel, K., Boxhammer, T., Budenbender, J., Deckelnick, M., et al. (2013a). Technical Note: a mobile sea-going mesocosm system – new opportunities for ocean change research. *Biogeosciences* 10, 1835–1847. doi: 10.5194/bg-10-1835-2013
- Riebesell, U., and Gattuso, J. P. (2015). Lessons learned from ocean acidification research. *Nat. Clim. Chang.* 5, 12–14. doi: 10.1038/nclimate2456

- Riebesell, U., Gattuso, J. P., Thingstad, T. F., and Middelburg, J. J. (2013b). Arctic ocean acidification: pelagic ecosystem and biogeochemical responses during a mesocosm study. *Biogeosciences* 10, 5619–5626. doi: 10.5194/bg-10-5619-2013
- Rousseau, V., Chretiennot-Dinet, M.-J., Jacobsen, A., Verity, P. G., and Whipple, S. (2007). The life cycle of Phaeocystis: state of knowledge and presumptive role in ecology. *Biogeochemistry* 83, 29–47. doi: 10.1007/s10533-007-9085-3
- Sabine, C. L., Feely, R. A., Gruber, N., Key, R. M., Lee, K., Bullister, J. L., et al. (2004). The oceanic sink for anthropogenic CO₂. *Science* 305, 367–371. doi: 10.1126/science.1097403
- Sala, M. M., Aparicio, F. L., Balague, V., Boras, J. A., Borrull, E., Cardelus, C., et al. (2015). Contrasting effects of ocean acidification on the microbial food web under different trophic conditions. *ICES J. Mar. Sci.* 73, 670–679. doi: 10.1093/icesjms/fsv130
- Sangra, P., Pascual, A., Rodriguez-Santana, A., Machin, F., Mason, E., McWilliams, J. C., et al. (2009). The Canary Eddy Corridor: a major pathway for long-lived eddies in the subtropical North Atlantic. *Deep Sea Res. I Oceanogr. Res. Pap.* 56, 2100–2114. doi: 10.1016/j.dsr.2009.08.008
- Sangra, P., Pelegri, J. L., Hernandez-Guerra, A., Arregui, I., Martin, J. M., Marrero-Diaz, A., et al. (2005). Life history of an anticyclonic eddy. *J. Geophys. Res.* 110, C3. doi: 10.1029/2004JC002526
- Schulz, K. G., Bellerby, R. G. J., Brussaard, C. P. D., Büdenbender, J., Czerny, J., Engel, A., et al. (2013). Temporal biomass dynamics of an Arctic plankton bloom in response to increasing levels of atmospheric carbon dioxide. *Biogeosciences* 10, 161–180. doi: 10.5194/bg-10-161-2013
- Schulz, K. G., and Riebesell, U. (2013). Diurnal changes in seawater carbonate chemistry speciation at increasing atmospheric carbon dioxide. *Mar. Biol.* 160, 1889–1899. doi: 10.1007/s00227-012-1965-y
- Sharp, J. H. (1974). Improved analysis for “particulate” organic carbon and nitrogen from seawater. *Limnol. Oceanogr.* 19, 984–989. doi: 10.4319/lo.1974.19.6.0984
- Signorini, S. R., Franz, B. A., and McClain, C. R. (2015). Chlorophyll variability in the oligotrophic gyres: mechanisms, seasonality and trends. *Front. Mar. Sci.* 2:1. doi: 10.3389/fmars.2015.00001
- Smith, S. V. (1985). Physical, chemical and biological characteristics of CO₂ gas flux across the air-water interface. *Plant Cell Environ.* 8, 387–398. doi: 10.1111/j.1365-3040.1985.tb01674.x
- Tagliabue, A., Sallee, J. B., Bowie, A. R., Levy, M., Swart, S., and Boyd, P. W. (2014). Surface-water iron supplies in the Southern Ocean sustained by deep winter mixing. *Nat. Geosci.* 7, 314–320. doi: 10.1038/ngeo2101
- Utermöhl, V. H. (1931). Neue Wege in der quantitativen Erfassung des Planktons. (Mit besondere Berücksichtigung des Ultraplanktons). *Verhandlungen der Internationalen Vereinigung für Theoretische und Angewandte Limnologie* 5, 567–595.
- Weatherall, P., Marks, K. M., Jakobsson, M., Schmitt, T., Tani, S., Arndt, J. E., et al. (2015). A new digital bathymetric model of the world's oceans. *Earth Space Sci.* 2, 331–345. doi: 10.1002/2015EA000107
- Wittmann, A. C., and Pörtner, H.-O. (2013). Sensitivities of extant animal taxa to ocean acidification. *Nat. Clim. Chang.* 3, 995–1001. doi: 10.1038/nclimate1982
- Wolf-Gladrow, D., and Riebesell, U. (1997). Diffusion and reactions in the vicinity of plankton: a refined model for inorganic carbon transport. *Mar. Chem.* 59, 17–34. doi: 10.1016/S0304-4203(97)00069-8
- Yamamoto-Kawai, M., McLaughlin, F. A., Carmack, E. C., Nishino, S., and Shimada, K. (2009). Aragonite undersaturation in the Arctic Ocean: effects of ocean acidification and sea ice melt. *Science* 326, 1098–1100. doi: 10.1126/science.1174190
- Zeebe, R. E., and Wolf-Gladrow, D. (2001). *CO₂ in Seawater: Equilibrium, Kinetics, Isotopes: Equilibrium, Kinetics, Isotopes*. Amsterdam: Elsevier.

Conflict of Interest Statement: The authors declare that the research was conducted in the absence of any commercial or financial relationships that could be construed as a potential conflict of interest.

Copyright © 2017 Taucher, Bach, Boxhammer, Nauendorf, The Gran Canaria KOSMOS Consortium, Achterberg, Algueró-Muñoz, Arístegui, Czerny, Esposito, Guan, Haunost, Horn, Ludwig, Meyer, Spisla, Sswat, Stange and Riebesell. This is an open-access article distributed under the terms of the Creative Commons Attribution License (CC BY). The use, distribution or reproduction in other forums is permitted, provided the original author(s) or licensor are credited and that the original publication in this journal is cited, in accordance with accepted academic practice. No use, distribution or reproduction is permitted which does not comply with these terms.



Ocean Acidification Experiments in Large-Scale Mesocosms Reveal Similar Dynamics of Dissolved Organic Matter Production and Biotransformation

Maren Zark^{1*}, Nadine K. Broda¹, Thomas Hornick², Hans-Peter Grossart^{2,3}, Ulf Riebesell⁴ and Thorsten Dittmar¹

¹ Research Group for Marine Geochemistry (ICBM-MPI Bridging Group), Institute for Chemistry and Biology of the Marine Environment, Carl von Ossietzky University of Oldenburg, Oldenburg, Germany, ² Experimental Limnology, Leibniz-Institute of Freshwater Ecology and Inland Fisheries, Stechlin, Germany, ³ Institute for Biochemistry and Biology, University of Potsdam, Potsdam, Germany, ⁴ GEOMAR Helmholtz Centre for Ocean Research Kiel, Kiel, Germany

OPEN ACCESS

Edited by:

Christel Hassler,
Université de Genève, Switzerland

Reviewed by:

Wei-dong Zhai,
Shandong University, China
Elvira Pulido-Villena,
Mediterranean Institute of
Oceanography - MIO, France

*Correspondence:

Maren Zark
maren.zark@uni-oldenburg.de

Specialty section:

This article was submitted to
Marine Biogeochemistry,
a section of the journal
Frontiers in Marine Science

Received: 22 March 2017

Accepted: 07 August 2017

Published: 05 September 2017

Citation:

Zark M, Broda NK, Hornick T,
Grossart H-P, Riebesell U and
Dittmar T (2017) Ocean Acidification
Experiments in Large-Scale
Mesocosms Reveal Similar Dynamics
of Dissolved Organic Matter
Production and Biotransformation.
Front. Mar. Sci. 4:271.
doi: 10.3389/fmars.2017.00271

Dissolved organic matter (DOM) represents a major reservoir of carbon in the oceans. Environmental stressors such as ocean acidification (OA) potentially affect DOM production and degradation processes, e.g., phytoplankton exudation or microbial uptake and biotransformation of molecules. Resulting changes in carbon storage capacity of the ocean, thus, may cause feedbacks on the global carbon cycle. Previous experiments studying OA effects on the DOM pool under natural conditions, however, were mostly conducted in temperate and coastal eutrophic areas. Here, we report on OA effects on the existing and newly produced DOM pool during an experiment in the subtropical North Atlantic Ocean at the Canary Islands during an (1) oligotrophic phase and (2) after simulated deep water upwelling. The last is a frequently occurring event in this region controlling nutrient and phytoplankton dynamics. We manipulated nine large-scale mesocosms with a gradient of $p\text{CO}_2$ ranging from ~ 350 up to $\sim 1,030 \mu\text{atm}$ and monitored the DOM molecular composition using ultrahigh-resolution mass spectrometry via Fourier-transform ion cyclotron resonance mass spectrometry (FT-ICR-MS). An increase of $37 \mu\text{mol L}^{-1}$ DOC was observed in all mesocosms during a phytoplankton bloom induced by simulated upwelling. Indications for enhanced DOC accumulation under elevated CO_2 became apparent during a phase of nutrient recycling toward the end of the experiment. The production of DOM was reflected in changes of the molecular DOM composition. Out of the 7,212 molecular formulae, which were detected throughout the experiment, $\sim 50\%$ correlated significantly in mass spectrometric signal intensity with cumulative bacterial protein production (BPP) and are likely a product of microbial transformation. However, no differences in the produced compounds were found with respect to CO_2 levels. Comparing the results of this experiment with a comparable OA experiment in the Swedish Gullmar Fjord, reveals similar succession patterns for individual compound pools during a phytoplankton bloom

and subsequent accumulation of these compounds were observed. The similar behavior of DOM production and biotransformation during and following a phytoplankton bloom irrespective of plankton community composition and CO₂ treatment provides novel insights into general dynamics of the marine DOM pool.

Keywords: dissolved organic matter, ocean acidification, ultrahigh resolution mass spectrometry, FT-ICR-MS, molecular composition, subtropical North Atlantic, mesocosm experiment

INTRODUCTION

The global ocean currently takes up about 25% of all annually emitted anthropogenic CO₂ (Le Quéré et al., 2013). Once dissolved in seawater, most of the CO₂ is transported into deep waters via thermohaline circulation and the biological pump. A smaller fraction of the CO₂, however, forms carbonic acid and causes a decline in pH in the surface ocean (Zhai and Zhao, 2016). This process is commonly referred to as ocean acidification (OA). Under a business-as-usual climate scenario, surface ocean pH could be reduced by 0.4 units until the end of the century compared to pre-industrial levels (IPCC, 2014). OA may impact physiology of marine organisms, structure of phytoplankton communities, and the biogeochemical cycling of elements (Riebesell et al., 2007, 2017; Kroeker et al., 2010; Dutkiewicz et al., 2015).

One important pool in the marine carbon cycle that may be affected by OA is dissolved organic matter (DOM). It holds a similar amount of carbon as all living biomass on Earth (Hedges, 1992). This huge carbon pool is mainly produced by marine primary producers and consumed and biotransformed within the microbial loop at the bottom of the marine food web (Azam et al., 1983; Carlson et al., 2007). A stimulation of marine primary production by OA (Riebesell, 2000; Engel et al., 2013; Eberlein et al., 2017) may consequently lead to enhanced production of DOM and subsequently stimulate microbial mineralization (Grossart et al., 2006; Piontek et al., 2010). Thus, concurrent OA-induced changes in degradation and transformation processes affect DOM quantity and quality and have the potential to impact the biogeochemical carbon cycle (Moran et al., 2016).

The surface ocean contains a large fraction of labile DOM that is readily respired to CO₂. Only a smaller fraction of marine primary production is channeled into more recalcitrant DOM fractions (Hansell et al., 2012). This recalcitrant DOM is of importance in terms of oceanic carbon storage and may be altered in a more acidified ocean. So far, OA experiments monitored mainly bulk dissolved organic carbon (DOC) concentrations by neglecting the quality of DOM pools. Thereby, the effect of elevated CO₂ on bulk DOC concentrations in seawater was reported to be positive in large-scale mesocosm and incubation experiments (e.g., Czerny et al., 2013; Engel et al., 2013). However, other studies report no or even negative effects (Yoshimura et al., 2010; Engel et al., 2014; MacGilchrist et al., 2014; Zark et al., 2015a). In contrast, monitoring the molecular DOM composition via FT-ICR-MS may reveal changes in the quality of the accumulating DOM fraction. FT-ICR-MS is to

date the only available analytical technique that holds the power to resolve the molecular masses of more than 60% of intact molecules in DOM (Mopper et al., 2007; Dittmar et al., 2008). In a previous long-term mesocosm experiment in the Swedish Gullmar Fjord, OA effects on DOM molecular composition were analyzed for the first time in an ultrahigh resolution by using Fourier-transform ion cyclotron resonance mass spectrometry (FT-ICR-MS). This study revealed no effects of elevated *p*CO₂ as projected for the end of this century on the DOM pool size and molecular composition in this eutrophic temperate system (Zark et al., 2015a). To what extent these findings can be extrapolated to other regions, in particular less eutrophic open waters, is presently unknown. Microbial communities in surface waters of oligotrophic areas experience less variability in pH than in coastal regions (Hofmann et al., 2011) and are hence less adapted to rapid changes in pH (Salisbury et al., 2008; Joint et al., 2011).

In this study, we tested the effects of OA on the DOM molecular composition in a subtropical system under oligotrophic conditions and in response to simulated upwelling of nutrient-rich deep water. Oligotrophic areas comprise ~30% of the global oceanic primary production and changes in DOM accumulation in these areas may have significant impacts on the marine carbon cycle (Longhurst et al., 1995). So far, effects of OA in oligotrophic environments remain largely unknown, since most community-level field experiments were conducted under nutrient replete conditions. To bridge this knowledge gap, we performed a large-scale pelagic mesocosm experiment in the subtropical North Atlantic Ocean off the coast of Gran Canaria. This area is part of the Canary Current system, where upwelling of nutrient-rich deep water seasonally induces phytoplankton blooms (Aristegui et al., 2009) and controls net production of DOC by input of additional nutrients (Romera-Castillo et al., 2016). Nine sea-going mesocosm systems were deployed, two of them served as controls with ambient *p*CO₂ levels and seven others were artificially enriched with CO₂. A gradient design with a range of *p*CO₂ levels from ~350 to ~1,030 μatm was chosen to test for the presence of a threshold for detecting *p*CO₂ induced effects. After ~3 weeks, we added ~8,000 L of nutrient-rich deep-sea water to each mesocosm to simulate an upwelling event and monitored responses for another ~5 weeks (Taucher et al., 2017). DOC and dissolved organic nitrogen (DON) concentrations were measured as well as the changes in molecular DOM composition via FT-ICR-MS over the course of the oligotrophic phase and an upwelling-induced phytoplankton bloom. Specifically, we aimed for DOM that accumulates on timescales of weeks or longer, because it represents the non-labile fraction of DOM and is most important for carbon storage. We hypothesize that the effect of increased *p*CO₂ on the amount of primary production channeled

via the microbial loop into the more recalcitrant DOM pool is more pronounced under oligotrophic compared to eutrophic conditions.

MATERIALS AND METHODS

Experimental Set-Up

The mesocosm experiment was performed from September to November 2014 at the Plataforma Oceánica de Canarias (PLOCAN) on Gran Canaria, Spain. A technical description of the Kiel Off-Shore Mesocosms for Ocean Simulations (KOSMOS) facility and the experimental design is given in Riebesell et al. (2013) and Schulz et al. (2013). In brief, nine cylindrical mesocosms of $\sim 35 \text{ m}^3$ volume were deployed in the Bay of Gando (Figure 1) and filled at the same time with seawater from the Atlantic. The mesocosms were manipulated with CO_2 to reach average $p\text{CO}_2$ levels of 450 (M5), 560 (M3), 670 (M7), 720 (M4), 890 (M2), and $1,030 \mu\text{atm}$ (M8) between day 1 and day 55 (rounded values). The remaining two mesocosms were used as controls at ambient $p\text{CO}_2$ -values of 350 (M9) to $370 \mu\text{atm}$ (M1). Initial manipulations with CO_2 were done by stepwise addition of CO_2 saturated seawater (days 0, 2, 4, and 6). All mesocosms were open to the atmosphere and CO_2 enriched water had to be added at several time points to keep the $p\text{CO}_2$ level close to the target (days 21 and 38). After CO_2 manipulation, the pH was on average 0.26 units lower in the enriched mesocosms compared to the controls. To simulate a naturally occurring upwelling event we added about 8,000 L deep-sea water ($62 \mu\text{mol L}^{-1}$ DOC, $17 \mu\text{mol L}^{-1}$ combined NO_3^- and NO_2^-) to each of the mesocosms on day 23. It has to be noted that one of the mesocosms with moderate $p\text{CO}_2$ treatment (M6) was damaged on day 26 and had to be excluded from all statistical and graphical analyses. Comprehensive information about experiment design and basic parameters is provided in an overview by Taucher et al. (2017).

Sample Preparation and Bulk Analysis

Representative samples were collected for both, the mesocosms and the surrounding Atlantic water, every other day from boats between 09:00 a.m. and 12:00 a.m. local time, starting from the day after the mesocosm bags were closed (day -3). We used 5 L integrating water samplers (IWS, Hydrobios) collecting a representative sample for the upper 13 m of the water column. Carbonate chemistry parameters such as pH and $p\text{CO}_2$ were calculated from total alkalinity (TA) and dissolved inorganic carbon (DIC) using CO_2SYS (Pierrot et al., 2006) and dissociation constants of Lueker et al. (2000) as described in Taucher et al. (2017). In brief, TA analyses were carried out via potentiometric titration (Metrohm 862 Titrosampler) after Dickson et al. (2003) and DIC concentrations were determined by infrared absorption of CO_2 purged from an acidified sample (MARIANDA AIRICA system with LI-COR LI-7000). Concentrations of chlorophyll *a* (Chl *a*) and other phytoplankton pigments were analyzed by high performance liquid chromatography (HPLC). Therefore, samples (500–1,000 mL) were collected by filtration onto glass fiber filters (GF/F

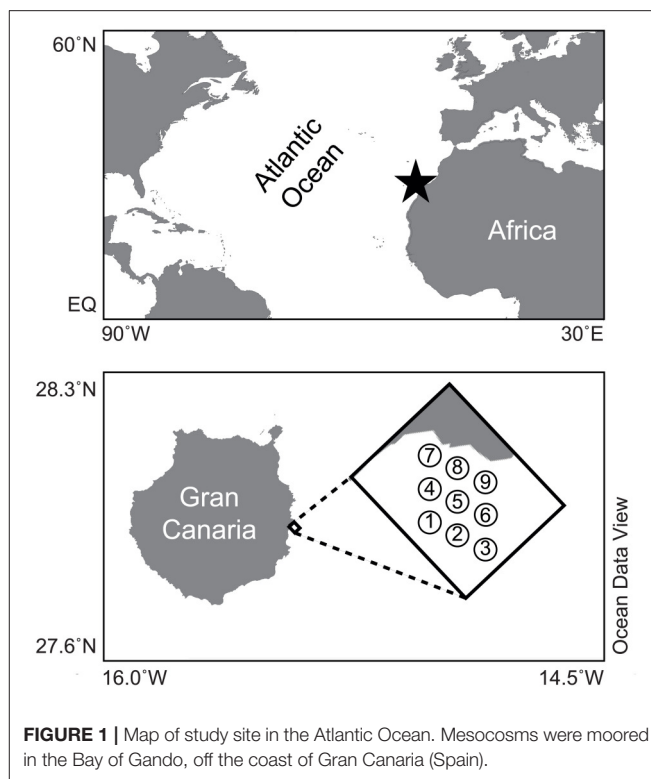


FIGURE 1 | Map of study site in the Atlantic Ocean. Mesocosms were moored in the Bay of Gando, off the coast of Gran Canaria (Spain).

Whatman, nominal pore size of $0.7 \mu\text{m}$) and stored in cryovials at -80°C . For the HPLC analyses, samples were extracted in acetone (100%) in plastic vials by homogenization of the filters using glass beads in a cell mill. After centrifugation (10 min, 5,200 rpm, 4°C) the supernatant was filtered through $0.2 \mu\text{m}$ PTFE filters (VWR International). From this, phytoplankton pigment concentrations were determined using a Thermo Scientific HPLC Ultimate 3000 with Eclipse XDB-C8 $3.5 \mu\text{m}$ 4.6×150 column.

For dissolved organic carbon (DOC) and total dissolved nitrogen (TDN) analysis, samples were collected into pre-rinsed 250 mL polycarbonate bottles (Nalgene) in triplicate. The samples were then filtered through a syringe with $0.7 \mu\text{m}$ GF/F pre-combusted (400°C , 4 h) glass microfiber filters (Whatman) into pre-combusted 20 mL glass vials (400°C , 4 h) with acid-rinsed Teflon caps (Wheaton). Directly after filtration, we acidified samples with HCl (25%, analysis grade, Carl Roth) to pH 2. The analysis of DOC and TDN concentrations was done via a high-temperature catalytic oxidation method (Qian and Mopper, 1996) using a Shimadzu TOC-VCPH/CPN Total Organic Carbon Analyzer, equipped with ASI V auto sampler and TNM-1 module for the determination of TDN. The accuracy of the measurement was controlled with Florida Strait Water reference material (D.A. Hansell, University of Miami, Florida) for every run. The error for DOC and TDN analysis was on average 4 and 10%, respectively. Average concentrations were calculated for each mesocosm and time point from triplicates. We calculated dissolved organic nitrogen (DON) concentrations from TDN by subtracting the concentration of all dissolved inorganic nitrogen species (DIN). DIN is the sum of nitrate,

nitrite and ammonium concentrations that were measured using a segmented flow analyzer (SEAL QuAAtro).

Molecular Characterization

Samples for molecular DOM characterization were collected from the IWS sampler into 2 L acid-rinsed polycarbonate bottles (Nalgene). The samples were transported to shore and stored at *in situ* water temperatures in the dark until processing on the same day. After filtration through 0.7 μm GF/F glass microfiber filters (Whatman) using manual vacuum pumps (<200 mbar) we acidified samples with HCl (25%, analysis grade, Carl Roth) to pH 2. Samples were stored at 4°C in the dark until subsequent solid phase extraction (SPE) according to Dittmar et al. (2008). We used a commercially available modified styrene divinyl benzene polymer resin (PPL, 1 g, Agilent). Prior to use, cartridges were soaked in methanol (HPLC grade, Sigma-Aldrich) overnight, and rinsed sequentially with methanol and 0.01 mol L⁻¹ HCl in ultrapure water. After loading the samples onto the cartridges they were rinsed with 0.01 mol L⁻¹ HCl to remove all remaining salts and dried with nitrogen gas (analysis grade, Air Liquide). The extracted DOM was eluted with 6 mL methanol and stored in pre-combusted glass vials at 20°C. Extraction efficiencies for this method are typically $>60\%$ on a carbon basis (Stubbins and Dittmar, 2012; Green et al., 2014). Especially colloidal matter and small ionic compounds may escape extraction and are likely lost from our analytical window. For this study the average extraction efficiency was $34 \pm 4\%$ across all mesocosms. Despite the relatively low recovery, SPE-DOC concentrations followed the general succession of DOC concentrations and can hence be considered as representative. Procedural blanks were prepared by processing ultrapure water the same way as DOM samples. The detection limit for solid phase extractable DOC (SPE-DOC) was lower than the detection limit for regular DOC samples (Stubbins and Dittmar, 2012) due to concentration by a factor of hundred. SPE-DOC concentrations in the resulting blank extracts were slightly above detection limit but did not exceed a concentration level of 12.3 $\mu\text{mol L}^{-1}$.

We used FT-ICR mass spectrometry for molecular characterization of the DOM pool. Thereby, individual compounds can be resolved from the complex mixture and due to the high mass accuracy, molecular formulae can be assigned. Molecular formulae may be grouped into categories according to indices derived from elemental composition ("Aliphatics" $\text{H/C} \geq 1.5$, "CRAM O-poor" $\text{H/C} < 1.5$ & $\text{AI}_{\text{mod}} \leq 0.5$ & $\text{O/C} \leq 5$, "CRAM O-rich" $\text{H/C} < 1.5$ & $\text{AI}_{\text{mod}} \leq 0.5$ & $\text{O/C} > 5$, "Polyphenols" $0.5 < \text{AI}_{\text{mod}} \leq 0.66$, "Polycyclic aromatics" $\text{AI}_{\text{mod}} > 0.66$) (Koch and Dittmar, 2006; Riedel et al., 2016). This is not meant to be an unambiguous identification of molecular structures.

Mass spectra were obtained on a 15 Tesla Solarix FT-ICR-MS system (Bruker Daltonics) equipped with an electrospray ionization source (ESI, Bruker Apollo II) applied in negative ionization mode. Methanol extracts were diluted with ultrapure water and methanol to give a final concentration of 15 mg C L⁻¹ in a 1:1 mixture (v/v) of methanol (HPLC grade, Sigma-Aldrich) and ultra-pure water. For each measurement we accumulated

500 scans in the mass window of 150–2,000 Da. We calibrated spectra internally with a reference mass list using the Bruker Daltonics Data Analysis software package. The mass error of the calibration was <0.06 ppm for all samples. To remove noise a method detection limit following the guidelines of Riedel and Dittmar (2014) was applied. Compounds detected in procedural blanks were removed. We further found a group of likely contaminants ($n = 50$), which continuously increased in all mesocosms. These compounds were excluded from statistical analysis, as some of them correspond to known constituents of detergents. During previous mesocosm experiments using the identical setup, however, no such contamination could be observed (Zark et al., 2015a).

All 89 samples from a total of 10 time points (79 samples from mesocosms and 10 from the Atlantic) were analyzed via FT-ICR-MS in random order. To test the reproducibility and stability of the FT-ICR-MS analysis, we analyzed DOM extract of North Equatorial Pacific Intermediate Water (NEqPIW) twice per day (Green et al., 2014). MATLAB routines developed by our working group were applied for molecular formula assignment and further data processing. All molecules were detected as singly-charged ions and molecular formulae were assigned based on the criteria by Koch et al. (2007) and Rossel et al. (2013), under consideration of the elements C, H, O, N, S, and P.

Bacterial Protein Production

Rates of bacterial protein production (BPP) were determined by incorporation of ¹⁴C-leucine (Simon and Azam, 1989) modified after Grossart et al. (2006) and Allgaier et al. (2008). Triplicates and a formol-killed control were incubated *in situ* with ¹⁴C-Leu (318 mCi mmol⁻¹; Hartmann Analytic) at a concentration, which ensured saturation of the bacterial uptake systems. Incubation was performed for 1 h in dark at *in situ* temperature and gentle moving of closed containers in a water bath to prevent settling of particles. After fixation with 2% formalin, samples were filtered onto 5.0 μm nitrocellulose filters (Sartorius AG) for the particle associated bacteria fraction and extracted with ice-cold 5% trichloroacetic acid (TCA) for 5 min. Thereafter, filters were rinsed twice with ice-cold 5% TCA, once with ethanol (50% v/v) and mixed with liquid scintillation cocktail (Ultima Gold™, Perkin Elmer). For the free-living bacteria the filtrate was filtered on 0.2 μm nitrocellulose filters (Sartorius) and processed in the same way. The incorporated leucine was measured as disintegrations per minute (dpm) on a liquid scintillation analyzer (TriCarb 2810 TR, Perkin Elmer). The sum of incorporated ¹⁴C-leucine of both size-fractions was converted into BPP by using an intracellular isotope dilution factor of 2 (Kirchman, 1993). A factor of 0.86 was used to convert the produced protein in carbon (Simon and Azam, 1989). Standard deviation of triplicate measurements was usually $<15\%$. Cumulative BPP was determined by summing up the average rates per day of experiment.

Statistical Analysis of FT-ICR-MS Data

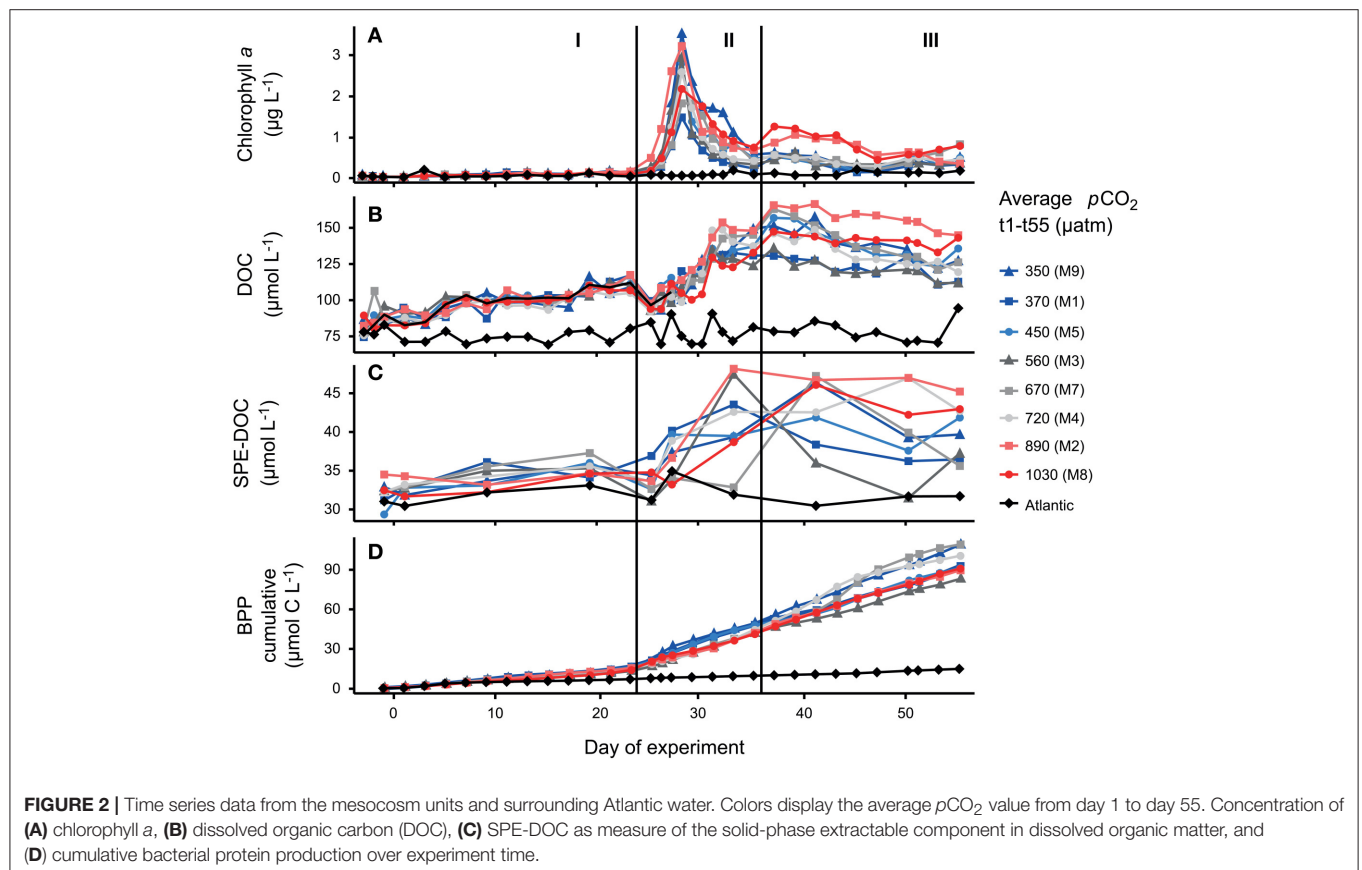
All statistical analyses were based on normalized peak magnitudes of FT-ICR-MS signals. Variations in the molecular

DOM composition were characterized by principal components analysis (PCA). Additionally, a Bray-Curtis based distance matrix was calculated. This method from ecology aims at quantification of the dissimilarity of different ecological sites based on the counts of individual species (Bray and Curtis, 1957). In analogy, we calculated the dissimilarity of all mesocosms at each time point throughout the experiment based on normalized peak magnitudes of the individual DOM compounds. The dissimilarity may reach values between 0 (the two mesocosms share all molecular formulae in similar abundances) and 1 (the mesocosms share no molecular formulae). Thereby, a general comparison of the molecular diversity between samples can be obtained. We further calculated Pearson product-moment correlation coefficients (r) for the co-correlation of individual relative signal intensities of each detected molecular formula with cumulative BPP over time (Figure 4C). This statistical approach results in Pearson correlation coefficients (r) for all molecular formulae of each individual mesocosm (Figure 4B). Pearson correlation coefficients can range from -1 (negative linear relationship) to 1 (positive linear relation). We then used the obtained correlation coefficients for a follow-up Pearson correlation between the mesocosm units that aimed at revealing similar temporal dynamics of DOM molecular formulae (Figure 4A). All statistical analyses were performed with the software package R (Version 3.0.2, package “vegan,” Oksanen et al., 2013).

RESULTS

DOC Production after a Phytoplankton Bloom Induced by Artificial Upwelling

Prior to the addition of CO_2 , mesocosms showed similar conditions after a short equilibration period (Figures 2A–D). After CO_2 addition, $p\text{CO}_2$ inside the mesocosms showed temporal fluctuations throughout the experiment due to outgassing and repeated additions of CO_2 that were done to readjust the gradient. An overview on the temporal succession of $p\text{CO}_2$ in the experiment is provided by Taucher et al. (2017). The temporal succession of phytoplankton biomass was similar for all mesocosms and can be divided into three phases that were driven by different processes. The first phase of the experiment was characterized by oligotrophic conditions (phase I) with stable and low chlorophyll a concentrations (Figure 2A). During this phase, an increase in DOC concentration was observed (Figure 2B) from $80 \pm 5 \mu\text{mol L}^{-1}$ on day 3 to $112 \pm 5 \mu\text{mol L}^{-1}$ on day 23 (mean \pm SD), while BPP remained stable (Figure 2D). A similar trend was not observed for the samples from the Atlantic. Immediately after the start of phase II, with addition of nutrient-rich deep water, chlorophyll a rapidly increased in all mesocosms (Figure 2A). A maximum of $3.5 \mu\text{g L}^{-1}$ was reached on day 28 which is within the range of chlorophyll a (Chl a) maxima in winter months and is typical for the subtropical oligotrophic Atlantic after upwelling events at this time of the year (Neuer



et al., 2007). The bloom was dominated by diatoms (~70% of Chl *a*) as the most abundant group, but also included other groups such as dinoflagellates, prymnesiophytes (*Phaeocystis*) and cyanobacteria (e.g., *Synechococcus*) (Taucher et al., 2017). A sharp decrease of DOC from day 23 to day 25 occurred due to dilution by the injected deep water. At the same time, cumulative BPP increased from 41.8 ± 3.1 to $54.5 \pm 4.4 \mu\text{mol C L}^{-1}$ (Figure 2D). DOC concentrations increased to a maximum of $149 \pm 12 \mu\text{mol L}^{-1}$ after the decay of the bloom on day 37 (Figure 2B). Inorganic nutrients were again depleted from day 30 until the end of the experiment. At the beginning of phase III, a second phytoplankton bloom developed in mesocosms M2 and M8, sustained from recycled production with a low Chl *a* concentration ($0.7 \mu\text{g L}^{-1}$ on day 37, Figure 2A). Cumulative BPP increased constantly during phase III and bacterial activity remained on a high level during the post-bloom (Figure 2D).

Apart from these general trends, the two mesocosms with the highest $p\text{CO}_2$ treatments (1,030 and $890 \mu\text{atm } p\text{CO}_2$) showed higher Chl *a* and DOC concentrations during recycled production in post-bloom phase III. This trend is significant in a linear regression of both, DOC and Chl *a* with phase-averages of $p\text{CO}_2$ ($p < 0.05$) (Supplementary Materials Figure 1). It has to be noted that the plankton community composition in both high CO_2 treatments was clearly different from the other treatments and may have accounted for the differences in both, DOC and Chl *a* (Taucher et al., 2017). There were no differences with CO_2 between treatments for phases I and II.

The Succession of Molecular DOM Composition

Taken together, a total of 7,212 intact compounds with assigned molecular formulae were identified across all mesocosm samples after removal of contaminant signals. For further statistical analysis, the 5,205 molecular formulae with highest signal intensities were selected from each sample. This number was chosen because it was the lowest number in a single sample across the entire sample set. SPE-DOC concentrations in the collected DOM extracts reflect the same general trends as DOC concentration (Figure 2C) and our analysis can thus be considered representative for the fraction in DOM that showed variability during the experiment. FT-ICR-MS signal intensities followed an overall similar pattern with a bell-shaped distribution along the mass axis and an intensity weighted maximum at 372 Da. Using PCA, we could summarize 60% of the total variability of the complex molecular information in a single component (PC1). This component correlated significantly in a Pearson's product-moment correlation with DOC and showed a highly reproducible trend among all independent mesocosm units over time (Pearson, $r = 0.60$, $p < 0.0001$, $n = 79$). Thus, it represents the accumulating molecular signature (Supplementary materials Figure 2). A positive correlation was observed for PC3 with CO_2 (Pearson, $r = 0.20$, $p < 0.05$, $n = 79$). This component, however, explains only 6% of the total observed variability. In agreement to the results from PCA, the dissimilarity on a Bray-Curtis level from on average 8.7% in phase I and phase II, which is within our analytical error, increased to 14.4% in phase

III (Supplementary materials Figure 3), but without indications for a trend associated to $p\text{CO}_2$ levels and the same amount of variability was observed for comparing control to control mesocosms and control to high CO_2 mesocosms.

To compare the succession of DOM on a molecular level between individual mesocosm units in more detail, we performed targeted statistical analysis on specific compound groups using cumulative BPP as proxy. We assume that molecular formulae showing close coupling to cumulative BPP in their succession of signal intensities represent the DOM that is a product of bacterial transformation of freshly produced carbon. This fraction of the marine DOM pool accumulates over timescales of weeks to months and is most important in terms of carbon storage. A Pearson correlation of the normalized signal intensities with cumulative BPP for the individual mesocosms revealed that 50% of all detected molecular formulae ($n = 3,583$) were showing significant correlations with cumulative BPP (Pearson, $p < 0.05$) (Figure 3). This is in good agreement to the results from Bray-Curtis based dissimilarity analysis. No differences were observed

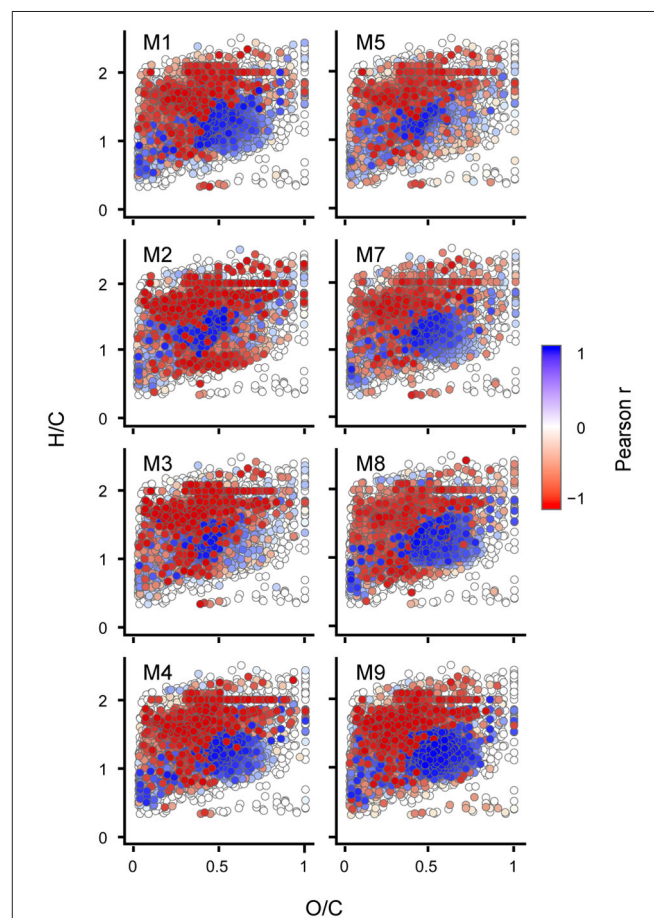


FIGURE 3 | Trends of individual molecular compounds displayed in van Krevelen space. Each dot represents one molecular formula ($n = 7,212$). Pearson's product-moment correlation of cumulative bacterial protein production (BPP) with relative signal intensities for the individual mesocosm units. The color displays the Pearson correlation coefficient (r) with values between -1 (negative linear relation) and 1 (positive linear relation).

in the type of accumulating molecular formulae between CO_2 levels.

To test for generality of these results, we applied the same proxy approach to published molecular DOM data from a mesocosm experiment performed in a eutrophic and temperate environment in the Swedish Gullmar Fjord (Zark et al., 2015a,b). For the fraction of common molecular formulae present in both studies ($n = 3,972$), we searched for molecular formulae showing co-correlation with cumulative BPP (Figure 4C) by calculating Pearson's product-moment correlation coefficients (r) for each individual molecular formula (Figure 4B). In a second step, Pearson's product-moment correlation coefficients between individual mesocosms were calculated to test whether molecular formulae show the same co-correlation patterns in the two experiments contrasting in location and habitat features (Figure 4A). The result was highly significant with average Pearson correlation coefficients of $r = 0.71$ for this study and $r = 0.68$ for the eutrophic study in the Swedish Fjord (Pearson, $p < 0.0001$). The average of the Pearson correlation coefficients between both experiments was lower, but also highly significant ($r = 0.46$, $p < 0.0001$). Grouping the molecular formulae into molecular categories confirmed this finding (Figure 5). While aliphatic compounds were not produced over the course of both experiments (Figures 5A,B), highly unsaturated compounds, also known as carboxyl-rich alicyclic molecules (CRAM) (Hertkorn et al., 2006) decreased in relative intensity (Figures 5C,D,E,F). It should be mentioned that these molecular categories are deduced from elemental compositions only, without further structural information (Šantl-Temkiv et al.,

2013). The overall percentages of the individual compound groups varied with trophic, i.e., between the eutrophic and oligotrophic systems (Figure 5). Most importantly, however, there were no major differences in the most abundant compound groups.

DISCUSSION

CO_2 Effects on the Marine DOM Pool

No differences were observed between the mesocosms during DOC production in phases I and II with respect to bulk parameters and DOM molecular composition. The increase in DOC concentration in phase I was presumably caused by several factors. In the beginning of phase I a bloom of unicellular picocyanobacteria occurred, followed by a dust event from day 16 to day 22 which induced an increase of diatom biomass (Taucher et al., 2017). Concentrations of DOC and SPE-DOC started to diverge between treatments with the onset of recycled production in phase III, after inorganic nutrients added by the deep water injection had been consumed. DOC concentrations were highest in the two mesocosms with highest $p\text{CO}_2$ (890 and $1,030 \mu\text{atm}$) during this period. This is likely an indirect effect of differences in plankton community structure, which were induced by elevated $p\text{CO}_2$ and remained apparent in all three phases of the experiment (Taucher et al., 2017). Our findings provide evidence for the existence of a threshold for indirect $p\text{CO}_2$ -effects on DOC concentrations above $\sim 890 \mu\text{atm}$ $p\text{CO}_2$. Doubtlessly, this estimate is very coarse considering the chosen $p\text{CO}_2$ levels, spatial limitations of the mesocosms, the

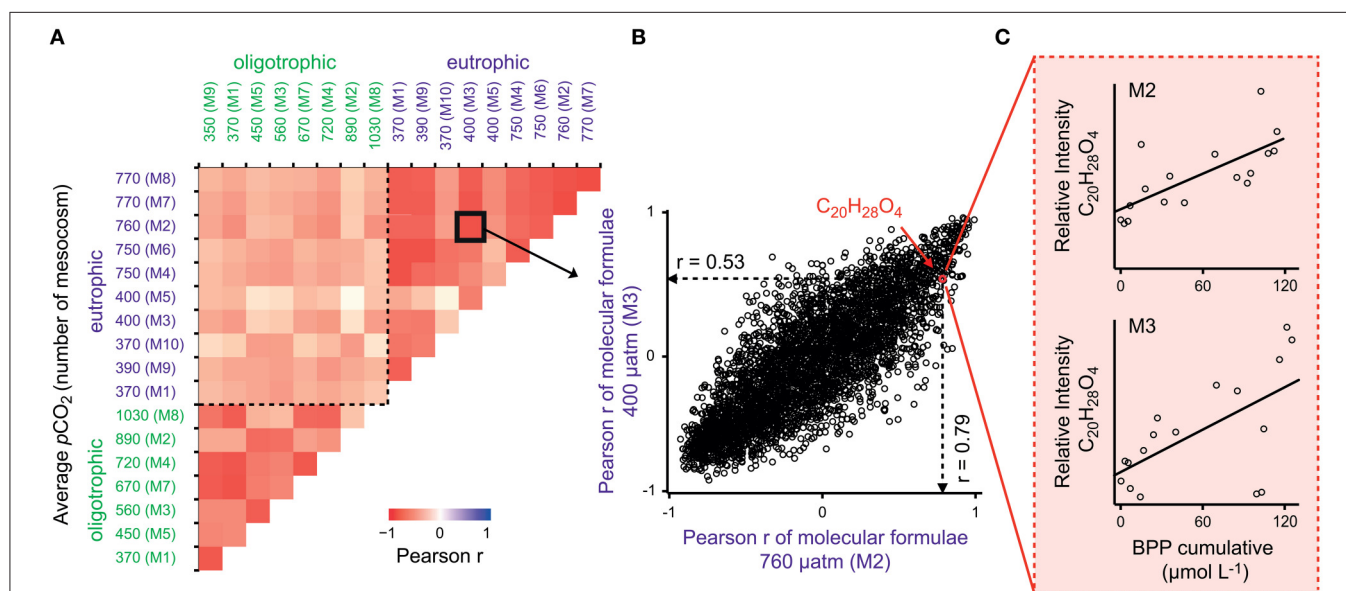
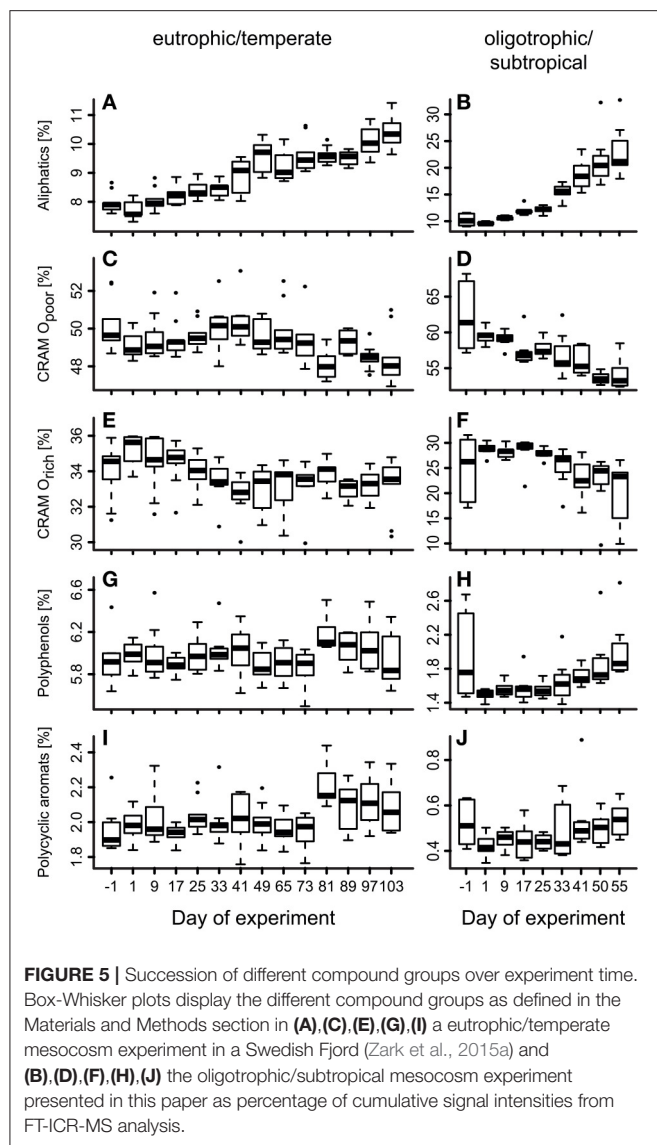


FIGURE 4 | Production of similar compounds in all mesocosms. (A) Pearson's product-moment correlation between individual mesocosms in a coastal mesocosm study in a Swedish Fjord (Zark et al., 2015a) and in the presented oligotrophic mesocosm experiment. The calculation is based on (B) Pearson product-moment correlation coefficients (r) from (C) correlation of relative signal intensities of molecular formulae with cumulative BPP. This statistical analysis illustrates the similarities in succession of molecular compounds between the experiments. The color scale displays the Pearson correlation coefficient (r) with values between -1 (negative linear relation) and 1 (positive linear relation). Similar compounds correlate with cumulative BPP in all mesocosms with an overall highly significant correlation of $r = 0.45$ ($p < 0.0001$, $n = 3,972$).



lack of replicates, and the fact that only a short time period was monitored compared to the time scales typically used for projections. Nevertheless, they are consistent with previous mesocosm experiments, for example with studies conducted in Finland (Paul et al., 2015) and in the Arctic (Czerny et al., 2013; Engel et al., 2013) where higher DOC accumulation was observed under strongly elevated $p\text{CO}_2$ levels of up to $1,420 \mu\text{atm}$. In agreement to the proposed threshold, it was reported that lower maximum target levels of $\sim 700\text{--}800 \mu\text{atm}$ $p\text{CO}_2$ showed no significant effect on DOC concentration (MacGilchrist et al., 2014; Zark et al., 2015a). These studies, however, were all conducted in coastal areas under eutrophic conditions. Studies conducted under oligotrophic conditions in the Mediterranean Sea without artificial addition of nutrients showed no effect on chlorophyll *a* and DOC accumulation under higher $p\text{CO}_2$ levels of up to $\sim 1,000 \mu\text{atm}$ (Maugendre et al., 2017). Incubation studies using water from the oligotrophic Okhotsk Sea even show

higher DOC removal under enhanced CO_2 (Yoshimura et al., 2010). Conclusively, the effect of $p\text{CO}_2$ on DOM quantity appears to be ambiguous in the literature, most likely because it may strongly depend on the environmental settings, particularly the respective location, nutritional status and organismic community composition.

Production of a Fraction of Compounds with Similar Molecular Formulae in All Mesocosms

In a previous mesocosm experiment in a Swedish Fjord with elevated $p\text{CO}_2$ levels of $760 \mu\text{atm}$, we observed no effects of $p\text{CO}_2$ on DOM compounds being consumed or produced over time (Zark et al., 2015a; Bach et al., 2016). The same was true for this study in the subtropical North Atlantic Ocean. Despite indications for DOC accumulation, the overall effect of $p\text{CO}_2$ on DOM bulk molecular composition, if present, is smaller than the variance between control replicates toward the end of the experiment. Nevertheless, it is possible that some DOM compounds are produced by phytoplankton and quickly recycled by bacteria as a response to elevated CO_2 levels. Such enhanced cycle would not necessarily leave detectable imprints in the DOM molecular composition of our samples, because our sampling frequency did not resolve the relevant time scales and possibly also because of rapid aggregation of biopolymers to particles (Engel et al., 2004, 2014; Taucher et al., 2015). Furthermore, CO_2 may have a strong impact on specific DOM degradation processes which become not apparent in bulk analyses (Allgaier et al., 2008; Bergen et al., 2016).

To improve our current understanding of the underlying DOM dynamics, cumulative BPP was used as proxy to assess in more detail the $p\text{CO}_2$ -induced differences in the accumulating DOM fraction over time. It is important to differentiate between DOM reactivity fractions because DOM with short turnover times does not significantly contribute to oceanic carbon export, unless it aggregates to larger particles which sink to the bottom and get buried in the sediment. On the other hand, longer-lived DOM compounds may contribute to carbon sequestration into the oceans interior. Due to the sampling frequency and duration, we covered mainly two operationally-defined reactivity fractions of DOM in our study, i.e., labile and semi-labile DOM. A major fate of photosynthetically produced labile DOM is quick turnover within the microbial loop on timescales of hours to days (Ducklow et al., 2001; Hansell, 2013), whereas semi-labile DOM resists microbial degradation in the surface ocean and accumulates over months and years before it is transported to depths of $>100 \text{ m}$ (Hansell et al., 2012). We assumed that semi-labile DOM compounds accumulate as a result of bacterial activity and thus correlate with cumulative BPP. It has to be noted, that other cumulative data may be also used as proxy for the accumulating DOM, but may not be environmentally meaningful. Refractory and ultra-refractory DOM may also have been produced by microbial transformation or other processes during our study, but cannot be separated from semi-labile DOM, since the lifetime of both reactivity fractions exceeds by far the duration of our experiment. However, it should be noted that

due to our sampling frequency (every second day) highly labile DOM was not resolved as well.

We found that half of the detected molecular formulae showed significant ($p < 0.05$) correlation with cumulative BPP similar for all mesocosms over time. This finding is remarkable, given the fact that the plankton community composition inside the mesocosms differed in relation to the $p\text{CO}_2$ level (Taucher et al., 2017). Whereas, freshly produced DOM from different phytoplankton species is clearly distinct in its individual chemical composition (Landa et al., 2014), the accumulating DOM fraction in our experiment, which remains after an initially rapid remineralization and microbial degradation of the highly labile compounds, was not. This notion may be explained by functional redundancy either in plankton communities regarding production of similarly stable compounds, or in degradation processes. Our results from a natural system support previous small-scale mesocosm experiments indicating production of similar compounds over long timescales despite variability in phytoplankton composition (Osterholz et al., 2015).

Applying the same approach to the molecular DOM data from our experiment in a Swedish Fjord (Zark et al., 2015a,b), we found a similar fraction of molecular formulae in both, the oligotrophic North Atlantic Ocean and the eutrophic fjord system. In both experiments, they significantly correlated with cumulative BPP in a similar manner. These findings suggest that compounds with the same elemental composition also show the same spatial and temporal dynamics in production and degradation. The formation of similar molecular compounds following the breakdown of the phytoplankton bloom, independent of environmental conditions such as phytoplankton community structure and acidification, indicates a rather universal microbial DOM transformation in different ecosystems. This finding points toward a high resilience of processes shaping the molecular DOM signature in complex pelagic communities.

CONCLUSION

DOM concentration and composition in our large-scale mesocosm experiments showed the same succession independent of $p\text{CO}_2$ treatment. OA induced effects became only apparent at the two highest CO_2 , i.e., levels $>890 \mu\text{atm}$, through elevated DOC concentrations during the last experimental phase. However, molecular DOM pool composition remained the same. Regarding climate scenarios, the obtained $p\text{CO}_2$ threshold level will be reached under the “business as usual emission” scenario until the end of the century (IPCC, 2014; Gattuso et al., 2015). However, the observed trends were not pronounced and can only serve as an indicator. If excess DOC was available in a future high CO_2 ocean, it could function as nutrient for new production. Alternatively, it could be sequestered and may thereby cause a negative feedback to the climate system. $p\text{CO}_2$ levels below $\sim 890 \mu\text{atm}$ did not reveal significant differences in DOM quality and molecular

compound groups show similar dynamics over the succession of phytoplankton blooms in two highly contrasting environments, i.e., a temperate eutrophic vs. a subtropical oligotrophic system. This finding indicates a high resilience of microbial DOM transformation processes independent of any environmental variable leading to generally very similar temporal dynamics of DOM groups following phytoplankton blooms. Comparing different large-scale OA mesocosm experiments, thus, provides valuable insights into the biogeochemical dynamics of DOM compounds.

AUTHOR CONTRIBUTIONS

All authors were involved in conceiving the study. MZ, UR, TH, and NB took the samples. MZ and NB conducted solid-phase extractions. FT-ICR-MS analysis was performed by MZ. TH and HG analyzed BPP rates. Statistical analyses were done by MZ and TD. MZ wrote the manuscript with comments from all other authors.

FUNDING

Financial support for this study was provided by the German Ministry of Education and Research (BMBF, FKZ 03F06550 and FKZ 03F07280) through the BIOACID (Biological Impacts of Ocean ACIDification) project. UR received additional funding from the Leibniz Award 2012 by the German Research Foundation (DFG).

ACKNOWLEDGMENTS

We thank the team of the Gran Canaria mesocosm experiment in 2014, in particular A. Ludwig for the logistical organization and coordination. We also thank the staff of the Plataforma Oceánica de Canarias (PLOCAN) for hosting our team, sharing their research facilities, and providing technical assistance. We thank the captain and crew of RV *Hesperides* for deploying and recovering the mesocosms (cruise 29HE20140924) and RV *Poseidon* for transporting the mesocosms and providing support in testing the deep water collector during cruise POS463. The authors furthermore thank K. Klaproth, M. Friebe, and I. Ulber for technical support with FT-ICR-MS and DOC/TDN analysis. We acknowledge A. Nauendorf for the analysis of Chl *a* concentrations, J. Meyer for carbonate chemistry measurements, and Eliesabeth Walter for support of BPP measurements. Nutrient concentrations were kindly provided by E. Achterberg and M. Esposito. All DOM data is archived at the PANGAEA data library (pangaea.de/10.1594/PANGAEA.869453) and will be made available upon request.

SUPPLEMENTARY MATERIAL

The Supplementary Material for this article can be found online at: <http://journal.frontiersin.org/article/10.3389/fmars.2017.00271/full#supplementary-material>

REFERENCES

- Allgaier, M., Vogt, M., Thyrhaug, R., Riebesell, U., and Grossart, H.-P. (2008). Coupling of heterotrophic bacteria to phytoplankton bloom development at different pCO₂ levels: a mesocosm study. *Biogeosciences* 5, 317–359. doi: 10.5194/bg-5-1007-2008
- Aristegui, J., Barton, E. D., Álvarez-Salgado, X. A., Santos, A. M. P., Figueiras, F. G., Kifani, S., et al. (2009). Sub-regional ecosystem variability in the Canary Current upwelling. *Prog. Oceanogr.* 83, 33–48. doi: 10.1016/j.pocean.2009.07.031
- Azam, F., Fenchel, T., Field, J. G., Gray, J. S., Meyer-Reil, L. A., and Thingstad, F. (1983). The ecological role of water-column microbes in the sea. *Mar. Ecol. Prog. Ser.* 10, 257–263. doi: 10.3354/meps010257
- Bach, L. T., Taucher, J., Boxhammer, T., Ludwig, A., The Kristineberg, KOSMOS Consortium, Achterberg, E. P., et al. (2016). Influence of ocean acidification on a natural winter-to-summer plankton succession: first insights from a long-term mesocosm study draw attention to periods of low nutrient concentrations. *PLoS ONE* 11:e0159068. doi: 10.1371/journal.pone.0159068
- Bergen, B., Endres, S., Engel, A., Zark, M., Dittmar, T., Sommer, U., et al. (2016). Acidification and warming affect prominent bacteria in two seasonal phytoplankton blooms. *Environ. Microbiol.* 18, 4579–4595. doi: 10.1111/1462-2920.13549
- Bray, J. R., and Curtis, J. T. (1957). An ordination of the upland forest communities of Southern Wisconsin. *Ecol. Monogr.* 27, 325–349. doi: 10.2307/1942268
- Carlson, C. A., Del Giorgio, P. A., and Herndl, G. J. (2007). Microbes and the dissipation of energy and respiration: from cells to ecosystems. *Oceanography* 20, 89–100. doi: 10.5670/oceanog.2007.52
- Czerny, J., Schulz, K. G., Boxhammer, T., Bellerby, R. G. J., Büdenbender, J., Engel, A., et al. (2013). Implications of elevated CO₂ on pelagic carbon fluxes in an Arctic mesocosm study - an elemental mass balance approach. *Biogeosciences* 10, 3109–3125. doi: 10.5194/bg-10-3109-2013
- Dickson, A. G., Afghan, J. D., and Anderson, G. C. (2003). Reference materials for oceanic CO₂ analysis: a method for the certification of total alkalinity. *Mar. Chem.* 80, 185–197. doi: 10.1016/S0304-4203(02)00133-0
- Dittmar, T., Koch, B., Hertkorn, N., and Kattner, G. (2008). A simple and efficient method for the solid-phase extraction of dissolved organic matter (SPE-DOM) from seawater. *Limnol. Oceanogr. Methods* 6, 230–235. doi: 10.4319/lom.2008.6.230
- Ducklow, H. W., Steinberg, D. K., and Buesseler, K. O. (2001). Upper ocean carbon export and the biological pump. *Oceanography* 14, 50–58. doi: 10.5670/oceanog.2001.06
- Dutkiewicz, S., Morris, J. J., Follows, M. J., Scott, J., Levitan, O., Dyhrman, S. T., et al. (2015). Impact of ocean acidification on the structure of future phytoplankton communities. *Nat. Clim. Change* 5, 1002–1006. doi: 10.1038/nclimate2722
- Eberlein, T., Wohrlab, S., Rost, B., John, U., Bach, L. T., Riebesell, U., et al. (2017). Effects of ocean acidification on primary production in a coastal North Sea phytoplankton community. *PLoS ONE* 12:e0172594. doi: 10.1371/journal.pone.0172594
- Engel, A., Borchard, C., Piontek, J., Schulz, K. G., Riebesell, U., and Bellerby, R. (2013). CO₂ increases ¹⁴C primary production in an Arctic plankton community. *Biogeosciences* 10, 1291–1308. doi: 10.5194/bg-10-1291-2013
- Engel, A., Piontek, J., Grossart, H.-P., Riebesell, U., Schulz, K. G., and Sperling, M. (2014). Impact of CO₂ enrichment on organic matter dynamics during nutrient induced coastal phytoplankton blooms. *J. Plankton Res.* 36, 641–657. doi: 10.1093/plankt/ftb125
- Engel, A., Thoms, S., Riebesell, U., Rochelle-Newall, E., and Zondervan, I. (2004). Polysaccharide aggregation: a sink of marine dissolved organic carbon. *Nature* 428, 929–932. doi: 10.1038/nature02453
- Gattuso, J.-P., Magnan, A., Billé, R., Cheung, W. W. L., Howes, E. L., Joos, F., et al. (2015). Contrasting futures for ocean and society from different anthropogenic CO₂ emissions scenarios. *Science* 349, aac4722. doi: 10.1126/science.aac4722
- Green, N. W., Perdue, E. M., Aiken, G. R., Butler, K. D., Chen, H., Dittmar, T., et al. (2014). An intercomparison of three methods for the large-scale isolation of oceanic dissolved organic matter. *Mar. Chem.* 161, 14–19. doi: 10.1016/j.marchem.2014.01.012
- Grossart, H.-P., Allgaier, M., Passow, U., and Riebesell, U. (2006). Testing the effect of CO₂ concentration on the dynamics of marine heterotrophic bacterioplankton. *Limnol. Oceanogr.* 51, 1–11. doi: 10.4319/lo.2006.51.1.0001
- Hansell, D. A. (2013). Recalcitrant dissolved organic carbon fractions. *Annu. Rev. Mar. Sci.* 5, 421–445. doi: 10.1146/annurev-marine-120710-100757
- Hansell, D. A., Carlson, C. A., and Schlitzer, R. (2012). Net removal of major marine dissolved organic carbon fractions in the subsurface ocean. *Global Biogeochem. Cycles* 26:GB1016. doi: 10.1029/2011GB004069
- Hedges, J. I. (1992). Global biogeochemical cycles: progress and problems. *Mar. Chem.* 39, 67–93. doi: 10.1016/0304-4203(92)90096-S
- Hertkorn, N., Benner, R., Frommberger, M., Schmitt-Kopplin, P., Witt, M., Kaiser, K., et al. (2006). Characterization of a major refractory component of marine dissolved organic matter. *Geochim. Cosmochim. Acta* 70, 2990–3010. doi: 10.1016/j.gca.2006.03.021
- Hofmann, G. E., Smith, J. E., Johnson, K. S., Send, U., Levin, L. A., et al. (2011). High-frequency dynamics of ocean pH: a multi-ecosystem comparison. *PLoS ONE* 6:e28983. doi: 10.1371/journal.pone.0028983
- IPCC (2014). “Climate Change 2014: impacts, adaptation, and vulnerability. Part A: global and sectoral aspects,” in *Contribution of Working Group II to the Fifth Assessment Report of the Intergovernmental Panel on Climate Change* (Cambridge; New York, NY: Cambridge University Press).
- Joint, I., Doney, S. C., and Karl, D. M. (2011). Will ocean acidification affect marine microbes? *ISME J.* 5, 1–7. doi: 10.1038/ismej.2010.79
- Kirchman, D. L. (1993). “Leucine incorporation as a measure of biomass production by heterotrophic bacteria,” in *Handbook of Methods in Aquatic Microbial Ecology*, eds P. F. Kemp, B. F. Sherr, E. B. Sherr, and J. J. Cole (Boca Raton, FL: Lewis), 509–512.
- Koch, B. P., and Dittmar, T. (2006). From mass to structure: an aromaticity index for high-resolution mass data of natural organic matter. *Rapid Commun. Mass Spectrom.* 20, 926–932. doi: 10.1002/rcm.2386
- Koch, B. P., Dittmar, T., Witt, M., and Kattner, G. (2007). Fundamentals of molecular formula assignment to ultrahigh resolution mass data of natural organic matter. *Anal. Chem.* 79, 1758–1763. doi: 10.1021/ac061949s
- Kroeker, K. J., Kordas, R. L., Crim, R. N., and Singh, G. G. (2010). Meta-analysis reveals negative yet variable effects of ocean acidification on marine organisms. *Ecol. Lett.* 13, 1419–1434. doi: 10.1111/j.1461-0248.2010.01518.x
- Landa, M., Cottrell, M. T., Kirchman, D. L., Kaiser, K., Medeiros, P. M., Tremblay, L., et al. (2014). Phylogenetic and structural response of heterotrophic bacteria to dissolved organic matter of different chemical composition in a continuous culture study. *Environ. Microbiol.* 16, 1668–1681. doi: 10.1111/1462-2920.12242
- Le Queré, C., Peters, G. P., Andres, R. J., Andrew, R. M., Boden, T., and Ciais, P. (2013). Global carbon budget 2013. *Earth Syst. Sci. Data* 6, 689–760. doi: 10.5194/essdd-6-689-2013
- Longhurst, A., Sathyendranath, S., Platt, T., and Caverhill, C. (1995). An estimate of global primary production in the ocean from satellite radiometer data. *J. Plankt. Res.* 17, 1245–1271. doi: 10.1093/plankt/17.6.1245
- Lueker, T. J., Dickson, A. G., and Keeling, C. D. (2000). Ocean pCO₂ calculated from dissolved inorganic carbon, alkalinity, and equations for K₁ and K₂: validation based on laboratory measurements of CO₂ in gas and seawater at equilibrium. *Mar. Chem.* 70, 105–119. doi: 10.1016/S0304-4203(00)00022-0
- MacGilchrist, G. A., Shi, T., Tyrell, T., Richier, S., Moore, C. M., Dumousseaud, C., et al. (2014). Effects of enhanced pCO₂ levels on the production of dissolved organic carbon and transparent exopolymer particles in short-term bioassay experiments. *Biogeosciences* 11, 3695–3706. doi: 10.5194/bg-11-3695-2014
- Maugendre, L., Gattuso, J.-P., Poulton, A. J., Dellisanti, W., Gaubert, M., Guieu, C., et al. (2017). No detectable effect of ocean acidification on plankton metabolism in the NW oligotrophic Mediterranean Sea: results from two mesocosm studies. *Estuar. Coast. Shelf Sci.* 186, 89–99. doi: 10.1016/j.ecss.2015.03.009
- Mopper, K., Stubbins, A., Ritchie, J. D., Bialk, H. M., and Hatcher, P. G. (2007). Advanced instrumental approaches for characterization of marine dissolved organic matter: extraction techniques, mass spectrometry, and nuclear magnetic resonance. *Chem. Rev.* 107, 419–442. doi: 10.1021/cr050359b
- Moran, M. A., Kujawinski, E. B., Stubbins, A., Fatland, R., Aluwihare, L. I., Buchan, A., et al. (2016). Deciphering ocean carbon in a changing world. *Proc. Natl. Acad. Sci. U.S.A.* 113, 3143–3151. doi: 10.1073/pnas.1514645113
- Neuer, S., Cianca, A., Helmke, P., Freudenthal, T., Davenport, R., Meggers, H., et al. (2007). Biogeochemistry and hydrography in the eastern subtropical North

- Atlantic gyre. Results from the European time-series station ESTOC. *Prog. Oceanogr.* 72, 1–29. doi: 10.1016/j.pcean.2006.08.001
- Oksanen, J., Blanchet, F. G., Kindt, R., Legendre, P., Minchin, P. R., O'Hara, R. B., et al. (2013). *Vegan: Community Ecology Package*. R package version 2.0-10. Available online at: <http://CRAN.R-project.org/package=vegan>
- Osterholz, H., Niggemann, J., Giebel, H.-A., Simon, M., and Dittmar, T. (2015). Inefficient microbial production of refractory dissolved organic matter in the ocean. *Nat. Commun.* 6, 7422. doi: 10.1038/ncomms8422
- Paul, A. J., Bach, L. T., Schulz, K.-G., Boxhammer, T., Czerny, J., Achterberg, E. P., et al. (2015). Effect of elevated CO₂ on organic matter pools and fluxes in a summer Baltic Sea plankton community. *Biogeosciences* 12, 6181–6203. doi: 10.5194/bg-12-6181-2015
- Pierrot, D. E., Lewis, E., and Wallace, D. W. R. (2006). *MS Excel Program Developed for CO₂ System Calculations*. ORNL/CDIAC-105a, Carbon Dioxide Information Analysis Center, Oak Ridge National Laboratory, U.S. Department of Energy, Oak Ridge, TN.
- Piontek, J., Lunau, M., Händel, N., Borchard, C., Wurst, M., and Engel, A. (2010). Acidification increases microbial polysaccharide degradation in the ocean. *Biogeosciences* 7, 1615–1624. doi: 10.5194/bg-7-1615-2010
- Qian, J., and Mopper, K. (1996). Automated high-performance, high-temperature combustion total organic carbon analyzer. *Anal. Chem.* 68, 3090–3097. doi: 10.1021/ac960370z
- Riebesell, U. (2000). Carbon fix for a diatom. *Nature* 407, 959–960. doi: 10.1038/35039665
- Riebesell, U., Bach, L. T., Bellerby, R. G. J., Bermúdez Monsalve, J. R., Boxhammer, T., Czerny, J., et al. (2017). Competitive fitness of a predominant pelagic calcifier impaired by ocean acidification. *Nat. Geosci.* 10, 19–23. doi: 10.1038/ngeo2854
- Riebesell, U., Czerny, J., von Bröckel, K., Boxhammer, T., Büdenbender, J., Deckelnick, M., et al. (2013). Technical note: a mobile sea-going mesocosm system - new opportunities for ocean change research. *Biogeosciences* 10, 1835–1847. doi: 10.5194/bg-10-1835-2013
- Riebesell, U., Schulz, K. G., Bellerby, R. G. J., Botros, M., Fritsche, P., Meyerhöfer, M., et al. (2007). Enhanced biological carbon consumption in a high CO₂ ocean. *Nature* 450, 545–549. doi: 10.1038/nature06267
- Riedel, T., and Dittmar, T. (2014). A method detection limit for the analysis of natural organic matter via Fourier transform ion cyclotron resonance mass spectrometry. *Anal. Chem.* 86, 8876–8882. doi: 10.1021/ac501946m
- Riedel, T., Zark, M., Vähätalo, A. V., Niggemann, J., Spencer, R. G. M., Hernes, P. J., et al. (2016). Molecular signatures of biogeochemical transformations in dissolved organic matter from ten world rivers. *Front. Earth Sci.* 4:85. doi: 10.3389/feart.2016.00085
- Romera-Castillo, C., Letscher, R. T., and Hansell, D. A. (2016). New nutrients exert fundamental control on dissolved organic carbon accumulation in the surface Atlantic Ocean. *Proc. Natl. Acad. Sci. U.S.A.* 113, 10497–10502. doi: 10.1073/pnas.1605344113
- Rossel, P. E., Vähätalo, A. V., Witt, M., and Dittmar, T. (2013). Molecular composition of dissolved organic matter from a wetland plant (*Juncus effusus*) after photochemical and microbial decomposition (1.25 yr): common features with deep sea dissolved organic matter. *Org. Geochem.* 60, 62–71. doi: 10.1016/j.orggeochem.2013.04.013
- Salisbury, J., Green, M., Hunt, C., and Campbell, J. (2008). Coastal acidification by rivers: a threat to shellfish? *Eos* 89, 513. doi: 10.1029/2008EO500001
- Šantl-Temkiv, T., Finster, K., Dittmar, T., Hansen, B. M., Thyraug, R., and Nielsen, N. W. (2013). Hailstones: a window into the microbial and chemical inventory of a storm cloud. *PLoS ONE* 8:e53550. doi: 10.1371/journal.pone.0053550
- Schulz, K. G., Bellerby, R. G. J., Brussaard, C. P. D., Büdenbender, J., Czerny, J., Engel, A., et al. (2013). Temporal biomass dynamics of an Arctic plankton bloom in response to increasing levels of atmospheric carbon dioxide. *Biogeosciences* 10, 161–180. doi: 10.5194/bg-10-161-2013
- Simon, M., and Azam, F. (1989). Protein content and protein synthesis rates of planktonic marine bacteria. *Mar. Ecol. Prog. Ser.* 51, 201–213. doi: 10.3354/meps051201
- Stubbins, A., and Dittmar, T. (2012). Low volume quantification of dissolved organic carbon and dissolved nitrogen. *Limnol. Oceanogr. Methods* 10, 347–352. doi: 10.4319/lom.2012.10.347
- Taucher, J., Bach, L. T., Boxhammer, T., Achterberg, E. P., Algueró-Muñoz, M., Aristegui, J., et al. (2017). Influence of ocean acidification and deep water upwelling on oligotrophic plankton communities in the subtropical North Atlantic: insights from an *in situ* mesocosm study. *Front. Earth. Sci.* 4:85. doi: 10.3389/feart.2017.00085
- Taucher, J., Jones, J., James, A., Brzezinski, M. A., Carlson, C. A., Riebesell, U., et al. (2015). Combined effects of CO₂ and temperature on carbon uptake and partitioning by the marine diatoms *Thalassiosira weissflogii* and *Dactylosolen fragilissimus*. *Limnol. Oceanogr.* 60, 901–919. doi: 10.1002/lno.10063
- Yoshimura, T., Nishioka, J., Suzuki, K., Hattori, H., Kiyosawa, H., and Watanabe, Y. W. (2010). Impacts of elevated CO₂ on organic carbon dynamics in nutrient depleted Okhotsk Sea surface waters. *J. Exp. Mar. Biol. Ecol.* 395, 191–198. doi: 10.1016/j.jembe.2010.09.001
- Zark, M., Riebesell, U., and Dittmar, T. (2015a). Effects of ocean acidification on marine dissolved organic matter are not detectable over the succession of phytoplankton blooms. *Sci. Adv.* 1:e1500531. doi: 10.1126/sciadv.1500531
- Zark, M., Riebesell, U., and Dittmar, T. (2015b). Dissolved organic matter molecular composition and concentrations from a large scale mesocosm study KOSMOS 2013 (Kristineberg) on ocean acidification. *PANGAEA*. doi: 10.1594/PANGAEA.846137
- Zhai, W., and Zhao, H. (2016). Quantifying air-sea re-equilibration-implied ocean surface CO₂ accumulation against recent atmospheric CO₂ rise. *J. Oceanogr.* 72, 651. doi: 10.1007/s10872-016-0350-8

Conflict of Interest Statement: The authors declare that the research was conducted in the absence of any commercial or financial relationships that could be construed as a potential conflict of interest.

Copyright © 2017 Zark, Broda, Hornick, Grossart, Riebesell and Dittmar. This is an open-access article distributed under the terms of the Creative Commons Attribution License (CC BY). The use, distribution or reproduction in other forums is permitted, provided the original author(s) or licensor are credited and that the original publication in this journal is cited, in accordance with accepted academic practice. No use, distribution or reproduction is permitted which does not comply with these terms.



Photochemical vs. Bacterial Control of H₂O₂ Concentration Across a pCO₂ Gradient Mesocosm Experiment in the Subtropical North Atlantic

Mark J. Hopwood^{1*}, Ulf Riebesell¹, Javier Aristegui², Andrea Ludwig¹, Eric P. Achterberg¹ and Nauzet Hernández²

¹ GEOMAR Helmholtz Centre for Ocean Research Kiel, Kiel, Germany, ² Instituto de Oceanografía y Cambio Global (IOCAG), Universidad de Las Palmas de Gran Canaria (ULPGC), Las Palmas, Spain

OPEN ACCESS

Edited by:

Jörg Wiedenmann,
University of Southampton,
United Kingdom

Reviewed by:

Marta Plavsic,
Rudjer Boskovic Institute, Croatia
Bernhard Riegl,
Nova Southeastern University,
United States

*Correspondence:

Mark J. Hopwood
mhopwood@geomar.de

Specialty section:

This article was submitted to
Marine Biogeochemistry,
a section of the journal
Frontiers in Marine Science

Received: 25 July 2017

Accepted: 14 March 2018

Published: 27 March 2018

Citation:

Hopwood MJ, Riebesell U, Aristegui J,
Ludwig A, Achterberg EP and
Hernández N (2018) Photochemical
vs. Bacterial Control of H₂O₂
Concentration Across a pCO₂
Gradient Mesocosm Experiment in the
Subtropical North Atlantic.
Front. Mar. Sci. 5:105.
doi: 10.3389/fmars.2018.00105

In the surface ocean, microorganisms are both a source of extracellular H₂O₂ and, via the production of H₂O₂ destroying enzymes, also one of the main H₂O₂ sinks. Within microbial communities, H₂O₂ sources and sinks may be unevenly distributed and thus microbial community structure could influence ambient extracellular H₂O₂ concentrations. Yet the biogeochemical cycling of H₂O₂ and other reactive oxygen species (ROS) is rarely investigated at the community level. Here, we present a time series of H₂O₂ concentrations during a 28-day mesocosm experiment where a pCO₂ gradient (400–1,450 μatm) was applied to subtropical North Atlantic waters. Pronounced changes in H₂O₂ concentration were observed over the duration of the experiment. Initially H₂O₂ concentrations in all mesocosms were strongly correlated with surface H₂O₂ concentrations in ambient seawaters outside the mesocosms which ranged from 20 to 92 nM over the experiment duration (Spearman Rank Coefficients 0.79–0.93, *p*-values < 0.001–0.015). After approximately 9 days of incubation however, H₂O₂ concentrations had increased across all mesocosms, later reaching >300 nM in some mesocosms (2–6 fold higher than ambient seawaters). The correlation with ambient H₂O₂ was then no longer significant (*p* > 0.05) in all treatments. Furthermore, changes in H₂O₂ could not be correlated with inter-day changes in integrated irradiance. Yet H₂O₂ concentrations in most mesocosms were inversely correlated with bacterial abundance (negative Spearman Rank Coefficients ranging 0.59–0.94, *p*-values < 0.001–0.03). Our results therefore suggest that ambient H₂O₂ concentration can be influenced by microbial community structure with shifts toward high bacterial abundance correlated with low extracellular H₂O₂ concentrations. We also infer that the nature of mesocosm experiment design, i.e., the enclosure of water within open containers at the ocean surface, can strongly influence extracellular H₂O₂ concentrations. This has potential chemical and biological implications during incubation experiments due to the role of H₂O₂ as both a stressor to microbial functioning and a reactive component involved in the cycling of numerous chemical species including, for example, trace metals and haloalkanes.

Keywords: hydrogen peroxide, H₂O₂, mesocosm, Atlantic, pCO₂

INTRODUCTION

Reactive oxygen species (ROS) are ubiquitous in sunlit natural surface waters (Van Baalen and Marler, 1966; Moore et al., 1993; Miller and Kester, 1994). The most extensively measured ROS in the marine environment, H₂O₂, is present in the surface mixed layer at concentrations on the order of 10–100 nM (Price et al., 1998; Yuan and Shiller, 2001; Gerringa et al., 2004). In the surface ocean, H₂O₂ is known to be mainly produced by photochemistry (Fujiwara et al., 1993; Micinski et al., 1993) with a poorly quantified fraction produced via biochemical processes (Palenik et al., 1987; Croot et al., 2005; Milne et al., 2009). Biochemical processes are also used to explain H₂O₂ production in the dark (Palenik and Morel, 1988; Moffett and Zafiriou, 1990; Vermilyea et al., 2010).

H₂O₂ can cross cell membranes and cause a wide range of cellular damage, a process generically referred to as oxidative stress (Seaver and Imlay, 2001; Lesser, 2006; Imlay, 2008). Extracellular H₂O₂ is however not generally considered to be a major constraint on cellular growth under natural conditions in the marine environment because most microorganisms are thought to produce catalase and peroxidase enzymes which control H₂O₂ decomposition rates in the surface ocean (Moffett and Zafiriou, 1990; Petasne and Zika, 1997). However, recent work has challenged the assumption that extracellular H₂O₂ at nanomolar concentrations does not negatively influence cellular metabolism in surface seawater. The susceptibility of a range of marine microorganisms to H₂O₂ (Bogosian et al., 2000; Morris et al., 2011) and measurable effects on primary metabolism at extracellular H₂O₂ concentrations within the range of surface marine concentrations (Morris et al., 2011; Baltar et al., 2013) have been demonstrated. Furthermore, it has been suggested that microbes sensitive to H₂O₂ may not be cultivable under normal laboratory conditions (Morris et al., 2008, 2011), which may have severely biased our historical understanding of ROS interactions with marine microorganisms.

H₂O₂ production rates, decomposition rates, and effects on cellular functioning may vary widely at the species level (Palenik et al., 1987; Baltar et al., 2013). Furthermore, cross-group interactions may be important in regulating ambient extracellular H₂O₂ concentrations (Morris et al., 2011). Investigations at the community level are therefore required in order to comprehensively understand the interaction between biological processes and ROS in seawater. Mesocosm studies are one approach by which this could be achieved, yet rapid decay rates mean that investigating ROS during an offshore mesocosm experiment, with a setup for example as per Taucher (2017, this Research Topic), would be logistically challenging. A mesocosm experiment on a smaller and more accessible scale, with a similar pCO₂ gradient and timespan, was therefore conducted in the subtropical waters of Gran Canaria in March 2016. Our objective was to compare changes in ROS and other short-lived reactive species over the timescale of an induced phytoplankton bloom across a broad pCO₂ gradient. The pCO₂ gradient was designed to encompass pCO₂ under all plausible future climate scenarios until 2100 (IPCC Working Group 1, 2014) with the addition of some higher end-members to investigate potential thresholds

with respect to CO₂-sensitive ecological and biogeochemical processes.

MATERIALS AND METHODS

Mesocosm Design

The mesocosm study, conducted in Taliarte Harbor, Gran Canaria in March 2016, used eight thermoplastic polyurethane bags with a 2 m diameter, a depth of ~3 m, a starting volume of ~8,000 L, and no lid or screen on top. The bags were mounted on a buoyant frame which was allowed to drift ~2–3 m away from a sampling jetty. After filling with ambient seawater (on 1 March, experiment day –4), pumped from outside Taliarte Harbor (depth 15 m), the mesocosms were allowed to function without nutrient addition for 21 days (**Supplementary Figure 1**). A pCO₂ gradient across the eight mesocosms was induced on day 0 by the addition of varying volumes of filtered, CO₂ saturated seawater using a custom made “spider” distribution device described by Riebesell et al. (2013). The pCO₂ gradient (400–1,450 µatm) was designed to be similar to that used during the offshore KOSMOS mesocosm experiment conducted in Gando Bay, Gran Canaria in September/October 2014 (Taucher, 2017, this Research Topic). A further top-up of pCO₂ saturated seawater was then made to the mesocosms as necessary to maintain the pCO₂ gradient (**Supplementary Figure 1**) following CO₂ outgassing. The precise volume of each mesocosm was determined (on day 18) by measuring salinity before, and after, the addition of 40 L freshwater to each mesocosm, similar to Czerny et al. (2013). A single macronutrient addition (3.1 µM nitrate, 1.5 µM silicate, and 0.2 µM phosphate) was then made (after day 18 sampling).

Analysis

H₂O₂ samples were collected in opaque 125 mL high density polyethylene (HDPE) bottles (Nalgene) which were pre-cleaned (1 day soak in detergent, 1 week soak in 1 M HCl, three rinses with de-ionized water; 18.2 MΩ·cm, Milli-Q, Millipore) and dried in a laminar flow hood prior to use. Sample bottles were rinsed once with seawater and filled with no headspace by gently submerging the bottles within the mesocosms. Chlorophyll a, bacterial abundance, chromophoric dissolved organic matter (CDOM) and macronutrient concentrations were determined from depth integrated water samples collected using 2.5 m long custom-made samplers with an internal volume of ~10 L. These samplers were constructed from polypropylene tubing with valves at both ends. After filling, by submerging into the mesocosms and closing the valves, the samplers were removed and gently inverted to facilitate mixing. Samplers were then slowly drained through 1 cm diameter silicone tubing into pre-rinsed (de-ionized water and then mesocosm water) 25 L transparent HDPE containers, which were then transferred to shaded boxes and moved to a dark, refrigerated room for sub-sampling. Analysis of chlorophyll a and macronutrients then began immediately.

Chlorophyll a was measured by fluorometry as per Welschmeyer (1994) and macronutrient concentrations (nitrate + nitrite, phosphate, silicate) were determined by colorimetry as per Hansen and Koroleff (1999). CDOM absorption spectra

were measured with a 100 cm, 250 μ L capillary (LPC100CM) connected via an optical fiber to a light source (DH2000BAC) and a USB2000+UV-VIS ES detector (Ocean Optics). The system was controlled using Spectra-suite software (Ocean Optics). Samples were injected into the capillary with a peristaltic pump at a flow rate of 1 mL min⁻¹. Relative molecular weight was estimated from CDOM absorption by deriving the slope ratio (S_R) as the ratio of the slope of the shorter wavelength region (275–295 nm) to that of the longer wavelength region (350–400 nm; Helms et al., 2008). The spectral slopes were calculated from the linear regression of the log-transformed absorption spectra.

H₂O₂ was always analyzed within 1 h of collection via flow injection analysis (FIA) using the Co(II) catalyzed oxidation of luminol (Yuan and Shiller, 1999). A FIA system was assembled and operated exactly as per Hopwood et al. (2017) resulting in a detection limit of <1 nM. Calibrations were run daily, and with every new reagent batch, by at least six standard additions of diluted H₂O₂ (TraceSelect, Fluka) to aged (stored at room temperature for >48 h) seawater (unfiltered). The stability of H₂O₂ stock solution was checked by measuring absorbance at 240 nm using a quartz 10 cm cell and a USB4000 spectrometer (Ocean Optics). H₂O₂ (TraceSelect, Fluka) was sequentially diluted weekly to create stock solutions of 100 mM and 100 μ M using de-ionized water. With respect to the measurement of chemical species other than H₂O₂, the H₂O₂ luminol based FIA method is expected to be robust for measurements in oxygenated surface seawater (Yuan and Shiller, 1999, 2004).

Bacterial counts were obtained on depth integrated water samples. Two mL water samples were fixed with 1% paraformaldehyde (final concentration) and stored at -80°C until analysis. Samples were analyzed by flow cytometry (FACSCalibur, Becton Dickinson), with a 15 mW laser set to excite at 488 nm (Gasol and del Giorgio, 2000). Subsamples (400 μ L) for the determination of heterotrophic bacteria were stained with the fluorochrome SybrGreen-I (4 μ L) at room temperature for 20 min and run at a flow rate of 16 μ L min⁻¹. Cells were enumerated in a bivariate plot of 90° light scatter and green fluorescence. Molecular Probes latex beads (1 μ m) were used as internal standards.

Ancillary Measurements

A CTD cast (using a CTD60M, Sea and Sun Technology) was conducted every sample collection day in all mesocosms. Additionally, a CTD cast was conducted on the sampling jetty adjacent to the mesocosms where a H₂O₂ sample in ambient seawater was also collected alongside every mesocosm sampling event. Photosynthetically active radiation (PAR) data was obtained from an ELDONET (Häder and Lebert, 2006) monitoring site located <200 m from the mesocosm jetty. Complete diurnal light profiles were available for experiment day 7 onwards, excluding days 12 and 13.

The diurnal change in H₂O₂ concentration in ambient seawater, and inside two mesocosms, was monitored by setting up FIA equipment on the mesocosm sampling jetty with a PTFE sampling line weighted to float ~10 cm below the water surface. Seawater was pumped continuously using a peristaltic pump

(MiniPuls 3, Gilson) with a time delay between water inflow and analysis of ~60–120 s. The sample line was used without a filter and visually inspected regularly for blockage. Calibration was undertaken three times in every 24 h period by 6–8 standard additions of H₂O₂ into aged (>48 h in the dark) seawater. A coiled 3 m PTFE sample line, which could be extended to the bottom of the mesocosms, was used to determine whether H₂O₂ was vertically homogenous within the mesocosm bags. During the diurnal experiment monitoring ambient seawater, salinity was measured regularly (<3 h intervals) using a LF 325 conductivity meter (WTW) which was calibrated before use with a KCl solution.

During rain events, rainwater was collected by deploying open low density polyethylene (LDPE) bags adjacent to the mesocosms. Rainwater was diluted prior to analysis by spiking 200 μ L unfiltered rainwater into 50 mL aged seawater with the H₂O₂ concentration in seawater measured before, and after, the rainwater spike.

RESULTS

Mesocosm Time Series

Time series for the core parameters discussed herein are included in **Supplementary Datasheet 1**. Initial measurements in the mesocosms (2 March 2016, experiment day -3, after filling the mesocosms—but before any treatments were applied) verified that the enclosed waters were close to identical with respect to H₂O₂ concentration. Differences between the eight enclosures (range 38.3–40.9 nM, mean 39.3 \pm 0.8 nM) were small compared to the detection limit of the analytical method (<1 nM; Croot et al., 2004; Hopwood et al., 2017) and the standard deviation of quadruple measurements of H₂O₂ in seawater collected on the sample jetty (mean 3.3 nM over the experiment duration). Depth profiles within a mesocosm bag (~3 m depth) were conducted on day 25 mid-afternoon, when any stratification was expected to be maximal, and verified that H₂O₂ concentration was relatively well-mixed with only a slight vertical gradient (increasing from 43 to 51 nM bottom-top, mean 47 \pm 3.5 nM). On day 12, surface seawater collected using a small inflatable boat showed a range of H₂O₂ concentrations at different locations around Taliarte Harbor (39 \pm 9.9 nM, n = 4), outside the harbor within 150 m of the coastline (63 \pm 1.8 nM, n = 3) and outside the harbor >400 m offshore (38 \pm 5.6 nM, n = 4). Ambient seawater concentrations within the harbor (used to determine a background concentration for comparison with the mesocosms) were therefore similar to those found in near-shore waters.

The imposition of a large pCO₂ gradient across the mesocosm bags after sampling on day 0 had no clear prolonged effect on observed H₂O₂ concentrations (**Figure 1A**). Temporal trends in H₂O₂ concentration were relatively similar in all mesocosms until day 9 of the experiment with the standard deviation ranging from 0.7 to 13 nM. Data for mesocosm 1 are shown only until day 3, after which exchange with surrounding seawater occurred following leakage, and monitoring was thus discontinued. After day 9 the enclosed waters diverged and some mesocosms experienced swings to very high (>300 nM) H₂O₂ concentrations compared to ambient water (**Figure 1A**).

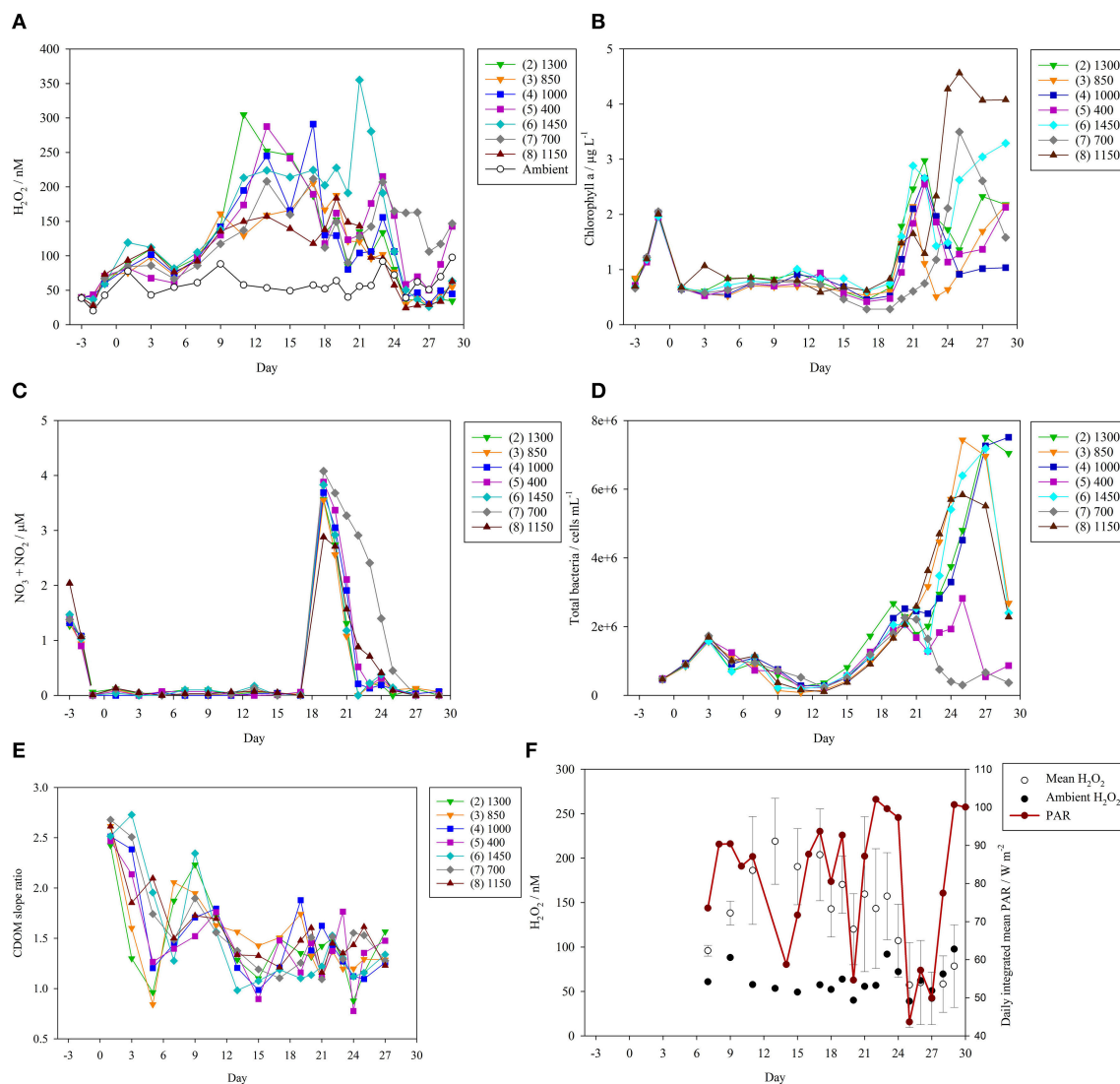


FIGURE 1 | Time series of core parameters over the experiment duration. The eight mesocosms (numbered 1–8) were subject to a pCO₂ gradient (400–1,450 µatm) imposed by the addition of CO₂ saturated, filtered seawater on day 0 (5 March 2016). Labels refer to target pCO₂ levels (µatm) which were obtained on pCO₂ addition days (see **Supplementary Figure 1**). The 550 µatm pCO₂ mesocosm (1) was discontinued after day 3 due to leakage and exchange with outside seawater and so no data is shown. **(A)** H₂O₂ concentrations (nM) during the mesocosm experiment. H₂O₂ concentration was also measured in ambient surface seawater outside the mesocosms (open circles). **(B)** Chlorophyll a concentrations (µg L⁻¹, depth integrated samples) throughout the experiment. **(C)** Nitrate + nitrite concentrations (µM, depth integrated samples) throughout the experiment. One macronutrient addition (3.1 µM nitrate, 1.5 µM silicate, and 0.2 µM phosphate) was made on day 18 to stimulate a phytoplankton bloom. **(D)** Total bacteria (cells mL⁻¹) during the mesocosm experiment. **(E)** Chromophoric dissolved organic matter (CDOM) slope ratio (S_R), a dimensionless parameter that is inversely proportional to molecular weight. **(F)** Photosynthetically active radiation (PAR, mean irradiance integrated over each experiment day, W m⁻²), available only for experiment day 7 onwards, compared to ambient seawater and mean (±standard deviation) mesocosm H₂O₂ concentration.

Over the duration of the mesocosm experiment, ambient surface seawater H₂O₂ concentrations ranged from only 20–92 nM.

The initial nitrate concentration present in ambient seawater was depleted rapidly after filling of the mesocosms (**Figure 1C**). Nitrate + nitrite fell to <0.1 µM in all mesocosms by day -1. Nitrate concentration then remained depleted until the macronutrient addition on day 18 (macronutrient addition occurred after sampling on day 18). Correspondingly, a small

peak in chlorophyll a was observed in all mesocosms on day -1 (**Figure 1B**). Chlorophyll a then declined to low concentrations until a larger peak following the macronutrient addition on day 18. Maximum chlorophyll a was then observed in most mesocosms on days 21–22.

A notable exception to the general trend in mesocosm H₂O₂ under post-bloom conditions was mesocosm 7 (700 µatm pCO₂). On days 25–27, H₂O₂ concentrations in the majority of mesocosms dropped below those measured in ambient

seawater, but H₂O₂ in mesocosm 7 always remained >100 nM (**Figure 1A**). Mesocosm 7 was also anomalous with respect to the bloom development. In mesocosm 7 only it appeared that grazing may have impeded bloom development after nutrient addition (this was consistent with higher meso-zooplankton abundances in mesocosm 7, data not shown), as evidenced by a noticeably slower decline in nitrate concentration (**Figure 1C**) and a late peak in chlorophyll *a* (**Figure 1B**).

Bacterial abundance was similar in all mesocosms until after nutrient addition (**Figure 1D**). Unlike chlorophyll *a* however, an increase in bacterial abundance was evident in all treatments prior to the nutrient addition on day 18. A small dip in bacterial abundance was then evident in most mesocosms between days 19 and 22. Under post-bloom conditions bacterial abundance was lowest in the anomalous treatment (700 μ atm) and the 400 μ atm pCO₂ mesocosm with notably elevated abundances in all pCO₂ enriched treatments. The observed trend in bacterial abundance can be interpreted as resulting from grazing pressure, and enhanced growth rates post-nutrient addition. Bacterial abundance pre-nutrient addition was inversely related to nanoeukaryotes' abundance due to grazing pressure. The increase in bacterial abundance from day 13 reflected a decline in the abundance of nanoeukaryotes. After nutrient addition (day 18), grazing on bacteria was probably considerable, but bacterial growth was enhanced sufficiently to overcome grazing pressure (except in the anomalous treatment). An in depth discussion of phytoplankton community structure over the experiment duration will be presented in a companion text.

The trend in CDOM over the experiment duration was similar across all pCO₂ treatments. The generally higher *S_R* at the start of the experiment (**Figure 1E**) corresponds to lower mean molecular weight and suggests an overall increase in CDOM molecular weight over the experiment duration. Photochemical bleaching would be expected to have had the opposite effect; to have produced low molecular weight CDOM from high molecular weight CDOM (i.e., to have increased *S_R*). Thus, the overall trend suggests that bacterial production of high molecular weight CDOM exceeded the rate of photochemical bleaching. Only between experiment days 7 and 13 was a sustained increase in *S_R* evident across most mesocosms and this corresponded to a temporary decline in bacterial abundance (**Figure 1D**).

Photosynthetically active radiation (PAR) data was available from day 7 until the end of the mesocosm experiment (**Figure 1F**) from a recording site close to the mesocosm jetty (<200 m displacement). Integrated daily PAR was subject to notable variations over the duration of the experiment ranging from a mean irradiance of 44 (day 25) to 102 (day 22) W m⁻².

Diurnal Cycling of H₂O₂

The diurnal cycling of H₂O₂ was followed both in ambient seawater (**Figure 2**) and inside mesocosm numbers 6 (1,450 μ atm pCO₂, **Figure 3A**) and 5 (400 μ atm pCO₂, **Figure 3B**) on days 22 and 23, respectively. Gaps in the data series corresponded to periods when standard additions were analyzed, the FIA instrument was cleaned, or malfunctions occurred such as air bubbles which occasionally resulted in missed data collection points. Generally, a clear increase in H₂O₂ associated with

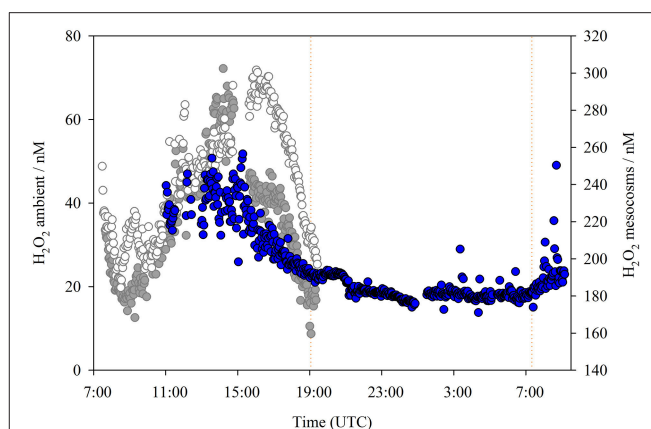
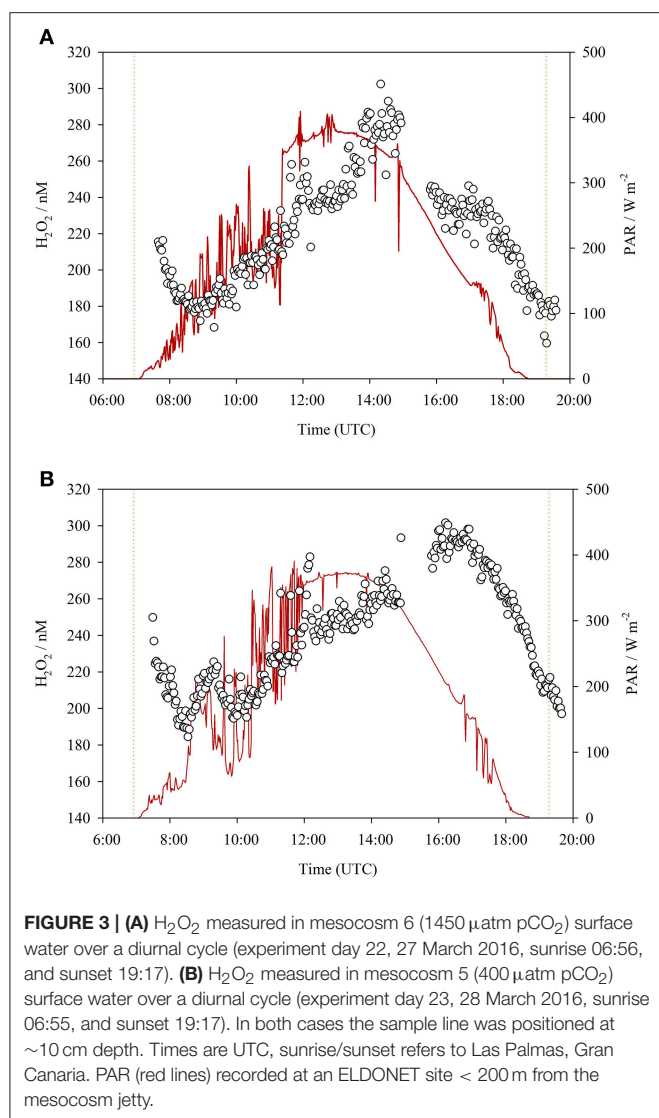


FIGURE 2 | H₂O₂ concentrations (nM) in ambient waters adjacent to the mesocosm sampling jetty over a complete diurnal cycle at ~2 min resolution (blue circles), superimposed on H₂O₂ concentrations for different days (as per **Figure 3**) from within the 1,450 μ atm pCO₂ (dark gray) and 400 μ atm pCO₂ (light gray) mesocosms. Ambient H₂O₂ concentration data collected 5–6 March 2016. All times are UTC, sunrise/sunset (illustrated) refers to Las Palmas: sunrise (5 March) 7:21, sunset (5 March) 19:04, sunrise (6 March) 07:20. The sample line was positioned at ~10 cm depth. There was no large change in surface salinity over the experiment duration (range 0.2 practical salinity units).

daylight was evident in all three diurnal datasets (**Figures 2, 3**). Yet H₂O₂ concentrations were much higher throughout the diurnal cycle within the mesocosms compared to ambient waters. In all three diurnal cycles, peak H₂O₂ concentration occurred mid-late afternoon (times refer to UTC). In the two mesocosms where diurnal H₂O₂ concentration was followed, the range between peak and minimum H₂O₂ was similar (180–300 nM, mesocosm 5, day 23; 160–300 nM, mesocosm 6, day 22), despite the pronounced difference in pCO₂ (400 μ atm [5] compared 1,450 μ atm [6]) and the 2 h offset between the timing of peak daytime H₂O₂ concentration (**Figure 3**). In ambient seawater, the amplitude of diurnal variation in H₂O₂ (~20–30 nM, **Figure 2**) was very similar to that reported previously in the central Atlantic Ocean (25 nM, Yuan and Shiller, 2001).

Two curious features were notable in both mesocosm diurnal cycles (**Figure 3**). These features could only be observed by virtue of the very high data resolution and, to some extent, also the relatively high H₂O₂ concentrations within the mesocosms compared to ambient waters. First, peak H₂O₂ concentrations occurred >1 h after peak irradiance. PAR data from ELDONET was not available for the seawater diurnal study date (**Figure 2**), but noting the timing of peak H₂O₂, there was likely approximately a 1 h offset between peak irradiance and peak H₂O₂ here also. Second, the net decline in H₂O₂ concentration which occurred in the dark continued until sometime after sunrise in both mesocosm studies (**Figure 3**). An increase in H₂O₂ was not apparent until after PAR increased above ~100 W m⁻². This was not apparent in the ambient seawater study (**Figure 2**) where a relatively stable concentration of 18.1 ± 1.3 nM was maintained from 21:11 to 07:20 (sunrise) with a sustained rise in H₂O₂ thereafter. This time offset could



simply therefore have related to the incident solar angle as the mesocosm walls may have reduced the rate of light induced H₂O₂ formation at low incident solar angles.

Minor H₂O₂ Additions From Rainwater

The open design of the mesocosms created the potential for significant atmospheric deposition of H₂O₂. Rain water H₂O₂ concentrations were quantified for the two rainfall events during the mesocosm experiment with sufficient amounts of deposition (>1 mm) to facilitate sampling (Table 1) and were similar to values reported elsewhere over the Atlantic (Zika et al., 1982; Kieber et al., 2001). H₂O₂ concentrations in rainwater are thought to be sufficiently high to offset the expected beneficial effect of rainwater derived nutrient and micro-nutrient addition on primary production when rainwater is mixed with seawater (Willey et al., 2004) unless the dilution factor is high. The calculated H₂O₂ addition to mesocosms resulting from rainfall in Gran Canaria was however modest relative to the mesocosm

TABLE 1 | Contribution of rainwater events to H₂O₂ concentrations in the mesocosms.

Location	Date and time	Rainfall (mm)	Rainwater H ₂ O ₂ (μM)	Calculated H ₂ O ₂ increase in mesocosms (nM)
Taliarte, Gran Canaria	21/03/16 07:00 (day 16)	1	20.5	6
	30/03/16 17:30 (day 25)	3	44.4	40

H₂O₂ concentrations due to the low ratio of rain:mesocosm volume (Table 1).

DISCUSSION

Diurnal Cycling of H₂O₂

Photochemical processes are thought to be the dominant influence on ambient H₂O₂ concentrations in the surface ocean (O'Sullivan et al., 2005; Steigenberger and Croot, 2008), with large scale spatial variations typically explained in terms of latitudinal changes in light and ocean temperature (Yocis et al., 2000; Yuan and Shiller, 2001). In the high-resolution temporal experiments a clear diurnal cycle in H₂O₂ concentration was evident, both inside and outside the mesocosm bags (Figures 2, 3). The amplitude of H₂O₂ concentration over a diurnal cycle was however much greater inside the mesocosms (100 nM compared to 20–30 nM in ambient seawater). H₂O₂ concentrations over the 28 day duration of the mesocosm experiment (Figure 1A) were always measured at 14:00–15:00 (UTC) daily to ensure that the month long data series was not affected unduly by diurnal variation.

During overnight monitoring of ambient H₂O₂ it appeared that an equilibrium concentration of 18 nM was maintained in the dark (Figure 2). This was indicative of a dark production mechanism, such as that highlighted in prior work (Palenik and Morel, 1988; Moffett and Zafiriou, 1990), sufficient to offset H₂O₂ decay. Whilst photochemical processes are no doubt a major source of H₂O₂, inter-day changes in integrated PAR were only significantly correlated with the H₂O₂ trend in ambient seawater (Spearman rank correlation 0.73, *p* value 0.002, *n* = 14) and in the 400 μatm mesocosm (Table 2). In all other mesocosms there was no apparent correlation between integrated daily PAR and H₂O₂ concentration from days 7–29.

The two high-resolution diurnal cycles within mesocosms (Figure 3) revealed some interesting features that would not be apparent at lower H₂O₂ concentrations (due to the increased signal:noise ratio) or reduced sampling resolution. An offset between irradiance and H₂O₂ concentration was reflected in the later delayed peak in H₂O₂ compared to maximum irradiance. Partial shading of the mesocosms in the early morning and late afternoon could create a local PAR exposure that was reduced compared to that reported by a mounted sensor. However, as the displacement of the sensor was <200 m from the mesocosms, this could not explain the offset between peak H₂O₂ and peak irradiance in the mid-afternoon. Instead, we suggest that net

TABLE 2 | Spearman rank correlation coefficients and *p* values for H₂O₂ concentration time series in each mesocosm compared to: baseline H₂O₂ concentration in ambient seawater (nM), chlorophyll *a* (μg L⁻¹), total bacteria (cells mL⁻¹), colored dissolved organic matter slope ratio (*S_R*), and daily integrated mean photosynthetically active radiation (PAR, W m⁻²).

Mesocosm (number) pCO ₂ (μatm)	Spearman rank correlation coefficient									
	Baseline H ₂ O ₂			Chlorophyll <i>a</i>		Bacteria		CDOM <i>S_R</i>		PAR
	Day -3 to 9	Day 11+	All days	Day 11+	All days	Day 11+	All days	Day 11+	All days	Days 7+
(5) 400	0.86	NSR	0.48	NSR	NSR	NSR	NSR	NSR	NSR	0.58
(7) 700	0.79	NSR	0.42	NSR	NSR	NSR	NSR	NSR	-0.51	NSR
(3) 850	0.81	NSR	NSR	-0.58	-0.47	-0.85	-0.52	0.70	NSR	NSR
(4) 1000	0.81	NSR	NSR	NSR	NSR	-0.87	-0.50	NSR	NSR	NSR
(8) 1150	0.86	NSR	NSR	-0.78	-0.53	-0.83	-0.56	NSR	NSR	NSR
(2) 1300	0.83	NSR	NSR	-0.61	-0.46	-0.94	-0.58	NSR	NSR	NSR
(6) 1450	0.93	NSR	NSR	NSR	NSR	-0.59	NSR	NSR	NSR	NSR
P VALUES										
(5) 400	0.0018	0.44	0.019	0.29	0.87	0.15	0.59	0.92	0.50	0.028
(7) 700	0.015	0.23	0.040	0.74	0.91	0.081	0.16	0.85	0.035	0.13
(3) 850	0.0096	0.76	0.33	0.035	0.030	<0.001	0.023	0.010	0.17	0.66
(4) 1000	0.0096	0.82	0.12	0.098	0.36	<0.001	0.028	0.97	0.99	0.20
(8) 1150	0.0018	0.67	0.57	<0.001	0.013	<0.001	0.013	0.72	0.54	0.92
(2) 1300	0.0053	0.73	0.38	0.025	0.034	<0.001	0.010	0.60	0.54	0.70
(6) 1450	<0.001	0.70	0.46	0.17	0.60	0.031	0.28	0.85	0.20	0.22

NSR, no significant relationship (*P* > 0.05). Highly significant correlations (*P* 0.010 or less) are highlighted. Mesocosm 1 (550 μatm pCO₂), was excluded due to the lack of data after day 3.

biological production of H₂O₂ is slightly offset from irradiance. A critical factor, not measured herein, which likely affects the net rate of change in H₂O₂ concentration during daylight hours is the production rate of peroxidase or catalase enzymes. This process is known to be diurnally variable, with oxidative defenses more active during daylight hours (Morris et al., 2016). Whilst it is not clear if this response under natural conditions is triggered by increasing H₂O₂ induced stress or by a circadian rhythm, the rate and efficiency (which may also change with incident light) of enzymatic H₂O₂ removal are likely to be key influences on the shape of the diurnal H₂O₂ trend.

Correlation of H₂O₂ in Mesocosms With Core Parameters

Between days -3 and 9 the range of H₂O₂ within the different mesocosms was small (<45 nM) and the behavior of chlorophyll *a* and nitrate very similar across all mesocosms (Figures 1A–C). During this early phase, H₂O₂ inside and outside the mesocosms was relatively well correlated across all pCO₂ conditions (positive Spearman Rank Coefficients of 0.79–0.93). Combined with the comparability of the diurnal H₂O₂ cycle in 400 and 1,450 μatm pCO₂ mesocosms (Figure 3), despite the extreme pCO₂ difference, this suggests that the direct effect of the pCO₂ gradient (applied after day 0) on H₂O₂ concentrations was minimal.

In contrast to the early stage of the experiment, H₂O₂ concentrations in the mesocosms diverged after day 9 and there was then no longer a statistically significant relationship between the paired H₂O₂ concentrations in and outside the mesocosm (Spearman Rank Correlation *P* > 0.05, Table 2) for any pCO₂

treatment. If irradiance was the dominant factor controlling extracellular H₂O₂ concentrations throughout the experiment, we would expect H₂O₂ concentrations to have remained similar across all mesocosms and to remain correlated with H₂O₂ in ambient water outside the mesocosms. Yet this was not the case. Variations in daily integrated PAR, available from day 7 onwards, could explain some of the variation in background seawater H₂O₂, but inter-day changes in PAR were only significantly correlated with H₂O₂ in the 400 μatm mesocosm (Table 2).

Formation of ROS generally increases with dissolved organic carbon concentration in estuarine waters and this is specifically linked to the presence of terrestrially derived humic material (Timko et al., 2014) which has a relatively large component of CDOM. However, CDOM properties are not clearly linked to increasing H₂O₂ concentrations in offshore seawater (O'Sullivan et al., 2005). The general decline in *S_R* throughout the mesocosms (from day 1 to day 27, Figure 1E) suggested that *in situ* production of higher molecular weight CDOM was sufficient to offset photo bleaching. However, this was not clearly related to any change in H₂O₂ concentration as no clear correlation was found between *S_R* and H₂O₂ either over the whole experiment or specifically for days 11+ (Table 2).

Similarly, the overall trend in H₂O₂ concentration could not be related directly to macronutrient depletion. The observed nitrate concentrations were similar across all mesocosms until after the addition of macronutrients on day 18 (Figure 3) and there was no consistent trend in H₂O₂ concentration in the days immediately following this addition. Most mesocosms obtained the highest measured H₂O₂ concentration between days 9–18. Yet mesocosm 6 was notable for obtaining a peak H₂O₂

concentration 3 days after the nutrient addition. A sustained drop in H₂O₂ concentration across all mesocosms (apart from the anomalous mesocosm 7) was only observed between days 23–25. The lowest H₂O₂ concentrations, both within the mesocosm experiment and relative to ambient seawater, were observed in this post-bloom phase when bacterial abundance peaked (Figure 1D) and when daily integrated PAR was persistently low for 3 days (Figure 1F).

A Contribution to H₂O₂ From Mesocosm Design?

H₂O₂ concentrations might be expected to be generally higher inside the mesocosms due to the nature of their design. Sunlight is attenuated with depth, so in a natural surface mixed layer H₂O₂ is formed predominantly at the surface and then physically mixed throughout the surface mixed layer (Johnson et al., 1989; Miller and Kester, 1994), although sub-surface H₂O₂ peaks can occasionally be observed at the chlorophyll *a* maxima (Yuan and Shiller, 2001; Croot et al., 2005; Steigenberger and Croot, 2008). The confinement of the surface 3 m within the mesocosm bags used here thereby encloses the water with the highest light exposure and, throughout most of this experiment, a high level of biological activity relative to ambient seawater, whilst removing the physical processes that would constantly act to mix H₂O₂ into deeper waters. The enclosure of seawater was thereby a likely factor contributing to the high H₂O₂ concentrations occurring during the middle (days 9–18) of the mesocosm experiment. Yet this alone does not explain the divergence in H₂O₂ levels between the various mesocosms after day 9 (Figure 1A). The timings of the initial mini-bloom after the mesocosms were filled, of the macronutrient addition and the subsequent bloom were (with the exception of mesocosm 7) relatively uniform (Figures 1B,C).

A Link Between Community Structure and Extracellular H₂O₂?

Two possible explanations for why H₂O₂ concentrations were so variable between mesocosms, which are not mutually exclusive, are that either the biological H₂O₂ source(s) or the biological H₂O₂ sink(s) varied because of different microbial communities across the pCO₂ gradient. An anti-correlation between bacterial abundance and extracellular H₂O₂ concentrations is therefore intriguing. Microorganisms are simultaneously both a H₂O₂ source and a H₂O₂ sink. ROS are generated as waste products from aerobic cellular metabolism (Kruk, 1998; Apel and Hirt, 2004), with H₂O₂ produced both directly and from the decay of other ROS (for example, the enzyme superoxide dismutase produces H₂O₂ from O₂^{•−}; McCord and Fridovich, 1969). Conversely, biological H₂O₂ sinks arise from both synthesis of H₂O₂ destroying enzymes (catalase and peroxidase) and also, under some circumstances, serendipitously with increasing biomass. The quenching of extracellular H₂O₂ with increasing biomass is referred to as “self-shading” and has been described both in monocultures of *Prochlorococcus*, which lacks catalase-peroxidase genes (Morris et al., 2011) and at the community level (Barros and Colepiccolo, 2003). It

presumably arises from physical shading and/or non-enzymatic ROS sinks.

The anti-correlation between H₂O₂ concentrations in each mesocosm both with chlorophyll *a* and with total bacterial abundance over the duration of the experiment (Table 2) was statistically significant in most mesocosms. Overall there was a significant ($P < 0.05$) anti-correlation between chlorophyll *a* and H₂O₂ concentrations with negative correlation coefficients (Table 2) in mesocosms 3, 4, 8, and 2 (850–1,300 μatm pCO₂). The anti-correlation was slightly stronger when the initial phase of the experiment (Days −3 to 9, when the range of H₂O₂ concentrations across all mesocosms was relatively narrow) was excluded. A negative relationship between chlorophyll *a* and H₂O₂ concentrations could arise from an increasing biological H₂O₂ sink simply due to self-shading associated with increasing biomass, yet no correlation with chlorophyll *a* was found either at low (400, 700 μatm) or at the highest (1,450 μatm) pCO₂ treatments. For bacteria, the correlation followed the same pattern as chlorophyll *a* with respect to pCO₂, yet the effect was stronger and more significant. From day 11 onwards, the intermediate pCO₂ mesocosms (850–1,300 μatm) all exhibited a strong negative correlation (Spearman Rank Coefficients of −0.83 to −0.94) between bacteria cell counts and H₂O₂ concentration (P values < 0.001). This suggests that under post-bloom conditions, bacteria were an important net-sink for extracellular H₂O₂.

As both cellular H₂O₂ production and defense mechanism activity vary over diurnal cycles and at the species level, it is difficult to separate the source and sink terms within separate mesocosms and over the pCO₂ gradient. Yet in any case, the effects of a pCO₂ gradient on H₂O₂ concentration were apparently indirect, resulting from changes to bacterial abundance and community composition rather than directly arising as a consequence of perturbing the carbonate system alone.

Effects of Elevated H₂O₂ Under Experimental Conditions?

Reported H₂O₂ concentrations in seawater incubated under laboratory conditions are typically 100–300 nM (e.g., Coe et al., 2016), but can be much higher depending on the buffer composition and irradiance exposure (Morris and Zinser, 2013). In a spot-check of baseline H₂O₂ concentrations in incubated seawater (with added nutrients) in our own laboratory, we found 42 ± 50 nM H₂O₂ in freshly made mixtures (made from seawater which was previously stored in the dark for >1 year) and 180 ± 130 nM in the same water after 72 h of incubation subject to a diel light cycle. In all these cases, the H₂O₂ concentrations in seawater incubated under laboratory conditions are thereby at the mid-high end of the range observed in the surface ocean (Price et al., 1998; Yuan and Shiller, 2001; Hopwood et al., 2017).

The unmodified concentrations of H₂O₂ in growth media are sufficiently high to prevent the cultivation of some microorganisms, including strains of *Prochlorococcus*, under laboratory conditions (Morris et al., 2011). However, uncertainties remain about what the effects of elevated H₂O₂ are

at the community level. Whilst H₂O₂ is not widely investigated during mesocosm studies, field evidence suggests that increases in H₂O₂ to concentrations less than the peaks observed here (**Figure 1A**) can affect a broad range of biogeochemical processes. Additions of 10–100 nM H₂O₂ to water from 100 m in the North Atlantic were found to reduce the extracellular activity of β -glucosidase, alkaline phosphatase, and leucine aminopeptidase by 20–80% with the inhibition effect consistently strongest on β -glucosidase (Baltar et al., 2013). A similar small absolute increase of only 30 nM is reported to suppress rates of ammonia oxidation to below detection in surface (10 m depth) Antarctic seawater (Tolar et al., 2016) where the initial natural concentration of H₂O₂ was low (14 nM). Additional specific effects of increasing extracellular H₂O₂ concentrations in seawater can also be deduced from laboratory experiments. For example, an increase on the order of 100 nM H₂O₂ is sufficient to measurably decrease the half-life of Fe(II), thereby theoretically decreasing dissolved Fe bioavailability (González-Davila et al., 2005), and to double brominating activity in some diatoms (Hughes and Sun, 2016).

A particularly curious phenomenon observed here was the extremely high H₂O₂ concentrations observed during the pre-bloom phase of the experiment (**Figure 1A**). It is questionable to what extent this phenomenon would occur in a natural environment because small-scale mesocosms inevitably fail to mimic the mixing processes that occur within the natural water column. Nevertheless, the potential for oxidative stress from extracellular ROS to be increased under natural, or incubated, oligotrophic conditions should be investigated concurrently with other stressors to understand the interactive effect(s) on microbial functioning. As outlined above, the sensitivity of some enzymatic processes to increasing extracellular H₂O₂ concentrations and the involvement of H₂O₂ in the biogeochemical cycling of various chemicals including the micronutrient Fe, means that large perturbations to H₂O₂ during mesocosm experiments are undesirable.

CONCLUSIONS

During the progression of a 28 day mesocosm experiment in North Atlantic waters an applied pCO₂ gradient (400–1,450 μ atm) had no discernable direct effect upon extracellular H₂O₂ concentrations. Whilst a clear diurnal trend in H₂O₂ was observed, both within high/low pCO₂ mesocosms and in ambient waters, inter-day variation in PAR was not correlated with mesocosm H₂O₂ concentrations.

The general elevation of H₂O₂ above ambient North Atlantic concentrations was attributed to the effect of enclosing seawater in an open mesocosm at the ocean surface. Yet during the pre-bloom phase of the experiment, unexpected swings occurred to H₂O₂ concentrations >300 nM. Across the majority of mesocosms, bacteria appeared to be a net-sink for H₂O₂, particularly under post-bloom conditions. Thus,

microbial community structure does appear to strongly influence extracellular H₂O₂ concentrations.

Given the multitude of possible direct and indirect, chemical and biological effects of large changes to H₂O₂ concentrations, it is important to consider to what extent ROS are a source of oxidative stress in the natural surface ocean and how well experiments manipulate the natural environment with respect to this stressor.

AUTHOR CONTRIBUTIONS

All authors contributed to the design of the study. Fieldwork and analytical work was conducted by MH, UR, AL, JA, and NH. MH wrote the initial draft of the manuscript and then all authors contributed to its revision.

FUNDING

Funding for this mesocosm study was provided by the Kiel Excellence Cluster The Future Ocean and by the German Research Foundation (DFG) through the Leibniz Award 2012 to UR. MH and EA gratefully acknowledge financial aid from the European Commission (OCEAN-CERTAIN, FP7-ENV-2013-6.1-1; no: 603773) and the Collaborative Research Centre 754 (SFB 754) Climate-Biogeochemistry Interactions in the Tropical Ocean funded by the German Research Foundation (DFG). JA was supported by a Helmholtz International Fellow Award, 2015 (Helmholtz Association, Germany). NH was partially supported by the FLUXES project (CTM2015-69392-C3-1-R) funded by the Spanish government (Plan Nacional I+D).

ACKNOWLEDGMENTS

The KOSMOS/PLOCAN teams assisting with all aspects of mesocosm organization are thanked for logistical support. Leila Kittu and Syrmalenia Kotronaki are thanked for chlorophyll a and macronutrient data. Labview software for operating the H₂O₂ FIA system was designed by P. Croot, M. Heller, C. Neill, and W. King. Statistics were performed in SigmaPlot.

SUPPLEMENTARY MATERIAL

The Supplementary Material for this article can be found online at: <https://www.frontiersin.org/articles/10.3389/fmars.2018.00105/full#supplementary-material>

Supplementary Figure 1 | Mesocosm timeline labeled with experiment days (used throughout the text). Day –4, when the mesocosms were filled, was 1 March 2016. A pH gradient was imposed on day 0 by the addition of CO₂ saturated, filtered seawater. Further pCO₂ additions were then made as necessary to compensate for out-gassing. The volume of each mesocosm was determined on day 18 by measuring the change in salinity resulting from a freshwater addition. A single macronutrient spike was then added after sampling on day 18.

Supplementary Datasheet 1 | Mesocosm time series data for core parameters used: chlorophyll a, nitrate + nitrite, hydrogen peroxide, bacterial abundance and CDOM SR.

REFERENCES

- Apel, K., and Hirt, H. (2004). Reactive oxygen species: metabolism, oxidative stress, and signal transduction. *Annu. Rev. Plant Biol.* 55, 373–399. doi: 10.1146/annurev.arplant.55.031903.141701
- Baltar, F., Reinthaler, T., Herndl, G. J., and Pinhassi, J. (2013). Major effect of hydrogen peroxide on bacterioplankton metabolism in the Northeast Atlantic. *PLoS ONE* 8:e61051. doi: 10.1371/journal.pone.0061051
- Barros, M. P., and Colepiccolo, P. (2003). Self-shading protects phytoplankton communities against H₂O₂-induced oxidative damage. *Aquat. Microb. Ecol.* 30, 275–282. doi: 10.3354/ame030275
- Bogosian, G., Aardema, N. D., Bourneuf, E. V., Morris, P. J. L., and O'Neil, J. P. (2000). Recovery of hydrogen peroxide-sensitive culturable cells of *Vibrio vulnificus* gives the appearance of resuscitation from a viable but nonculturable state. *J. Bacteriol.* 182, 5070–5075. doi: 10.1128/JB.182.18.5070-5075.2000
- Coe, A., Ghizzoni, J., LeGault, K., Biller, S., Roggensack, S. E., and Chisholm, S. W. (2016). Survival of *Prochlorococcus* in extended darkness. *Limnol. Oceanogr.* 61, 1375–1388. doi: 10.1002/lno.10302
- Croot, P. L., Laan, P., Nishioka, J., Strass, V., Cisewski, B., Boye, M., et al. (2005). Spatial and temporal distribution of Fe(II) and H₂O₂ during EisenEx, an open ocean mesocosm iron enrichment. *Mar. Chem.* 95, 65–88. doi: 10.1016/j.marchem.2004.06.041
- Croot, P. L., Streu, P., Peeken, I., Luchte, K., and Baker, A. R. (2004). Influence of the ITCZ on H₂O₂ in near surface waters in the equatorial Atlantic Ocean. *Geophys. Res. Lett.* 31:L23S04. doi: 10.1029/2004GL020154
- Czerny, J., Schulz, K. G., Krug, S. A., Ludwig, A., and Riebesell, U. (2013). Technical note: the determination of enclosed water volume in large flexible-wall mesocosms KOSMOS. *Biogeosciences* 10, 1937–1941. doi: 10.5194/bg-10-1937-2013
- Fujiwara, K., Ushiroda, T., Takeda, K., Kumamoto, Y., and Tsubota, H. (1993). Diurnal and seasonal distribution of hydrogen-peroxide in seawater of the seto inland sea. *Geochem. J.* 27, 103–115. doi: 10.2343/geochemj.27.103
- Gasol, J. M., and del Giorgio, P. A. (2000). Using flow cytometry for counting natural planktonic bacteria and understanding the structure of planktonic bacterial communities. *Sci. Mar.* 64, 197–224. doi: 10.3989/scimar.2000.64n2197
- Gerringa, L. J. A., Rijkenberg, M. J. A., Timmermans, R., and Buma, A. G. J. (2004). The influence of solar ultraviolet radiation on the photochemical production of H₂O₂ in the equatorial Atlantic Ocean. *J. Sea Res.* 51, 3–10. doi: 10.1016/j.seares.2003.03.002
- González-Davila, M., Santana-Casiano, J. M., and Millero, F. J. (2005). Oxidation of iron (II) nanomolar with H₂O₂ in seawater. *Geochim. Cosmochim. Acta* 69, 83–93. doi: 10.1016/j.gca.2004.05.043
- Häder, D.-P., and Lebert, M. (2006). “Eldonet—European light dosimeter network BT - environmental UV radiation: impact on ecosystems and human health and predictive models,” in *Proceedings of the NATO Advanced Study Institute on Environmental UV Radiation: Impact on Ecosystems and Human Health*, eds F. Ghetti, G. Checcucci, and J. F. Bornman (Dordrecht: Springer Netherlands), 95–108.
- Hansen, H. P., and Koroleff, F. (1999). “Determination of nutrients,” in *Methods of Seawater Analysis*, eds K. Grasshoff, K. Kremling, and M. Ehrhardt (New York, NY: Wiley-VCH Verlag GmbH), 159–228.
- Helms, J. R., Stubbins, A., Ritchie, J. D., Minor, E. C., Kieber, D. J., and Mopper, K. (2008). Absorption spectral slopes and slope ratios as indicators of molecular weight, source, and photobleaching of chromophoric dissolved organic matter. *Limnol. Oceanogr.* 53, 955–969. doi: 10.4319/lo.2008.53.3.0955
- Hopwood, M. J., Rapp, I., Schlosser, C., and Achterberg, E. P. (2017). Hydrogen peroxide in deep waters from the Mediterranean Sea, South Atlantic and South Pacific Oceans. *Sci. Rep.* 7:43436. doi: 10.1038/srep43436
- Hughes, C., and Sun, S. (2016). Light and brominating activity in two species of marine diatom. *Mar. Chem.* 181, 1–9. doi: 10.1016/j.marchem.2016.02.003
- Imlay, J. A. (2008). Cellular defenses against superoxide and hydrogen peroxide. *Annu. Rev. Biochem.* 77, 755–776. doi: 10.1146/annurev.biochem.77.061606.161055
- IPCC Working Group 1 (2014). *IPCC Fifth Assessment Report (AR5) - The Physical Science Basis*. IPCC Working Group.
- Johnson, K. S., Willason, S. W., Wiesenburg, D. A., Lohrenz, S. E., and Arnone, R. A. (1989). Hydrogen peroxide in the western Mediterranean Sea: a tracer for vertical advection. *Deep Sea Res. Oceanogr. Res. Pap.* 36, 241–254. doi: 10.1016/0198-0149(89)90136-2
- Kieber, R. J., Peake, B., Willey, J. D., and Jacobs, B. (2001). Iron speciation and hydrogen peroxide concentrations in New Zealand rainwater. *Atmos. Environ.* 35, 6041–6048. doi: 10.1016/S1352-2310(01)00199-6
- Kruk, I. (1998). *Environmental Toxicology and Chemistry of Oxygen Species, 1st Edn*. Berlin; Heidelberg: Springer-Verlag.
- Lesser, M. P. (2006). Oxidative stress in marine environments: biochemistry and physiological ecology. *Annu. Rev. Physiol.* 68, 253–278. doi: 10.1146/annurev.physiol.68.040104.110001
- McCord, J. M., and Fridovich, I. (1969). Superoxide dismutase. An enzymic function for erythrocyte (hemocuprein). *J. Biol. Chem.* 244, 6049–6055.
- Micinski, E., Ball, L. A., and Zafriou, O. C. (1993). Photochemical oxygen activation: superoxide radical detection and production rates in the eastern Caribbean. *J. Geophys. Res. Ocean.* 98, 2299–2306. doi: 10.1029/92JC02766
- Miller, W. L., and Kester, D. R. (1994). Peroxide variations in the Sargasso Sea. *Mar. Chem.* 48, 17–29. doi: 10.1016/0304-4203(94)90059-0
- Milne, A., Davey, M. S., Worsfold, P. J., Achterberg, E. P., and Taylor, A. R. (2009). Real-time detection of reactive oxygen species generation by marine phytoplankton using flow injection-chemiluminescence. *Limnol. Oceanogr.* 7, 706–715. doi: 10.4319/lom.2009.7.706
- Moffett, J. W., and Zafriou, O. C. (1990). An investigation of hydrogen peroxide chemistry in surface waters of Vineyard Sound with H₂¹⁸O₂ and ¹⁸O₂. *Limnol. Oceanogr.* 35, 1221–1229. doi: 10.4319/lo.1990.35.6.1221
- Moore, C. A., Farmer, C. T., and Zika, R. G. (1993). Influence of the Orinoco River on hydrogen peroxide distribution and production in the eastern Caribbean. *J. Geophys. Res.* 98:2289. doi: 10.1029/92JC02767
- Morris, J. J., Johnson, Z. I., Szul, M. J., Keller, M., and Zinser, E. R. (2011). Dependence of the cyanobacterium *Prochlorococcus* on hydrogen peroxide scavenging microbes for growth at the ocean's surface. *PLoS ONE* 6:e16805. doi: 10.1371/journal.pone.0016805
- Morris, J. J., Johnson, Z. I., Wilhelm, S. W., and Zinser, E. R. (2016). Diel regulation of hydrogen peroxide defenses by open ocean microbial communities. *J. Plankton Res.* 38, 1103–1114. doi: 10.1093/plankt/fbw016
- Morris, J. J., Kirkegaard, R., Szul, M. J., Johnson, Z. I., and Zinser, E. R. (2008). Facilitation of robust growth of *Prochlorococcus* colonies and dilute liquid cultures by “helper” heterotrophic bacteria. *Appl. Environ. Microbiol.* 74, 4530–4534. doi: 10.1128/AEM.02479-07
- Morris, J., and Zinser, E. R. (2013). Continuous hydrogen peroxide production by organic buffers in phytoplankton culture media. *J. Phycol.* 49, 1223–1228. doi: 10.1111/jpy.12123
- O'Sullivan, D. W., Neale, P. J., Coffin, R. B., Boyd, T. J., and Osburn, C. L. (2005). Photochemical production of hydrogen peroxide and methylhydroperoxide in coastal waters. *Mar. Chem.* 97, 14–33. doi: 10.1016/j.marchem.2005.04.003
- Palenik, B., and Morel, F. M. M. (1988). Dark production of H₂O₂ in the Sargasso Sea. *Limnol. Oceanogr.* 33, 1606–1611. doi: 10.4319/lo.1988.33.6_part_2.1606
- Palenik, B., Zafriou, O. C., and Morel, F. M. M. (1987). Hydrogen peroxide production by a marine phytoplankter. *Limnol. Oceanogr.* 32, 1365–1369. doi: 10.4319/lo.1987.32.6.1365
- Petasne, R. G., and Zika, R. G. (1997). Hydrogen peroxide lifetimes in South Florida coastal and offshore waters. *Mar. Chem.* 56, 215–225. doi: 10.1016/S0304-4203(96)00072-2
- Price, D., Mantoura, R. F. C., and Worsfold, P. J. (1998). Shipboard determination of hydrogen peroxide in the western Mediterranean sea using flow injection with chemiluminescence detection. *Anal. Chim. Acta* 377, 145–155. doi: 10.1016/S0003-2670(98)00621-7
- Riebesell, U., Czerny, J., Von Bröckel, K., Boxhammer, T., Büdenbender, J., Deckelnick, M., et al. (2013). Technical note: a mobile sea-going mesocosm system - new opportunities for ocean change research. *Biogeosciences* 10, 1835–1847. doi: 10.5194/bg-10-1835-2013
- Seaver, L. C., and Imlay, J. A. (2001). Hydrogen peroxide fluxes and compartmentalization inside growing *Escherichia coli*. *J. Bacteriol.* 183, 7182–7189. doi: 10.1128/JB.183.24.7182-7189.2001
- Steigenberger, S., and Croot, P. L. (2008). Identifying the processes controlling the distribution of H₂O₂ in surface waters along a meridional transect in the eastern Atlantic. *Geophys. Res. Lett.* 35:L03616. doi: 10.1029/2007GL032555
- Taucher, J. (2017). Influence of ocean acidification and deep water upwelling on oligotrophic plankton communities in the subtropical North

- Atlantic: insights from an *in situ* Mesocosm study. *Front. Mar. Sci.* 4:85. doi: 10.3389/fmars.2017.00085
- Timko, S. A., Romera-Castillo, C., Jaffé, R., and Cooper, W. J. (2014). Photo-reactivity of natural dissolved organic matter from fresh to marine waters in the Florida Everglades, USA. *Environ. Sci. Process. Impacts* 16, 866–878. doi: 10.1039/C3EM00591G
- Tolar, B., Powers, L., Miller, W., Wallsgrove, N., Popp, B., and Hollibaugh, J. (2016). Ammonia oxidation in the ocean can be inhibited by nanomolar concentrations of hydrogen peroxide. *Front. Mar. Sci.* 3:237. doi: 10.3389/fmars.2016.00237
- Van Baalen, C., and Marler, J. E. (1966). Occurrence of hydrogen peroxide in sea water. *Nature* 211:951. doi: 10.1038/211951a0
- Vermilyea, A. W., Hansard, S. P., and Voelker, B. M. (2010). Dark production of hydrogen peroxide in the Gulf of Alaska. *Limnol. Oceanogr.* 55, 580–588. doi: 10.4319/lo.2009.55.2.0580
- Welschmeyer, N. A. (1994). Fluorometric analysis of chlorophyll a in the presence of chlorophyll b and pheopigments. *Limnol. Oceanogr.* 39, 1985–1992. doi: 10.4319/lo.1994.39.8.1985
- Willey, J. D., Kieber, R. J., and Avery, G. B. (2004). Effects of rainwater iron and hydrogen peroxide on iron speciation and phytoplankton growth in seawater near Bermuda. *J. Atmos. Chem.* 47, 209–222. doi: 10.1023/B:JOCH.0000021087.19846.e1
- Yocis, B. H., Kieber, D. J., and Mopper, K. (2000). Photochemical production of hydrogen peroxide in Antarctic Waters. *Deep. Res. I* 47, 1077–1099. doi: 10.1016/S0967-0637(99)00095-3
- Yuan, J. C., and Shiller, A. M. (1999). Determination of subnanomolar levels of hydrogen peroxide in seawater by reagent-injection chemiluminescence detection. *Anal. Chem.* 71, 1975–1980. doi: 10.1021/ac981357c
- Yuan, J., and Shiller, A. (2001). The distribution of hydrogen peroxide in the southern and central Atlantic ocean. *Deep Sea Res. II Top. Stud. Oceanogr.* 48, 2947–2970. doi: 10.1016/S0967-0645(01)00026-1
- Yuan, J., and Shiller, A. M. (2004). Hydrogen peroxide in deep waters of the North Pacific Ocean. *Geophys. Res. Lett.* 31:L01310. doi: 10.1029/2003GL018439
- Zika, R., Saltzman, E., Chameides, W. L., and Davis, D. D. (1982). H₂O₂ levels in rainwater collected in south Florida and the Bahama Islands. *J. Geophys. Res.* 87:5015. doi: 10.1029/JC087iC07p05015

Conflict of Interest Statement: The authors declare that the research was conducted in the absence of any commercial or financial relationships that could be construed as a potential conflict of interest.

Copyright © 2018 Hopwood, Riebesell, Aristegui, Ludwig, Achterberg and Hernández. This is an open-access article distributed under the terms of the Creative Commons Attribution License (CC BY). The use, distribution or reproduction in other forums is permitted, provided the original author(s) and the copyright owner are credited and that the original publication in this journal is cited, in accordance with accepted academic practice. No use, distribution or reproduction is permitted which does not comply with these terms.



Ocean Acidification-Induced Restructuring of the Plankton Food Web Can Influence the Degradation of Sinking Particles

Paul Stange¹, Jan Taucher^{1*}, Lennart T. Bach¹, María Algueró-Muñiz², Henriette G. Horn², Luana Krebs³, Tim Boxhammer¹, Alice K. Nauendorf¹ and Ulf Riebesell¹

¹ GEOMAR Helmholtz Centre for Ocean Research Kiel, Kiel, Germany, ² Helmholtz Centre for Polar and Marine Research, Alfred Wegener Institute, Biologische Anstalt Helgoland, Helgoland, Germany, ³ Swiss Federal Institute of Technology, Zurich, Switzerland

OPEN ACCESS

Edited by:

Hongbin Liu,
Hong Kong University of Science and
Technology, Hong Kong

Reviewed by:

Toshi Nagata,
The University of Tokyo, Japan
Hiroaki Saito,
The University of Tokyo, Japan

*Correspondence:

Jan Taucher
jtaucher@geomar.de

Specialty section:

This article was submitted to
Marine Biogeochemistry,
a section of the journal
Frontiers in Marine Science

Received: 31 May 2017

Accepted: 09 April 2018

Published: 25 April 2018

Citation:

Stange P, Taucher J, Bach LT,
Algueró-Muñiz M, Horn HG, Krebs L,
Boxhammer T, Nauendorf AK and
Riebesell U (2018) Ocean
Acidification-Induced Restructuring of
the Plankton Food Web Can Influence
the Degradation of Sinking Particles.
Front. Mar. Sci. 5:140.
doi: 10.3389/fmars.2018.00140

Ocean acidification (OA) is expected to alter plankton community structure in the future ocean. This, in turn, could change the composition of sinking organic matter and the efficiency of the biological carbon pump. So far, most OA experiments involving entire plankton communities have been conducted in meso- to eutrophic environments. However, recent studies suggest that OA effects may be more pronounced during prolonged periods of nutrient limitation. In this study, we investigated how OA-induced changes in low-nutrient adapted plankton communities of the subtropical North Atlantic Ocean may affect particulate organic matter (POM) standing stocks, POM fluxes, and POM stoichiometry. More specifically, we compared the elemental composition of POM suspended in the water column to the corresponding sinking material collected in sediment traps. Three weeks into the experiment, we simulated a natural upwelling event by adding nutrient-rich deep-water to all mesocosms, which induced a diatom-dominated phytoplankton bloom. Our results show that POM was more efficiently retained in the water column in the highest CO₂ treatment levels (>800 μatm pCO₂) subsequent to this bloom. We further observed significantly lower C:N and C:P ratios in post-bloom sedimented POM in the highest CO₂ treatments, suggesting that degradation processes were less pronounced. This trend is most likely explained by differences in micro- and mesozooplankton abundance during the bloom and post-bloom phase. Overall, this study shows that OA can indirectly alter POM fluxes and stoichiometry in subtropical environments through changes in plankton community structure.

Keywords: sinking, particles, degradation, elemental stoichiometry, plankton, food-webs, ocean acidification, zooplankton

INTRODUCTION

The increase in anthropogenic carbon dioxide (CO₂) emissions during the last century has led to atmospheric CO₂ concentrations that are unprecedented in the recent geological history (IPCC, 2014). About 25% of these emissions is taken up by the oceans each year (Le Quéré et al., 2016). While this dampens the atmospheric CO₂ increase, it also results in shifts in carbonate chemistry

and a reduction of seawater pH, commonly referred to as ocean acidification (OA) (Wolf-Gladrow et al., 1999; Caldeira and Wickett, 2003). Estimates predict a 0.3–0.4 reduction in surface pH until the end of this century (Orr et al., 2005), which is expected to have significant impacts on physiological processes of marine biota (Doney et al., 2009).

Results from more than a decade of OA research have shown that responses differ substantially between marine organisms (Wittmann and Pörtner, 2013). While these studies helped in developing a principal understanding of how OA affects the physiology of single species, we are still largely lacking the understanding of how OA effects may manifest on the community level (Riebesell and Gattuso, 2015). Existing “whole community” studies show that both direct effects of OA on single species (Riebesell et al., 2017) and indirect effects through changes in plankton community structure (Hall-Spencer et al., 2008; Fabricius et al., 2011; Schulz et al., 2013; Paul et al., 2015; Bach et al., 2016; Gazeau et al., 2016) can significantly influence biogeochemical cycles in the ocean.

Mesocosm experiments with entire plankton communities allow us to investigate how OA induced changes in community structure may affect processes of biogeochemical cycles, e.g., the production and quality of particulate organic matter (POM). Changes in elemental stoichiometry of POM have the potential to influence the partitioning of carbon between the ocean and atmosphere, which is particularly important in the context of climate change. In an *in situ* mesocosm experiment in a Norwegian fjord, Riebesell et al. (2007) observed increased carbon to nitrogen (C:N) ratios in POM under elevated levels of CO₂. The authors attributed these changes to an increase in carbon overconsumption in the dominant phytoplankton groups and outlined the possibility of a more efficient carbon pump under future ocean conditions once this carbon-enriched POM sinks out of the surface ocean. Using a global biogeochemical model, Oschlies et al. (2008) extrapolated these findings to the global ocean and found that the enhanced carbon export may lead to an expansion in suboxic water volume by up to 50% until the end of this century.

Recent mesocosm experiments showed that OA effects can be particularly pronounced during extended periods of low inorganic nutrient concentrations (Paul et al., 2015; Sala et al., 2015; Bach et al., 2016; Thomson et al., 2016). We therefore conducted an *in situ* mesocosm experiment in the eastern subtropical Atlantic Ocean off the coast of Gran Canaria (Canary Islands)—a region characterized by low concentrations of inorganic nutrients in particular during fall when the study took place (Aristegui et al., 2001). Halfway through the study we simulated an upwelling event of nutrient-rich water by adding collected deep-water to each mesocosm (see Taucher et al., 2017). Mesoscale upwelling events are naturally occurring frequently south of the Canary Islands, as this region is characterized by a distinct eddy-corridor (Sangrà et al., 2009). In this paper we address how OA induced changes in plankton community structure could influence the elemental composition and degradation of sinking POM.

MATERIALS AND METHODS

Experimental Design

From September to December 2014 we conducted a pelagic *in situ* mesocosm study in Gando Bay (27° 55' 41" N, 15° 21' 55" W) off the coast of Gran Canaria (Canary Islands). We deployed nine “Kiel Off-Shore Mesocosms for Ocean Simulations” (KOSMOS, M1-M9), each consisting of a floatation frame and a mounted bag (2 m diameter) made of 1 mm thick thermoplastic polyurethane foil (Riebesell et al., 2013). Once deployed, the initially folded bags were lowered to a depth of 13 m and thereby filled with approximately 35 m³ of seawater. The bags were sealed at the bottom and top with a net (mesh size of 3 mm) already before deployment in order to exclude unequally distributed nekton and large zooplankton (e.g., fish or jellyfish) from the experiment. The lowered bags were left open for 4 days to allow water exchange and ensure similar starting conditions in all mesocosms. Subsequently, the water bodies inside the mesocosms were enclosed by lifting the upper part of the bags above the sea surface, while divers simultaneously closed the bottom of each mesocosm with sediment traps. The collection cylinders of these traps were connected to silicon tubes, which were fixed to the floatation frames above sea surface (Boxhammer et al., 2016). Closing the mesocosms marked the start of the experiment on September 27, 4 days before the first CO₂ addition.

To simulate different OA scenarios, we added different amounts of CO₂-saturated seawater to the mesocosms. In order to reduce the immediate stress response, the addition was conducted gradually in 4 consecutive steps. The first addition was performed on the October 1 and marks the beginning of the experimental manipulation (day 0 = t0). Target concentrations were reached after the 4th addition on October 7. **Table 1** depicts the mean CO₂ concentrations in the respective mesocosms.

On October 23 (t22) approximately 85 m³ of deep-water were collected with a deep-water collecting system (described in detail by Taucher et al., 2017) from 650 m depth, approximately 7.5 km northeast of the study site. The collector was moored adjacent to the mesocosms. During the night between t23 and t24, approximately 20% of each mesocosms' volume was removed and replaced by equivalent amounts of nutrient-rich deep-water. Exact mixing ratios were calculated based on previously determined mesocosm volumes and target nutrient concentrations (Taucher et al., 2017). In total, the study lasted 61 days with the last sampling on t55 and t57 for the water column and sediment trap, respectively.

Alongside the regular sampling routine, we dedicated extensive effort to continuous maintenance of each mesocosm, including cleaning of the mesocosm walls. While divers regularly cleaned the outside, a cleaning ring was used to wipe the inside of the walls every week (Riebesell et al., 2013). This procedure prohibits wall growth, except for the flange ring connecting the mesocosm to the sediment trap and the funnel of the sediment trap, which are too narrow to be cleaned with the ring. Cleaning of these parts was thus performed by divers inside the mesocosms on t56, after the last sampling of the water column.

Sampling Procedure

Water Column

Samples were taken every second day between 9 a.m. and 12 p.m. We used two sampling systems simultaneously: (1) an integrating water sampler (IWS, HYDRO-BIOS, Kiel) for parameters that are sensitive to gas exchange or contamination and require low amounts of sample volume (e.g., carbonate chemistry) and (2) a vacuum pumping system for parameters that require large amounts of sample volume (e.g., particulate matter) (Taucher et al., 2017). Both systems allowed for integrated sampling of the entire water column of each mesocosm from 0 to 13 m water depth. All water column parameters presented in this study are thus given as integrated values for each mesocosm on the respective sampling day. Sampling was conducted every second day except for the time directly after deep-water addition (t25–t33), where samples were taken every day. Water collected with the pumping system was stored in 20 L carboys and transferred in a temperature-controlled room (set to *in situ* temperature) once they were transported back to the laboratory facilities. Carboys were always carefully mixed before withdrawing subsample volume in order to avoid sinking bias.

Additionally, net hauls were conducted on nine occasions during the 61 days experiment in order to estimate the abundance of mesozooplankton (e.g., copepods, appendicularians). Sampling frequency was restricted to one net haul every 4th sampling day in order to avoid overfishing. Samples were taken using an Apstein net (55 μ m mesh size, 17 cm diameter opening) with a sampling volume of 295 L per haul. The net content was transferred into 500 mL Kautex bottles and immediately preserved with 4% formaldehyde buffered with sodium tetraborate solution until identification.

For the determination of microzooplankton abundances, 250 mL of unfiltered seawater was taken from the 20 L carboys and filled into brown glass bottles. Samples were preserved using acidic Lugol's solution (1–2% final concentration) and stored in the dark until enumeration with an inverse light microscope (section Zooplankton Counts).

Environmental boundary conditions [*in situ* temperature, salinity, pH, dissolved oxygen, chlorophyll *a*, and photosynthetically active radiation (PAR)] were monitored inside each mesocosm and in the surrounding seawater every sampling day using a hand-held self-logging CTD probe (CTD60M, Sea and Sun Technologies).

Sediment Trap

Sedimented POM was collected from each mesocosm every 48 h starting at t-3. Sampling was always carried out before the water column samples were taken to avoid re-suspension of sedimented matter. A detailed description of the sampling procedure is provided by Boxhammer et al. (2016). Briefly, sedimented material was pumped into 5 L Schott Duran glass bottles through the silicon tube connecting the collection cylinder of the sediment trap to the surface. All samples were collected within 0.5–1 h and immediately stored in large coolers filled with seawater and additional cool packs for the remaining sampling procedure to avoid warming and minimize bacterial degradation of the material. Once collection was finished,

sediment trap samples were transported to the land-based facilities and processed as described in section POM in Sediment Trap Samples.

Sample Analysis

Chlorophyll *a* and Phytoplankton Pigments

Chlorophyll *a* and phytoplankton pigment concentrations were determined using reverse-phase high-performance liquid chromatography (HPLC). For this, we filtered up to 1.5 L of seawater onto glass fiber filters (nominal pore size of 0.7 μ m, 25 mm diameter, Whatman) by gentle vacuum filtration (<200 mbar). During filtration, samples were covered with aluminum foil to reduce exposure to light. Pigments were extracted in acetone (90%) by homogenization of the filters with glass beads in a cell mill. Samples were then centrifuged (10 min, 5,200 rpm, 4°C) and the supernatant was filtered through 0.2 μ m PTFE filters (VWR International). Pigment concentrations were determined in the supernatant by reverse-phase high-performance liquid chromatography (HPLC; Thermo Scientific HPLC Ultimate 3000 with an Eclipse XDB-C8 3.5 μ 4.6 \times 150 column; Van Heukelem and Thomas, 2001).

Contributions of individual phytoplankton groups to total chlorophyll *a* were then calculated using the software CHEMTAX (Mackey et al., 1996).

Zooplankton Counts

Mesozooplankton was analyzed quantitatively and taxonomically using a stereomicroscope (Olympus SZX9). Copepod abundances include copepodites as well as adults. Microzooplankton abundances were determined following the method described by Utermöhl (1931) using an inverted microscope (Zeiss Axiovert 25). Only the dominant groups of microzooplankton were counted, i.e., ciliates and heterotrophic dinoflagellates.

POM in Water Column Samples

For the determination of total particulate carbon (TPC), as well as particulate organic carbon, nitrogen and phosphorous (POC, PON, POP), we took up to 1 L subsample from the 20 L carboys. Subsamples were filtered with a gentle vacuum (<200 mbar) onto combusted glass fiber filters (nominal pore size of 0.7 μ m, 25 mm diameter, Whatman). Filters for the determination of TPC were dried at 60°C over night and transferred into tin cups until analysis. Filters for POC and PON analysis were stored in combusted glass petri dishes at –20°C, while POP filters were directly transferred into 40 mL glass bottles and frozen at –20°C. POC, PON filters were fumed with hydrochloric acid (37%) for 2 h before measurement in order to remove particulate inorganic carbon (PIC). Concentrations of TPC, POC and PON were determined using an elemental CN analyser (EuroEA) following Sharp (1974).

POP filters were placed in 40 mL of deionized water with oxidizing decomposition reagent ("Oxisolve," Merck) and autoclaved for 30 min in a pressure cooker to oxidize the particulate organic phosphorus to orthophosphate. After cooling, POP concentrations were determined by spectrophotometric

analysis analogous to the method for dissolved inorganic phosphate, following Hansen and Koroleff (1999).

POM in Sediment Trap Samples

Quantities of the sediment trap material suspended in the 5 L bottles (see section Sediment Trap) were determined gravimetrically after transport to the laboratory. Afterwards, we homogenized the suspended material in the sampling bottles by gently mixing, to take subsamples for a variety of parameters, which are not considered any further in this study. Total subsample volume was small (generally <10% of bulk sample volume). The remaining bulk sample was transferred stepwise into 800 mL beakers and centrifuged therein with $5,236 \times g$ for 10 min (6–16 KS centrifuge, SIGMA). The supernatant was then carefully decanted while the sedimented pellets were transferred into 110 mL centrifuge tubes. This procedure was repeated until the entire sample was centrifuged and transferred. For further compression, the 110 mL tubes were centrifuged a second time at $5,039 \times g$ for 10 min (3K12 centrifuge, SIGMA) and the suspension was decanted. The remaining pellets were immediately deep frozen at -20°C and stored in small plastic screw cap cups. The centrifugation method was chosen over filtration since the latter only works with very small volumes of sedimented samples, due to the rapid clogging of the filter. A small sample volume of a rather patchy sample would then increase the error of later analyses for biogeochemical parameters. Concentrating the sample by centrifugation allows for an easier homogenization by grinding and thus reduces the error in later analyses.

The decanted supernatant was visually inspected for translucency and discarded unless there were still large amounts of organic material present in the supernatant. Between t35 and t49 we observed strongly elevated sedimentation and sample volumes increased drastically. During this period, translucency of the supernatant decreased as a larger proportion of the suspended matter could not be concentrated by centrifugation. We therefore pipetted small subsamples of the homogenized supernatant onto glass fiber filters (nominal pore size of $0.7 \mu\text{m}$, 25 mm diameter, Whatman). All filters were deep-frozen at -20°C immediately after filtration for subsequent analysis of TPC, POC, PON, and POP as described for water column samples. In some cases the particle density of the original samples was too low for centrifugation to compress the sedimented matter into transferrable pellets (t21–t33 for M2 and t31–t33 for M8). In these cases we filtered subsamples of up to 100 mL for POM analysis of the entire samples as described for the supernatant at strongly elevated sedimentation.

The frozen centrifuge pellets were freeze-dried and ground to a very fine and homogenous powder as described in Boxhammer et al. (2016). This powder was then subsampled for the determination of TPC, POC, PON and POP. Duplicate subsamples of 2 mg were taken for the determination of TPC and transferred into tin cups. Additionally, two similar subsamples were transferred into silver cups and acidified before measurement to remove the inorganic carbon fraction (acidified for 1 h with 1 M HCl and dried at 50°C overnight). All four subsamples were measured using an elemental

analyser (Euro EA-CN, Hekatech), which was calibrated with acetanilide ($\text{C}_8\text{H}_9\text{NO}$) and soil standard (Hekatech, catalog number HE33860101) prior to each measurement run. PIC was then calculated from total and organic carbon content. For the analysis of POP, subsamples of 2 mg were transferred into 40 mL glass vials and analyzed similar to the water column samples, as described above. In this study, sediment trap data are presented as daily fluxes, which we calculated by dividing the sediment trap data of each sampling point (every 48 h) by 2. Furthermore, the daily fluxes were normalized for mesocosm volume. Volume determination is described in the introductory paper to this special issue by Taucher et al. (2017).

Estimating Degradation of Sinking Particles Based on Stoichiometry

Preferential remineralization of nitrogen and phosphorus over carbon is commonly observed in sinking POM, which leads to increasing elemental ratios (C:N, C:P) with depth (Sambrotto et al., 1993; Thomas et al., 1999; Schneider et al., 2003). We calculated the changes in elemental ratios between POM collected in the sediment trap and POM sampled from the water column and defined this ratio as the stoichiometry-based degradation index (SDI), as it gives an indication of the extent of degradation on sinking PM.

$$SDI_{\text{CN}} = \text{C:N}_{\text{sink}} / \text{C:N}_{\text{susp}} \quad (1)$$

$$SDI_{\text{CP}} = \text{C:P}_{\text{sink}} / \text{C:P}_{\text{susp}} \quad (2)$$

Here, a value of 1 indicates identical elemental ratios of POM suspended in the water column (e.g., C:N_{susp}) and POM collected in the sediment trap (e.g., C:N_{sink}), while values >1 denote higher C:N ratios in the sedimented POM compared to the water column, thus indicating preferential remineralization of nitrogen.

The SDI was calculated on a daily basis and does therefore not account for the time lag between POM production and sinking of POM to the sediment traps (Stange et al., 2017). The reason for this was that the time lag could only be accurately determined during the bloom, when clear peaks in biomass production and POM flux to the sediment traps were observed. It is, however, unlikely that a time lag of approximately 10 days, as observed between the peak of POM production in the water column and the peak of POM sedimentation, is the same for the entire experiment. We thus decided to calculate the SDI using the water column and sediment trap measurements of the same day. Nevertheless, calculating the SDI with a constant time lag of 10 days still resulted in similar trends and significant effects that were comparable to the ones reported in Table 3.

Data Analysis and Statistical Approach

To facilitate statistical analysis and a quantitative description of the data, we divided the dataset in three experimental phases based on the chlorophyll *a* development. A detailed description of the determination of the experimental phases is given in section Chlorophyll *a* and Experimental Phases. We applied linear regression analysis to determine the relationship between

average $p\text{CO}_2$ and average response of the variables during each phase. The model results were checked for normality and homoscedasticity. A linear regression was performed for several reasons. First of all, a non-linear analysis requires an underlying hypothesis of a non-linear relationship between predictor and response variable. Since there was no physiological reason to suspect a non-linear relationship, a linear model is more conservative and prevents the risk of overfitting. Furthermore, our analyses did not aim to identify a certain $p\text{CO}_2$ level as a tipping point, but rather aimed to verify whether there is an overall effect. Cases where a non-linear relation may be underlying are discussed as such in the text. Unfortunately, Mesocosm 6 was irreparably damaged on t26 and thus excluded from the statistical analysis of phases II and III. Statistical analyses were undertaken using the software R, version 3.3.1 (R Core Team, 2013).

RESULTS

Chlorophyll *a* and Experimental Phases

The experiment started in oligotrophic conditions, with very low concentrations of inorganic nutrients (Figure S5) and chlorophyll

a (Figure 1A). Chlorophyll *a* concentration during phase I (t-3–t24) averaged at approximately $0.1 \mu\text{g L}^{-1}$. On t24 we added nutrient-rich deep-water to the mesocosms in order to simulate an eddy-induced upwelling event (for a detailed description of the deep-water addition see Taucher et al., 2017). The deep-water addition increased inorganic nutrient concentrations to approximately 3.15 , 0.17 , and $1.60 \mu\text{mol L}^{-1}$ for $\text{NO}_3^- + \text{NO}_2^-$, PO_4^{3-} , and Si(OH)_4 , respectively. This stimulated the rapid development of a phytoplankton bloom in phase II (t25–t35) with a peak in chlorophyll *a* at t28 (Figure 1). The inorganic nutrients were quickly depleted and reached values close to detection limit between t28 and t30 (Figure S5). After the peak on t28 chlorophyll *a* concentrations decreased rapidly in all mesocosms until they reached a minimum at t35. In the post-bloom phase (phase III, t37–t55) inorganic nutrients and chlorophyll *a* concentrations remained low, except for the two mesocosms with highest CO_2 , which displayed elevated chlorophyll *a* until the end of the experiment. Experimental phases were defined differently for the POM flux to the sediment traps, as described in section Sediment Trap. We further observed a well-mixed water column regarding the *in situ* temperature and salinity throughout the experiment (Taucher et al., 2017).

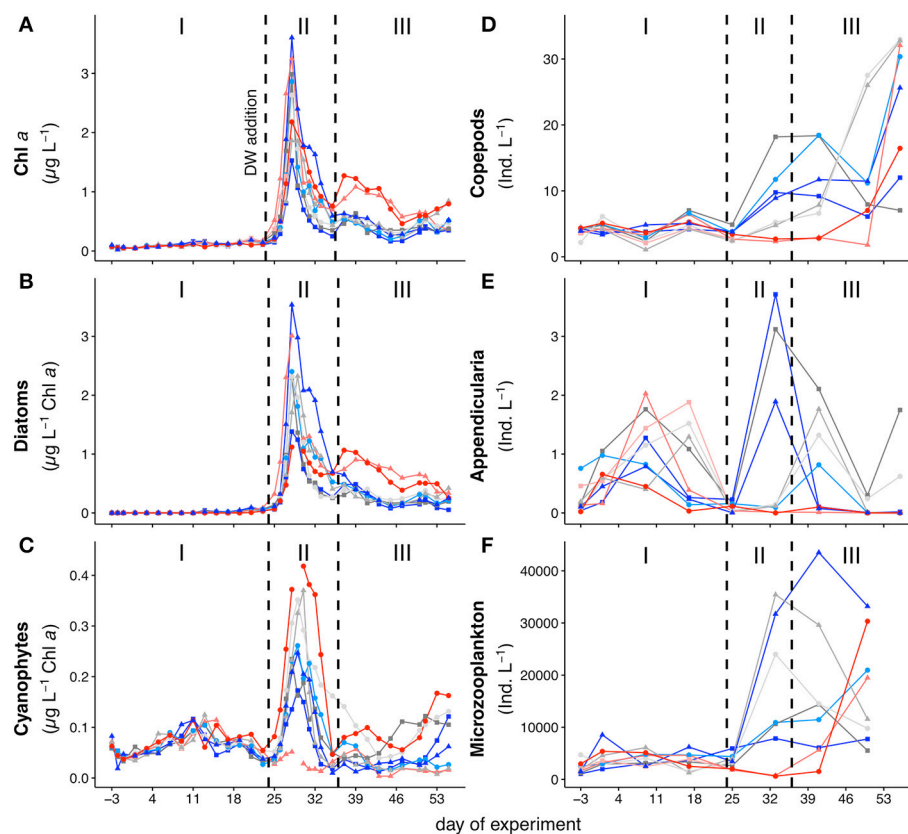











FIGURE 1 | Development of (A) chlorophyll *a* concentrations. (B) Abundances of diatoms, and (C) abundances of cyanophytes. (D–F) depict zooplankton abundances over the course of the experiment with (B) copepods, including both adult and all copepodite stages, (C) appendicularians, and (D) protozoan microzooplankton, mostly ciliates and heterotrophic dinoflagellates. The three different phases are indicated with I, II and III and separated by the dashed vertical lines. Note that the first dashed line also depicts the time of deep-water addition. Colors and symbols are described in Table 1.

TABLE 1 | Average values for seawater $p\text{CO}_2$ for each experimental phase, defined in section Chlorophyll *a* and Experimental Phases.

Mesocosm ID	Symbol	Water column $p\text{CO}_2$ [μatm]			Sediment trap $p\text{CO}_2$ [μatm]		
		Phase I (t-3–t24)	Phase II (t25–t35)	Phase III (t37–t55)	Phase _{sed} I (t-3–t33)	Phase _{sed} II (t35–t45)	Phase _{sed} III (t47–t55)
M1		401	374	326	392	333	318
M9		406	343	297	382	292	299
M5		502	404	427	464	406	431
M3		636	493	546	578	536	533
M7		746	571	672	678	632	671
M4		800	620	710	729	697	682
M6		976	–	–	970	–	–
M2		1050	748	830	930	807	802
M8		1195	902	944	1080	940	897

$p\text{CO}_2$ values were calculated from the combination of TA and DIC using CO_2SYS (Pierrot et al., 2006) with the carbonate dissociation constants (K_1 and K_2) of Lueker et al. (2000). A detailed description of the determination of the carbonate chemistry is given by Taucher et al. (2017).

Temporal Dynamics in Plankton Community Composition

Figures 1B,C shows the development of cyanophytes and diatoms over the course of the experiment. We only focused on these groups since they had by far the largest contribution to total chlorophyll *a* concentrations during the respective experimental phases. During the oligotrophic phase I, (pico-)cyanobacteria (*Synechococcus* sp.) were the dominant phytoplankton group, with a contribution of 70–80% to total chlorophyll *a* (Figures S1A,B). Abundances of this group increased toward t11 and decreased afterwards until the deep-water addition on t24. We observed a significant positive effect of $p\text{CO}_2$ on the abundance of cyanophytes during phase I ($p = 0.002$, $F = 26.67$).

Following the deep-water addition on t24, the phytoplankton community underwent significant changes. Throughout phases II and III, large chain-forming diatoms, such as *Leptocylindrus* sp., *Guinardia* sp., and *Bacteriastrum* sp. dominated the phytoplankton community with a contribution to total chlorophyll *a* concentrations of 50–70% (Figure S1B). While their overall abundance decreased toward the end of the experiment, diatoms were still the dominant phytoplankton group throughout phase III. This dominance was particularly pronounced in both high CO_2 mesocosms (M2 and M8, see Figure 1B) and we observed a significant positive effect of $p\text{CO}_2$ on the abundance of diatoms during phase III ($p = 0.026$, $F = 8.71$). Plankton community structure and species succession during this study closely resembled those during natural bloom events in the Canary Islands region (Basterretxea and Arístegui, 2000; Arístegui et al., 2004) and are thus representative for natural marine ecosystems of the study area.

Figures 1B–D shows the temporal development of micro- and mesozooplankton abundances in all mesocosms. For the purpose of this study, we only differentiated between copepods, appendicularians and microzooplankton. Abundances of copepods were constantly low throughout phase I of the experiment. Appendicularian abundances increased during phase I in all mesocosms, but declined again and reached a

minimum right after deep-water addition. Phase II and III were characterized by higher abundances of both groups in all mesocosms, except in M2 and M8. While abundances of appendicularians in those two mesocosms remained low until the end of the experiment, copepod abundances increased from t50 to the last sampling day. Microzooplankton abundances were overall low during phase I of the experiment and started to increase in all mesocosms after t25, but remained comparably low in M2 and M8.

Temporal Dynamics of POM Water Column

The temporal development of POC, PON, and POP in the water column is shown in Figures 2A–C. Water column POC and PON concentrations were only determined from t9 onwards as we did not have sufficient filtration volume during the first couple of days. Concentrations of all three parameters remained low from t9 onwards, but increased slightly toward the end of phase I (t17–t23). With the addition of deep-water at t24, POM increased rapidly in the water column and peaked between t30 and t31 in all mesocosms. After the peak in phase II, most POM was retained in the water column and only slowly decreased during phase III. We observed a slight but significant negative effect of $p\text{CO}_2$ on POP during phase I (Table 2), but this effect vanished during the subsequent phases. During phase III, concentrations of water column POC, PON and POP were elevated in the two highest CO_2 mesocosms (M2 and M8), but we did not detect an overall significant effect of $p\text{CO}_2$.

Sediment Trap

Peaks in POM sedimentation were temporally delayed to POM concentration peaks in the water column. This temporal delay can be explained by particle aggregation dynamics, as the rapid growth rate of phytoplankton due to the pulsed nutrient addition first resulted in an increasing abundance of smaller particles. The POM formed in the water column thus only started to sink after larger aggregates had formed several days

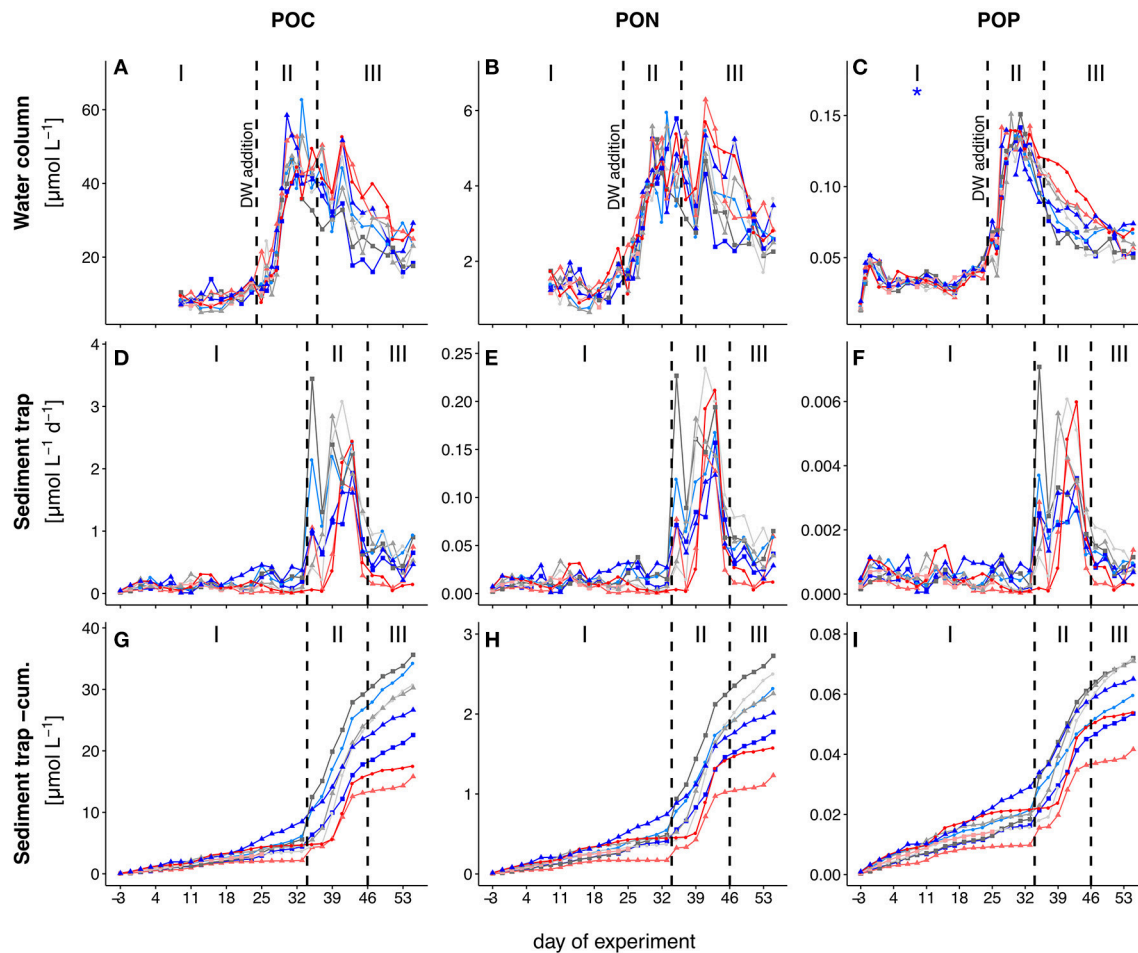


FIGURE 2 | Temporal development of standing stocks and fluxes of total particulate carbon (TPC; **A,D,G**), nitrogen (TPN; **B,E,H**) and phosphorus (TPP; **C,F,I**). (**A–C**) and (**D–F**) depict POM concentrations from the water column and daily flux to the sediment trap, respectively. (**G–I**) show the cumulative flux of POM to the sediment trap. Colored lines depict the different mesocosms. The three different phases are indicated with I, II, and III and separated by the dashed vertical lines. Note that the first dashed line in (**A–C**) also depicts the time of deep-water addition. Colors and symbols are described in **Table 1**. The * denotes a statistically significant positive (red) or negative (blue) effect of CO_2 during the respective experimental phase.

after the peak in the water column (Taucher et al., in review). Due to this delay, and in order to correctly compare water column and sedimented POM, we define experimental phases differently for the sediment trap material (phase_{sed} I = t-3–t33; phase_{sed} II = t35–t45; phase_{sed} III = t47–t55). While this approach does not take into account the influence of changes in sinking velocity of sedimenting particles on the time lag between OM production in the water column and its sedimentation to the sediment trap, we argue that in this experiment differences in aggregation dynamics were the main driver of this delay.

Total POM fluxes to the sediment trap were low throughout phase_{sed} I (**Figures 2D–F**). The onset of increased POM fluxes to the sediment trap followed water column POM build-up with a temporal delay of approximately 10 days. After an initial peak in POM flux on t35 (phase_{sed} II), we observed rather low sedimentation rates on t37. This changed again on t39, after which sedimentation rates stayed high until t43. M3 and M5

had the largest contribution to the initial peak on t35, while the remaining mesocosms showed highest sedimentation rates on t39 and t43. Rates decreased during the last phase_{sed} (t45 to t55) but were still higher than in phase_{sed} I. The two mesocosms with highest CO_2 concentrations (M2, M8) showed particularly low sedimentation rates during phase_{sed} III. However, we did not detect a significant effect of $p\text{CO}_2$ in the regression analysis (**Table 2**).

The analysis of filters taken due to low translucency of the supernatant during the period of high sedimentation (t35–t49; described in section POM in Sediment Trap Samples) contributed generally less than 4% to the total concentration of the respective parameter and was thus neglected. The cleaning of the lowest segment of the mesocosms and sediment trap walls on the last day of the experiment (day 57) resulted in strongly elevated sedimentation rates since there was considerable growth of benthic autotrophs on this segment (Figure S2). We thus excluded this day from the analysis.

TABLE 2 | Statistical results from the linear regression analysis on response means over the respective phases.

	Phase	Water column			Sediment trap		
		<i>p</i>	<i>R</i> ²	<i>F</i>	<i>P</i>	<i>R</i> ²	<i>F</i>
POC	I	0.943	0.000	0.006	0.062	0.414	4.942
	II	0.951	0.000	0.004	0.523	0.071	0.461
	III	0.110	0.369	3.503	0.274	0.195	1.45
PON	I	0.368	0.117	0.924	0.086	0.362	3.975
	II	0.568	0.057	0.365	0.815	0.009	0.059
	III	0.209	0.247	1.971	0.553	0.062	0.394
POP	I	0.019 (–)	0.569	9.268	0.279	0.164	1.372
	II	0.171	0.287	2.42	0.889	0.003	0.021
	III	0.151	0.311	2.702	0.616	0.045	0.280
C:N	I	0.002 (–)	0.759	22.09	0.605	0.040	0.293
	II	0.649	0.037	0.229	0.295	0.179	1.314
	III	0.075	0.436	4.641	0.012 (–)	0.682	12.85
N:P	I	0.218	0.208	1.833	0.019 (–)	0.571	9.321
	II	0.986	0.000	0.000	0.135	0.331	2.975
	III	0.857	0.006	0.035	0.287	0.185	1.362
C:P	I	0.539	0.056	0.417	0.006 (–)	0.684	15.12
	II	0.710	0.025	0.152	0.154	0.306	2.666
	III	0.353	0.145	1.015	0.037 (–)	0.545	7.186

Mesocosm 6 was lost after phase I and was thus not considered in the analysis in phases II and III (df for phase I = 7, and for phases II and III = 6).

Significant *p*-values (*p* < 0.05) are highlighted in bold. We indicate the trend of the effect in brackets behind the *p*-value, with (+) indicating a positive and (–) and negative trend.

Dynamics in Elemental Stoichiometry

Water Column

We observed higher ratios of C:N (POC:PON), N:P (PON:POP), and C:P (POC:POP) compared to Redfield proportions (C:N:P = 106:16:1) throughout almost the entire experiment (Figures 3A–C). The only exceptions were C:N ratios during phase I (t9–t13) and during the phytoplankton bloom right after the addition of deep-water (t25–t28). We observed a small peak in C:N stoichiometry between t17 and t19 in all mesocosms. C:N ratios subsequently declined until the deep-water addition and fluctuated close to Redfield proportions of approximately 6–7 from t25–t28. C:N ratios increased profoundly directly after the bloom peak and nutrient depletion (t29 until t32). After this transient peak, C:N decreased toward the end of the experiment. Statistical analysis of C:N ratios averaged over the entire experiment did not reveal a significant effect of *p*CO₂. However, when we tested each phase individually, we observed a significantly negative effect of *p*CO₂ on C:N during phase I (see Table 2). We also found a borderline insignificant positive effect on C:N during phase III. However, the lack of significance was likely due to the effect being exclusively driven by both high CO₂ mesocosms instead of a linear relationship (see Figure S3C).

Both N:P and C:P did not show a clear change during phase I. Similar to C:N, we observed minimum values for both ratios right after deep-water addition. While C:P also increased rapidly

after t28 and stayed constant afterwards, N:P was characterized by a comparably slow and steady increase toward the end of the experiment. We neither observed significant treatment effects on C:P and N:P when averaged over the entire time, nor for any of the three phases individually.

Sediment Trap

C:N and C:P ratios of sediment trap material were above Redfield and also higher than in water column POM (Figures 3D,F). This difference was less pronounced in the N:P ratios (Figure 3E). We observed a slow and steady increase in all ratios over the course of the experiment. After t19, the variability between mesocosms increased in N:P and C:P and stayed high until the end of the experiment. We observed a significant negative effect of *p*CO₂ on the C:N ratio in sedimented POM during phase_{sed} III (see Table 2) as well as on N:P during phase_{sed} I and C:P during phases_{sed} I and III. These CO₂ effects were driven primarily by the very low values in the two highest CO₂ mesocosms (M2 and M8) (Figures 3D–F).

Temporal Development of the SDI

SDI_{CN} was above 1 in all mesocosms throughout the experiment, with only few exceptions (see Figure 4A). This shows that C:N ratios in the sediment trap were higher compared to those in the water column for most of the time. There was no clear trend of *SDI_{CN}* over time, however, the ratio fluctuated in all mesocosms from the beginning up until t39 and stayed more or less constant after that. We observed a significant positive treatment effect of CO₂ on *SDI_{CN}* during phase I and a highly significant negative treatment effect during phase III (see Table 3).

SDI_{CP} did not strongly deviate from one during the majority of phase I except for the first two sampling days (Figure 4B). *SDI_{CP}* increased during phase II and remained elevated throughout phase III except for mesocosms M4, M2 and M8. We observed significant negative CO₂ treatment effects on *SDI_{CP}* during phases II and III.

DISCUSSION

Temporal Development of POM Standing Stocks

CO₂-related differences in standing stocks and elemental composition of POM were detected primarily after the phytoplankton bloom in phase II and more pronounced during phase III (Figures 2, 3). In particular, we observed that in both mesocosms with highest *p*CO₂, post-bloom water column POM remained at high concentrations longer than in low and intermediate treatment levels. This led to less sedimentation of POC, PON, and POP to the sediment trap during the study period under high *p*CO₂ (see the cumulative plots of sedimented matter in Figures 2G–I). However, the CO₂ trend was not linear, but driven almost entirely by the two mesocosms with highest *p*CO₂ (M2 and M8, Figures S3A,B). There are three possible explanations for the observed differences in post-bloom water column POM retention: Differences in (1) particle load with ballasting minerals, such as calcite, opal or lithogenic material, (2) grazing and thus repackaging by micro- and mesozooplankton, or (3) the rate of sinking particle formation (aggregation rate).

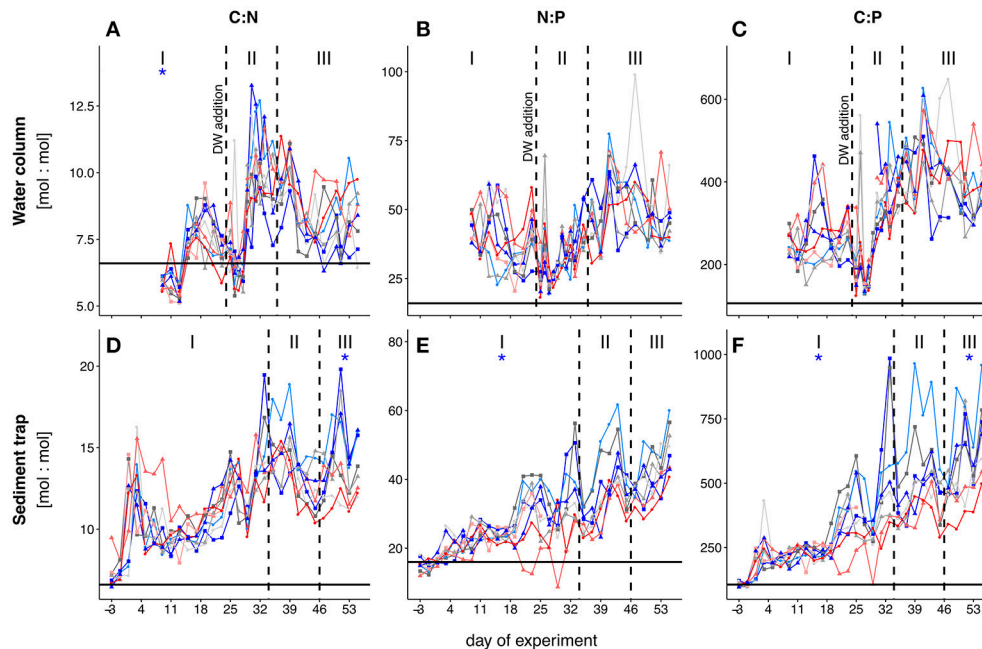


FIGURE 3 | Temporal development of POM elemental stoichiometries in the water column (A–C) and the sediment trap samples (D–F). Black horizontal lines indicate Redfield proportions for the respective elemental ratios (C:N = 6.6, N:P = 16, C:P = 106). Colored lines depict the different mesocosms. The three different phases are indicated with I, II and III and separated by the dashed vertical lines. Note that the phases for water column and sediment trap POM have been defined differently (see section Chlorophyll *a* and Experimental Phases). Colors and symbols are described in **Table 1**. The * denotes a statistically significant positive (red) or negative (blue) effect of CO₂ during the respective experimental phase.

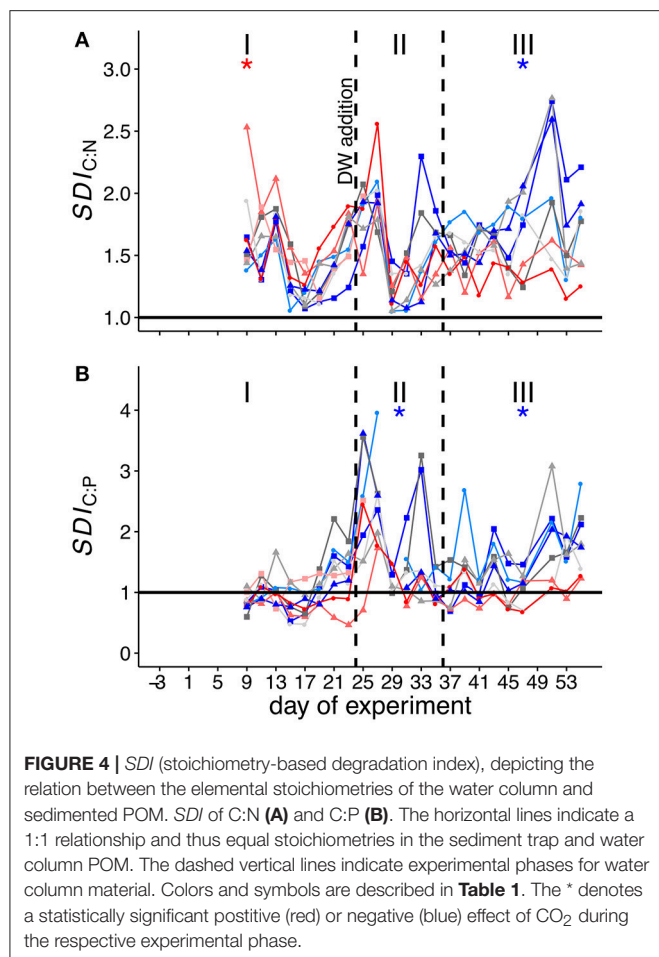
PIC/POC and biogenic silica (BSi)/POC ratios (Figure S4) did not give an indication for a lower ballasting effect in mesocosms M2 and M8 after the bloom and we have no reason to expect a differing supply of airborne lithogenic material to individual mesocosms. We thus conclude that the difference in POM retention was most likely driven by differences in food-web dynamics and/or aggregation processes. Indeed, abundances of the dominant groups of mesozooplankton, i.e., copepods and appendicularians, as well as microzooplankton abundances were particularly low in both high CO₂ mesocosms during phases II and III (**Figures 1D–F**). Although the difference in grazer abundance was mainly driven by M2 and M8, the linear regression analysis revealed significantly lower abundances of copepods on t41 with increasing pCO₂ ($F = 5.469$, $p = 0.05$). These results are further supported by the results of the multivariate analysis using Bray–Curtis dissimilarity, which showed that M2 and M8 were particularly different to the other mesocosms in terms of their plankton community composition (Taucher et al., 2017). The lower abundance of grazers in the highest CO₂ treatment levels may have resulted in reduced consumption and repackaging of POM, which in turn translated into a longer residence time of phytoplankton cells and aggregates in the water column. On the other hand, the comparatively high abundances of zooplankton grazers in the other mesocosms resulted in higher clearance rates of approximately 9 L d^{−1} (assuming an a mean abundance of 10 ind. L^{−1} with an average body size of less than 500 μm; Kiørboe, 2011), which further illustrates the strong influence of

zooplankton grazing on controlling and modifying the elemental flux to the sediment traps.

The increased retention of water column POM in M2 and M8 may also be explained by lower aggregation rates. While possibly lower turbulence inside the mesocosms compared to the surrounding water column may result in overall lower aggregation rates, the similarly mixed water columns did not suggest strong differences in turbulence between the individual mesocosms. This suggests that other processes were the key drivers of the difference in OM retention in the water column. Differences in phytoplankton community composition, nutritional status and growth phase of the cells can profoundly influence the coagulation efficiency (Kiørboe et al., 1990; Kiørboe and Hansen, 1993; Burd and Jackson, 2009). However, measurements of the *in situ* particle size spectrum by Taucher et al. (in review) did not reveal CO₂ related differences for the start and rate of aggregate formation. We thus conclude that the increased retention of water column POM under elevated CO₂ is primarily driven by differences in zooplankton abundance.

Temporal Development of Element Stoichiometry

Elemental ratios in water column POM were much higher than Redfield values for the majority of time during the experiment. This deviation is likely caused by very low concentrations of all major inorganic nutrients. Exceptions to this trend were observed in water column C:N ratios, which were substantially lower in the middle of phase I and right before the deep-water



addition. We observed a small bloom of cyanophytes (mainly *Synechococcus* sp.) during phase I, with a peak in abundances around t11 (Figure 1C). While nutrient concentrations were generally low throughout phase I (mean concentrations of $\text{NO}_3^- + \text{NO}_2^- = 0.05 \mu\text{mol L}^{-1}$ and $\text{PO}_4^{3-} = 0.03 \mu\text{mol L}^{-1}$; Figure S5), excess phosphate was available during phase I (mean $\text{NO}_3^- + \text{NO}_2^- / \text{PO}_4^{3-} = 2$). *Synechococcus* has been shown to have particularly low intercellular C:N ratios during exponential growth (Bertilsson et al., 2003). Since this group dominated the phytoplankton community during phase I, it is likely that their C:N signature is reflected in the C:N ratios of water column POM. The small bloom of cyanophytes collapsed after t11 and water column C:N increased correspondingly in the following days. During this period, we observed a significantly negative effect of $p\text{CO}_2$ on water column C:N ratios (Figure 3A). This effect again correlates well with the significantly higher abundances of cyanobacteria observed under elevated levels of CO₂ during that phase.

With the addition of deep-water on t24, inorganic nutrient limitation was relieved for about 4 days. Consequently, C:N and C:P ratios of water column POM declined immediately after the addition on t24 and stayed low until t28 (Figures 3A,C). C:N and C:P increased rapidly back to elevated values as soon as inorganic nutrients from deep-water addition were depleted. This

TABLE 3 | Statistical results from the linear regression analysis on response means over the respective phases.

	Phase	<i>p</i>	<i>R</i> ²	<i>F</i>
<i>SDI_{CN}</i>	I	0.037 (+)	0.483	6.543
	II	0.847	0.007	0.041
	III	0.002 (–)	0.814	26.21
<i>SDI_{CP}</i>	I	0.366	0.118	0.936
	II	0.047 (–)	0.51	6.245
	III	0.049 (–)	0.503	6.061

Mesocosm 6 was lost after phase I and was thus not considered in the analysis in phases II and III (df for phase I = 7, and for phases II and III = 6).

Significant *p*-values (*p* < 0.05) are highlighted in bold. We indicate the trend of the effect in brackets behind the *p*-value, with (+) indicating a positive and (–) and negative trend.

indicates carbon overconsumption, a mechanism observed in many groups of marine phytoplankton, particularly in diatoms, under nutrient-deplete conditions (Toggweiler, 1993; Riebesell et al., 2007). Indeed, diatoms were the dominant phytoplankton group during the bloom in all mesocosms, with a contribution of >60% to the total chlorophyll *a* concentrations (Taucher et al., 2017). Additionally, the overall low N:P ratios throughout the experiment suggests that the community was mainly phosphate-limited throughout the experiment (Figure 3B).

We observed a borderline insignificant effect (*p* = 0.075) of $p\text{CO}_2$ on the elemental stoichiometry of water column POM during phase III of the experiment. We argue that our analysis did not reveal a significant effect as the difference in C:N wasn't linear, but solely driven by both mesocosms with highest $p\text{CO}_2$ (Figure S3C). This difference is likely caused by differences in phytoplankton community composition. Abundances of large diatoms were significantly increased in both mesocosms with highest $p\text{CO}_2$ during phase III (Figure 1B) and they continued to increase even after the supplied nutrients were depleted on t28. The difference in abundance thus likely increased the magnitude of carbon overconsumption in the two highest CO₂ treatments, resulting in slightly higher C:N ratios in M2 and M8.

Influence of Community Structure on the Degradation of Sinking POM

SDI_{CN} and *SDI_{CP}* were larger than 1 for the majority of the experiment. This shows that elemental ratios of sedimented POM were overall elevated compared to those of POM suspended in the water column. A similar trend has also been observed to a lesser degree in a previous study (Czerny et al., 2013), and was interpreted as an indication for preferential remineralization of both N and P relative to C in sinking organic material (Sambrotto et al., 1993; Thomas et al., 1999; Schneider et al., 2003).

We observed a significant positive effect of $p\text{CO}_2$ on *SDI_{CN}* during phase I, suggesting that degradation processes were more pronounced under high CO₂ before the deep-water addition. This trend reversed during and after the bloom and a significant negative effect of $p\text{CO}_2$ was detected for *SDI_{CP}* during phase II and *SDI_{CN}* and *SDI_{CP}* during phase III. In order to identify the mechanisms responsible for the observed differences, we evaluated the processes, which have the potential to alter C:N

and C:P stoichiometry in sinking POM. These include the degradation of POM by grazers (protozoans and metazoans) and bacteria.

Zooplankton grazers are known to assimilate nitrogen and phosphorus more efficiently than carbon in order to maintain homeostasis, i.e., keeping their elemental composition constant (Checkley and Entzeroth, 1985; Daly et al., 1999). The excess carbon is either respired, internally stored in lipid reservoirs (e.g., in overwintering copepods in the Arctic), or defecated, resulting in fecal pellets with substantially higher C:N ratios than sinking aggregates or marine phytoplankton (Gerber and Gerber, 1979; Small et al., 1983; Daly et al., 1999). Another pathway that has the potential to impact the stoichiometry of sinking POM is bacterial degradation. It has been shown that the rapid decrease of sinking particulate matter with depth is partly associated with degradation processes by particle-attached bacteria (Smith et al., 1992; Ploug and Grossart, 2000). However, production rates of free-living and particle-associated bacteria were not significantly different in the high CO₂ treatments throughout the experiment (Hornick, unpublished data). Furthermore, CO₂-related differences in zooplankton abundances between mesocosms only manifested during phase II and III (see **Figure 1**). We can therefore only speculate that the higher *SDI_{CN}* under elevated levels of CO₂ during phase I is most likely related to differences in the quality of the sinking POM. Contrastingly, the significant negative effects of *pCO₂* on *SDI_{CN}* and *SDI_{CP}* during phase II and III are indicative for slower degradation of sinking organic material, which correlates well with the lower abundances of micro- and mesozooplankton during these periods.

In an earlier study by Riebesell et al. (2007), increased consumption of dissolved inorganic carbon (DIC) with increasing levels of seawater *pCO₂* was observed in an enclosed natural plankton community. The authors extrapolated these results and argued that this increased consumption may translate to enhanced carbon relative to nitrogen drawdown from the euphotic zone. In this study, we also observed slightly higher C:N ratios in water column POM in both mesocosms with highest *pCO₂* (**Figure 3A**), indicating that elevated levels of CO₂ may indeed promote carbon overconsumption. However, our results show that the degradation by micro- and mesozooplankton tightly controlled the fate of POM stoichiometry with depth, with the possibility to reverse CO₂ trends in elemental stoichiometry observed in the surface. We thus argue that changes in the elemental stoichiometry of suspended POM in the surface cannot be extrapolated to depth without estimating the degradation processes, which in turn are controlled by the plankton community structure.

CONCLUSION

In the present study, we show that OA induced changes in plankton community structure can significantly influence the degradation of sinking POM. We found that C:N ratios in suspended POM were slightly elevated after a diatom-dominated phytoplankton bloom in the two mesocosms with highest *pCO₂*, most likely due to enhanced carbon overconsumption. Yet, POM collected in the sediment traps showed significantly

lower C:N ratios under high CO₂ conditions. This indicates that degradation of sinking matter was less pronounced under elevated levels of CO₂, which we mainly attribute to the lower abundances of micro- and mesozooplankton in those mesocosms during and after the phytoplankton bloom. These trends only manifested during post-bloom conditions, 4 weeks into the experiment, when differences in community structure were most pronounced. Our findings underline that CO₂ induced changes in elemental stoichiometry of sinking POM are ultimately controlled by the plankton community structure. In particular, our results highlight the importance of micro- and mesozooplankton grazers on the transformation of sinking organic matter and we suggest that extrapolations of biogeochemical processes to global scales cannot be made without considering the entire planktonic food web.

AUTHOR CONTRIBUTIONS

UR, JT, LB, TB, and PS: contributed to the design of the study; LK, TB, and PS: analyzed sediment trap samples; MA-M and HH: analyzed the zooplankton samples; AN: analyzed the water column samples; PS interpreted the data and wrote the manuscript with comments from all co-authors.

FUNDING

This project was funded by the German Federal Ministry of Education and Research (BMBF) in the framework of the coordinated project BIOACID—Biological Impacts of Ocean Acidification, phase 2 (FKZ 03F06550). UR received additional funding from the Leibniz Award 2012 by the German Research Foundation (DFG).

ACKNOWLEDGMENTS

The authors of this paper are very thankful to the entire Gran Canaria KOSMOS consortium for their contribution to this experiment. We also would like to thank the Oceanic Platform of the Canary Islands (Plataforma Oceánica de Canarias, PLOCAN) for sharing their expertise and research facilities, and providing us with all the necessary tools to successfully conduct our research. Another special thanks goes to the Marine Science and Technology Park (Parque Científico Tecnológico Marino, PCTM) and the Spanish Bank of Algae (Banco Español de Algas, BEA), both from the University of Las Palmas (ULPGC), who provided additional facilities to run experiments, measurements, and analyses.

We are also thankful for the great support by the captain and crew of RV *Hesperides* for deploying and recovering the mesocosms (cruise 29HE20140924), and RV *Poseidon* for transporting the mesocosms and their support in testing the deep water collector during cruise POS463.

SUPPLEMENTARY MATERIAL

The Supplementary Material for this article can be found online at: <https://www.frontiersin.org/articles/10.3389/fmars.2018.00140/full#supplementary-material>

REFERENCES

- Aristegui, J., Barton, E. D., Tett, P., Montero, M. F., García-Muñoz, M., Basterretxea, G., et al. (2004). Variability in plankton community structure, metabolism, and vertical carbon fluxes along an upwelling filament (Cape Juby, NW Africa). *Prog. Oceanogr.* 62, 95–113. doi: 10.1016/j.pocean.2004.07.004
- Aristegui, J., Hernández-León, S., Montero, M. F., and Gómez, M. (2001). The seasonal planktonic cycle in coastal waters of the Canary Islands. *Sci. Mar.* 65, 51–58. doi: 10.3989/scimar.2001.65s151
- Bach, L. T., Taucher, J., Boxhammer, T., Ludwig, A., Achterberg, E. P., Algueró-Muñoz, M., et al. (2016). Influence of Ocean acidification on a natural winter-to-summer plankton succession: first insights from a long-term mesocosm study draw attention to periods of low nutrient concentrations. *PLoS ONE* 11:e0159068. doi: 10.1371/journal.pone.0159068
- Basterretxea, G., and Aristegui, J. (2000). Mesoscale variability in phytoplankton biomass distribution and photosynthetic parameters in the Canary-NW African coastal transition zone. *Mar. Ecol. Prog. Ser.* 197, 27–40. doi: 10.3354/meps197027
- Bertilsson, S., Berglund, O., Karl, D. M., and Chisholm, S. W. (2003). Elemental composition of marine *Prochlorococcus* and *Synechococcus*: implications for the ecological stoichiometry of the sea. *Limnol. Oceanogr.* 48, 1721–1731. doi: 10.4319/lo.2003.48.5.1721
- Boxhammer, T., Bach, L. T., Czerny, J., and Riebesell, U. (2016). Technical note: sampling and processing of mesocosm sediment trap material for quantitative biogeochemical analysis. *Biogeosciences* 13, 2849–2858. doi: 10.5194/bg-13-2849-2016
- Burd, A. B., and Jackson, G. A. (2009). Particle aggregation. *Ann. Rev. Mar. Sci.* 1, 65–90. doi: 10.1146/annurev.marine.010908.163904
- Caldeira, K., and Wickett, M. E. (2003). Oceanography: anthropogenic carbon and ocean pH. *Nature* 425:365. doi: 10.1038/425365a
- Checkley, D. M., and Entzeroth, L. C. (1985). Elemental and isotopic fractionation of carbon and nitrogen by marine, planktonic copepods and implications to the marine nitrogen cycle. *J. Plankton Res.* 7, 553–568. doi: 10.1093/plankt/7.4.553
- Czerny, J., Schulz, K. G., Boxhammer, T., Bellerby, R. G. J., Büdenbender, J., Engel, A., et al. (2013). Implications of elevated CO₂ on pelagic carbon fluxes in an Arctic mesocosm study - an elemental mass balance approach. *Biogeosciences* 10, 3109–3125. doi: 10.5194/bg-10-3109-2013
- Daly, K. L., Wallace, D. W. R., Smith, W. O., Skoog, A., Lara, R., Gosselin, M., et al. (1999). Non-Redfield carbon and nitrogen cycling in the Arctic: effects of ecosystem structure and dynamics. *J. Geophys. Res. Ocean.* 104, 3185–3199. doi: 10.1029/1998JC900071
- Doney, S. C., Fabry, V. J., Feely, R. A., and Kleypas, J. A. (2009). Ocean acidification: the other CO₂ problem. *Ann. Rev. Mar. Sci.* 1, 169–192. doi: 10.1146/annurev.marine.010908.163834
- Fabricius, K. E., Langdon, C., Uthicke, S., Humphrey, C., Noonan, S., De'ath, G., et al. (2011). Losers and winners in coral reefs acclimatized to elevated carbon dioxide concentrations. *Nat. Clim. Chang.* 1, 165–169. doi: 10.1038/nclimate1122
- Gazeau, F., Sallon, A., Maugendre, L., Louis, J., Dellisanti, W., Gaubert, M., et al. (2016). First mesocosm experiments to study the impacts of ocean acidification on plankton communities in the NW Mediterranean Sea (MedSea project). *Estuar. Coast. Shelf Sci.* 138, 11–29. doi: 10.1016/j.ecss.2016.05.014
- Gerber, R. P., and Gerber, M. B. (1979). Ingestion of natural particulate organic matter and subsequent assimilation, respiration and growth by tropical lagoon zooplankton. *Mar. Biol.* 52, 33–43. doi: 10.1007/BF00386855
- Hall-Spencer, J. M., Rodolfo-Metalpa, R., Martin, S., Ransome, E., Fine, M., Turner, S. M., et al. (2008). Volcanic carbon dioxide vents show ecosystem effects of ocean acidification. *Nature* 454, 96–99. doi: 10.1038/nature07051
- Hansen, H. P., and Koroleff, F. (1999). "Determination of nutrients," in *Methods of Seawater Analysis*, eds K. Grasshoff, K. Kremling, and M. Ehrhardt (Weinheim: Wiley-VCH Verlag GmbH), 159–228.
- IPCC (2014). "Technical summary," in *Climate Change 2013 - The Physical Science Basis*, ed Intergovernmental Panel on Climate Change (Cambridge: Cambridge University Press), 31–116.
- Kjørboe, T. (2011). How zooplankton feed: mechanisms, traits and trade-offs. *Biol. Rev.* 86, 311–339. doi: 10.1111/j.1469-185X.2010.00148.x
- Kjørboe, T., and Hansen, J. L. S. (1993). Phytoplankton aggregate formation: observations of patterns and mechanisms of cell sticking and the significance of exopolymeric material. *J. Plankton Res.* 15, 993–1018. doi: 10.1093/plankt/15.9.993
- Kjørboe, T., Andersen, K. P., and Dam, H. G. (1990). Coagulation efficiency and aggregate formation in marine phytoplankton. *Mar. Biol.* 107, 235–245. doi: 10.1007/BF01319822
- Le Quéré, C., Andrew, R. M., Canadell, J. G., Sitch, S., Korsbakken, J. I., Peters, G. P., et al. (2016). Global Carbon Budget 2016. *Earth Syst. Sci. Data* 8, 605–649. doi: 10.5194/essd-8-605-2016.
- Lueker, T. J., Dickson, A. G., and Keeling, C. D. (2000). Ocean pCO₂ calculated from dissolved inorganic carbon, alkalinity, and equations for K₁ and K₂: validation based on laboratory measurements of CO₂ in gas and seawater at equilibrium. *Mar. Chem.* 70, 105–119. doi: 10.1016/S0304-4203(00)00022-0
- Mackey, M., Mackey, D., Higgins, H., and Wright, S. (1996). CHEMTAX - a program for estimating class abundances from chemical markers: application to HPLC measurements of phytoplankton. *Mar. Ecol. Prog. Ser.* 144, 265–283. doi: 10.3354/meps144265
- Orr, J. C., Fabry, V. J., Aumont, O., Bopp, L., Doney, S. C., Feely, R. A., et al. (2005). Anthropogenic ocean acidification over the twenty-first century and its impact on calcifying organisms. *Nature* 437, 681–686. doi: 10.1038/nature04095
- Oschlies, A., Schulz, K. G., Riebesell, U., and Schmittner, A. (2008). Simulated 21st century's increase in oceanic suboxia by CO₂-enhanced biotic carbon export. *Global Biogeochem. Cycles* 22:GB4008. doi: 10.1029/2007GB003147
- Paul, A. J., Bach, L. T., Schulz, K. G., Boxhammer, T., Czerny, J., Achterberg, E. P., et al. (2015). Effect of elevated CO₂ on organic matter pools and fluxes in a summer Baltic Sea plankton community. *Biogeosciences* 12, 6181–6203. doi: 10.5194/bg-12-6181-2015
- Pierrot, D., Lewis, E., and Wallace, D. W. R. (2006). *MS Excel Program Developed for CO₂ System Calculations*. ORNL/CDIAC-105a.
- Ploug, H., and Grossart, H.-P. (2000). Bacterial growth and grazing on diatom aggregates: respiratory carbon turnover as a function of aggregate size and sinking velocity. *Limnol. Oceanogr.* 45, 1467–1475. doi: 10.4319/lo.2000.45.7.1467
- R Core Team (2013). *R: A Language and Environment for Statistical Computing*.
- Riebesell, U., and Gattuso, J. (2015). Lessons learned from ocean acidification research. *Nat. Publ. Gr.* 5, 12–14. doi: 10.1038/nclimate2456
- Riebesell, U., Bach, L. T., Bellerby, R. G. J., Monsalve, J. R. B., Boxhammer, T., Czerny, J., et al. (2017). Competitive fitness of a predominant pelagic calcifier impaired by ocean acidification. *Nat. Geosci.* 10, 19–23. doi: 10.1038/ngeo2854
- Riebesell, U., Czerny, J., von Bröckel, K., Boxhammer, T., Büdenbender, J., Deckelnick, M., et al. (2013). Technical Note: a mobile sea-going mesocosm system - new opportunities for ocean change research. *Biogeosciences* 10, 1835–1847. doi: 10.5194/bg-10-1835-2013
- Riebesell, U., Schulz, K. G., Bellerby, R. G. J., Botros, M., Fritzsche, P., Meyerhöfer, M., et al. (2007). Enhanced biological carbon consumption in a high CO₂ ocean. *Nature* 450, 545–548. doi: 10.1038/nature06267
- Sala, M. M., Aparicio, F. L., Balagué, V., Boras, J. A., Borrull, E., Cardelús, C., et al. (2015). Contrasting effects of ocean acidification on the microbial food web under different trophic conditions. *ICES J. Mar. Sci. J. du Cons.* 73, 670–679. doi: 10.1093/icesjms/fsv130
- Sambrotto, R. N., Savidge, G., Robinson, C., Boyd, P., Takahashi, T., Karl, D. M., et al. (1993). Elevated consumption of carbon relative to nitrogen in the surface ocean. *Nature* 363, 248–250. doi: 10.1038/363248a0
- Sangrà, P., Pascual, A., Rodríguez-Santana, Á., Machín, F., Mason, E., McWilliams, J. C., et al. (2009). The canary eddy corridor: a major pathway for long-lived eddies in the subtropical North Atlantic. *Deep. Res. Part I Oceanogr. Res. Pap.* 56, 2100–2114. doi: 10.1016/j.dsr.2009.08.008
- Schneider, B., Schlitzer, R., Fischer, G., and Nothig, E. M. (2003). Depth-dependent elemental compositions of particulate organic matter (POM) in the ocean. *Glob. Biogeochem. Cycles* 17:1032. doi: 10.1029/2002GB001871
- Schulz, K. G., Bellerby, R. G. J., Brussaard, C. P. D., Büdenbender, J., Czerny, J., Engel, A., et al. (2013). Temporal biomass dynamics of an Arctic plankton bloom in response to increasing levels of atmospheric carbon dioxide. *Biogeosciences* 10, 161–180. doi: 10.5194/bg-10-161-2013
- Sharp, J. H. (1974). Improved analysis for particulate organic carbon and nitrogen from seawater. *Limnol. Oceanogr.* 19, 984–989. doi: 10.4319/lo.1974.19.6.0984
- Small, L. F., Fowler, S. W., Moore, S. A., and LaRosa, J. (1983). Dissolved and fecal pellet carbon and nitrogen release by zooplankton in tropical

- waters. *Deep Sea Res. Part A. Oceanogr. Res. Pap.* 30, 1199–1220. doi: 10.1016/0198-0149(83)90080-8
- Smith, D. C., Simon, M., Alldredge, A. L., and Azam, F. (1992). Intense hydrolytic enzyme activity on marine aggregates and implications for rapid particle dissolution. *Nature* 359, 139–142. doi: 10.1038/359139a0
- Stange, P., Bach, L. T., Le Moigne, F. A. C., Taucher, J., Boxhammer, T., and Riebesell, U. (2017). Quantifying the time lag between organic matter production and export in the surface ocean: implications for estimates of export efficiency. *Geophys. Res. Lett.* 44, 268–276. doi: 10.1002/2016GL070875
- Taucher, J., Bach, L. T., Boxhammer, T., Achterberg, E. P., Algueró-Muñoz, M., Aristegui, J., et al. (2017). Influence of ocean acidification on oligotrophic plankton communities in the subtropical North Atlantic: an *in situ* mesocosm study reveals community-wide responses to elevated CO₂ during a simulated deep water upwelling event. *Front. Mar. Sci.* 4:2800. doi: 10.3389/fmars.2017.00085
- Thomas, H., Ittekkot, V., Osterroht, C., and Schneider, B. (1999). Preferential recycling of nutrients—the ocean's way to increase new production and to pass nutrient limitation? *Limnol. Oceanogr.* 44, 1999–2004.
- Thomson, P., Davidson, A., and Maher, L. (2016). Increasing CO₂ changes community composition of pico- and nano-sized protists and prokaryotes at a coastal Antarctic site. *Mar. Ecol. Prog. Ser.* 554, 51–69. doi: 10.3354/meps11803
- Toggweiler, J. R. (1993). Carbon overconsumption. *Nature* 363, 210–211. doi: 10.1038/363210a0
- Utermöhl, V. H. (1931). Neue wege in der quantitativen Erfassung des Planktons (mit besonderer Berücksichtigung des Ultraplanktons). *Verhandlungen der Int. Vereinigung für Theor. und Angew. Limnol.* 5, 567–596.
- Van Heukelem, L., and Thomas, C. S. (2001). Computer-assisted high-performance liquid chromatography method development with applications to the isolation and analysis of phytoplankton pigments. *J. Chromatogr. A* 910, 31–49. doi: 10.1016/S.0378-4347(00)00603-4
- Wittmann, A. C., and Pörtner, H.-O. (2013). Sensitivities of extant animal taxa to ocean acidification. *Nat. Clim. Chang.* 3, 995–1001. doi: 10.1038/nclimate1982
- Wolf-Gladrow, D. A., Riebesell, U., Burkhardt, S., and Bijma, J. (1999). Direct effects of CO₂ concentration on growth and isotopic composition of marine plankton. *Tellus* 51B, 461–476. doi: 10.3402/tellusb.v51i2.16324

Conflict of Interest Statement: The authors declare that the research was conducted in the absence of any commercial or financial relationships that could be construed as a potential conflict of interest.

Copyright © 2018 Stange, Taucher, Bach, Algueró-Muñoz, Horn, Krebs, Boxhammer, Nauendorf and Riebesell. This is an open-access article distributed under the terms of the Creative Commons Attribution License (CC BY). The use, distribution or reproduction in other forums is permitted, provided the original author(s) and the copyright owner are credited and that the original publication in this journal is cited, in accordance with accepted academic practice. No use, distribution or reproduction is permitted which does not comply with these terms.



High CO₂ Under Nutrient Fertilization Increases Primary Production and Biomass in Subtropical Phytoplankton Communities: A Mesocosm Approach

Nauzet Hernández-Hernández¹, Lennart T. Bach², María F. Montero¹, Jan Taucher², Isabel Baños¹, Wanchun Guan^{2,3}, Mario Espósito², Andrea Ludwig², Eric P. Achterberg², Ulf Riebesell² and Javier Arístegui^{1*}

OPEN ACCESS

Edited by:

Christel Hassler,
Université de Genève, Switzerland

Reviewed by:

Chiara Lombardi,
National Agency for New
Technologies, Energy and Sustainable
Economic Development, Italy
Jie Xu,

South China Sea Institute of
Oceanology (CAS), China

*Correspondence:

Javier Arístegui
javier.aristegui@ulpgc.es

Specialty section:

This article was submitted to
Marine Biogeochemistry,
a section of the journal
Frontiers in Marine Science

Received: 30 March 2018

Accepted: 30 May 2018

Published: 19 June 2018

Citation:

Hernández-Hernández N, Bach LT,
Montero MF, Taucher J, Baños I,
Guan W, Espósito M, Ludwig A,
Achterberg EP, Riebesell U and
Arístegui J (2018) High CO₂ Under
Nutrient Fertilization Increases Primary
Production and Biomass in
Subtropical Phytoplankton
Communities: A Mesocosm
Approach. *Front. Mar. Sci.* 5:213.
doi: 10.3389/fmars.2018.00213

¹ Instituto de Oceanografía y Cambio Global, Universidad de Las Palmas de Gran Canaria, Las Palmas, Spain, ² GEOMAR
Helmholtz Center for Ocean Research, Kiel, Germany, ³ Department of Marine Biotechnology, School of Laboratory Medicine
and Life Science, Wenzhou Medical University, Wenzhou, China

The subtropical oceans are home to one of the largest ecosystems on Earth, contributing to nearly one third of global oceanic primary production. Ocean warming leads to enhanced stratification in the oligotrophic ocean but also intensification in cross-shore wind gradients and thus in eddy kinetic energy across eastern boundary regions of the subtropical gyres. Phytoplankton thriving in a future warmer oligotrophic subtropical ocean with enhanced CO₂ levels could therefore be patchily fertilized by increased mesoscale and submesoscale variability inducing nutrient pumping into the surface ocean. Under this premise, we have tested the response of three size classes (0.2–2, 2–20, and >20 μm) of subtropical phytoplankton communities in terms of primary production, chlorophyll and cell biomass, to increasing CO₂ concentrations and nutrient fertilization during an *in situ* mesocosm experiment in oligotrophic waters off of the island of Gran Canaria. We found no significant CO₂-related effect on primary production and biomass under oligotrophic conditions (phase I). In contrast, primary production, chlorophyll and biomass displayed a significant and pronounced increase under elevated CO₂ conditions in all groups after nutrient fertilization, both during the bloom (phase II) and post-bloom (phase III) conditions. Although the relative increase of primary production in picophytoplankton (250%) was 2.5 higher than in microphytoplankton (100%) after nutrient fertilization, comparing the high and low CO₂ treatments, microphytoplankton dominated in terms of biomass, contributing >57% to the total. These results contrast with similar studies conducted in temperate and cold waters, where consistently small phytoplankton benefitted after nutrient additions at high CO₂, pointing to different CO₂-sensitivities across plankton communities and ecosystem types in the ocean.

Keywords: ocean acidification, nutrient fertilization, mesocosm, size-fractionated primary production, phytoplankton community structure, subtropical North Atlantic

INTRODUCTION

With a surface area of more than 200 million square kilometers, subtropical oligotrophic waters form the largest ecosystem of the world's surface oceans, covering more than 60% of total ocean surface (Longhurst et al., 1995). These extensive areas are typically characterized by a deep and nutrient-poor mixed layer, which is prevented from mixing with deeper nutrient-rich waters by a strong, almost permanent thermocline. Consequently, both phytoplankton biomass and primary production are low during most of the year. Despite its low productivity per surface area (Longhurst et al., 1995), more than 30 million tons of carbon dioxide (CO₂) are photosynthetically fixed into organic compounds every day, contributing nearly one third of total oceanic primary production (Field et al., 1998; Behrenfeld et al., 2001, 2006), and thus playing a key role in the global carbon cycle (Falkowski, 1994; Falkowski et al., 2000).

Climate change is inducing physical and chemical changes in the marine environment, with profound consequences for ocean productivity (Bopp et al., 2001; Gruber, 2011; Doney et al., 2012; IPCC, 2014). The anthropogenic release of CO₂ through human activity since the beginning of the industrial revolution is leading to an increase of the partial pressure of this greenhouse gas in the ocean, and consequently both pH and calcium carbonate saturation states (Ω) are declining rapidly, a process termed "ocean acidification" (Caldeira and Wickett, 2003; Sarmiento et al., 2004). Furthermore, as a consequence of increasing atmospheric greenhouse gas concentrations, the surface ocean is warming at a higher rate than the deep ocean, which may lead to a strengthening of the water column stratification (IPCC, 2014 and references therein).

Whereas increasing oceanic CO₂ levels are hypothesized to boost ocean productivity by relieving CO₂ limitation of the Ribulose-1,5-bisphosphate carboxylase/oxygenase (RubisCO) enzyme (Beardal and Raven, 2004; Reinfelder, 2011; Mackey et al., 2015), a more stratified ocean would lead to a decrease in nutrient supply to the euphotic layer and therefore a potential reduction of autotrophic productivity (Bopp et al., 2001; Steinacher et al., 2010). Nevertheless, it has been predicted that the heterogeneous warming of oceans and continents, may enhance upwelling-favorable winds in Eastern Boundary Current Systems (Bakun, 1990; Sydeman et al., 2014; García-Reyes et al., 2015). Stronger cross-shore wind gradients would lead to an intensification of the eddy kinetic energy fields across eastern boundary regions of the subtropical Gyres, favoring the upward pumping of nutrients driven by upwelling processes. Phytoplankton thriving in a future warmer and acidified oligotrophic subtropical ocean could therefore be patchily fertilized by increased mesoscale and submesoscale processes inducing nutrient pumping into the ocean surface.

Investigations of CO₂-related effects on marine productivity have experienced a remarkable surge over the last years (Riebesell and Gattuso, 2015). Theoretical studies based on chlorophyll-dependent models predict a decrease in phytoplankton chlorophyll concentration, and consequently in primary production, in a warmer, acidified and more stratified ocean (Behrenfeld et al., 2006; Marinov et al., 2010; Steinacher et al.,

2010). On the other hand, experimental studies have reported contrasting results about the potential effects of increasing CO₂ on marine productivity in natural assemblages (Table 1). Whereas, some authors reported increased photosynthetic rates with increasing CO₂ (Hein and Sand-Jensen, 1997; Riebesell et al., 2007; Bellerby et al., 2008; Tortell et al., 2008; Egge et al., 2009; Engel et al., 2013; Eberlein et al., 2017), others have not observed significant relationships between marine productivity and ocean acidification (Tortell et al., 2002; Delille et al., 2005; Hare et al., 2007; Feng et al., 2009; Tanaka et al., 2013; Maugendre et al., 2017). Most of the experiments, however, have been carried out in nutrient-rich systems, with only a few performed in low-nutrient regions (Yoshimura et al., 2009; Maugendre et al., 2017). Thus, there is a severe lack of information on how ocean acidification could affect primary production in subtropical oligotrophic regions.

This study investigates how an acidified and patchily fertilized subtropical ocean impacts marine autotrophic productivity. For this, we carried out a mesocosm experiment off the coast of Gran Canaria (Canary Islands) during the autumn of 2014. We studied the response of size-fractionated primary production, chlorophyll *a* and biomass of the phytoplankton community to enhanced CO₂ levels and nutrient fertilization to investigate which size-fraction, if any, responds more readily to these short-term perturbations.

METHODS

Set-Up and Sampling

The experiment was carried out in Gando Bay (27°55' 41'' N, 15° 21' 55'' W), Gran Canaria (Canary Island), as part of the BIOACID (Biological Impacts of Ocean ACIDification) project. Nine KOSMOS (Kiel Off-Shore Mesocosms for future Ocean Simulations; Riebesell et al., 2013) were deployed and enclosed ~35 m³ of low-nutrient low-chlorophyll water off the east coast of Gran Canaria. In order to achieve a *p*CO₂ gradient from ~400 μ atm to partial pressures corresponding to the year 2150 (~1,000 μ atm) according to the RCP8.5 scenario (IPCC, 2014), seven mesocosms were gradually enriched at the start of the experiment over a period of 7 days (from *t*₀ to *t*₆), via the addition of different amounts of filtered CO₂-saturated seawater. Unfortunately, one of the high-CO₂ mesocosms (M6) was damaged on *t*₂₆, and hence was not considered in the data analyses. Two more CO₂ addition were carried out on *t*₂₄ and *t*₃₈ to counteract the loss of CO₂ due to outgassing and biological uptake. The average *p*CO₂ concentrations along the whole experiment for each of the remaining six mesocosms were: M5 (448 μ atm), M3 (563 μ atm), M7 (668 μ atm), M4 (716 μ atm), M2 (887 μ atm), and M8 (1025 μ atm). Two other mesocosms - M1 (369 μ atm) and M9 (352 μ atm) - remained untreated, serving as controls (ambient *p*CO₂) (Figure 1). The volumes of CO₂-saturated seawater added to achieve the *p*CO₂ gradient varied from 77 L in M5 to 382 L in M8. After 24 days, between 7.5 and 9.0 m³ of nutrient-rich deep water was added to each mesocosm with the purpose of simulating a natural fertilization event (Figure 2). During the 56 day experimental period, integrated

TABLE 1 | Published studies on the effect of ocean acidification on primary production in plankton communities.

Location	Experiment	Method	Total	PP _{DOC}	SF	References
Atlantic Ocean	Culture	¹⁴ C	+			Hein and Sand-Jensen, 1997
Peruvian upwelling	Microcosm	¹⁴ C	NS			Tortell et al., 2002
Raune Fjord (Norway)	Mesocosm	¹⁴ C	NS			Delille et al., 2005
Bering Sea	Microcosm	¹⁴ C	NS			Hare et al., 2007
Raune Fjord (Norway)	Mesocosm	DIC	+			Riebesell et al., 2007
Raune Fjord (Norway)	Mesocosm	C _T	+			Bellerby et al., 2008
Ross Sea	Microcosm	¹⁴ C	+			Tortell et al., 2008
Raune Fjord (Norway)	Mesocosm	¹⁴ C	+		*	Egge et al., 2009
Raune Fjord (Norway)	Mesocosm	O ₂	NS			Egge et al., 2009
North Atlantic Ocean	Microcosm	¹⁴ C	NS			Feng et al., 2009
BATS (North Atlantic)	Microcosm	¹⁴ C	NS			Lomas et al., 2012
Kongs Fjord (Norway)	Mesocosm	¹⁴ C	+	+		Engel et al., 2013
Kongs Fjord (Norway)	Mesocosm	O ₂	NS			Tanaka et al., 2013
Mediterranean Sea	Mesocosm	¹⁴ C	NS			Maugendre et al., 2017
Mediterranean Sea	Mesocosm	O ₂	NS			Maugendre et al., 2017
Gullmar Fjord (Sweden)	Mesocosm	¹⁴ C	+			Eberlein et al., 2017

"Total" refers to the whole community, excluding the dissolved fraction (PP_{DOC}) in ¹⁴C-based experiments. SF, size fractionated in the particulate organic fraction. NS, Not significant; +, Enhanced; *, Positive effect only in the size-fraction <1 μm.

water samples (0–13 m) were collected by means of depth-integrated water samplers (IWS, HYDRO-BIOS, Kiel), on days –1, 1, 5, 9, 13, 17, 21, 25, 27, 29, 31, 33, 35, 37, 41, 45, 50, and 55, from each of the nine mesocosms, plus an extra sample from ambient waters outside the mesocosms (referred to as Atlantic; A). Once on land, subsamples were taken for primary production, chlorophyll *a*, phytoplankton abundances, as well as for dissolved inorganic carbon and inorganic nutrients. More detailed information concerning the experimental set-up (CO₂ manipulation, deep water addition, sampling, etc.) is provided by Taucher et al. (2017).

pCO₂ and Inorganic Nutrients

Partial pressure of CO₂ (pCO₂) was derived from total alkalinity (TA) and dissolved inorganic carbon (DIC) data, following Pierrot et al. (2006) and Lueker et al. (2000). TA was measured by means of a Metrohm 862 Compact Titrator and a 907 Titrando unit. DIC was determined by infrared absorption using a LI-COR LI-700 on an ARICA system (MIRANDA, Kiel). Inorganic nutrients (NO₃[–], NO₂[–], PO₄^{3–}, and Si(OH)₄) were determined by colorimetric methods following Murphy and Riley (1962) and Hansen and Grasshoff (1983). Ammonium (NH₄⁺) was fluorometrically analyzed following Holmes et al. (1999). A SEAL Analytical QuAAtro AutoAnalyzer connected to a JASCO Model FP-2020 Intelligent Fluorescence Detector and a SEAL Analytical XY2 autosampler was used to measure NO₃[–], NO₂[–], PO₄^{3–}, Si(OH)₄, and NH₄⁺. For details on the methodology of these measurements see Taucher et al. (2017).

Chlorophyll *a*

For chlorophyll *a* analysis, 500 ml of sea water were sampled and filtered sequentially through 20, 2, and 0.2 μm pore-size Whatman polycarbonate filters under low vacuum pressure.

Filters were kept frozen at –20°C until analysis. Before chlorophyll determination, pigments were extracted using 10 ml of 90% acetone at 4°C in the dark for 24 h. Extracts were measured fluorometrically, before and after acidification, by means of a Turner Designs bench fluorometer 10-AU, previously calibrated with pure chlorophyll *a* (Sigma Chemical), following Holm-Hansen et al. (1965). The collected material on the 20, 2, and 0.2 μm filters was used to measure the corresponding microplankton (Chl_{Micro}), nanoplankton (Chl_{Nano}) and picoplankton (Chl_{Pico}) chlorophyll concentrations, respectively. Total chlorophyll (Chl_{Tot}) was derived from the sum of the three size fractions.

Phytoplankton Abundance and Biomass

Prochlorococcus and *Synechococcus* type cyanobacteria and small photosynthetic eukaryotic cells (picoeukaryotes) were enumerated with a FACScalibur (Becton and Dickinson) flow cytometer. Picoeukaryotes, *Prochlorococcus* and *Synechococcus* samples (about 1 mL) were analyzed in fresh material 30–60 min after subsampling from the carboys. *Prochlorococcus* were recurrently observed in Atlantic waters, but vanished inside all the mesocosms after 2 days. Thus, we did not use their abundances to compute biomass. Phytoplankton groups were identified by their signatures in a plot of side scatter (SSC) vs. red (FL3) and orange (FL2) fluorescence. Samples were run at 60 μL min^{–1}. A suspension of yellow-green 1 μm latex beads (~10⁵ beads mL^{–1}) was added as an internal standard (Polysciences, Inc.). Pigmented nanoeukaryotes (2–20 μm) were counted on fresh samples with a Cytobuoy cytometer (Dubelaar and Gerritzen, 2000), provided with flow-image. Samples (about 3 ml) were analyzed *in vivo* for 7 min at a flow rate of 300 μL min^{–1}. Microphytoplankton (mostly diatoms and dinoflagellates) were fixed with alkaline Lugol's iodine (1% final

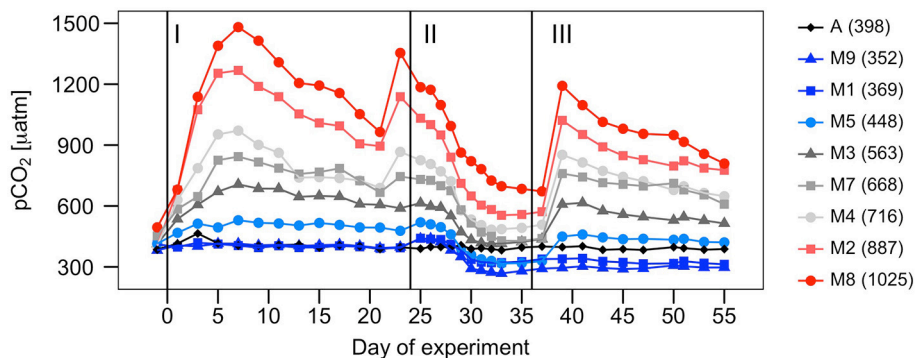


FIGURE 1 | Temporal development of $p\text{CO}_2$ (μatm) over the course of the experiment in the mesocosms (MX) and the surrounding Atlantic waters (A). Vertical lines separate the three phases of the experiment. Values in parentheses indicate average $p\text{CO}_2$ concentrations for each mesocosm along the whole experiment.

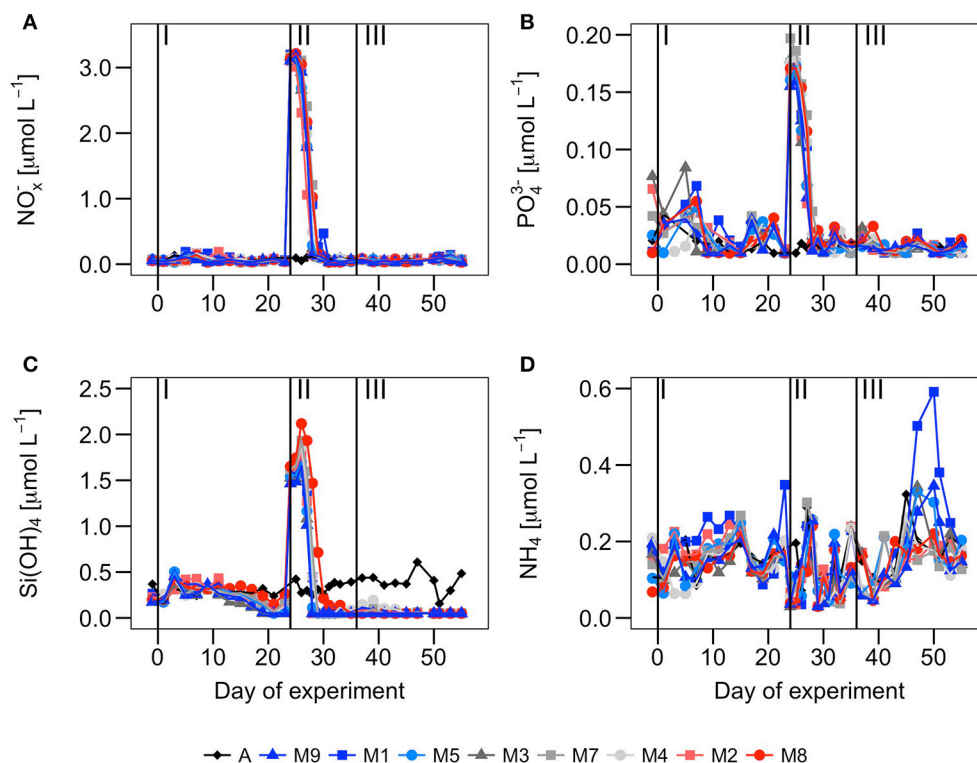


FIGURE 2 | Temporal development of (A) nitrate + nitrite (NO_x^-) ($\mu\text{mol}\cdot\text{L}^{-1}$), (B) phosphate ($\mu\text{mol}\cdot\text{L}^{-1}$), (C) silicate ($\mu\text{mol}\cdot\text{L}^{-1}$) and (D) ammonium ($\mu\text{mol}\cdot\text{L}^{-1}$) over the course of the experiment. Vertical lines separate the three phases of the experiment.

concentration), sedimented in Utermöhl chambers and counted by means of an inverted microscope (Utermöhl, 1931).

Biomass of *Synechococcus* and picoeukaryotes were estimated by multiplying their abundances by the average cell carbon content obtained for each group, using the conversion factors obtained by MF Montero (unpublished) from samples collected in coastal waters of Gran Canaria: 120 fgC/cell (*Synechococcus*), 420 fgC/cell (picoeukaryotes). Nanoeukaryotes' abundances were converted into biomass using an estimated average biovolume of $20\ \mu\text{m}^3$ for organisms between 2 and $6\ \mu\text{m}$ and a biovolume

of $125\ \mu\text{m}^3$ for organisms between 6 and $11\ \mu\text{m}$, applying the conversion factor of $220\ \text{fgC}\ \mu\text{m}^{-3}$ proposed by Borsheim and Bratbak (1987). Biovolumes and conversion factors used for diatoms and dinoflagellates were calculated following Menden-Deuer and Lessard (2000). Picoplankton biomass (B_{Pico}) was calculated as the sum of the biomasses of *Synechococcus* and picoeukaryotes, nanoplankton biomass (B_{Nano}) as the sum of all nanoeukaryotes' biomass, and microplankton biomass (B_{Micro}) as the sum of the diatoms and dinoflagellates biomass. Total biomass (B_{Tot}) refers to the sum of all size fractions.

¹⁴C-Based Primary Production

Primary production was measured using the ¹⁴C method. Four culture flasks per mesocosm, and per ambient Atlantic seawater sample, were filled with 70 ml of water, and inoculated with 15 μCi of ¹⁴C-labeled sodium bicarbonate solution (NaH¹⁴CO₃; Perkin Elmer). Three of them were *in vitro* incubated for 12 h in a temperature-controlled chamber reproducing *in situ* daily average light and temperature, while the remaining flask was incubated at the same temperature under complete darkness to measure the dark carbon uptake. Sixty milliliter of the samples were filtered with a vacuum pump sequentially through 20, 2, and 0.2 μm pore-size Whatman polycarbonate filters, to allow calculation of the particulate organic carbon fixed by microplankton (PP_{Micro}), nanoplankton (PP_{Nano}) and picoplankton (PP_{Pico}), respectively. The total particulate organic carbon production (PP_{POC}) was derived from the sum of the three size fractions. Filters were then placed in 4 ml scintillation vials and exposed to concentrated HCl fumes overnight to remove ¹⁴C-labeled inorganic carbon. To estimate the amount of carbon fixation into the dissolved organic carbon fraction (PP_{DOC}), 5 ml of water sample was gently filtered onto 0.2 μm Whatman polycarbonate filter under low vacuum pressure. The filtrate was transferred to a 20 ml scintillation vial. Liquid samples were acidified with 100 μl of 50% HCl and placed in an orbital oscillator for 24 h. Finally, scintillation cocktail (Ultima Gold XR) was added to every sample, thoroughly mixed, and stored in darkness for another 24 h, prior to measuring radioactivity in a scintillation counter Beckman LS-6500. Primary production (μg C·L⁻¹·h⁻¹) was calculated according to:

$$PP = \left[\frac{V_S}{V_F} \right] \cdot \frac{DIC \cdot (DPM_S - DPM_D)}{DPM_A \cdot t_i}$$

where V_S is the volume of the sample (ml); V_F the filtered volume (ml); DIC the dissolved inorganic carbon of the sample (μg C·L⁻¹); DPM_S the disintegration per minute of the samples; DPM_D the disintegration per minute of the dark-incubated samples; DPM_A total initial addition of ¹⁴C and t_i the incubation time (h).

The percentage of extracellular carbon release (PER) was calculated as:

$$PER (\%) = \frac{PP_{DOC}}{PP_{TOT}} \times 100$$

being PP_{TOT} the sum of PP_{DOC} and PP_{POC}

Statistical Analysis

To investigate the potential effects of ocean acidification on autotrophic productivity throughout the three phases of the experiment, model II (Reduced Major Axis) linear regressions (Sokal and Rohlf, 2013) between primary production, chlorophyll and biomass and pCO_2 concentrations were performed for each phase using Matlab (The MathWorks, Inc, Natick, Massachusetts, United States). For that purpose, all datasets were averaged per mesocosm and phase. The confidence level for all analysis was set at 95% ($p < 0.05$).

RESULTS

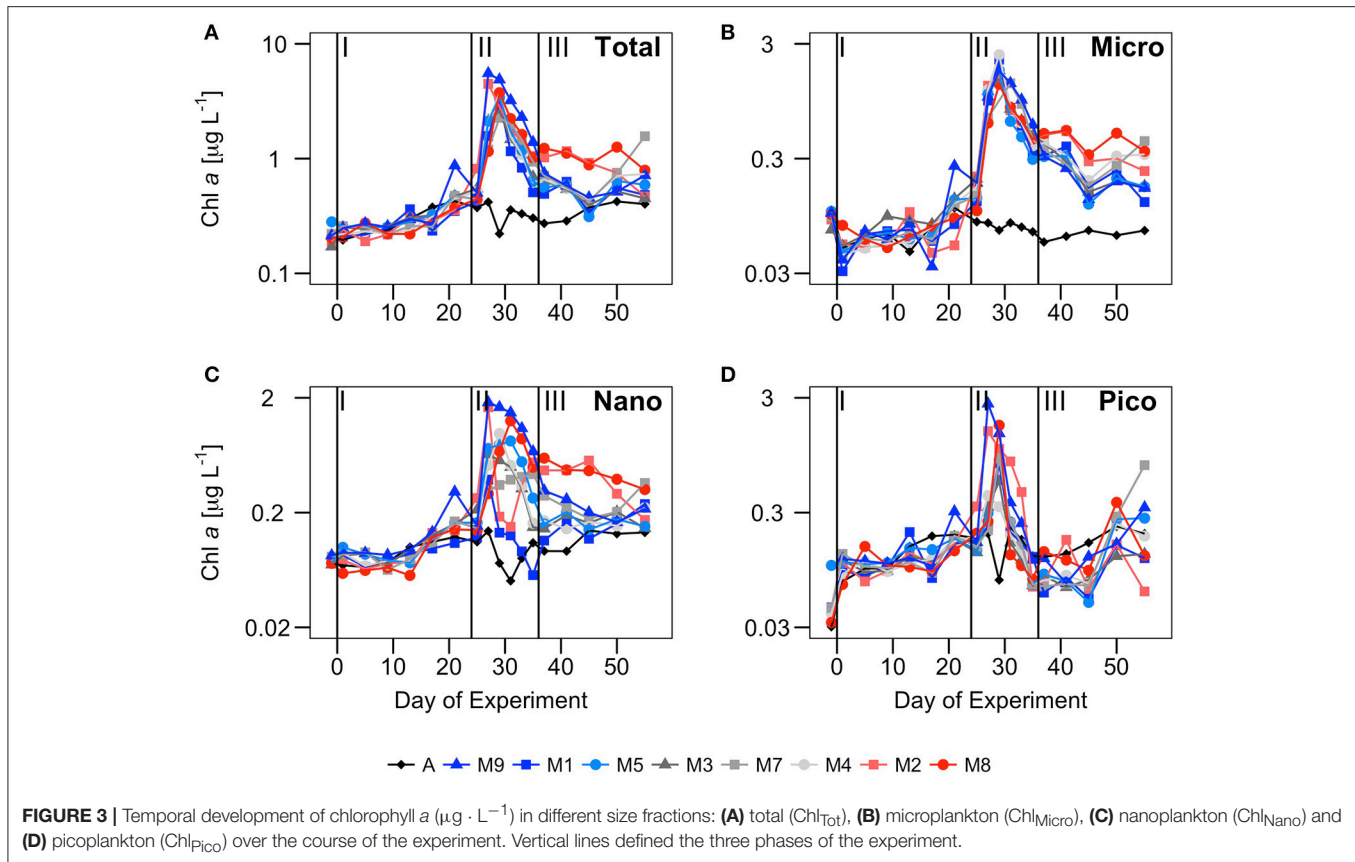
Temporal Development of Size-Fractionated Chlorophyll a and Autotrophic Biomass

Nutrient concentrations (Figure 2), together with the development of chlorophyll and biomass (Figures 3, 4), allowed the differentiation of three well-defined phases over the experimental period: The pre-bloom phase (I), from t_1 to t_{23} ; the bloom phase (II), from t_{25} to t_{35} ; and the post-bloom phase (III), from t_{37} until the end of the experiment (t_{55}).

During phase I, the waters inside the mesocosms were characterized by relatively low nutrient concentrations (similar to ambient Atlantic waters), low Chl_{Tot} , and low B_{Tot} (Figures 2–4). Two to three days after enclosing the water inside the mesocosm bags (t_1 – t_2), the concentration of all inorganic nutrients slightly increased both inside the mesocosms and in Atlantic waters. This suggests the influence of external inputs; perhaps caused by dust deposition on the surface waters (since during those days there was aerosols deposition with dust originating from NW Africa). Nitrate, phosphate and silicate displayed relative maxima around t_5 , dropping after t_{10} and reaching minimum values at t_{23} . Ammonia peaked around t_{10-15} and dropped to minimum values around t_{20} . The largest decrease in the mesocosm nutrient concentrations compared to the Atlantic waters was in the silicates, as a result of its consumption by diatoms (Taucher et al., 2017).

Total chlorophyll and biomass increased from t_0 to t_{23} , following a general inverse trend with nutrient concentrations (Figure 3). However, there were contrasting patterns between chlorophyll and biomass in the different size-fractions. There were no significant differences in chlorophyll concentrations between the mesocosms and Atlantic waters in any of the size fractions (Figure 3). In contrast, there were significant differences in biomass in the largest size fractions between mesocosms and Atlantic waters, suggesting a dominance of large mixotrophic organisms inside the mesocosms (Figure 4). Figure 5 illustrates the relative contributions of the different size fractions (averaged from all the mesocosms) to chlorophyll, biomass and primary production over the course of the experiment. During phase I, picophytoplankton (Pico) contributed >40% to Chl_{Tot} , but <40% to B_{Tot} , with no significant differences with ambient waters. Nanophytoplankton (Nano) contributed 30–35% to Chl_{Tot} , but dominated in biomass (about 50%), although differences between mesocosms and Atlantic waters were not significant. Diatoms and dinoflagellates (Micro) contributed about 25% to Chl_{Tot} but only 10–20% to B_{Tot} , with clear differences with respect to Atlantic waters, particularly after t_{10} .

Following the nutrient fertilization at t_{24} , Chl_{Tot} and B_{Tot} increased exponentially reaching maximum average values (3.4 ± 0.5 and $244 \pm 122 \mu g C \cdot L^{-1}$, respectively) at t_{29} (Figures 3, 4). Consequently, nutrient concentrations were rapidly utilized inside the mesocosms, dropping to levels similar to the Atlantic waters when the phytoplankton bloom was at its peak (Figure 2). There was an exception with silicates, whose values dropped even below the Atlantic values after the bloom, as result



of the large consumption by diatoms during phases II and III (Taucher et al., 2017). M8 and M2, the two mesocosms with highest CO₂ concentrations, were markedly elevated in biomass, both in the Micro and Nano fractions, compared to the other mesocosms (Figure 3). With the depletion of inorganic nutrients, the levels of chlorophyll as well as biomass decreased in the Pico and Nano fractions, with a change in the slopes at t₃₆, when nutrients were almost exhausted. Biomass of Micro decreased more smoothly, maintaining high values in the high CO₂ treatments during the start of phase III. chlorophyll and biomass in phase II were dominated by Micro, contributing 40–60%, with a slightly higher dominance in biomass than in chlorophyll. In contrast, Pico contributed on average only 10–35% to chlorophyll and biomass inside the mesocosms, with values significantly lower than in the Atlantic waters.

During phase III, nutrient concentrations remained low (Figure 2), with nitrate and phosphate occurring at similar levels compared to Atlantic waters, but silicate was almost depleted (due to the consumption by diatoms) to levels $<0.08 \mu\text{M}$, significantly below those of Atlantic waters. Only ammonium showed higher concentrations in some of the mesocosms, compared to Atlantic waters and phases I and II, probably due to higher excretion rates of grazers during this phase. Although Chl_{Tot} and B_{Tot} decreased with respect to phase II, they were still markedly higher than in Atlantic waters. The contribution

of the larger size fractions to chlorophyll and biomass were always higher in the mesocosms than in Atlantic waters, but with apparent differences between chlorophyll and biomass (Figure 5). Pico contributed in general to near 45% of Chl_{Tot} and 35% to B_{Tot} in Atlantic waters compared to $<25\%$ of Chl_{Tot} and $<10\%$ of B_{Tot} in the mesocosms. Nano and Micro contributed almost evenly to Chl_{Tot} in the mesocosms, but not to biomass.

Dynamics of Size-Fractionated ¹⁴C-Based Primary Production

Total primary production in the particulate fraction (PP_{POC}) displayed average rates in the mesocosms ($0.93 \pm 0.48 \mu\text{g C} \cdot \text{L}^{-1} \cdot \text{h}^{-1}$) that were almost double than in Atlantic waters ($0.56 \pm 0.24 \mu\text{g C} \cdot \text{L}^{-1} \cdot \text{h}^{-1}$) at the start of the experiment. Like chlorophyll and biomass, the rates increased 4 to 5-fold peaking at t_{10–12} in all size fractions (although more for the Pico), to decrease again to initial rates, just before nutrient fertilization (Figure 6). The greatest differences between Atlantic waters and mesocosms were observed in Pico. This fraction contributed $>50\%$ to PP_{POC} in phase I, compared to $\sim 30\%$ in Atlantic waters.

After nutrient fertilization (phase II), PP_{POC} increased more than 15 fold in all mesocosms, peaking at t₂₉ with the highest rates in M2, reaching $35 \mu\text{g C} \cdot \text{L}^{-1} \cdot \text{h}^{-1}$, compared to values $<2 \mu\text{g C} \cdot \text{L}^{-1} \cdot \text{h}^{-1}$ in Atlantic waters (Figure 6). Due

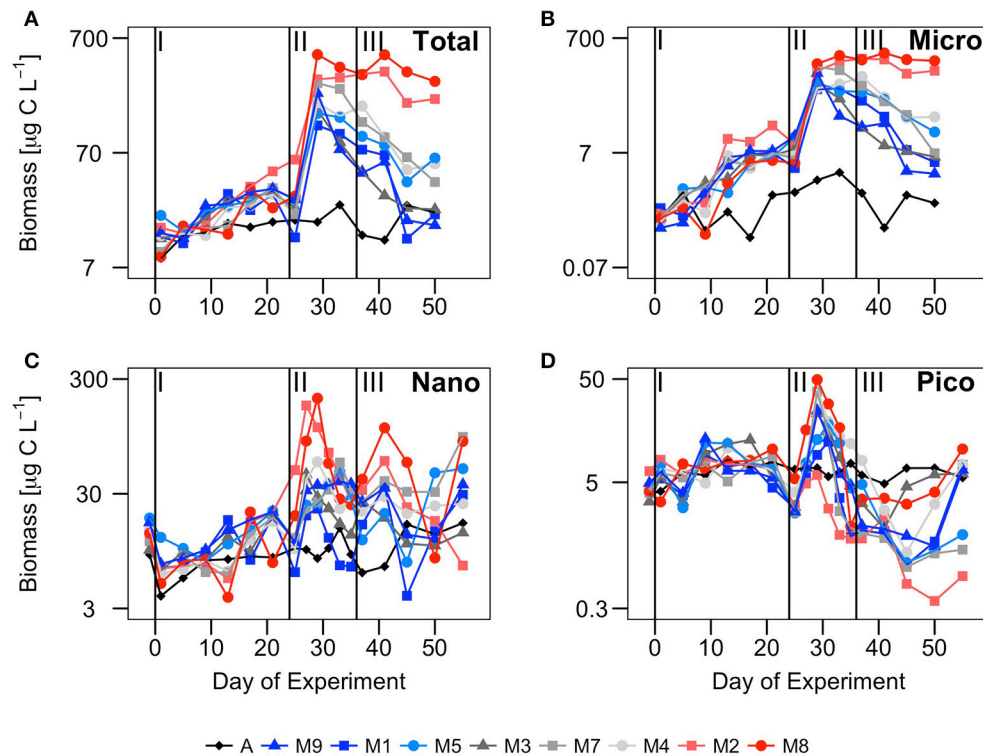


FIGURE 4 | Temporal development of biomass ($\mu\text{g C}\cdot\text{L}^{-1}$) in different size fractions: (A) total (B_{Tot}), (B) microplankton (B_{Micro}), (C) nanoplankton (B_{Nano}) and (D) picoplankton (B_{Pico}) over the course of the experiment. Vertical lines defined the three phases of the experiment.

to nutrient depletion, total PP_{POC} rates declined to $<4 \mu\text{g C}\cdot\text{L}^{-1}\cdot\text{h}^{-1}$ at t_{35} (end of phase II). Micro contributed almost a 75% to total PP_{POC} , even more than to chlorophyll and biomass (Figure 5), while the contribution of Pico was about 10%.

During phase III, PP_{POC} rates declined more smoothly than in phase II, following nutrient depletion, with higher rates in the mesocosms with higher CO₂ treatments (see following section). Like in phase II, the major contribution to total PP_{POC} was due to Micro (60–70%), while Pico and Nano contributed about 15–20% each.

The average rate of primary production contributing to the dissolved organic carbon fraction (PP_{DOC} ; Figure 7A) inside the mesocosms varied strongly during the course of the experiment, between $34.7 \mu\text{g C}\cdot\text{L}^{-1}\cdot\text{h}^{-1}$ in mesocosm M2 during the bloom phase and $0.23 \mu\text{g C}\cdot\text{L}^{-1}\cdot\text{h}^{-1}$ in mesocosm M7 during phase I. Its temporal development matched PP_{POC} dynamics, increasing with nutrient addition in t_{24} . However, the percentage of extracellular organic carbon release (PER; Figure 7B) decreased from the first week of the experiment (average $26.7 \pm 8.6\%$), to t_{29} , when primary production reached their maximum values and PER its average minimum value ($7.1 \pm 3.7\%$). In Atlantic waters, PP_{DOC} was similar (phase I) or lower (phases II and III) than in the experiments, but with higher and less stable PER, ranging from <10 to 35% (Figure 7B).

CO₂ Effects on Size-Fractionated Chlorophyll, Biomass and Primary Production

A total of 39 linear regressions were conducted to test potential CO₂ effects on total community and size-fractionated primary production, biomass and chlorophyll, and almost two thirds (28) showed statistically significant ($p < 0.05$) relationships (Tables 2 – 4, respectively). Total particulate primary production (PP_{POC}) remained unaffected during phase I, in contrast to B_{Tot} , B_{Nano} , Chl_{Nano} and Chl_{Tot} , which exhibited negative responses to increasing $p\text{CO}_2$. Negative responses (6) were only observed in the oligotrophic phase (phase I). Dissolved carbon production rate (PP_{DOC}) also presented a strong relationship with $p\text{CO}_2$, but a positive one. No statistically significant correlations with $p\text{CO}_2$ concentrations were found with the remaining parameters in phase I.

After nutrient fertilization in t_{24} , the majority of the CO₂ correlations (23 out of 26) were statistically significant and mostly positive (Tables 2 – 4). Fractionated primary production, biomass and chlorophyll, as well as PP_{POC} , B_{Tot} and Chl_{Tot} were positively related to increasing $p\text{CO}_2$ (except PP_{Nano}) in phase II. PP_{DOC} was statistically correlated with $p\text{CO}_2$ in phase III but not in phase II. We also observed strong significant and positive correlations between $p\text{CO}_2$ and both total and size-fractionated primary production,

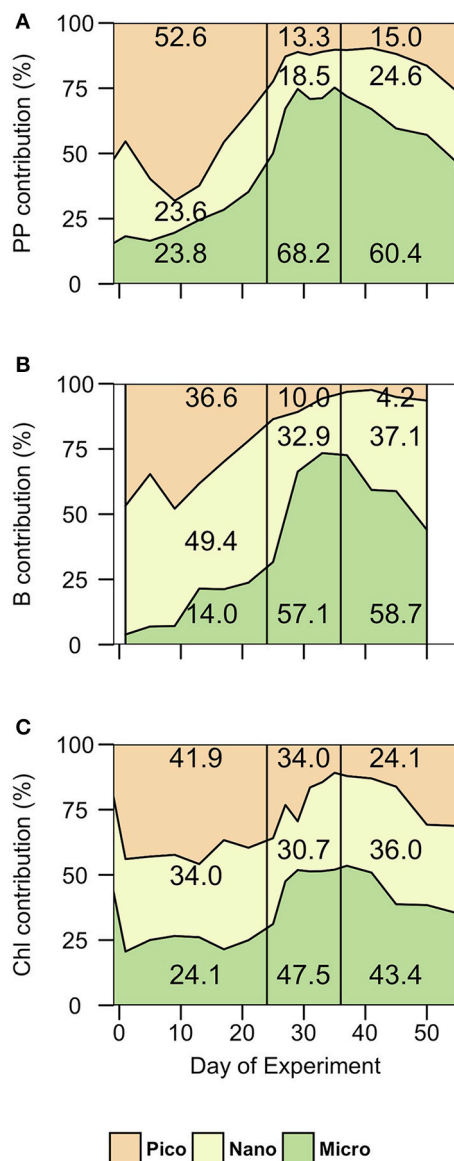


FIGURE 5 | Contribution (%) of each size fraction to (A) total particulate primary production (PP), (B) total biomass, and (C) total chlorophyll (Chl) in phase I (t_1 - t_{24}), phase II (t_{25} - t_{35}) and phase III (t_{36} - t_{55}). Micro, microplankton; Nano, nanoplankton; Pico, picoplankton.

biomass and chlorophyll during phase III (except in the Pico fraction).

DISCUSSION

CO₂ and Nutrient Impacts on Phytoplankton Biomass and Productivity

The eight mesocosms during phase I displayed similar behaviors to the Atlantic ambient waters, showing a phytoplankton community dominated in terms of biomass by small picophytoplankton and nanophytoplankton (Figure 5),

characteristic of the oligotrophic subtropical northeast Atlantic (Zubkov et al., 2000a,b; Aristegui and Montero, 2005; Figueiras et al., 2016), although with somewhat higher primary production and biomass.

Due to the low nutrient concentrations, PP_{POC} was low and relatively stable during phase I, showing no significant relationship with $p\text{CO}_2$. Although, theoretically, carbon fixation should be enhanced by high $p\text{CO}_2$ levels (Giordano et al., 2005; Reinfelder, 2011), the absence of a response of primary production to increasing CO₂ in oligotrophic waters dominated by small phytoplankton has been reported by other authors (Yoshimura et al., 2009; Maudendire et al., 2017). Surprisingly, both chlorophyll and biomass decreased with increasing $p\text{CO}_2$ during phase I (Tables 3, 4), even though primary production remained rather stable. Engel et al. (2013) observed the same behavior in a similar mesocosms study in Arctic waters. They hypothesized that either the enhancement of particle aggregation and settling as a consequence of increasing Transparent Exopolymer Particles (TEP), the increase in remineralization of phytoplankton cells, the nutrient competition between auto- and heterotrophic organisms, or a combination of the preceding processes, could explain the mismatch between PP_{POC} and its accumulation as biomass. Due to the lack of response of TEPs to increasing $p\text{CO}_2$ in our experiment (data not shown), the first hypothesis would not apply in our case. A more likely explanation would be that a fraction of primary production is channeled through the dissolved fraction increasing the DOC pool inside the mesocosms. This hypothesis agrees with both the observed higher values of PP_{DOC} in the high-CO₂ mesocosms, and the increase in DOC from t_3 to t_{23} reported by Zark et al. (2017) in this same study.

Nutrient fertilization triggered autotrophic phytoplankton community growth, with higher maximum biomass build-up in the high-CO₂ mesocosms. The bloom that occurred during phase II, coincided with an increase in primary production and biomass inside all mesocosms. As a consequence, major nutrients were depleted to values similar (such as $\text{NO}_3^- + \text{NO}_2^-$ and PO_4^{3-}) or lower (Si(OH)_4) to phase I. Linear regressions between PP_{POC}, B_{Tot} and Chl_{Tot} vs $p\text{CO}_2$ revealed significantly positive relationships in phase II, although the strongest relationships of PP_{POC}, B_{Tot} and Chl_{Tot} vs $p\text{CO}_2$ occurred in phase III. A positive effect of increasing $p\text{CO}_2$ in seawater on primary production has been reported by other authors, from single species' experiments (Beardal and Raven, 2004; Fu et al., 2007; Sobrino et al., 2008) to whole community level experiments (Egge et al., 2009; Engel et al., 2013). The positive effect of enhanced $p\text{CO}_2$ on primary production has been attributed to the relieve of CO₂ limitation of RubisCO (Giordano et al., 2005; Riebesell et al., 2007; Reinfelder, 2011; Mackey et al., 2015). The increase in the availability of CO₂ should thus produce an increase in photosynthetic rates, by relieving carbon limitation, or indirectly by lowering the energy required to concentrate CO₂ against a smaller concentration gradient.

In summary, our results show that all the positive significant correlations between plankton productivity and biomass and

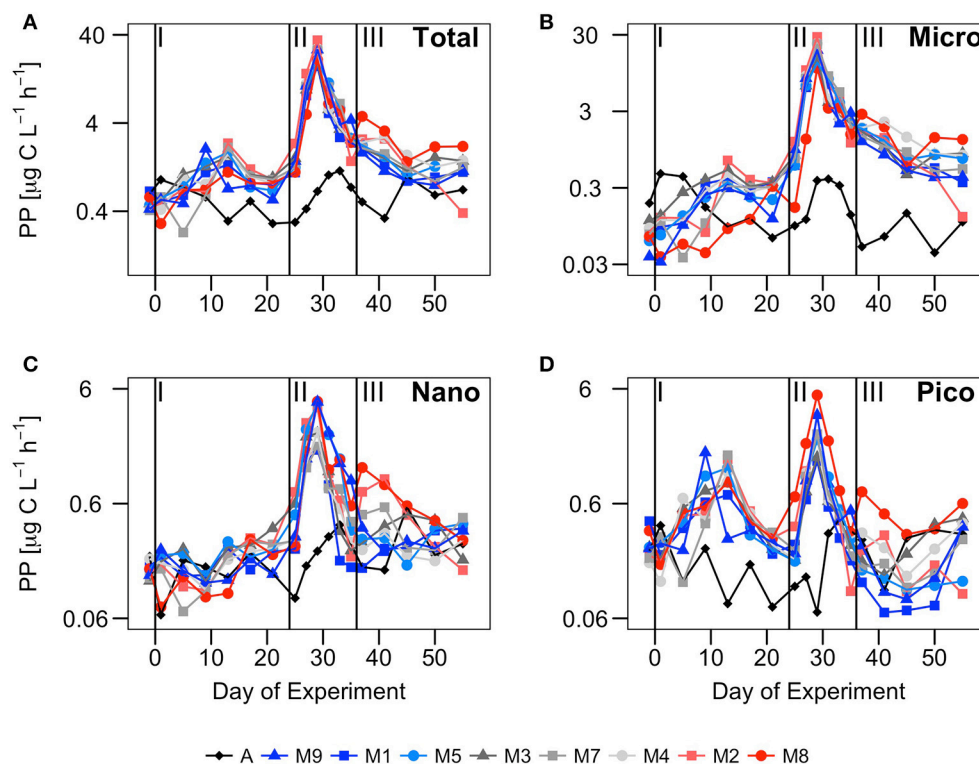


FIGURE 6 | Temporal development of primary production ($\mu\text{g C L}^{-1} \text{h}^{-1}$) in (A) the total particulate fraction (Total), and in the (B) microplankton (Micro), (C) nanoplankton (Nano) and (D) picoplankton (Pico) size fractions, over the course of the experiment. Vertical lines defined the three phases of the experiment. PP is represented in log scale to better illustrate the differences among mesocosms.

$p\text{CO}_2$ occur after nutrients addition, suggesting a synergistic effect of nutrients and CO₂. Indeed, as far as we know, the only ocean acidification mesocosm study carried out to test primary production responses in oligotrophic regions, report non-statistically significant effects of increasing $p\text{CO}_2$ on primary production under nutrient depleted conditions (Maugendre et al., 2017).

Community Structure Response to Elevated CO₂ and Nutrient Fertilization

During phase I, Pico contributed > 40% to Chl and > 50% to primary production, although Nano was the dominant size fraction in terms of biomass. A marked change in the phytoplankton community occurred after the fertilization through deep-water addition at the beginning of phase II and during phase III, where the community shifted to larger microphytoplankton (mostly diatoms; Taucher et al., 2017) with > 57% dominance in biomass and > 60% in primary production (Figure 5). Changes from small to large size fractions of phytoplankton have been described in the Canary Islands region, associated with transitional changes from oligotrophic to eutrophic conditions across upwelling filaments, eddies and fronts (Basterretxea and Arístegui, 2000; Arístegui et al., 2004).

Our results show that phytoplankton size-groups generally remained unresponsive during phase I to the increases in $p\text{CO}_2$, whereas all of them benefitted from the nutrient addition. This disagrees with a study by Egge et al. (2009), who reported non-significant changes in primary production among size fractions in a mesocosm experiment in Bergen (Norway), although differences in chlorophyll and biomass at group level have been observed during other mesocosm experiments (Brussaard et al., 2013; Schulz et al., 2017). For this present study, Taucher et al. (2017), using a non-metric multidimensional scaling (NMDS) analysis, described a significant effect of CO₂ on the whole planktonic community (including protozoa and mesozooplankton). The effect is apparent even in phase I, but became more pronounced after nutrient fertilization. They reported that the response of the community structure to CO₂ treatments emerges not from one or two dominant species but from overall shifts across the entire plankton community. At the phytoplankton level, we find in most cases a significant effect of CO₂ on primary production, biomass and chlorophyll *a* in all the size fractions during phases II and III, pointing to a size independent stimulation of nutrients and CO₂ over all the phytoplankton groups, which particularly benefited the increase of diatoms in absolute terms (Taucher et al., 2017). However, a closer look to the linear correlations reveals significant differences among regression

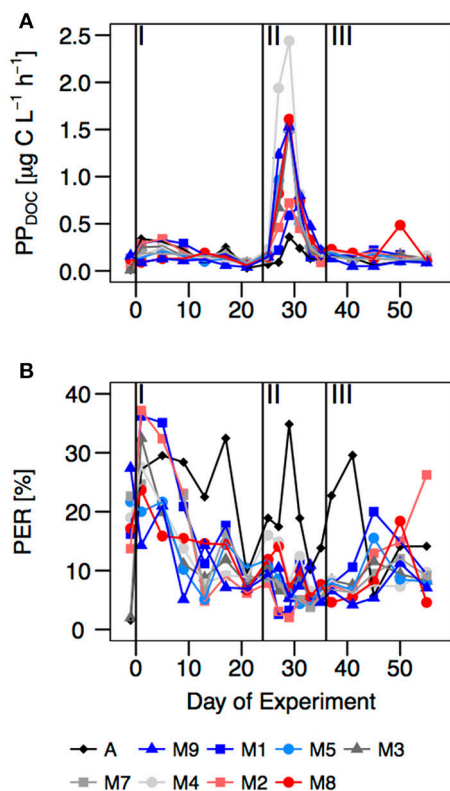


FIGURE 7 | Temporal development of **(A)** rates of dissolved primary production (PP_{DOC}) ($\mu\text{g C L}^{-1} \cdot \text{h}^{-1}$) and **(B)** the percentage of extracellular release (PER) (%) [$(PP_{DOC}/PP_{DOC}) \cdot 100$] over the course of the experiment. Vertical lines separate the three phases of the experiment.

slopes, indicating differences in size fractions responses. Indeed, the relative increase of primary production after nutrient additions display a clear size-related pattern, where small PP_{Pico} was enhanced about 250%, PP_{Nano} up to 150% and PP_{Micro} about 100% in the two high- CO_2 mesocosms compared to the two low- CO_2 mesocosms. Surprisingly, the highest relative change in biomass was observed in B_{Micro} followed by B_{Nano} and B_{Pico} . This could be partly explained by a more intense grazing pressure on the smallest size fractions compared to the largest ones.

A number of experimental and modeling studies have suggested the existence of potential winners and losers in a future acidified ocean (Dutkiewicz et al., 2013; Kroeker et al., 2013; Bach et al., 2017). In our mesocosm experiment, the shift from a cyanobacteria-dominated community to a large diatom-dominated community in the high CO_2 scenarios after nutrient fertilization, as well as the distinct size-related relative change observed among size-fractions, seems to support this hypothesis. Nevertheless, the fact that all phytoplankton size classes increased after nutrient addition in high CO_2 treatments, suggests that the entire phytoplankton community in subtropical regions would benefit in an acidified and patchily fertilized ocean, although larger cells could outcompete the smaller ones under high nutrient inputs.

TABLE 2 | Linear regressions statistics of the relationship between average primary production in the total particulate (PP_{POC}) and different size fractions (PP_{Micro} , PP_{Nano} , PP_{Pico}), as well as in the total dissolved fraction (PP_{DOC}), vs. pCO_2 levels for the three experimental phases.

	Parameter	Slope ($\times 10^4$)	R ²	F statistic	p-value
Phase I	PP_{POC}	-3.92 ± 2.11	0.02	3.45	0.11
Phase II		127.00 ± 36.00	0.70	12.27	0.03
Phase III		21.00 ± 5.57	0.64	14.74	<0.01
Phase I	PP_{Micro}	-2.39 ± 1.22	0.05	3.83	0.10
Phase II		95.00 ± 29.00	0.59	10.68	0.02
Phase III		13.00 ± 4.41	0.43	8.71	0.03
Phase I	PP_{Nano}	-0.94 ± 0.45	0.10	4.36	0.08
Phase II		24.00 ± 13.00	0.01	3.17	0.13
Phase III		6.27 ± 1.64	0.63	14.63	<0.01
Phase I	PP_{Pico}	1.75 ± 0.92	0.03	3.61	0.11
Phase II		23.00 ± 6.29	0.66	13.28	0.02
Phase III		5.17 ± 1.70	0.46	9.30	0.02
Phase I	PP_{DOC}	1.50 ± 0.47	0.65	10.25	0.03
Phase II		11.00 ± 5.92	0.01	3.21	0.12
Phase III		1.74 ± 0.53	0.51	10.60	0.02

Statistically significant correlations are indicated in bold.

TABLE 3 | Linear regressions statistics of the relationship between average total community biomass (B_{Tot}) and the biomass of the different size fractions (B_{Micro} , B_{Nano} , B_{Pico}) vs. pCO_2 levels for the three experimental phases.

	Parameter	Slope ($\times 10^4$)	R ²	F statistic	p-value
Phase I	B_{Tot}	-0.86 ± 0.43	0.07	4.07	0.09
Phase II		40.96 ± 7.15	0.83	32.86	<0.01
Phase III		53.75 ± 12.12	0.72	19.68	<0.01
Phase I	B_{Micro}	0.59 ± 0.29	0.07	4.07	0.09
Phase II		27.49 ± 5.69	0.76	23.37	<0.01
Phase III		48.89 ± 11.27	0.71	18.83	<0.01
Phase I	B_{Nano}	-0.55 ± 0.16	0.57	12.27	0.01
Phase II		11.96 ± 2.75	0.71	18.87	<0.01
Phase III		6.28 ± 2.10	0.44	8.94	0.02
Phase I	B_{Pico}	0.21 ± 0.11	0.02	3.51	0.11
Phase II		2.37 ± 0.41	0.85	32.87	<0.01
Phase III		0.64 ± 0.32	0.06	3.91	0.10

Statistically significant correlations are indicated in bold.

Biogeochemical Implications

Oligotrophic regions are expanding at an annual rate of 0.8–4.3%, with the North Atlantic subtropical Gyre showing the fastest annual expansion (Sarmiento et al., 2004; Polovina et al., 2008). Approximately 0.8 million km² of productive waters are being replaced annually by warmer stratified oligotrophic waters. Most models predict a decline in primary production as well as in

TABLE 4 | Linear regressions statistics of the relationship between average total community chlorophyll *a* (Chl_{Tot}) and the chlorophyll of the different size fractions (Chl_{Micro}, Chl_{Nano}, Chl_{Pico}) vs. *p*CO₂ levels for the three experimental phases.

	Parameter	Slope (x10 ⁴)	R ²	F statistic	p-value
Phase I	Chl _{Tot}	-1.27 ± 0.30	0.74	18.22	<0.01
Phase II		14.00 ± 4.98	0.46	7.74	0.04
Phase III		8.51 ± 1.92	0.72	19.72	<0.01
Phase I	Chl _{Micro}	-0.38 ± 0.14	0.47	7.87	0.04
Phase II		-5.39 ± 2.24	0.24	5.83	0.05
Phase III		3.33 ± 0.47	0.88	49.70	<0.01
Phase I	Chl _{Nano}	-0.53 ± 0.14	0.71	15.64	0.01
Phase II		8.34 ± 3.08	0.43	7.33	0.04
Phase III		4.77 ± 1.33	0.59	12.90	0.01
Phase I	Chl _{Pico}	-0.39 ± 0.11	0.58	12.46	0.01
Phase II		9.20 ± 3.83	0.32	5.79	0.06
Phase III		2.21 ± 1.15	0.04	3.71	0.10

Statistically significant correlations are indicated in bold.

the downward carbon fluxes in these regions by the end of the century (Riebesell et al., 2009; Gruber, 2011; Bopp et al., 2013), due to a reduction of vertical nutrient supply related with the shoaling of the mixed layer depth (Bopp et al., 2001; Marinov et al., 2010; Steinacher et al., 2010). Nevertheless, these models do not take into account the effect of mesoscale and submesoscale processes, such as eddies or fronts, which are known to play a key role in enhancing primary production (e.g. McGillicuddy et al., 2007; Sangrà et al., 2009) and export fluxes (Omand et al., 2015) in the ocean. Under an scenario of an acidified and warmer ocean, leading to an intensification of cross-shore wind gradients and eddy kinetic energy across eastern boundary regions (Bakun, 1990; Sydeman et al., 2014; García-Reyes et al., 2015), mesoscale variability would increase mixing and upwelling of deeper nutrient-rich water into the euphotic zone (Renault et al., 2016; Xiu et al., 2018). Our data suggest that a patchy nutrient pumping in a more acidified ocean would increase primary productivity in subtropical warm regions. Furthermore, community structure would shift from small to large cells, like diatoms, potentially leading to a more efficient carbon export to the deep ocean. The concomitant increase in dissolved organic carbon production (PP_{DOC}) may also contribute to the biological carbon pump, through particle aggregation and the subsequent increase of sinking rates (Engel et al., 2004, 2014; Schartau et al., 2007).

It has been estimated that mesoscale and submesoscale features account for 20–30% of the new primary production in the world's ocean (McGillicuddy et al., 2007). If global warming reinforces wind regimes in eastern boundary regions as predicted (Bakun, 1990; Sydeman et al., 2014), increasing the eddy kinetic energy field, new production could increase as well, counteracting the effect of enhanced stratification in subtropical regions. Nevertheless, further research is needed to constrain the synergistic or antagonistic effects of climate drivers on primary

production and plankton community structure in subtropical oligotrophic waters, the most extensive ecosystems of the world's ocean.

CONCLUSIONS

This is the first mesocosm study addressing the response, in terms of primary production and community structure, of size-fractionated (0.2–2, 2–20, and >20 μm) natural plankton communities in subtropical oligotrophic regions to increasing CO₂ concentrations and nutrient fertilization. Our results reveal a non-significant CO₂-related effect on PP and B under nutrient depleted conditions, with a phytoplankton dominance of small cyanobacteria. After nutrient fertilization, however, the community shifts toward larger phytoplankton, with a diatom-dominated community, showing a significant marked increase in PP, B and chlorophyll under higher CO₂ conditions in all groups. Our data suggest that in a future acidified subtropical ocean, mesoscale and submesoscale features—which are predicted to enhance under global warming in eastern boundary regions—would drive nutrient pumping to the surface ocean favoring the development of diatoms and increasing new production in the global ocean.

AUTHOR CONTRIBUTIONS

UR and JA: conceived and designed the experiment. All authors performed the experiment and analyzed the data. Wrote the paper: NH-H and JA with inputs from all co-authors.

FUNDING

The KOSMOS project was funded by the German Federal Ministry of Education and Research (BMBF) in the framework of the coordinated project BIOACID—Biological Impacts of Ocean Acidification, phase 2 (FKZ 03F06550). UR received additional funding from the Leibniz Award 2012 by the German Research Foundation (DFG). The Natural Environment Research Council provided funding for EA and ME as part of the UK Ocean Acidification Programme (NE/H017348/1). JA was supported by a Helmholtz International Fellow Award, 2015 (Helmholtz Association, Germany). NH-H was partially supported by KOSMOS funding during the experimental work, and by a grant of the Agencia Canaria de Investigación, Innovación y Sociedad de la Información (ACIISI) during the writing stage (TESIS2015010036). IB was supported by a FPI fellowship (BES-2016-078407) from the Spanish Ministry of Economy, Industry and Competitiveness (MINECO). NH-H, MM, IB, and JA benefited also from the FLUXES project (CTM2015-69392-C3-1-R) funded by the Spanish government (Plan Nacional I+D).

ACKNOWLEDGMENTS

We would like to thank the KOSMOS and the Plataforma Oceánica de Canarias (PLOCAN) teams assisting with

all aspects of the organization and logistical support before, during and after this mesocosms campaign, as well as to Minerva Espino and Acorayda González

(IOCAG, ULPGC) for their technical support in the sampling and analyses of phytoplankton and productivity data.

REFERENCES

- Aristegui, J., Barton, E. D., Tett, P., Montero, M. F., García-Muñoz, M., Basterretxea, G., et al. (2004). Variability in plankton community structure, metabolism, and vertical carbon fluxes along an upwelling filament (Cape Juby, NW Africa). *Prog. Oceanogr.* 62, 95–113. doi: 10.1016/j.pcean.2004.07.004
- Aristegui, J., and Montero, M. F. (2005). Temporal and spatial changes in plankton respiration and biomass in the Canary Islands region: the effect of mesoscale variability. *J. Mar. Syst.* 54, 65–82. doi: 10.1016/j.jmarsys.2004.07.004
- Bach, L. T., Alvarez-Fernandez, S., Hornick, T., Stühr, A., and Riebesell, U. (2017). Simulated ocean acidification reveals winners and losers in coastal phytoplankton. *PLoS ONE* 12:e0188198. doi: 10.1371/journal.pone.0188198
- Bakun, A. (1990). Global climate change and intensification of coastal ocean upwelling. *Science* 247, 198–201. doi: 10.1126/science.247.4939.198
- Basterretxea, G., and Aristegui, J. (2000). Mesoscale variability in phytoplankton biomass distribution and photosynthetic parameters in the Canary-NW African coastal transition zone. *Mar. Ecol. Prog. Ser.* 197, 27–40. doi: 10.3354/meps197027
- Beardal, J., and Raven, J. A. (2004). The potential effects of global climate change on microalgal photosynthesis, growth and ecology. *Phycologia* 43, 26–40. doi: 10.2216/10031-8884-43-1-26.1
- Behrenfeld, M. J., O'Malley, R. T., Siegel, D. A., McClain, C. R., Sarmiento, J. L., Feldman, G. C., et al. (2006). Climate-driven trends in contemporary ocean productivity. *Nature* 444, 752–755. doi: 10.1038/nature05317
- Behrenfeld, M. J., Randerson, J. T., McClain, C. R., Feldman, G. C., Los, S. O., Tucker, C. J., et al. (2001). Biospheric primary production during an ENSO transition. *Science* 291, 2594–2597. doi: 10.1126/science.1055071
- Bellerby, R. G. J., Schulz, K. G., Riebesell, U., Neill, C., Nondal, G., Heegaard, E., et al. (2008). Marine ecosystem community carbon and nutrient uptake stoichiometry under varying ocean acidification during the PeECE III experiment. *Biogeosciences* 5, 1517–1527. doi: 10.5194/bg-5-1517-2008
- Bopp, L., Monfray, P., Aumont, O., Dufresne, J.-L., Le Treut, H., Madec, G., et al. (2001). Potential impact of climate change on marine export production. *Global Biogeochem. Cycles* 15, 81–99. doi: 10.1029/1999GB001256
- Bopp, L., Resplandy, L., Orr, J. C., Doney, S. C., Dunne, J. P., Gehlen, M., et al. (2013). Multiple stressors of ocean ecosystems in the 21st century: projections with CMIP5 models. *Biogeosciences* 10, 6225–6245. doi: 10.5194/bg-10-6225-2013
- Borsheim, K. Y., and Bratbak, G. (1987). bacterivorous *Monas* sp. enriched from seawater. *Mar. Ecol. Prog. Ser.* 36, 171–175. doi: 10.3354/meps036171
- Brussaard, C. P. D., Noordeloos, A. A. M., Witte, H., Collenteur, M. C. J., Schulz, K., Ludwig, A., et al. (2013). Arctic microbial community dynamics influenced by elevated CO₂ levels. *Biogeosciences* 10, 719–731. doi: 10.5194/bg-10-719-2013
- Caldeira, K., and Wickett, M. E. (2003). Oceanography: anthropogenic carbon and ocean pH. *Nature* 425, 365–365. doi: 10.1038/425365a
- Delille, B., Harlay, J., Zondervan, I., Jacquet, S., Chou, L., Wollast, R., et al. (2005). Response of primary production and calcification to changes of pCO₂ during experimental blooms of the coccolithophorid *Emiliania huxleyi*. *Global Biogeochem. Cycles* 19, 1–14. doi: 10.1029/2004GB002318
- Doney, S. C., Ruckelshaus, M., Emmett Duffy, J., Barry, J. P., Chan, F., English, C. A., et al. (2012). Climate change impacts on marine ecosystems. *Ann. Rev. Mar. Sci.* 4, 11–37. doi: 10.1146/annurev-marine-041911-111611
- Dubelaar, G. B. J., and Gerritsen, P. L. (2000). Cytobuoy: a step forward towards using flow cytometry in operational oceanography. *Sci. Mar.* 64, 255–265. doi: 10.3989/scimar.2000.64n2255
- Dutkiewicz, S., Scott, J. R., and Follows, M. J. (2013). Winners and losers: ecological and biogeochemical changes in a warming ocean. *Global Biogeochem. Cycles* 27, 463–477. doi: 10.1002/gbc.20042
- Eberlein, T., Wohlrab, S., Rost, B., John, U., Bach, L. T., Riebesell, U., et al. (2017). Effects of ocean acidification on primary production in a coastal North Sea phytoplankton community. *PLoS ONE* 12:e0172594. doi: 10.1371/journal.pone.0172594
- Egge, J. K., Thingstad, T. F., Engel, A., Bellerby, R. G. J., Riebesell, U., Larsen, A., et al. (2009). Primary production during nutrient-induced blooms at elevated CO₂ concentrations. *Biogeosciences* 6, 877–885. doi: 10.5194/bg-6-877-2009
- Engel, A., Borchard, C., Piontek, J., Schulz, K. G., Riebesell, U., and Bellerby, R. (2013). CO₂ increases ¹⁴C primary production in an Arctic plankton community. *Biogeosciences* 10, 1291–1308. doi: 10.5194/bg-10-1291-2013
- Engel, A., Delille, B., Jacquet, S., Riebesell, U., Rochelle-newall, E., Terbrüggen, A., et al. (2004). Transparent exopolymer particles and dissolved organic carbon production by *Emiliania huxleyi* exposed to different CO₂ concentrations : a mesocosm experiment. *Aquat. Microb. Ecol.* 34, 93–104. doi: 10.3354/ame034093
- Engel, A., Piontek, J., Grossart, H. P., Riebesell, U., Schulz, K. G., and Sperling, M. (2014). Impact of CO₂ enrichment on organic matter dynamics during nutrient induced coastal phytoplankton blooms. *J. Plankton Res.* 36, 641–657. doi: 10.1093/plankt/ftt125
- Falkowski, P. G. (1994). The role of phytoplankton photosynthesis in global biogeochemical cycles. *Photosyn. Res.* 39, 235–258. doi: 10.1007/BF00014586
- Falkowski, P., Scholes, R. J., Boyle, E., Canadell, J., Canfield, D., Elser, J., et al. (2000). The global carbon cycle: a test of our knowledge of earth as a system. *Science* 290, 291–296. doi: 10.1126/science.290.5490.291
- Feng, Y., Hare, C. E., Leblanc, K., Rose, J. M., Zhang, Y., DiTullio, G. R., et al. (2009). Effects of increased pCO₂ and temperature on the north atlantic spring bloom. I. the phytoplankton community and biogeochemical response. *Mar. Ecol. Prog. Ser.* 388, 13–25. doi: 10.3354/meps08133
- Field, C. B., Behrenfeld, M. J., Randerson, J. T., and Falkowski, P. (1998). Primary production of the biosphere: integrating terrestrial and oceanic components. *Science* 281, 237–240. doi: 10.1126/science.281.5374.237
- Figueiras, F. G., Arbones, B., Montero, M. F., Barton, E. D., and Aristegui, J. (2016). Photophysiological variability and its influence on primary production in the NW Africa-Canary Islands coastal transition zone. *J. Mar. Syst.* 157, 92–100. doi: 10.1016/j.jmarsys.2016.01.003
- Fu, F. X., Warner, M. E., Zhang, Y., Feng, Y., and Hutchins, D. A. (2007). Effects of increased temperature and CO₂ on photosynthesis, growth, and elemental ratios in marine *Synechococcus* and *Prochlorococcus* (Cyanobacteria). *J. Phycol.* 43, 485–496. doi: 10.1111/j.1529-8817.2007.00355.x
- García-Reyes, M., Sydeman, W. J., Schoeman, D. S., Rykaczewski, R. R., Black, B. A., Smit, A. J., et al. (2015). Under pressure: climate change, upwelling, and eastern boundary upwelling ecosystems. *Front. Mar. Sci.* 2:109. doi: 10.3389/fmars.2015.00109
- Giordano, M., Beardall, J., and Raven, J. A. (2005). CO₂ concentrating mechanisms, environmental modulation, and evolution. *Annu. Rev. Plant Biol.* 56, 99–131. doi: 10.1146/annurev-arplant.56.032604.144052
- Gruber, N. (2011). Warming up, turning sour, losing breath: ocean biogeochemistry under global change. *Philos. Trans. R. Soc. A Math. Phys. Eng. Sci.* 369, 1980–1996. doi: 10.1098/rsta.2011.0003
- Hansen, H. P., and Grasshoff, K. (1983). “Automated chemical analysis,” in *Methods of Seawater Analysis*, eds K. Grasshoff, M. Ehrhardt, and K. Kremling (Weinheim: Verlag Chemie), 347–379.
- Hare, C. E., Leblanc, K., DiTullio, G. R., Kudela, R. M., Zhang, Y., Lee, P. A., et al. (2007). Consequences of increased temperature and CO₂ for phytoplankton community structure in the Bering Sea. *Mar. Ecol. Prog. Ser.* 352, 9–16. doi: 10.3354/meps07182
- Hein, M., and Sand-Jensen, K. (1997). CO₂ increases oceanic primary production. *Nature* 388, 526–527. doi: 10.1038/41457
- Holmes, R. M., Aminot, A., Kérouel, R., Hooker, B. A., and Peterson, B. J. (1999). A simple and precise method for measuring ammonium in marine and freshwater ecosystems. *Can. J. Fish. Aquat. Sci.* 56, 1801–1808. doi: 10.1139/f99-128

- Holm-Hansen, O., Lorenzen, C. J., Holmes, R. W., and Strickland, D. H. (1965). Fluorometric determination of chlorophyll. *ICES J. Mar. Sci.* 30, 3–15. doi: 10.1093/icesjms/30.1.3
- IPCC (2014). *Climate Change: 2014: Impacts, Adaption, and Vulnerability. Part A: Global and Sectoral Aspects. Contribution of Working Group II to the Fifth Assessment Report of the Intergovernmental Panel on Climate Change*. Cambridge, UK; New York, NY: Cambridge University Press.
- Kroeker, K. J., Kordas, R. L., Crim, R., Hendriks, I. E., Ramajo, L., Singh, G. S., et al. (2013). Impacts of ocean acidification on marine organisms: quantifying sensitivities and interaction with warming. *Glob. Chang. Biol.* 19, 1884–1896. doi: 10.1111/gcb.12179
- Lomas, M. W., Hopkinson, B. M., Losh, J. L., Ryan, D. E., Shi, D. L., Xu, Y., et al. (2012). Effect of ocean acidification on cyanobacteria in the subtropical North Atlantic. *Aquat. Microb. Ecol.* 66, 211–222. doi: 10.3354/ame01576
- Longhurst, A., Sathyendranath, S., Platt, T., and Caverhill, C. (1995). An estimate of global primary production in the ocean from satellite radiometer data. *J. Plankton Res.* 17, 1245–1271. doi: 10.1093/plankt/17.6.1245
- Lueker, T. J., Dickson, A. G., and Keeling, C. D. (2000). Ocean pCO₂ calculated from dissolved inorganic carbon, alkalinity, and equations for K₁ and K₂: validation based on laboratory measurements of CO₂ in gas and seawater at equilibrium. *Mar. Chem.* 70, 105–119. doi: 10.1016/S0304-4203(00)0022-0
- Mackey, K. R. M., Morris, J. J., Morel, F. M. M., and Kranz, S. A. (2015). Response of photosynthesis to ocean acidification. *Oceanography* 28, 74–91. doi: 10.5670/oceanog.2015.33
- Marinov, I., Doney, S. C., and Lima, I. D. (2010). Response of ocean phytoplankton community structure to climate change over the 21st century: partitioning the effects of nutrients, temperature and light. *Biogeosciences* 7, 3941–3959. doi: 10.5194/bg-7-3941-2010
- Maugendre, L., Gattuso, J. P., Poulton, A. J., Dellisanti, W., Gaubert, M., Guieu, C., et al. (2017). No detectable effect of ocean acidification on plankton metabolism in the NW oligotrophic Mediterranean Sea: results from two mesocosm studies. *Estuar. Coast. Shelf Sci.* 186, 89–99. doi: 10.1016/j.ecss.2015.03.009
- McGillicuddy, D. J., Anderson, L. A., Bates, N. R., Buesseler, K. O., Carlson, C. A., Davis, C. S., et al. (2007). Eddy/Wind interactions stimulate extraordinary mid-ocean blooms. *Science* 316, 1021–1026. doi: 10.1126/science.1136256
- Menden-Deuer, S., and Lessard, E. J. (2000). Carbon to volume relationships for dinoflagellates, diatoms, and other protist plankton. *Limnol. Oceanogr.* 45, 569–579. doi: 10.4319/lo.2000.45.3.0569
- Murphy, J., and Riley, J. P. (1962). A modified single solution method for the determination of phosphate in natural waters. *Anal. Chem. Acta* 27, 31–36. doi: 10.1016/S0003-2670(00)88444-5
- Omand, M. M., D'Asaro, E. A., Lee, C. M., Perry, M. J., Briggs, N., Cetini, I., et al. (2015). Eddy-driven subduction exports particulate organic carbon from the spring bloom. *Science* 348, 222–225. doi: 10.1126/science.1260062
- Pierrot, D. E., Lewis, E., and Wallace, D. W. R. (2006). *MS Excel Program Developed for CO₂ System Calculations*. Oak Ridge, TN: Carbon Dioxide Information Analysis Center (CDIAC).
- Polovina, J. J., Howell, E. A., and Abecassis, M. (2008). Ocean's least productive waters are expanding. *Geophys. Res. Lett.* 35, 2–6. doi: 10.1029/2007GL031745
- Reinfielder, J. R. (2011). Carbon concentrating mechanisms in eukaryotic marine phytoplankton. *Ann. Rev. Mar. Sci.* 3, 291–315. doi: 10.1146/annurev-marine-120709-142720
- Renault, L., Deutsch, C., McWilliams, J. C., Frenzel, H., Liang, J.-H., and Colas, F. (2016). Partial decoupling of primary productivity from upwelling in the California current system. *Nat. Geosci.* 9, 505–508. doi: 10.1038/ng eo2722
- Riebesell, U., Czerny, J., Von Bröckel, K., Boxhammer, T., Büdenbender, J., Deckelnick, M., et al. (2013). Technical Note: a mobile sea-going mesocosm system-New opportunities for ocean change research. *Biogeosciences* 10, 1835–1847. doi: 10.5194/bg-10-1835-2013
- Riebesell, U., and Gattuso, J.-P. (2015). Lessons learned from ocean acidification research. *Nat. Clim. Chang.* 5, 12–14. doi: 10.1038/nclimate2456
- Riebesell, U., Kortzinger, A., and Oschlies, A. (2009). Sensitivities of marine carbon fluxes to ocean change. *Proc. Natl. Acad. Sci. U.S.A.* 106, 20602–20609. doi: 10.1073/pnas.0813291106
- Riebesell, U., Schulz, K. G., Bellerby, R. G. J., Botros, M., Fritsche, P., Meyerhöfer, M., et al. (2007). Enhanced biological carbon consumption in a high CO₂ ocean. *Nature* 450, 545–548. doi: 10.1038/nature 06267
- Sangrà, P., Pascual, A., Rodríguez-Santana, Á., Machín, F., Mason, E., McWilliams, J. C., et al. (2009). The Canary Eddy Corridor: a major pathway for long-lived eddies in the subtropical North Atlantic. *Deep. Res. I Oceanogr. Res. Pap.* 56, 2100–2114. doi: 10.1016/j.dsr.2009.08.008
- Sarmiento, J. L., Slater, R., Barber, R., Bopp, L., Doney, S. C., Hirst, A. C., et al. (2004). Response of ocean ecosystems to climate warming. *Global Biogeochem. Cycles* 18:GB3003. doi: 10.1029/2003GB002134
- Schartau, M., Engel, A., Schröter, J., Thoms, S., Völker, C., and Wolf-Gladrow, D. (2007). Modelling carbon overconsumption and the formation of extracellular particulate organic carbon. *Biogeosciences* 4, 433–454. doi: 10.5194/bg-4-433-2007
- Schulz, K. G., Bach, L. T., Bellerby, R. G. J., Bermúdez, R., Büdenbender, J., Boxhammer, T., et al. (2017). Phytoplankton blooms at increasing levels of atmospheric carbon dioxide: experimental evidence for negative effects on prymnesiophytes and positive on small picoeukaryotes. *Front. Mar. Sci.* 4:64. doi: 10.3389/fmars.2017.00064
- Sobrinho, C., Ward, M. L., and Neale, P. J. (2008). Acclimation to elevated carbon dioxide and ultraviolet radiation in the diatom *Thalassiosira pseudonana*: effects on growth, photosynthesis, and spectral sensitivity of photoinhibition. *Limnol. Oceanogr.* 53, 494–505. doi: 10.4319/lo.2008.53.2.0494
- Sokal, R. R., and Rohlf, F. J. (eds.). (2013). *Biometry: The Principles and Practice of Statistics in Biological Research*. New York, NY: W. H. Freeman and Co.
- Steinacher, M., Joos, F., Frölicher, T. L., Bopp, L., Cadule, P., Cocco, V., et al. (2010). Projected 21st century decrease in marine productivity: a multi-model analysis. *Biogeosciences* 7, 979–1005. doi: 10.5194/bg-7-979-2010
- Sydesman, W. J., Garcia-Reyes, M., Schoeman, D. S., Rykaczewski, R. R., Thompson, S. A., Black, B. A., et al. (2014). Climate change and wind intensification in coastal upwelling ecosystems. *Science* 345, 77–80. doi: 10.1126/science.1251635
- Tanaka, T., Alliouane, S., Bellerby, R. G. B., Czerny, J., De Kluijver, A., Riebesell, U., et al. (2013). Effect of increased pCO₂ on the planktonic metabolic balance during a mesocosm experiment in an Arctic fjord. *Biogeosciences* 10, 315–325. doi: 10.5194/bg-10-315-2013
- Taucher, J., Bach, L. T., Boxhammer, T., Nauendorf, A., Achterberg, E. P., Algueró-Muñiz, M., et al. (2017). Influence of ocean acidification and deep water upwelling on oligotrophic plankton communities in the subtropical north atlantic: insights from an *in situ* mesocosm study. *Front. Mar. Sci.* 4:85. doi: 10.3389/fmars.2017.00085
- Tortell, P. D., DiTullio, G. R., Sigman, D. M., and Morel, F. M. M. (2002). CO₂ effects on taxonomic composition and nutrient utilization in an Equatorial Pacific phytoplankton assemblage. *Mar. Ecol. Prog. Ser.* 236, 37–43. doi: 10.3354/meps236037
- Tortell, P. D., Payne, C. D., Li, Y., Trimborn, S., Rost, B., Smith, W. O., et al. (2008). CO₂ sensitivity of southern ocean phytoplankton. *Geophys. Res. Lett.* 35, 1–5. doi: 10.1029/2007GL032583
- Utermöhl, H. (1931). Neue Wege in der quantitativen Erfassung des Plankton. (Mit besonderer Berücksichtigung des Ultraplanktons.). *SIL Proc. 1922-2010* 5, 567–596. doi: 10.1080/03680770.1931.11898492
- Xiu, P., Chai, F., Curchitser, E. N., and Castruccio, F. S. (2018). Future changes in coastal upwelling ecosystems with global warming: the case of the California current system. *Sci. Rep.* 8, 1–9. doi: 10.1038/s41598-018-21247-7
- Yoshimura, T., Nishioka, J., Suzuki, K., Hattori, H., Kiyosawa, H., and Watanabe, Y. W. (2009). Impacts of elevated CO₂ on phytoplankton community composition and organic carbon dynamics in nutrient-depleted Okhotsk Sea surface waters. *Biogeosci. Dis.* 6, 4143–4163. doi: 10.5194/bgd-6-4143-2009
- Zark, M., Broda, N. K., Hornick, T., Grossart, H.-P., Riebesell, U., and Dittmar, T. (2017). Ocean acidification experiments in large-scale mesocosms

- reveal similar dynamics of dissolved organic matter production and biotransformation. *Front. Mar. Sci.* 4:271. doi: 10.3389/fmars.2017.00271
- Zubkov, M. V., Sleight, M. A., and Burkill, P. H. (2000a). Assaying picoplankton distribution by flow cytometry of underway samples collected along a meridional transect across the Atlantic Ocean. *Aquat. Microb. Ecol.* 21, 13–20. doi: 10.3354/ame021013
- Zubkov, M. V., Sleight, M. A., Burkill, P. H., and Leakey, R. J. G. (2000b). Picoplankton community structure on the Atlantic Meridional Transect: a comparison between seasons. *Prog. Oceanogr.* 45, 369–386. doi: 10.1016/S0079-6611(00)00008-2

Conflict of Interest Statement: The authors declare that the research was conducted in the absence of any commercial or financial relationships that could be construed as a potential conflict of interest.

Copyright © 2018 Hernández-Hernández, Bach, Montero, Taucher, Baños, Guan, Espósito, Ludwig, Achterberg, Riebesell and Arístegui. This is an open-access article distributed under the terms of the Creative Commons Attribution License (CC BY). The use, distribution or reproduction in other forums is permitted, provided the original author(s) and the copyright owner are credited and that the original publication in this journal is cited, in accordance with accepted academic practice. No use, distribution or reproduction is permitted which does not comply with these terms.



Processes That Contribute to Decreased Dimethyl Sulfide Production in Response to Ocean Acidification in Subtropical Waters

Stephen D. Archer^{1*}, Kerstin Suffrian¹, Kevin M. Posman¹, Lennart T. Bach², Patricia A. Matrai¹, Peter D. Countway¹, Andrea Ludwig² and Ulf Riebesell²

¹ Bigelow Laboratory for Ocean Sciences, Boothbay, ME, United States, ² GEOMAR Helmholtz Centre for Ocean Research Kiel, Kiel, Germany

OPEN ACCESS

Edited by:

Christel Hassler,
Université de Genève, Switzerland

Reviewed by:

Katherina Petrou,
University of Technology Sydney,
Australia
William Sunda,
University of North Carolina at Chapel
Hill, United States

*Correspondence:

Stephen D. Archer
sarcher@bigelow.org

Specialty section:

This article was submitted to
Marine Biogeochemistry,
a section of the journal
Frontiers in Marine Science

Received: 31 March 2018

Accepted: 26 June 2018

Published: 23 July 2018

Citation:

Archer SD, Suffrian K, Posman KM,
Bach LT, Matrai PA, Countway PD,
Ludwig A and Riebesell U (2018)
Processes That Contribute to
Decreased Dimethyl Sulfide
Production in Response to Ocean
Acidification in Subtropical Waters.
Front. Mar. Sci. 5:245.
doi: 10.3389/fmars.2018.00245

Long-term time series data show that ocean acidification is occurring in the subtropical oceans. As a component of an *in situ* mesocosm experiment carried out off Gran Canaria in the subtropical North Atlantic, we examined the influence of ocean acidification on the net production of dimethylsulfide (DMS). Over 23 days under oligotrophic conditions, time-integrated DMS concentrations showed an inverse relationship of -0.21 ± 0.02 nmol DMS nmol⁻¹ H⁺ across the gradient of H⁺ concentration of 8.8–23.3 nmol l⁻¹, equivalent to a range of pCO₂ of 400–1,252 atm. Proportionally similar decreases in the concentrations of both dissolved and particulate dimethylsulfoniopropionate (DMSP) were observed in relation to increasing H⁺ concentration between the mesocosms. The reduced net production of DMSP with increased acidity appeared to result from a decrease in abundance of a DMSP-rich nanophytoplankton population. A ³⁵S-DMSP tracer approach was used to determine rates of dissolved DMSP catabolism, including DMS production, across the mesocosm treatments. Over a phase of increasing DMS concentrations during the experiment, the specific rates of DMS production were significantly reduced at elevated H⁺ concentration. These rates were closely correlated to the rates of net DMS production indicating that transformation of dissolved DMSP to DMS by bacteria was a major component of DMS production. It was not possible to resolve whether catabolism of DMSP was directly influenced by H⁺ concentrations or was an indirect response in the bacterial community composition associated with reduced DMSP availability. There is a pressing need to understand how subtropical planktonic communities respond to the predicted gradual prolonged ocean acidification, as alterations in the emission of DMS from the vast subtropical oceans could influence atmospheric chemistry and potentially climate, over a large proportion of the Earth's surface.

Keywords: DMS, DMSP, ocean acidification, bacterial metabolism, phytoplankton composition, subtropical North Atlantic, mesocosm experiment

INTRODUCTION

Recent estimates of the net flux of dimethyl sulfide (DMS) from the oceans of $20\text{--}28\text{ Tg S yr}^{-1}$ (Lana et al., 2011; Wang et al., 2015) represent the largest natural source of sulfur to the atmosphere. This has a substantial impact on atmospheric chemistry (Toumi, 1994; Johnson and Bell, 2008; Chen and Jang, 2012). In the atmosphere, DMS is oxidized primarily to sulfur dioxide, sulfuric acid and to methanesulfonic acid (MSA). Sulfuric acid is responsible for new aerosol particles and cloud condensation nuclei (Sipilä et al., 2010; Kirkby et al., 2011), while MSA often makes a major contribution to the growth of existing aerosols (Rinaldi et al., 2010). Hence, DMS emissions contribute to a reduction in radiative forcing through both a direct aerosol effect and an indirect affect from cloud reflectivity (Haywood and Boucher, 2000; Lohmann and Feichter, 2005). Natural sources of aerosols, particularly DMS and sulfur emission from volcanoes, represent major uncertainties in understanding the controls on aerosol-mediated reductions in radiative forcing, including the role of anthropogenically-derived aerosols (Carslaw et al., 2013). Improved understanding of what causes variations in the DMS source would therefore, potentially improve estimates of the sensitivity of the climate to anthropogenic greenhouse gas emissions.

DMS is a product primarily of marine microbial planktonic communities. The precursor to DMS, dimethylsulfoniopropionate (DMSP), mainly synthesized by microalgae, is transformed to dissolved DMS or DMSP, through active exudation, cell lysis during senescence, viral lysis and grazing by microzooplankton and mesozooplankton (reviewed in Stefels et al., 2007). Once in the dissolved phase, bacteria are thought to play the major role in degrading DMSP in the oceans. Radiolabelled tracer studies have shown that pelagic bacteria generally either cleave DMSP, generating DMS, or demethylate/demethylate DMSP to methylmercaptopropionate and methanethiol (Kiene et al., 2000). The relative magnitude of these catabolic pathways determines the DMS yield from dissolved DMSP consumption, which has been hypothesized to be a product of the sulfur demand of the bacteria (Kiene et al., 2000). Due to photochemical and biological consumption of DMS, only 2–10% of DMS production is emitted to the atmosphere (Bates et al., 1994; Archer et al., 2002). The fate of biologically transformed DMS is poorly understood but the most likely products in the pelagic environment are dimethylsulfoxide (DMSO) and sulfate (Kiene and Linn, 2000a; Vila-Costa et al., 2006; del Valle et al., 2007). One possibility is that DMS metabolism is routed through thiosulfate or tetrathionate (Boden et al., 2010), which is rapidly consumed to produce sulfate (Reisch et al., 2011).

There is mounting experimental evidence that DMS concentrations, and hence emissions, are likely to alter in response to ocean acidification. This stems, in particular, from a series of $p\text{CO}_2$ -perturbation experiments in natural seawater mesocosms. A compelling and consistent pattern of decreasing DMS concentrations with increased $p\text{CO}_2$ and associated proton concentrations $[\text{H}^+]_{\text{T}}$ $[\text{H}^+]$ in Norwegian coastal waters (Hopkins et al., 2010; Avgoustidi et al., 2012; Webb et al.,

2016b) has also been observed in the Baltic (Webb et al., 2016a), Arctic (Archer et al., 2013), and coastal waters of Korea in early summer (Park et al., 2014). In stark contrast, a comparable study during the winter in the Korean coastal mesocosms resulted in elevated DMS concentrations with increased acidity (Kim et al., 2010). Moreover, limited variation in DMS concentrations between levels of acidity was observed in one of the series of Norwegian mesocosm experiments (Wingenter et al., 2007; Vogt et al., 2008). Less consistent responses of DMS to ocean acidification have been observed in alternative experimental approaches. For instance, a series of microcosm experiments carried out in temperate waters of the north-west European Shelf, generally resulted in increased DMS concentrations in response to acidification (Hopkins and Archer, 2014), while a similar microcosm-based experiment in the Arctic observed decreased DMS concentrations in response to increased acidity in both high and reduced light conditions (Hussherr et al., 2017). There is a clear bias in this experimental evidence to both northern latitudes and coastal waters.

Studies of the impact of ocean acidification on planktonic communities have generally been carried out at higher latitudes because the greater solubility of CO_2 in colder waters means anthropogenic increases in atmospheric $p\text{CO}_2$ result in more rapid reduction of pH, reduced calcium carbonate saturation states and lower buffering capacity in these regions (Sabine et al., 2004). Nonetheless, ocean acidification is apparent in time series measurements in warmer ocean waters. For instance, the increasing trend in atmospheric $p\text{CO}_2$ has resulted in an increased seawater $p\text{CO}_2$ of $1.75 \pm 0.37\text{ }\mu\text{atm yr}^{-1}$ at the European Station for Time Series in the Ocean at the Canary Islands (ESTOC) over the period 1995–2004, and of $1.80 \pm 0.09\text{ }\mu\text{atm yr}^{-1}$ at the Bermuda Atlantic Time Series Study (BATS) from 1983 to 2011 (González-Dávila et al., 2010; Bates et al., 2012). Corresponding changes in pH were also recorded at the two sites, of $0.0018 \pm 0.0003\text{ units yr}^{-1}$ at ESTOC and $0.0017 \pm 0.0001\text{ units yr}^{-1}$ at BATS. These changes are equivalent to an increase of $\sim 0.4\text{ }\text{yr}^{-1}$ or $0.0031\text{ nmol yr}^{-1}$ in $[\text{H}^+]_{\text{T}}$. Hence, there is a pressing need to understand how planktonic communities of the subtropical and tropical oceans are going to respond to ocean acidification, including how this will influence DMS emissions.

The five subtropical ocean gyres cover approximately 40 % of the Earth's surface and are estimated to take up $0.353\text{ Pg C yr}^{-1}$ from the atmosphere, representing approximately 31% of the global uptake of atmospheric CO_2 by the oceans (Signorini et al., 2015). These regions may make an even larger proportional contribution to the global emission of DMS, with the area between 10 and 30°N and $10\text{--}30^\circ\text{S}$ contributing an estimated 41% of the global DMS flux (Lana et al., 2011). At a more regional level, DMS emissions from the vicinity of the Canary Islands influence aerosol composition and chemistry over the tropical North Atlantic. This is apparent in aerosol samples collected at the Cape Verde Atmospheric Observatory, in which the products of DMS oxidation, including MSA, make a significant contribution to the non-sea-salt sulfate content and aerosol mass in air that has passed close to the Canary Islands and Mauritanian upwelling region (Müller et al., 2010; Fomba et al., 2014).

A key objective of this study was to extend the latitudinal range of mesocosm experiments that have examined the DMS response to ocean acidification, to waters representative of the subtropical ocean gyres. The study examines the level and direction of response of the net production of DMS, DMSP and DMSO in oligotrophic waters of the subtropical North Atlantic, with an emphasis on improving our understanding of the mechanisms underlying the DMS response. In order to determine what may alter the sources of DMS in response to acidification, we also examined the link between changes in DMSP concentrations and the composition of the phytoplankton community. In addition, a radiolabelled tracer approach was used to determine how the catabolism of dissolved DMSP, including enzyme cleavage to DMS, responded to ocean acidification. The study identifies key mechanisms that may influence DMS concentrations in an increasingly acidifying ocean, providing new insights into the causes of decreasing DMS concentrations that have been observed in previous ocean acidification mesocosm experiments.

MATERIALS AND METHODS

Experimental Set-Up

The mesocosm experiment was conducted in Gando Bay, on the east coast of Gran Canaria (27° 55' 41'' N, 15° 21' 55'' W) in the subtropical North Atlantic. Sample processing, analysis and further experiments were conducted in the laboratories of Plataforma Oceánica de Canarias (PLOCAN), Gran Canaria. The full experiment took place from 23rd September to 25th November 2014. The 1st October, the day of the first CO₂ manipulation, was defined as *t*0. Routine sampling was conducted every second day, starting on *t*-3.

The design and deployment of the Kiel Off-Shore Mesocosms for future Ocean Simulations (KOSMOS) facility has previously been described in detail (Riebesell et al., 2013). The design, implementation and progression of this particular *in situ* mesocosm experiment are described by Taucher et al. (2017). Briefly, the set up consisted of nine cylindrical transparent thermoplastic polyurethane (TPU) enclosures, supported by a floating frame, and loosely covered by a polyvinyl (PVC) hood. Once deployed on *t*-8, the open cylinders were allowed to fill with ~32–38 m³ of natural seawater screened through a 3 mm mesh. Seawater was allowed to flush through the cylinders for ~4 days in order to capture a representative and similar plankton community in each enclosure. On *t*-4 the cylinders were sealed at the bottom by attachment of sediment traps. Hoods were installed and the tops of the mesocosms were lifted to a height of ~1.5 m above the sea surface to separate the enclosed water from the surrounding waters. During the experiment, the insides of the enclosures were cleaned with a cleaning ring on three occasions (*t*4, *t*10, *t*20) to minimize the build-up of a biofilm (Taucher et al., 2017).

Manipulation of Carbonate Chemistry

In order to generate a gradient in carbonate chemistry that mimicked potential future levels of ocean acidification, seven of the mesocosms had different volumes of 50 μm-filtered Atlantic seawater saturated with CO₂ added to them in four additions

between *t*0 and *t*6 (Taucher et al., 2017; **Table 1**). Filtered seawater that was not enriched with CO₂ was added to two of the mesocosms that remained at ambient pCO₂ levels, in order to replicate any physical disturbance applied during the CO₂-rich seawater additions. On each sampling day, total alkalinity (TA) was measured using a potentiometric titration approach and dissolved inorganic carbon (DIC) by infrared absorption (Taucher et al., 2017). Proton concentrations [H⁺]_T based on the total scale (pH_T) were calculated from TA and DIC in CO2SYS (Pierrot et al., 2006) using the carbonate dissociation constants K₁ and K₂ of Lueker et al. (2000).

Sampling

A 5 l depth-integrating water sampler (IWS, Hydrobios, Kiel, Germany) was used to collect an integrated sample from ~13 to 0 m from each mesocosm and the adjacent Atlantic Ocean in the morning of every sampling day. It should be noted that in contrast to the mesocosms, there is limited temporal continuity in the Atlantic water sampled from the vicinity of the mesocosm experiment. Samples for chemical analysis and rate measurements were subsampled from the IWS into biological oxygen demand (BOD) bottles using a standardized gas sampling protocol. Samples were transported and stored in the dark and at ambient seawater temperature in cool boxes until analysis. The strategy for processing samples is illustrated in **Figure 1**.

Quantification of Dimethylated Sulfur Compounds

DMS concentrations were measured using a purge system and cryogenic trap linked to a GC-8A gas chromatograph (Shimadzu, Japan) equipped with a flame photometric detector and sulfur-specific, Chromosil 330 PTFE packed column (Sigma Aldrich). Samples were purged with high purity He in 10 or 20 ml headspace vials at a flow rate of 55–60 ml min⁻¹ for 5 min.

TABLE 1 | Seawater pCO₂ and corresponding [H⁺]_T for each mesocosm (M) and the surrounding Atlantic water over the duration of the experimental period (*t*5–*t*23).

Mesocosm #	pCO ₂ (μatm kg ⁻¹)	[H ⁺] _T (nmol l ⁻¹)
	Mean (range)	Mean (range)
Atlantic	403 (18)	8.9 (0.5)
M1	400 (21)	8.8 (0.5)
M9	406 (22)	8.9 (0.5)
M5	505 (52)	10.6 (1.0)
M3	649 (117)	13.1 (2.1)
M7	772 (176)	15.2 (3.2)
M4	819 (282)	16.0 (4.9)
M6	1,001 (318)	19.0 (5.5)
M2	1,085 (373)	20.4 (6.4)
M8	1,252 (517)	23.3 (8.9)

Values are the mean of daily measurements and in parentheses, the range between maximum and minimum concentrations.

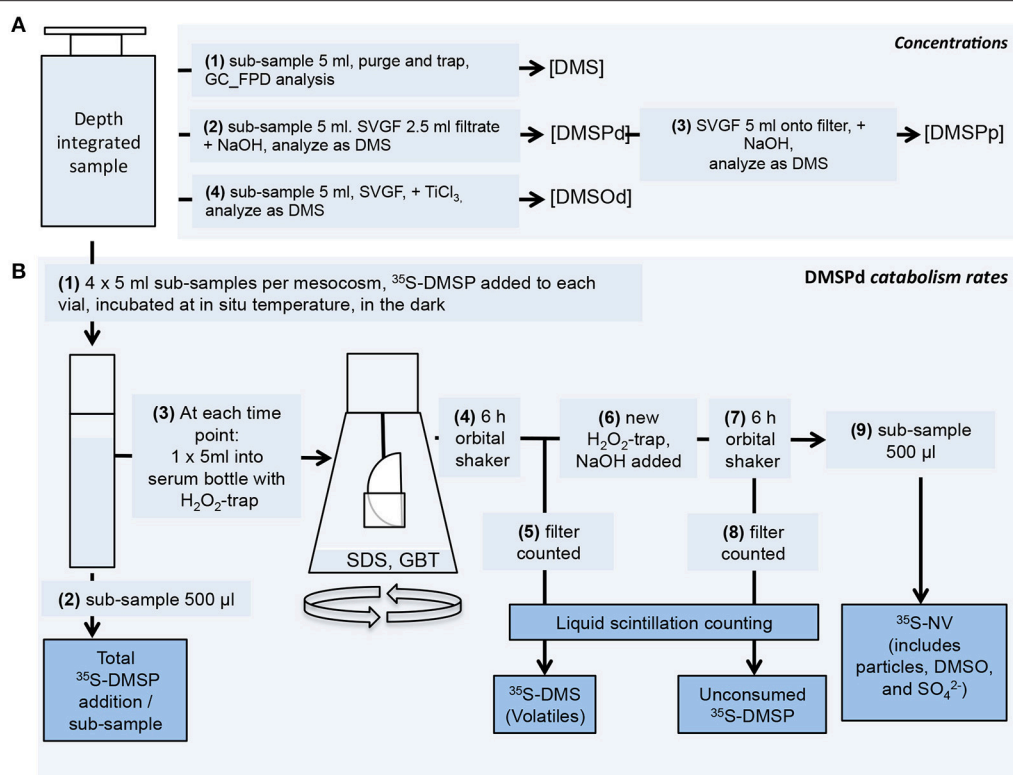


FIGURE 1 | Scheme used to process seawater samples. **(A)** Concentration measurement procedures for DMS, DMSP_d, DMSP_p and DMSO_d. **(B)** DMSP_d catabolic rate measurement procedures using ³⁵S-labeled DMSP. Further details of the procedures are described in the text.

To determine DMS concentrations in seawater ([DMS]), 5 ml of unfiltered seawater was transferred to a 10 ml headspace vial that was capped with a PTFE-coated crimp top and immediately analyzed. Unfiltered samples were used for [DMS] analysis for the entire experiment to minimize processing artifacts; for instance, due to cell disruption during filtration or exposure to the atmosphere. We are aware, however, that current standard procedures generally pre-filter samples to avoid DMS production during the purge and trap process. It is not clear which is the more accurate approach but tests of filtered vs. unfiltered samples generally demonstrated greater precision in unfiltered samples. For instance, triplicate analyses of samples from mesocosm M1 on *t*-3 gave results for the filtered samples that were ~25% lower with an average (\pm SD) of 1.00 (\pm 0.12) nmol l⁻¹ vs. unfiltered samples at 1.34 (\pm 0.01) nmol l⁻¹. DMS standards were prepared from 99.9% DMS (Sigma Aldrich) and MQ water.

Dissolved DMSP concentration [DMSP_d] was determined by the small volume drip filtration approach (Kiene and Slezak, 2006). A 5 ml sample was allowed to drip filter through a 25 mm GF/F and the first ~3 ml were collected in a glass vial containing 40 μl 50% H₂SO₄, to fix DMSP_d and remove DMS by oxidation. A 2.5 ml subsample was transferred to a 10 ml headspace vial to which 2.5 ml of 1 mol l⁻¹ NaOH was added and immediately crimp-capped in order to hydrolyse the DMSP to DMS. The samples were analyzed as described for DMS.

Particulate DMSP concentrations [DMSP_p] were determined using a solid phase micro extraction approach for DMS analysis (Yassaa et al., 2006). The GF/F filters were placed in 10 ml headspace vials with 5 ml 0.5 mol l⁻¹ NaOH and immediately crimp-capped. After \geq 6 h, DMS was sampled from the headspace using a 85 μm CAR/PDMS-solid phase micro extraction SPME fiber (Sigma Aldrich). The fibers were allowed to equilibrate in the headspace for 5 min and analyzed on a QP-2010 Ultra gas chromatograph with mass-spectrometric detector (Shimadzu, Japan). Ultra high purity He was used as the carrier gas at a flow rate of 0.85 ml min⁻¹ through a 30 m × 0.32 mm SPBTM-1 SULFUR column (Sigma Aldrich). The mass spectrometer was run in selected ion mode (SIM) to focus on the DMS parent ion *m/z* 62.06 and fragment ion *m/z* 47.05. Calibration standards were prepared and analyzed in the same manner as the samples using dilutions of the 99.9% DMS standard (Sigma Aldrich).

Quantification of dissolved DMSO [DMSO_d] closely followed the protocol of del Valle et al. (2007). Samples for [DMSO_d] were also prepared using the small volume drip filtration approach (Kiene and Slezak, 2006). The first 3 ml of filtrate were collected in a 10 ml headspace vial, sparged to eliminate DMS, crimped gastight, and frozen at -20°C. The samples were thawed for ~1 h then sparged again before DMSO was reduced to DMS by adding 400 μl of TiCl₃ 30% in 10% HCl, and incubated at 50°C for 30 min. After cooling to room temperature, samples were analyzed for DMS. A Na₂CO₃ trap was introduced before the

Nafion dryer in the purge and trap system to prevent acid vapors from entering the cryotrap and the gas chromatograph. DMSO standards were prepared from 99.9% DMSO standards (Fisher Scientific).

Rates of DMSPd Consumption and Transformation

Rates of DMSPd catabolism were determined using ^{35}S -DMSP as a tracer (Figure 1; Kiene and Linn, 2000a). The ^{35}S -DMSP was synthesized from L- ^{35}S -methionine with an initial specific activity of $1,175 \text{ Ci mmol}^{-1}$ (Perkin-Elmer, NEG009C) (Malmstrom et al., 2004). For each mesocosm, three or four discrete 5 ml seawater subsamples were spiked with ^{35}S -DMSP to a final concentration of $\leq 0.02 \text{ nmol l}^{-1}$, equivalent to an activity of $\leq 50,000 \text{ DPM ml}^{-1}$. Vials were incubated in the dark at ambient seawater temperature and sequentially sacrificed for analysis over an incubation period of typically $\sim 45 \text{ min}$, but up to 90 min in some cases. For each time point, metabolism of ^{35}S -DMSPd in the vial was stopped by addition of sodium dodecyl sulfate (0.2% final concentration) and glycine betaine (0.01% final concentration). The total amount of added ^{35}S -DMSP was determined from 500 μl subsamples added directly to Ecolume liquid scintillation cocktail (MP Biomedicals). The remaining 4.5 ml of subsample was transferred to a 120 ml serum vial and the volatile ^{35}S products were collected on hanging filter traps impregnated with H_2O_2 . Trapped volatile products were considered to be dominated by ^{35}S -DMS but it is possible that other products, including ^{35}S -methanethiol, were also trapped. The amount of ^{35}S -DMSP remaining in the subsample was then determined by alkaline hydrolysis to ^{35}S -DMS that was collected on a fresh H_2O_2 trap. The amount of non-volatile (NV) product was calculated from the difference between the total addition, DMS produced and DMSP remaining. Samples were analyzed on a Tri Carb 3100 TR liquid scintillation counter (Perkin Elmer) after overnight stabilization in the Ecolume scintillation cocktail.

Phytoplankton Abundance and Chlorophyll Concentration

Seawater for chlorophyll a measurements was collected from each mesocosm and the Atlantic with a manual vacuum pump system that was lowered steadily through the water column to acquire a depth-integrated sample from 0 to 13 m (see Taucher et al., 2017 for details on the pumping system and sample collection). Subsampled seawater was filtered on glass microfiber filters (Whatman, $0.7 \mu\text{m}$ nominal pore, $\Delta\text{pressure} = 200 \text{ mbar}$) which were put into cryovials and stored at -80°C . Chlorophyll a was extracted in 90% acetone and concentrations determined by means of reverse phase high performance liquid chromatography following Barlow et al. (1997).

Seawater for flow cytometry measurements was subsampled directly from the IWS on board the sampling boats and kept at seawater temperature in a coolbox until analysis about 2–6 h later. Measurements were performed with an Accuri C6 flow cytometer (BD Biosciences) as described in Bach et al. (2017). Briefly, fresh samples were counted for 10 min with the “fast” setting. Volume intake was verified regularly by weighing

the samples before and after measurements. Four different populations (picoeukaryotes, nanoeukaryotes, microeukaryotes, and *Synechococcus*) were distinguished based on their light scatter and fluorescence properties.

Statistical Analysis

Model 1 linear regression was used to determine the response of a variety of measured variables to increased acidity over distinct periods of the mesocosm experiment. The significance of the linear regression was determined by ANOVA. Hydrogen ion equivalent concentration $[\text{H}^+]_T$ is used as the basis to examine the response to ocean acidification, providing a linear scale against which to compare other parameters, as opposed to pH. Alterations in extracellular $[\text{H}^+]_T$ are likely to impact a greater proportion of the physiological processes that occur in heterotrophic and autotrophic microbes than changes in CO_2 availability *per se* (Raven, 2013). However, $[\text{H}^+]_T$ and pCO_2 are directly related in this context.

RESULTS

The full KOSMOS GC2 experiment took place over 55 d (Taucher et al., 2017); the results presented here are from Phase I of the experiment that ended on t_{23} , prior to the addition of deepwater to the mesocosms (M). The influence of the deepwater additions on DMS cycling will be presented as a separate study.

Initial Conditions in the Mesocosms

Seawater characteristics were typical of an oligotrophic, subtropical environment. Mean inorganic macronutrient concentrations across all mesocosms during Phase I were $60 \text{ nmol l}^{-1} \text{ NO}_3^-$, $160 \text{ nmol l}^{-1} \text{ NH}_4^+$, $26 \text{ nmol l}^{-1} \text{ PO}_4^{3-}$, and $260 \text{ nmol l}^{-1} \text{ Si(OH)}_4$. The initial water temperature decreased gradually from 24.5 to 24.0°C and salinity increased from 36.95 to 38.00 during Phase I. There was no evidence, from the salinity and temperature depth profiles, of water column stratification within the mesocosms or the surrounding waters in the Bay of Gando, during this experiment (Taucher et al., 2017). Surface photosynthetically active radiation (PAR) varied on a daily basis, from 40 to $100 \text{ mol m}^{-2} \text{ d}^{-1}$, and showed a gradual seasonal decline.

Carbonate Chemistry in the Mesocosms

At the time of closing the mesocosm bags (t_{-3}), the ambient water at the experimental site had a pCO_2 of $\sim 380 \mu\text{atm}$ and $[\text{H}^+]_T$ of 8.9 nmol l^{-1} . Manipulation of the carbonate chemistry in the mesocosms established an initial gradient in pCO_2 from ambient levels of $\sim 405 \mu\text{atm}$ (M1, M9) to $\sim 1,480 \mu\text{atm}$ in the highest CO_2 treatment (M8) and $[\text{H}^+]_T$ of 8.8 – 27.2 nmol l^{-1} . This manipulation over the course of 7 days equated to an average adjustment of pCO_2 of $\sim 140 \mu\text{atm d}^{-1}$ or $\sim 2.4 \text{ nmol l}^{-1} \text{ d}^{-1}$ in $[\text{H}^+]_T$ in the most acidified treatment. The average values from t_5 to t_{23} are shown in Table 1. Over time, pCO_2 and $[\text{H}^+]_T$ declined most rapidly in the highly acidified treatments. In general, the distinction in carbonate chemistry between treatments was maintained

throughout Phase I, except in the case of M4 and M7, in which $p\text{CO}_2$ and $[\text{H}^+]_{\text{T}}$ converged following $t11$ (Taucher et al., 2017).

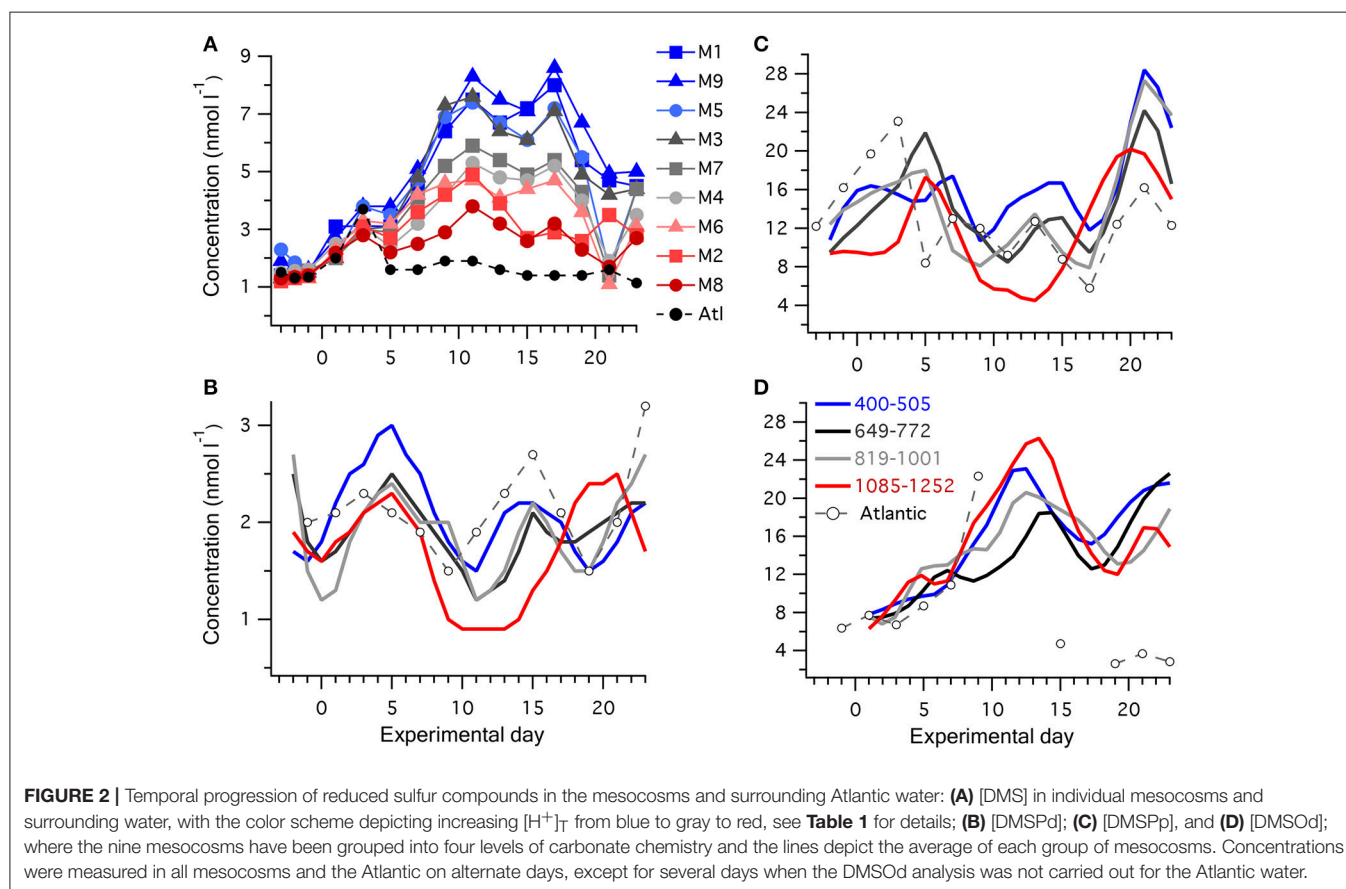
Temporal Trends in Reduced Sulfur Compounds

Initial concentrations of the reduced sulfur compounds were typical of subtropical oceanic waters (Dacey et al., 1998; Lana et al., 2011). At $t-3$, the average ($\pm\text{SD}$) for [DMS] was $1.5 \pm 0.4 \text{ nmol l}^{-1}$, [DMSPp] was $8.5 \pm 2.9 \text{ nmol l}^{-1}$ and [DMSPd] was $2.8 \pm 1.1 \text{ nmol l}^{-1}$, among the mesocosms (Figure 2). Measurements of [DMSOd] were not carried out until $t1$ when they averaged $7.3 \pm 1.1 \text{ nmol l}^{-1}$ (Figure 2), comparable to prior observations in open ocean waters (Simó et al., 1997; Hatton et al., 1998).

An initial general increase in [DMS] occurred in all mesocosms, and plateaued on $\sim t11$ (Figure 2A). [DMS] then stabilized until $\sim t17$, followed by relatively rapid decline until $t21$ (Figure 2A). This was in contrast to the surrounding Atlantic water, in which an initial 3-fold increase in [DMS] by $t3$ matched the pattern in the mesocosms but then dropped to $\sim 1 \text{ nmol l}^{-1}$ for the remainder of the experiment, presumably as a different water mass passed through the experimental site. In comparison to [DMS], lower relative changes in [DMSPd], and [DMSPp] occurred during Phase I of the experiment. To clearly illustrate the temporal trends in [DMSPp], [DMSPd], and

[DMSOd], the mesocosms have been grouped into four levels of carbonate chemistry manipulation (Figures 2B,C). [DMSPp] and [DMSPd] showed similar temporal patterns. Following closure of the mesocosms on $t-3$, [DMSPp] in general increased to a peak on $t5$ and then decreased from $t5$ to $t10$. Between $t10$ and $t17$, a second peak in [DMSPp] and [DMSPd] occurred in the majority of the mesocosms. This was followed by a rapid increase in [DMSPp] to a third peak at $t21$, at which point values exceeded 30 nmol l^{-1} in some of the mesocosms (Figure 2C).

The temporal pattern of [DMSOd] had a closer resemblance to the generally increasing trends in [DMS] rather than [DMSPp], with increasing concentrations that reached their highest levels between $t10$ and $t15$, declined between $t15$ and $t20$, and then increased again following $t20$ (Figure 2D). The average rate of increase in [DMSOd] between $t5$ and $t11$ of $2.0 \text{ nmol l}^{-1} \text{ d}^{-1}$ among all the mesocosms exceeded the average for [DMS] of $0.54 \text{ nmol l}^{-1} \text{ d}^{-1}$ by approximately 4-fold. The total increase in DMSOd during this period averaged 8.6 nmol l^{-1} among the mesocosms and was of a similar magnitude to the average decrease in [DMSPp] of 8.4 nmol l^{-1} , suggesting a stoichiometric relationship between DMSPp loss and DMSOd production. However, when examined at the level of individual mesocosms no clear patterns between temporal trends in [DMSOd] and [DMSPp] were apparent.



Relationship Between Acidity and Reduced Sulfur Compounds

Time-averaged [DMS], calculated from all the measurements that were carried out on alternate days between t_0 and t_{23} , was significantly decreased at higher $[H^+]_T$ (Figure 3A, Table 2). This response to increasing acidity began almost immediately following the addition of pCO_2 -enriched seawater at t_0 . This is apparent in the slope of the linear regression between [DMS] and

$[H^+]_T$ for individual sampling days, with a significant negative impact of increased acidity apparent at t_5 (Figure 3E). The degree of inhibition of net DMS production at higher acidity increased up to t_{17} and then decreased for the remaining period (Figure 3E).

The time-averaged concentrations of both DMSPd and DMSPp between t_0 and t_{23} showed a significant decrease as well in relation to average $[H^+]_T$ (Figures 3B,C, Table 2). This is also

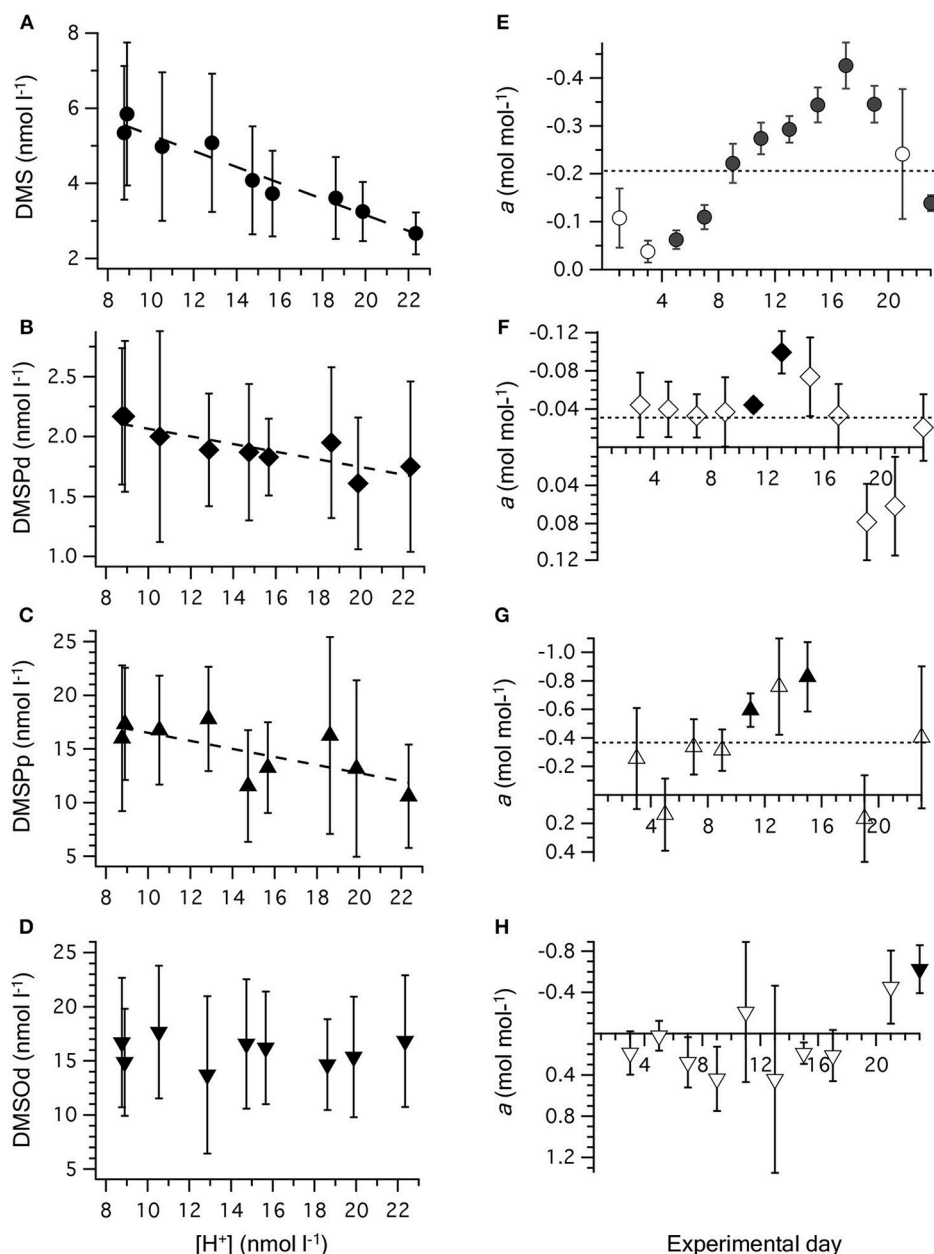


FIGURE 3 | Relationship between $[H^+]_T$ and concentrations of (A) DMS; (B) DMSPd; (C) DMSPp, and (D) DMSOd. Values are time-averaged from measurements on alternate days from t_1 to t_{23} . Error bars are the SD. The equations for the linear regressions are included in Table 2. The slope (\pm SE) of the linear regression between $[H^+]_T$ and concentration of reduced sulfur compounds on individual days is shown for: (E) DMS; (F) DMSPd; (G) DMSPp, and (H) DMSOd. Significant regressions ($P < 0.05$) are shown as bold symbols. The slope from the time-averaged data is shown as a dashed line. Error bars are the SE.

apparent in the results from individual days, although significant regressions between [DMSPd] or [DMSPp] and $[H^+]_T$ were observed on only 2 days in each case (Figures 3E,G). The level of reduction in concentration with $[H^+]_T$ was approximately 10-fold lower for DMSPd than DMSPp, reflecting the relative difference in concentrations (Table 2).

In contrast to the other sulfur compounds, [DMSOd] showed no significant relationship to the varied $[H^+]_T$ in

the mesocosms on the basis of time-averaged measurements (Figure 3D, Table 2). A significant reduction in [DMSOd] vs. $[H^+]_T$ for individual days was only observed at the end of Phase I of the experiment, at t_{23} (Figure 3H).

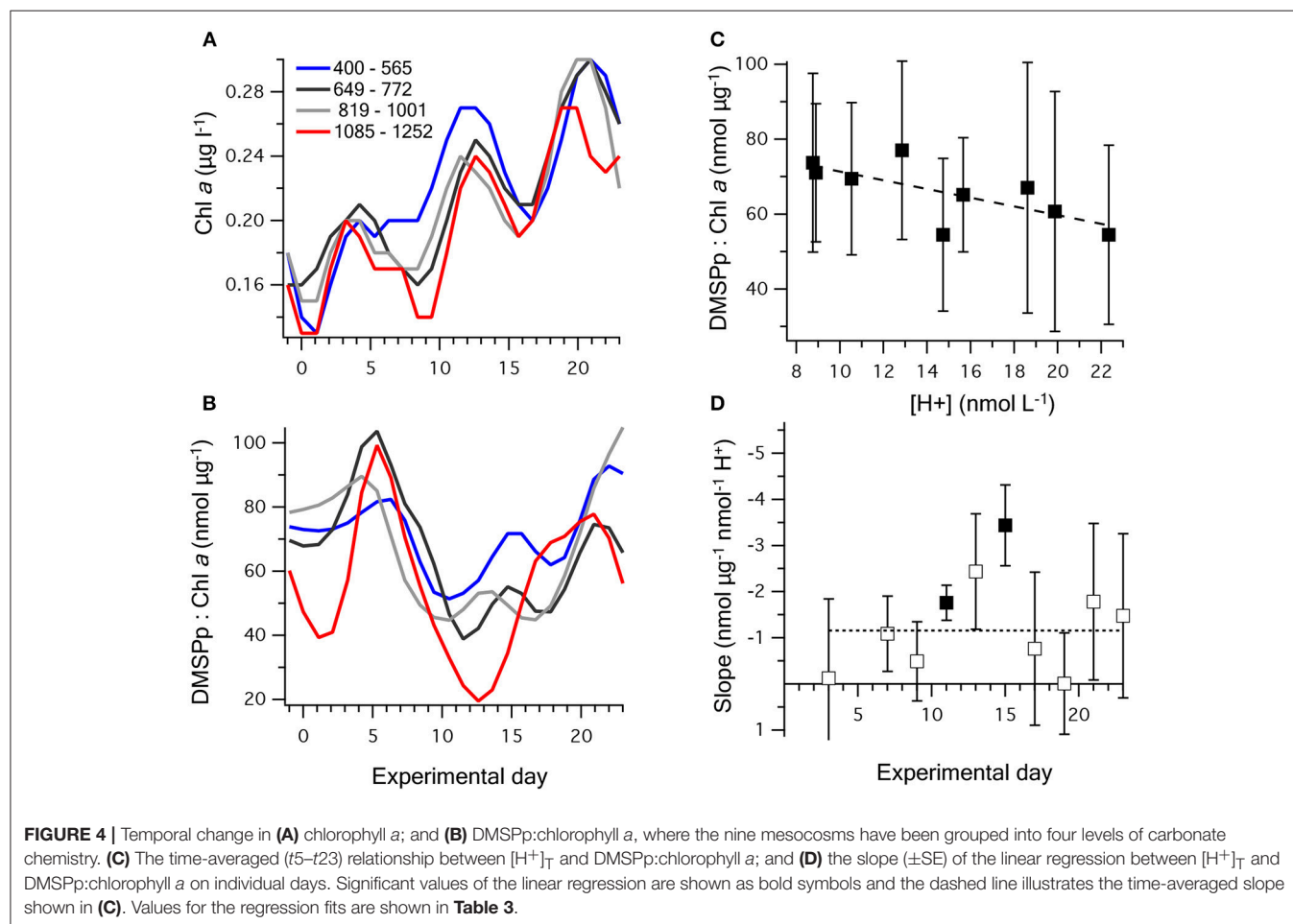
Phytoplankton and DMSPp

Chl *a* concentrations were generally low, starting at an average of $0.17 \pm 0.02 \mu\text{g l}^{-1}$ on t_{-1} , and gradually increased in all

TABLE 2 | Coefficients and levels of significance for the linear regressions of the time-averaged ($t_{5-t_{23}}$) concentrations (nmol l^{-1}) of DMS, DMSPd, DMSPp, and DMSOd vs. $[H^+]_T$ (nmol l^{-1}) in the nine mesocosms (Figure 3).

Variable	<i>a</i> (nmol nmol^{-1})	<i>b</i> (nmol l^{-1})	<i>P</i>	Proportional decrease (%)			
				RCP2.6	RCP4.5	RCP6.0	RCP8.5
DMS	-0.21, 0.02	7.4 ± 0.3	1.4×10^{-5}	5	12	19	33
DMSPd	-0.032, 0.007	2.4 ± 0.1	0.0037	2	5	8	13
DMSPp	-0.38, 0.15	20.3 ± 2.3	0.037	3	7	12	20
DMSOd	-0.012, 0.098	16.0 ± 1.5	0.91	ns	ns	ns	ns
DMSPp:Chl <i>a</i>	-1.16, 0.44	83.0 ± 6.7	0.032	2	5	8	14

Where *a* is the coefficient of the slope ($\pm\text{SE}$), *b* is the intercept ($\pm\text{SE}$), *P* is the significance of the *F*-value of the ANOVA of the regression, and ns is not significant at $P < 0.05$. A proportional decrease in each variable relative to values from the 1990s of pH 8.1 and $p\text{CO}_2$ of $350 \mu\text{atm}$, is shown for ocean pH predicted for 2,100 from the four representative concentration pathways (RCPs) of the IPCC (Bopp et al., 2013).



mesocosms to between 0.17 and $0.32 \mu\text{g l}^{-1}$ on $t23$. The three peaks in [DMSPp] (Figure 2C) are apparent in the temporal trends in Chl a concentration (Figure 4A), suggesting that the phytoplankton that synthesized DMSP made up a sizeable component of the total Chl a . The initial DMSP:Chl a ratio among the mesocosms, of $71 \pm 12 \text{ nmol } \mu\text{g}^{-1}$ on $t1$, increased to 96 ± 22 on $t5$ and then decreased in all mesocosms to 42 ± 11 on

$t11$ (Figure 4B). Following $t11$, DMSP:Chl a increased at varying rates in the mesocosms, with a noticeable lag of several days in mesocosms at the highest $[\text{H}^+]_{\text{T}}$ (Figure 4B). By $t23$, DMSP:Chl a varied from 34 to $130 \text{ nmol } \mu\text{g}^{-1}$ between mesocosms.

Between $t1$ and $t23$, the time-averaged DMSPp:Chl a showed a significant decreasing trend with $[\text{H}^+]_{\text{T}}$, with the strongest response between $t11$ and $t15$ (Figures 4C,D). This trend

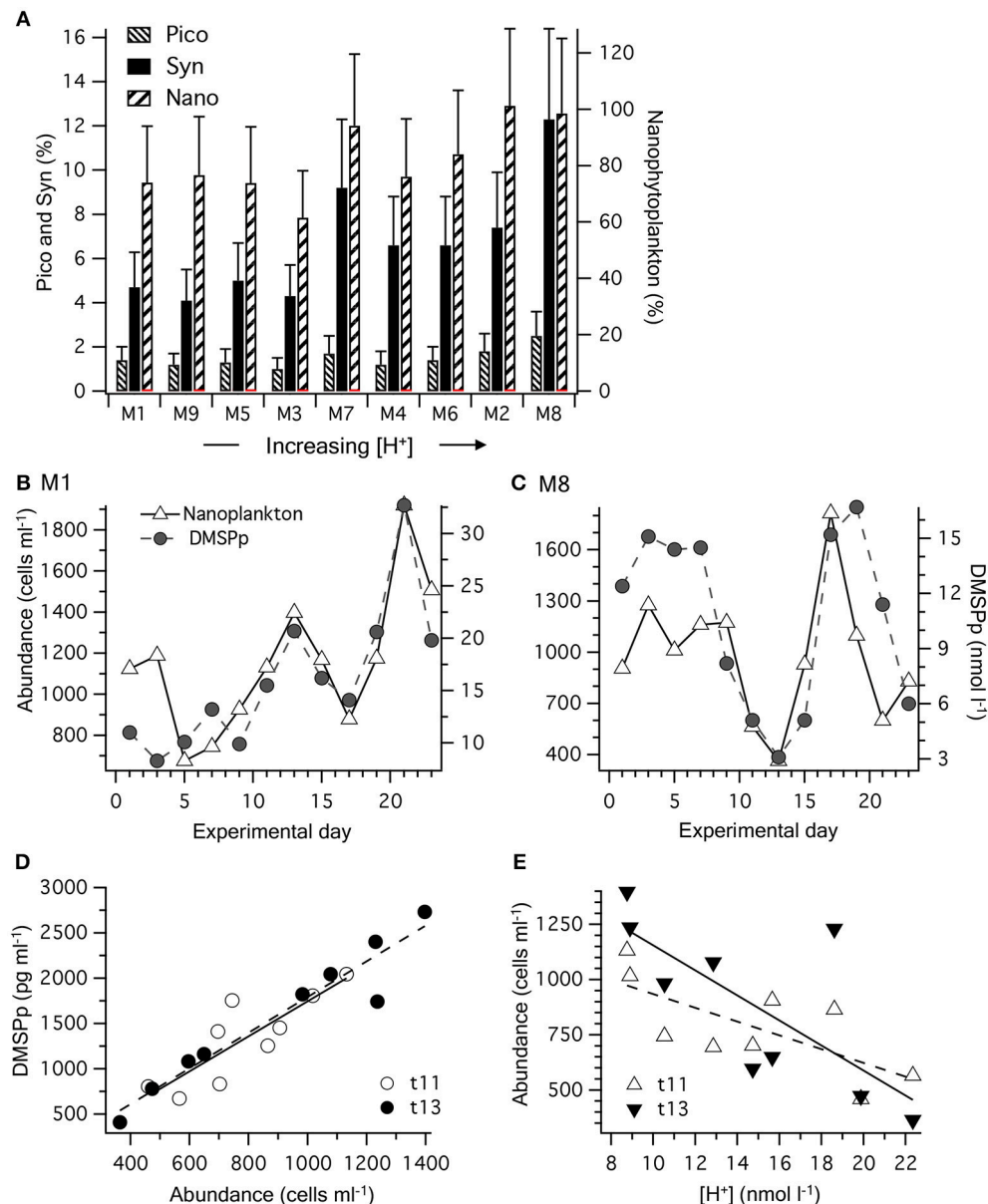


FIGURE 5 | Partition of DMSPp among phytoplankton functional groups: **(A)** time-averaged contribution to the total DMSPp pool based on values of DMSP cell content in each mesocosm (M) over the 23 days. Values are the average DMSP contribution based on cell-specific estimates from two different stations: *Synechococcus* spp.: 0.0013 – 0.0027 ; picoeukaryotes: 0.006 – 0.016 ; nanoeukaryotes: 0.92 – $1.60 \text{ pg DMSP cell}^{-1}$ (Archer et al., 2011). Error bars show the range. **(B)** Temporal progression of the nanophytoplankton population and [DMSPp] in M1 that experienced a time-averaged $[\text{H}^+]_{\text{T}}$ of 8.8 nmol l^{-1} ; and **(C)** M8 in which the $[\text{H}^+]_{\text{T}}$ averaged 23.3 nmol l^{-1} . **(D)** The relationship between nanophytoplankton abundance and [DMSPp] in the nine mesocosms on days $t11$ and $t13$. **(E)** the relationship between nanophytoplankton abundance and $[\text{H}^+]_{\text{T}}$ in the nine mesocosms on days $t11$ and $t13$. Values and levels of significance for the linear regressions are given in Table 3.

TABLE 3 | Coefficients and levels of significance for the linear regressions of: time-averaged ($t5$ – $t23$) DMSP:Chl a ($\text{nmol } \mu\text{g}^{-1}$) vs. $[\text{H}^+]_T$ (nmol l^{-1}) (**Figure 4**); the relationship between DMSPp (pg ml^{-1}) and abundance of nanophytoplankton (cells ml^{-1}) on $t11$ and $t13$ (**Figure 5D**); and the relationship between nanophytoplankton abundance and $[\text{H}^+]_T$ (nmol l^{-1}) on $t11$ and $t13$ (**Figure 5E**).

Variables	a	b	P
DMSPp:Chl a vs. $[\text{H}^+]_T$: $t5$ – $t23$	-1.16 ± 0.44	83.0 ± 6.7	0.032
DMSPp vs. nanophytoplankton: $t11$	1.93 ± 0.47	-184 ± 384	0.0047
DMSPp vs. nanophytoplankton: $t13$	1.98 ± 0.21	-176 ± 203	3.5×10^{-5}
Nanophytoplankton vs. $[\text{H}^+]_T$: $t11$	-31 ± 11	1247 ± 176	0.029
Nanophytoplankton vs. $[\text{H}^+]_T$: $t13$	-57 ± 20	1723 ± 303	0.023

Where a is the coefficient of the slope ($\pm\text{SE}$), b is the intercept ($\pm\text{SE}$), P is the significance of the F -value of the ANOVA of the regression.

was largely a product of reduced [DMSPp] at higher acidity (**Figure 2**), rather than increased Chl a concentration at lower acidity. This indicates that higher acidity caused a decrease in the DMSP-producing components of the planktonic communities or a decrease in cell-specific DMSP production, including during the period when net DMS production was highest from $t5$ to $t11$ (**Figure 4D**).

The contribution of phytoplankton functional groups to the DMSPp pool can be estimated based on cell DMSP content measured directly using flow cytometric sorting of specific phytoplankton groups from the eastern Tropical Atlantic (Archer et al., 2011; **Figure 5A**). The initial phytoplankton community in the mesocosms was dominated numerically by picophytoplankton, including the cyanobacteria *Synechococcus* sp. and *Prochlorococcus*, and picoeukaryote cells. Of these groups, *Synechococcus* sp. abundance increased fastest, from $\sim 10,000$ to $>50,000$ cells ml^{-1} by $t11$ and made up 70–80% of the Chl a during that period (Taucher et al., 2017). Based on the previously measured DMSP content (Archer et al., 2011), the contribution of *Synechococcus* sp. to DMSPp may have increased to a maximum of ~ 2 nmol l^{-1} by $t11$ – $t13$ and averaged 4–12 % of the total DMSPp over the course of the 23 days (**Figure 5A**). The picoeukaryote population declined from $\sim 3,000$ to $<1,000$ cells ml^{-1} between $t0$ and $t10$ and is estimated to have contributed <0.5 nmol l^{-1} DMSPp, equivalent to an average of 1–3% of the total DMSPp during the 23 day period (**Figure 5A**). The largest contribution to total DMSPp was most likely from a nanophytoplankton population of 2–8 μm cells that contributed an estimated average of 62–101 % of the total DMSPp among the mesocosms (**Figure 5A**). The abundance of the nanophytoplankton populations was closely related to the temporal trends in DMSPp in each mesocosm (**Figure 5B**). Indeed, [DMSPp] and nanophytoplankton abundance from $t1$ to $t23$ were significantly correlated in each of the nine mesocosms (Pearson correlation coefficient, $r = 0.62$ to 0.87 , p -value = 0.0002 – 0.0305).

This close relationship between DMSPp and nanophytoplankton was apparent on a daily basis over the range of $[\text{H}^+]_T$ in the mesocosms (**Figure 5D**). Significant linear regressions (p -value < 0.05) of [DMSPp] vs. nanophytoplankton abundance across all 9 mesocosms occurred on $t11$, $t13$, $t15$, $t21$,

and $t23$ and are shown for $t11$ and $t13$ (**Figure 5D**, **Table 3**). The slopes of the regressions indicate that the DMSP cell content of the nanophytoplankton population were 1.93 ± 0.47 and 1.98 ± 0.21 pg DMSP cell $^{-1}$ in the mesocosms on $t11$ and $t13$, respectively (**Figure 5D**, **Table 3**). Similar DMSP cell content of 2.13, 1.41, and 1.82 pg DMSP cell $^{-1}$ could be derived for $t15$, $t21$, and $t23$, respectively. These estimates of DMSP cell content are at the upper range of the values directly measured in flow cytometrically-sorted natural nanophytoplankton populations (0.92 – 1.60 pg DMSP cell $^{-1}$) that are used to determine the group specific contribution to total DMSPp (**Figure 5A**). Nanophytoplankton abundance also showed a significant inverse relationship to mesocosm $[\text{H}^+]_T$ on $t11$ and $t13$ (**Figure 5E**, **Table 3**), consistent with significant relationships between $[\text{H}^+]_T$ and DMSPp on those 2 days (**Figure 3G**, **Table 2**).

Microphytoplankton abundance between $t5$ and $t23$ was <100 cells ml^{-1} in all mesocosms. Even at such low abundance, large DMSP-rich cells may have made a sizeable contribution to the DMSPp pool, but this is difficult to assess from the available information.

Transformation of DMSPd

Measurements of ^{35}S -DMSP transformation were carried out on $t5$, $t9$, $t11$, $t13$, $t21$, and $t23$ for each of the mesocosms and the Atlantic water. Although ^{35}S -DMSP incubations were carried out on $t17$, an experimental error meant the results could not be interpreted. Examples of the results from ^{35}S -DMSP tracer experiments for M1 during the period from $t5$ to $t11$ are illustrated in **Figure 6**. The rate coefficients for consumption of DMSPd (kDMSPd), production of DMS (kDMS), and conversion to a non-volatile form (kNV) were calculated as the rate of change in the log-transformed fraction of the disintegrations per minute (DPM) for each component relative to the total DPM added to each incubation vial. The corresponding coefficients and rates of DMSPd consumption, DMS production and transformation to non-volatile products are shown in **Table 4**. At $[\text{H}^+]_T$ close to ambient levels in M1, DMSPd consumption, transformation to non-volatile products, and DMS production increased from $t5$ to $t11$, coinciding with increasing [DMS] over this period. Despite a decrease in [DMSPd] over time, the faster turnover of DMSPd and increased yield of DMS meant that production of DMS almost doubled from 0.12 to 0.20 nmol $\text{L}^{-1} \text{h}^{-1}$ from $t5$ to $t11$ (**Table 4**). The major part of the DMSPd pool was converted to non-volatile products, presumably including SO_4^{2-} and assimilation by bacteria (Kiene and Linn, 2000a).

Values of kDMS in all mesocosms increased over the course of the experiment, particularly between $t5$ and $t11$ (**Figure 7**), contributing to the observed increases in [DMS] seen in all the mesocosms. As is apparent in **Figure 7**, values of kDMS diverge between $t5$ and $t9$ in relation to $[\text{H}^+]_T$ in the different mesocosms and this pattern was maintained, to some extent, through to $t11$. A highly significant inverse relationship occurred between $[\text{H}^+]_T$ and kDMS on $t9$ (p -value: 0.0062) but the same relationship was not significant (p -value: < 0.05) on the other days when measurements were made. Significant relationships to $[\text{H}^+]_T$ were also not observed for kDMSPd and kNV for the individual days.

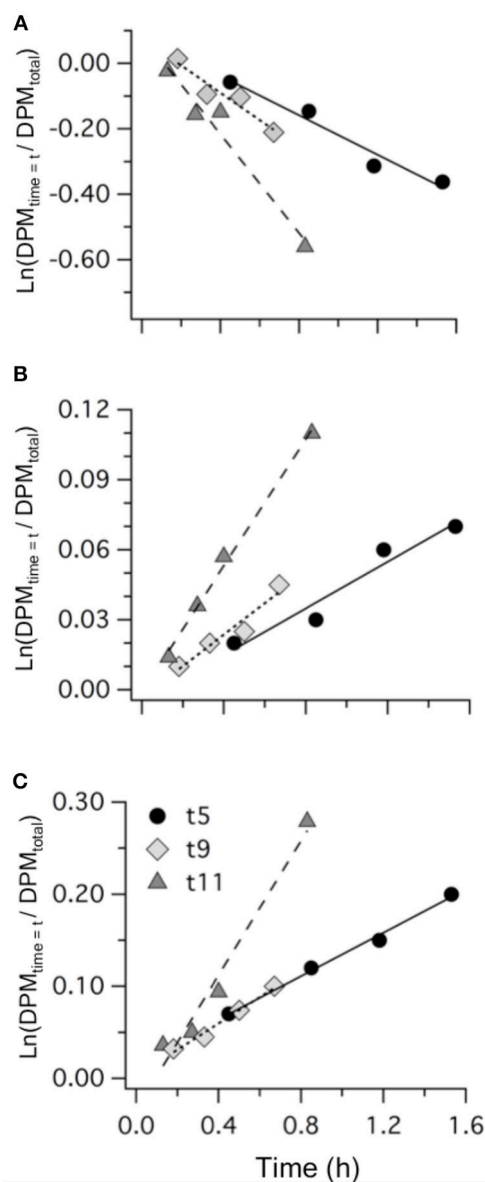


FIGURE 6 | Examples of the results from ^{35}S -DMSP addition experiments from mesocosm M1 on t_5 , t_9 , and t_{11} showing: **(A)** DMSPd consumption; **(B)** DMS production; and **(C)** formation of non-volatile (NV) products. Values are the natural log of the concentrations (DPM ml^{-1}) normalized to the initial concentration of ^{35}S -DMSP (DPM ml^{-1}). The slope of the linear regression provides the rate coefficients k_{DMSPd} , k_{DMS} , and k_{NV} (Table 4).

A general decrease in k_{DMS} between t_{21} and t_{23} accompanied a drop in $[\text{DMS}]$ that started at t_{17} in most of the mesocosms. This decrease in k_{DMS} and $[\text{DMS}]$ occurred despite increasing $[\text{DMSPd}]$ concentrations in the majority of mesocosms (Figure 2C) that were associated with expanding nanophytoplankton populations (Figures 5B,C). There was no apparent $[\text{H}^+]_{\text{T}}$ dependence in k_{DMS} or k_{DMSPd} on t_{21} or t_{23} .

The most striking features of the temporal trends in $[\text{DMS}]$ are the rapid increases between t_5 and t_{11} (Figure 2A) that

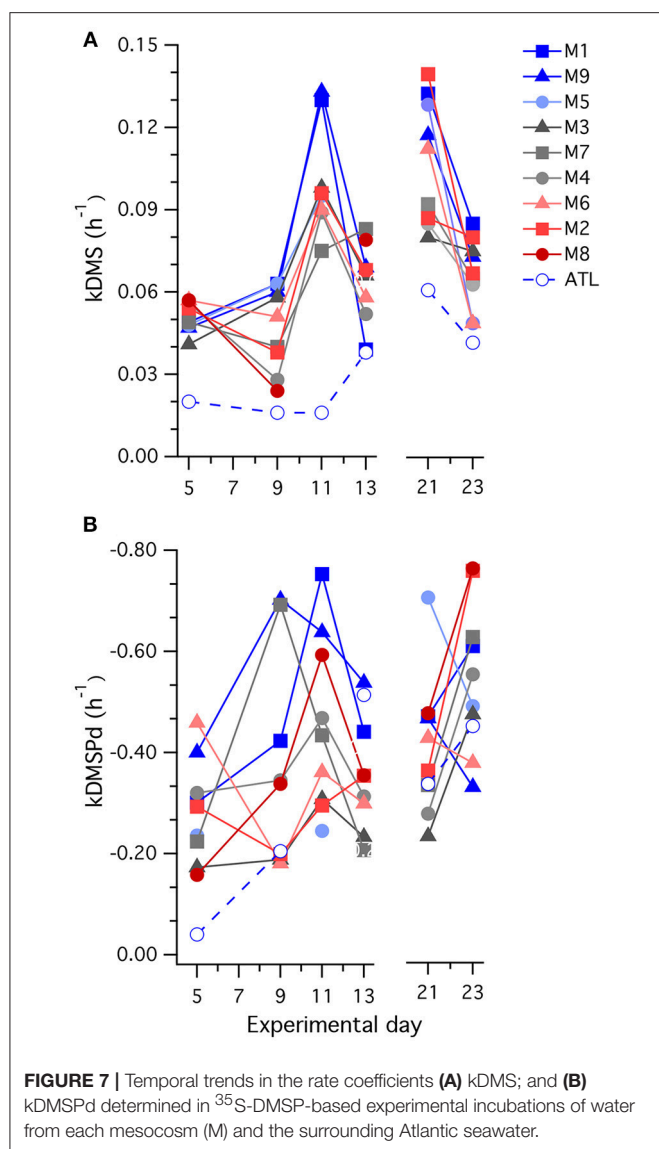
TABLE 4 | Rate coefficients and derived rates for mesocosm M1 on experimental days t_5 , t_9 , and t_{11} ; corresponding to the ^{35}S -DMSP-based experimental results shown in Figure 6.

Experimental day	t_5	t_9	t_{11}
k_{DMSPd} (h^{-1})	-0.30 ± 0.05	-0.42 ± 0.09	-0.76 ± 0.11
k_{DMS} (h^{-1})	0.049 ± 0.003	0.062 ± 0.011	0.131 ± 0.006
k_{NV} (h^{-1})	0.12 ± 0.01	0.13 ± 0.01	0.36 ± 0.05
$[\text{DMSPd}]$ (nmol l^{-1})	2.4	2.7	1.5
$[\text{DMS}]$ (nmol l^{-1})	3.1	6.4	7.5
DMSPd consumption ($\text{nmol l}^{-1} \text{ h}^{-1}$)	-0.62	-0.92	-0.78
DMS production ($\text{nmol l}^{-1} \text{ h}^{-1}$)	0.12	0.17	0.20
NV production ($\text{nmol l}^{-1} \text{ h}^{-1}$)	0.31	0.39	0.64
DMS yield (%)	19	19	26
DMSPd turnover (h)	3.8	2.9	1.9

Rate coefficients ($\pm \text{SE}$) were calculated from the slope of the relationships shown in Figure 6. Actual rates were calculated from the rate coefficients and $[\text{DMSPd}]$ measured in the same samples.

drive the observed response to $[\text{H}^+]_{\text{T}}$ between the mesocosms (Figure 3A). To explain this feature in a more comprehensive way, time-integrated rates are used to examine whether the differences in DMS production via cleavage of DMSPd to DMS contributed to the differences in net production of DMS between t_5 and t_{11} . The rate coefficients and rates of DMSPd transformation have been integrated over the 6 days between t_5 and t_{11} from the ^{35}S -DMSP-based incubations on t_5 , t_9 , and t_{11} (Figure 8, Table 5). Observed rates of net DMS production showed a highly significant relationship to $[\text{H}^+]_{\text{T}}$ when integrated between t_5 and t_{11} , varying from 0.68 to 0.23 $\text{nmol l}^{-1} \text{ d}^{-1}$ between mesocosms (Figure 8B, Table 6). The time-integrated k_{DMS} values showed a corresponding, significant inverse relationship to $[\text{H}^+]_{\text{T}}$ (Figure 8A, Table 6). Net DMS production in each mesocosm was significantly correlated to the corresponding values of k_{DMS} (Pearson's product-moment correlation, $r = 0.67$, $P = 0.049$) (Table 6). Time-integrated DMS production rates due to cleavage of DMSPd ranged from ~ 3.9 to $1.8 \text{ nmol l}^{-1} \text{ d}^{-1}$ across the $[\text{H}^+]_{\text{T}}$ gradient (Table 5), on average 6-fold higher than the net rates of DMS production (Figure 8B). These DMS production rates from the cleavage of DMSPd were also significantly related to $[\text{H}^+]_{\text{T}}$ between t_5 and t_{11} (Table 6). This indicates that variable specific rates of DMSPd cleavage to DMS (k_{DMS}) related to $[\text{H}^+]_{\text{T}}$ are at least in part, responsible for the observed differences in $[\text{DMS}]$ between the different levels of acidity.

Reduced k_{DMS} with increased $[\text{H}^+]_{\text{T}}$ contributed to the decreasing, although not significant, trend of the linear regression between k_{DMSPd} and $[\text{H}^+]_{\text{T}}$ (Figure 8). The non-significant regression, (Table 6) suggests DMSPd uptake and transformation in general, was inhibited by acidification during the peak of DMS net production (t_5 to t_{11}), possibly to a greater extent than k_{DMS} . Conversion to non-volatile products during this period accounted for an average of 79 % (range 49–95%) of



the DMSP consumption kNV and production of non-volatile products showed no significant relationship to $[H^+]_T$ when integrated over the time period (t_{5-t11}) or on individual days.

DISCUSSION

Environmental Context and Comparison to Previous Experiments

To the best of our knowledge, this *in situ* mesocosm experiment was the first that investigated the impact of increased acidity on DMS concentrations in a subtropical oligotrophic environment. This substantially extends the latitudinal and environmental range of mesocosm experiments that have examined the influence of ocean acidification on DMS concentrations. The Canaries Current flows NNE to SSW through the Canaries archipelago (Molina, 1976). Similar levels of long term change in carbonate chemistry and pH to those measured in the open

ocean to the north of the islands at ESTOC (see Introduction), would be expected to have occurred along the east coast of Gran Canaria, where this experiment was conducted. Moreover, there is growing evidence that planktonic communities in open ocean, low latitude environments may be more susceptible to ocean acidification because of the limited variability they normally experience in carbonate chemistry, compared to communities in shelf and coastal seas (Joint et al., 2011; Duarte et al., 2013). Although regional enhancement of nutrients and productivity may occur in the coastal waters around the islands and to the south of the Canaries (Aristegui et al., 1997), the initial experimental water had concentrations of nutrients and Chl *a*, and phytoplankton communities dominated by cyanobacteria and picophytoplankton (Taucher et al., 2017), that are similar to those observed further north at ESTOC (Neuer et al., 2007). Hence, the initial planktonic communities captured in the mesocosms are likely to have experienced day-to-day and seasonal variability in carbonate chemistry that is also representative of subtropical ocean waters.

Of the nine mesocosm experiments described so far that have investigated the DMS response to ocean acidification, including the present study, seven show a clear reduction in the time-integrated DMS concentration over the course of the experiments (reviewed in Hopkins et al., in preparation). This is despite being carried out in widely varied locations and environments by independent teams of researchers using differing experimental approaches. The similar set up of the present study and the Arctic experiment (Archer et al., 2013), in terms of mesocosm structure and volume, number, and range of $[H^+]_T$ treatments and the methods and duration of carbonate chemistry manipulation, enables a straightforward comparison of the DMS response to altered acidity. The linear decrease in time-averaged $[DMS]$ in relation to $[H^+]_T$ was remarkably similar in the two experiments, with slopes of 0.22 ± 0.3 and 0.21 ± 0.02 $nmol\ nmol^{-1}$ for the Arctic and sub-tropical experiments, respectively (Figure 3, Table 2). If the response observed in the mesocosm experiments is assumed to represent what may happen in the oceans over the next century, $[DMS]$ may decrease by 5–33%, depending on which IPCC representative concentration pathway (RCP) transpires (Table 2). This estimated decrease is based on the average change in ocean $[H^+]_T$ predicted using ten Earth System Models with marine biogeochemical components that were part of the Coupled Model Intercomparison Project 5 (CMIP5) (Bopp et al., 2013).

The relationships between $[DMS]$ and pH observed in mesocosm experiments, particularly the Arctic experiment, have been used as the basis for modeled predictions of the impact of ocean acidification on global DMS emissions and climate (Six et al., 2013; Schwinger et al., 2017). The study by Schwinger et al. (2017) used a fully coupled Earth system model to demonstrate a potential 31% decrease in DMS emissions by the year 2100, assuming a medium level, negative response of DMS production to pH. This level of decrease in DMS emissions could contribute an extra 0.3 K of global warming by the turn of the century, due to reduction in both cloud albedo and the aerosol direct effect, as the sulfate aerosol loading is decreased. Both modeling studies used the parameterization of Six et al. (2013) in which local DMS

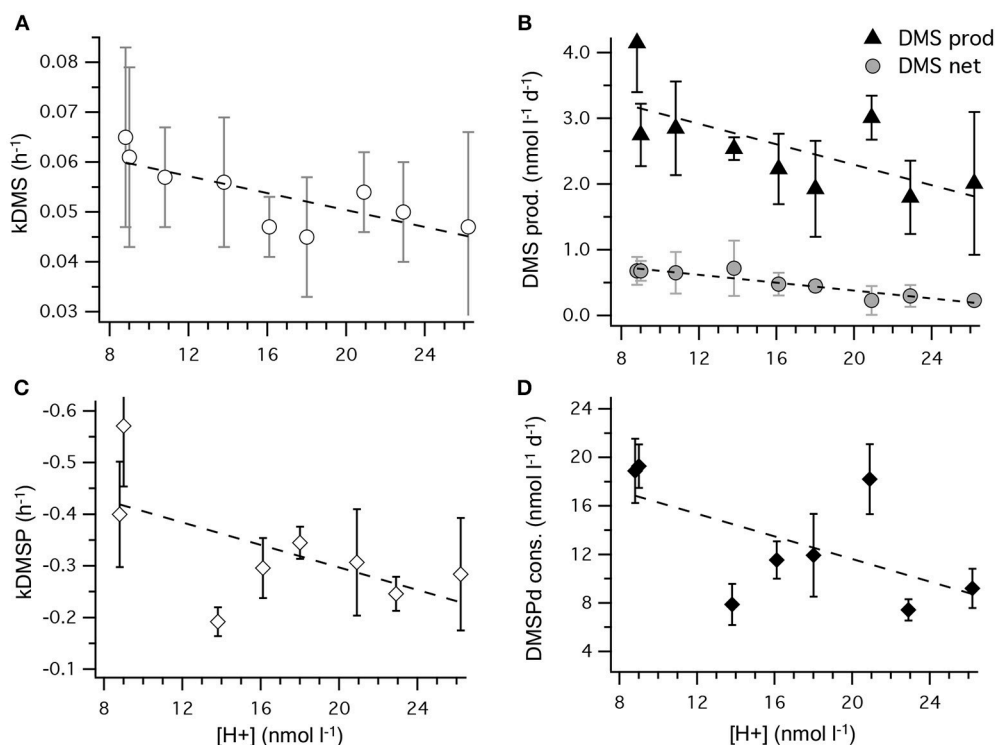


FIGURE 8 | Rates of DMSPd catabolism from ^{35}S -DMSP experiments, in relation to $[\text{H}^+]_{\text{T}}$ for the period of maximum net DMS production from t_5 to t_{11} . Values are average (\pm SD) daily rates integrated over the 6-day period: **(A)** kDMS; **(B)** DMS production from DMSPd and net DMS production; **(C)** kDMSPd; **(D)** DMSPd consumption (Table 6). Time-integrated values of kDMSPd and DMSPd consumption are not available for mesocosm 5.

production is modified by a pH-sensitive factor F ; in which $F = 1 - (\text{pH}_{\text{pi}} - \text{pH}) \cdot \gamma$, where γ is the slope of time-averaged [DMS] vs. pH and pH_{pi} is the pH value of the preindustrial undisturbed ocean determined in reference model runs. The similarity in γ between experiments conducted in Arctic waters and in the subtropical North Atlantic, supports the global extrapolation of the pH vs. [DMS] dependence used as a first approximation in the model studies. However, understanding the mechanistic basis of this common response is required for more robust model predictions and this will be the focus of the remaining discussion.

Mechanisms Driving the DMS Response

Compared to many other approaches, the large *in situ* mesocosm approach has advantages of scalability, in part because it effectively captures many of the natural ecological interactions that are important influences in the response of pelagic ecosystems. That said, there are several caveats that need to be made clear in interpreting the DMS response. Although the lack of continuity in the waters sampled outside the mesocosms needs to be considered, the increasing difference between [DMS] in the mesocosms vs. Atlantic waters (Figure 2A) as the experiment progressed, points to some characteristic of the mesocosm environment that causes enhanced production or inhibits DMS loss. This may also be true of the trends in [DMSOd] inside and outside the mesocosms, which appear similar in the early stages of the experiment but remain at a higher level in the

mesocosms toward the end of the experiment (Figure 2D). This is in contrast to the temporal trends in [DMSPd] and [DMSPp] that remain of a similar magnitude to the surrounding Atlantic waters throughout (Figures 2B,C). Two DMS removal processes, exchange with the atmosphere and photochemistry, are potentially affected by the enclosures and, as a result, net DMS production may be enhanced, leading to elevated [DMS]. In the Arctic mesocosm experiment, loss rates of added N_2O were slightly higher than predicted from the measured average wind speeds close to the mesocosms, counter-intuitively indicating an enhanced loss rate from the mesocosms (Czerny et al., 2013). This possibly results from perturbation of the air-sea interface due to the routine sampling and from interactions with the mesocosm walls (Czerny et al., 2013). Gas exchange rates were not measured directly during the present experiment and the closest wind speed recordings from nearby Las Palmas Airport averaged 5.3 m s^{-1} between t_0 and t_{23} , more than 2-fold higher than during the EPOCA experiment. Even though the magnitude of the DMS sea-to-air flux is uncertain, it is expected to have varied in direct proportion to [DMS] in each mesocosm and therefore, to have minimal influence on the relationship between $[\text{H}^+]_{\text{T}}$ and [DMS] across mesocosms.

Another DMS loss process potentially affected by the enclosures is photolysis, including photo-oxidation to DMSOd. The indirect photolysis of DMS requires photochemical production of oxidants derived from sources including

TABLE 5 | Concentrations and rates determined using the ^{35}S -DMSP approach during the period of rapid net production of DMS (t5–t11).

	M1	M9	M5	M3	M7	M4	M6	M2	M8	Atl
$[\text{H}^+]_{\text{T}}$ (nmol l $^{-1}$)	8.8	9.0	10.8	13.8	16.1	18.0	20.9	22.9	26.2	8.9
[DMSPd] (nmol l $^{-1}$)	2.5	1.9	2.0	1.9	1.9	1.7	2.1	1.3	1.6	1.8
[DMS] (nmol l $^{-1}$)	5.0	5.6	5.4	5.4	4.3	3.5	4.1	3.7	2.7	1.7
[DMSPp] (nmol l $^{-1}$)	11.5	15.9	15.5	17.5	11.7	11.0	11.5	11.0	11.6	11.2
[DMSOd] (nmol l $^{-1}$)	13.2	14.3	16.7	9.4	15.0	15.4	15.0	14.1	20.0	11.2
kDMS (h $^{-1}$) ^a	0.065	0.061	0.057	0.056	0.047	0.045	0.054	0.050	0.047	0.017
DMS production (nmol l $^{-1}$ d $^{-1}$) ^b	3.9	2.8	2.9	2.5	2.2	1.9	3.0	1.8	2.0	0.8
DMS net production (nmol l $^{-1}$ d $^{-1}$) ^c	0.68	0.68	0.65	0.72	0.48	0.45	0.23	0.30	0.23	0.05
DMS removal (nmol l $^{-1}$ d $^{-1}$) ^d	3.2	2.1	2.2	1.8	1.7	1.5	2.8	1.5	1.8	0.7
DMS turnover (d) ^e	1.6	2.8	3.0	3.5	2.8	1.5	2.7	3.0	2.9	2.5
kDMSPd (h $^{-1}$) ^a	−0.40	−0.57	−0.24*	−0.19	−0.30	−0.34	−0.40	−0.25	−0.28	−0.15
DMSPd consumption (nmol l $^{-1}$ d $^{-1}$) ^b	18.9	19.3	11.8*	7.9	11.5	11.9	18.2	7.4	9.2	5.7
DMSPd turnover (d) ^e	0.13	0.10	0.20*	0.24	0.17	0.14	0.13	0.19	0.19	0.44
DMS yield (%) ^f	21	14	23*	32	19	16	16	24	22	14
DMSPp turnover (d) ^g	0.61	0.82	1.31*	2.22	1.01	0.92	0.63	1.48	1.26	1.98
DMSOd net production (nmol l $^{-1}$ d $^{-1}$) ^c	2.4	1.9	2.0	−0.9	1.7	1.6	0.4	2.3	2.1	0.2

Values are the average of integrated daily data points ($n = 6$). Concentrations were measured each consecutive day. Experimental rates in each mesocosm (M) and Atlantic seawater were determined on t5, t9, and t11.

^aRate coefficients were calculated as shown in **Figure 6, Table 4**, with hourly rates extrapolated to a daily value.

^bRates were calculated from the rate coefficients and daily concentration.

^cDMS and DMSOd net production were calculated from the difference in daily values of [DMS] and [DMSOd].

^dDMS removal was calculated from the difference between DMS production from DMSPd and the DMS net production.

^eTurnover rates for each day were calculated from the removal or consumption rates and the daily concentration (e.g., [DMS]/DMS removal).

^fDMS yield was calculated from DMS production/DMSPd consumption.

^gThis only accounts for the DMSPp transformed to DMSPd. The turnover and rate measurements do not account for direct production of DMS from DMSPp. *a value for kDMSP was not obtained for the M5 sample on t9, values shown are averages of t5 and t11 measurements.

photo-excited chromophoric dissolved organic matter (CDOM), nitrate, bromide, and the carbonate system (Mopper and Kieber, 2002; Bouillon and Miller, 2005). In general, DMS photolysis is driven by wavelengths below 400 nm but varies in relation to the composition of potential oxidants. The transparency of the polyvinyl chloride (PVC) roofs and the thermoplastic polyurethane (TPU) walls of the mesocosms rapidly reduces below 400 nm (Riebesell et al., 2013). The magnitude of DMS photolysis within the mesocosms remains to be resolved but cannot be completely ruled out on the basis of the transparency of the construction materials. For instance, higher wavelengths of 380–400 nm were reported to dominate DMS photo-oxidation to DMSO in water from the equatorial Pacific (Kieber et al., 1996). Moreover, the elevated [DMSOd] in the mesocosms compared to the Atlantic waters on t15–t23 (**Figure 2**) suggest enhanced production of DMSO relative to the surrounding waters, possibly as a result of DMS photochemistry in the mesocosms. In a separate mesocosm experiment of similar design in Norwegian coastal waters, concentrations of DMSOd and particulate DMSO were reduced under high $[\text{H}^+]_{\text{T}}$ (Zindler-Schlundt et al., 2016). This was not apparent in the present experiment in oligotrophic waters, possibly reflecting variations in the balance between biological and photochemical processes that control [DMSOd] at different latitudes and in different water types.

Changes in Community Composition and DMSPp

Understanding how environmental pressures on physiology influence the composition of planktonic communities will help

TABLE 6 | Coefficients of the linear regressions between $[\text{H}^+]_{\text{T}}$ in the mesocosms and the time-integrated coefficients and rates of DMS and DMSP metabolism between t5 and t11 (**Figure 8**), where a is the coefficient of the slope (\pm SE), b is the intercept (\pm SE), P is the significance of the F -value of the ANOVA of the regression.

Relationship	a	b	P
kDMS vs. $[\text{H}^+]_{\text{T}}$	-0.00085 ± 0.00026	0.067 ± 0.005	0.015
DMS from DMSPd vs. $[\text{H}^+]_{\text{T}}$	-0.078 ± 0.033	3.9 ± 0.6	0.049
DMS net production vs. $[\text{H}^+]_{\text{T}}$	-0.030 ± 0.004	3.9 ± 0.6	0.00026
kDMSP vs. $[\text{H}^+]_{\text{T}}$	-0.011 ± 0.006	-0.51 ± 0.11	0.12
DMSPd consumption vs. $[\text{H}^+]_{\text{T}}$	-0.47 ± 0.26	21.0 ± 4.7	0.13
net DMS production vs. kDMS	19.6 ± 8.2	0.56 ± 0.44	0.049

The relationship between kDMS and net DMS production is not shown in **Figure 8** but is given in the Table.

in predicting how ecosystem functions respond to climate change and ocean acidification. These adjustments in composition are likely to impact resource allocation by communities, including to biogeochemically important compounds like DMSP. Over the range of reduced pH predicted for the different RCPs (Bopp et al., 2013), this experiment suggests a decrease of between 3 and 20% in [DMSPp] and a corresponding decrease of 2–14% for DMSPp:Chl a may occur in subtropical waters (**Figures 3, 4; Table 2**). This seeming reduced investment by the community in DMSP synthesis in response to increased acidity is in contrast

to the experiment in Arctic waters, during which time-averaged total DMSP increased in relation to $[H^+]_T$ and no significant decrease in DMSP:Chl *a* vs. $[H^+]_T$ was apparent (Archer et al., 2013).

Reduced net growth of the nanophytoplankton population in relation to $[H^+]_T$ during the first phase of this subtropical experiment (Figure 5, Table 3) appears to explain the observed reduction in time-averaged [DMSP] with increasing acidity (Figure 3, Table 2). Furthermore, reduced competitiveness among nanophytoplankton in the face of increased ocean acidity may be a more general phenomenon. A recent review of experiments that have examined phytoplankton community composition in relation to increased pCO_2 and $[H^+]_T$ found a negative impact on nanoflagellates, specifically prymnesiophytes (Haptophyta), in seven of 16 studies, and a positive impact in only one experiment (Schulz et al., 2017). The composition of the nanophytoplankton populations in the present study is unclear at this time, but the estimated cell quota of ~ 2 pg DMSP cell⁻¹ from the regression between cell abundance and [DMSP] (Figure 5) is consistent with high DMSP-producing taxa such as prymnesiophytes that can accumulate intracellular DMSP concentrations of >100 mmol l⁻¹ cell volume and range in size from 2 to 10 μ m in diameter (Keller et al., 1989).

Growth rates of the calcifying prymnesiophyte *E. huxleyi* have been shown to be adversely affected by increased $[H^+]_T$ rather than changes in carbonation *per se* (Bach et al., 2011). It may be that increased $[H^+]_T$ similarly affects other species of nanophytoplankton and was responsible for reducing the growth rates and competitiveness of the nanophytoplankton populations in the present study. How exactly $[H^+]_T$ may impact growth rates is unclear but maintaining intracellular pH homeostasis in the face of increasing extracellular $[H^+]_T$ may incur physiological costs for some taxa of microalgae (Taylor et al., 2012). This may potentially have led to reduced growth rates of DMSP-producing nanophytoplankton in the more acidified mesocosms during the early stages of the experiment.

Catabolism of DMSP and Production of DMS

The ³⁵S-DMSP-based measurements of DMSPd catabolism provide additional insights into the mechanisms that result in reduced [DMS] in relation to $[H^+]_T$ in this and, possibly, other mesocosm experiments. The ³⁵S-DMSP approach used in the present study was chosen to specifically test if bacterial populations altered rates of DMSPd consumption and/or the proportion of DMSPd converted to DMS in the face of ocean acidification. The rates of DMSPd transformation that were measured in the mesocosm samples are generally consistent with previous measurements using the ³⁵S-DMSP-tracer approach (reviewed in Kiene et al., 2000; Lizotte et al., 2017). For instance, values of kDMSPd integrated from *t*5 to *t*11 ranged between -0.19 and -0.40 h⁻¹, equivalent to turnover times of the DMSPd pool of 6.3–1.3 h, respectively; confirming the rapid utilization of this labile compound by planktonic microbes (Table 5). For comparison, Kiene and Linn (2000b) recorded similar rates of kDMSPd of -0.06 to -0.28 h⁻¹, equivalent to turnover times for DMSPd of 17.3–4.1 h in the near surface (1–10 m) oligotrophic waters of the Gulf of Mexico. In oligotrophic waters during

summer in the northwestern Mediterranean, Vila-Costa et al. (2008) also measured similar rates of kDMSPd of -0.09 to -0.26 h⁻¹ that are equivalent to turnover times for DMSPd of 10.9–3.8 h.

During this subtropical experiment, rates of kDMS were determined from the production rate of ³⁵S-DMS from ³⁵S-DMSP. The yield of DMS from consumed DMSPd varied between 8 and 46% for individual samples over the course of the experiment (data not shown), with time-integrated values at the height of DMS net production (*t*5–*t*11) of 14 to 32% among the $[H^+]_T$ treatments (Table 5). Few directly comparable data for DMS yields exist from warm oceanic regions. Kiene and Linn (2000b) measured values of 5–6% in the oceanic waters of the Gulf of Mexico and Sargasso Sea. Generally lower values of 4–18% have been determined in temperate waters using similar ³⁵S-DMSP-based approaches (Zubkov et al., 2001; Merzouk et al., 2008; Lizotte et al., 2017).

Other processes, including production of DMS directly by DMSP-producers, through grazing processes, or due to viral infection and lysis, may have contributed to the significant differences in concentration and net production of DMS between $[H^+]_T$ treatments (Figures 3, 8) but were not quantified. However, two observations indicate that catabolism of DMSPd made an important contribution to the trends between [DMS] and $[H^+]_T$: (i) there was a significant correlation between the time integrated kDMS and net DMS production rates during the peak of DMS production (see Results section); and (ii) estimates of DMS production from DMSPd were on average 6-fold higher than net DMS production rates (Figure 8).

The response of kDMS in the mesocosms extrapolates to a decrease of 3 and 13% by 2100 for RCP2.6 and RCP8.5 respectively, based on the global ocean pH shifts predicted by Bopp et al. (2013). It also seems likely that a $[H^+]_T$ -related decrease in DMSPd consumption in general occurred during the *t*5–*t*11 period (Figure 8). In contrast, no significant response to $[H^+]_T$ was observed in the measurements of community bacterial production during this period, based on the incorporation into protein of ¹⁴C-leucine (Zark et al., 2017). In all mesocosms, bacterial production more than doubled from initial rates of ~ 6 –12 μ g C l⁻¹ d⁻¹ on *t*1 to 24–38 μ g C l⁻¹ d⁻¹ by *t*5 and then gradually declined before increasing again after *t*15–*t*17 to reach values of 20–42 μ g C l⁻¹ d⁻¹ by *t*23 (Hornick, pers comm.). Our data show that the response of DMSPd catabolism to ocean acidification is not closely linked to the response of the bulk community bacterial production. This emphasizes the complexity of bacterial communities and the variety of ways in which bacterial processes or different components of the community may respond to environmental stresses.

Possibly the largest uncertainty associated with the ³⁵S-DMSPd-tracer approach is conversion of the rate coefficients, kDMS, kDMSPd and kNV (h⁻¹), to production or loss rates (nmol l⁻¹ h⁻¹) based on measured [DMSPd]. The introduction of a small volume, gravity filtration (SVGF) approach to determine [DMSPd] has substantially reduced estimates of [DMSPd] over earlier techniques (Kiene and Slezak, 2006). This has the knock-on effect of reducing estimates of DMSPd loss and DMS production rate. Our analysis of DMSPd provided

values that ranged from 0.8 to 3.9 nmol l⁻¹ and averaged 1.9 nmol l⁻¹ (Figure 2), consistent with other studies using the same approach. Nonetheless, it has been shown that the amount of bioavailable DMSPd in seawater may be lower than even SVGF-based measures of [DMSPd] (Li et al., 2009). Potential inaccuracies in determining [DMSPd] do not alter the fact that elevated [H⁺]_T had a negative influence on the rate at which the pool of bioavailable DMSPd was converted to DMS, evident as a significant decrease in the time-integrated (*t*₅–*t*₁₁) rate of kDMS (Figure 8).

Our experiment demonstrated that both DMSPd catabolism in general and DMSPd cleavage, specifically, may be affected by ocean acidification to an extent that partially explains observed decreases in [DMS]. Whether this is due to a direct effect of increased [H⁺]_T on DMSP metabolism or is an indirect response to [H⁺]_T-driven changes in the composition and availability of resources, is not obvious. The contrasting temporal patterns in [DMS] and kDMS compared to [DMSPp] and nanophytoplankton abundance following *t*₁₇ suggests a shift in the resource coupling between DMSP-producing nanophytoplankton and the bacterial populations compared to the period of rapid net DMS production earlier in the experiment.

The physiological basis of the [H⁺]_T dependence of DMSPd cleavage to DMS observed in the present study warrants further investigation. The DMSP lyase DddY is a periplasmic enzyme associated with the cell surface (Yoch et al., 1997), and may be directly susceptible to variations in external [H⁺]_T. However, the DddY of *Alcaligenes* sp., for instance, has a *K_m* of 1–2 mmol l⁻¹, and DddY-producing bacteria may thrive only in DMSPd-rich microenvironments (de Souza and Yoch, 1996). Most lyase and demethylation enzymes involved in DMSP catabolism are cytoplasmic and may be protected from external changes in pH by the maintenance of intracellular pH homeostasis. The uptake of leucine by dominant components of the bacterioplankton, including SAR11, in North Atlantic waters appeared to be unaffected by short term (2 h) increases in acidity, indicating that oceanic bacteria may be tolerant to changes in pH (Hartmann et al., 2015). An enduring challenge remains to establish whether the indirect consequences of acidification, including changes in phytoplankton composition and alterations in resource availability, have a greater influence on the biogeochemical function of bacterial communities than direct effects on physiology.

CONCLUSION

As anthropogenic sources of atmospheric sulfur decrease, it becomes increasingly important to understand how natural sources, particularly DMS emissions from the oceans, will respond to environmental changes and influence atmospheric chemistry and climate. This experiment demonstrated the potential for decreased DMS emissions from the vast subtropical oceans that could result as the oceans acidify over the next century and beyond. This confirms results from similar experiments conducted in more northern latitudes in coastal seas, indicating that similar pH-sensitive and/or pCO₂-sensitive

mechanisms may influence DMS concentrations generally, with possible implications for the global sulfur budget and climate.

It was possible to distinguish several, interrelated causes of the decreased net production of DMS due to increased acidity. Higher levels of acidity decreased the abundance of nanophytoplankton populations that dominated the production of DMSPp. This had the effect of decreasing the availability of DMSPd. Bacterial populations may have responded to this decreased substrate availability by decreasing the specific rate at which they catabolized DMSPd, particularly the rate at which DMSPd was cleaved to DMS. Whether this change in DMSP catabolism was the result of a physiological response by the existing bacterial populations or reflected a change in taxonomic composition, remains to be established. A direct effect of increased acidity on DMSP uptake or catabolism cannot be discounted, especially as variations in DMS concentrations between treatments were detected earlier in the experiment than variations in the nanophytoplankton abundance or DMSP pools. Although no relationship was observed between DMSOd concentrations and levels of acidity, conversion of DMS is likely to have contributed to the increasing concentrations of DMSOd that developed in the mesocosms.

The more mechanistic understanding of the processes driving reduced [DMS] with increasing [H⁺]_T observed in this sub-tropical experiment may help to explain similar results in previous mesocosm experiments. If so, these processes may present mechanistic solutions to incorporate into predictive Earth system models, potentially providing more robust predictions of changes in DMS emissions and the consequences for climate. It remains to be resolved how the processes that drive the decreases in DMS concentration in response to increasing ocean acidity will impact DMS emissions on longer, more realistic timescales than the duration of mesocosm experiments. Future predictions may need to also embrace how the adaptive capacity, and potential for geographical redistribution, of key microbial components of the planktonic community may influence DMS cycling.

AUTHOR CONTRIBUTIONS

All authors were involved in designing the study. LB, AL, UR, KS, KP, and SA took part in the experiment. GC and GC/MS analysis was carried out by KS and KP. KS and SA carried out the ³⁵S-rate measurements. Data interpretation and manuscript writing was carried out by SA and KS with input from all other authors.

ACKNOWLEDGMENTS

We thank all the team of the Gran Canaria KOSMOS experiment for their assistance, support and bonhomie. We would also like to thank the Plataforma Oceánica de Canarias (PLOCAN) for sharing their research facilities with us and for their thoughtful hospitality and considerable support. We also thank the captain and crew of RV *Hesperides* for deploying and recovering the mesocosms (cruise 29HE20140924). Ron Kiene, University of South Alabama, kindly provided protocols for the synthesis of

³⁵S-DMSP. We gratefully acknowledge financial support from the National Science Foundation, United States (NSF project OCE-1316133 to SA, PM, and PC). Funding from the German Federal Ministry of Education and Research (BMBF) in the

framework of the coordinated project BIOACID—Biological Impacts of Ocean Acidification, phase 2 (FKZ 03F06550) largely supported the project. UR received additional funding from the Leibniz Award 2012 by the German Research Foundation (DFG).

REFERENCES

- Archer, S. D., Gilbert, F. J., Nightingale, P. D., Zubkov, M. V., Taylor, A. H., Smith, G. C., et al. (2002). Transformation of dimethylsulphoniopropionate to dimethyl sulphide during summer in the North Sea with an examination of key processes via a modelling approach. *Deep Sea Res. II* 49, 3067–3101. doi: 10.1016/S0967-0645(02)00072-3
- Archer, S. D., Kimmance, S. A., Stephens, J. A., Hopkins, F. E., Bellerby, R. G. J., Schulz, K. G., et al. (2013). Contrasting responses of DMS and DMSP to ocean acidification in Arctic waters. *Biogeosciences* 10, 1893–1908. doi: 10.5194/bg-10-1893-2013
- Archer, S. D., Tarran, G. A., Stephens, J. A., Butcher, L. J., and Kimmance, S. A. (2011). Combining flow sorting with gas chromatography to determine phytoplankton group-specific intracellular content of dimethylsulphoniopropionate (DMSP). *Aquat. Microb. Ecol.* 62, 109–121. doi: 10.3354/AME01464
- Aristegui, J., Tett, P., Hernández-Guerra, A., Basterretxea, G., Montero, M. F., Wild, K., et al. (1997). The influence of island-generated eddies on chlorophyll distribution: a study of mesoscale variation around Gran Canaria. *Deep Sea Res. I* 44, 71–96. doi: 10.1016/S0967-0637(96)00093-3
- Avgoustidi, V., Nightingale, P. D., Joint, I., Steinke, M., Turner, S. M., Hopkins, F. E., et al. (2012). Decreased marine dimethyl sulfide production under elevated CO₂ levels in mesocosm and in vitro studies. *Environ. Chem.* 9, 399–404. doi: 10.1071/EN11125
- Bach, L. T., Riebesell, U., and Schulz, K. G. (2011). Distinguishing between the effects of ocean acidification and ocean carbonation in the coccolithophore *Emiliania huxleyi*. *Limnol. Oceanogr.* 56, 2040–2050. doi: 10.4319/lo.2011.56.6.2040
- Bach, L. T., Alvarez-Fernandez, S., Hornick, T., Stühr, A., and Riebesell, U. (2017). Simulated ocean acidification reveals winners and losers in coastal phytoplankton. *PLoS ONE* 12:e0188198. doi: 10.1371/journal.pone.0188198
- Barlow, R. G., Cummings, D. G., and Gibb, S. W. (1997). Improved resolution of mono- and divinyl chlorophylls a and b and zeaxanthin and lutein in phytoplankton extracts using reverse phase C-8 HPLC. *Mar. Ecol. Prog. Ser.* 161, 303–307.
- Bates, N. R., Best, M. H. P., Neely, K., Garley, R., Dickson, A. G., and Johnson, R. J. (2012). Detecting anthropogenic carbon dioxide uptake and ocean acidification in the North Atlantic Ocean. *Biogeosciences* 9, 2509–2522. doi: 10.5194/bg-9-2509-2012
- Bates, T. S., Kiene, R. P., Wolfe, G. V., Matrai, P. A., Chavez, F. P., Buck, K. R., et al. (1994). The cycling of sulfur in surface seawater of the Northeast Pacific. *J. Geophys. Res.* 99, 7835–7843. doi: 10.1029/93JC02782
- Boden, R., Kelly, D. P., Murrell, J. C., and Schäfer, H. (2010). Oxidation of dimethylsulfide to tetrathionate by *Methylophaga thiooxidans* sp. nov.: a new link in the sulfur cycle. *Environ. Microbiol.* 12, 2688–2699. doi: 10.1111/j.1462-2920.2010.02238.x
- Bopp, L., Resplandy, L., Orr, J. C., Doney, S. C., Dunne, J. P., Gehlen, M., et al. (2013). Multiple stressors of ocean ecosystems in the 21st century: projections with CMIP5 models. *Biogeosciences* 10, 6225–6245. doi: 10.5194/bg-10-6225-2013
- Bouillon, R. C., and Miller, W. L. (2005). Photodegradation of dimethyl sulfide (DMS) in natural waters: laboratory assessment of the nitrate-photolysis-induced DMS oxidation. *Environ. Sci. Tech.* 39, 9471–9477. doi: 10.1021/es048022z
- Carslaw, K. S., Lee, L. A., Reddington, C. L., Pringle, K. J., Rap, A., Forster, P. M., et al. (2013). Large contribution of natural aerosols to uncertainty in indirect forcing. *Nature* 503, 67–74. doi: 10.1038/nature12674
- Chen, T. Y., and Jang, M. (2012). Secondary organic aerosol formation from photooxidation of a mixture of dimethyl sulfide and isoprene. *Atmos. Environ.* 46, 271–278. doi: 10.1016/j.atmosenv.2011.09.082
- Czerny, J., Schulz, K. G., Ludwig, A., and Riebesell, U. (2013). A simple method for air–sea gas exchange measurements in mesocosms and its application in carbon budgeting. *Biogeosciences* 10, 11989–12017. doi: 10.5194/bg-10-1379-2013
- Dacey, J. W., Howse, F. A., Michaels, A. F., and Wakeham, S. G. (1998). Temporal variability of dimethylsulfide and dimethylsulfoniopropionate in the Sargasso Sea. *Deep Sea Res. I* 45, 2085–2104. doi: 10.1016/S0967-0637(98)00048-X
- del Valle, D. A., Kieber, D. J., John, B., and Kiene, R. P. (2007). Light-stimulated production of dissolved DMSO by a particle-associated process in the Ross Sea, Antarctica. *Limnol. Oceanogr.* 52, 2456–2466. doi: 10.4319/lo.2007.52.6.2456
- de Souza, M. P., and Yoch, D. C. (1996). “N-terminal amino acid sequences and comparison of DMSP lyases from *Pseudomonas dooudoroffii* and *Alcaligenes* strain M3A,” in *Biological and Environmental Chemistry of DMSP and Related Sulfonium Compounds*, eds M. D. Keller, R. D. Kiene, G. O. Kirst, and P. T. Visscher (Boston, MA: Springer), 293–304.
- Duarte, C. M., Hendriks, I. E., Moore, T. S., Olsen, Y. S., Steckbauer, A., Ramajo, L., et al. (2013). Is ocean acidification an open-ocean syndrome? Understanding anthropogenic impacts on seawater pH. *Est. Coasts* 36, 221–236. doi: 10.1007/s12237-013-9594-3
- Fomba, K. W., Müller, K., van Pinxteren, D., Poulain, L., van Pinxteren, M., and Herrmann, H. (2014). Long-term chemical characterization of tropical and marine aerosols at the Cape Verde Atmospheric Observatory (CVAO) from 2007 to 2011. *Atmos. Chem. Phys.* 14, 8883–8904. doi: 10.5194/acp-14-8883-2014
- González-Dávila, M., Santana-Casiano, J. M., Rueda, M. J., and Llinas, O. (2010). The water column distribution of carbonate system variables at the ESTOC site from 1995 to 2004. *Biogeosciences* 7, 3067–3081. doi: 10.5194/bg-7-3067-2010
- Hartmann, M., Hill, P. G., Tynan, E., Achterberg, E. P., Leakey, R. J., and Zubkov, M. V. (2015). Resilience of SAR11 bacteria to rapid acidification in the high-latitude open ocean. *FEMS Microbiol. Ecol.* 92:fiv161. doi: 10.1093/femsec/fiv161
- Hatton, A. D., Turner, S. M., Malin, G., and Liss, P. S. (1998). Dimethylsulphoxide and other biogenic sulphur compounds in the Galapagos Plume. *Deep Sea Res. II* 45, 1043–1053. doi: 10.1016/S0967-0645(98)00017-4
- Haywood, J., and Boucher, O. (2000). Estimates of the direct and indirect radiative forcing due to tropospheric aerosols: a review. *Rev. Geophys.* 38, 513–543. doi: 10.1029/1999RG000078
- Hopkins, F. E., and Archer, S. D. (2014). Consistent increase in dimethyl sulfide (DMS) in response to high CO₂ in five shipboard bioassays from contrasting NW European waters. *Biogeosciences* 11, 4925–4940. doi: 10.5194/bg-11-4925-2014
- Hopkins, F. E., Turner, S. M., Nightingale, P. D., Steinke, M., Bakker, D., and Liss, P. S. (2010). Ocean acidification and marine trace gas emissions. *Proc. Natl. Acad. Sci. U.S.A.* 107, 760–765. doi: 10.1073/pnas.0907163107
- Husscherr, R., Levasseur, M., Lizotte, M., Tremblay, J. É., Mol, J., Helmuth, T., et al. (2017). Impact of ocean acidification on Arctic phytoplankton blooms and dimethyl sulfide concentration under simulated ice-free and under-ice conditions. *Biogeosciences* 14, 2407–2427. doi: 10.5194/bg-14-2407-2017
- Johnson, M. T., and Bell, T. G. (2008). Coupling between dimethylsulfide emissions and the ocean-atmosphere exchange of ammonia. *Environ. Chem.* 5, 259–267. doi: 10.1071/EN08030
- Joint, I., Doney, S. C., and Karl, D. M. (2011). Will ocean acidification affect marine microbes? *ISME J.* 5, 1–7. doi: 10.1038/ismej.2010.79
- Keller, M. D., Bellows, W. K., and Guillard, R. R. L. (1989). “Dimethyl sulfide production in marine phytoplankton,” in *Biogenic Sulfur in the Environment*, eds E. S. Saltzman and W. J. Cooper (American Chemical Society), 183–200.
- Kieber, D. J., Jiao, J., Kiene, R. P., and Bates, T. S. (1996). Impact of dimethylsulfide photochemistry on methyl sulfur cycling in the equatorial Pacific Ocean. *J. Geophys. Res. Oceans* 101, 3715–3722. doi: 10.1029/95JC03624

- Kiene, R., and Linn, L. (2000a). The fate of dissolved dimethylsulfoniopropionate (DMSP) in seawater: tracer studies using ^{35}S -DMSP. *Geochim. Cosmochim. Acta* 64, 2797–2810. doi: 10.1016/S0016-7037(00)00399-9
- Kiene, R. P., and Linn, L. J. (2000b). Distribution and turnover of dissolved DMSP and its relationship with bacterial production and dimethylsulfide in the Gulf of Mexico. *Limnol. Oceanogr.* 45, 849–861. doi: 10.4319/lo.2000.45.4.0849
- Kiene, R. P., Linn, L. J., and Bruton, J. A. (2000). New and important roles for DMSP in marine microbial communities. *J. Sea Res.* 43, 209–224. doi: 10.1016/S1385-1101(00)00023-X
- Kiene, R. P., and Slezak, D. (2006). Low dissolved DMSP concentrations in seawater revealed by small volume gravity filtration and dialysis sampling. *Limnol. Oceanogr. Methods* 4, 80–95. doi: 10.4319/lom.2006.4.80
- Kim, J. M., Lee, K., Yang, E. J., Shin, K., Noh, J. H., Park, K. T., et al. (2010). Enhanced production of oceanic dimethylsulfide resulting from CO_2 -induced grazing activity in a high CO_2 world. *Environ. Sci. Tech.* 44, 8140–8143. doi: 10.1021/es102028k
- Kirkby, J., Curtius, J., Almeida, J., Dunne, E., Duplissy, J., Ehrhart, S., et al. (2011). Role of sulphuric acid, ammonia and galactic cosmic rays in atmospheric aerosol nucleation. *Nature* 476, 429–433. doi: 10.1038/nature10343
- Lana, A., Bell, T., Sim, R., Vallina, S. M., Ballabrera-Poy, J., Kettle, A. J., et al. (2011). An updated climatology of surface dimethylsulfide concentrations and emission fluxes in the global ocean. *Glob. Biogeochem. Cycles* 25:GB1004. doi: 10.1029/2010GB003850
- Li, C. X., Yang, G. P., and Kiene R. P. (2009). “Bio-availability and turnover of dissolved dimethylsulfoniopropionate (DMSP) in coastal waters of the Gulf of Mexico,” in *Abstracts of the SOLAS Open Science Conference 2009* (Barcelona).
- Lizotte, M., Levasseur, M., Law, C. S., Walker, C. F., Safi, K. A., Marriner, A., et al. (2017). Dimethylsulfoniopropionate (DMSP) and dimethyl sulfide (DMS) cycling across contrasting biological hotspots of the New Zealand subtropical front. *Ocean Sci.* 13, 961–982. doi: 10.5194/os-13-961-2017
- Lohmann, U., and Feichter, J. (2005). Global indirect aerosol effects: a review. *Atmos. Chem. Phys.* 5, 715–737. doi: 10.5194/acp-5-715-2005
- Lueker, T. J., Dickson, A. G., and Keeling, C. D. (2000). Ocean pCO_2 calculated from dissolved inorganic carbon, alkalinity, and equations for K_1 and K_2 : validation based on laboratory measurements of CO_2 in gas and seawater at equilibrium. *Mar. Chem.* 70, 105–119. doi: 10.1016/S0304-4203(00)00022-0
- Malmstrom, R. R., Kiene, R. P., Cottrell, M. T., and Kirchman, D. L. (2004). Contribution of SAR11 bacteria to dissolved dimethylsulfoniopropionate and amino acid uptake in the North Atlantic ocean. *Appl. Environ. Microbiol.* 70, 4129–4135. doi: 10.1128/AEM.70.7.4129-4135.2004
- Merzouk, A., Levasseur, M., Scarratt, M., Michaud, S., Lizotte, M., Rivkin, R. B., et al. (2008). Bacterial DMSP metabolism during the senescence of the spring diatom bloom in the Northwest Atlantic. *Mar. Ecol. Progr. Ser.* 369, 1–11. doi: 10.3354/meps07664
- Molina, R. (1976). Consideraciones Sobre la Corriente de Canarias, Asamblea Nacional de Geodesia y Geofísica. *Comunicaciones* 3, 1567–1588.
- Mopper, K., and Kieber, D. J. (2002). “Photochemistry and the cycling of carbon, sulfur, nitrogen and phosphorus,” in *Biogeochemistry of Marine Dissolved Organic Matter*, eds D. A. Hansell and C. A. Carlson (San Diego, CA: Academic Press), 455–503.
- Müller, K., Lehmann, S., Pinxteren, D. V., Gnauk, T., Niedermeier, N., Wiedensohler, A., et al. (2010). Particle characterization at the Cape Verde atmospheric observatory during the 2007 RHaMBLE intensive. *Atmos. Chem. Phys.* 10, 2709–2721. doi: 10.5194/acp-10-2709-2010
- Neuer, S., Cianca, A., Helmke, P., Freudenthal, T., Davenport, R., Meggers, H., et al. (2007). Biogeochemistry and hydrography in the eastern subtropical North Atlantic gyre. Results from the European time-series station ESTOC. *Progr. Oceanogr.* 72, 1–29. doi: 10.1016/j.pocan.2006.08.001
- Park, K. T., Lee, K., Shin, K., Yang, E. J., Hyun, B., Kim, J. M., et al. (2014). Direct linkage between dimethyl sulfide production and microzooplankton grazing, resulting from prey composition change under high partial pressure of carbon dioxide conditions. *Environ. Sci. Tech.* 4750–4756. doi: 10.1021/es403351h
- Pierrot, D., Lewis, E., and Wallace, D. W. R. (2006). *MS Excel Program Developed for CO_2 System Calculations*. ORNL/CDIAC-105a. Oak Ridge, TN: Carbon Dioxide Information Analysis Center, Oak Ridge National Laboratory, US Department of Energy.
- Raven, J. A. (2013). “Half a century of pursuing the pervasive proton,” in *Progress in Botany*, eds U. Lüttge, W. Beyschlag, D. Francis, and J. Cushman (Berlin; Heidelberg, Springer), 3–34. doi: 10.1007/978-3-642-30967-0_1
- Reisch, C. R., Moran, M. A., and Whitman, W. B. (2011). Bacterial catabolism of dimethylsulfoniopropionate (DMSP). *Front. Microbiol.* 2:172. doi: 10.3389/fmicb.2011.00172
- Riebesell, U., Czerny, J., Von Bröckel, K., Boxhammer, T., Büdenbender, J., Deckelnick, M., et al. (2013). Technical note: a mobile sea-going mesocosm system - new opportunities for ocean change research. *Biogeosciences* 10, 1835–1847. doi: 10.5194/bg-10-1835-2013
- Rinaldi, M., Decesari, S., Finessi, E., Giulianelli, L., Carbone, C., Fuzzi, S., et al. (2010). Primary and secondary organic marine aerosol and oceanic biological activity: recent results and new perspectives for future studies. *Adv. Meteorol.* 2010:310682. doi: 10.1155/2010/310682
- Sabine, C. L., Feely, R. A., Gruber, N., Key, R. M., Lee, K., Bullister, J. L., et al. (2004). The oceanic sink for anthropogenic CO_2 . *Science* 305, 367–371. doi: 10.1126/science.1097403
- Schulz, K. G., Bach, L. T., Bellerby, R. G., Bermúdez, R., Büdenbender, J., Boxhammer, T., et al. (2017). Phytoplankton blooms at increasing levels of atmospheric carbon dioxide: experimental evidence for negative effects on prymnesiophytes and positive on small picoeukaryotes. *Front. Mar. Sci.* 4, 1–18. doi: 10.3389/fmars.2017.00064
- Schwinger, J., Tjiputra, J., Goris, N., Six, K. D., Kirkevåg, A., Seland, Ø., et al. (2017). Amplification of global warming through pH dependence of DMS production simulated with a fully coupled Earth system model. *Biogeosciences* 14, 3633–3648. doi: 10.5194/bg-14-3633-2017
- Signorini, S. R., Franz, B. A., and McClain, C. R. (2015). Chlorophyll variability in the oligotrophic gyres: mechanisms, seasonality and trends. *Front. Mar. Sci.* 2:1. doi: 10.3389/fmars.2015.00001
- Simó, R., Grimalt, J. O., and Albaigés, J. (1997). Dissolved dimethylsulphide, dimethylsulphoniopropionate and dimethylsulphoxide in western Mediterranean waters. *Deep Sea Res. II* 44, 929–950. doi: 10.1016/S0967-0645(96)00099-9
- Sipilä, M., Berndt, T., Petäjä, T., Brus, D., Vanhanen, J., Stratmann, F., et al. (2010). The role of sulfuric acid in atmospheric nucleation. *Science* 327, 1243–1246. doi: 10.1126/science.1180315
- Six, K. D., Kloster, S., Ilyina, T., Archer, S. D., Zhang, K., and Maier-Reimer, E. (2013). Global warming amplified by reduced sulphur fluxes as a result of ocean acidification. *Nat. Clim. Chang.* 3, 975–978. doi: 10.1038/nclimate1981
- Stefels, J., Steinke, M., Turner, S., Malin, G., and Belviso, S. (2007). Environmental constraints on the production and removal of the climatically active gas dimethylsulphide (DMS) and implications for ecosystem modelling. *Biogeochemistry* 83, 245–275. doi: 10.1007/s10533-007-9091-5
- Taucher, J., Bach, L. T., Boxhammer, T., Nauendorf, A., Achterberg, E. P., Algueró-Muñoz, M., et al. (2017). Influence of ocean acidification and deep water upwelling on oligotrophic plankton communities in the subtropical North Atlantic: insights from an in situ mesocosm study. *Front. Mar. Sci.* 4:85. doi: 10.3389/fmars.2017.00085
- Taylor, A. R., Brownlee, C., and Wheeler, G. L. (2012). Proton channels in algae: reasons to be excited. *Trends Plant Sci.* 17, 675–684. doi: 10.1016/j.tplants.2012.06.009
- Toumi, R. (1994). BrO as a sink for dimethylsulphide in the marine atmosphere. *Geophys. Res. Letts.* 21, 117–120. doi: 10.1029/93GL03536
- Vila-Costa, M., del Valle, D. A., González, J. M., Slezak, D., Kiene, R. P., Sánchez, O., et al. (2006). Phylogenetic identification and metabolism of marine dimethylsulfide-consuming bacteria. *Environ. Microbiol.* 8, 2189–2200. doi: 10.1111/j.1462-2920.2006.01102.x
- Vila-Costa, M., Kiene, R. P., and Simó, R. (2008). Seasonal variability of the dynamics of dimethylated sulfur compounds in a coastal northwest Mediterranean site. *Limnol. Oceanogr.* 53, 198–211. doi: 10.4319/lo.2008.53.1.0198
- Vogt, M., Steinke, M., Turner, S., Paulino, A., Meyerhöfer, M., Riebesell, U., et al. (2008). Dynamics of dimethylsulphoniopropionate and dimethylsulphide under different CO_2 concentrations during a mesocosm experiment. *Biogeosciences* 5, 407–419. doi: 10.5194/bg-5-407-2008
- Wang, S., Elliott, S., Maltrud, M., and Cameron-Smith, P. (2015). Influence of explicit *Phaeocystis* parameterizations on the global distribution of

- marine dimethyl sulfide. *J. Geophys. Res. Biogeosci.* 120, 2158–2177. doi: 10.1002/2015JG003017
- Webb, A. L., Leedham-Elvidge, E., Hughes, C., Hopkins, F. E., Malin, G., Bach, L. T., et al. (2016a). Effect of ocean acidification and elevated CO₂ on trace gas production by a Baltic Sea summer phytoplankton community. *Biogeosciences* 13, 4595–4613. doi: 10.5194/bg-13-4595-2016
- Webb, A. L., Malin, G., Hopkins, F. E., Ho, K. L., Riebesell, U., Schulz, K. G., et al. (2016b). Ocean acidification has different effects on the production of dimethylsulfide and dimethylsulfoniopropionate measured in cultures of *Emiliania huxleyi* and a mesocosm study: a comparison of laboratory monocultures and community interactions. *Environ. Chem.* 13, 314–329. doi: 10.1071/EN14268
- Wingenter, O. W., Haase, K. B., Zeigler, M., Blake, D. R., Rowland, F. S., Sive, B. C., et al. (2007). Unexpected consequences of increasing CO₂ and ocean acidity on marine production of DMS and CH₂ClI: potential climate impacts. *Geophys. Res. Letts.* 34:L05710. doi: 10.1029/2006GL028139
- Yassaa, N., Colomb, A., Lochte, K., Peeken, I., and Williams, J. (2006). Development and application of a headspace solid-phase microextraction and gas chromatography/mass spectrometry method for the determination of dimethylsulfide emitted by eight marine phytoplankton species. *Limnol. Oceanogr. Methods* 4, 374–381. doi: 10.4319/lom.2006.4.374
- Yoch, D. C., Ansedé, J. H., and Rabinowitz, K. S. (1997). Evidence for intracellular and extracellular dimethylsulfoniopropionate (DMSP) lyases and DMSP uptake sites in two species of marine bacteria. *Appl. Environ. Microbiol.* 63, 3182–3188.
- Zark, M., Broda, N. K., Hornick, T., Grossart, H. P., Riebesell, U., and Dittmar, T. (2017). Ocean acidification experiments in large-scale mesocosms reveal similar dynamics of dissolved organic matter production and biotransformation. *Front. Mar. Sci.* 4:271. doi: 10.3389/fmars.2017.00271
- Zindler-Schlundt, C., Lutterbeck, H., Endres, S., and Bange, H. W. (2016). Environmental control of dimethylsulfoxide (DMSO) cycling under ocean acidification. *Environ. Chem.* 13, 330–339. doi: 10.1071/EN14270
- Zubkov, M. V., Fuchs, B. M., Archer, S. D., Kiene, R. P., Amann, R., and Burkill, P. H. (2001). Linking the composition of bacterioplankton to rapid turnover of dissolved dimethylsulphoniopropionate in an algal bloom in the North Sea. *Environ. Microbiol.* 3, 304–311. doi: 10.1046/j.1462-2920.2001.00196.x

Conflict of Interest Statement: The authors declare that the research was conducted in the absence of any commercial or financial relationships that could be construed as a potential conflict of interest.

Copyright © 2018 Archer, Suffrian, Posman, Bach, Matrai, Countway, Ludwig and Riebesell. This is an open-access article distributed under the terms of the Creative Commons Attribution License (CC BY). The use, distribution or reproduction in other forums is permitted, provided the original author(s) and the copyright owner(s) are credited and that the original publication in this journal is cited, in accordance with accepted academic practice. No use, distribution or reproduction is permitted which does not comply with these terms.



Plankton Community Respiration and ETS Activity Under Variable CO₂ and Nutrient Fertilization During a Mesocosm Study in the Subtropical North Atlantic

Alba Filella¹, Isabel Baños¹, María F. Montero¹, Nauzet Hernández-Hernández¹, Adriana Rodríguez-Santos¹, Andrea Ludwig², Ulf Riebesell² and Javier Arístegui^{1*}

¹ Instituto de Oceanografía y Cambio Global, Universidad de Las Palmas de Gran Canaria, Las Palmas, Spain, ² Biological Oceanography, GEOMAR Helmholtz Centre for Ocean Research Kiel, Kiel, Germany

OPEN ACCESS

Edited by:

Hongbin Liu,
Hong Kong University of Science
and Technology, Hong Kong

Reviewed by:

J. Michael Beman,
University of California, Merced,
United States
Carol Robinson,
University of East Anglia,
United Kingdom

*Correspondence:

Javier Arístegui
javier.aristegui@ulpgc.es

Specialty section:

This article was submitted to
Marine Biogeochemistry,
a section of the journal
Frontiers in Marine Science

Received: 29 March 2018

Accepted: 13 August 2018

Published: 28 August 2018

Citation:

Filella A, Baños I, Montero MF,
Hernández-Hernández N,
Rodríguez-Santos A, Ludwig A,
Riebesell U and Arístegui J (2018)
Plankton Community Respiration
and ETS Activity Under Variable CO₂
and Nutrient Fertilization During
a Mesocosm Study in the Subtropical
North Atlantic. *Front. Mar. Sci.* 5:310.
doi: 10.3389/fmars.2018.00310

The enzymatic electron transport system (ETS) assay is frequently used as a proxy of respiratory activity in planktonic communities. It is thought to estimate the maximum overall activity of the enzymes associated with the respiratory ETS systems in both eukaryotic and prokaryotic organisms. Thus, in order to derive actual respiration rates (R) from ETS it is necessary to determine empirical R/ETS conversion algorithms. In this study we explore the temporal development of R and ETS activity in natural plankton communities (from bacteria to large phytoplankton) enclosed in mesocosms, treated with different CO₂ concentrations. The experiment lasted 30 days, during which abrupt changes in community structure and biomass occurred through a sharp transition from oligotrophy (phase I) to highly eutrophic conditions (phase II) after nutrient-induced fertilization (day 18). R and ETS did not show any response to CO₂ under oligotrophic conditions, but R increased significantly more in the two high CO₂ mesocosms after fertilization, coinciding with a sharp rise in large phytoplankton (mostly diatoms). R and ETS were significantly correlated only during the eutrophic phase. The R/ETS ranged more than threefold in magnitude during the experiment, with phase-averaged values significantly higher under oligotrophic conditions (0.7–1.1) than after nutrient fertilization (0.5–0.7). We did not find any significant relationship between R/ETS and community structure or biomass, although R correlated significantly with total biomass after fertilization in the four mesocosms. Multiple stepwise regression models show that large phytoplankton explains most of the variance in R during phases I (86%) and II (53%) and of ETS (86%) during phase II, while picophytoplankton contributes up to 73% to explain the variance in the ETS model during phase I. Our results suggest that R/ETS may be too variable in the ocean as to apply constant values to different communities living under contrasting environmental conditions. Controlled experiments with natural communities, like the present one, would help to constrain the range of variability of the R/ETS ratio, and to understand the factors driving it.

Keywords: plankton respiration, ETS activity, R/ETS, ocean acidification, nutrient fertilization, mesocosm, subtropical North Atlantic

INTRODUCTION

Respiration is a key factor in organic carbon utilization and energy flow in oceanic ecosystems. It is regarded to be an ubiquitous process, occurring at all depths and in all regions, so it can be used as an indicator of community metabolism for aquatic ecology studies (del Giorgio and Williams, 2005). The rates of community respiration are, however, generally low and consequently difficult to measure in the ocean, particularly in the deep cold waters, where long term (>24 h) *in vitro* incubations are necessary to measure significant changes in oxygen concentration. Several studies have reported changes in bacterial abundance, phylogenetic composition (e.g., Massana et al., 2001) and metabolic rates (Jürgens et al., 2000; Massana et al., 2001; Gattuso et al., 2002) during ≥ 24 h incubations, caused by a number of factors, like bacterivory pressure (Hopkinson et al., 1989) or changes in inorganic and organic nutrients inside the incubation bottles (Gasol and Morán, 1999). Other studies, however, have shown that *in vitro* incubations may not drastically affect the respiratory rates of bacterial populations, in spite of shifts in the bacterial assemblage composition during the incubation (e.g., Baltar et al., 2012).

In order to overcome the potential difficulties in measuring community respiration by oxygen consumption during long incubation periods, other alternative approaches have been used (see review in Robinson and Williams, 2005). Among these, Packard (1971) introduced the electron transport system (ETS) assay as an index of potential respiration for planktonic organisms. The determination of ETS activity in plankton is thought to estimate, under saturation of substrates, the maximum overall capacity of the enzymes associated with the respiratory ETS (i.e., the potential respiration) in both eukaryotic and prokaryotic organisms (Packard, 1985). Since the introduction of the ETS method, this approach has been widely used to estimate the respiratory activity of specific components of marine plankton (e.g., Kenner and Ahmed, 1975; King and Packard, 1975; Christensen et al., 1980; Bidigare et al., 1982; Finlay et al., 1983; Packard et al., 1983; Packard, 1985; Hernández-León, 1988; Schalk, 1988; Martinez, 1991). However, like other enzymatic methods, the ETS represents a proxy of activity, which needs to be transformed to actual respiration rates (R) by means of a R/ETS ratio or relationship. Paradoxically, few studies have investigated the variability of R/ETS, with the aim to elucidate whether ETS could be universally used to derive actual respiration in marine ecosystems (Packard and Williams, 1981; Vosjan et al., 1987, 1990; Mimura et al., 1988; Arístegui and Montero, 1995; Arístegui et al., 2005; Reinthaler et al., 2006). Published empirical R/ETS ratios for bacteria, phytoplankton and zooplankton show a wide range of values (0.2 to >1), with large standard deviations (Table 1), suggesting that it may vary with community structure and specific metabolism of the different members of the community. Unfortunately, the meager database on R/ETS is insufficient to conclude on the causes of its variability. In spite of this, R has been frequently inferred from ETS using constant R/ETS ratios, sometimes without any reasoning for the selection of the applied conversion factor (e.g., Bangqin et al., 2005; Ramírez et al., 2006).

Here we aim to contribute to the understanding of the causes and magnitude of variability of R, ETS, and their ratio. This is the first study where R and ETS are simultaneously measured under controlled conditions, inside mesocosms, during a relatively long period of time (30 days), where the ecosystem undergoes sharp changes in nutrients and CO₂ concentrations. The objective of our work was twofold. First, to investigate how the variability in the structure and biomass of the autotrophic and heterotrophic communities, under different trophic conditions (oligotrophic versus eutrophic environments), may affect community respiration, ETS activity and the R/ETS index. We wanted to test whether pulses in nutrient fertilization (e.g., due to local upwelling events) could modify the community structure, and how this is reflected in the respiratory metabolism of the whole community, estimated both as oxygen consumption and respiratory enzymatic activity. Second, to examine the effects of acidification on plankton community respiration, with the aim of predicting how different CO₂ scenarios due to anthropogenic activities might affect plankton respiration in a future ocean. In case there is a response to high CO₂ concentrations, we wanted to investigate whether it is due to a direct effect on the specific metabolism of the organisms, or rather to an indirect effect caused by the changes in community composition and total planktonic biomass.

MATERIALS AND METHODS

Experimental Design and Sampling

The study (KOSMOS Gran Canaria 2016) was carried out at the pier of Taliarte, Gran Canaria (Canary Islands), from 2nd March to 5th April 2016. Eight 11 m³ mesocosm bags were installed and supplied with seawater pumped directly from the adjacent offshore waters outside the harbor. Different pCO₂ levels were applied to each mesocosm in a random distribution: the gradient spanned from 400 μ atm (the present-day level in the atmosphere and sea surface) up to 1450 μ atm (simulating a future scenario of an acidified surface ocean). We chose the following four mesocosms for our study: M5, M6, M7, and M8 with target pCO₂ levels of 400, 1450, 700, and 1150 μ atm, respectively, although actual values varied during the different phases of the experiment (see Hopwood et al., 2018).

Depth-integrated water samples were collected using 2.5 m long custom-made samplers with an internal volume of 10 L, constructed from polypropylene tubing with valves at both ends. Samples were collected every 2 days, from the beginning of the experiment (t1) until the depletion of nutrients (t17) (phase I: t1–t17). On t18, a single macronutrient addition was applied to reach the following concentrations: 3.1 μ mol L⁻¹ nitrate, 1.5 μ mol L⁻¹ silicate, and 0.2 μ mol L⁻¹ phosphate. Then, the sampling was changed to daily in order to closely follow the development of the phytoplankton bloom (t19–t25). Over the last days (t25–t29), the sampling shifted again to every 2nd day (phase II: t18–t29). A wide variety of measurements were carried out in the mesocosms to study the effects of acidification on both ecological and biogeochemical processes (see Hopwood et al., 2018, for

TABLE 1 | Published empirical actual respiration to ETS ratios (R/ETS) [means and standard deviations (SD)] for various groups of marine organisms and for freshwater and marine plankton communities.

Location	R/ETS Average \pm SD (n)	Organisms	Reference
Cultures	0.43 \pm 0.09(98)	Senescent bacteria	Christensen et al., 1980
	5.02 \pm 1.45(49)	Active bacteria	
Cultures	0.75 \pm 0.16	Bacteria	Packard, 1985
Cultures	0.71 \pm 0.23(11)	Phytoplankton	Martinez, 1992
Cultures	0.17 \pm 0.01(106)	Phytoplankton	Kenner and Ahmed, 1975
Cultures	0.25 \pm 0.02(6)	Protozoa	Finlay et al., 1983
Canadian lakes	0.22 \pm 0.11(60)	Microplankton	del Giorgio, 1992
Med Sea (SML)	1.09 \pm 0.71(22)	Microplankton	Mimura et al., 1988
Banda Sea	0.32 \pm 0.71(10)	Microplankton	Vosjan and Nieuwland, 1987
North Sea	0.23 \pm 0.71(9)	Microplankton	Vosjan et al., 1990
Gulf of Maine	0.25 \pm 0.05(14)	Microplankton	Packard and Williams, 1981
Oceanic regions	0.89 \pm 0.4(197)	Microplankton	Aristegui and Montero, 1995
Subtropical NE Atlantic	1.14 \pm 0.22(4)	Microplankton	Hernández-León et al., 1999
Mesopelagic NE Atlantic	0.68 \pm 0.11(28)	Bacterioplankton	Aristegui et al., 2005
Bathypelagic N Atlantic	5.3	Bacterioplankton	Reinthal et al., 2006

n, number of observations; SML, surface micro layer.

additional information on the water samplers and set up of the experiment).

Community Respiration

Community respiration (R) was determined by oxygen consumption in borosilicate bottles. Water samples (5 L) were carefully siphoned using a silicone tube into four replicate “time-zero” and “dark” 125 mL-BOD bottles. Dark bottles were kept in a temperature-controlled chamber (21°C) at *in situ* temperature for ~24 h. R was estimated from the difference in oxygen concentration between the time-zero and dark bottles.

Dissolved oxygen was measured by the Winkler technique, following the recommendations of Carrit and Carpenter (1966), Bryan et al. (1976), and Grasshoff et al. (1983). The entire contents of the bottles were titrated during ~3 min by means of an automated, precise titration system, with colorimetric end-point detection (Williams and Jenkinson, 1982). The precision achieved in replicates was %CV < 0.07.

Enzymatic ETS Activity

ETS activity was measured by means of the tetrazolium reduction technique according to Aristegui and Montero (1995). Briefly, a tetrazolium salt [2-(4-iodophenyl)-3-(4-nitrophenyl)-5-phenyl tetrazolium chloride salt (INT)] is incorporated through the respiratory ETS and subsequently reduced by dehydrogenase enzymes to a non-fluorescent formazan crystal, INT-formazan. The amount of INT-formazan produced can be estimated from its absorption at 490 nm and be converted to the equivalent oxygen utilization. Seawater (about 3 L of the same carboy where water was collected for R) were poured into acid-cleaned plastic carboys, before being filtered through 47 mm Whatman GF/F filters, at a low vacuum pressure (<1/3 atm). The filters were immediately flash-frozen in liquid nitrogen and stored at -80°C until being assayed in the laboratory within a few

weeks. ETS determinations were carried out according to the Kenner and Ahmed (1975) modification of the tetrazolium reduction technique as described in Aristegui and Montero (1995). An incubation time of 15 min at 18°C was used. ETS activities measured at 18°C were converted to activities at *in situ* temperature by using the Arrhenius equation. A mean activation energy of 16 kcal mole⁻¹ was used (Aristegui and Montero, 1995).

Chlorophyll a

Samples (250–500 mL) for chlorophyll a (Chla) were filtered and collected on GF/F Whatman glass-fiber filters (nominal pore size of 0.7 µm). Chla was estimated fluorometrically by means of a Turner Designs bench fluorometer, previously calibrated with pure chlorophyll a (Sigma Co.), as described in Strickland and Parsons (1960). Pigments were extracted in cold acetone (4°C) for 24 h. For the final determination of Chla, the acetone extracts were acidified allowing Chla and phaeopigments to be independently estimated.

Prokaryotic and Eukaryotic Abundances and Biomasses

We used a FACScalibur (Becton and Dickinson) flow cytometer to look for heterotrophic bacteria (HB), small photosynthetic eukaryotic cells (picoeukaryotes), and *Prochlorococcus* and *Synechococcus* type cyanobacteria. Sea water samples (about 1 mL) were analyzed 30–60 min after sampling. *Prochlorococcus* was not found in the samples throughout the experiment. In other similar experiments we observed that *Prochlorococcus* vanished during the 1st day of enclosure in the mesocosms. Heterotrophic bacteria (HB) were fixed with a 2% final concentration of formaldehyde, after keeping them 30 min at 4°C, and then stored frozen in liquid nitrogen until analysis. Subsamples (400 µL) were stained with the fluorochrome SYBR

Green I, Molecular Probes (final concentration 1000× dilution of the commercial product) at room temperature before analyses. HB were identified by their signatures in a plot of side scatter (SSC) versus green fluorescence (FL1). Samples were run at low speed for HB ($16 \mu\text{L min}^{-1}$) and medium speed for the other photosynthetic cells ($60 \mu\text{L min}^{-1}$). A suspension of yellow-green $1 \mu\text{m}$ latex beads ($\sim 10^5$ – 10^6 beads mL^{-1}) was added as an internal standard (Polysciences, Inc., Warrington, PA, United States). Pigmented nanoeukaryotes (2 – $20 \mu\text{m}$; Nano) were counted on fresh samples with a Cytobuoy cytometer (Dubelaar and Gerritzen, 2000), provided with flow-image. Samples (about 3 – 5 mL) were analyzed *in vivo* for 7 min at a flow rate of $300 \mu\text{L min}^{-1}$. Microphytoplankton (mostly diatoms and dinoflagellates; Micro) were fixed with alkaline Lugol's iodine (1% final concentration), sedimented in Utermöhl chambers and counted by means of an inverted microscope.

Biomass of picoplankton (Pico: *Synechococcus* and picoeukaryotes) and HB were estimated by multiplying their abundances by the average cell carbon content for each group, using the conversion factors obtained by MF Montero (unpublished) from samples collected in coastal waters of Gran Canaria: 18 fgC/cell (bacteria), 120 fgC/cell (*Synechococcus*), 420 fgC/cell (picoeukaryotes). Nanoeukaryotes' abundances were converted into biomass using an estimated average biovolume of $20 \mu\text{m}^3$ for organisms between 2 and $6 \mu\text{m}$ and a biovolume of $125 \mu\text{m}^3$ for organisms between 6 and $11 \mu\text{m}$, applying the conversion factor of $220 \text{ fgC } \mu\text{m}^3$ proposed by Borsheim and Bratbak (1987). Measured average biovolumes for the different diatoms and dinoflagellates species were used to estimate their biomass using the biovolume-carbon conversion factors given by Menden-Deuer and Lessard (2000).

Total Organic Carbon (TOC) and Chromophoric Organic Carbon (CDOM)

TOC in seawater was measured using a Shimadzu TOC-V analyzer. Samples were collected in 10 mL high-density polyethylene bottles (Nalgene®) and stored at -20°C . Prior to that, bottles were acid-cleaned, flushed with MQ water and dried. Before analysis, samples were acidified with $50 \mu\text{L}$ of 50% phosphate, and sparged with CO_2 -free air for 2 min to remove inorganic carbon. To ensure the precision and accuracy of the measurement, reference Sargasso Sea deep-water samples (44 – $45 \mu\text{M C}$) and blank reference water, distributed by the Rosenstiel School of Marine and Atmospheric Science (University of Miami), were analyzed daily. TOC concentrations were determined from standard curves (30 – $200 \mu\text{M C}$) of potassium hydrogen phthalate produced every day (Thomas et al., 1995).

CDOM absorption spectra were measured with a 100 cm, $250 \mu\text{L}$ capillary (LPC100CM) connected via an optical fiber to a light source (DH2000BAC) and a USB2000+UV-VIS ES detector (Ocean Optics). The system was controlled using Spectra-suite software (Ocean Optics). Samples were injected into the capillary with a peristaltic pump at a flow rate of 1 mL min^{-1} . Relative molecular weight was estimated from CDOM absorption by deriving the slope ratio (SR), calculated as the ratio of the slope of the shorter wavelength region (275 – 295 nm) to that of the

longer wavelength region (350 – 400 nm) (Helms et al., 2008). The spectral slopes were calculated from the linear regression of the log-transformed absorption spectra.

Statistical Analysis

Model II (Reduced Major Axis) linear regressions were conducted to determine potential correlations between log-normalized data of R and ETS activity, for the whole study and for each of the phases. Statistical significance was accepted for p -values higher than 0.05 (95% of confidence level). In order to quantify the error of the correlation predictors and to compare between the different models, the Mean Absolute Percentage Error (MAPE) was calculated.

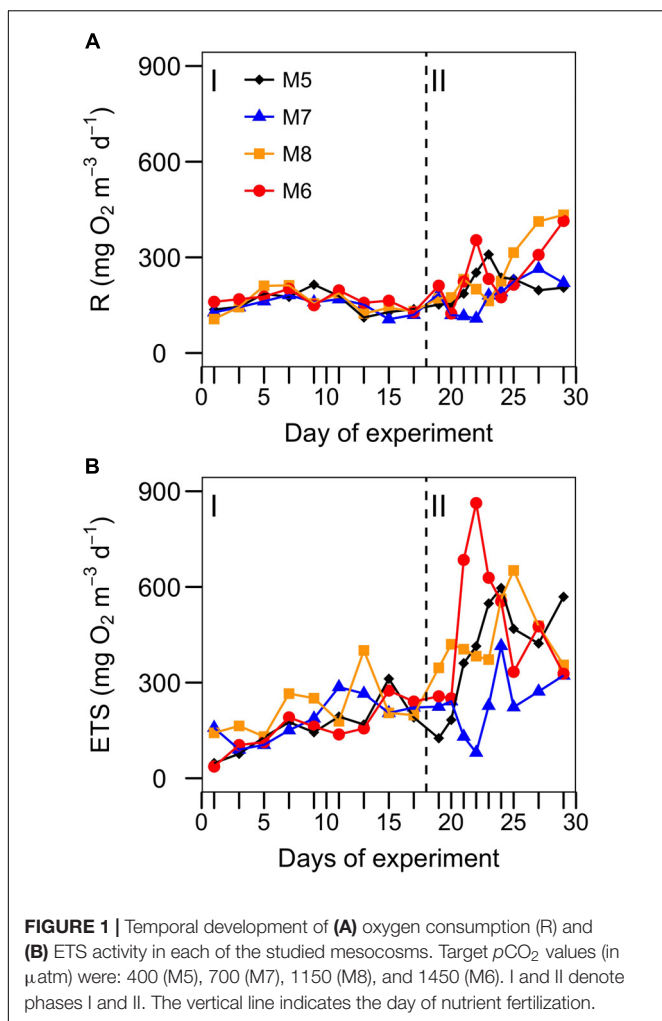
To investigate the variables (Micro, Nano, Pico and HB biomass, Chla and TOC) that influence R and ETS activity during the two phases, multivariate regression models were fitted via Stepwise Multiple Linear Regressions (SMLR). Models were built both by adding predictor variables to an initial model in which R and ETS would not be correlated with any predictor variable (Forward SMLR method), and by removing predictor variables from a full model in which R and ETS would be correlated with all predictor variables (Backward SMLR method). The selection of the best explanatory model was based on Akaike's Information Criterion (AIC). The model with lower AIC was considered as the best explanatory option for our data. All data were tested for multicollinearity using Variance Inflation Factors (VIF). Models were graphically tested for homoscedasticity. The contribution of every statistically significant predictor variable to the explained variance (R^2) was quantified calculating the Relative Importance (RI; %) using the LMG method (Lindeman et al., 1980). All statistical computations were performed using R software¹.

RESULTS

Community Respiration (R) and ETS Activity

The rates of R over the course of the experiment ranged from 106 to $433 \text{ mg O}_2 \text{ m}^{-3} \text{ d}^{-1}$, with the highest values at the end of the experiment in the mesocosms with highest CO_2 concentrations (Figure 1A). These rates are about 2–7 times higher than average values reported for open ocean waters of the Canary Islands (Aristegui and Montero, 1995). Despite the different concentrations of CO_2 in the mesocosms, a common general trend was observed during phase I (from t1 to t17). R increased from t1 to t5 to t10 and decreased thereafter until nutrient fertilization (t18). ETS activity showed a steadier increase from t1 to t17, also with no significant differences among mesocosms during phase I (Figure 1B). After nutrient fertilization (phase II), R in M5, M6, and M8 increased and peaked on days t21–t23, decreasing toward the end of the experiment. R in M6 and M8 – the two mesocosms with the highest CO_2 – started to increase after t23 reaching the highest rates at t29. R in M7 showed a delayed pattern with respect to other mesocosms, decreasing at t20–22 and peaking at t27. ETS

¹<http://www.r-project.org>



during phase II showed similar trends as R, except at the end of the experiment, where ETS decreased in M6 and M8, while R increased.

Influence of Community Structure on R and ETS

The temporal development of the planktonic community, from HB to microplankton (Micro: diatoms and dinoflagellates), is represented in **Figure 2**. There were significant correlations between total biomass and R for all the mesocosms only during phase II, while ETS only correlated with total biomass in M5 in phases I and II (**Table 2**). Some patterns of R and ETS can be attributed to changes in community structure. The relatively higher values of R from days t5 to t10 coincided with a transition period, with a decreasing pattern in the biomass of HB and Micro and increased biomass of nanoeukaryotes (Nano) (**Figure 2**). After nutrient fertilization (t18), the peaks of R and ETS observed on t21–24 in M5, M6, and M8 coincided both with peaks in Chla and in biomass of Nano. M7 behaved differently with respect to the other mesocosms in terms of the development of Chla and planktonic organisms. The

exceptionally high zooplankton concentration observed in this mesocosm after nutrient fertilization (data not shown), probably prevented the fast development of the phytoplankton bloom (as occurred in the other mesocosms), showing a delay of several days in the Nano burst and thus in the increase in Chla, R, and ETS. The further increase in R with maximum rates at the end of the experiment in the two highest CO_2 treatments matched the highest Chla and biomasses of HB and Micro (mostly large diatoms; data not shown) in M6 and M8, although HB decreased sharply the last day of the experiment in the two mesocosms. On the contrary, M5 and M7 presented lower Micro and HB biomasses with a relative dominance of Nano and picophytoplankton (Pico: *Synechococcus* + picoeukaryotes). Indeed, average planktonic biomasses at the different mesocosms show a transition in M5 and M7 from a diatom-dominated (phase I) to a Nano-dominated community, decreasing in total biomass, while in M6 and M8, the diatom-dominated community of phase I shifted to a co-dominance of HB and large diatoms (but see discussion below), with a clear increase in total biomass (**Figure 3**).

Relationship Between R and ETS

R and ETS show a significant, although weak, positive correlation ($r^2 = 0.31$, $P < 0.001$) for the whole experiment (**Table 3**). However, when splitting the data set into the two phases, the relationship of R and ETS before and after fertilization turns out to be very different (**Figure 4** and **Table 3**): Phase I shows no significant correlation ($r^2 = 0.02$, $P > 0.05$), while the two variables are significantly correlated during phase II ($r^2 = 0.38$, $P < 0.0001$), when the phytoplankton bloomed after nutrient fertilization.

The average R/ETS ratios for all the mesocosms were markedly different during the two phases, being close to 1 in phase I and about 0.5 (except in M7) in phase II (**Table 4**).

DISCUSSION

One of the goals of this study was to explore the effect of CO_2 concentration on the respiratory metabolism. Linear regression analysis detected no significant relationship (F -test, $p > 0.05$) between R and CO_2 in any of the mesocosms, agreeing with previous observations by other authors (Egge et al., 2007; Li and Gao, 2012; Motegi et al., 2013; Tanaka et al., 2013). However, when looking into the temporal development of R and ETS during the experiment (**Figures 1A,B**), we observed significant enhancements of R (but not ETS) at high CO_2 during the last 5 days of the experiment. These results contrast with the conclusions of Spilling et al. (2016) from another recent ocean acidification mesocosm experiment performed in the Baltic Sea. They observed that lower R and bacterial remineralization occurred at elevated CO_2 levels, resulting in high dissolved organic carbon accumulation. Although they discussed several mechanisms that might explain their results, they also acknowledge that the cause for reduced respiration at high CO_2 remains unresolved. In our study, the high R associated with high CO_2 treatments is probably not due to a direct effect

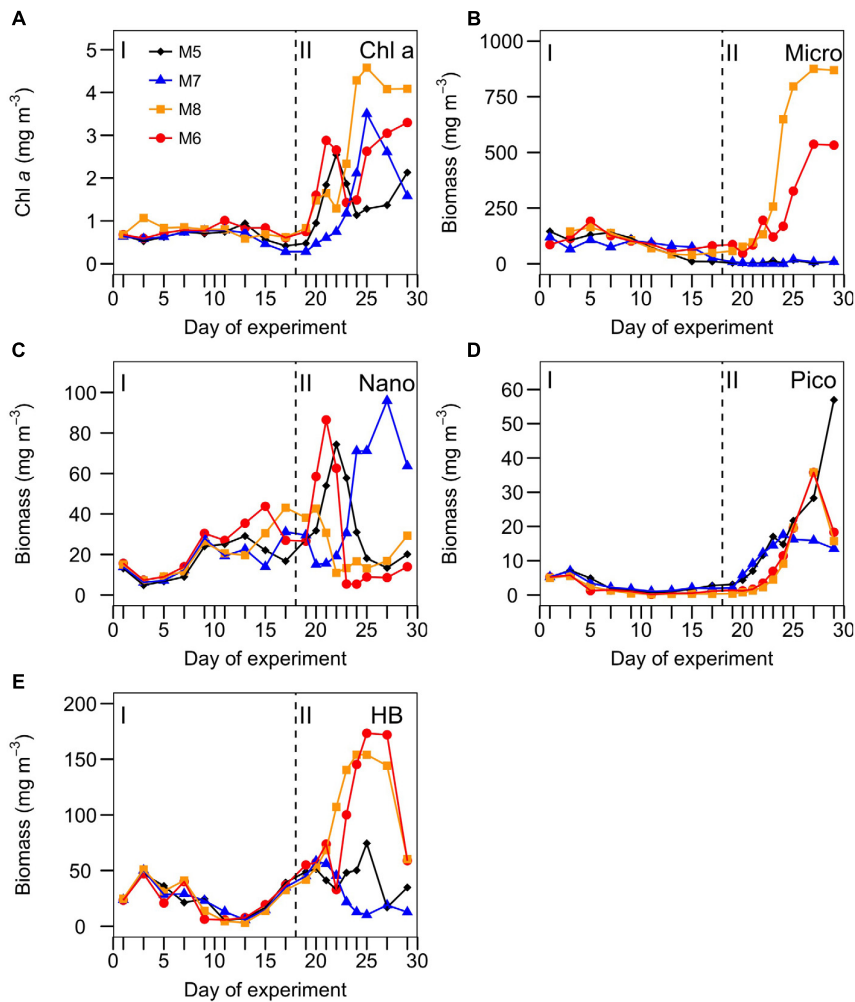


FIGURE 2 | Temporal development of (A) chlorophyll a, and biomasses (in mg C m⁻³) of (B) microphytoplankton (diatoms + autotrophic and mixotrophic dinoflagellates), (C) nanophytoplankton (pigmented nanoeukaryotes), (D) picophytoplankton (picoeukaryotes + *Synechococcus*), and (E) heterotrophic bacteria (HB) in the studied mesocosms. Target pCO₂ values (in μatm) were: 400 (M5), 700 (M7), 1150 (M8), and 1450 (M6). I and II denote phases I and II. The vertical line indicates the day of nutrient fertilization.

TABLE 2 | Pearson pairwise correlation coefficients between community respiration (R) and ETS activity and the biomass of heterotrophic bacteria (HB), picophytoplankton (Pico), nanophytoplankton (Nano) and microphytoplankton (Micro), and the sum of all them (Total), during the two phases (I and II) of the experiment (target pCO₂ concentrations in brackets).

Phase	Variable	M5 (400)		M7 (700)		M8 (1150)		M6 (1450)	
		R	ETS	R	ETS	R	ETS	R	ETS
I	HB	0.03	0.16	0.00	0.56*	0.08	0.28	0.00	0.00
	Pico	0.01	0.44*	0.04	0.78**	0.11	0.21	0.03	0.35
	Nano	0.03	0.27	0.02	0.70**	0.26	0.10	0.12	0.30
	Micro	0.31	0.50*	0.14	0.02	0.51*	0.21	0.18	0.05
	Total	0.33	0.61**	0.11	0.20	0.35	0.32	0.08	0.01
II	HB	0.00	0.02	0.65**	0.4	0.06	0.45*	0.04	0.00
	Pico	0.31	0.72**	0.08	0.02	0.65**	0.31	0.24	0.01
	Nano	0.13	0.00	0.87**	0.45*	0.01	0.18	0.01	0.00
	Micro	0.08	0.02	0.36	0.07	0.64**	0.32	0.58*	0.01
	Total	0.43*	0.44*	0.58*	0.23	0.63**	0.34	0.40*	0.01

All data were previously log transformed. *p ≤ 0.05, **p ≤ 0.01.

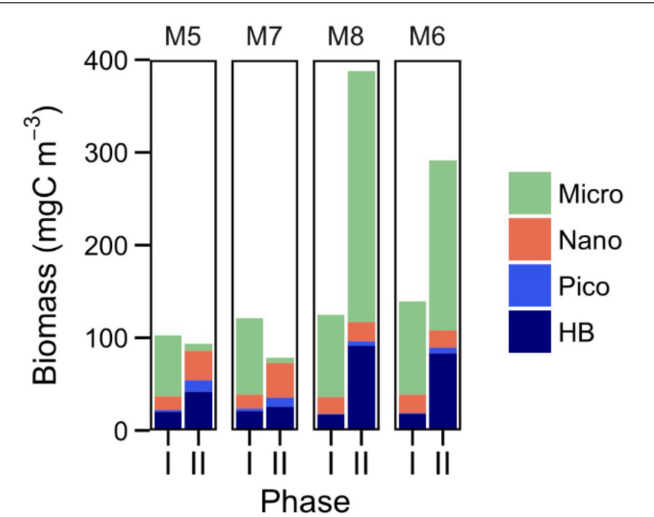


FIGURE 3 | Average biomasses (mg C m^{-3}) of heterotrophic bacteria (HB), picophytoplankton (picoeukaryotes + *Synechococcus*), nanophytoplankton (pigmented nanoeukaryotes), and microphytoplankton (diatoms and autotrophic + mixotrophic dinoflagellates), during the two phases of the experiment for each of the studied mesocosms.

on the specific metabolism of the organisms but to the increase in total planktonic biomass at the end of the experiment. HB increased in abundance in phase II right after the Nano decline (probably relieving the grazing pressure on HB) in parallel to the Micro rise, with both groups together reaching the highest biomasses (Figures 2, 3). Other studies carried out in mesocosms show a similar trend, with increased bacterial abundance and metabolism stimulated after the development of phytoplankton blooms (Grossart et al., 2006; Endres et al., 2014; Bergen et al., 2016).

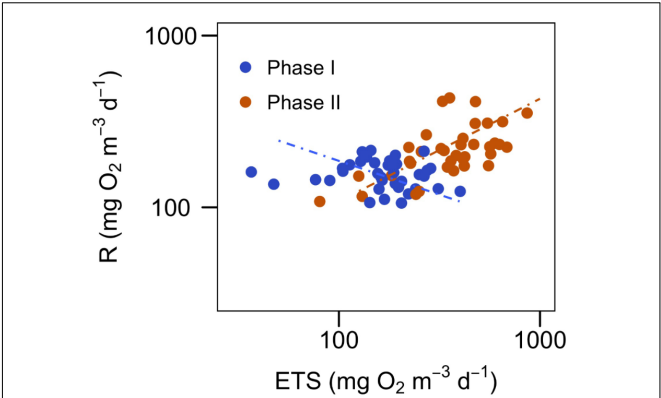


FIGURE 4 | Relationship between community respiration (R) and ETS activity for the two phases of the experiment (see Table 3 for the statistics of the regressions). Data are log transformed for the regression analysis.

M6 holds the highest plankton biomass in phase I, as well as in phase II (together with M8). This is reflected in higher concentrations of total organic carbon (TOC) excreted by the phytoplankton and accumulated during the experiment in M6 during phase I, and M6 and M8 during phase II (Figure 5A). The molecular weight of the colored dissolved organic matter (CDOM) – represented by the slope ratio (SR) – increased during the course of the experiment in all the mesocosms (Figure 5B; decreasing SR), suggesting that bacterial production of high molecular weight CDOM exceeded the rate of photochemical bleaching, responsible of breaking high molecular weight into low molecular weight organic compounds. Indeed, the only change in the decreasing trend of SR during phase I occurred around t10, when bacterial biomass was at its minimum (Figures 2E, 5B). Moreover, in the two mesocosms with highest CO₂ there were significant correlations (Pearson

TABLE 3 | Regression statistics for the relationship between actual respiration (R) and ETS activity in our study (phases I and II), compared with the study of Arístegui and Montero (1995) (A&M95) (see their Figures 2, 6).

Study	<i>n</i>	Slope (± se)	y-intercept (± se)	<i>r</i> ²	<i>F</i>	Significance (<i>F</i> -test)	CF	MAPE (%)
This study (Ph. I+II)	72	0.508* (0.058)	1.050* (0.138)	0.31	77.4	<0.001	1.04	21
This study (Phase I)	36	−0.393 ^{NS} (0.090)	3.057* (0.260)	0.02	19.3	>0.1	1.02	15
This study (Phase II)	36	0.672* (0.058)	0.616* (0.259)	0.38	44.0	<0.001	1.04	20
A&M95 [§]	197	0.750* (0.031)	0.357* (0.057)	0.75	578.2	<0.0001	1.08	34
A&M95 + Phases I+II	269	0.865* (0.024)	0.186* (0.046)	0.80	1272.1	<0.001	1.09	34
A&M95 + Phase I	233	0.896* (0.030)	0.111* (0.046)	0.75	882.8	<0.001	1.10	35
A&M95 + Phase II	233	0.844* (0.024)	0.286* (0.046)	0.83	1290.0	<0.001	1.07	33

Values (in $\text{mg O}_2 \text{ m}^{-3} \text{ d}^{-1}$) were log transformed to compute regression statistics. The data are fitted to the model $\log R = a(\pm \text{se}) + b(\pm \text{se}) \times \log \text{ETS}$, where *a* is the slope and *b* the intercept. The correction factor (CF) is used to convert from log to arithmetic scales. $\text{CF} = \text{antilog}(1.513 \times \text{RMS})$, RMS being the square of the mean residual value of each regression. *n*, number of data; se, standard error. **P* < 0.001; NS, not significant; MAPE, Mean Absolute Percentage Error.

TABLE 4 | Average (\pm SD) ratios of R/ETS from the two phases of the experiment: before (Phase I: t1–t17) and after (Phase II: t19–t29) fertilization, in the four mesocosms studied (target $p\text{CO}_2$ concentrations in brackets).

	Phase I	Phase II
M5 (400)	0.98 ± 0.31	0.52 ± 0.43
M7 (700)	0.79 ± 0.37	0.75 ± 0.56
M8 (1150)	0.73 ± 0.46	0.59 ± 0.99
M6 (1450)	1.06 ± 0.31	0.52 ± 0.43

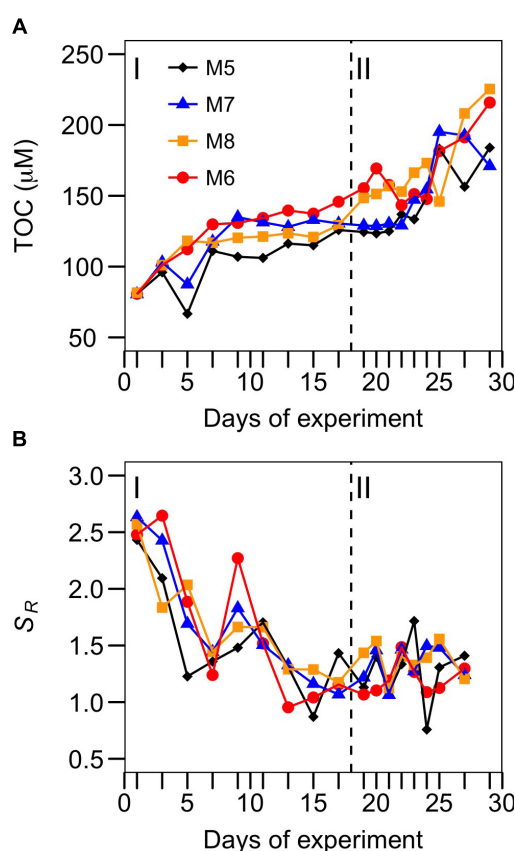


FIGURE 5 | Temporal development of (A) total organic carbon (TOC) and (B) the slope ratio (S_R) of chromophoric organic matter, as an index of molecular weight (see text for details) for each of the studied mesocosms. Target $p\text{CO}_2$ values (in μatm) were: 400 (M5), 700 (M7), 1150 (M8), and 1450 (M6).

pairwise coefficient) between TOC and HB biomass ($r = 0.55$, $p < 0.05$ for M6; $r = 0.64$, $p < 0.01$ for M8), suggesting a strong link between organic carbon dynamics and bacterial biomass.

The specific contribution of HB to R and ETS, however, is uncertain. Multiple stepwise regressions (Table 5) show that R and ETS, average over the mesocosms, can be mostly explained by the phytoplankton community. Large phytoplankton explains most of the variance in R during phases I (86%) and II (53%) and of ETS (86%) during phase II, while picophytoplankton contributes up to 73% to explain the variance in the ETS model during phase I.

Past studies on plankton respiration reported significant correlations between ETS and Chla, (e.g., Packard et al., 1983; Martinez, 1991; del Giorgio, 1992; Estrada et al., 1992; Packard and Christensen, 2004), suggesting that when seawater Chla is high, respiratory activity is mainly due to phytoplankton (Harrison, 1986; Martinez, 1991; Packard and Christensen, 2004). Our results, however, in spite of the large contribution of phytoplankton to biomass, show values ranging from 4 to 13 $\text{mg O}_2 \text{ mg Chla}^{-1} \text{ d}^{-1}$, which are similar to those reported by Martinez et al. (1990) for the western Mediterranean Sea ($2\text{--}10 \text{ mg O}_2 \text{ mg Chla}^{-1} \text{ d}^{-1}$). In our study, in spite of the phytoplankton dominance during the two periods (Figure 3), ETS and R do not consistently correlate with Micro biomass, which largely contributes to total biomass in most of the mesocosms and phases. R, however, correlates with total biomass in the four mesocosms during phase II (Table 2), when diatoms' biomass increased. This lack of a consistent correlation could result from the presence of a complex and variable in time planktonic community (Figures 2, 3), where HB do not seem to be a key player in the total community respiration. Indeed, recent studies from the North Atlantic indicate that the contribution of bacterial respiration to total community respiration may be highly variable, ranging from <5 to $>75\%$ (García-Martín et al., 2017, 2018).

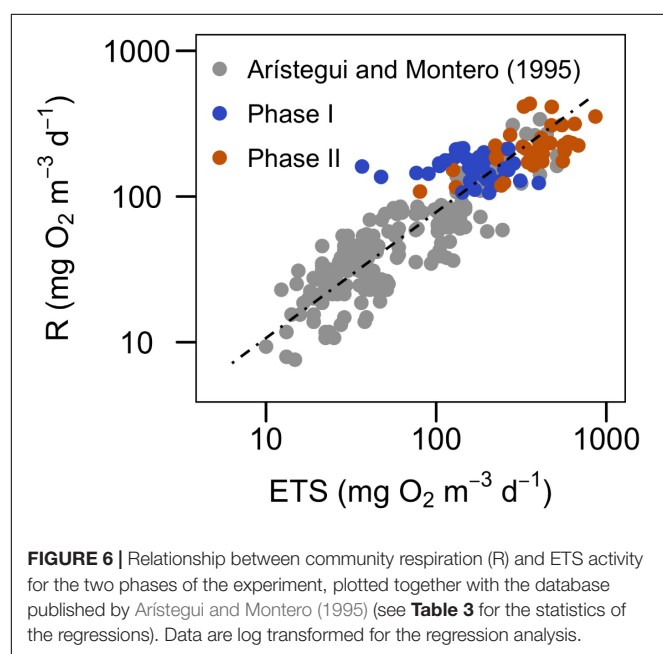
Earlier studies showed that the R/ETS ratio may vary depending on the planktonic community structure and seasonality (e.g., Hobbie et al., 1972), with a general perception that autotrophic organisms have lower R/ETS ratios than heterotrophs (Kenner and Ahmed, 1975; Span, 1988; del Giorgio, 1992). Photosynthesis, like respiration, involves an ETS. Therefore, when autotrophs dominate the plankton community, the ETS assay would measure the potential activity of both processes, yielding higher ETS estimates, and hence lower R/ETS, than measured taking into account only the respiratory process (Packard, 1985). Supporting this hypothesis, Martinez, 1991) reported the highest values of ETS at the chlorophyll maximum layer for all the sampled stations during a cruise in the Barents Sea. Conversely, R/ETS would be higher with increased bacteria contribution to overall respiration (Fuhrman and Azam, 1980; Williams, 1984; Harrison, 1986). In our experiment, the R/ETS ratios were lower during the second period, after nutrient fertilization, coinciding with the phytoplankton bloom and the rise of diatoms. Our phase-average R/ETS data show significant variability between mesocosms during the course of the experiment (ranging from 0.5 to >1). This is however not surprising when looking at the published R/ETS ratios that span several fold (0.2 to >1) in phytoplankton cultures and natural samples (Table 1).

The application of a regression equation has been found to be a more reliable approach than the use of a mean R/ETS ratio to transform ETS activity to actual respiratory rates (e.g., Packard and Williams, 1981), but unfortunately there are very few published studies from natural communities to compare with. The only study where community R/ETS from different marine biogeographical regions (spanning from polar to tropical waters) are compared was published by Arístegui and Montero (1995).

TABLE 5 | Stepwise multiple linear regression statistics between actual respiration (R) and ETS activity and plankton biomasses (Micro, Nano, Pico, HB), Chlorophyll (Chla) and Total Organic Carbon (TOC) during the two phases (I and II) of the experiment.

Phase	Y	X _i	R ² -adj	p-value	F-statistic	RI (%)
I	R	Micro	0.35	<0.001	9.99	85.64
		Pico				14.36
	ETS	Micro	0.43	<0.001	13.56	26.95
		Pico				73.05
II	R	Micro	0.57	<0.001	14.93	53.33
		Nano				15.50
		Pico				31.17
	ETS	Micro	0.18	0.023	4.302	86.45
		Nano				13.55

Y, Dependent variable; X_i, Statistically significant predictor variables; R²-adj, Adjusted correlation coefficient; RI (%), Relative importance.

**FIGURE 6 |** Relationship between community respiration (R) and ETS activity for the two phases of the experiment, plotted together with the database published by Arístegui and Montero (1995) (see Table 3 for the statistics of the regressions). Data are log transformed for the regression analysis.

Their study shows that in all except one of the regions, measured R and ETS were significantly positively correlated, although the slopes and y-intercept of the regression equations differ up to 50% among regions. The regression equation obtained, considering all their data together, yields a mean error of $\pm 34\%$ in the prediction of R from ETS, similar to the errors obtained applying the equation at each area, but much lower than applying an average R/ETS ratio (Arístegui and Montero, 1995). The regression between R and ETS in our study (even if we use only the data from phase II) yields a lower slope, a higher y-intercept and a lower r^2 than the general equation for the global ocean (Table 3). The error in the prediction of R from ETS using only the data of phase II yields a mean error of $\pm 20\%$, even lower than when including the data in the global equation. However, if we include the dataset of this study in the global equation of Arístegui and Montero (Figure 6 and Table 3), the slope, y-intercept and r^2 do not change significantly, although the correlation is higher if we only include the data from phase II. All our data are placed

in the highest range of the regression, closely together with the data from the eutrophic ecosystems of the Gulf of California and Baltic Sea (Figure 6; Arístegui and Montero, 1995). Nevertheless, the variability in the slopes and intercepts of our data with respect to the global equation raises the question of whether we can universally use a single R/ETS relationship to derive R from ETS activity in different communities and environmental conditions.

CONCLUSION

This work represents one of the few studies where actual respiration rates (R) and ETS activity are measured simultaneously in natural marine communities. Moreover, it is the only study where R and ETS are measured under controlled conditions – inside mesocosms – and during a relatively long period of time (30 days), where the community undergoes drastic changes in nutrient and CO₂ concentrations, as well as community structure.

R and ETS do not show any significant correlation with CO₂ or community structure for the whole experiment, although R increased in the high CO₂ treatments at the end of the experiment, matching the rise in diatoms after nutrient fertilization (phase II). Only during this phase R correlates significantly with total biomass in all the mesocosms.

The temporal development of R and ETS can be mostly explained by changes in the phytoplankton community. Large phytoplankton explains most of the variance in R during phases I and II and of ETS during phase II, while picophytoplankton contributes to explain the variance in ETS during phase I.

The R/ETS ratio ranged more than threefold in magnitude during the experiment. The average R/ETS is higher under nutrient depleted conditions (0.7–1.1), compared to the bloom period after nutrient fertilization, where the ratios reached lower and more similar values among the mesocosms (0.5–0.7).

Our results (together with other published studies) indicate that R/ETS may be too variable as to apply constant ratios in different marine regions and trophic conditions. The application of a regression equation is a more reliable approach than the use of a mean R/ETS ratio to transform ETS activity to actual respiratory rates. Nevertheless, further research, like the one

carried out in this study, is necessary to constraint the variability of the R/ETS and to elucidate the universality of this equation.

AUTHOR CONTRIBUTIONS

UR and JA conceived and designed the experiment. All authors performed the experiment and analyzed the data. JA and AF with input from all co-authors wrote the paper.

FUNDING

The KOSMOS project was funded by the German Federal Ministry of Education and Research (BMBF) in the framework of the coordinated project BIOACID – Biological Impacts of Ocean Acidification, phase II (FKZ 03F06550). UR received additional funding from the Leibniz Award 2012 by the German Research Foundation (DFG). JA was supported by a Helmholtz International Fellow Award, 2015 (Helmholtz Association,

Germany). IB was supported by a FPI fellowship (BES-2016-078407) from the Spanish Ministry of Economy, Industry and Competitiveness (MINECO). NH-H was partially supported by KOSMOS funding during the experimental work, and by a grant of the Agencia Canaria de Investigación, Innovación y Sociedad de la Información (ACIISI) during the writing stage (TESIS2015010036). JA, MM, IB, and NH-H benefited also from the FLUXES project (CTM2015-69392-C3-1-R) funded by the Spanish government (Plan Nacional I+D).

ACKNOWLEDGMENTS

We would like to thank the KOSMOS team and the Plataforma Oceánica de Canarias (PLOCAN) assisting with all aspects of the organization and logistical support before, during and after this mesocosms campaign, as well as to Minerva Espino and Acorayda González (IOCAG, ULPGC) for their technical support in the sampling and analyses of data.

REFERENCES

- Aristegui, J., Duarte, C. M., Gasol, J. M., and Alonso-Sáez, L. (2005). Active mesopelagic prokaryotes support high respiration in the subtropical northeast Atlantic Ocean. *Geophys. Res. Lett.* 32:L03608. doi: 10.1029/2004GL021863
- Aristegui, J., and Montero, M. F. (1995). The relationship between community respiration and ETS activity in the ocean. *J. Plankton Res.* 17, 1563–1571. doi: 10.1093/plankt/17.7.1563
- Baltar, F., Lindh, M. V., Parparov, A., Berman, T., and Pinhassi, J. (2012). Prokaryotic community structure and respiration during long-term incubations. *MicrobiologyOpen* 1, 214–224. doi: 10.1002/mbo3.25
- Bangqin, H., Huasheng, H., Xiangzhong, X., and Yuan, L. (2005). Study on respiratory electron transport system (ETS) of phytoplankton in Taiwan Strait and Xiamen Harbour. *Chin. J. Oceanol. Limnol.* 23, 176–182. doi: 10.1007/BF02894235
- Bergen, B., Endres, S., Engel, A., Zark, M., Dittmar, T., Sommer, U., et al. (2016). Acidification and warming effect prominent bacteria in two seasonal phytoplankton bloom mesocosms. *Environ. Microbiol.* 18, 4579–4595. doi: 10.1111/1462-2920.13549
- Bigdare, R. R., King, F. D., and Biggs, D. C. (1982). Glutamate dehydrogenase (GDH) and respiratory electron-transport-system (ETS) activities in Gulf of Mexico zooplankton. *J. Plankton Res.* 4, 895–911. doi: 10.1093/plankt/4.4.895
- Borsheim, K. Y., and Bratbak, G. (1987). Cell volume to cell carbon conversion factors of a bacterivorous *Monas* sp. enriched from seawater. *Mar. Ecol. Prog. Ser.* 36, 171–175. doi: 10.3354/meps036171
- Bryan, J. R., Riley, J. P., and Williams, P. L. (1976). A Winkler procedure for making precise measurements of oxygen concentration for productivity and related studies. *J. Exp. Mar. Biol. Ecol.* 21, 191–197. doi: 10.1016/0022-0981(76)90114-3
- Carrit, D. E., and Carpenter, J. H. (1966). Recommendation procedure for Winkler analyses of sea water for dissolved oxygen. *J. Mar. Res.* 24, 313–318.
- Christensen, J. P., Owens, T. G., Devol, A. H., and Packard, T. T. (1980). Respiration and physiological state in marine bacteria. *Mar. Biol.* 55, 267–276. doi: 10.1007/bf00393779
- del Giorgio, P. A. (1992). The relationship between ETS (electron transport system) activity and oxygen consumption in lake plankton: a cross-system calibration. *J. Plankton Res.* 14, 1723–1741. doi: 10.1093/plankt/14.12.1723
- del Giorgio, P. A., and Williams, P. L. B. (2005). “The global significance of respiration in aquatic ecosystems: from single cells to the biosphere,” in *Respiration in Aquatic Ecosystems*, eds P. A. del Giorgio and P. J. B. Williams (Oxford: Oxford University Press), 267–303. doi: 10.1093/acprof:oso/9780198527084.003.0014
- Dubelaar, G. B. J., and Gerritzen, P. L. (2000). CytoBuoy: a step forward towards using flow cytometry in operational oceanography. *Sci. Mar.* 64, 255–265. doi: 10.3989/scimar.2000.64n2255
- Engel, A., Thingstad, T. F., Engel, A., Bellerby, R. G. J., and Riebesell, U. (2007). Primary production during nutrient-induced blooms at elevated CO₂ concentrations. *Biogeosciences* 6, 877–885. doi: 10.5194/bg-6-877-2009
- Endres, S., Galgani, L., Riebesell, U., Schulz, K. G., and Engel, A. (2014). Stimulated bacterial growth under elevated pCO₂: results from an off-shore mesocosm study. *PLoS One* 9:e99228. doi: 10.1371/journal.pone.0099228
- Estrada, M., Martinez, R., and Mathot, S. (1992). Respiratory electron transport activity in plankton of the Weddell and Scotia Seas during late spring—early summer: relationships with other biological parameters. *Polar Biol.* 12, 35–42. doi: 10.1007/BF00239963
- Finlay, B., Span, A., and Ochsenbein-Gattlen, C. (1983). Influence of physiological state on indices of respiration rate in protozoa. *Comp. Biochem. Physiol.* 74, 211–219. doi: 10.1016/0300-9629(83)90590-X
- Fuhrman, J. A., and Azam, F. (1980). Bacterioplankton secondary production estimates for coastal waters of British Columbia, Antarctica, and California. *Appl. Environ. Microbiol.* 39, 1085–1095.
- García-Martín, E. E., Aranguren-Gassis, M., Hartmann, M., Zubkov, M. V., and Serret, P. (2017). Contribution of bacterial respiration to plankton respiration from 50°N to 44°S in the Atlantic Ocean. *Prog. Oceanogr.* 158, 99–108. doi: 10.1016/j.pocean.2016.11.006
- García-Martín, E. E., Daniels, C. J., Davidson, K., Davis, C. E., Mahaffey, C., Mayers, K. M. J., et al. (2018). Seasonal changes in plankton respiration and bacterial metabolism in a temperate shelf sea. *Prog. Oceanogr.* (in press). doi: 10.1016/j.pocean.2017.12.002
- Gasol, J. M., and Morán, X. A. (1999). Effects of filtration on bacterial activity and picoplankton community structure as assessed by flow cytometry. *Aquat. Microbial Ecol.* 16, 251–264. doi: 10.3354/ame016251
- Gattuso, J. P., Peduzzi, S., Pizay, M. D., and Tonolla, M. (2002). Changes in freshwater bacterial community composition during measurements of microbial and community respiration. *J. Plankton Res.* 24, 1197–1206. doi: 10.1093/plankt/24.11.1197
- Grasshoff, K., Ehrhardt, M., and Kremling, K. (eds) (1983). *Determination of oxygen. Methods of Seawater Analysis*. Weinheim: Verlag Chemie, 61–72.
- Grossart, H. P., Allgaier, M., Passow, U., and Riebesell, U. (2006). Testing the effect of CO₂ concentration on the dynamics of marine heterotrophic bacterioplankton. *Limnol. Oceanogr.* 51, 1–11. doi: 10.4319/lo.2006.51.1.0001
- Harrison, W. G. (1986). Respiration and its size-dependence in microplankton populations from surface waters of the Canadian Arctic. *Polar Biol.* 6, 145–152. doi: 10.1007/BF00274877

- Helms, J. R., Stubbins, A., Ritchie, J. D., Minor, E. C., Kieber, D. J., and Mopper, K. (2008). Absorption spectral slopes and slope ratios as indicators of molecular weight, source, and photobleaching of chromophoric dissolved organic matter. *Limnol. Oceanogr.* 53, 955–969. doi: 10.4319/lo.2008.53.3.0955
- Hernández-León, S. (1988). Gradients of mesozooplankton biomass and ETS activity in the wind-shear area as evidence of an island mass effect in the Canary Island waters. *J. Plankton Res.* 10, 1141–1154. doi: 10.1093/plankt/10.6.1141
- Hernández-León, S., Postel, L., Aristegui, J., Gómez, M., Montero, M. F., Torres, S., et al. (1999). Large-scale and mesoscale distribution of plankton biomass and metabolic activity in the Northeastern Central Atlantic. *J. Oceanogr.* 55, 471–482. doi: 10.1023/A:100782292
- Hobbie, J. E., Holm-Hansen, O., Packard, T. T., Pomeroy, L. R., Sheldon, R. W., Thomas, J. P., et al. (1972). A study of the distribution and activity of microorganisms in ocean water. *Limnol. Oceanogr.* 17, 544–555. doi: 10.4319/lo.1972.17.4.0544
- Hopkinson, C. S. J., Sherr, B., and Wiebe, W. J. (1989). Size-fractionated metabolism of coastal microbial plankton. *Mar. Ecol. Prog. Ser.* 51, 155–166. doi: 10.3354/meps051155
- Hopwood, M. J., Riebesell, U., Aristegui, J., Ludwig, A., Achterberg, E. P., and Hernández, N. (2018). Photochemical versus bacterial control of H₂O₂ concentration across a pCO₂ gradient mesocosm experiment in the subtropical North Atlantic. *Front. Mar. Sci.* 5:105. doi: 10.3389/fmars.2018.00105
- Jürgens, K., Gasol, J. M., and Vague, D. (2000). Bacteria-flagellate coupling in microcosm experiments in the Central Atlantic Ocean. *J. Exp. Mar. Biol. Ecol.* 245, 127–147. doi: 10.1016/S0022-0981(99)00156-2
- Kenner, R. A., and Ahmed, S. I. (1975). Measurements of electron transport activities in marine phytoplankton. *Mar. Biol.* 33, 119–127. doi: 10.1007/BF00390716
- King, F. D., and Packard, T. T. (1975). Respiration and the activity of the respiratory electron transport system in marine zooplankton. *Limnol. Oceanogr.* 20, 849–854. doi: 10.4319/lo.1975.20.5.0849
- Li, W., and Gao, K. (2012). A marine secondary producer respire and feeds more in a high CO₂ ocean. *Mar. Pollut. Bull.* 64, 699–703. doi: 10.1016/j.marpolbul.2012.01.033
- Lindeman, R. H., Merenda, P. F., and Gold, R. Z. (1980). *Introduction to Bivariate and Multivariate Analysis*. Glenview, IL: Scott Foresman.
- Martinez, R. (1991). Biomass and respiratory ETS activity of microplankton in the Barents Sea. *Polar Res.* 10, 193–200. doi: 10.3402/polar.v10i1.6738
- Martinez, R. (1992). Respiration and respiratory electron transport activity in marine phytoplankton: growth rate dependence and light enhancement. *J. Plankton Res.* 14, 789–797. doi: 10.1093/plankt/14.6.789
- Martinez, R., Arnone, R. A., and Velasquez, Z. (1990). Chlorophyll a and respiratory electron transport system activity in microplankton from the surface waters of the western Mediterranean. *J. Geophys. Res.* 95, 1615–1622. doi: 10.1029/JC095iC02p01615
- Massana, R., Pedrós-Álió, C., Casamayor, E. O., and Gasol, J. M. (2001). Changes in marine bacterioplankton phylogenetic composition during incubations designed to measure biogeochemically significant parameters. *Limnol. Oceanogr.* 46, 1181–1188. doi: 10.4319/lo.2001.46.5.1181
- Menden-Deuer, S., and Lessard, E. J. (2000). Carbon to volume relationships for dinoflagellates, diatoms, and other protist plankton. *Limnol. Oceanogr.* 45, 569–579. doi: 10.4319/lo.2000.45.3.0569
- Mimura, T., Romano, J. C., and de Souza-Lima, Y. (1988). Microbiomass structure and respiratory activity of microneuston and microplankton in the northwestern Mediterranean Sea influenced by Rhone River water. *Mar. Ecol. Prog. Ser.* 49, 151–162. doi: 10.3354/meps049151
- Motegi, C., Tanaka, T., Piontek, J., Brussaard, C. P. D., Gattuso, J. P., and Weinbauer, M. G. (2013). Effect of CO₂ enrichment on bacterial metabolism in an Arctic fjord. *Biogeosciences* 10, 3285–3296. doi: 10.5194/bg-10-3285-2013
- Packard, T. T. (1971). The measurement of respiratory electron transport activity in marine phytoplankton. *J. Mar. Res.* 29, 235–244.
- Packard, T. T. (1985). Measurement of electron transport activity of microplankton. *Adv. Aqua. Microbiol.* 3, 207–261.
- Packard, T. T., and Christensen, J. P. (2004). Respiration and vertical carbon flux in the Gulf of Maine water column. *J. Mar. Res.* 62, 93–115. doi: 10.1357/00222400460744636
- Packard, T. T., Garfield, P. C., and Martinez, R. (1983). Respiration and respiratory enzyme activity in aerobic and anaerobic cultures of the marine denitrifying bacterium, *Pseudomonas perfectomarinus*. *Deep Sea Res. A* 30, 227–243. doi: 10.1016/0198-0149(83)90008-0
- Packard, T. T., and Williams, P. J. L. (1981). Rates of respiratory oxygen-consumption and electron-transport in surface seawater from the northwest Atlantic. *Oceanol. Acta* 4, 351–358.
- Ramírez, T., Liger, E., Mercado, J. M., Cortés, D., Vargas-Yañez, M., Sebastián, M., et al. (2006). Respiratory ETS activity of plankton in the northwestern Alboran Sea: seasonal variability and relationship with hydrological and biological features. *J. Plankton Res.* 28, 629–641. doi: 10.1093/plankt/fbi146
- Reinthal, T., Van Aken, H., Veth, C., Aristegui, J., Robinson, C., Williams, P. J. L. B., et al. (2006). Prokaryotic respiration and production in the meso- and bathypelagic realm of the eastern and western North Atlantic basin. *Limnol. Oceanogr.* 51, 1262–1273. doi: 10.4319/lo.2006.51.3.1262
- Robinson, C., and Williams, P. J. B. (2005). “Respiration and its measurement in the surface waters,” in *Respiration in Aquatic Ecosystems*, eds P. A. del Giorgio and P. J. B. Williams (New York, NY: Oxford University Press), 147–180. doi: 10.1093/acprof:oso/9780198527084.003.0009
- Schalk, P. H. (1988). Respiratory electron transport system (ETS) activities in zooplankton and micronekton of the Indo-Pacific region. *Mar. Ecol. Prog. Ser.* 44, 25–35. doi: 10.3354/meps044025
- Span, A. S. (1988). Metabolic activity as reflected by ETS and BOD in a shallow eutrophic lake. *Arch. Hydrobiol* 31, 141–147.
- Spilling, K., Schulz, K. G., Paul, A. J., Boxhammer, T., Achterberg, E. P., Hornick, T., et al. (2016). Effects of ocean acidification on pelagic carbon fluxes in a mesocosm experiment. *Biogeosciences* 13:6081. doi: 10.5194/bg-13-6081-2016
- Strickland, J. D. H., and Parsons, T. R. (1960). *A Manual of Sea Water Analysis*. Ottawa, ON: Bulletin Fisheries Research Board of Canada.
- Tanaka, T., Alliouane, S., Bellerby, R. G. B., Czerny, J., De Kluijver, A., Riebesell, U., et al. (2013). Effect of increased pCO₂ on the planktonic metabolic balance during a mesocosm experiment in an Arctic fjord. *Biogeosciences* 10:315. doi: 10.5194/bg-10-315-2013
- Thomas, C., Cauwet, G., and Minster, J. F. (1995). Dissolved organic carbon in the equatorial Atlantic Ocean. *Mar. Chem.* 49, 155–169. doi: 10.1016/0304-4203(94)00061-H
- Vosjan, J. H., and Nieuwland, G. (1987). Microbial biomass and respiratory activity in the surface waters of the east Banda Sea and northwest Arafura Sea (Indonesia) at the time of the southeast monsoon. *Limnol. Oceanogr.* 32, 767–775. doi: 10.4319/lo.1987.32.3.0767
- Vosjan, J. H., Nieuwland, G., Ernst, W., and Bluszcz, T. (1987). Shipboard comparison of two methods of extraction and measurements of ATP applied to Antarctic water samples. *Netherlands J. Sea Res.* 21, 107–112. doi: 10.1016/0077-7579(87)90026-3
- Vosjan, J. H., Tijssen, S. B., Nieuwland, G., and Wetsteyn, F. J. (1990). Oxygen regime, respiratory activity and biomass of microorganisms, and the carbon budget in the Fladen Ground area (Northern North Sea) during spring. *Netherlands J. Sea Res.* 25, 89–99. doi: 10.1016/0077-7579(90)90011-5
- Williams, P. L. (1984). A review of measurements of respiration rates of marine plankton populations. *Heterotr. Activity* 15, 357–389. doi: 10.1007/978-1-4684-9010-7_16
- Williams, P. L., and Jenkinson, N. W. (1982). A transportable microprocessor-controlled precise Winkler titration suitable for field station and shipboard use. *Limnol. Oceanogr.* 27, 576–584. doi: 10.4319/lo.1982.27.3.0576

Conflict of Interest Statement: The authors declare that the research was conducted in the absence of any commercial or financial relationships that could be construed as a potential conflict of interest.

Copyright © 2018 Filella, Baños, Montero, Hernández-Hernández, Rodríguez-Santos, Ludwig, Riebesell and Aristegui. This is an open-access article distributed under the terms of the Creative Commons Attribution License (CC BY). The use, distribution or reproduction in other forums is permitted, provided the original author(s) and the copyright owner(s) are credited and that the original publication in this journal is cited, in accordance with accepted academic practice. No use, distribution or reproduction is permitted which does not comply with these terms.



Response of Subtropical Phytoplankton Communities to Ocean Acidification Under Oligotrophic Conditions and During Nutrient Fertilization

Jan Taucher^{1*}, Javier Aristegui², Lennart T. Bach¹, Wanchun Guan³, María F. Montero², Alice Nauendorf¹, Eric P. Achterberg¹ and Ulf Riebesell¹

¹ GEOMAR Helmholtz Centre for Ocean Research Kiel, Kiel, Germany, ² Instituto de Oceanografía y Cambio Global, Universidad de Las Palmas de Gran Canaria, Las Palmas, Spain, ³ Department of Marine Biotechnology, School of Laboratory Medicine and Life Science, Wenzhou Medical University, Wenzhou, China

OPEN ACCESS

Edited by:

Claire Mahaffey,
University of Liverpool,
United Kingdom

Reviewed by:

Karin M. Björkman,
University of Hawaii, United States
John Patrick Dunne,
Geophysical Fluid Dynamics
Laboratory-NOAA, United States

*Correspondence:

Jan Taucher
jtaucher@geomar.de

Specialty section:

This article was submitted to
Marine Biogeochemistry,
a section of the journal
Frontiers in Marine Science

Received: 31 May 2018

Accepted: 28 August 2018

Published: 20 September 2018

Citation:

Taucher J, Aristegui J, Bach LT,
Guan W, Montero MF, Nauendorf A,
Achterberg EP and Riebesell U (2018)
Response of Subtropical
Phytoplankton Communities to Ocean
Acidification Under Oligotrophic
Conditions and During Nutrient
Fertilization. *Front. Mar. Sci.* 5:330.
doi: 10.3389/fmars.2018.00330

The subtropical oceans are home to the largest phytoplankton biome on the planet. Yet, little is known about potential impacts of ocean acidification (OA) on phytoplankton community composition in the vast oligotrophic ecosystems of the subtropical gyres. To address this question, we conducted an experiment with 9 *in situ* mesocosms (~35 m³) off the coast of Gran Canaria in the eastern subtropical North Atlantic over a period of 9 weeks. By establishing a gradient of *p*CO₂ ranging from ~350 to 1,025 μatm, we simulated carbonate chemistry conditions as projected until the end of the twenty-first century. Furthermore, we injected nutrient-rich deep water into the mesocosms halfway through the experiment to simulate a natural upwelling event, which regularly leads to patchy nutrient fertilization in the study region. The temporal developments of major taxonomic groups of phytoplankton were analyzed by flow cytometry, pigment composition and microscopy. We observed distinct shifts in phytoplankton community structure in response to high CO₂, with markedly different patterns depending on nutrient status of the system. Phytoplankton biomass during the oligotrophic phase was dominated by picocyanobacteria (*Synechococcus*), which constituted 60–80% of biomass and displayed significantly higher cell abundances at elevated *p*CO₂. The addition of deep water triggered a substantial bloom of large, chain-forming diatoms (mainly *Guinardia striata* and *Leptocylindrus danicus*) that dominated the phytoplankton community during the bloom phase (70–80% of biomass) and until the end of the experiment. A CO₂ effect on bulk diatom biomass became apparent only in the highest CO₂ treatments (>800 μatm), displaying elevated concentrations especially in the stationary phase after nutrient depletion. Notably, these responses were tightly linked to distinct interspecific shifts within the diatom assemblage, particularly favoring the largest species *Guinardia striata*. Other taxonomic groups contributed less to total phytoplankton biomass, but also displayed distinct responses to OA treatments. For instance, higher CO₂ favored the occurrence of prymnesiophyceae (*Phaeocystis globosa*) and dictyochophyceae, whereas dinoflagellates were negatively

affected by increasing CO₂. Altogether, our findings revealed considerable shifts in species composition in response to elevated CO₂ and/or lower pH, indicating that phytoplankton communities in the subtropical oligotrophic oceans might be profoundly altered by ocean acidification.

Keywords: ocean acidification, phytoplankton, marine ecology, diatoms, oligotrophic oceans, upwelling, Canary Islands, subtropical North Atlantic

INTRODUCTION

Oceanic uptake of anthropogenic CO₂ leads to pronounced shifts in seawater carbonate chemistry and a decrease in pH, a process commonly termed “ocean acidification” (OA) (Wolf-Gladrow and Riebesell, 1997; Caldeira and Wickett, 2003).

Intensive research efforts over the past decade have demonstrated that OA can substantially influence the physiological performance of marine phytoplankton (Riebesell and Tortell, 2011; Dutkiewicz et al., 2015). A wealth of laboratory studies, mostly with single species cultures, has shown highly variable physiological sensitivities of taxa to changing carbonate chemistry. Such differential sensitivities to OA could alter phytoplankton species composition and succession patterns, with important implications for entire pelagic food webs.

Following these considerations, more recent work has illuminated how OA effects manifest themselves on the level of ecological communities by investigating CO₂-sensitivities of entire plankton communities in larger volume incubations (up to 80 m³) under close-to-natural conditions (Riebesell et al., 2013; Gazeau et al., 2016).

Most of these studies have reported pronounced effects of simulated OA on plankton communities in different ocean regions, e.g., in the Arctic Ocean, several locations in subpolar temperate waters and in the Mediterranean Sea (Bach et al., 2017; Maugendre et al., 2017; Schulz et al., 2017). These studies demonstrated that OA may lead to distinct “winners and losers” within the plankton community, sometimes with wider-reaching impacts on higher trophic levels and biogeochemical cycles (Sswat et al., 2018; Stange et al., 2018).

However, geographical coverage of such studies is still sparse and to date virtually nothing is known about OA impacts on phytoplankton communities in the oligotrophic regions of the subtropical ocean. These vast “ocean deserts” cover more than 60% of the ocean surface area, making them the largest ecosystem in the surface ocean (Longhurst et al., 1995; McClain et al., 2004). Physical conditions are typically characterized by a nutrient-poor surface layer, which is separated from deeper nutrient-rich waters by a strong and almost permanent thermocline. As a result, primary production (per unit surface area) in these waters is usually low-yet, their immense size makes the contribution of oligotrophic waters to global primary production significant (Signorini et al., 2015).

However, despite generally low nutrient levels, (sub-)mesoscale phenomena like eddies frequently inject nutrients into the surface layer, thus stimulating biological productivity in oligotrophic oceans worldwide (Mahadevan, 2016; McGillicuddy, 2016). Such local increases in chlorophyll

and primary production associated with nutrient pumping in eddies have been also reported from the subtropical ocean in the Canary Current System, where mesoscale variability is particularly intense (Aristegui et al., 1997; Sangra et al., 2009; Schütte et al., 2016).

Predicting how the subtropical oligotrophic ocean will respond to climate change remains very difficult: On the one hand, increasing temperatures are expected to result in an expansion of oligotrophic gyres due to stronger thermal stratification (Polovina et al., 2008; Bopp et al., 2013). On the other hand, future changes in wind patterns as a result of global warming are predicted to increase upwelling-favorable winds in Eastern Boundary Current Systems, which would also lead to an increase of eddy kinetic energy and associated upward pumping of nutrients in these regions (Bakun, 1990; García-Reyes et al., 2015; Xiu et al., 2018).

Considering the global importance of subtropical oligotrophic ocean ecosystems and our sparse knowledge about their potential responses to OA, the goal of the present study was to investigate how increasing CO₂ and lower pH affect phytoplankton community composition in these oceanic regions. The experiment was designed in a way, that allowed us to investigate phytoplankton responses to OA during oligotrophic periods as well as under the influence of patchy nutrient fertilization typical of the study region. The present study complements the findings of a companion paper in this Frontiers Research Topic, which addresses the effects of OA on size fractionated PP and biomass (Hernández-Hernández et al., 2018).

MATERIALS AND METHODS

Mesocosm Experiment Set Up

We conducted a pelagic *in situ* experiment with large-volume mesocosms in Gando Bay, Gran Canaria for a period of 62 days from September to December 2014.

The setup consisted of nine pelagic mesocosms (M1–M9), each extending to a depth of 15 m (13 m bag and 2 m conical sediment trap attached to the bottom of the bag) and enclosing about 35 m³ of the natural water column (Riebesell et al., 2013; Taucher et al., 2017). One mesocosm (M6) was lost due to irreparable damage a few days after deep-water addition, and was thus excluded from analysis in the present study.

The mesocosms were treated with different amounts of CO₂-enriched seawater following the method described in Riebesell et al. (2013). Briefly, natural seawater was enriched with pure CO₂ in a large mixing tank, filled into 20 L bottles and added

to the mesocosms with a special distribution device (“spider”), that allows distributing the water uniformly within a radius of ~ 1 m. By constantly pulling the spider up and down inside the mesocosms, we ensured homogenous CO_2 enrichment throughout the entire water columns. CO_2 enrichment was carried out at the beginning of the experiment, and two more times (day 22 and 38) to maintain carbonate chemistry within target levels. Based on these CO_2 manipulations, we simulated various scenarios of OA, i.e., seawater carbonate chemistry conditions that are within RCP pathways projected until the end of the twenty-first century (IPCC, 2014). Average $p\text{CO}_2$ during the experiment ranged between ~ 350 and $1,000 \mu\text{atm}$ in the different mesocosms (Table 1).

After an oligotrophic phase of almost 4 weeks, we used a specifically developed deep-water collector to obtain $\sim 85 \text{ m}^3$ of nutrient-rich deep water (from 650 m depth) and by addition to the mesocosms simulate an upwelling event typical for the study region. Therefore, we replaced $\sim 20\%$ of the mesocosms’ volumes with deep water during the night of day 24–25. Deep water addition had only a marginal effect on the carbonate system, with in the control mesocosms $p\text{CO}_2$ in the control mesocosms increasing by a maximum of $40 \mu\text{atm}$.

Based on the timing of deep-water addition and the temporal development of chlorophyll *a*, the experiment can be divided into three distinct phases: (I) the oligotrophic phase until t23, (II) the phytoplankton bloom between t25 and t35, and (III) the post-bloom phase from t37 until the end of the study. For a comprehensive description of experimental design and technical details, please refer to Taucher et al. (2017).

Sample Collection and Measurements

Phytoplankton Community Composition

Samples for phytoplankton were collected every second day with a custom-built pump system that created a gentle vacuum (<150 mbar) and allowed for depth-integrated samples that rapidly collect large volumes of water distributed evenly throughout the water column of the mesocosms.

Subsamples for chlorophyll *a* (Chl *a*) and other phytoplankton pigments were collected onto glass fiber filters (GF/F Whatman, pore size: $0.7 \mu\text{m}$) and analyzed by reverse-phase high-performance liquid chromatography (HPLC) on a Thermo Scientific HPLC Ultimate 3000 as described in Taucher et al. (2017). Contributions of individual phytoplankton groups to total Chl *a* were then estimated using the CHEMTAX software, which classifies phytoplankton based on taxon-specific pigment ratios (Mackey et al., 1996). Applied pigment ratios corresponded to those of the original work by Mackey et al. (1996).

We used three different flow cytometers to optimize coverage of the wide size spectrum of phytoplankton cells and particles during our study. Size classes are based on previously examined relationships between forward or sideward scatter and cell size and should thus be considered as an approximation. Furthermore, we differentiated between phytoplankton groups based on their patterns in plots of forward or side scatter (FSC or SSC) vs. red (FL3) and orange (FL2) fluorescence.

Presented data for *Prochlorococcus*, *Synechococcus* and picoeukaryotes ($<2 \mu\text{m}$) were obtained by analyzing subsamples

of seawater (about 1 ml) with a FACScalibur (Becton and Dickinson) flow cytometer. Nanophytoplankton ($2\text{--}20 \mu\text{m}$) was enumerated with an Accuri C6 (BD Biosciences) from $650 \mu\text{l}$ subsamples. Microphytoplankton ($>20 \mu\text{m}$), including large chain-forming diatoms were counted with a Cytosense system (subsample $\sim 10 \text{ ml}$; Dubelaar and Gerritzen, 2000). Note that counting single diatom cells within a chain with the pulse-shape approach of the Cytosense was not successful during our study. Thus, our counts represent the number of diatom chains (and single cells) rather than the total abundance of diatom cells.

Samples for microscopy were obtained every 4 days, fixed with acidic Lugol solution and analyzed using the Utermöhl technique (Utermöhl, 1958), with classification until the lowest possible taxonomic level (species or genus). Biovolume for the different diatom species were calculated based on measurements of cell length and width (approximately 50 cells measured per species) and subsequent conversion into volume assuming cylindrical geometry for the present species (Menden-Deuer and Lessard, 2000).

Carbonate Chemistry and Nutrients

Partial pressure of aqueous CO_2 ($p\text{CO}_2$) was derived from total alkalinity and dissolved inorganic carbon using CO2SYS (Pierrot et al., 2006). Inorganic nutrients $\text{NO}_3^- + \text{NO}_2^-$, PO_4^{3-} , and Si(OH)_4 were determined colorimetrically following Murphy and Riley (1962) and Hansen and Koroleff, (1999). Ammonium (NH_4^+) was fluorometrically measured following Holmes et al. (1999). For a more detailed description of these measurements see Taucher et al. (2017).

Statistical Analysis

To examine potential effects of OA on the abundance and biomass of the different phytoplankton taxa, we applied simple linear regression analysis. Therefore, we computed temporal averages of the datasets for the different experimental phases (see above), using the respective average $p\text{CO}_2$ as the explanatory variable. Statistical significance was assumed for $p < 0.05$.

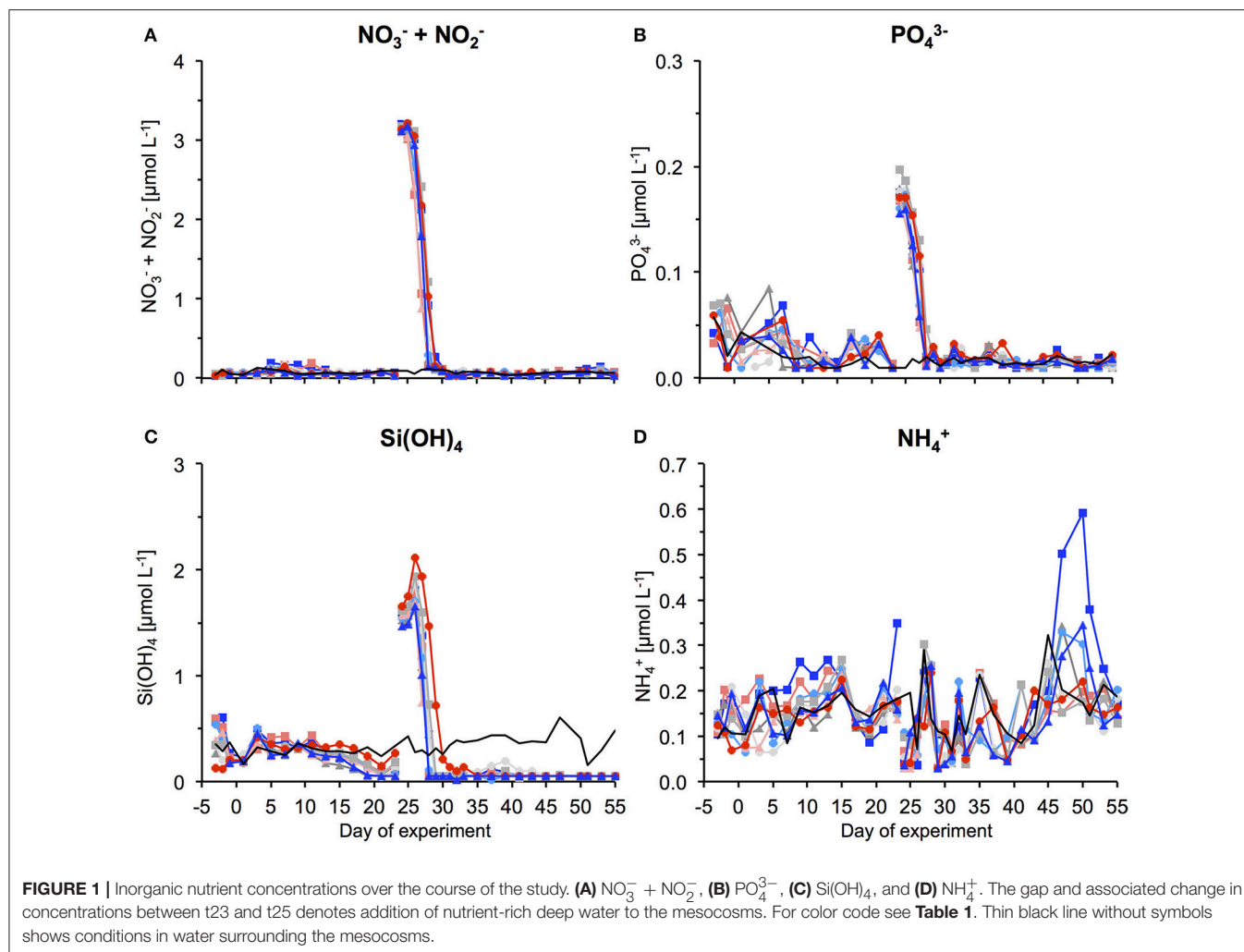
RESULTS

Phase I: Oligotrophic Conditions

During the oligotrophic phase with low nutrient concentrations (Figure 1), chl *a* concentrations of the different phytoplankton groups remained consistently low, fluctuating around a total $\sim 0.1 \mu\text{g L}^{-1}$ until day 23 (Figure 2). Based on CHEMTAX analysis of pigment composition and flow cytometry, biomass of the phytoplankton community was dominated by picocyanobacteria (*Synechococcus*), which constituted 70–80% of total chl *a* in the mesocosms. Comparison of temporal patterns and treatment differences between flow cytometry and pigment-based CHEMTAX analysis revealed that cyanobacteria biomass was almost exclusively composed of *Synechococcus* (Figures 2, 3). *Prochlorococcus* was present ($\sim 10^4\text{--}10^5 \text{ cells ml}^{-1}$) only during the first few days of the experiment, but disappeared from the mesocosms around day 10 (Supplementary Material). The remaining biomass during this period was mainly composed of prymnesiophytes (identified

TABLE 1 | $p\text{CO}_2$ treatment of mesocosms (average over the study period), as well as symbols and color-code for figures.

Mesocosm	M1	M2	M3	M4	M5	M7	M8	M9
$p\text{CO}_2$ (μatm)	369	887	563	716	448	668	1,025	352
Symbol	■	■	▲	●	●	■	●	▲



as *Phaeocystis globosus*), dinoflagellates, and diatoms, which increased in biomass from day 15 onwards (**Figure 2**).

Elevated CO_2 significantly increased the abundance and biomass of *Synechococcus* under oligotrophic conditions, as indicated by flow cytometry and pigment analysis (**Tables 2, 3**). We could distinguish between two distinct *Synechococcus* populations based on their fluorescence patterns in flow cytometry analysis. We here refer to them as the high and low fluorescence populations (high-FL and low-FL). While both populations were similarly abundant (between 20,000 and 40,000 cells ml^{-1}), they clearly differed in their response to CO_2 : while the high-FL cluster did not show a statistically significant response to CO_2 (but a rather negative trend), the cell densities of the low-FL population were significantly enhanced with increasing CO_2 (**Figures 3A–C**).

Most other groups did not display a response to CO_2 treatments during oligotrophic conditions, except for prymnesiophytes, which were negatively affected by increasing CO_2 during this phase I (**Table 3**).

Phase II: Phytoplankton Bloom

By addition of deep water, inorganic nutrients concentrations were increased to 3.15, 0.17, and 1.60 $\mu\text{mol L}^{-1}$ for $\text{NO}_3^- + \text{NO}_2^-$, PO_4^{3-} , and Si(OH)_4 , respectively (**Figure 1**). In response to this nutrient fertilization, a phytoplankton bloom developed rapidly, visible both by a sharp increase in chl *a* concentrations and corresponding increases in cell numbers counted by flow cytometry and microscopy (**Figures 2–5**).

With the development of the bloom, the phytoplankton community quickly shifted toward the dominance of diatoms,

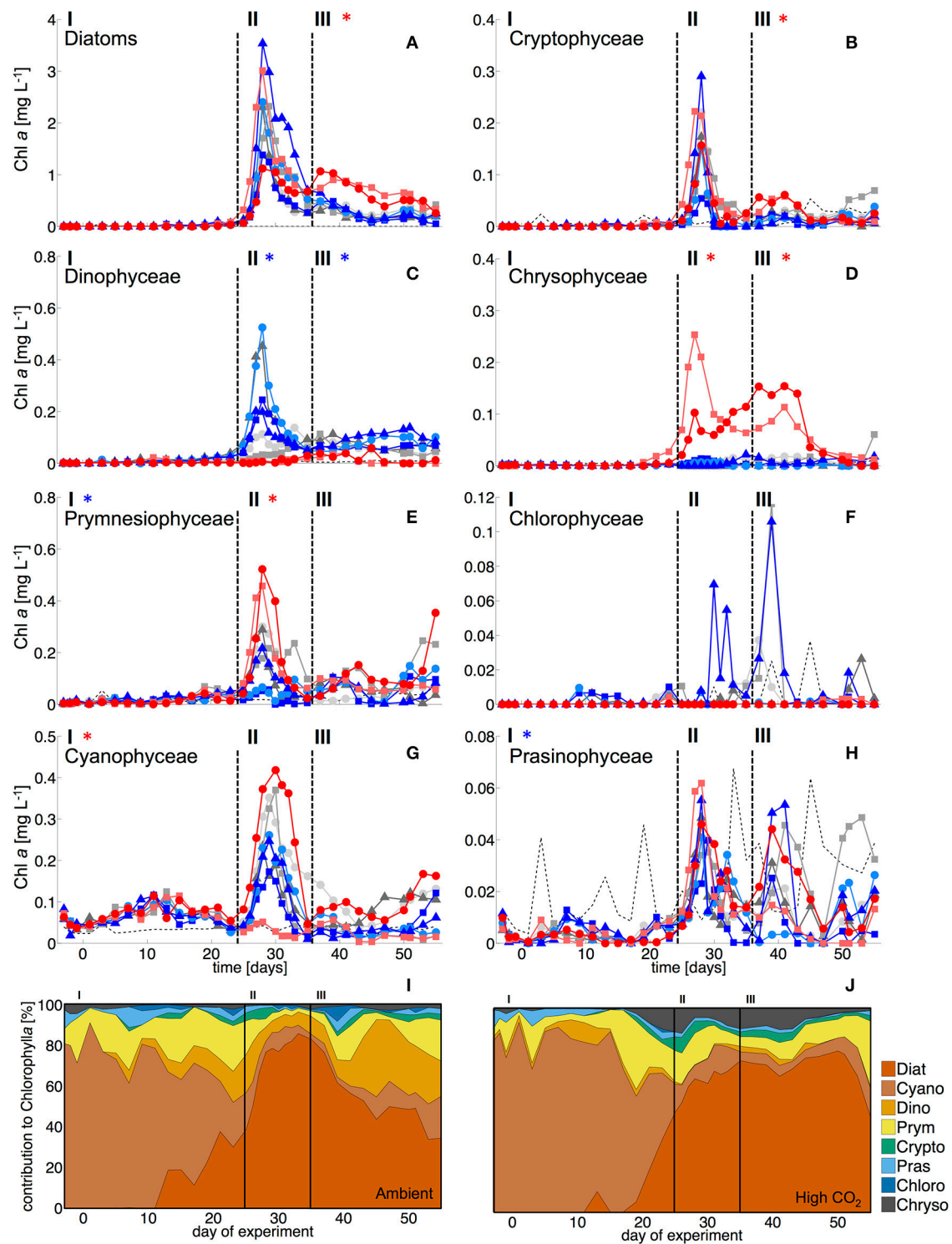
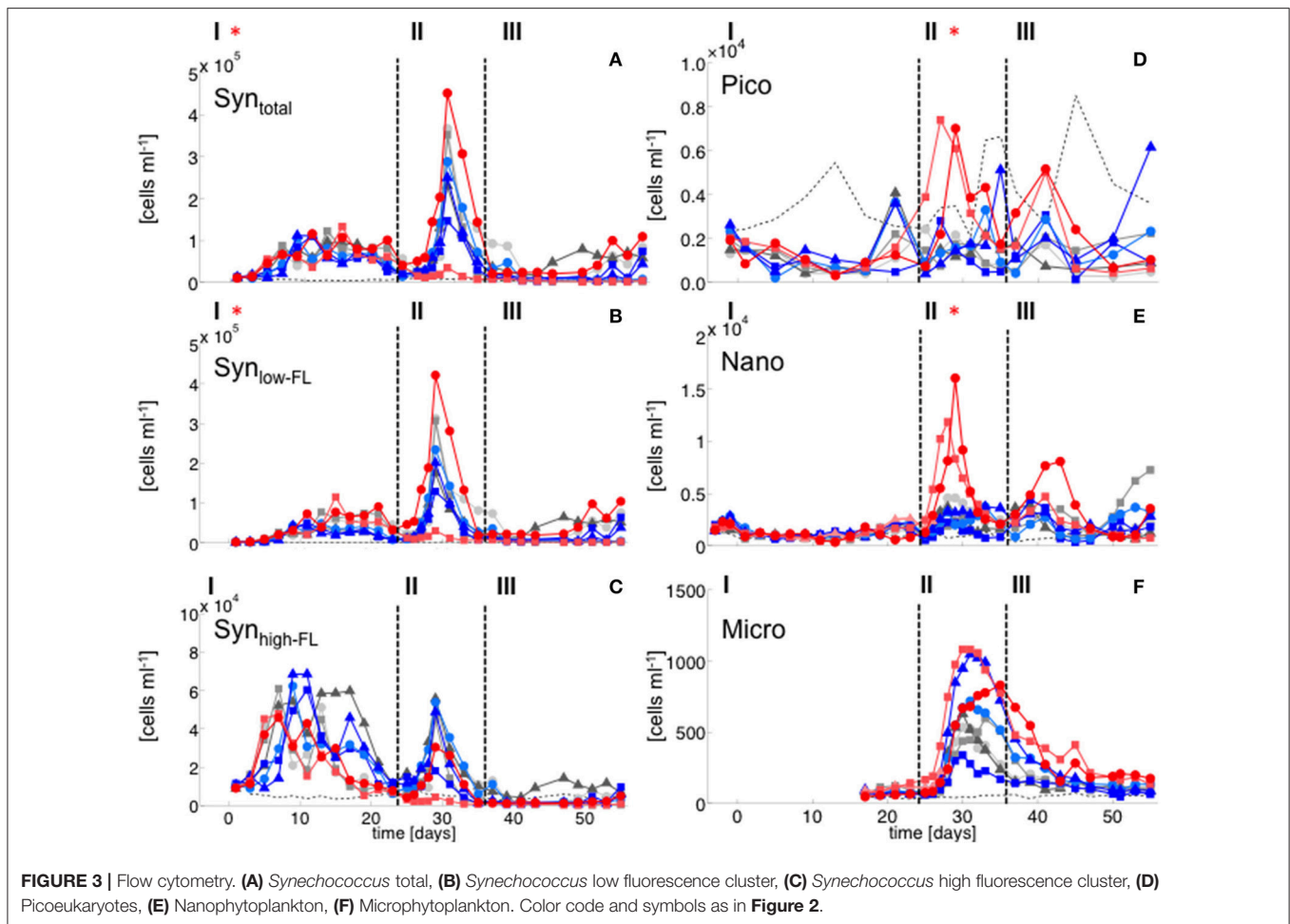


FIGURE 2 | Biomass of phytoplankton groups based on pigment analysis and CHEMTAX. Dashed vertical lines denote different experimental phases (I–III, see section Methods). **(A)** Diatoms, **(B)** Cryptophyceae, **(C)** Dinophyceae, **(D)** Chrysophyceae (mainly reflecting the signal of the Dictyochophyceae *Vicicitus globosus*), **(E)** Prymnesiophyceae (mostly *Phaeocystis globosus*), **(F)** Chlorophyceae, **(G)** Cyanophyceae (mostly *Synechococcus*), and **(H)** Prasinophyceae. Asterisks denote statistically significant effect of CO₂ during this phase (red = positive, blue = negative). **(I, J)** Relative composition of total phytoplankton chl a under **(I)** ambient CO₂ (M1, M9) and **(J)** in the high CO₂ mesocosms (M2, M8).



which constituted up to 80% of total biomass (Figure 2). The most important species were *Guinardia striata*, *Leptocylindrus danicus*, *Bacteriastrium delicatulum*, and *Nitzschia* sp. *Guinardia striata* dominated the diatom community in terms of biovolume, constituting ~50 to >90% of diatom biovolume throughout the study (Figure 4).

The peak in diatom biomass (based on CHEMTAX) was reached on day 28 in all mesocosms, i.e., only 3 days after deep-water addition and declined steadily until day 35, when biomass started to fluctuate around post-bloom levels. The bloom peak was somewhat delayed for larger microphytoplankton (counted by flow cytometry) and the dominant diatom species in particular. Here, highest abundances were reached between day 30 and 40 (Figures 3F, 4).

The abundance and biomass of other phytoplankton groups also increased substantially during the bloom, with some groups also displaying significant responses to CO₂. Data from flow cytometry indicated that abundances of pico- and nanophytoplankton increased with elevated CO₂ (Figure 3; Table 2).

Furthermore, analysis of CHEMTAX data revealed positive CO₂ effects on prymnesiophytes and chrysophytes (Table 3). Microscopy and visual inspection of sediment trap material

indicated high (but very patchy) abundances of *Phaeocystis globosa* colonies. Since this species is usually identified as a prymnesiophyte in CHEMTAX analysis (Mackey et al., 1996; Zapata et al., 2004), this suggests that this species also dominated the signal and CO₂ effect on this group in our study. Chrysophyte biomass consisted mainly of *Vicicitus globosus* (dictyochophyceae). Species of this group have long been classified as chrysophyceae and have only recently been ordered into a separate taxonomic class (actinochrysophyceae; Mikrjukov and Patterson, 2001; Lee, 2008). Yet, based on their pigment signature, particularly the marker pigment 19'-butanoyloxyfucoxanthin (Chang et al., 2012), they are still identified as chrysophyceae in CHEMTAX analysis.

In contrast, dinoflagellate biomass was significantly lower under high CO₂ conditions, not even indicating any signs of population growth in the highest treatments. This pattern was visible both in bulk dinoflagellate biomass (Figure 2), as well as for individual taxa (Figure 5).

Diatoms, the dominant group during the phytoplankton bloom, did not display a clear response to CO₂ in terms of bulk biomass based on CHEMTAX analysis. However, microscopic analysis revealed differential CO₂ effects on the various diatom species. *Guinardia striata* abundances were significantly elevated

TABLE 2 | Results of linear regression for CO₂ effects on phytoplankton groups based on flow cytometry.

	Phase	R ² adj.	p-value	F-value	β ₀	β ₁	Δ _{800–400μatm} [%]
Syn (total)	I	0.68	0.007	16.11	40,766	19.37	+16.0
	II	0.00	0.38	0.91	43,341	84.22	
	III	0.00	0.44	0.67	10,204	30.91	
Pico	I	0.00	0.520	0.46	1,313	−0.22	
	II	0.47	0.037	7.09	−221.1	4.01	+116.0
	III	0.00	0.871	0.03	15,091	0.18	
Nano	I	0.20	0.126	3.01	1,333	−0.24	
	II	0.67	0.008	15.28	−931.6	7.34	+146.5
	III	0.17	0.166	2.48	13,322	1.70	
Micro	I	–	–	–	–	–	
	II	0.00	0.414	0.77	−95.1	0.21	
	III	0.28	0.099	3.79	21.7	0.18	

Intercept β₀ and the slope β₁ are given in (cells ml^{−1}). Significant effects ($p < 0.05$) are marked in bold and are listed with the relative change (Δ) for a pCO₂ doubling from 400 to a 800 μatm as calculated from the regression coefficients ($Y = \beta_0 + \beta_1 \text{ pCO}_2$).

in the high CO₂ mesocosms, whereas a negative CO₂ effect was detected for *Leptocylindrus* (Figure 4; Table 4). As a consequence, the composition of the diatom assemblage shifted substantially in response to increasing CO₂, with *Guinardia striata* being virtually the only species present in noticeable numbers in the high CO₂ mesocosms (Figures 4E,F).

Phase III: Post-bloom

The CO₂-related patterns in phytoplankton composition that emerged during the bloom prevailed during most of the post-bloom phase. During this period, the CO₂ effect on diatoms also manifested itself in bulk diatom biomass derived from CHEMTAX: In the high CO₂ mesocosms diatom biomass was significantly elevated compared to ambient conditions (by about 2-fold) until the end of the experiment (Figure 3). This pattern was mostly driven by the *Guinardia striata*, which strongly dominated the biomass of diatoms and overall phytoplankton in the high CO₂ treatments (Figure 4). This trend was also visible in the microphytoplankton group (based on flow cytometry), although slightly non-significant (Figure 3; Table 2). Besides diatoms, the most prominent treatment effect during the post-bloom phase was the persisting negative CO₂ effect on dinoflagellates, which remained almost absent under high CO₂ conditions (Figure 2; Table 5).

DISCUSSION

Response of Individual Phytoplankton Taxa to Simulated Ocean

Acidification—Physiological Drivers and the Potential Role of Zooplankton Grazing *Synechococcus*

During the oligotrophic (N-limited) phase until day 24, cyanophyceae (almost exclusively *Synechococcus*) dominated the phytoplankton community and displayed a distinct positive response to simulated OA (Figures 2, 3; Tables 2, 3). This observation is consistent with laboratory-based experiments by

Fu et al. (2007), who found increased net growth rates of *Synechococcus* at high CO₂. Other studies have reported more variable effects of OA conditions on *Synechococcus* (Lomas et al., 2012; Bach et al., 2017; Schulz et al., 2017). Besides differences in the experimental setup (e.g., nutrient replete vs. deplete conditions, N vs. P limitation), the most likely explanation for these variable responses of *Synechococcus* to CO₂ is the enormous intraspecific diversity within this taxon (Hunter-Cevera et al., 2016). Even in our study, we could distinguish between two clearly distinct *Synechococcus* clusters based on their fluorescence (FL) properties in flow cytometry analysis, likely resulting from differences in light adaptation. While the high-FL (low light adapted) cluster had lower abundances and displayed a rather negative CO₂ trend, the low-FL (high light adapted) constituted the majority of the overall population and also drove the positive response to CO₂ during the oligotrophic phase (Figure 3).

Since abundances of micro- and mesozooplankton did not display any CO₂ effects during this period (Algueró et al., in review), it seems unlikely that indirect effects mediated by grazing can explain the observed patterns. Thus, a fertilizing effect of CO₂ on the growth rate of *Synechococcus* seems to be the most likely explanation for our results.

Dictyochophyceae

As described in the Results section, chrysophyte biomass consisted mainly of *Vicicitus globosus* (dictyochophyceae), which occurred in considerably higher abundances in the high CO₂ mesocosms. Possible explanations and implications for the food web are discussed in a separate paper (Riebesell et al., in review). However, for the scope of the present study, it should be noted that *Vicicitus globosus* is known as a harmful algal bloom (HAB) species that produces hemolytic cytotoxins (Chang, 2015) and may thus have affected mixotrophic phytoplankton (see Discussion on dinoflagellates below). However, direct toxic effects on other phytoplankton seem very unlikely, as most groups did not show a negative response in mesocosms with high CO₂ (M2 and M8) that would match the patterns of chrysophyceae biomass (i.e., *Vicicitus globosus*), and diatoms and

TABLE 3 | Results of linear regression for CO₂ effects on phytoplankton groups based on pigment analysis (HPLC) and CHEMTAX.

	Phase	R ² adj.	p-value	F-value	β ₀	β ₁	Δ _{800–400μatm} [%]
Diatom	I	0.48	0.057	5.533	0.024	−1.6e ^{−5}	−36.6
	II	0.00	0.519	0.469	1.252	−4.9e ^{−4}	
	III	0.52	0.026	8.713	0.016	5.9e ^{−4}	+93.7
Cyano	I	0.79	0.002	26.67	0.059	1.3e ^{−5}	+7.9
	II	0.00	0.363	0.97	0.067	1.3e ^{−4}	
	III	0.05	0.290	1.34	0.018	5.8e ^{−5}	
Dino	I	0.40	0.055	5.62	0.014	−8.6e ^{−6}	
	II	0.50	0.030	8.00	0.256	−2.9e ^{−4}	−82.5
	III	0.52	0.008	15.38	0.119	−1.0e ^{−4}	−53.3
Prymnesio	I	0.46	0.039	6.88	0.026	−10.0e ^{−6}	−17.9
	II	0.68	0.007	15.89	−0.030	2.6e ^{−4}	+139.6
	III	0.14	0.193	2.15	0.031	6.7e ^{−5}	
Crypto	I	0.00	0.494	0.53	0.002	8.0e ^{−7}	
	II	0.06	0.272	1.46	0.021	5.1e ^{−5}	
	III	0.63	0.012	12.79	−2.96e ^{−4}	3.1e ^{−5}	+102.5
Prasino	I	0.53	0.024	9.03	0.005	−2.0e ^{−6}	−19.3
	II	0.40	0.055	5.67	0.013	1.3e ^{−5}	
	III	0.00	0.541	0.42	0.009	8.0e ^{−6}	
Chloro	I	0.20	0.148	2.75	0.002	−1.7e ^{−6}	
	II	0.08	0.249	1.63	0.010	−1.3e ^{−5}	
	III	0.00	0.433	0.71	0.010	−8.6e ^{−6}	
Chryso	I	0.05	0.289	1.35	4.10e ^{−4}	1.8e ^{−6}	
	II	0.47	0.036	7.20	−0.071	1.8e ^{−4}	NA*
	III	0.58	0.017	10.75	−0.033	8.9e ^{−5}	NA*

Intercept β₀ and the slope β₁ are given in (μg Chl a L^{−1}). Significant effects (*p* < 0.05) are marked in bold and are listed with the relative change (Δ) for a pCO₂ doubling from 400 to a 800 μatm as calculated from the regression coefficients (*Y* = β₀ + β₁ pCO₂). *Note that chrysophytes were not present in the ambient pCO₂ mesocosms, thus no relative change was computed.

prymnesiophyceae even reached highest biomass concentrations in the high CO₂ treatments (Figure 3, 4).

Diatoms

Starting with the bloom onset on day 25, diatoms began to dominate phytoplankton biomass for the rest of the experiment. While no treatment-related differences were detectable during the bloom phase (II), diatom biomass was significantly elevated in the high CO₂ mesocosms in the post-bloom phase (III), displaying a much longer retention of biomass in the water column than under ambient conditions. These observations are consistent with previous evidence, which found CO₂ effects on diatom population densities to be most pronounced under post-bloom conditions when nutrients were exhausted (Taucher et al., 2015).

The effect of simulated OA on bulk diatom biomass in our experiment, was tightly coupled to distinct taxonomic shifts within the diatom assemblage. Most prominently, elevated CO₂ had a significant positive effect of on cell densities of the dominant species *Guinardia striata*, a taxon that forms twisted chains from relatively large-sized cells (~170 × 17 μm in this study). In contrast, abundances of *Leptocylindrus danicus* (~30 × 7 μm) were highest in the ambient CO₂ treatment and decreased significantly with increasing CO₂ (Figure 4).

A direct negative physiological effect seems unlikely, since previous studies have rather reported positive effects of CO₂ on this taxon (Reul et al., 2014; Tatters et al., 2018). Thus, it seems more likely that *Leptocylindrus danicus* was outcompeted by *Guinardia striata*, possibly because the latter benefited stronger from CO₂ fertilization and could therefore take up a large portion of nutrients after deep-water addition. In that sense, our findings are consistent with previous theoretical and experimental studies, which predicted that increasing CO₂ would affect larger species more than smaller ones (Wolf-Gladrow and Riebesell, 1997; Wu et al., 2014; Taucher et al., 2015). The reason is that larger cells (with lower surface-to-volume ratios) can rely less on diffusive uptake of CO₂ and thus need to invest more resources into carbon concentrating mechanisms (CCM). Elevated CO₂ can increase the proportion of diffusive carbon uptake, in turn leading to a down-regulation of CCMs and accelerated growth (Giordano et al., 2005).

Clearly, the possible role of an indirect CO₂ effect mediated by grazing cannot be excluded, as micro- and mesozooplankton abundances were lower in the high CO₂ treatments during the bloom and early post-bloom phase (Algueró et al, in review). For the dominant species *Guinardia striata*, its large cell and chain size and the relatively small size of zooplankton during

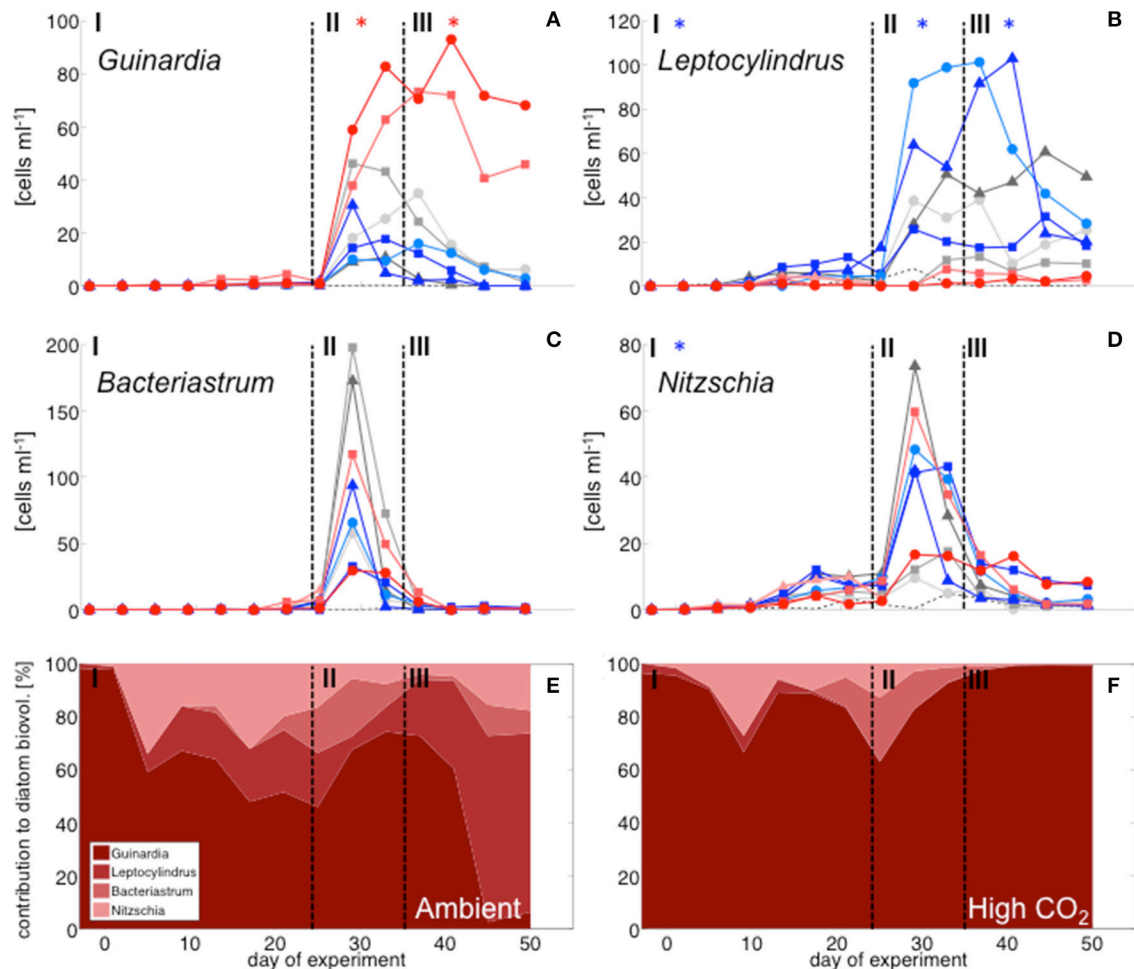


FIGURE 4 | Diatom community composition derived from microscopy. Abundance of (A) *Guinardia striata*, (B) *Leptocylindrus danicus*, (C) *Bacteriastrum delicatulum*, and (D) *Nitzschia* sp. Color code and symbols as in Figure 2. (E,F): relative contribution of different taxa to total diatom biovolume under (E) ambient CO₂ (M1, M9) and (F) in the high CO₂ mesocosms (M2, M8).

the experiment (mainly copepods < 1 mm) make it unlikely that abundances of this diatom species were strongly affected by mesozooplankton grazing. However, it is possible that top-down control to some extent influenced the population size of the smaller species *Leptocylindrus danicus* before and/or during the bloom stage, thus keeping their abundance lower and thereby indirectly favoring the proliferation of *Guinardia striata*.

Altogether, our findings suggest that increasing CO₂ might have highly variable effects on the competitive capabilities of different diatom species, which may ultimately translate into substantial taxonomic shifts during diatom blooms with ongoing OA.

Prymnesiophyceae (*Phaeocystis Globosa*)

During the phytoplankton bloom, *Phaeocystis globosa* formed large colonies (several mm in diameter) that were very patchily distributed within the water column. Moreover, part of their biomass was present as colonies temporarily attached to the mesocosm walls, a phenomenon that has been observed

previously for this species (Rousseau et al., 2007). Thus, quantifying their abundance by microscopy was not possible. However, earlier studies have shown that *Phaeocystis globosa* taxa possess a characteristic pigment signature, particularly with respect to the accessory pigment 19'-hexanoyloxyfucoxanthin and its content relative to the more common fucoxanthin (Vaulot et al., 1994; Zapata et al., 2004). Thus, based on CHEMTAX analysis and visual inspection of *Phaeocystis globosa* colonies, we are confident that most biomass classified as prymnesiophyceae was constituted by *Phaeocystis globosa* in our study.

In our experiment, prymnesiophyceae formed a substantial bloom with considerably elevated biomass with increasing CO₂ (see Figure 2E). Although occurrences of *Phaeocystis* taxa are rather uncommon at low latitudes (Vogt et al., 2012), occasional blooms in subtropical waters have been observed previously, particularly after upwelling events (Long et al., 2007). In terms of potential OA impacts, previous work has found subtle to moderate increases of physiological rates and colony formation of

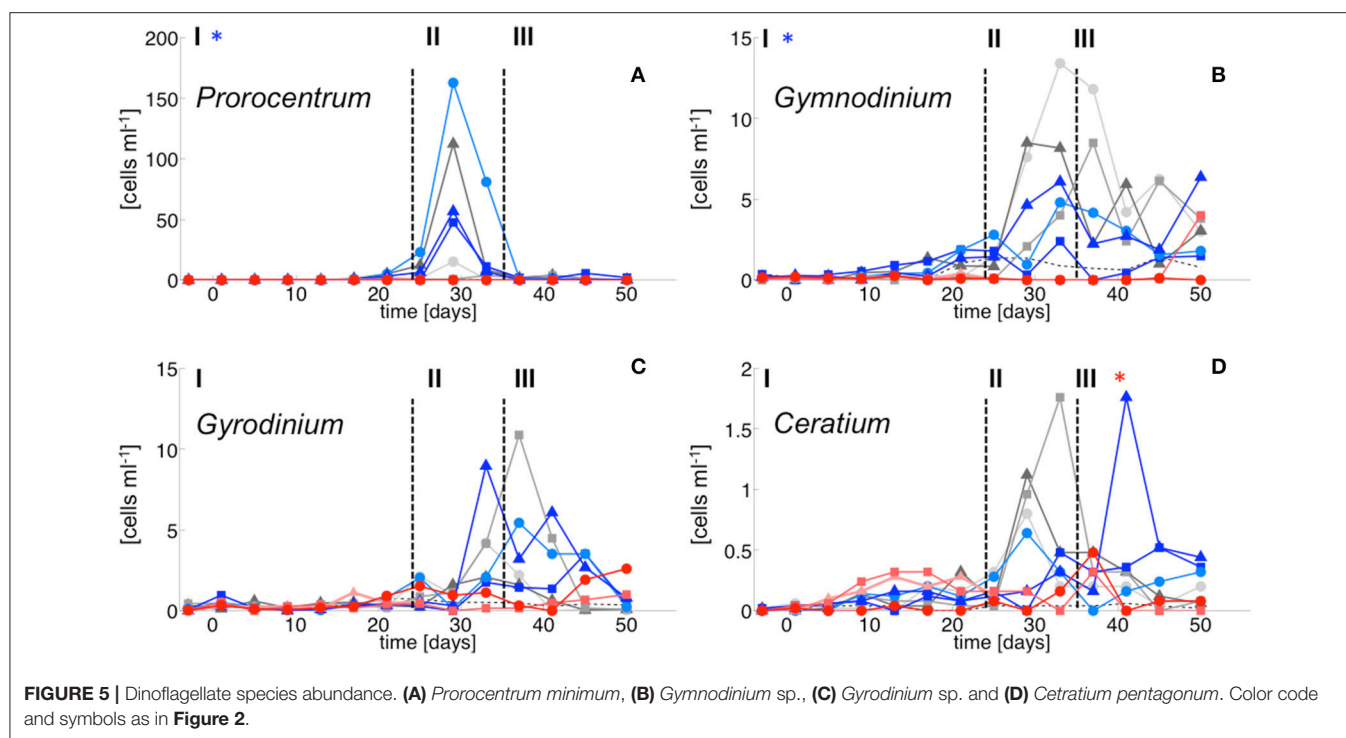


TABLE 4 | Results of linear regression for CO₂ effects on diatom species counted by light microscopy.

	Phase	R^2 adj.	p -value	F -value	β_0	β_1	$\Delta_{800-400\mu\text{atm}}$ [%]
<i>Guinardia</i>	I	0.11	0.226	1.82	0.07	$7.4e^{-4}$	
	II	0.75	0.033	22.04	-0.02	$6.8e^{-3}$	+279.5
	III	0.67	0.008	15.21	-0.04	$1.0e^{-2}$	+1,826.6
<i>Leptocylindrus</i>	I	0.51	0.029	8.19	5.55	$-4.3e^{-3}$	-45.6
	II	0.43	0.046	6.29	69.50	$-8.1e^{-3}$	-91.4
	III	0.52	0.027	8.47	74.75	$-8.0e^{-3}$	-70.1
<i>Bacteriastrum</i>	I	0.00	0.371	0.94	-0.08	$4.2e^{-4}$	
	II	0.00	0.910	0.01	-0.08	$6.2e^{-3}$	
	III	0.05	0.281	1.40	0.21	$2.0e^{-3}$	
<i>Nitzschia</i>	I	0.70	0.006	17.07	5.24	$-3.1e^{-3}$	-30.3
	II	0.00	0.380	0.86	35.49	$-2.2e^{-2}$	
	III	0.00	0.599	0.31	3.55	$3.3e^{-3}$	

Intercept β_0 and the slope β_1 are given in (cells ml⁻¹). Significant effects ($p < 0.05$) are marked in bold and are listed with the relative change (Δ) for a pCO₂ doubling from 400 to a 800 μatm as calculated from the regression coefficients ($Y = \beta_0 + \beta_1 \text{ pCO}_2$).

Phaeocystis globosa at elevated CO₂ (Rost et al., 2003; Wang et al., 2010). Thus, similar to CO₂ effects on other phytoplankton types during our experiment, beneficial effects of CO₂ fertilization are the most obvious explanation for the proliferation of prymnesiophyceae (i.e., *Phaeocystis globosa*) under simulated OA conditions.

Indirect CO₂ effects by grazing may have contributed to this pattern to some extent. However, as mentioned earlier, a large portion *Phaeocystis globosa* biomass was present in the form of large colonies during our study. The formation of such colonies has been demonstrated to act as a defense strategy, i.e., reducing feeding pressure by size-selective grazers (Jakobsen and

Tang, 2002). Therefore, a strong indirect CO₂ effect through zooplankton grazing seems unlikely in our study.

Dinoflagellates

Dinoflagellates are a diverse taxonomic group of eukaryotes which acquire energy through photosynthesis or heterotrophy, or a combination of both known as mixotrophy (Stoecker et al., 2017). Our data on dinoflagellate biomass are based on their contribution to chl *a* (based on CHEMTAX), thus considering auto- and mixotrophic taxa with a pigment composition characteristic for Dinophyceae, particularly regarding the marker pigment peridinin (Mackey et al., 1996). Accordingly, this

TABLE 5 | Results of linear regression for CO₂ effects on dinoflagellate species counted by light microscopy.

	Phase	R ² adj.	p-value	F-value	β ₀	β ₁	Δ _{800–400μatm} [%]
<i>Prorocentrum</i>	I	0.47	0.025	8.05	1.02	−8.7e ^{−4}	−51.5
	II	0.23	0.127	3.13	74.25	−9.2e ^{−2}	
	III	9.12	0.215	1.96	2.26	−0.2e ^{−2}	
<i>Gymnodinium</i>	I	0.55	0.013	10.97	0.77	−6.4e ^{−4}	−49.6
	II	0.15	0.330	1.08	5.96	−5.4e ^{−3}	
	III	0.00	0.791	0.08	3.41	−1.0e ^{−3}	
<i>Gyrodinium</i>	I	0.00	0.871	0.03	0.29	−2.0e ^{−5}	
	II	0.00	0.374	0.92	2.60	−1.8e ^{−3}	
	III	0.00	0.254	1.59	3.44	−2.7e ^{−3}	
<i>Ceratium</i>	I	0.00	0.728	0.13	0.08	2.0e ^{−5}	
	II	0.00	0.567	0.37	0.56	−3.4e ^{−4}	
	III	0.49	0.033	7.65	0.65	−6.5e ^{−4}	

Intercept β₀ and the slope β₁ are given in (cells ml^{−1}). Significant effects ($p < 0.05$) are marked in bold and are listed with the relative change (Δ) for a pCO₂ doubling from 400 to a 800 μatm as calculated from the regression coefficients ($Y = \beta_0 + \beta_1 \text{ pCO}_2$).

pigment-based approach excludes heterotrophic species and likely also a large portion of mixotrophic (non-peridinin containing) species that acquire kleptochloroplasts from other phytoplankton.

Notably, dinoflagellates were the only phytoplankton group displaying a clear negative response to high CO₂ throughout the study. This trend emerged already during the oligotrophic phase (although borderline non-significant, **Table 3**), prevailing and even amplifying throughout the bloom and entire post-bloom phase (see regression slopes in **Table 3**). In fact, the development of a dinoflagellate bloom or even an increase in population densities was not detectable in the high CO₂ mesocosms (M2 and M8), which largely drove the CO₂ effect detected by linear regression.

Microscopic counts suggested that dinoflagellate biomass was mainly comprised of *Prorocentrum minimum*, *Gyrodinium* sp., *Gymnodinium* sp., and *Ceratium pentagonum*. Since these taxa also contain peridinin they probably constituted most of the CHEMTAX signal. Indeed, temporal patterns and the low abundances of dinoflagellates in the high CO₂ mesocosms appear very similar between CHEMTAX data and microscopic counts of these species (**Figures 2, 5**). On a species basis, linear regression detected significant effects only for some taxa and time periods, mainly because the CO₂ effect appeared very non-linear, being mostly driven by the high CO₂ mesocosms (M2 and M8).

Based on previous empirical evidence, it seems unlikely that the strongly reduced dinoflagellate numbers under high CO₂ were driven by a direct physiological effect. In fact, most laboratory studies so far have reported dinoflagellates to be resilient or rather benefit from increasing pCO₂ (Fu et al., 2008; Eberlein et al., 2014).

Furthermore, differences in grazing pressure by mesozooplankton cannot explain the observed pattern, as mesozooplankton abundances were lowest in the high CO₂ treatments. Thus, one would have expected the opposite pattern.

Considering that all dinoflagellate taxa examined in our study are known to be mixotrophic (Stoecker, 1999; Stoecker et al.,

2017), it seems more likely that dinoflagellates were indirectly affected by elevated CO₂ via food-web effects. The presence of toxic *Vicicitus globosus* cells (classified as chrysophyceae by CHEMTAX), which occurred only in the high CO₂ mesocosms may have impaired the growth of dinoflagellates. Laboratory-based experiments have demonstrated that *Vicicitus globosus* can have cytotoxic effects (i.e., lysis) on other microalgae, including dinoflagellates (Chang, 2015). Furthermore, there is some evidence that *Phaeocystis globosa* can have similar toxic effects (Peng et al., 2005). Since CO₂ had also a positive effect on *Phaeocystis globosa* biomass, this may have further contributed to the decline of mixotrophic dinoflagellates under OA conditions. However, the fact that CO₂ trends on dinoflagellates were mainly driven by the two mesocosms with highest CO₂ (M2 and M8) rather points toward growth inhibition by *Vicicitus. globosus*, which was only present in these two mesocosms.

CONCLUSION

Our *in situ* mesocosm experiment provides the first evidence of OA impacts on phytoplankton community structure in the subtropical oligotrophic ocean. Under typical nutrient-poor and low chl *a* conditions, *Synechococcus* dominated phytoplankton biomass and seemed to profit from simulated OA. The phytoplankton bloom that developed after deep-water addition was strongly dominated by diatoms, which were retained much longer in the water column under OA conditions. These patterns were the result of distinct taxonomic shifts within the diatom assemblage, with a clear tendency toward larger species (here *Guinardia striata*) benefitting from increasing CO₂. Considering that other taxa (*Phaeocystis globosa*, dictyochophyceae, dinoflagellates) were also significantly affected by increasing pCO₂, the overall phytoplankton community composition, including bulk chl *a* biomass, was considerably altered by simulated OA. Notably, some of the high CO₂/low pH effects observed during the bloom emerged already during the oligotrophic phase and were then amplified by nutrient

fertilization (e.g., the negative effect on dinoflagellates). So far, there have been only few studies that investigated the response of plankton communities to OA under nutrient-poor conditions. Evidence from this earlier work is contrasting: Mesocosm studies in the Mediterranean Sea reported phytoplankton communities to be rather resilient to increasing $p\text{CO}_2$, with no effects on total biomass and only subtle changes in taxonomic composition (Maugendre et al., 2017). However, these studies were rather short (12–20 days), and other recent work has shown that it may take more than a month until OA effect manifest themselves on the community level (Bach et al., 2017). In fact, other studies found ecological impacts of OA to be even more pronounced under nutrient-depleted conditions than during blooms (Paul et al., 2015; Sala et al., 2015; Bach et al., 2016). Our findings from the subtropical eastern North Atlantic are in support of the latter, indicating that phytoplankton communities in these regions might undergo distinct taxonomic shifts in response to increasing CO_2 . If our findings from this experiment hold true on larger spatial and temporal scales, then we can expect phytoplankton community composition in the subtropical oligotrophic ocean to be considerably altered by ongoing OA over the coming decades.

AUTHOR CONTRIBUTIONS

UR, JT, LB, JA, and EA: conceived and designed the experiment. All authors performed the experiment and analyzed the data. JT with input from all co-authors wrote the paper.

REFERENCES

- Aristegui, J., Tett, P., Hernandez-Guerra, A., Basterretxea, G., Montero, M. F., Wild, K., et al. (1997). The influence of island-generated eddies on chlorophyll distribution: A study of mesoscale variation around Gran Canaria. *Deep-Sea Res. Part I Oceanogr. Res. Papers* 44, 71–96. doi: 10.1016/S0967-0637(96)00093-3
- Bach, L. T., Alvarez-Fernandez, S., Hornick, T., Stühr, A., and Riebesell, U. (2017). Simulated ocean acidification reveals winners and losers in coastal phytoplankton. *PLoS ONE* 12:e0188198. doi: 10.1371/journal.pone.0188198
- Bach, L. T., Taucher, J., Boxhammer, T., Ludwig, A., Achterberg, E. P., Algüero-Muñiz, M., et al. (2016). Influence of ocean acidification on a natural winter-to-summer plankton succession: first insights from a long-term mesocosm study draw attention to periods of low nutrient concentrations. *PLoS ONE* 11:e0159068. doi: 10.1371/journal.pone.0159068
- Bakun, A. (1990). Global climate change and intensification of coastal ocean upwelling. *Science* 247, 198–201. doi: 10.1126/science.247.4939.198
- Bopp, L., Resplandy, L., Orr, J. C., Doney, S. C., Dunne, J. P., Gehlen, M., et al. (2013). Multiple stressors of ocean ecosystems in the 21st century: projections with CMIP5 models. *Biogeosciences* 10, 6225–6245. doi: 10.5194/bg-10-6225-2013
- Caldeira, K., and Wickett, M. E. (2003). Anthropogenic carbon and ocean pH. *Nature* 425, 365–365. doi: 10.1038/425365a
- Chang, F. H. (2015). Cytotoxic effects of vicinitus globosus (Class Dictyochophyceae) and Chattonella marina (Class Raphidophyceae) on rotifers and other microalgae. *J. Mar. Sci. Eng.* 3, 401–411. doi: 10.3390/jmse3020401
- Chang, F. H., McVeagh, M., Gall, M., and Smith, P. (2012). Chattonella globosa is a member of Dictyochophyceae: reassignment to Vicinitus gen. nov., based on molecular phylogeny, pigment composition, morphology and life history. *Phycologia* 51, 403–420. doi: 10.2216/10-104.1

FUNDING

This study was supported by the German Federal Ministry of Science and Education (BMBF) in the framework of the BIOACID II project (FKZ 03F06550). UR received additional funding from the Leibniz Award 2012 by the German Research Foundation (DFG). JA was supported by a Helmholtz International Fellow Award, 2015 (Helmholtz Association, Germany). JA and MM benefited also from the FLUXES project (CTM2015-69392-C3-1-R) funded by the Spanish government (Plan Nacional I + D).

ACKNOWLEDGMENTS

We would like to thank the KOSMOS and the Plataforma Oceánica de Canarias (PLOCAN) teams assisting with all aspects of the organization and logistical support before, during and after this mesocosms campaign. Furthermore, we thank the captain and crew of RV *Hesperides* for deploying and recovering the mesocosms (cruise 29HE20140924), and RV *Poseidon* for transporting the mesocosms and support in collecting deep water during cruise POS463.

SUPPLEMENTARY MATERIAL

The Supplementary Material for this article can be found online at: <https://www.frontiersin.org/articles/10.3389/fmars.2018.00330/full#supplementary-material>

- Dubelaar, G. B. J., and Gerritzen, P. L. (2000). CytoBuoy: a step forward towards using flow cytometry in operational oceanography. *Sci. Mar.* 64, 255–265. doi: 10.3989/scimar.2000.64n2255
- Dutkiewicz, S., Morris, J. J., Follows, M. J., Scott, J., Levitan, O., Dyhrman, S. T., et al. (2015). Impact of ocean acidification on the structure of future phytoplankton communities. *Nat. Clim. Change Adv.* 5, 1002–1006. doi: 10.1038/nclimate2722
- Eberlein, T., Van de Waal, D. B., and Rost, B. (2014). Differential effects of ocean acidification on carbon acquisition in two bloom-forming dinoflagellate species. *Physiol. Plant.* 151, 468–479. doi: 10.1111/pp.12137
- Fu, F. X., Warner, M. E., Zhang, Y. H., Feng, Y. Y., and Hutchins, D. A. (2007). Effects of increased temperature and CO_2 on photosynthesis, growth, and elemental ratios in marine *Synechococcus* and *Prochlorococcus* (Cyanobacteria). *J. Phycol.* 43, 485–496. doi: 10.1111/j.1529-8817.2007.00355.x
- Fu, F. X., Zhang, Y. H., Warner, M. E., Feng, Y. Y., Sun, J., and Hutchins, D. A. (2008). A comparison of future increased CO_2 and temperature effects on sympatric *Heterosigma akashiwo* and *Prorocentrum minimum*. *Harmful Algae* 7, 76–90. doi: 10.1016/j.hal.2007.05.006
- García-Reyes, M., Sydeman, W. J., Schoeman, D. S., Rykaczewski, R. R., Black, B. A., Smit, A. J., et al. (2015). Under pressure: climate change, upwelling, and eastern boundary upwelling ecosystems. *Front. Mar. Sci.* 2:109. doi: 10.3389/fmars.2015.00109
- Gazeau, F., Sallon, A., Maugendre, L., Louis, J., Dellisanti, W., Gaubert, M., et al. (2016). First mesocosm experiments to study the impacts of ocean acidification on plankton communities in the NW Mediterranean Sea (MedSeA project). *Estuarine Coast. Shelf Sci.* 186, 11–29. doi: 10.1016/j.ecss.2016.05.014
- Giordano, M., Beardall, J., and Raven, J. A. (2005). CO_2 concentrating mechanisms in algae: mechanisms, environmental modulation, and evolution. *Annu. Rev. Plant Biol.* 56, 99–131. doi: 10.1146/annurev.arplant.56.032604.144052

- Hansen, H. P., and Koroleff, F. (1999). "Determination of nutrients," in *Methods of Seawater Analysis*, eds K. Grasshoff, K. Kremling, and M. Ehrhardt (Weinheim: Wiley-VCH Verlag GmbH), 159–228.
- Hernández-Hernández, N., Bach, L. T., Montero, M. F., Taucher, J., Baños, I., Guan, W., et al. (2018). High CO₂ under nutrient fertilization increases primary production and biomass in subtropical phytoplankton communities: a mesocosm approach. *Front. Mar. Sci.* 5:213. doi: 10.3389/fmars.2018.00213
- Holmes, R. M., Aminot, A., Kerouel, R., Hooker, B. A., and Peterson, B. J. (1999). A simple and precise method for measuring ammonium in marine and freshwater ecosystems. *Can. J. Fish. Aquat. Sci.* 56, 1801–1808. doi: 10.1139/f99-128
- Hunter-Cevera, K. R., Post, A. F., Peacock, E. E., and Sosik, H. M. (2016). Diversity of *Synechococcus* at the Martha's vineyard coastal observatory: insights from culture isolations, clone libraries, and flow cytometry. *Microb. Ecol.* 71, 276–289. doi: 10.1007/s00248-015-0644-1
- IPCC (2014). *Climate Change 2013: The Physical Science Basis. Working Group I Contribution to the Fifth Assessment Report of the Intergovernmental Panel on Climate Change*. Cambridge; New York, NY: Cambridge University Press.
- Jakobsen, H. H., and Tang, K. W. (2002). Effects of protozoan grazing on colony formation in *Phaeocystis globosa* (Prymnesiophyceae) and the potential costs and benefits. *Aquat. Microb. Ecol.* 27, 261–273. doi: 10.3354/ame027261
- Lee, R. E. (2008). "Heterokontophyta, dictyochophyceae," in *Phycology*, ed R. E. Lee (Cambridge: Cambridge University Press), 359–364.
- Lomas, M. W., Hopkinson, B. M., Losh, J. L., Ryan, D. E., Shi, D. L., Xu, Y., et al. (2012). Effect of ocean acidification on cyanobacteria in the subtropical North Atlantic. *Aquat. Microb. Ecol.* 66, 211–222. doi: 10.3354/ame01576
- Long, J. D., Frischer, M. E., and Robertson, C. Y. (2007). A *phaeocystis globosa* bloom associated with upwelling in the subtropical South Atlantic Bight. *J. Plankton Res.* 29, 769–774. doi: 10.1093/plankt/fbm058
- Longhurst, A. R., Sathyendranath, S., Platt, T., and Caverhill, C. (1995). An estimate of global primary production in the ocean from satellite radiometer data. *J. Plankton Res.* 17, 1245–1271. doi: 10.1093/plankt/17.6.1245
- Mackey, M. D., Mackey, D. J., Higgins, H. W., and Wright, S. W. (1996). CHEMTAX—a program for estimating class abundances from chemical markers: application to HPLC measurements of phytoplankton. *Mar. Ecol. Prog. Ser.* 144, 265–283. doi: 10.3354/meps144265
- Mahadevan, A. (2016). "The impact of submesoscale physics on primary productivity of plankton," in *Annual Review of Marine Science*, Vol. 8, eds C. A. Carlson, and S. J. Giovannoni (Palo Alto, CA: Annual Reviews), 161–184.
- Maugendre, L., Guieu, C., Gattuso, J. P., and Gazeau, F. (2017). Ocean acidification in the Mediterranean Sea: pelagic mesocosm experiments. A synthesis. *Estuarine Coast. Shelf Sci.* 186, 1–10. doi: 10.1016/j.ecss.2017.01.006
- McClain, C. R., Signorini, S. R., and Christian, J. R. (2004). Subtropical gyre variability observed by ocean-color satellites. *Deep Sea Res. Part II Topical Stud. Oceanogr.* 51, 281–301. doi: 10.1016/j.dsr2.2003.08.002
- McGillicuddy, D. J. (2016). "Mechanisms of physical-biological-biogeochemical interaction at the oceanic mesoscale," in *Annual Review of Marine Science*, Vol. 8, eds C. A. Carlson, S. J. Giovannoni (Palo Alto, CA: Annual Reviews), 125.
- Menden-Deuer, S., and Lessard, E. J. (2000). Carbon to volume relationships for dinoflagellates, diatoms, and other protist plankton. *Limnol. Oceanogr.* 45, 569–579. doi: 10.4319/lo.2000.45.3.0569
- Mikrjukov, K. A., and Patterson, D. J. (2001). Taxonomy and phylogeny of heliozoa. III. Actinophryids. *Acta Protozool.* 40, 3–25.
- Murphy, J., and Riley, J. P. (1962). A modified single solution method for the determination of phosphate in natural waters. *Anal. Chim. Acta* 27, 31–36. doi: 10.1016/S0003-2670(00)88444-5
- Paul, A. J., Bach, L. T., Schulz, K. G., Boxhammer, T., Czerny, J., Achterberg, E. P., et al. (2015). Effect of elevated CO₂ on organic matter pools and fluxes in a summer Baltic Sea plankton community. *Biogeosciences* 12, 6181–6203. doi: 10.5194/bg-12-6181-2015
- Peng, X. C., Yang, W. D., Liu, J. S., Peng, Z. Y., Lu, S. H., and Ding, W. Z. (2005). Characterization of the hemolytic properties of an extract from *Phaeocystis globosa* Scherffel. *J. Integr. Plant Biol.* 47, 165–171. doi: 10.1111/j.1744-7909.2005.00039.x
- Pierrot, D. E., Lewis, E., and Wallace, D. W. R. (2006). *MS Excel Program Developed for CO₂ System Calculations*. ORNL/CDIAC-105a. Oak Ridge, TN: Carbon Dioxide Information Analysis Center, Oak Ridge National Laboratory, U.S. Department of Energy.
- Polovina, J. J., Howell, E. A., and Abecassis, M. (2008). Ocean's least productive waters are expanding. *Geophys. Res. Lett.* 35, L0361. doi: 10.1029/2007GL031745
- Reul, A., Munoz, M., Bautista, B., Neale, P. J., Sobrino, C., Mercado, J. M., et al. (2014). Effect of CO₂, nutrients and light on coastal plankton. III. Trophic cascade, size structure and composition. *Aquat. Biol.* 22, 59–76. doi: 10.3354/ab00585
- Riebesell, U., Czerny, J., von Brockel, K., Boxhammer, T., Budenbender, J., Deckelnick, M., et al. (2013). Technical note: a mobile sea-going mesocosm system—new opportunities for ocean change research. *Biogeosciences* 10, 1835–1847. doi: 10.5194/bg-10-1835-2013
- Riebesell, U., and Tortell, P. D. (2011). "Effects of ocean acidification on pelagic organisms and ecosystems," in *Ocean Acidification*, eds J. P. Gattuso, and L. Hansson (New York, NY: Oxford University Press), 99–121.
- Rost, B., Riebesell, U., Burkhardt, S., and Sultemeyer, D. (2003). Carbon acquisition of bloom-forming marine phytoplankton. *Limnol. Oceanogr.* 48, 55–67. doi: 10.4319/lo.2003.48.1.0055
- Rousseau, V., Chrétiennot-Dinet, M.-J., Jacobsen, A., Verity, P. G., and Whipple, S. (2007). The life cycle of *Phaeocystis*: state of knowledge and presumptive role in ecology. *Biogeochemistry* 83, 29–47. doi: 10.1007/s10533-007-9085-3
- Sala, M. M., Aparicio, F. L., Balague, V., Boras, J. A., Borrell, E., Cardelus, C., et al. (2015). Contrasting effects of ocean acidification on the microbial food web under different trophic conditions. *Ices J. Mar. Sci.* 73, 670–679. doi: 10.1093/icesjms/fsv130
- Sangra, P., Pascual, A., Rodríguez-Santana, A., Machin, F., Mason, E., McWilliams, J. C., et al. (2009). The canary eddy corridor: a major pathway for long-lived eddies in the subtropical North Atlantic. *Deep Sea Res. Part I Oceanogr. Res. Papers* 56, 2100–2114. doi: 10.1016/j.dsr.2009.08.008
- Schulz, K. G., Bach, L. T., Bellerby, R. G. J., Bermúdez, R., Budenbender, J., Boxhammer, T., et al. (2017). Phytoplankton blooms at increasing levels of atmospheric carbon dioxide: experimental evidence for negative effects on prymnesiophytes and positive on small picoeukaryotes. *Front. Mar. Sci.* 4:64. doi: 10.3389/fmars.2017.00064
- Schütte, F., Brandt, P., and Karstensen, J. (2016). Occurrence and characteristics of mesoscale eddies in the tropical northeastern Atlantic Ocean. *Ocean Sci.* 12, 663–685. doi: 10.5194/os-12-663-2016
- Signorini, S. R., Franz, B. A., and McClain, C. R. (2015). Chlorophyll variability in the oligotrophic gyres: mechanisms, seasonality and trends. *Front. Mar. Sci.* 2:1. doi: 10.3389/fmars.2015.00001
- Sswat, M., Stiasny, M. H., Taucher, J., Algueró-Muñoz, M., Bach, L. T., Jutfelt, F., et al. (2018). Food web changes under ocean acidification promote herring larvae survival. *Nat. Ecol. Evol.* 2, 836–840. doi: 10.1038/s41559-018-0514-6
- Stange, P., Taucher, J., Bach, L. T., Algueró-Muñoz, M., Horn, H. G., Krebs, L., et al. (2018). Ocean acidification-induced restructuring of the plankton food web can influence the degradation of sinking particles. *Front. Mar. Sci.* 5:140. doi: 10.3389/fmars.2018.00140
- Stoecker, D. K. (1999). Mixotrophy among dinoflagellates. *J. Eukaryotic Microbiol.* 46, 397–401. doi: 10.1111/j.1550-7408.1999.tb04619.x
- Stoecker, D. K., Hansen, P. J., Caron, D. A., Mitra, A., and Annual, R. (2017). Mixotrophy in the marine plankton. *Annu. Rev. Mar. Sci.* 9, 311–335. doi: 10.1146/annurev-marine-010816-060617
- Tatters, A. O., Schnetzer, A., Xu, K., Walworth, N. G., Fu, F. X., Spackeen, J. L., et al. (2018). Interactive effects of temperature, CO₂ and nitrogen source on a coastal California diatom assemblage. *J. Plankton Res.* 40, 151–164. doi: 10.1093/plankt/fbx074
- Taucher, J., Bach, L. T., Boxhammer, T., Nauendorf, A., Consortium, T. G. C. K., Achterberg, E. P., et al. (2017). Influence of ocean acidification and deep water upwelling on oligotrophic plankton communities in the subtropical north atlantic: insights from an *in situ* mesocosm study. *Front. Mar. Sci.* 4:85. doi: 10.3389/fmars.2017.00085
- Taucher, J., Jones, J., James, A., Brzezinski, M. A., Carlson, C. A., Riebesell, U., et al. (2015). Combined effects of CO₂ and temperature on carbon uptake and partitioning by the marine diatoms *Thalassiosira weissflogii* and *Dactyliosolen fragilissimus*. *Limnol. Oceanogr.* 60, 901–919. doi: 10.1002/lno.10063
- Utermöhl, H. (1958). *Zur Vervollkommnung Der Quantitativen Phytoplankton-Methodik*. Stuttgart: Schweizerbart.
- Vaulot, D., Birritt, J. L., Marie, D., Casotti, R., Veldhuis, M. J. W., Kraay, G. W., et al. (1994). Morphology, ploidy, pigment composition, and genome size of

- cultured strains of *Phaeocystis* (Prymnesiophyceae). *J. Phycol.* 30, 1022–1035. doi: 10.1111/j.0022-3646.1994.01022.x
- Vogt, M., O'Brien, C., Peloquin, J., Schoemann, V., Breton, E., Estrada, M., et al. (2012). Global marine plankton functional type biomass distributions: *Phaeocystis* spp. *Earth Syst. Sci. Data* 4, 107–120. doi: 10.5194/essd-4-107-2012
- Wang, Y., Smith, W. O., Wang, X. D., and Li, S. S. (2010). Subtle biological responses to increased CO₂ concentrations by *Phaeocystis globosa* Scherffel, a harmful algal bloom species. *Geophys. Res. Lett.* 37. doi: 10.1029/2010GL042666
- Wolf-Gladrow, D., and Riebesell, U. (1997). Diffusion and reactions in the vicinity of plankton: a refined model for inorganic carbon transport. *Mar. Chem.* 59, 17–34. doi: 10.1016/S0304-4203(97)00069-8
- Wu, Y., Campbell, D. A., Irwin, A. J., Suggett, D. J., and Finkel, Z. (2014). Ocean acidification enhances the growth rate of larger diatoms. *Limnol. Oceanogr.* 59, 1027–1034. doi: 10.4319/lo.2014.59.3.1027
- Xiu, P., Chai, F., Curchitser, E. N., and Castruccio, F. S. (2018). Future changes in coastal upwelling ecosystems with global warming: the case of the California current system. *Sci. Rep.* 8: 2866. doi: 10.1038/s41598-018-21247-7
- Zapata, M., Jeffrey, S. W., Wright, S. W., Rodriguez, F., Garrido, J. L., and Clementson, L. (2004). Photosynthetic pigments in 37 species (65 strains) of Haptophyta: implications for oceanography and chemotaxonomy. *Mar. Ecol. Prog. Ser.* 270, 83–102. doi: 10.3354/meps270083

Conflict of Interest Statement: The authors declare that the research was conducted in the absence of any commercial or financial relationships that could be construed as a potential conflict of interest.

Copyright © 2018 Taucher, Arístegui, Bach, Guan, Montero, Nauendorf, Achterberg and Riebesell. This is an open-access article distributed under the terms of the Creative Commons Attribution License (CC BY). The use, distribution or reproduction in other forums is permitted, provided the original author(s) and the copyright owner(s) are credited and that the original publication in this journal is cited, in accordance with accepted academic practice. No use, distribution or reproduction is permitted which does not comply with these terms.



Response of Pelagic Calcifiers (Foraminifera, Thecosomata) to Ocean Acidification During Oligotrophic and Simulated Up-Welling Conditions in the Subtropical North Atlantic Off Gran Canaria

Silke Lischka*, Paul Stange and Ulf Riebesell

GEOMAR Helmholtz Centre for Ocean Research Kiel, Biological Oceanography, Kiel, Germany

OPEN ACCESS

Edited by:

Christel Hassler,
Université de Genève, Switzerland

Reviewed by:

Michal Kucera,
University of Bremen, Germany
Michaël Hermoso,
Sorbonne Universités, France

*Correspondence:

Silke Lischka
slischka@geomar.de

Specialty section:

This article was submitted to
Marine Biogeochemistry,
a section of the journal
Frontiers in Marine Science

Received: 26 April 2018

Accepted: 28 September 2018

Published: 24 October 2018

Citation:

Lischka S, Stange P and Riebesell U
(2018) Response of Pelagic Calcifiers
(Foraminifera, Thecosomata) to Ocean
Acidification During Oligotrophic and
Simulated Up-Welling Conditions in
the Subtropical North Atlantic Off Gran
Canaria. *Front. Mar. Sci.* 5:379.
doi: 10.3389/fmars.2018.00379

Planktonic Foraminifera and thecosome pteropods are major producers of calcite and aragonite in the ocean and play an important role for pelagic carbonate flux. The responses of planktonic foraminifers to ocean acidification (OA) are variable among the species tested and so far do not allow for reliable conclusion. Thecosome pteropods respond with reduced calcification and shell dissolution to OA and are considered at high risk especially at high latitudes. The present investigation was part of a large-scale *in situ* mesocosm experiment in the oligotrophic waters of the eastern subtropical North Atlantic. Over 62 days, we measured the abundance and vertical flux of pelagic foraminifers and thecosome pteropods as part of a natural plankton community over a range of OA scenarios. A bloom phase was initiated by the introduction of deep-water collected from approx. 650 m depth simulating a natural up-welling event. Foraminifers occurred throughout the entire experiment in both the water column and the sediment traps. Pteropods were present only in small numbers and disappeared after the first two weeks of the experiment. No significant CO₂ related effects were observed for foraminifers, but cumulative sedimentary flux was reduced at the highest CO₂ concentrations. This flux reduction was most likely accompanying an observed flux reduction of particulate organic matter (POM) so that less foraminifers were intercepted and transported downward.

Keywords: ocean acidification, pteropods, foraminifers, mesocosm experiment, oligotrophic ocean, subtropical, North Atlantic, export flux

1. INTRODUCTION

The global ocean absorbs yearly about 27% of the anthropogenically emitted CO₂ (Rhein et al., 2013; Le Quéré et al., 2015) whereby the seawater chemistry is changed and the pH, the carbonate ion concentration [CO₃²⁻] and the saturation states (Ω) of the calcium carbonates (CaCO₃) calcite (ca) and aragonite (ar) decline (Zeebe and Wolf-Gladrow, 2001). This phenomenon is termed ocean

acidification (OA). Presently, the mean ocean surface pH ranges between 7.8 and 8.4 and models project a further decrease of 0.1–0.4 units by the end of this century (Ciais et al., 2013). OA has the potential to impact marine life on organismal and ecosystem levels (e.g., Wittmann and Pörtner, 2013; Dutkiewicz et al., 2015; Hammill et al., 2017; Riebesell et al., 2017). Calcifying organisms are particularly sensitive because shell and skeleton formation becomes increasingly difficult with decreasing calcium carbonate saturation states (Guinotte and Fabry, 2008; Doney et al., 2009; Kroeker et al., 2010, 2013). The ability of calcifiers to deal with OA conditions therefore critically depends on how much they are able to regulate intracellular pH during calcification (Stumpp et al., 2012). Foraminifers for example can elevate the pH at calcification site by one unit above seawater pH (Bentov et al., 2009; de Nooijer et al., 2009). CaCO_3 saturation states are generally highest in the tropics and lowest at high latitudes, because CO_2 solubility increases with decreasing temperature (Fabry et al., 2008). The higher CO_2 solubility in cold water intensifies this process due to increased uptake from the atmosphere. In contrast, the warm surface waters of the tropics and subtropics will not become aragonite or calcite undersaturated over the range of CO_2 concentrations projected for this century (Ciais et al., 2013), although in some upwelling regions shoaling aragonite saturation horizons intrude on the depth ranges of calcifying planktonic organisms (Feely et al., 2004).

The vertical and temporal distribution of planktonic foraminifers (Protozoa) is mainly controlled by sea surface temperature (SST), hydrography and phytoplankton biomass in the productive surface layers (Schiebel and Hemleben, 2000; Wilke et al., 2009). Similar relationships determine the occurrence of pteropods (metazoa, pelagic gastropods) (Almogi-Labin et al., 1988; Fischer et al., 1996). Planktonic foraminifers and euthecosomatous (shell-bearing) pteropods are the major calcifiers among marine zooplankton (Fabry et al., 2008). Pelagic Foraminifera make their shells (or tests) of calcite, whereas pteropods produce shells of aragonite, a metastable form of CaCO_3 that is 50% more soluble than calcite (Mucci, 1983). Both groups are wide-spread in the ocean and contribute significantly to particulate inorganic carbon (PIC) and they also contribute to particulate organic carbon (POC) flux to depth (Schiebel, 2002; Tsurumi et al., 2005; Wilke et al., 2009). On a global mean, 25% of total calcite production of planktonic foraminifers sinks to the deep ocean sediment surface which is equivalent to about 32–80% of total calcite flux to the deep ocean (Schiebel, 2002). Pteropods are more patchily distributed and thus aragonite flux rates show a high temporal and regional variability, but occasionally they can dominate carbonate flux (Bathmann et al., 1991; Schiebel, 2002). The contribution of aragonite to the total calcium carbonate flux oceanwide was estimated to ~12% (Berner and Honjo, 1981), but in some areas it can amount to >50% of total CaCO_3 flux (Lalli and Gilmer, 1989). The contribution of pteropods to global pelagic carbonate production is estimated to 20–42% (Bednaršek et al., 2012a).

Due to their aragonitic shell, thecosome pteropods are particularly threatened by OA because their shells dissolve easily when Ω_{ar} is nearing 1 and calcification rates decline with

decreasing Ω_{ar} (Comeau et al., 2010a,b; Lischka et al., 2011; Bednaršek et al., 2012b, 2014). Also, their survival is affected by pCO_2 and habitat suitability is declining where the occurrence of undersaturated water with respect to aragonite is increasing (Lischka et al., 2011; Bednaršek et al., 2014; Thabet et al., 2015). No true OA perturbation studies are currently available on planktonic foraminifera. Studies that are available do not allow for clear distinction of confounding factors (e.g., Lombard et al., 2010; Keul et al., 2013). For benthic foraminifers, lab experiments revealed a range of responses to OA that include positive and negative correlations with pCO_2 depending on species (e.g., Schmidt et al., 2014). Survivorship of large benthic foraminifers for example was unaffected (McIntyre-Wressnig et al., 2013; Schmidt et al., 2014; Prazeres et al., 2018). Growth and calcification of benthic species increased in response to elevated pCO_2 (Vogel and Uthicke, 2012), yet net calcification rates of the planktonic foraminifer *Neogloboquadrina pachyderma* decreased under low pH conditions and in combination with elevated temperature this effect was moderated. Survival was not affected at all (Manno et al., 2012). Field observations underline that there is no simple relationship between abundance and growth of planktonic foraminifers and environmental conditions (e.g., carbonate saturation, temperature, productivity, optimum growth conditions) with substantial interspecies- and intraspecies-specific variations (Gonzalez-Mora et al., 2008; Beer et al., 2010; Weinkauff et al., 2016). Shell weight of *Globigerinoides ruber* from the Arabian Sea for example could be related to anthropogenic induced OA scenarios but also to periods of different upwelling intensities (de Moel et al., 2009). Studies along natural CO_2 gradients revealed that densities and diversity of benthic foraminifer assemblages declined sharply with increasing pCO_2 at pH levels of <7.9 (>700 $\mu\text{atm pCO}_2$) (Dias et al., 2010; Uthicke et al., 2013). On the other hand, modern *Globigerina bulloides* from the Southern Ocean had 30–35% lower shell weights as compared to the underlying Holocene-aged sediments (Moy et al., 2009). This finding is consistent with Davis et al. (2017) who found in laboratory experiments with *Globigerinoides bulloides* calcification and oxygen consumption to decrease with declining pH conditions. It should be noted, however, that most of the species tested, especially the benthic ones, bear symbionts which may mitigate the response to OA by CO_2 -fertilization through the symbionts. With respect to the ability of organisms to cope with elevated pCO_2 in the long run, insights from natural habitats may be more conclusive than results from short-term lab experiments can suggest (Vogel and Uthicke, 2012).

For pteropods, most of these studies were conducted in polar regions. In some areas of the Arctic Ocean aragonite undersaturation is starting already now and will continue to expand and intensify in the coming decades. In tropical regions, Ω_{ar} will stay well above 1 even beyond the end of this century and thus, OA may affect calcification rates but probably not cause shell dissolution in these regions. For foraminifers, IPCC projections for tropical regions for the second half of this century correspond with pH ranges for which drastic decrease of densities and diversity of benthic foraminifers have been described (Ciais et al., 2013; Uthicke et al., 2013).

One of the most pressing questions in OA research is, how OA effects described for single species play out at the community level with respect to species abundance and diversity, trophic interactions, and elemental cycling, including the vertical flux of carbon and carbonate. In this regard, large-scale *in situ* mesocosm experiments enclosing natural plankton communities provide a powerful approach to gain a more realistic insight into how OA effects on individual organisms translate to the community level. Recent mesocosm experiments performed in the Baltic Sea, the Skagerrak, and the Mediterranean Sea suggest OA effects on plankton communities may be stimulated during times of low inorganic nutrient concentrations (Paul et al., 2015; Sala et al., 2016; Bach, et al., 2016). Possible OA effects on plankton communities in the oligotrophic waters of the North Atlantic subtropical gyres have not yet been studied. The oligotrophic waters around the Canary Islands in the subtropical North Atlantic are characterized by low nutrient concentrations during most of the year (Aristegui et al., 1997), but regular upwelling events of deep water through island-induced eddy formation as well as upwelling filaments reaching out to the Canary Islands from the West-African coast provide for frequent nutrient pulses and accompanying bloom situations (Aristegui et al., 2001; Sangra et al., 2009).

In this study, we intended to test how possible OA responses of the plankton community may change during a temporary shift from oligotrophic to eutrophic conditions. To simulate this, we conducted a 9-week CO₂-manipulated mesocosm experiment to which we added natural nutrient-rich deep-water collected in the field midway of the experiment to mimic a natural upwelling event (Taucher et al., 2017). As part of the Gran Canaria KOSMOS study, described in detail in Taucher et al. (2017), this paper focusses on possible OA effects on the occurrence and succession of pelagic calcifiers (thecosome pteropods, heteropods, planktonic foraminifers) in the water column of the mesocosms and on their vertical flux to the sediment traps. Establishing OA conditions through the addition of different amounts of CO₂-enriched seawater to the mesocosms assured a realistic OA scenario. Thus, this study provided the unique opportunity to investigate for the first time the impact of OA on pelagic calcifiers on ecosystem-level.

2. METHODS

2.1. Mesocosm Set-Up

To investigate OA effects on a natural plankton community in the oligotrophic subtropical North Atlantic, nine off-shore pelagic mesocosms (KOSMOS: “Kiel Off-Shore Mesocosms for Ocean Simulations”) were deployed and moored on 23 September 2014 in the northern Gando Bay at 27° 55'41" N, 15° 21'55" W (Gran Canaria). Approximate bottom depth at the mooring site was ~ 20–25 m. The bags of the mesocosms extended down to 13 m and were closed with a 2 m long conical sediment trap that allows for regular collection of settled material via a vacuum pump system. After deployment, the bags were initially kept open and submerged to ~ 1 m below the ocean surface so that a free exchange with the surrounding plankton community and water was ensured for 4 days. During this time, the upper











and lower end of the bags were covered with a 3 mm mesh to exclude larger plankton (Cnidaria) and fish. The experiment started on 27 September 2014, when these nets were removed and simultaneously the sediment traps were attached to the bottom and the mesocosm bags pulled up to above the ocean surface to isolate the enclosed plankton community from the surrounding water masses. The water volumes right before deep-water addition ranged between 31.57 and 37.75 m³ (Taucher et al., 2017). The first CO₂ addition was performed on 1 October and is denoted day 0 (t0), i.e., the start of the experiment was 4 days prior to the first CO₂ manipulation and is denoted day -4 (t-4). The experiment lasted for 62 days with the last sampling day on 27 November (t57). To simulate a natural upwelling event, on t24 we injected deep water in each of the mesocosms. For this 20% of the enclosed water was substituted with deep water collected at 650 m depth to simulate the input of comparable amounts of inorganic nutrients as observed during natural upwelling events in this region (Aristegui et al., 1997; Neuer et al., 2007). Deep-water volumes added to the mesocosms ranged between 7.50 and 8.95 m³ (Taucher et al., 2017).

OA was simulated by adding different amounts of CO₂-saturated seawater to seven of the nine mesocosms according to Riebesell et al. (2013) to set up an initial pCO₂ gradient from ambient levels of ~400 μatm to a maximum concentration of ~1,480 μatm in the highest CO₂ treatment. A detailed description of the CO₂ manipulations is given in Taucher et al. (2017). In short, about 1,500 L natural pre-filtered seawater was collected from Melenara Bay using a pipe and bubbled with pure CO₂ gas until saturation. Before filling the CO₂-saturated seawater in 20 L containers and subsequent boat-transport to the mesocosms, it was filtered again (20 μm). The different amounts of CO₂-saturated seawater were added to the mesocosms with a special distribution device that assures uniform distribution within a radius of ~1 m (Riebesell et al., 2013). The volume of CO₂-saturated seawater needed to reach target pCO₂ levels in the mesocosms was calculated from measured DIC and TA concentrations. Determination of the carbonate system was part of the regular sampling effort carried out every second day. CO₂ additions were done stepwise over 7 days to allow for gradual acclimation of the plankton community, and thus final starting conditions were reached on t6. To compensate for a CO₂ loss through air-sea gas exchange, two further CO₂ manipulations were conducted on t21 prior to the deep-water addition (oligotrophic phase) and on t38 during the post-bloom phase. The CO₂ gradient was chosen according to IPCC scenarios projected for this century. M1 and M9 served as controls and were not CO₂ manipulated. Manipulations resulted in average pCO₂ values over the experiment duration (t1–t55) ranging from 352 μatm to 1,025 μatm (Table 1). Unfortunately, M6 was lost on t27 due to strong currents (Taucher et al., 2017).

2.2. Sampling and Enumeration of Calcifiers in the Water Column

Mesozooplankton net sampling was conducted vertically with an Apstein net of 55 μm mesh size and 17 cm diameter aperture.

TABLE 1 | Mesocosm set-up with mean $p\text{CO}_2$ [μatm], mean pH_T (total scale), mean carbonate ion concentration [CO_3^{2-}], mean Ω_{calcite} (Ω_{ca}), and mean $\Omega_{\text{aragonite}}$ (Ω_{ar}) values, averaged over the whole experimental duration (t1–t55; except for M6).

Mesocosm	Symbol	$p\text{CO}_2$	pH_T	$[\text{CO}_3^{2-}]$	Ω_{ca}	Ω_{ar}	Note
M1		369 (43)	8.09 (0.04)	248 (17.5)	5.8 (0.4)	3.8 (0.26)	Control
M9		352 (60)	8.11 (0.06)	260 (26.5)	6.11 (0.62)	4.02 (0.40)	Control
M5		448 (67)	8.02 (0.06)	221 (22.9)	5.19 (0.54)	3.41 (0.35)	
M3		563 (86)	7.94 (0.06)	190 (21)	4.47 (0.49)	2.94 (0.32)	
M7		668 (121)	7.78 (0.07)	170 (25)	3.99 (0.59)	2.63 (0.39)	
M4		716 (136)	7.86 (0.08)	162 (23.6)	3.8 (0.56)	2.5 (0.37)	
M6		970 (126)	7.74 (0.05)	129 (14.5)	3.03 (0.34)	2.0 (0.23)	Mean t1–t26 lost on t27
M2		887 (206)	7.78 (0.09)	140 (25.7)	3.29 (0.6)	2.16 (0.4)	
M8		1025 (230)	7.72 (0.09)	125 (22.1)	2.93 (0.52)	1.93 (0.34)	
Atlantic		399 (15)	8.06 (0.01)	227 (4.8)	5.37 (0.11)	3.53 (0.08)	

Carbonate system parameters were calculated from measured DIC and TA concentrations (Taucher et al., 2017). The standard deviation is given in brackets. Definition of symbols and color-code used in the figures.

All mesocosms were sampled evenly, i.e., the same amount of net hauls was taken from all mesocosms on each sampling event. The first net hauls were taken on t-3, the day after mesocosm closure. Beginning on t1, further net hauls were done on a regular 8 days basis. However, due to adverse weather conditions, sampling on t49 had to be shifted to t50 resulting in a 9 days interval between t41 and t50. Additional net samples were also taken at experiment closure (t56). Sampling depth was 13 m to avoid resuspension of material from the sediment trap zone resulting in 295 L of total filtered water volume. Net hauls were always done between 14:00 and 16:00 CET. After retrieval of the net, zooplankton was quantitatively rinsed into sample bottles with filtered seawater and stored in cooled containers to prevent them from heating. Samples were brought back to PLOCAN (Platforma Oceánica de Canarias) where the research campaign was hosted (Taucher et al., 2017). Back in the PLOCAN laboratories, samples were immediately preserved in 70% ethanol.

Calcifiers [Thecosomata, Pterotracheoidea (formerly heteropods), and Foraminifera] were counted and identified under a WILD M3B stereomicroscope assuming 100% filtering efficiency of the net. Abundances were calculated as individuals m^{-3} . Foraminifera had a strong tendency to clump together with their spines and therefore accurate enumeration was not possible without prior sorting of the individuals and likewise it was not possible to assure accurate splitting to estimate abundances from subsamples. Therefore, all calcifiers were counted and identified from the whole sample after species identification and abundance determination of the bulk zooplankton was completed (Algueró-Muñoz et al. submitted). As identification and enumeration of all foraminifer specimen was not possible on the species level due to their small size, the species inventory was determined on some representative specimen only under higher magnification on a Keyence microscope (model number of microscope: VH-Z250R, model number of computer: VHX-700FD) with the help of Dr. N. Keul at Kiel University, but enumerations were done on family level (Globigerinidae). The same approach was applied to the sediment trap samples.

2.3. Sampling and Enumeration of Calcifiers in the Sediment Trap Material

The sediment traps were emptied every 2 days using a manual vacuum pump to collect the settled material via a silicon tube connected to the collection cylinder of the sediment trap (Riebesell et al., 2013; Boxhammer et al., 2015). Pteropods, heteropods, and foraminifera were counted prior to processing of these samples for quantification and characterization of bulk particulate matter. Initially, we tried to count representatives of the three groups from the whole sediment sample. However, from t5 onwards, samples became too voluminous and foraminifera too abundant that regular every other day counting became too laborious and time-consuming. Therefore, enumeration of foraminifera had to be restricted to 50 ml subsamples from t5 onwards. Pteropods and heteropods, however, were much less abundant and were not found representatively in subsamples, and hence were continually counted from the complete sample until t35. On that day, sedimentation had increased even stronger due to enhanced production in the water column in response to the deep-water addition on t24 and it was no longer possible to enumerate pteropods and heteropods from the complete sediment trap samples. Thus, from t35 onwards, only the 50 ml subsamples were checked for the occurrence of calcifiers.

2.4. Statistics

We performed statistical analyses on the abundance of planktonic Foraminifera (all belong to the family Globigerinidae) in the water column and on the flux of Globigerinidae and the sexual stage of *Orbulina universa* to the sediment traps. GLM (generalized linear mixed models) or GAMM (generalized additive mixed model) with a Gaussian distribution were used to test whether $p\text{CO}_2$ had an effect on the temporal development of abundances. “Mesocosm” was included as random intercept. In case of GAMM a smoother on experiment day was included. $p\text{CO}_2$ was used as continuous explanatory variable for each t-day to account for the change over time due to biological activity. We log-transformed flux data of Globigerinidae, because

preceding GLM models suggested significance for CO₂ but model validation showed strong variance heterogeneity especially due to the factor experiment day that could not be adequately captured by different variance structures tested. M6 was excluded from all analyses because it was lost on t26. t-3 data were excluded from analyses of water column data to assure equally spaced data. All analyses were carried out with R using the package nlme, mgcv, Hmisc and MASS. All plots were done in ggplot (R Core Team, 2013).

Pelagic mollusks occurred only very shortly during the first days of the experiment, both in the water column and sediment traps. In the water column, the spherical stage of *Orbulina universa* was only found on t9. Thus, sampling frequency was comparatively low for these groups and, therefore, we did not do any statistical analyzes on the temporal trends in the different mesocosms.

3. RESULTS

3.1. Percent Contribution of Calcifiers to the Mesozooplankton Community in the Water Column

The abundance of pelagic calcifiers in the mesocosms was generally low throughout the study. Among the three groups of calcifying zooplankton, foraminifers were most numerous. Thecosome pteropods and heteropods (Pterotracheidae) were present only during the first days of the experiment and were virtually absent from t9 onwards. Highest contributions of pteropods were 1.7% (M6, t9) and of heteropods 0.7% (M8, t1) of the total mesozooplankton abundance (data not shown). Foraminifers were present during the whole study and contributed between 0.2 and 11.3% to the total mesozooplankton abundance with some exceptional peaks in M7 on t9, in M8 on t33, and in M2 on t50. In the surrounding Atlantic water, pteropods were always found during the study period (0.7–6%) with a contribution peak on t25 but heteropods were only occasionally identified with very low contributions (max. 0.4%). As in the mesocosms, foraminifers occurred continually in the Atlantic but had somewhat lower contributions as in the mesocosms (1–6%). Representatives of both groups were mostly smaller than 200 μm , many of them even smaller than 100 μm in size. Only very few larger pteropods (older stage of *Creseis* sp.) were found.

3.2. Temporal Dynamics of Calcifiers

3.2.1. Water Column

3.2.1.1. Pteropoda and Heteropoda

Abundances of thecosome pteropods in the mesocosms varied between 0 and 86 ind. m^{-3} and of heteropods between 0 and 32 ind. m^{-3} (Figures 1A,B). Compared to the mesocosms, numbers of pteropods in the surrounding Atlantic water were higher (18–157 ind. m^{-3}), and those of heteropods lower (0–11 ind. m^{-3}). In the mesocosms, both groups had abundance peaks during the first days (t-3, t1). As mentioned above already, pteropods and heteropods almost completely disappeared after t9/t17 in the mesocosms. Deep-water addition on t24 did not have an obvious effect on the occurrence of pteropods and heteropods in

the water column. Abundances showed no trend with the CO₂ concentration over time.

3.2.1.2. Dominant pteropod and heteropod species/genus

Most pteropod specimen found were *Heliconoides inflatus* with a maximum abundance of 86 ind. m^{-3} . Occasionally, specimen of *Limacina trochiformis* (max. 4 ind. m^{-3}) and embryonal stages of some cavolinid thecosomes were found. Cavolinids most likely belonged to the genus *Creseis* sp. or *Styliola* sp. and reached maximum numbers of 61 ind. m^{-3} (data not shown). Heteropods identified in the samples belonged exclusively to the family Atlantidae (genus *Atlanta*) and the individuals found were all juvenile stages. In the surrounding Atlantic water, *Heliconoides inflatus* was present during the study period (18–157 ind. m^{-3}). *L. trochiformis* was not found, *Creseis* sp. and *Styliola* sp. as well as heteropods occurred only sporadically at low numbers (max. 4 and 11 ind. m^{-3} , respectively).

3.2.1.3. Dominant foraminiferan species/groups

Of the planktonic foraminiferans (family Globigerinidae), the most abundant species that we identified were *Globigerinoides ruber*, *Globigerina bulloides*, *Globigerinella siphonifera*, and *Orbulina universa* (Figure 2A). The abundances of Globigerinidae ranged between 18 and 610 ind. m^{-3} (Atlantic: 25–103 ind. m^{-3}). Temporarily, we found the sexual stage of *O. universa* in the mesocosms with peak abundances of 68 ind. m^{-3} on t9, but we did not find it in the net samples taken in the surrounding Atlantic water (Figure 2B). Occasionally, we also found a few specimen of the planktonic *Globorotalia* but these were too rare to analyze quantitatively. We also occasionally found many specimen of the benthic *Tretomphalus* with floating chambers in the net samples. These were, despite their abundance, not considered in the analysis, because they are not part of the normal pelagic community. Most likely, the mesocosms acted as artificial substrate for these benthic foraminifer species and reproduction may have been stimulated by nutrient fertilization after the deep-water addition. However, as mentioned already, they are not part of the pelagic community and therefore are not further considered here.

Abundances of Globigerinidae were not significantly affected by CO₂ (GAMM, $p = 0.39$) over time.

3.2.2. Sediment Trap

3.2.2.1. Pteropoda and Heteropoda

Peak occurrence of pelagic mollusks in the sediment traps was around t5 shortly after their abundance peak in the water column (Figures 1C,D) with a maximum time delay between peak abundance in the water column and in the sediment traps of 4 days. Sedimentation peaks of pteropods and heteropods were highest in M3, M4, and M5. A small increase in flux of both groups, pteropods and heteropods, in M1, M9, and M5 followed on t19. After that pelagic mollusks were absent, both in the sediment traps and the water column. Strikingly though, the total flux differed considerably from the abundance of pelagic mollusks in the water column (Figures 1E, F). This flux deficit is most likely due to the difficulty to find remains of these fragile organisms in the sediment traps.

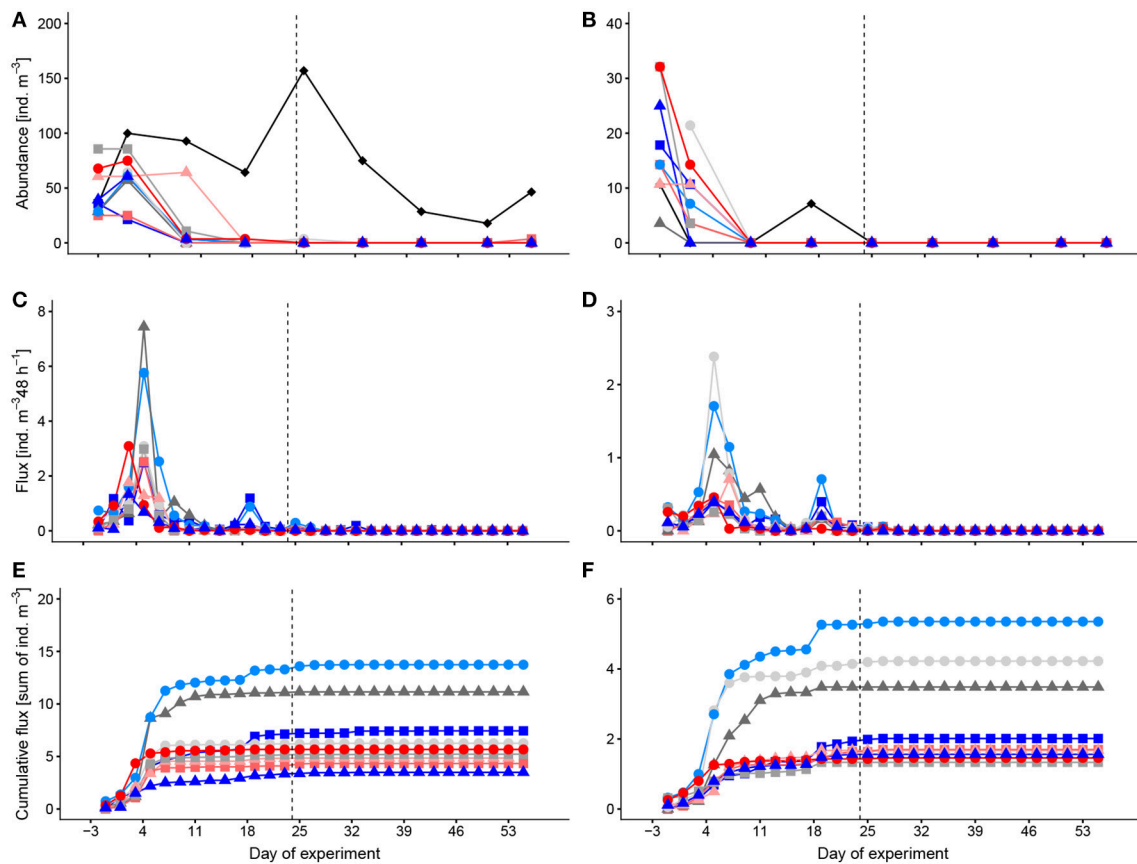


FIGURE 1 | Temporal development of standing stocks and flux to the sediment traps of thecosome Pteropoda (A,C,E) and Heteropoda (B,D,F). (A,B) abundances in the water column, (C,D) flux to the sediment trap per 48 h, (E,F) cumulative flux to the sediment trap. Colors and symbols are described in Table 1. Dashed line indicates the time of deep-water addition. Note different scales.

3.2.2.2. Foraminifera, Globigerinidae

The main flux of Globigerinidae and of the spherical stage of *Orbulina universa* was around t9–t15 only shortly after their main peaks in the water column (t1, t9; Figures 2C–F). The spherical stage of *O. universa* occurred in the sediments of most mesocosms [especially in M4, M8, and M2, (Figures 2D, F)] at low numbers also during the remainder of the experiment, indicating that net sampling failed to collect this stage in the water column after t9 (Figure 2B). The occurrence of the spherical stage of *O. universa* more or less throughout the experiment points to ongoing reproduction that likely was continuous. Reproduction and development is also indicated by comparing the abundance of Globigerinidae in the water column with the cumulative flux that the standing stock in the water column is continuously replenished.

The cumulative flux of Globigerinidae on the last sampling day (t55) is shown in Figure 3. The flux was lowest in one of the control mesocosms (M1, 361 ind. m⁻³ 48 h⁻¹) and the two high CO₂ mesocosms (M2, M8, 321 and 343 ind. m⁻³ 48 h⁻¹, respectively). The trend of the data resembles an optimum curve with highest flux at mid CO₂ levels. Interestingly, a similar trend was not found in the water column. GAMM on the flux of Globigerinidae revealed no significant effect of pCO₂ ($p = 0.05$).

Also the flux of the sexual stage of *Orbulina universa* was not impacted by CO₂ concentration (GLM, $p = 0.84$).

4. DISCUSSION

4.1. Pteropods and Heteropods

4.1.1. General Considerations

The occurrence of pteropods and heteropods in the mesocosms was only low and too short to allow for any sound conclusion on possible CO₂ effects. Therefore, we restrict the discussion to some general considerations of what might have caused the quick disappearance of pelagic gastropods in the mesocosms in this particular study. Pteropods vanished in the mesocosms soon after the experiment had started, whereas they occurred continuously in the surrounding Atlantic water during the entire study. Also heteropods did not occur in the mesocosms for very long but they were also rare in the outside Atlantic. Survival of pteropods in our previous mesocosm experiments was variable and it is difficult to explain what causes success or failure. In general, pteropods are very delicate against captivity and until now cannot really be cultivated over an entire reproductive cycle (Howes et al., 2014). The most likely explanation for their quick disappearance is entrapment in the sediment traps in the course

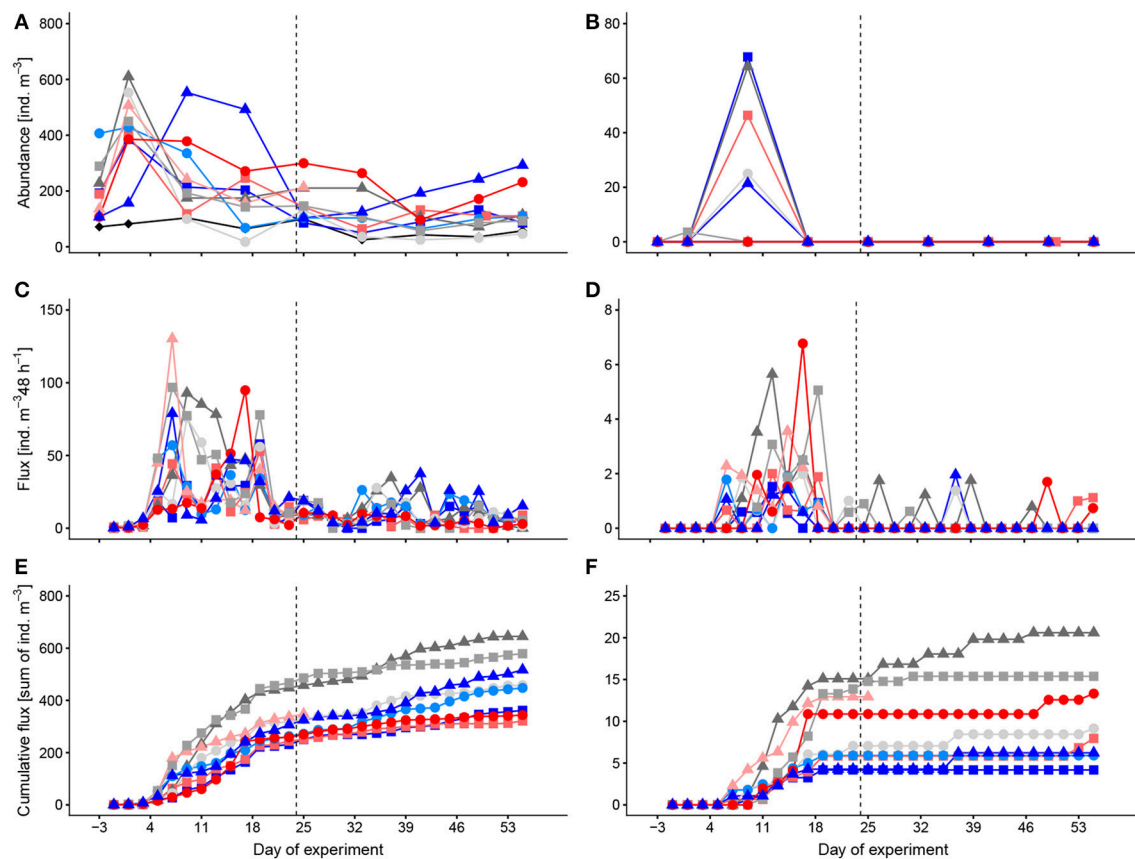


FIGURE 2 | Temporal development of standing stocks and flux to the sediment traps of Globigerinidae (A,C,E) and the sexual stage of *Orbulina universa* (B,D,F). (A,B) abundances in the water column, (C,D) flux to the sediment trap per 48 h, (E,F) cumulative flux to the sediment trap. Colors and symbols are described in Table 1. Dashed line indicates the time of deep-water addition. Note different scales.

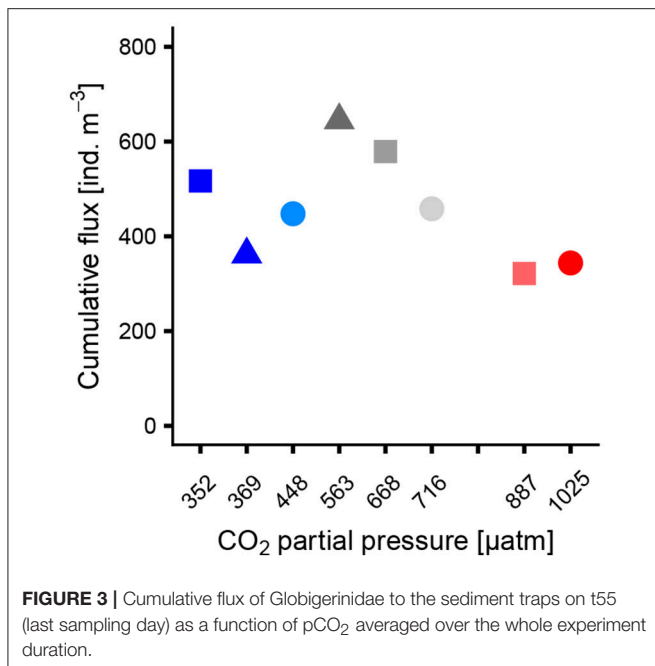
of their natural vertical migration. *Heliconoides inflatus*, the most dominant pteropod species in our experiment, performs diurnal vertical migrations in the upper 300 m (Bé and Gilmer, 1977). To descend pteropods can either rapidly sink down through a retraction of the wings into the shell or swim down. Rapid sinking is also used as escape reaction that can be easily initiated (Tsurumi et al., 2005) when accidentally bouncing against the mesocosm bags. Either way, the negative buoyancy of pteropods facilitates rapid sinking (Lalli and Gilmer, 1989), and in our study they may have accidentally fallen into the sediment trap of the mesocosm, where they entangled with the sedimented material and eventually died. Also in the mesocosm study performed in the Arctic, adult *Limacina helicina* vanished from the water column within a week most likely because they accumulated and died in the sediment traps (Niehoff et al., 2013). In contrast, all stages (veligers to adults) of the smaller North Atlantic species *Limacina retroversa* survived well throughout a 40 day long mesocosm experiment in the Norwegian Raunefjord conducted in 2011 (Howes et al., 2014, J. Büdenbender and U. Riebesell unpublished). During another mesocosm study in Raunefjord in 2015, however, *L. retroversa* early developmental stages (veligers, juveniles) occurred during the full duration of the experiment (45 days), but adult specimen were mainly found during the first days

and were extremely rare after that (Lischka et al. unpublished). Given that *Limacina* spp. also migrate vertically, some favoring factor(s) must have contributed to their survival in the Bergen experiments in contrast to the Gran Canaria experiment. Reasons could be for example lower loss to the sediment traps due to less pronounced vertical migration behavior because of the longer day length at Raunefjord compared to the Canary region. However, the same explanation cannot hold for the Arctic study. Thus, so far no consistent picture emerges to explain loss or upkeep of pteropods in the mesocosms. In general, OA has the potential to affect standing stocks of pteropods negatively and to lower their calcification and, thus their contribution to the vertical flux of aragonite and calcite.

4.2. Planktonic Foraminifera

4.2.1. Species Inventory and Habitat Conditions in the Mesocosms

Mesocosms cannot provide optimal living conditions for planktonic foraminifera because they have characteristic depth habitats that can differ considerably between species, (Hull et al., 2011; Rebotim et al., 2017) and they migrate vertically during their life cycles. (Hemleben et al., 1989; Bijma et al., 1990). Accordingly, they can be found primarily in open



waters (Rebotim et al., 2017). Thus, their natural vertical living range exceeds mesocosm depth and it is likely, that specimen enclosed in the mesocosms were advected into Gando Bay. These ecologic characteristics likely impacted on the flux observed to the sediment traps. The average living depth of the species enclosed in the mesocosms varies between 40 and 60 m for *Globigerionoides ruber*, around 80 m for *Globigerinella siphonifera* and *Orbulina universa* and 100 m for *Globigerina bulloides* (Wilke et al., 2009; Rebotim et al., 2017). The vast majority of export flux of planktonic foraminifera is generated below 100 m depth and consists mostly of empty adult specimen (Erez and Honjo, 1981). Thus, considering vertical movements related to the species' life cycles and their preferred living depths, it is likely that not only dead shells were collected in the mesocosm sediment traps but that also living (juvenile) specimen were passively intercepted not able to leave again and continue growing. This process may have dominated flux of these protozoans in the mesocosms and depleted water column stocks over time. We frequently counted individuals of different size in the sediment trap samples supporting this assumption. However, this is a general problem for vertically migrating zooplankton kept in closed systems that also applied equally to all mesocosms in our experiment. It probably generated an off-set to natural flux but shouldn't impede observe a general CO₂ impact across our set-up.

Globigerinidae species enclosed in the mesocosms are typical for the Canary Island region and the subtropical eastern North Atlantic. Also reported numbers of Globigerinidae in the winter season are in the same range of what we found though they were somewhat higher in the mesocosms (Wilke et al., 2009; Rebotim et al., 2017). Wilke et al. for example indicate concentrations of Globigerinidae of up to 300 individuals m⁻³, while Rebotim et al. found densities of around 80–100 m⁻³. After some initial high

values of about 600 individuals m⁻³, densities in the mesocosms stayed quite stable between about 100–200 m⁻³. These higher densities in the mesocosms are most likely due to the small mesh size used in our study (55 µm) compared to ≥100 µm meshes used in the field studies. Moreover these studies only considered individuals larger than 100 µm whereas we counted all specimen found independent of size. However, when considering particular species, *Orbulina universa* had peak numbers (on t9) that were ~30 times higher than maximum densities reported by Rebotim and co-workers. These numbers bargained for the sexual stage of *O. universa* that is very easy to identify, i.e., we can exclude false identification. An overestimation of the filtered volume and calculated densities is unlikely since the lack of currents in the mesocosms allowed for more or less strictly vertical net hauls. Possibly it could be an artifact of the rather small volume filtered and patchy distribution in the mesocosm. As such high numbers were only found at the beginning of the experiment, another possible explanation could be some small scale eddies occurring prior mesocosm closure leading to short-term concentrations of pre-adult specimen that were then enclosed in the mesocosms. Lack of potential predators such as pelagic fish may be another reason enabling such high densities.

4.2.2. Succession and Flux of Globigerinidae

Foraminifers thrived well and reproduced in the mesocosms throughout the experiment. The most obvious evidence for most likely unsynchronized reproduction is the continuous occurrence of the spherical stage of *Orbulina universa* in the sediment traps more or less throughout the experiment. Constant replenishment is also suggested from the fact, that flux did not lead to deplete conditions in the water column despite we have to assume that also juvenile living specimen were passively caught in the traps as mentioned above. We exclude the possibility that the observed continuous flux was not due to reproduction but reflected maturation of juveniles smaller than the plankton net mesh-size (i.e., "not visible" in our water column densities). Firstly, because we found the same size spectrum of individuals in both, the water column and the sediment traps meaning that the visually identifiable minimum size was consistent. Secondly, as continuous flux continued throughout the experiment, a life span >4 weeks must be assumed for a large portion of the population enclosed in the mesocosms because the experiment lasted 54 days. Planktonic foraminifers usually have short life-cycles (lunar, semi-lunar), (Bijma et al., 1990; Schiebel et al., 1997) thus it is unlikely that the continuous occurrence of foraminifers can be explained by a successive prolongation of life-cycles of (very) small juveniles enclosed at experiment start that successively sustained population densities and flux. A certain portion of the small juveniles would have needed to arrest development in order to provide for a continuous replenishment or flux of organisms over time. Thirdly, even if it was the case that small juveniles matured that were not caught with our net and contributed significantly to continuous flux, water column densities should have decreased over time but they remained fairly constant.

We found no relation between the abundance and succession of foraminifers and the CO₂ concentrations in the mesocosms, i.e., Globigerinidae seemed to do equally well under the

CO₂ concentration range applied. However, our taxonomic resolution was low and we were not able to impose size-normalized weight of specimen of the different species to infer on calcification. Thus, we cannot say anything on possible CO₂-sensitivities on shell calcification or dissolution. But generally speaking, the present study concurs with previous work that showed no major vulnerability of growth rates of some large benthic foraminifer species to OA exposure in short term (up to 12 weeks) aquarium experiments (Vogel and Uthicke, 2012).

Despite more or less stable abundances of Globigerinidae in the water column in all mesocosms, flux to the sediment traps was reduced in the two high CO₂ mesocosms during the post-bloom phase. Possibly, this reduced flux is in relation with the reduced POM flux described for the two high CO₂ mesocosms as a consequence of delayed development of zooplankton (Stange et al., 2018; Algueró-Muñiz et al. submitted). Foraminifers might have become attached to sinking particles (POM) and transported downward that way. If so, a lower POM flux could also have lead to a lower flux of foraminifers. Similarly low flux, however, was also observed in one control mesocosm. Thus, we cannot be sure to what extent reduced POM flux or any other unknown factors contributed to flux reduction. Interestingly though, the observed zooplankton developmental delay was not found for planktonic foraminifers. This is discussed as a possible consequence of the occurrence of a harmful algae bloom in the two high CO₂ mesocosms (Algueró-Muñiz et al. submitted; Riebesell et al., unpublished). Apparently, planktonic foraminifers had different sensitivities against this bloom compared to the remaining micro- and mesozooplankton community.

With respect to planktonic Foraminifera, field and laboratory observations on their response to OA provide an inconclusive picture, ranging from evidence for impaired calcification and growth to no reaction. The same applies to benthic foraminifera, where some taxa have even shown positive response to OA. As a result, no prediction of the effect of OA on planktonic foraminifera can be made on ecosystem level and new data are required particularly from field experiments.

4.2.3. Conclusion

Mesocosms cannot provide optimal living conditions for migrating zooplankton. This can bias specific response patterns especially those that are closely connected with species life cycles and migration patterns. Notably, in our study, this applied to the flux of planktonic Foraminifera. But this is a general problem true for each of the mesocosms, meaning a bias occurs consistently. Thus, differences that can be found between different treatment levels should still inform of possible treatment effects.

The present study did not reveal any statistically proven CO₂-related trends on community level with respect to the

abundance, succession and flux of planktonic Foraminifera and thecosome pteropods. In case of pteropods and heteropods, their occurrence in the mesocosms was too short to allow for any sound conclusion. With respect to foraminifers, the low taxonomic resolution and methodological constraints in our study did not allow for more detailed analyses of possible OA effects on individual species (e.g., calcification, carbon/carbonate flux), and the resulting difficulty to adequately connect their development in the water column in relation to their different life cycles with the observed flux to the sediment traps. Flux in the two high CO₂ mesocosms could have been impacted by reduced POM flux that was in connection with CO₂ concentrations. But this conclusion conflicts with also reduced flux in one control mesocosm where POM flux was not reduced (Stange et al., 2018). Future studies looking at community-level response of planktonic foraminifers should include species-level identification and biomass/calcite mass determination to allow for more in-depth investigation of possible OA effects. This can only be done, however, if a substantially higher amount of time can be invested.

AUTHOR CONTRIBUTIONS

SL, PS, and UR conceived, designed, and performed the experiment. SL analyzed the data. SL with input from all co-authors wrote the paper.

FUNDING

This project was funded by the German Federal Ministry of Education and Research (BMBF) in the framework of the coordinated project BIOACID–Biological Impacts of Ocean Acidification, phase 2 (FKZ 03F06550). UR received additional funding from the Leibniz Award 2012 by the German Research Foundation (DFG).

ACKNOWLEDGMENTS

We would like to thank the Oceanic Platform of the Canary Islands (Plataforma Oceánica de Canarias, PLOCAN) for their kind hospitality and great logistic support. We also gratefully acknowledge the captain and crew of RV Hesperides for deploying and recovering the mesocosms (cruise 29HE20140924), and RV Poseidon for transporting the mesocosms and support in testing the deep water collector during cruise POS463.

Many thanks are due to Isabel Dörner for her invaluable help with checking sediment trap samples for pteropods and foraminifers on site. We are also thankful to Dr. Scarlett Sett and Kaden Griffith who helped counting pelagic calcifiers in the zooplankton net and sediment-trap samples back home. Dr. Nina Keul is acknowledged for identification of foraminifer species. Dr. Lennart Bach provided carbonate system data.

REFERENCES

- Almogi-Labin, A., Hemleben, C., and Deuser, W. (1988). Seasonal variation in the flux of euthecosomatous pteropods collected in a deep sediment trap in the sargossa sea. *Deep Sea Res. Part I Oceanogr. Res. Pap.* 35, 441–464.
- Aristegui, J., Hernández-Léon, S., Montero, F., and Gómez, M. (2001). The seasonal planktonic cycle in coastal waters of the canary islands. *Sci. Mar.* 65, 51–58.
- Aristegui, J., Tett, P., Hernandez-Guerra, A., Basterretxea, G., Montero, M., Wild, K., et al. (1997). The influence of island-generated eddies on chlorophyll distribution: a study of mesoscale variation around gran canaria. *Deep Sea Res. I* 44, 71–96.
- Bach, L. T., Taucher, J., Boxhammer, T., Ludwig, A., The Kristineberg KOSMOS Consortium, Achterberg, EP, et al. (2016). Influence of ocean acidification on a natural winter-to-summer plankton succession: First insights from a long-term mesocosm study draw attention to periods of low nutrient concentrations. *PLoS ONE* 11:e0159068. doi: 10.1371/journal.pone.0159068
- Bathmann, U., Noji, T., and von Bodungen, B. (1991). Sedimentation of pteropods in the norwegian sea in autumn. *Deep Sea Res.* 38, 1341–1360.
- Bé, A., and Gilmer, R. (1977). *Oceanic Micropalaeontology*, volume 1, chapter A zoogeographic and taxonomic review of euthecosomatous Pteropoda. London: Academic Press, 773–808.
- Bednaršek, N., Možina, J., Vogt, M., O'Brien, C., and Tarling, G. (2012a). The global distribution of pteropods and their contribution to carbonate and carbon biomass in the modern ocean. *Earth Syst. Sci. Data* 4, 167–186. doi: 10.5194/essd-4-167-2012
- Bednaršek, N., Tarling, G., Bakker, D., Fielding, S., and Feely, R. (2014). Dissolution dominating calcification process in polar pteropods close to the point of aragonite undersaturation. *PLoS ONE* 9:e0109183. doi: 10.1371/journal.pone.0109183
- Bednaršek, N., Tarling, G., Bakker, D., Fielding, S., Jones, E., Venables, H., et al. (2012b). Extensive dissolution of live pteropods in the southern ocean. *Nat. Geosci.* 5, 881–885. doi: 10.1038/ngeo1635
- Beer, C., Schiebel, R., and Wilson, P. (2010). Testing planktic foraminiferal shell weight as a surface water $[CO_3^{2-}]$ proxy using plankton net samples. *Geology* 38, 103–106. doi: 10.1130/G30150.1
- Bentov, S., Brownlee, C., and Erez, J. (2009). The role of seawater endocytosis in the biomineralization process in calcareous foraminifera. *Proc. Natl. Acad. Sci. U.S.A.* 106, 21500–21504. doi: 10.1073/pnas.0906636106
- Berner, R., and Honjo, S. (1981). Pelagic sedimentation of aragonite: its geochemical significance. *Science* 211, 940–942.
- Bijma, J., Erez, J., and Hemleben, C. (1990). Lunar and semi-lunar reproductive cycles in some spinose planktonic foraminifera. *J. Foraminif. Res.* 20, 117–127.
- Boxhammer, T., Bach, LT, Czerny, J., and Riebesell, U. (2015). Technical note: Sampling and processing of mesocosm sediment trap material for quantitative biogeochemical analysis. *Biogeosciences* 13, 2849–2858. doi: 10.5194/bg-13-2849-2016
- Ciais, P., Sabine, C., Bala, G., Bopp, L., Brovkin, V., Canadell, J., et al. (2013). "Climate Change 2013: The Physical Science Basis," in *Contribution of Working Group I to the Fifth Assessment Report of the Intergovernmental Panel on Climate Change*, chapter Carbon and Other Biogeochemical Cycles. Cambridge: New York, NY: Cambridge University Press, 465–570.
- Comeau, S., Gorsky, G., Alliouane, S., and Gattuso, J. (2010a). Larvae of the pteropod *Cavolinia inflexa* exposed to aragonite undersaturation are viable but shell-less. *Mar. Biol.* 157, 2341–2345. doi: 10.1007/s00227-010-1493-6
- Comeau, S., Jeffree, R., Teyssié, J., and Gattuso, J. (2010b). Response of the arctic pteropod *Limacina helicina* to projected future environmental conditions. *PLoS ONE* 5:e11362. doi: 10.1371/journal.pone.0011362
- Davis, C., Rivest, E., Hill, T., Gaylord, B., Russell, A., and Sanford, E. (2017). Ocean acidification compromises a planktic calcifier with implications for global carbon cycling. *Sci. Rep.* 7:2225. doi: 10.1038/s41598-017-01530-9
- de Moel, H., Ganssen, G., Peeters, F., Jung, S., Kroon, D., Brummer, G., et al. (2009). Planktic foraminiferal shell thinning in the arabian sea due to anthropogenic ocean acidification? *Biogeosciences* 6, 1917–1925. doi: 10.5194/bg-6-1917-2009
- de Nooijer, L., Toyofuku, T., and Kitazato, H. (2009). Foraminifera promote calcification by elevating their intracellular ph. *Proc. Natl. Acad. Sci. U.S.A.* 8, 15374–15378. doi: 10.1073/pnas.0904306106
- Dias, B., Hart, M., Smart, C., and Hall-Spencer, J. (2010). Modern seawater acidification: the response of foraminifera to high-co₂ conditions in the mediterranean sea. *J. Geol. Soc.* 167, 843–846. doi: 10.1144/0016-76492010-050
- Doney, S., Fabry, V., Feely, R., and Kleypas, J. (2009). Ocean acidification: The other co₂ problem. *Ann. Rev. Mar. Sci.* 1, 169–192. doi: 10.1146/annurev.marine.010908.163834
- Dutkiewicz, S., Morris, J., Follows, M., Scott, J., Levitan, O., Dyhrm, S., et al. (2015). Impact of ocean acidification on the structure of future phytoplankton communities. *Nat. Clim. Chang.* 5, 1002–1006. doi: 10.1038/NCLIMATE2722
- Erez, J., and Honjo, S. (1981). Comparison of isotopic composition of planktonic foraminifera in plankton tows, sediment-raps and sediments. *Palaeogeogr. Palaeoclimatol. Palaeoecol.* 33, 129–156.
- Fabry, V., Seibel, B., Feely, R., and Orr, J. (2008). Impacts of ocean acidification on marine fauna and ecosystem processes. *ICES J. Mar. Sci.* 65, 414–432. doi: 10.1093/icesjms/fsn048
- Feely, R., Sabine, C., Lee, K., Berelson, W., Kleypas, J., Fabry, V., et al. (2004). Impact of anthropogenic co₂ on the caco₃ system in the oceans. *Science* 305, 362–366. doi: 10.1126/science.1097329
- Fischer, G., Donner, B., Ratmeyer, V., Davenport, R., and Wefer, G. (1996). Distinct year-to-year particle flux variations off cape blanc during 1988–1991: Relation to delta18o-deduced sea-surface temperatures and trade winds. *J. Mar. Res.* 54, 73–98.
- Gonzalez-Mora, B., Sierro, F., and Flores, J. (2008). Controls of shell calcification in planktonic foraminifera. *Quat. Sci. Rev.* 27, 956–961. doi: 10.1016/j.quascirev.2008.01.008
- Guinotte, J., and Fabry, V. (2008). Ocean acidification and its potential effects on marine ecosystems. *Ann. N. Y. Acad. Sci.* 1134, 320–342. doi: 10.1196/annals.1439.013
- Hammill, E., Johnson, E., Atwood, T., Harianto, J., Hinchliffe, C., Calosi, P., et al. (2017). Ocean acidification alters zooplankton communities and increases top-down pressure of a cubozoan predator. *Glob. Chang. Biol.* 24, e128–e138. doi: 10.1111/gcb.13849
- Hemleben, C., Spindler, M., and Anderson, O. (eds.). (1989). *Modern planktonic Foraminifera*. Berlin: Springer-Verlag.
- Howes, E., Bednaršek, N., Büdenbender, J., Comeau, S., Doubleday, A., Gallagher, S., et al. (2014). Sink and swim: a status review of thecosome pteropod culture techniques. *J. Plankton Res.* 36, 299–315. doi: 10.1093/plankt/fbu002
- Hull, P., Osborn, K., Norris, R., and Robison, B. (2011). Seasonality and depth distribution of a mesopelagic foraminifer, *Hastigerinella digitata*, in monterey bay, California. *Limnol. Oceanogr.* 56, 562–576. doi: 10.4319/lo.2011.56.2.0562
- Keul, N., Langer, G., Nooijer, L., and Bijma, J. (2013). Effect of ocean acidification on the benthic foraminifera *Ammonia* sp. is caused by a decrease in carbonate ion concentration. *Biogeosciences* 10, 6185–6198. doi: 10.5194/bg-10-6185-2013
- Kroeker, K., Kordas, R., Crim, R., Hendriks, I., Ramajo, L., Singh, G., et al. (2013). Impacts of ocean acidification on marine organisms: quantifying sensitivities and interaction with warming. *Glob. Chang. Biol.* 19, 1884–1896. doi: 10.1111/gcb.12179
- Kroeker, K., Kordas, R., Crim, R., and Singh, G. (2010). Meta-analysis reveals negative yet variable effects of ocean acidification on marine organisms. *Ecol. Lett.* 13, 1419–1434. doi: 10.1111/j.1461-0248.2010.01518.x
- Lalli, C., and Gilmer, R. (1989). *Pelagic Snails: The Biology of Holoplanktonic Gastropod Molluscs*. Stanford, CA: Stanford University Press.
- Le Quéré, C., Moriarty, R., Andrew, R., Peters, G., Ciais, P., Friedlingstein, P., et al. (2015). Global carbon budget 2014. *Earth Syst. Sci. Data* 7, 47–85. doi: 10.5194/essd-7-47-2015
- Lischka, S., Büdenbender, J., Boxhammer, T., and Riebesell, U. (2011). Impact of ocean acidification and elevated temperatures on early juveniles of the polar shelled pteropod *Limacina helicina*: mortality, shell degradation, and shell growth. *Biogeosciences* 8, 919–932. doi: 10.5194/bg-8-919-2011
- Lombard, F., da Rocha, R., Bijma, J., and Gattuso, J.-P. (2010). Effect of carbonate ion concentration and irradiance on calcification in planktonic foraminifera. *Biogeosciences* 7, 247–255. doi: 10.5194/bg-7-247-2010

- Manno, C., Morata, N., and Bellerby, R. (2012). Effect of ocean acidification and temperature increase on the planktonic foraminifer *Neoglobobulimina pachyderma* (sinistral). *Polar Biol.* 35, 1311–1319. doi: 10.1007/s00300-012-1174-7
- McIntyre-Wressnig, A., Bernhardt, J., McCorkle, D., and Hallock, P. (2013). Non-lethal effects of ocean acidification on the symbiont-bearing benthic foraminifer *Amphistegina gibbosa*. *Mar. Ecol. Prog. Ser.* 472:45–60. doi: 10.3354/meps09918
- Moy, A., Howard, W., Bray, S., and Trull, T. (2009). Reduced calcification in modern southern ocean planktonic foraminifera. *Nat. Geosci.* 2, 276–280. doi: 10.1038/ngeo460
- Mucci, A. (1983). The solubility of calcite and aragonite in seawater at various salinities, temperatures, and one atmosphere total pressure. *Am. J. Sci.* 283, 780–799.
- Neuer, S., Cianca, A., Helmke, P., Freudenthal, T., Davenport, R., Meggers, H., et al. (2007). Biogeochemistry and hydrography in the eastern subtropical north atlantic gyre. results from the european time-series station estoc. *Prog. Oceanogr.* 72, 1–29. doi: 10.1016/j.pocean.2006.08.001
- Niehoff, B., Schmidthusen, T., Knüppel, N., Daase, M., Czerny, J., and Boxhammer, T. (2013). Mesozooplankton community development at elevated CO₂ concentrations: results from a mesocosm experiment in an arctic fjord. *Biogeosciences* 10, 1391–1406. doi: 10.5194/bg-10-1391-2013
- Paul, A., Bach, L., Schulz, K., Boxhammer, T., Czerny, J., Achterberg, E., et al. (2015). Effect of elevated CO₂ on organic matter pools and fluxes in a summer, post spring-bloom baltic sea plankton community. *Biogeosciences* 12, 6181–6203. doi: 10.5194/bg-12-6181-2015
- Prazeres, M., Uthicke, S., and Pandolfi, J. (2018). Ocean acidification induces biochemical and morphological changes in the calcification process of large benthic foraminifera. *Proc. R. Soc. B.* 282, 20142782. doi: 10.1098/rspb.2014.2782
- R Core Team (2013). *R: A Language and Environment for Statistical Computing*. Vienna: R Foundation for Statistical Computing. ISBN 3-900051-07-0.
- Rebotim, A., Voelker, A., Jonkers, L., Waniek, J., Meggers, H., Schiebel, R., et al. (2017). Factors controlling the depth habitat of planktonic foraminifera in the subtropical eastern north atlantic. *Biogeosciences* 14, 827–859. doi: 10.5194/bg-14-827-2017
- Rhein, M., Rintoul, S., Aoki, S., Campos, E., Chambers, D., Feely, R., et al. (2013). *chapter Observations: Ocean, Climate Change 2013: The Physical Science Basis. Contribution of Working Group I to the Fifth Assessment Report of the Intergovernmental Panel on Climate Change*. Cambridge, UK and New York, NY: Cambridge University Press, 255–315.
- Riebesell, U., Bach, L., Bellerby, R., Bermudez Monsalve, R., Czerny, J., Larsen, A., et al. (2017). Competitive fitness of a predominant pelagic calcifier impaired by ocean acidification. *Nat. Geosci.* 10, 19–23. doi: 10.1038/ngeo2854
- Riebesell, U., Czerny, J., von Bröckel, K., Boxhammer, T., Büdenbender, J., Deckelnick, M., et al. (2013). Technical note: A mobile sea-going mesocosm system – new opportunities for ocean change research. *Biogeosciences* 10, 1835–1847. doi: 10.5194/bg-10-1835-2013
- Sala, M., Aparicio, F., Balagué, V., Boras, J., Borrell, E., Cardelús, C., et al. (2016). Contrasting effects of ocean acidification on the microbial food web under different trophic conditions. *ICES J. Mar. Sci.* 73, 670–679. doi: 10.1093/icesjms/fsv130
- Sangra, P., Pascual, A., Rodríguez-Santana, A., Machín, F., Mason, E., McWilliams, J., et al. (2009). The canary eddy corridor: A major pathway for long-lived eddies in the subtropical north atlantic. *Deep Sea Res. I* 56, 2100–2114. doi: 10.1016/j.dsr.2009.08.008
- Schiebel, R. (2002). Planktic foraminiferal sedimentation and the marine calcite budget. *Glob. Biogeochem. Cycles* 16:1065. doi: 10.1029/2001GB001459
- Schiebel, R., Bijma, J., and Hemleben, C. (1997). Population dynamics of the planktic foraminifer *Globigerina bulloides* from the eastern north atlantic. *Deep Sea Res. I* 44, 1701–1713.
- Schiebel, R., and Hemleben, C. (2000). Interannual variability of planktic foraminiferal populations and test flux in the eastern north atlantic ocean (jgofs). *Deep Sea Res. Part II Top. Stud. Oceanogr.* 47, 1809–1852. doi: 10.1016/S0967-0645(00)00008-4
- Schmidt, C., Kucera, M., and Uthicke, S. (2014). Combined effects of warming and ocean acidification on coral reef foraminifera *Marginopora vertebralis* and *Heterostegina depressa*. *Coral Reefs* 33, 805–818. doi: 10.1007/s00338-014-1151-4
- Stange, P., Taucher, J., Bach, L., Algueró-Muñoz, M., Horn, H., Krebs, L., et al. (2018). Ocean acidification-induced restructuring of the plankton food web can influence the degradation of sinking particles. *Front. Mar. Sci.* 5:140. doi: 10.3389/fmars.2018.00140
- Stump, M., Hu, M., Melzner, F., Gutowska, M., Dorey, N., Himmerkus, N., et al. (2012). Acidified seawater impacts sea urchin larvae ph regulatory systems relevant for calcification. *Proc. Natl. Acad. Sci. U.S.A.* 109, 18192–18197. doi: 10.1073/pnas.1209174109
- Taucher, J., Bach, L., Boxhammer, T., Nauendorf, A., The Gran Canaria KOSMOS Consortium, Achterberg, EP, et al. (2017). Influence of ocean acidification and deep water upwelling on oligotrophic plankton communities in the subtropical north atlantic: Insights from an *in situ* mesocosm study. *Front. Mar. Sci.* 4:85. doi: 10.3389/fmars.2017.00085
- Thabet, A., Maas, A., Lawson, G., and Tarrant, A. (2015). Life cycle and early development of the thecosomatous pteropod *Limacina retroversa* in the gulf of maine, including the effect of elevated CO₂ levels. *Mar. Biol.* 162, 2235–2249. doi: 10.1007/s00227-015-2754-1
- Tsurumi, M., Mackas, D., Whitney, A., DiBacco, C., Galbraith, M., and Wong, C. (2005). Pteropods, eddies, carbon flux, and climate variability in the alaska gyre. *Deep Sea Res. Part II* 52, 1037–1052. doi: 10.1016/j.dsr.2005.02.005
- Uthicke, S., Momigliano, P., and Fabricius, K. (2013). High risk of extinction of benthic foraminifera in this century due to ocean acidification. *Sci. Rep.* 3:1796. doi: 10.1038/srep01769
- Vogel, N., and Uthicke, S. (2012). Calcification and photobiology in symbiont-bearing benthic foraminifera and responses to a high CO₂ environment. *J. Exp. Mar. Biol. Ecol.* 424–425:15–24. doi: 10.1016/j.jembe.2012.05.008
- Weinkauff, M., Kunze, J., Waniek, J., and Kucera, M. (2016). Seasonal variation in shell calcification of planktonic foraminifera in the ne atlantic reveals species-specific response to temperature, productivity, and optimum growth conditions. *PLOS ONE* 11:e0148363. doi: 10.1371/journal.pone.0148363
- Wilke, I., Meggers, H., and Bickert, T. (2009). Depth habitats and seasonal distributions of recent planktic foraminifera in the canary islands region (29°N) based on oxygen isotopes. *Deep Sea Res. Part I Oceanogr. Res. Pap.* 56, 89–106. doi: 10.1016/j.dsr.2008.08.001
- Wittmann, A., and Pörtner, H. (2013). Sensitivities of extant animal taxa to ocean acidification. *Nat. Clim. Chang.* 3, 995–1001. doi: 10.1038/NCLIMATE1982
- Zeebe, R., and Wolf-Gladrow, D. (2001). *CO₂ in Seawater: Equilibrium, Kinetics, Isotopes*. (Amsterdam: Elsevier Science).

Conflict of Interest Statement: The authors declare that the research was conducted in the absence of any commercial or financial relationships that could be construed as a potential conflict of interest.

Copyright © 2018 Lischka, Stange and Riebesell. This is an open-access article distributed under the terms of the Creative Commons Attribution License (CC BY). The use, distribution or reproduction in other forums is permitted, provided the original author(s) and the copyright owner(s) are credited and that the original publication in this journal is cited, in accordance with accepted academic practice. No use, distribution or reproduction is permitted which does not comply with these terms.



Analyzing the Impacts of Elevated- CO_2 Levels on the Development of a Subtropical Zooplankton Community During Oligotrophic Conditions and Simulated Upwelling

María Algueró-Muñiz^{1*}†, Henriette G. Horn^{1,2†}, Santiago Alvarez-Fernandez¹, Carsten Spisla^{1,3}, Nicole Aberle^{1,4}, Lennart T. Bach³, Wanchun Guan⁵, Eric P. Achterberg³, Ulf Riebesell³ and Maarten Boersma^{1,6}

OPEN ACCESS

Edited by:

Marius Nils Müller,
Federal University of Pernambuco,
Brazil

Reviewed by:

Soultana Zervoudaki,
Hellenic Centre for Marine Research
(HCMR), Greece
Jun Sun,
Tianjin University of Science
and Technology, China

*Correspondence:

María Algueró-Muñiz
maria.alguero@awi.de

† These authors have contributed
equally to this work

Specialty section:

This article was submitted to
Marine Biogeochemistry,
a section of the journal
Frontiers in Marine Science

Received: 28 March 2018

Accepted: 05 February 2019

Published: 25 February 2019

Citation:

Algueró-Muñiz M, Horn HG,
Alvarez-Fernandez S, Spisla C,
Aberle N, Bach LT, Guan W,
Achterberg EP, Riebesell U and
Boersma M (2019) Analyzing
the Impacts of Elevated- CO_2 Levels
on the Development of a Subtropical
Zooplankton Community During
Oligotrophic Conditions
and Simulated Upwelling.
Front. Mar. Sci. 6:61.
doi: 10.3389/fmars.2019.00061

¹ Biologische Anstalt Helgoland, Alfred-Wegener-Institut Helmholtz-Zentrum für Polar- und Meeresforschung, Bremerhaven, Germany, ² Department of Estuarine and Delta Systems, NIOZ Royal Netherlands Institute for Sea Research and Utrecht University, Yerseke, Netherlands, ³ GEOMAR Helmholtz Centre for Ocean Research Kiel, Kiel, Germany, ⁴ Department of Biology, Trondheim Biological Station, Norwegian University of Science and Technology, Trondheim, Norway, ⁵ Department of Marine Biotechnology, School of Laboratory Medicine and Life Science, Wenzhou Medical University, Wenzhou, China, ⁶ Department of Biology/Chemistry, University of Bremen, Bremen, Germany

Ocean acidification (OA) is affecting marine ecosystems through changes in carbonate chemistry that may influence consumers of phytoplankton, often via trophic pathways. Using a mesocosm approach, we investigated OA effects on a subtropical zooplankton community during oligotrophic, bloom, and post-bloom phases under a range of different $p\text{CO}_2$ levels (from ~ 400 to $\sim 1480 \mu\text{atm}$). Furthermore, we simulated an upwelling event by adding 650 m-depth nutrient-rich water to the mesocosms, which initiated a phytoplankton bloom. No effects of $p\text{CO}_2$ on the zooplankton community were visible in the oligotrophic conditions before the bloom. The zooplankton community responded to phytoplankton bloom by increased abundances in all treatments, although the response was delayed under high- $p\text{CO}_2$ conditions. Microzooplankton was dominated by small dinoflagellates and aloricate ciliates, which were more abundant under medium- to high- $p\text{CO}_2$ conditions. The most abundant mesozooplankters were calanoid copepods, which did not respond to CO_2 treatments during the oligotrophic phase of the experiment but were found in higher abundance under medium- and high- $p\text{CO}_2$ conditions toward the end of the experiment, most likely as a response to increased phyto- and microzooplankton standing stocks. The second most abundant mesozooplankton taxon were appendicularians, which did not show a response to the different $p\text{CO}_2$ treatments. Overall, CO_2 effects on zooplankton seemed to be primarily transmitted through significant CO_2 effects on phytoplankton and therefore indirect pathways. We conclude that elevated $p\text{CO}_2$ can change trophic cascades with significant effects on zooplankton, what might ultimately affect higher trophic levels in the future.

Keywords: microzooplankton, mesozooplankton, mesocosms, ocean acidification, nutrients, *Oncaea*, trophic transfer efficiency

INTRODUCTION

Anthropogenic emissions are increasing atmospheric CO₂ concentrations from pre-industrial levels of ~280 µatm to current levels of over 400 µatm, and increases up to 1000 µatm by the end of the century are projected for the RCP8.5 emission scenario (IPCC, 2013). The oceans act as carbon sinks, absorbing about one third of the anthropogenic CO₂ emission (Sabine et al., 2004). This oceanic CO₂ uptake causes a shift in carbonate chemistry with a decrease in seawater pH, commonly known as ocean acidification (OA). Recent years of intense research have shown that OA may cause substantial changes to marine ecosystems (IPCC, 2013; Kroeker et al., 2013).

Despite the large body of literature related to biological responses to OA, most studies investigated single species responses, which may rarely provide a sufficient basis to understand long-term responses in complex ecological environments (Harley, 2011; Queirós et al., 2015). Moreover, changes in pCO₂ may promote changes in trophic interactions, leading to the dampening or amplification of single species effects and hence promoting shifts in community composition (Lischka et al., 2011; Rossoll et al., 2012, 2013). Consequently, *in situ* community studies are important in order to evaluate OA effects at the level of assemblages and ecosystems (Guinotte and Fabry, 2008; Riebesell and Gattuso, 2015).

Focusing on marine plankton, nutrient conditions can determine how communities respond to OA (Alvarez-Fernandez et al., 2018), being the most noticeable pCO₂ effects often observed under limiting inorganic nutrient conditions (Paul et al., 2015; Sala et al., 2015; Bach et al., 2016b). This is because elevated CO₂ levels cause an increase in phytoplankton standing stocks—more pronounced in smaller-sized taxa—and this effect on primary producers may be transferred differently into heterotroph primary consumers depending on the inorganic nutrient availability (Alvarez-Fernandez et al., 2018). The present study focussed on an oligotrophic system around the island of Gran Canaria within the Canary Archipelago, located in the subtropical North Atlantic Ocean. Despite its overall oligotrophic character, this region experiences a short-term period of deep-water nutrient inputs in later winter (February–March) (de León and Braun, 1973; Cianca et al., 2007) as well as recurrent mesoscale upwelling events that act as an offshore pump of organic matter and carbon (Sangrà et al., 2009). The so-called *late winter bloom* usually causes an increase in primary production and chlorophyll *a* concentration in the euphotic zone (Menzel and Ryther, 1961; Aristegui et al., 2001). Typically, mesozooplankton grazing pressure exerted on phytoplankton is low in the study area (Aristegui et al., 2001; Hernández-León et al., 2004), and mesozooplankters are considered to feed on microzooplankton which, in turn, control primary production (Hernández-León et al., 2001; Quevedo and Anadón, 2001; Calbet and Alcaraz, 2007). The microzooplankton community is usually dominated by small dinoflagellates and aloricate ciliates (Quevedo and Anadón, 2001), while the most important mesozooplankton during the annual cycle are copepods (Hernández-León et al., 2007). However, the plankton community typically changes during bloom conditions

(Aristegui et al., 2001; Hernández-León et al., 2004; Schmoker et al., 2012). An increase in copepod abundances follows the increase in primary production, and a trophic cascade caused by the consumption of microzooplankton by mesozooplankton allows a further increase in autotrophic biomass by the combined effect of top-down control and nutrient remineralization (Hernández-León, 2009; Schmoker et al., 2012). This bloom situation may cause a reduction in the efficiency of the food web, considering that trophic transfer efficiency (i.e., zooplankton growth per unit phytoplankton production) tends to be diminished under nutrient enrichment conditions due to the limited capacity of grazers to use the boosted algae production (Calbet et al., 1996; Kemp et al., 2001; Calbet et al., 2014).

In order to assess the impacts of OA on zooplankton communities we must consider not only direct effects on zooplankton caused by pH reductions, but also effects that reach consumers indirectly, through trophic pathways (Boersma et al., 2008; Rossoll et al., 2012; Cripps et al., 2016). Detrimental indirect pCO₂ effects have been described in single species of herbivores (Schoo et al., 2013; Meunier et al., 2016) and secondary consumers (Lesniewski et al., 2015). In the case of copepods, bottom-up influences of OA seem to be largely associated with interspecific differences among prey items with regard to their sensitivity to elevated pCO₂ levels, as observed when analyzing the cellular stoichiometry of copepods' photosynthetic preys (Isari et al., 2015; Meunier et al., 2016). In turn, microzooplankton may be affected by the effect of high pCO₂ levels on phytoplankton availability or quality such as an increase in picophytoplankton standing stock or changes in their cellular carbon-to-nutrient ratios (Bach et al., 2016b; Meunier et al., 2016). In addition, a high pCO₂ scenario is likely to favor harmful algal blooms (Wells et al., 2015) with substantial consequences for energy transfer from primary producers to consumers within marine communities.

Plankton community OA studies to date have been mostly carried out in relatively eutrophic environments (but see Sala et al., 2015; Gazeau et al., 2017), and led to varying conclusions. Some studies showed the lack of major effects of elevated pCO₂ levels in micro- (Aberle et al., 2013; Horn et al., 2016) and mesozooplankton abundances (Niehoff et al., 2013), while others detected both changes in community size distributions and biomass (Lischka et al., 2017; Taucher et al., 2017b) as well as positive bottom-up pCO₂ responses on mesozooplankton abundances (Algueró-Muñiz et al., 2017). Inorganic nutrient availability can control these different responses to OA in planktonic communities, thereby the nutrient-deplete phases could determine the transfer of the pCO₂ effects on primary producers to primary consumers (Alvarez-Fernandez et al., 2018). Taking this into account, studying OA effect in oligotrophic systems—which represent most of the global surface ocean—becomes of paramount importance. To accomplish this goal, we performed an experiment that allowed us to study the contrast between nutrient-depleted and nutrient-replete periods. Our aim was to analyze the effects of OA on the development of an autumn zooplankton community from the subtropical North Atlantic, including a simulated bloom situation. We assessed the effects of pCO₂ on (1) the abundance of subtropical

micro- and mesozooplankton under oligotrophic and upwelling conditions, (2) the size and reproductive output of an important copepod species and (3) the trophic efficiency within the plankton community under different conditions.

MATERIALS AND METHODS

Mesocosms Setup and Experimental Design

The experiment was conducted from 27th September (t-4) until 26th November 2014 (t56) within the framework of the BIOACID II project (Biological Impacts of Ocean ACIDification) and was hosted by the Plataforma Oceánica de Canarias (PLOCAN, Spain). In order to study the effects of changing carbonate chemistry conditions on the plankton community succession, nine mesocosms (KOSMOS, M1–M9: “Kiel Off-Shore Mesocosms for Ocean Simulation”), were deployed in Gando Bay (27°55′41″ N, 15°21′55″ W), on the west coast of Gran Canaria (Canary Islands, Spain) (Taucher et al., 2017a). The nine cylindrical mesocosm units (13 m deep, 2 m diameter) enclosed water volumes ($\sim 35 \text{ m}^3$) sealed by sediment traps installed at the bottom of each mesocosm bag (Boxhammer et al., 2016). Target $p\text{CO}_2$ was reached at the beginning of the experiment by adding CO_2 saturated seawater to the mesocosms following the protocol described in Riebesell et al. (2013). The carbonate

chemistry of the enclosed seawater was manipulated by stepwise additions of CO_2 -saturated seawater in four steps over 7 days. Two further CO_2 additions were conducted on days 21 and 38 to compensate for the loss of CO_2 through air-sea gas exchange. As $p\text{CO}_2$ treatments we established a gradient from current levels to end-of-century scenarios, representing IPCC predictions for mitigation scenarios (RCP 2.6) as well as medium (RCP 6.0) and high (RCP 8.5) $p\text{CO}_2$ levels (IPCC, 2013). The mean $p\text{CO}_2$ values per mesocosms between t1 and t55 were M1 = 369, M2 = 887, M3 = 563, M4 = 716, M5 = 448, M7 = 668, M8 = 1025 and M9 = 352 μatm . Analyzing the oligotrophic phase of the experiment, we could differentiate three $p\text{CO}_2$ groups by a k -means cluster analysis (Jain, 2010). The outcome showed three distinguishable clusters: low- $p\text{CO}_2$ (M1, M9, M5; $k = 460 \mu\text{atm}$) medium- $p\text{CO}_2$ (M3, M7, M4; $k = 721 \mu\text{atm}$) and high- $p\text{CO}_2$ levels (M2, M8; $k = 1111 \mu\text{atm}$) (Figure 1A) which were used for the analyses presented throughout this paper. Unfortunately, we detected a hole in the enclosure bag of the third high- $p\text{CO}_2$ mesocosm (M6 = 976 μatm) on t27, so M6 was excluded from sampling and analyses after that date.

To simulate a natural upwelling event, we collected deep water ($\sim 84 \text{ m}^3$) from 650 m depth on t22, as described by Taucher et al. (2017a). From each mesocosm, a defined volume of water was removed from 5 m depth with a submersible pump (Grundfos SP-17-5R). Consequently, in a process of $\sim 9 \text{ h}$ duration during the night of t24, deep water was pumped into the mesocosms,

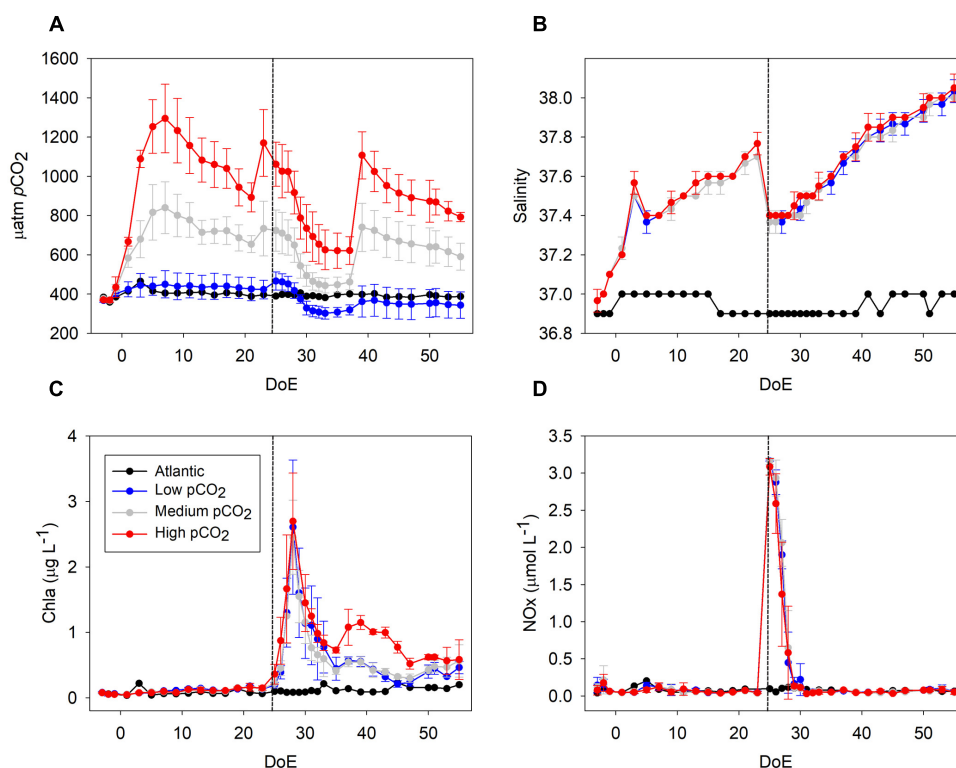


FIGURE 1 | Development of core parameters throughout the experiment. **(A)** $p\text{CO}_2$ (μatm), **(B)** salinity, **(C)** Chla ($\mu\text{g L}^{-1}$), **(D)** NOx (nitrate + nitrite; $\mu\text{mol L}^{-1}$). The addition of deep water (DW) in the mesocosms took place during the night between the 24th and 25th day of experiment (DoE); dashed line. Note that a clear draw down of CO_2 occurred during the phytoplankton bloom (t25–t35). Color code: black = Atlantic, blue = low- $p\text{CO}_2$, gray = medium- $p\text{CO}_2$, red = high- $p\text{CO}_2$.

TABLE 1 | Generalized additive mixed model (GAMM) structures.

Models	Meaning
$s(DoE)$	Temporal trend
$s(DoE) : pCO_2$	Effect of pCO_2 on the temporal trend
$s(DoE) + pCO_2$	Temporal trend and an independent pCO_2 effect on abundances

DoE, day of experiment.

reaching a mixing ratio of $\sim 20\%$ and a total mesocosm volume of $\sim 35 \text{ m}^3$ [see **Table 1** from Taucher et al. (2017a)]. Continuous up and down movement of the injection device during deep-water addition ensured homogenous vertical distribution of deep water inside the mesocosms.

All sampling methods and analyses are described in detail in the overview paper provided by Taucher et al. (2017a). Briefly, regular sampling — conducted every 2nd day before deep water addition, daily after t25 — included CTD casts, water column sampling, and sediment sampling. CTD casts were carried out with a hand-held CTD probe (CTD60M, Sea and Sun Technologies) in each mesocosm and in the surrounding water. Thereby we obtained vertical profiles of temperature, salinity (**Figure 1B**), pH, dissolved oxygen, chlorophyll *a*, and photosynthetically active radiation (PAR). Vertical profiles of temperature and salinity showed a uniform distribution of both variables, indicating that there was no stratification and that the water columns in the mesocosms were well-mixed throughout the entire study period (Taucher et al., 2017a). Water column samples were collected with integrating water samplers (IWS, Hydrobios, Kiel), in which a total volume of 5 L from 0 to 13 m depth was collected evenly through the water column. This water was either used for samples sensitive to contamination such as nutrient analyses, which were directly filled into separate containers on board, or stored in carboys for later subsampling for parameters such as phytoplankton and microzooplankton. Some analyses required larger volumes of water than could be sampled with the IWS in a reasonable time frame, e.g., pigment samples for reverse-phase high-performance liquid chromatography (HPLC) analysis. To enable a faster water collection, we used a custom-built pump system connected to a 20 L carboy. By creating a gentle vacuum and moving the inlet of the tube evenly up and down in the mesocosm during pumping, samples similar to those from the IWS were obtained. All carboys were protected from sunlight during sampling and stored in a temperature-controlled room at 16°C upon arrival on shore. Before taking subsamples from the carboys, they were carefully mixed to avoid a bias due to particle sedimentation.

Pigments such as Chlorophyll *a* (Chl*a* in the following) were analyzed using HPLC (**Figure 1C**). Nutrients (nitrate + nitrite (NO_x), **Figure 1D**) were measured using an autoanalyzer (SEAL Analytical, QuAAtro) coupled to an autosampler (SEAL Analytical, XY2). NO_x are presented here as a proxy for inorganic nutrients spec [see PO_4^{3-} , $Si(OH)_4$ and NH_4^+ dynamics in Taucher et al. (2017a)]. Phytoplankton samples for microscopy were obtained every 4 days and fixed with Lugol's solution. They were analyzed using the Utermöhl (1958) technique and

classified to the lowest possible taxonomical level. Biomass of phytoplankton was estimated by using conversion factors, as detailed in **Supplementary Table S1** (Tomas and Hasle, 1997; Ojeda, 1998; Leblanc et al., 2012).

Zooplankton: Sampling and Analysis

For the analysis of the microzooplankton community (microZP) —the size class of 20–200 μm — samples from the IWS were taken every 8 days until day 50. 250 mL of mesocosm water was transferred into brown glass bottles, fixed with acidic Lugol's solution (1–2% final concentration), and stored in the dark. MicroZP was counted and identified with an inverted microscope (Axiovert 25, Carl Zeiss) using the Utermöhl (1958). 50 mL of each sample was transferred into a sedimentation chamber and allowed to settle for 24 h prior to counting. Depending on plankton abundances, the whole or half of the chamber was counted at 100-fold magnification to achieve a count of at least 300–400 individuals for the most common taxa. MicroZP was identified to the lowest possible level (genus or species level) and otherwise grouped into size classes according to their distinct morphology. MicroZP were grouped into ciliates (aloricate and loricate) and dinoflagellates (athecate and thecate, size classes: small ($<25 \mu\text{m}$) and large ($>25 \mu\text{m}$)). As most dinoflagellates are capable of heterotrophic feeding (Calbet and Alcaraz, 2007), they can be considered as mixotrophic and were thus included in the microZP. Only few dinoflagellate taxa such as *Ceratium* or *Dinophysis* are considered to be predominantly autotrophic and were thus included in the phytoplankton (Tomas and Hasle, 1997). MicroZP biovolumes were estimated using geometric proxies obtained from literature (Ojeda, 1998; Hillebrand et al., 1999; Montagnes et al., 2001; Schmoker et al., 2014), and transformed to carbon biomass using conversion factors provided by Putt and Stoecker (1989) and Menden-Deuer and Lessard (2000) for ciliates and dinoflagellates, respectively (see **Supplementary Table S1**).

The mesozooplankton community (mesoZP) was sampled in the mesocosms by vertical net hauls with an Apstein net (55 μm mesh size, 17 cm diameter) equipped with a closed cod end. Sampling depth was restricted to 13 m to avoid resuspension of the material accumulated in the sediment traps at 15 m depth. Every net haul consisted in total filtered volume of 295 L. One net haul per mesocosm was carried out once every 8 days, always during the same time of the day (2–4 pm local time) to avoid diel differences in community composition. Samples were rinsed on board with filtered sea water, collected in containers and brought to the on-shore laboratory (PLOCAN, $\sim 4 \text{ nm}$ distance), where samples were preserved in denatured ethanol. For transportation, the samples were placed in cooling boxes until fixation of the organisms.

During analysis, organisms were sorted using a stereomicroscope (Olympus SZX9) and classified to the lowest possible taxonomical level. Copepodites and adults were classified together on a species/genus level, with the exception of the genus *Oncaea*, for which adults and copepodites were considered separately for a more in-depth study of this copepod. Nauplii from different species were pooled together. Taxonomical analysis was carried out focusing on copepods as the most

abundant group (Boltovskoy, 1999). Every sample was sieved using a 50 μm mesh, rinsed with fresh water and divided with a Folsom plankton splitter (1:2, 1:4). Abundant species/taxa (>200 individuals in an aliquot) were only counted from subsamples, while less abundant species/taxa were counted from the whole sample. An in depth analysis of the succession of calcifying zooplankton is provided by Lischka et al. (2018).

As a proxy to explore the system's energy transfer efficiency from producers to consumers (i.e., trophic transfer efficiency, TTE), we used the quotient autotrophy:heterotrophy (A:H) adapted from Calbet et al. (1996, 2014). This proxy was based on phytoplankton (Guan, 2018), heterotrophic microZP and mesoZP abundances transformed into biomass (see **Supplementary Table S1** for further details). Low TTE is indicated by a higher biomass A:H ratio, hence TTE and A:H are inversely correlated.

***Oncaea* spp. Development**

Oncaea is a common genus in the Canary Current System, where it has been typically recorded during the upwelling season (Hernández-León, 1998; Huskin et al., 2001; Hernández-León et al., 2007). *Oncaea* spp. is of special interest for this study because of (1) its trophic interaction with appendicularians (Go et al., 1998), which in turn may benefit from increased $p\text{CO}_2$ levels and nutrient enrichment conditions (Troedsson et al., 2013) and (2) to our knowledge, poecilostomatoid copepods had not been studied in an OA context before. Hence, despite being not the most abundant mesoZP taxon within the mesocosms (Poecilostomatoida; 8% total mesoZP catch) we focused on the condition of *Oncaea* to investigate direct and/or indirect $p\text{CO}_2$ effects on the female copepod length and reproductive output. Females were sorted from the same samples used for species determination, i.e., one sample per mesocosms (M1–M9) every 8 days during the whole study period (see section “Zooplankton: Sampling and Analysis”). The whole sample was scanned under the stereomicroscope (Olympus SZX9) and the first 20 adult females per sample were selected. Prosome length of every individual was measured, and females were classified regarding sexual development (mature/immature) and presence or absence of egg sacks. Females with developing egg sacks were classified as mature, while females which did not present any egg sack or eggs inside the prosome were rated as immature individuals.

Statistical Analyses

We used non-metric multidimensional scaling (NMDS) as exploratory analysis to describe the zooplankton community development in the mesocosms throughout the experiment. In our case the data matrix comprised abundances of each phytoplankton, microZP and mesoZP taxon in each mesocosm and on each sampling day (69 MK_timestep \times 96 taxa). The treatment effect was assessed by using permutation tests on the community position in the NMDS space. These permutations check if the area of clusters formed by the treatment in the NMDS are smaller than randomized samples of the same size (Legendre and Anderson, 1999). In a complementary approach, we applied an ANalysis Of SIMilarity (ANOSIM) test (Clarke, 1993) as a post-analysis to compare the mean of ranked dissimilarities

between $p\text{CO}_2$ treatments to the mean of ranked dissimilarities within treatments. This analysis tests the assumption that ranges of (ranked) dissimilarities within groups are equal, or at least very similar (Buttigieg and Ramette, 2014).

To describe the temporal trends of each taxon during this experiment we used generalized additive mixed models (GAMMs) (Wood, 2006; Zuur et al., 2009) with a Gamma distribution and a logarithmic link. Three different kinds of models were fitted to each abundance group (**Table 1**).

Each of these models allowed the abundance temporal trend to vary differently between $p\text{CO}_2$ treatments, representing (a) an equal temporal trend for all mesocosms [$s(\text{DoE})$], (b) an effect of $p\text{CO}_2$ on the temporal trend [$s(\text{DoE});p\text{CO}_2$], and (c) an equal temporal trend with an independent $p\text{CO}_2$ effect [$s(\text{DoE}) + p\text{CO}_2$]. This way, potential differences between $p\text{CO}_2$ treatments could be detected as either (b) changes in phenology or (c) an increase/decrease of overall abundance. If necessary, models were fitted with an autocorrelation structure of first order to account for temporal autocorrelation in the data (Zuur et al., 2009). Statistically significant models were compared by the coefficient of determination (R^2), which indicates the proportion of the variance in the dependent variable that is predictable from the independent variables. For each taxon, the model with the highest R^2 was considered to best represent the abundance data. Models presented here accounted from t1, whilst t-3 abundances have been included in the figures to illustrate conditions prior to $p\text{CO}_2$ manipulations within the mesocosms.

Differences in the condition of *Oncaea* females were analyzed by generalized linear mixed models (GLMMs) comparing the potential effect of $p\text{CO}_2$ and time on development, prosome length and reproductive output. The effect of the day of experiment (t1–t56) and $p\text{CO}_2$ treatment (low-, medium-, and high- $p\text{CO}_2$) on the studied parameters as well as their interaction were considered in the models. A Poisson distribution with a log link was used for the GLMM of count data, while length data was analyzed with a Gamma distribution. Unfortunately, the relatively low zooplankton sampling frequency did not allow for testing $p\text{CO}_2$ effects on a continuous manner. As an alternative, different $p\text{CO}_2$ levels were grouped in low-, medium-, and high- $p\text{CO}_2$ by a k -means cluster analysis, as described in Section “Mesocosms Setup and Experimental Design.”

We used R [version 3.0.2, (R Core Team, 2012)] to fit abundance data with the GAMMs and GLMs. The significance level for all statistical analysis was set to $p < 0.05$.

RESULTS

Community Change

The 2-dimensional representation of the community (NMDS) showed a strong trend in time (plankton succession), and a divergence of this trend from ca. t25 between the high- $p\text{CO}_2$ mesocosms and the low- and medium- ones (**Figure 2**). Treatments followed a similar trend from t-3 until t17, but tended to separate afterwards, matching the simulated upwelling caused by deep water addition (t24). Permutation tests (with 999 permutations) did not show the areas (i.e., clusters of samples)

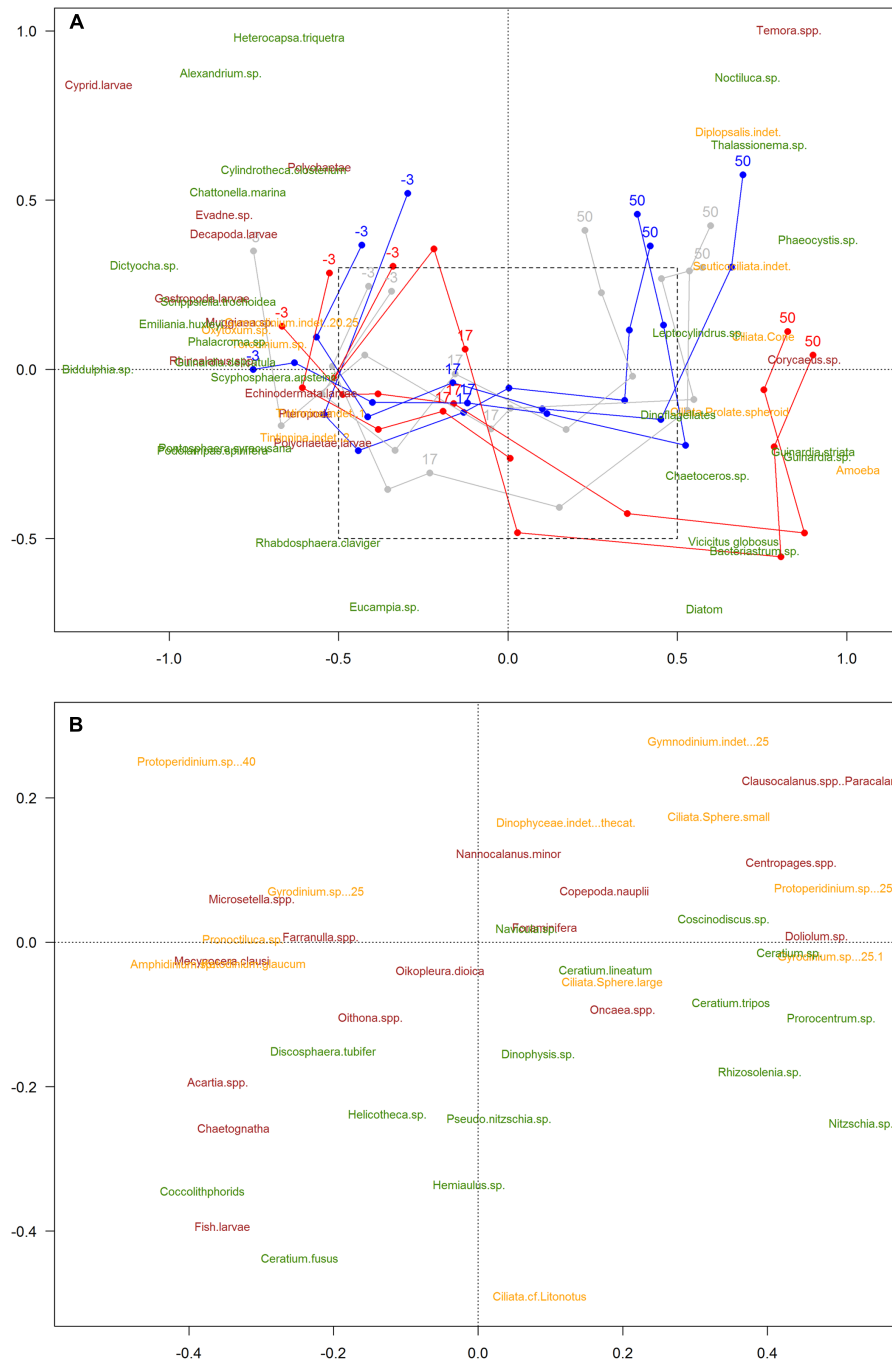


FIGURE 2 | Non-metric Multidimensional Scaling analysis (NMDS) of the plankton community (stress value = 0.18). Color code: blue = low- $p\text{CO}_2$ (M1, M5, and M9), gray = medium- $p\text{CO}_2$ (M3, M4, and M7), red = high- $p\text{CO}_2$ [M2, M6 (until t27), M8]. Only common species (>0.5% total abundances) represented. Taxa names: phytoplankton (green), microzooplankton (yellow), mesozooplankton (burgundy). The numbers -3, 17, and 51 indicate sampling days; lines represent patterns. Species are positioned in the graph according to their relative abundance during the experiment. Days of experiment included in the NMDS analysis were limited to t50, due to the absence of microZP samples for t56. Amplified area (B) is a zoom-in for a clearer view of the species that overlapped in the middle of the first graph [not shown in (A) for the sake of clarity].

representing the different $p\text{CO}_2$ treatments to be significantly smaller than randomized areas, indicating that the variation due to CO_2 is smaller than the changes over time (i.e., natural succession) (ANOSIM test, p -value = 0.246). Areas representing

the sampling day were significantly different from randomized areas using the same test, indicating a temporal trend (p -value = 0.001). Moreover, results for the interaction between sampling day and $p\text{CO}_2$ treatment (ANOSIM test, p -value = 0.001)

matched with the NMDS, suggesting that there was a significant effect of $p\text{CO}_2$ on plankton succession, ultimately affecting the plankton community development after the simulated upwelling event. Consequently, the plankton community developed differently within the different $p\text{CO}_2$ treatments, the largest difference being in the high- $p\text{CO}_2$ mesocosms.

Zooplankton Temporal Trends

In view of zooplankton abundance and Chla levels we could define three experimental phases: pre-bloom (from t1 until deep water addition on t24), phytoplankton bloom phase (t25–35) and post-bloom phase (from t35 until the end of the experiment), as shown in **Figure 1C**.

The microzooplankton (microZP) community comprised 13 different taxonomic groups of heterotrophic dinoflagellates and ciliates. Temporal trends of total microZP were affected by $p\text{CO}_2$ [$s(\text{DoE})\text{:Treat}$, **Table 2**], resulting in higher abundances under the high- $p\text{CO}_2$ treatment on the last sampling day. Averaged microZP abundances at the beginning of the experiment (t1) were $4.5 \cdot 10^6 \pm 2.89 \cdot 10^6$ individuals per m^3 for the low-, $3.45 \cdot 10^6 \pm 8.03 \cdot 10^5$ for the medium-, and $4.07 \cdot 10^6 \pm 9.36 \cdot 10^5$ for the high- $p\text{CO}_2$ treatments, respectively. After deep water addition (t24), abundances increased in all treatments, especially in the medium- $p\text{CO}_2$ treatment. Maximum values were reached at the end of the experiment (t50) in the high- $p\text{CO}_2$ treatment with $2.14 \cdot 10^7 \pm 8.94 \cdot 10^6$ individuals per m^3 ($1.44 \cdot 10^7 \pm 6.61 \cdot 10^6$ and $1.52 \cdot 10^7 \pm 1.08 \cdot 10^7$ individuals per

m^3 in the low- and medium- $p\text{CO}_2$ treatments, respectively). MicroZP responded rapidly to phytoplankton bloom formation following the simulated upwelling (t23/24) and showed the strongest increase in abundance in the medium- $p\text{CO}_2$ treatment. On t50, however, abundances in the medium- $p\text{CO}_2$ treatment decreased again while a pronounced increase in the high- $p\text{CO}_2$ was observed (**Figure 3G**).

Aloricate ciliates, mainly represented by specimen $<30 \mu\text{m}$, accounted for $\sim 26\%$ on average of total microZP abundances. Ciliate abundance was lower in high- $p\text{CO}_2$ during the bloom phase and increased after t35, matching with Chla decrease (**Figure 1**). An effect of $p\text{CO}_2$ on the temporal trend was detected on these ciliate abundances [$s(\text{DoE})\text{:Treat}$], indicating a direct link between CO_2 -enhanced phytoplankton growth and increases in ciliate abundance under high- $p\text{CO}_2$ conditions (**Table 2** and **Figure 3A**). Aloricate ciliates were clearly dominant while loricate ciliates, mainly represented by tintinnids, accounted for only $\sim 2.5\%$ of total microZP abundance. No significant $p\text{CO}_2$ effect was detected on the temporal trend of loricate ciliates [$s(\text{DoE}) + \text{Treat}$], even though abundances were higher at lower $p\text{CO}_2$ during the oligotrophic phase of the experiment (**Table 2** and **Figure 3B**). Most dinoflagellates in low- and medium- $p\text{CO}_2$ treatments responded to the deep-water addition and followed the Chla build-up and decrease (**Figure 1**) resulting in an increase in dinoflagellates abundance following the addition (t24), although only some ($>25 \mu\text{m}$ athecate) responded to high- $p\text{CO}_2$ at the end of the experiment (**Figures 3C–F**). Small athecate dinoflagellate abundances (**Figure 3C**) were higher under high- $p\text{CO}_2$ conditions during most of the oligotrophic phase, although highest abundances were recorded under medium- $p\text{CO}_2$ treatment toward the end of the experiment [$s(\text{DoE})\text{:Treat}$]. The most abundant group within the dinoflagellates were small thecate dinoflagellates. The best fitting model was an interaction of $p\text{CO}_2$ and the temporal trend resulting in higher abundances at medium $p\text{CO}_2$ in the second half of the experiment [$s(\text{DoE})\text{:Treat}$]. Thus, higher abundances of this group were recorded at medium- and low- $p\text{CO}_2$ treatments during the bloom, followed by a subsequent decrease in the post-bloom phase (**Table 2** and **Figure 3D**). Large athecate dinoflagellates (**Figure 3E**) showed a similar trend during the bloom phase, but abundance resulted to be ultimately higher under low- $p\text{CO}_2$ toward the end of the experiment [$s(\text{DoE})\text{:Treat}$]. Large thecate dinoflagellates (**Figure 3F**) responded differently than other dinoflagellates, reaching lowest abundance before deep water addition and increasing again when the phytoplankton bloom decayed, independent of the $p\text{CO}_2$ treatment [$s(\text{DoE}) + \text{Treat}$]. Large dinoflagellates were mainly represented by the genus *Gyrodinium*, comprising $\sim 12\%$ of the total microZP abundances. Small dinoflagellates from the genera *Protoperidinium* and *Gymnodinium* accounted for ~ 22 and 20% total microZP abundances, respectively.

The mesozooplankton (mesoZP) community was dominated by copepods and comprised 28 different species or taxonomic groups (see **Table 3**). Nauplii were counted from the net hauls ($>55 \mu\text{m}$) and thus included in the mesoZP category, although we are aware that early copepod life stages would in principle belong to microZP when strictly following Sieburth et al.'s (1978)

TABLE 2 | Zooplankton GAMM analyses.

Microzooplankton	Model	Edf	F		R^2 -adj.	Dev. Expl. (%)
Aloricate ciliates	$s(\text{DoE})\text{:Treat}$	4.106	11.26	***	0.69	72.6
Loricate ciliates	$s(\text{DoE}) + \text{Treat}$	6.779	579.2	***	0.753	79
Athe. dinoflag. $<25 \mu\text{m}$	$s(\text{DoE})\text{:Treat}$	4.035	3.287	*	0.38	39.3
Thec. dinoflag. $<25 \mu\text{m}$	$s(\text{DoE})\text{:Treat}$	5.219	7.227	***	0.438	55.1
Athe. dinoflag. $>25 \mu\text{m}$	$s(\text{DoE})\text{:Treat}$	5.388	13.191	***	0.385	79.7
Thec. dinoflag. $>25 \mu\text{m}$	$s(\text{DoE}) + \text{Treat}$	6.886	91.33	***	0.113	32.2
Total microZP	$s(\text{DoE})\text{:Treat}$	3.568	6.259	*	0.488	42.3
Mesozooplankton						
Calanoida	$s(\text{DoE})\text{:Treat}$	3.062	37.07	***	0.726	81.4
Cyclopoida	$s(\text{DoE})$	6.275	19	***	0.289	36.7
Harpacticoida	$s(\text{DoE})$	1	87.91	***	0.756	37.9
Poecilostomatoida	$s(\text{DoE})\text{:Treat}$	5.95	7.664	***	0.382	37.4
Nauplii	$s(\text{DoE})\text{:Treat}$	1.372	5.912	**	0.329	40.6
<i>O. dioica</i>	$s(\text{DoE})$	5.739	3.98	**	0.151	13.6
mesoZP total catch	$s(\text{DoE})\text{:Treat}$	3.596	5.786	***	0.571	67.1
Oncaea spp.						
Adults	$s(\text{DoE})\text{:Treat}$	2.144	7.533	**	0.204	9.37
Copepodites	$s(\text{DoE})\text{:Treat}$	2.062	5.914	***	0.146	17.2

Models defined the temporal trend of the abundances alone [$s(\text{DoE})$], or within an interaction with the $p\text{CO}_2$ treatments [$s(\text{DoE})\text{:Treat}$]. Only significant values (p -value < 0.05) are presented. DoE, day of experiment; edf, estimated degrees of freedom; Dev. Expl., deviance explained. Significance codes: <0.001 '***' 0.001 '***' 0.01 '**' 0.05 .

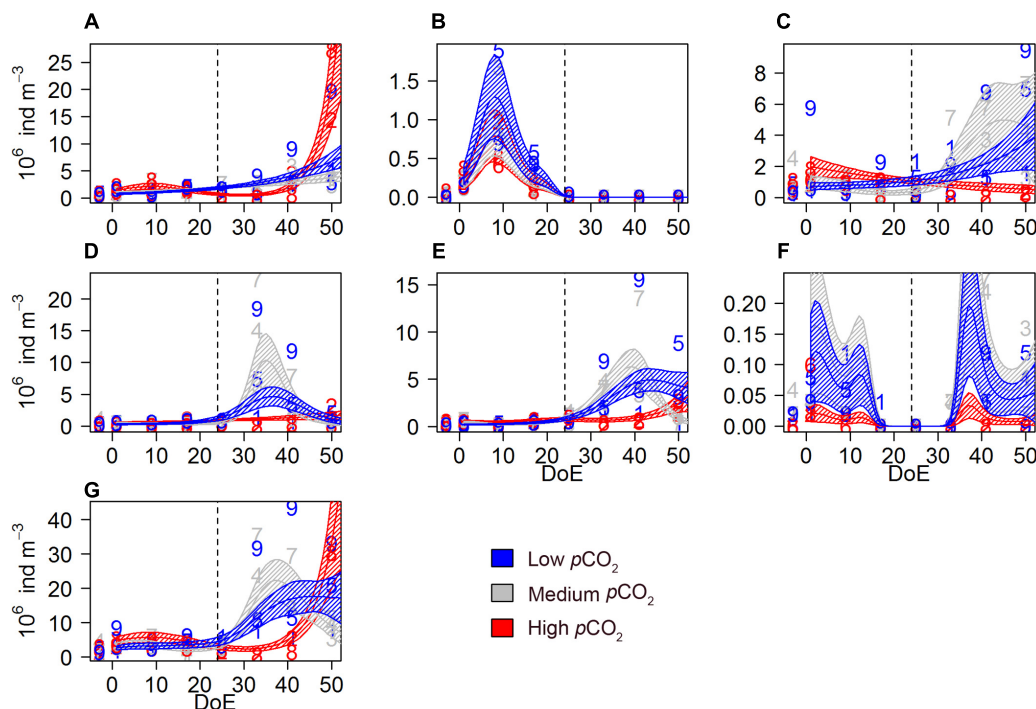


FIGURE 3 | Microzooplankton abundances during the study period. **(A)** aloricate ciliates, **(B)** loricate ciliates, **(C)** small athecate dinoflagellates (<25 μm), **(D)** small thecate dinoflagellates (<25 μm), **(E)** large athecate dinoflagellates (>25 μm), **(F)** large thecate dinoflagellates (>25 μm), **(G)** total microZP. Color code: blue = low- $p\text{CO}_2$ (M1, M5, and M9), gray = medium- $p\text{CO}_2$ (M3, M4, and M7), red = high- $p\text{CO}_2$ (M2, M6, and M8). DoE, day of experiment. Note that, for a better visibility of the data, y-axes have been adapted to abundances in each panel. Numbers represent abundances for the respective mesocosm (e.g., 9 for M9). Solid lines = prediction from Generalized Additive Mixed Models (GAMMs) (smoother trends p -value < 0.05); shaded area = confidence interval. Dashed line: t24, deep water addition.

size definition. Total mesoZP catch showed a different temporal trend for each $p\text{CO}_2$ treatment [$s(\text{DoE})$:*Treat*, **Table 2**]. Averaged mesoZP abundances at the beginning of the experiment (t1) varied between 4730 ± 1202 (low- $p\text{CO}_2$), 6023 ± 982 (medium- $p\text{CO}_2$), and 5242 ± 369 (high- $p\text{CO}_2$) individuals per m^3 , respectively. Our results showed that mesoZP abundances increased after deep water addition (t24), although this increase

was delayed in the high- $p\text{CO}_2$ treatment. Highest averaged abundances were recorded for all three treatments on the last sampling day (**Figure 4**): 23038 ± 9230 individuals per m^3 in low- $p\text{CO}_2$, 25295 ± 14196 in medium- $p\text{CO}_2$ and 24403 ± 10928 in high- $p\text{CO}_2$.

Different responses to $p\text{CO}_2$ treatments were observed among the studied copepod orders. All copepods, including nauplii, represented $\sim 90\%$ of total mesozooplankton abundances. Calanoid copepods were mainly represented by *Clausocalanus* spp. and *Paracalanus* spp. (including e.g., *Clausocalanus furcatus*, *C. arcuicornis*, *Paracalanus indicus*), and accounted for 7–89% (average = 38%) of the total mesozooplankton abundances. An increase in calanoid abundances was detected after deep water addition (t24) in low- and medium- $p\text{CO}_2$. Calanoida evolved similarly within the low- and the medium- $p\text{CO}_2$ treatments until $\sim t40$. Afterwards, abundances under medium- $p\text{CO}_2$ and high- $p\text{CO}_2$ treatments increased, resulting in abundances higher than those in low- $p\text{CO}_2$ mesocosms on the last sampling day (**Figure 4A**). Hence, a significant interaction between $p\text{CO}_2$ and temporal trend abundances was detected on calanoid abundances [$s(\text{DoE})$:*Treat*, **Table 2**] resulting in higher abundances under elevated $p\text{CO}_2$ conditions (medium- and high-) during the last two sampling days.

Cyclopoid copepods abundance (**Figure 4B**) decreased throughout the experiment independently of the treatment

TABLE 3 | Complete list of mesoZP species and taxa detected in the mesocosms registered throughout the study period.

(1) Foraminifera	(15) <i>Farranula</i> spp.
(2) Hydromedusae	(16) <i>Mecynocera clausi</i>
(3) <i>Muggiaea</i> sp.	(17) <i>Microsetella</i> spp.
(4) <i>Doliolum</i> sp.	(18) <i>Nannocalanus minor</i>
(5) Gastropoda larvae	(19) <i>Oithona</i> spp.
(6) Pteropoda	(20) <i>Oncaea</i> spp.
(7) Polychaete larvae	(21) <i>Rhincalanus</i> spp.
(8) Polychaete	(22) <i>Temora</i> spp.
(9) <i>Evadne</i> sp.	(23) Chaetognatha
(10) Copepoda nauplii	(24) Cyprid larvae
(11) <i>Acartia</i> spp.	(25) Decapoda larvae
(12) <i>Centropages</i> spp.	(26) Echinodermata larvae
(13) <i>Clausocalanus</i> spp./ <i>Paracalanus</i> spp.	(27) <i>Oikopleura dioica</i>
(14) <i>Corycaeus</i> sp.	(28) Fish larvae

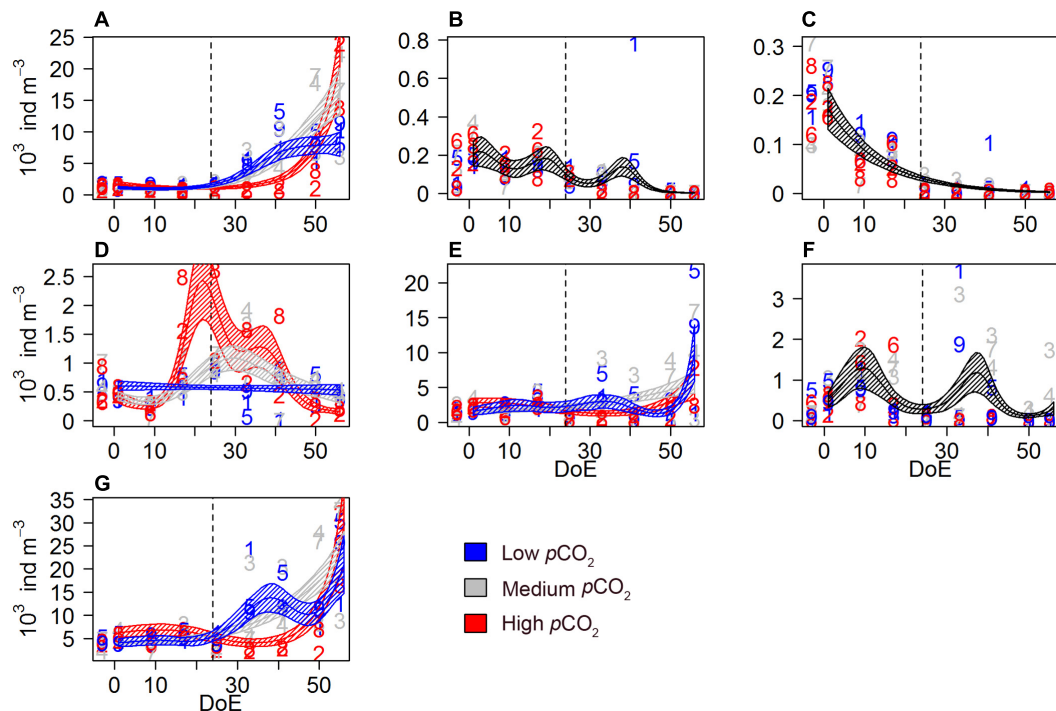


FIGURE 4 | Mesozooplankton abundances during the study period. **(A)** Calanoida, **(B)** Cyclopoida, **(C)** Harpacticoida, **(D)** Poecilostomatoida, **(E)** copepod nauplii, **(F)** *O. dioica*, **(G)** mesozooplankton total catch. Color code: blue = low- $p\text{CO}_2$ (M1, M5, and M9), gray = medium- $p\text{CO}_2$ (M3, M4, and M7), red = high- $p\text{CO}_2$ (M2, M6, and M8). Note that the black lines indicate that the model prediction for the three treatments is the same. DoE, day of experiment. For a better visibility of the data, y-axes have been adapted to abundances in each panel. Numbers represent abundances for the respective mesocosm (e.g., 9 for M9). Solid lines = prediction from Generalized Additive Mixed Models (GAMMs) (smoother trends p -value < 0.05); shaded area = confidence interval. Dashed line: t24, deep water addition.

[$s(\text{DoE})$, Table 2]. This order of copepods was mainly represented by *Oithona* spp. Harpacticoid copepod abundances (Figure 4C) decreased from the start of the experiment, and no $p\text{CO}_2$ effect was detected [$s(\text{DoE})$, Table 2]. This order of copepods was only represented by *Microsetella* spp. during this experiment. A significant effect of $p\text{CO}_2$ on the temporal trend was detected on poecilostomatoid copepods (Figure 4D), mainly represented by *Oncaea* spp. [$s(\text{DoE})$:Treat, Table 2]. Poecilostomatoids abundance was highest in high- $p\text{CO}_2$, increasing until ~t25 and decreasing gradually afterwards until the end of the experiment. A similar trend was observed under medium- $p\text{CO}_2$ while abundances under low- $p\text{CO}_2$ conditions did not vary much during the experiment. $p\text{CO}_2$ had an effect on the temporal trend of nauplii abundances [$s(\text{DoE})$:Treat, Table 2], which accounted for ~33% of total mesozooplankton abundances. An increase in nauplii abundances under low- and medium- $p\text{CO}_2$ conditions was detected after the deep-water addition (t24), with maximum abundances under the medium- $p\text{CO}_2$ treatment, while at high- $p\text{CO}_2$ abundances did not increase until the last sampling day (Figure 4E).

The appendicularia population — represented by the species *Oikopleura dioica* — was mainly composed by juveniles and accounted for 0–40% (average = 8%) of total mesozooplankton catch. We could not detect a $p\text{CO}_2$ effect on *O. dioica* during the experiment, even though they were completely absent in the high- $p\text{CO}_2$ treatment after deep water addition [$s(\text{DoE})$, Table 2

and Figure 4F]. The absence of a detectable effect could be attributed to the strong within-treatment variability.

Genus *Oncaea*

A significant effect of $p\text{CO}_2$ on the temporal trend was detected on both adults and copepodites [$s(\text{DoE})$:Treat], although no reaction to deep water addition (t24) was observed. Elevated $p\text{CO}_2$ levels resulted in higher abundances for both adults (only under high- $p\text{CO}_2$) and copepodites (under both medium- and high- $p\text{CO}_2$ conditions) (Figure 5 and Table 2).

A GLMM detected a negative $p\text{CO}_2$ effect on females' sexual development, resulting in higher number of immature females under high- $p\text{CO}_2$ conditions [$s(\text{DoE})$:Treat, Table 2 and Figure 6]. Approximately 60% of the females in the high- $p\text{CO}_2$ mesocosms were classified as immature, versus ~30% in medium- and ~36% low- $p\text{CO}_2$ treatments over the whole duration of the experiment. The number of immature females at high- and low- $p\text{CO}_2$ increased during the experiment while it decreased under medium- $p\text{CO}_2$ (Figure 6A). There were no significant differences between the numbers of mature females without egg sacks across treatments (Figure 6B). In contrast, the number of females carrying eggs during the experiment was significantly different across treatments. At high- $p\text{CO}_2$ there were no egg-carrying females after t24, and a clear increase in numbers could only be detected at medium- $p\text{CO}_2$ (Figure 6C). Thus, we observed a clear negative effect at high- $p\text{CO}_2$ on *Oncaea*

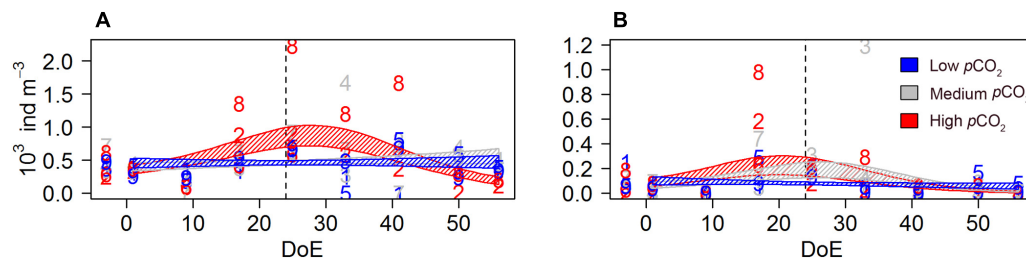


FIGURE 5 | *Oncaea* spp. abundances during the study period. **(A)** Adults, **(B)** copepodites. Color code: blue = low- $p\text{CO}_2$ (M1, M5, and M9), gray = medium- $p\text{CO}_2$ (M3, M4, and M7), red = high- $p\text{CO}_2$ (M2, M6, and M8). DoE, day of experiment. Numbers represent abundances per mesocosm (e.g., 9 for M9). Solid lines = prediction from Generalized Additive Mixed Models (GAMMs) (smoother trends p -value < 0.05); shaded area = confidence interval. Dashed line: t24, deep water addition.

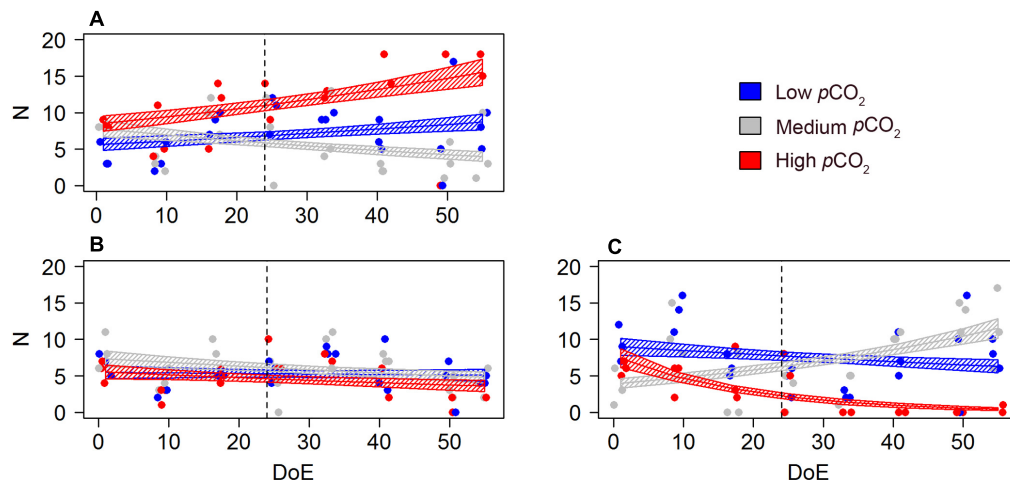


FIGURE 6 | $p\text{CO}_2$ effect on *Oncaea* spp. females' development and offspring (N). **(A)** number of immature females, **(B)** number of mature females (no egg sack), **(C)** number of egg-carrying females. Color code: blue = low- $p\text{CO}_2$ (M1, M5, and M9), gray = medium- $p\text{CO}_2$ (M3, M4, and M7), red = high- $p\text{CO}_2$ (M2, M6, and M8). DoE, day of experiment. Solid lines = GLMM predictions (p -value > 0.05). Dashed area = GLMM predictions confidence interval.

TABLE 4 | *Oncaea* females' condition.

<i>Oncaea</i> females	Model	Edf	Null deviance	p -value	Pseudo- R^2
Number of immature females	DoE:Treat	5	226.62	**	0.620
Number of egg-carrying females	DoE:Treat:egg sack	11	6.769	***	0.598
Length of females (immature)	DoE:Treat	5	17.97	**	0.065
Length of females (mature)	DoE:Treat:eggs	11	19.585	***	0.104

Summary of GLMs on mature and immature individuals ($n = 20$ females per mesocosms). Models (GLMMs) defined the $p\text{CO}_2$ effect in time of *Oncaea* spp. females' development and offspring DoE:Treat. DoE, day of experiment; edf, estimated degrees of freedom. Signif. codes: 0 '***' 0.001 '**' 0.01 '*' 0.05.

potential offspring (Table 4 and Figure 6), represented by females carrying an egg-sack.

The model revealed a negative effect of the $p\text{CO}_2$ treatment on the prosome length of mature and immature *Oncaea* females (Table 4 and Figure 7), although this result must be taken with caution due to the relatively weak fit of our models (pseudo- $R^2 \sim 0.1$, Table 4). Pooling together mature and immature individuals, females' prosome length was slightly shorter under high- $p\text{CO}_2$ conditions (0.45 ± 0.058 mm) when compared to medium- $p\text{CO}_2$ (0.56 ± 0.085 mm) and low- $p\text{CO}_2$ (0.52 ± 0.082 mm).

Trophic Transfer Efficiency (TTE)

The simulated upwelling induced a phytoplankton bloom (t25–t35) and amplified differences in succession patterns and food-web structure under high- $p\text{CO}_2$ conditions (Figure 8). In the high- $p\text{CO}_2$ mesocosms the phytoplankton bloom lasted for longer than in the other two treatments, and zooplankton responses were not detected until the bloom decayed (\sim t48). MicroZP abundance built up only in high- $p\text{CO}_2$ treatment, while we observed an increase in mesoZP abundances in both medium- and high- $p\text{CO}_2$ conditions toward the end of the experiment.

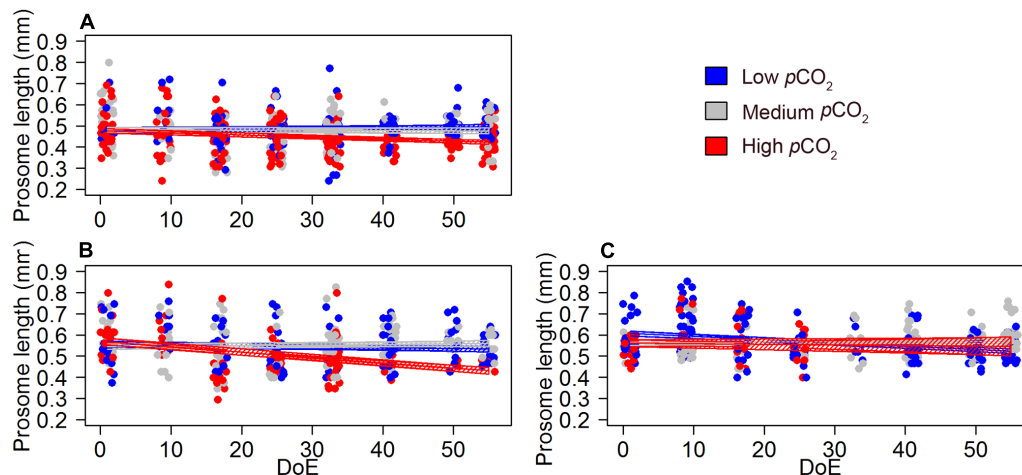


FIGURE 7 | $p\text{CO}_2$ effect on *Oncaea* females' development and offspring (length). **(A)** length of immature females, **(B)** length of mature females (no egg-sack), **(C)** length of egg-carrying females. Color code: blue = low- $p\text{CO}_2$ (M1, M5, and M9), gray = medium- $p\text{CO}_2$ (M3, M4, and M7), red = high- $p\text{CO}_2$ (M2, M6, and M8). DoE, day of experiment. Solid lines = GLMM predictions (p -value > 0.05). Dashed area = GLMM predictions confidence interval.

Generalized additive mixed models revealed a significant $p\text{CO}_2$ effect on the temporal trend of the A:H ratio [$s(\text{DoE}): \text{Treat}$, p -value < 0.05, **Figure 9**]. The model detected highest A:H ratio at the end of the phytoplankton bloom (~t35) in the high- $p\text{CO}_2$ treatment. During the post-bloom phase (i.e., after t35), the A:H ratio responded to the differential increase in microZP and mesoZP abundances (see **Figures 3G, 4G**). Hence, A:H in high- $p\text{CO}_2$ decreased faster than in the other two treatments, overlapping low- $p\text{CO}_2$ A:H on t50, when highest values corresponded to medium- $p\text{CO}_2$ treatment.

DISCUSSION

The main objective of this study was to analyze the effect of OA on the zooplankton community from subtropical waters during pre-bloom, bloom and post-bloom conditions. During the oligotrophic phase of this experiment we could not detect important differences in total zooplankton abundances between the treatments (**Figures 3G, 4G**). However, after the simulated upwelling, the zooplankton community under high- $p\text{CO}_2$ conditions evolved significantly differently compared to the low- and medium- $p\text{CO}_2$ conditions (**Figure 2**). Overall, higher zooplankton abundances were observed at elevated $p\text{CO}_2$ conditions (medium- and high-) in the post-bloom phase. This result matches with a previous KOSMOS study in coastal mesotrophic conditions (Bach et al., 2016b) where certain groups of consumers capitalized on CO_2 -enhanced phytoplankton biomass, resulting in higher zooplankton abundances under moderate IPCC end-of-century $p\text{CO}_2$ scenarios (RCP6.0) (Horn et al., 2016; Algueró-Muñiz et al., 2017). However, unexpectedly, both microZP and mesoZP abundances (**Figures 3G, 4G**) increased much later in the experiment under high- $p\text{CO}_2$ than under medium- and low- $p\text{CO}_2$. In the following, we will discuss the differences in zooplankton densities as well as the timing of bloom development.

$p\text{CO}_2$ Effects on Zooplankton Densities

As reported by other authors (e.g., Isari et al., 2015), responses to OA are not only dependent on species-specific sensitivities, but, much more importantly, depend on CO_2 effects on the community and the trophic interactions taking place in a species' natural habitat. In fact, most of the reported effects of OA on planktonic communities need to be attributed to these community effects, as many indicate a positive effect of OA (or rather carbon availability) on the plankton (Algueró-Muñiz et al., 2017; Taucher et al., 2017b). The temporal trends in major microZP groups (aloricate ciliates, small dinoflagellates) and Calanoida (**Figures 3, 4**, respectively) were most likely triggered by the food supply for microZP combined with the preference of most copepods for heterotrophic protists (Suzuki et al., 1999; Turner, 2004). As expected, picoplanktonic phytoplankton were a dominant component during the oligotrophic phase and large chain-forming diatoms dominated during the nutrient induced bloom (Taucher et al., 2017a). Diatoms are an ideal food source for larger mesoZP and this direct consumption of mesoZP on phytoplankton might have caused a release of microZP from grazing pressure after the deep-water addition.

The initial microZP abundance, as well as their taxonomic composition, was in agreement with those reported previously for the same area (Ojeda, 1998; Schmoker et al., 2014). During the post-bloom phase, microZP was dominated by dinoflagellates <25 μm and aloricate ciliates. Ciliates and dinoflagellates are the main grazers on phytoplankton in marine systems, especially oligotrophic ones and also contribute to a large part to the copepod diets (Calbet, 2008). This is attributed to their appropriate size and high nutritional quality of microZP relative to phytoplankton (Stoecker and Capuzzo, 1990) and the dominance of small-sized phytoplankton in oligotrophic systems which is outside the food spectrum of many mesozooplankters (Kleppel, 1993). Previous OA studies reported a tolerance of microZP communities toward high CO_2 concentrations, or only

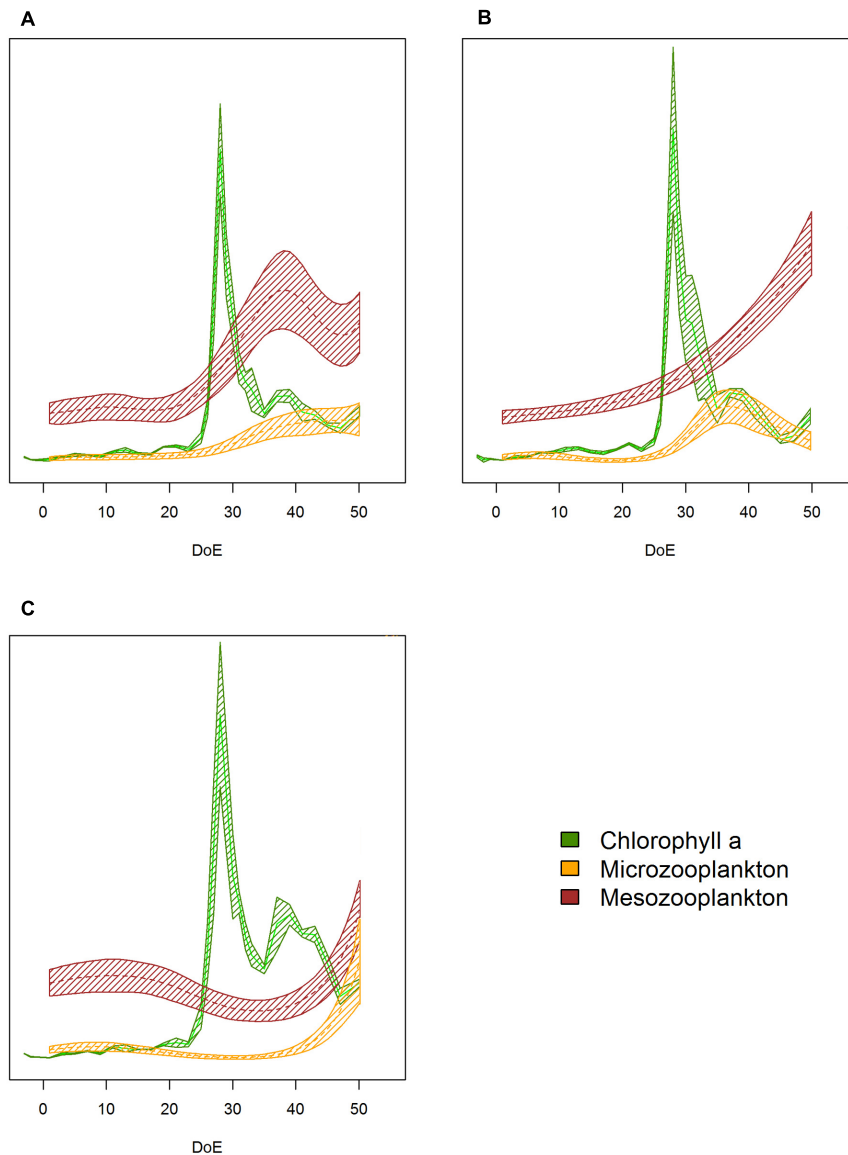
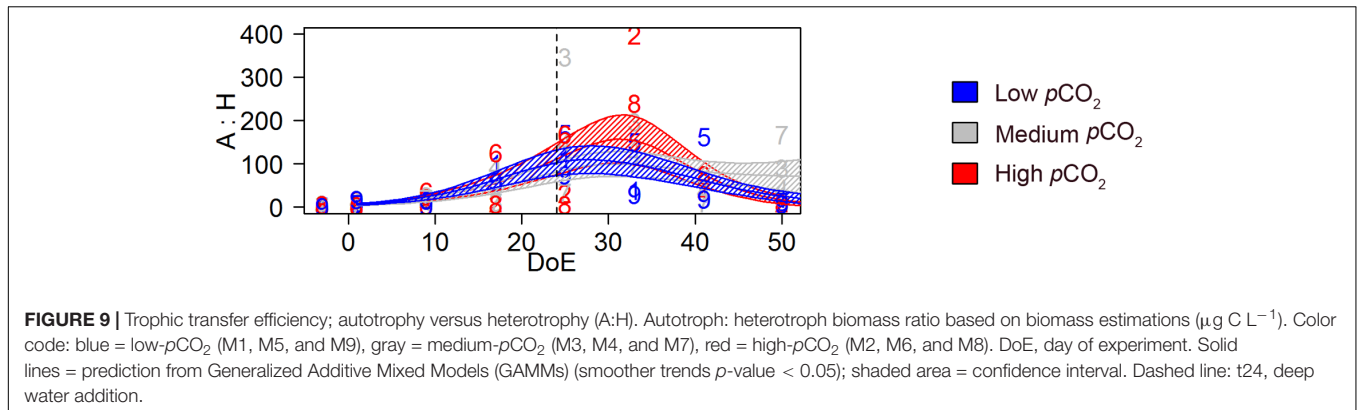


FIGURE 8 | Plankton succession trends. **(A)** Low- $p\text{CO}_2$ treatment, **(B)** medium- $p\text{CO}_2$ treatment, **(C)** high- $p\text{CO}_2$ treatment. Note that trends have been transformed to be in a 0 to 1 scale to enhance plankton succession visibility. Color code: green = Chla, yellow = microZP abundance, burgundy = mesoZP abundance. DoE, day of experiment. Solid lines = prediction from Generalized Additive Mixed Models (GAMMs) (smoother trends p -value < 0.05); shaded area = confidence interval.

very subtle changes in the community (Suffrian et al., 2008; Aberle et al., 2013; Horn et al., 2016; Lischka et al., 2017) while other studies showed detrimental (Calbet et al., 2014) or even positive effects (Rose et al., 2009). In this study, an increase in aloricate ciliate abundances was observed in all treatments in response to the deep water-induced phytoplankton bloom, although the increase showed a considerable time-lag relative to the phytoplankton bloom, especially at high CO_2 conditions. In contrast to aloricate ciliates, loricate ciliates played a minor role in this experiment and showed only a very small peak during the oligotrophic phase. Loricate ciliates started to decline after t10 and were virtually absent after deep water addition (see Figure 3).

For dinoflagellates, especially small-sized athecates, we expected a positive effect of high- $p\text{CO}_2$ levels due to findings from previous OA studies conducted in oligotrophic (Sala et al., 2015) and eutrophic regions (Horn et al., 2016). During the oligotrophic phase of the experiment, this expectation was confirmed since higher abundances of small athecate dinoflagellates at high- $p\text{CO}_2$ were also found in our study. However, after deep water addition overall dinoflagellate abundances were higher at low- and medium- $p\text{CO}_2$ conditions. Unlike ciliates, heterotrophic dinoflagellates are known to feed on phytoplankton of various sizes up to several times larger than their body size and have been shown to prey on bloom-forming diatoms including taxa as, e.g., *Thalassiosira* (Sherr and Sherr, 2007). The abundance



of diatoms, however, was higher at high- $p\text{CO}_2$ compared to the low- and medium- $p\text{CO}_2$ conditions (Taucher et al., 2017a). Thus, the effect of high $p\text{CO}_2$ on dinoflagellates was most likely an indirect one based on changes in the phytoplankton community and more precisely, on prey edibility (see section “ $p\text{CO}_2$ Effects on Zooplankton Bloom Timing”).

Calanoida were positively affected by medium- and high- $p\text{CO}_2$, although the trend was only visible during the last two sampling days. These results match with previous outcomes described for copepodites and adult *Pseudocalanus acuspes* in eutrophic waters and $p\text{CO}_2$ levels of $\sim 760 \mu\text{atm}$ (Algueró-Muñiz et al., 2017; Taucher et al., 2017b), suggesting a benefit of realistic end-of-century $p\text{CO}_2$ levels on calanoid copepods through higher food availability. Small planktonic copepods are dominant in the plankton communities in many parts of the world's oceans and therefore important members of pelagic food webs (Turner, 2004). Thus, a positive $p\text{CO}_2$ effect on these major zooplankton components could have a crucial impact on the transfer of energy to higher trophic levels thus affecting, e.g., future fisheries (Moyano et al., 2009; Sswat et al., 2018).

Copepod species that do not exhibit vertical migration behavior are considered as evolutionarily less exposed to high- $p\text{CO}_2$ levels compared to other copepods, and typically more sensitive to OA (Fitzer et al., 2012; Lewis et al., 2013). Accordingly, we expected cyclopoid (dominated by *Oithona*) and harpacticoid copepods (dominated by *Microsetella*) to show lower abundances under elevated $p\text{CO}_2$ conditions as neither species shows diel migration (Maar et al., 2006). However, during this experiment, elevated $p\text{CO}_2$ did not cause a significant effect on Cyclopoida and Harpacticoida abundances, according to the GAMM analyses (Figures 4B,C). The reason for the decay in Cyclopoida and Harpacticoida abundances is not entirely clear but could be due to the distribution of the copepods in the water column, closer to the mesocosm sediment traps. Such a loss through sedimentation was previously observed in other mesocosm experiments during periods of low food availability (Bach et al., 2016a; Algueró-Muñiz et al., 2017). *Oithona* and *Microsetella* have been reported to concentrate on marine snow (Ohtsuka et al., 1993; Koski et al., 2005) and during the present experiment, the cumulative flux of particulate organic matter to the sediment traps increased after deep water addition (Stange et al., 2018). This might have promoted a downward migration

of *Microsetella* —already from the beginning of the experiment on — to enhance their feeding on sinking material, preventing us to sample them in the net hauls.

$p\text{CO}_2$ Effects on Zooplankton Bloom Timing

Where the observed response of the zooplankton densities is in line with previously published results, the differences in timing of the blooms were rather unexpected. In fact, zooplankton density increases after the simulated upwelling under high- $p\text{CO}_2$ treatment were much slower than under the low and medium treatments. The most probable explanation for this observation lies in the differences in taxonomy of the phytoplankton responding to the nutrient addition of the upwelling. The phytoplankton bloom in the high- $p\text{CO}_2$ mesocosms (M2 and M8) was dominated by *Vicicitus globosus* (Dictyochophyceae) which bloomed only in the high- $p\text{CO}_2$ mesocosms from t25 until t47 (Riebesell et al., 2018). Harmful or non-edible for zooplankton, it seems likely that *V. globosus* caused adverse effects on the plankton community. MicroZP as potential grazers were most likely affected by the inadequacy of the available phytoplankton food (Chang, 2015), thus preventing the subsequent increase in mesoZP abundances. This is even more likely considering that once the phytoplankton bloom ceased in the high- $p\text{CO}_2$ treatments, microZP started to increase in numbers at a time point when they were already decreasing at low and medium- $p\text{CO}_2$. The tolerance to harmful algae has previously been described for copepod species closely related to those recorded in the mesocosms such as *Paracalanus parvus* (tolerant to *Chattonella antiqua*) and *Oncaea venusta* (tolerant to *Karenia brevis*) (Turner and Tester, 1989). Although *Paracalanus* sp. nauplii may exhibit adverse effects from feeding upon *Alexandrium tamiyavanichii* (Silva et al., 2013), we did not detect negative effects on nauplii abundances when relating them to the harmful algae abundance, but a delay in the reaction time likewise in aloricate ciliates, dinoflagellates and calanoid copepods. Accordingly, we based our conclusions for copepods on temporal trends and $p\text{CO}_2$ treatments rather than on possible effects of inedible/harmful food items. Our results suggest that copepods reacted to the different $p\text{CO}_2$ levels only after their preferred prey [i.e., heterotrophic protists (Turner, 2004)] reacted

to the stimulated bloom, thus highlighting the importance of microZP in bloom situations within oligotrophic ecosystems (Calbet and Alcaraz, 2007; Calbet, 2008).

***p*CO₂ Effects on *Oncaea* and *O. dioica* Interactions in Pre- and Post-bloom Conditions**

Oncaea's feeding strategies are associated with surface materials, such as fine particles, bacteria, or the tegument fluid of gelatinous zooplankton (*Sagitta* spp., *Oikopleura* spp. and *Salpa* spp.) (Go et al., 1998). During this study, abundances of *Oncaea* spp. and *O. dioica* were inversely correlated, as previously observed at other study sites (Itoh et al., 2014). *Oncaea* was positively affected by *p*CO₂, recording higher abundances under medium- and high-*p*CO₂ treatments from (approximately) the beginning of the experiment until the end of the phytoplankton bloom, on t35 (Figure 4D). The *O. dioica* trends showed some similarities with other studies at elevated nutrient concentrations (Troedsson et al., 2013). We did not detect a significant *p*CO₂ effect on *O. dioica* when considering the whole experimental period (Figure 4F), what agrees with previous results from Troedsson et al. (2013) and Winder et al. (2017) on the tolerance of appendicularians to OA. After deep water addition, we observed that *O. dioica* completely disappeared under high-*p*CO₂ while *Oncaea* abundances were higher than in the other two treatments, suggesting a top-down control of *Oncaea* on *O. dioica* abundances. Hence, the fact that during the last sampling days *Oncaea* spp. abundances decayed in the high-*p*CO₂ treatment might reflect the scarcity of *O. dioica* as food resource (Go et al., 1998).

Concerning the condition of *Oncaea* females (Figures 6, 7), we observed smaller individuals, as well as a higher number of immature females and a lower number of egg-carrying mature females in the high-*p*CO₂ treatment. These results are in line with previous studies in calanoid copepods which also observed a decrease in copepod size (Garzke et al., 2015) and fecundity loss (Thor and Dupont, 2015) caused by increased CO₂ levels. However, unlike the major sensitivities to OA previously described for early life stages of calanoid copepods (Pedersen et al., 2013; Algueró-Muñiz et al., 2017), we did not observe a stronger *p*CO₂ effect on *Oncaea* copepodites than on adults (Figure 5), suggesting differences between poecilostomatoids and calanoids in their offspring responses to expected future OA levels. We conclude that the negative *p*CO₂ effect detected on *Oncaea* females' reproductive output might affect food web interactions in the long term in those tropical and subtropical communities dominated by this species (e.g., Böttger-Schnack, 1994), especially in those where oncaeid copepods are the main prey for larvae and juvenile fish (Itoh et al., 2014). The lack of published OA research on *Oncaea* spp. (Poecilostomatoida) makes the analysis presented here of special relevance and calls for multigenerational OA studies on this species.

Influence of OA on the Transfer of Energy Within the Plankton Community

As discussed above, community effects and trophic interactions can alter sensitivities to OA (Rossoll et al., 2013), which in

turn may have an effect on the efficiency of the food web (Calbet et al., 2014; Cripps et al., 2016; Algueró-Muñiz et al., 2017). The autotrophic community was expected to experience an increase in biomass (Gismervik et al., 2002) responding to the nutrient input created by the deep water addition. Thus, a significant effect of CO₂ on plankton succession was observed after deep water addition (Taucher et al., 2017a), suggesting that phytoplankton blooms are boosted at elevated *p*CO₂. This situation could in turn cause a CO₂-dependant reduction in trophic efficiency after deep water addition, due to the limited capacity of micro- and mesoZP grazers to exploit the elevated phytoplankton productivity (Calbet et al., 2014). Accordingly, the A:H ratio (autotrophy/heterotrophy) proposed as a proxy for the trophic efficiency of the system was highest during the phytoplankton built-up at high-*p*CO₂. TTE decreased in all three *p*CO₂ treatments during the phytoplankton bloom (t25–t35), and lowest TTE was detected under high-*p*CO₂ conditions, likely because under these conditions microZP was limited by inadequate food items thus leading to a delayed response of microZP after phytoplankton bloom initiation, consequently affecting mesoZP production. These results are in line with previous studies (Calbet et al., 2014; Cripps et al., 2016) which point at a more-autotrophic and less efficient food web under higher *p*CO₂ conditions when the consumers mismatch the phytoplankton bloom (Edwards and Richardson, 2004; Calbet et al., 2014), as observed during this experiment until ~t40. Similarly than Calbet et al. (2014) and Cripps et al. (2016), we did not account for nanoplankton to estimate TTE in our study, what might have incurred in an underestimation of the system efficiency when considering phytoplankton as the only carbon source for zooplankton. The increase in calanoid copepod abundance observed in both high- and medium-*p*CO₂ treatments toward the end of the experiment points at *p*CO₂-induced effects under nutrient-replete conditions, which could travel up the food web reaching secondary consumers, as previously observed in eutrophic systems (Algueró-Muñiz, 2017; Sswat et al., 2018). In case of the medium-*p*CO₂ treatment, an increased grazing pressure of copepods (Calanoida) on dinoflagellates could explain that TTE in medium-*p*CO₂ was lower than in the other two treatments after the phytoplankton bloom. Our results thus suggest that *p*CO₂ effects on plankton succession depend on the coupling of the phytoplankton bloom with microZP and mesoZP grazers, ultimately affecting the development of the plankton community and the energy transfer efficiency of the system.

Based on this study, end-of-century *p*CO₂ levels are not expected to cause major effects on subtropical zooplankton communities during oligotrophic phases. However, during bloom and post-bloom conditions, elevated *p*CO₂ might promote higher zooplankton abundances by bottom-up effects of CO₂-enhanced primary production. Hence, *p*CO₂-fertilized phytoplankton productivity would reach grazers through trophic cascades, which might in turn be disrupted when CO₂ benefits harmful algae. These *p*CO₂ effects on plankton communities could be specially relevant in oligotrophic environments with short bloom periods such as the Canary Islands, where zooplankton biomass has been shown to have direct implications

on larval abundance in different fish species during late winter bloom (Moyano et al., 2009). Therefore, a positive effect of $p\text{CO}_2$ on zooplankton abundance after a bloom event might eventually benefit larval recruitment, and consequently have an effect on future fisheries.

DATA AVAILABILITY

All zooplankton abundance data are archived at the PANGAEA data library, <https://doi.pangaea.de/10.1594/PANGAEA.887283>.

ETHICS STATEMENT

No specific permission was required for activities related to field sampling. The field location was not privately owned or protected, and neither regulated animals, endangered nor protected species were involved.

AUTHOR CONTRIBUTIONS

UR, MA-M, HH, NA, LB, WG, EA, and MB conceived and designed the experiments. MA-M, HH, CS, LB, WG, and UR performed the experiments. MA-M, HH, SA-F, LB, WG, and EA analyzed the data. MA-M and HH contributed equally to this work. MA-M wrote this paper with input from all co-authors.

REFERENCES

- Aberle, N., Schulz, K. G., Stühr, A., Malzahn, A. M., Ludwig, A., and Riebesell, U. (2013). High tolerance of microzooplankton to ocean acidification in an Arctic coastal plankton community. *Biogeosciences* 10, 1471–1481. doi: 10.5194/bg-10-1471-2013
- Algueró-Muniz, M. (2017). *Zooplankton Community Responses to Ocean Acidification*. Ph.D. thesis, University of Bremen, Bremen. Available at: <https://elib.suub.uni-bremen.de/peid/D00106079.html>
- Algueró-Muñiz, M., Alvarez Fernandez, S., Thor, P., Bach, L. T., Esposito, M., Horn, H. G., et al. (2017). Ocean acidification effects on mesozooplankton community development: results from a long-term mesocosm experiment. *PLoS One* 12:e0175851. doi: 10.1371/journal.pone.0175851
- Alvarez-Fernandez, S., Bach, L. T., Taucher, J., Riebesell, U., Sommer, U., Aberle, N., et al. (2018). Plankton responses to ocean acidification: the role of nutrient limitation. *Progr. Oceanogr.* 165, 11–18. doi: 10.1016/j.pocean.2018.04.006
- Aristegui, J., Hernández-León, S., Montero, M. F., and Gómez, M. (2001). The seasonal planktonic cycle in coastal waters of the Canary Islands. *Sci. Mar.* 65, 51–58. doi: 10.3989/scimar.2001.65s151
- Bach, L. T., Boxhammer, T., Larsen, A., Hildebrandt, N., Schulz, K. G., and Riebesell, U. (2016a). Influence of plankton community structure on the sinking velocity of marine aggregates. *Glob. Biogeochem. Cycles* 30, 1145–1165. doi: 10.1002/2016GB005372
- Bach, L. T., Taucher, J., Boxhammer, T., Ludwig, A., Consortium, T. K. K., Achterberg, E. P., et al. (2016b). Influence of ocean acidification on a natural winter-to-summer plankton succession: First insights from a long-term mesocosm study draw attention to periods of low nutrient concentrations. *PLoS One* 11:e0159068. doi: 10.1371/journal.pone.0159068

FUNDING

Financial support for this study was provided by the German Ministry of Education and Research through phase II (BMBF, FKZ 03F0655A and 03F0655B) and III (BMBF, FKZ 03F0728B) of the BIOACID (Biological Impacts of Ocean ACIDification) project.

ACKNOWLEDGMENTS

We want to acknowledge the Plataforma Oceánica de Canarias (PLOCAN) for hosting and supporting us during this experiments. We also want to thank the Captain and crew of RV Hespérides for deploying and recovering the mesocosms (cruise 29HE20140924), as well as RV Poseidon for transporting the mesocosms and supporting in testing the deep-water collector (cruise POS463). We are grateful to “The Gran Canaria KOSMOS Consortium” (Taucher et al., 2017a) for all the help and support received during on-site work. We also thank Saskia Ohse for technical support with carbon content analyses, Barbara Niehoff for her advice on *Oncaea* condition analyses and Silke Lischka for calcifiers abundances data.

SUPPLEMENTARY MATERIAL

The Supplementary Material for this article can be found online at: <https://www.frontiersin.org/articles/10.3389/fmars.2019.00061/full#supplementary-material>

- Boersma, M., Aberle, N., Hantzsch, F. M., Schoo, K. L., Wiltshire, K. H., and Malzahn, A. M. (2008). Nutritional limitation travels up the food chain. *Int. Rev. Hydrobiol.* 93, 479–488. doi: 10.1002/iroh.200811066
- Boltovskoy, D. (1999). *South Atlantic Zooplankton*. Leiden: Backhuys Publishers.
- Böttger-Schnack, R. (1994). The microcopepod fauna in the Eastern Mediterranean and Arabian Seas: a comparison with the Red Sea fauna. *Hydrobiologia* 292, 271–282. doi: 10.1007/bf00229951
- Boxhammer, T., Bach, L. T., Czerny, J., and Riebesell, U. (2016). Technical note: sampling and processing of mesocosm sediment trap material for quantitative biogeochemical analysis. *Biogeosciences* 13, 2849–2858. doi: 10.5194/bg-13-2849-2016
- Buttigieg, P. L., and Ramette, A. (2014). A guide to statistical analysis in microbial ecology: a community-focused, living review of multivariate data analyses. *FEMS Microbiol. Ecol.* 90, 543–550. doi: 10.1111/1574-6941.12437
- Calbet, A. (2008). The trophic roles of microzooplankton in marine systems. *ICES J. Mar. Sci.* 65, 325–331. doi: 10.1093/icesjms/fsn013
- Calbet, A., and Alcaraz, M. (2007). “Microzooplankton, key organisms in the pelagic food web,” in *Fisheries and Aquaculture: Towards Sustainable Aquatic Living Resources Management*, ed. P. Safran (Oxford: Encyclopedia of Life Support Systems (EOLSS) UNESCO Eolss Publishers).
- Calbet, A., Alcaraz, M., Saiz, E., Estrada, M., and Trepas, I. (1996). Planktonic herbivorous food webs in the Catalan Sea (NW Mediterranean): temporal variability and comparison of indices of phyto-zooplankton coupling based on state variables and rate processes. *J. Plankton Res.* 18, 2329–2347. doi: 10.1093/plankt/18.12.2329
- Calbet, A., Sazhin, A. F., Nejstgaard, J. C., Berger, S. A., Tait, Z. S., Olmos, L., et al. (2014). Future climate scenarios for a coastal productive planktonic food web resulting in microplankton phenology changes and decreased trophic transfer efficiency. *PLoS One* 9:e94388. doi: 10.1371/journal.pone.0094388

- Chang, F. (2015). Cytotoxic Effects of *Vicicitus globosus* (Class Dictyochophyceae) and *Chattonella marina* (Class Raphidophyceae) on rotifers and other microalgae. *J. Mar. Sci. Eng.* 3:401. doi: 10.3390/jmse3020401
- Cianca, A., Helmke, P., Mouriño, B., Rueda, M. J., Llinás, O., and Neuer, S. (2007). Decadal analysis of hydrography and in situ nutrient budgets in the western and eastern North Atlantic subtropical gyre. *J. Geophys. Res.* 112:C07025. doi: 10.1029/2006JC003788
- Clarke, K. R. (1993). Non-parametric multivariate analyses of changes in community structure. *Aust. J. Ecol.* 18, 117–143. doi: 10.1111/j.1442-9993.1993.tb00438.x
- Cripps, G., Flynn, K. J., and Lindeque, P. K. (2016). Ocean acidification affects the phyto-zoo plankton trophic transfer efficiency. *PLoS One* 11:e0151739. doi: 10.1371/journal.pone.0151739
- de León, A. R., and Braun, J. G. (1973). Annual cycle of primary production and its relation to nutrients in the Canary Islands waters. *Boln. Inst. Esp. Oceanogr.* 167, 1–24.
- Edwards, M., and Richardson, A. J. (2004). Impact of climate change on marine pelagic phenology and trophic mismatch. *Nature* 430, 881–884. doi: 10.1038/nature02808
- Fitzer, S. C., Caldwell, G. S., Close, A. J., Clare, A. S., Upstill-Goddard, R. C., and Bentley, M. G. (2012). Ocean acidification induces multi-generational decline in copepod naupliar production with possible conflict for reproductive resource allocation. *J. Exp. Mar. Biol. Ecol.* 41, 30–36. doi: 10.1016/j.jembe.2012.03.009
- Garzke, J., Ismar, S. M. H., and Sommer, U. (2015). Climate change affects low trophic level marine consumers: warming decreases copepod size and abundance. *Oecologia* 177, 849–860. doi: 10.1007/s00442-014-3130-4
- Gazeau, F., Sallon, A., Maugendre, L., Louis, J., Dellisanti, W., Gaubert, M., et al. (2017). First mesocosm experiments to study the impacts of ocean acidification on plankton communities in the NW Mediterranean Sea (MedSea project). *Estuar. Coast. Shelf Sci.* 186(Part A), 11–29. doi: 10.1016/j.ecss.2016.05.014
- Gismervik, I., Olsen, Y., and Vadstein, O. (2002). Micro- and mesozooplankton response to enhanced nutrient input – a mesocosm study. *Hydrobiologia* 484, 75–87. doi: 10.1023/a:1021300920641
- Go, Y.-B., Oh, B.-C., and Terazaki, M. (1998). Feeding behavior of the poecilostomatoid copepods *Oncaea* spp. on chaetognaths. *J. Mar. Syst.* 15, 475–482. doi: 10.1016/S0924-7963(97)00038-9
- Guan, W. (2018). *KOSMOS 2014 Mesocosm Study: Phytoplankton Abundance, Pangaia*. Available at: <https://doi.pangaia.de/10.1594/PANGAEA.879600>.
- Guinotte, J. M., and Fabry, V. J. (2008). “Ocean acidification and its potential effects on marine ecosystems,” in *Year in Ecology and Conservation Biology 2008*, eds R. S. Ostfeld and W. H. Schlesinger (New York, NY: Annals of the New York Academy of Sciences), 320–342. doi: 10.1196/annals.1439.013
- Harley, C. D. G. (2011). Climate change, keystone predation, and biodiversity loss. *Science* 334, 1124–1127. doi: 10.1126/science.1210199
- Hernández-León, S. (1998). Annual cycle of epipelagic copepods in Canary Island waters. *Fish. Oceanogr.* 7, 252–257. doi: 10.1046/j.1365-2419.1998.00071.x
- Hernández-León, S. (2009). Top-down effects and carbon flux in the ocean: a hypothesis. *J. Mar. Syst.* 78, 576–581. doi: 10.1016/j.jmarsys.2009.01.001
- Hernández-León, S., Almeida, C., Bécognée, P., Yebra, L., and Aristegui, J. (2004). Zooplankton biomass and indices of grazing and metabolism during a late winter bloom in subtropical waters. *Mar. Biol.* 145, 1191–1200. doi: 10.1007/s00227-004-1396-5
- Hernández-León, S., Almeida, C., Gómez, M., Torres, S., Montero, I., and Portillo-Hahnefeld, A. (2001). Zooplankton biomass and indices of feeding and metabolism in island-generated eddies around Gran Canaria. *J. Mar. Syst.* 30, 51–66. doi: 10.1016/S0924-7963(01)00037-9
- Hernández-León, S., Gómez, M., and Aristegui, J. (2007). Mesozooplankton in the Canary Current System: the coastal-ocean transition zone. *Progr. Oceanogr.* 74, 397–421. doi: 10.1016/j.pocean.2007.04.010
- Hillebrand, H., Dürselen, C.-D., Kirschtel, D., Pollinger, U., and Zohary, T. (1999). Biovolume calculation for pelagic and benthic microalgae. *J. Phycol.* 35, 403–424. doi: 10.1046/j.1529-8817.1999.3520403.x
- Horn, H. G., Sander, N., Stuh, A., Algueró-Muñiz, M., Bach, L. T., Löder, M. G. J., et al. (2016). Low CO₂ sensitivity of microzooplankton communities in the Gullmar Fjord, Skagerrak: evidence from a long-term mesocosm study. *PLoS One* 11:e0165800. doi: 10.1371/journal.pone.0165800
- Huskin, I., Anadón, R., Medina, G., Head, R. N., and Harris, R. P. (2001). Mesozooplankton distribution and copepod grazing in the subtropical Atlantic near the Azores: influence of mesoscale structures. *J. Plankton Res.* 23, 671–691. doi: 10.1093/plankt/23.7.671
- IPCC (2013). “Climate change 2013: the physical science basis,” in *Contribution of Working Group I to the Fifth Assessment Report of the Intergovernmental Panel on Climate Change*, eds T.F. Stocker, D. Qin, G.-K. Plattner, M. Tignor, S.K. Allen, J. Boschung et al. (Cambridge: Cambridge University Press).
- Isari, S., Zervoudaki, S., Peters, J., Papantoniou, G., Pelejero, C., and Saiz, E. (2015). Lack of evidence for elevated CO₂-induced bottom-up effects on marine copepods: a dinoflagellate–calanoid prey–predator pair. *ICES. J. Mar. Sci.* 73, 650–658. doi: 10.1093/icesjms/fsv078
- Itoh, H., Nakata, K., Sasaki, K., Ichikawa, T., and Hidaka, K. (2014). Seasonal and diel changes in the vertical distribution of oncaeid copepods in the epipelagic zone of the Kuroshio Extension region. *Plankton Benthos Res.* 9, 1–14. doi: 10.3800/pbr.9.1
- Jain, A. K. (2010). Data clustering: 50 years beyond K-means. *Pattern Recognit. Lett.* 31, 651–666. doi: 10.1016/j.patrec.2009.09.011
- Kemp, W. M., Brooks, M. T., and Hood, R. R. (2001). Nutrient enrichment, habitat variability and trophic transfer efficiency in simple models of pelagic ecosystems. *Mar. Ecol. Progr. Ser.* 223, 73–87. doi: 10.3354/meps223073
- Kleppel, G. S. (1993). On the diets of calanoid copepods. *Mari. Ecol. Progr. Ser.* 99, 183–195. doi: 10.3354/meps099183
- Koski, M., Kiørboe, T., and Takahashi, K. (2005). Benthic life in the pelagic: aggregate encounter and degradation rates by pelagic harpacticoid copepods. *Limnol. Oceanogr.* 50, 1254–1263. doi: 10.4319/lo.2005.50.4.1254
- Kroeker, K. J., Kordas, R. L., Crim, R., Hendriks, I. E., Ramajo, L., Singh, G. S., et al. (2013). Impacts of ocean acidification on marine organisms: quantifying sensitivities and interaction with warming. *Glob. Change Biol.* 19, 1884–1896. doi: 10.1111/gcb.12179
- Leblanc, K., Aristegui, J., Armand, L., Assmy, P., Beker, B., Bode, A., et al. (2012). A global diatom database: abundance, biovolume and biomass in the world ocean. *Earth Syst. Sci. Data* 4, 149–165. doi: 10.5194/essd-4-149-2012
- Legendre, P., and Anderson, M. J. (1999). Distance-based redundancy analysis: testing multispecies responses in multifactorial ecological experiments. *Ecol. Monogr.* 69, 1–24. doi: 10.1890/0012-9615(1999)069[0001:DBRATM]2.0.CO;2
- Lesniewski, T. J., Gambill, M., Holst, S., Peck, M. A., Algueró-Muñiz, M., Haunost, M., et al. (2015). Effects of food and CO₂ on growth dynamics of polyps of two scyphozoan species (*Cyanea capillata* and *Chrysaora hysoscella*). *Mar. Biol.* 162, 1371–1382. doi: 10.1007/s00227-015-2660-6
- Lewis, C. N., Brown, K. A., Edwards, L. A., Cooper, G., and Findlay, H. S. (2013). Sensitivity to ocean acidification parallels natural pCO₂ gradients experienced by Arctic copepods under winter sea ice. *Proc. Natl. Acad. Sci. U.S.A.* 110, E4960–E4967. doi: 10.1073/pnas.1315162110
- Lischka, S., Bach, L. T., Schulz, K. G., and Riebesell, U. (2017). Ciliate and mesozooplankton community response to increasing CO₂ levels in the Baltic Sea: insights from a large-scale mesocosm experiment. *Biogeosciences* 14, 447–466. doi: 10.5194/bg-14-447-2017
- Lischka, S., Büdenbender, J., Boxhammer, T., and Riebesell, U. (2011). Impact of ocean acidification and elevated temperatures on early juveniles of the polar shelled pteropod *Limacina helicina*: mortality, shell degradation, and shell growth. *Biogeosciences* 8, 919–932. doi: 10.5194/bg-8-919-2011
- Lischka, S., Stange, P., and Riebesell, U. (2018). Response of pelagic calcifiers (Foraminifera, Thecosomata) to ocean acidification during oligotrophic and simulated up-welling conditions in the Subtropical North Atlantic off Gran Canaria. *Front. Mar. Sci.* 5:379. doi: 10.3389/fmars.2018.00379
- Maar, M., Visser, A. W., Nielsen, T. G., Stips, A., and Saito, H. (2006). Turbulence and feeding behaviour affect the vertical distributions of *Oithona similis* and *Microsetella norvegica*. *Mar. Ecol. Progr. Ser.* 313, 157–172. doi: 10.3354/meps313157
- Menden-Deuer, S., and Lessard, E. J. (2000). Carbon to volume relationships for dinoflagellates, diatoms, and other protist plankton. *Limnol. Oceanogr.* 45, 569–579. doi: 10.4319/lo.2000.45.3.0569
- Menzel, D. W., and Ryther, J. H. (1961). Zooplankton in the Sargasso Sea off Bermuda and its relation to organic production. *J. Conseil* 26, 250–258. doi: 10.1093/icesjms/26.3.250

- Meunier, C. L., Algueró-Muñiz, M., Horn, H. G., Lange, J. A. F., and Boersma, M. (2016). Direct and indirect effects of near-future pCO₂ levels on zooplankton dynamics. *Mar. Freshw. Res.* 68, 373–380. doi: 10.1071/MF15296
- Montagnas, D. J. S., Strüder-Kypke, M. C., Kypke, M. R., Agatha, S., and Warwick, J. (2001). *The Planktonic Ciliate Project: The User-Friendly Guide to Coastal Planktonic Ciliates*. Available at: <http://www.zooplankton.cn/ciliate>
- Moyano, M., Rodríguez, J. M., and Hernández-León, S. (2009). Larval fish abundance and distribution during the late winter bloom off Gran Canaria Island, Canary Islands. *Fish. Oceanogr.* 18, 51–61. doi: 10.1111/j.1365-2419.2008.00496.x
- Niehoff, B., Schmithusen, T., Knuppel, N., Daase, M., Czerny, J., and Boxhammer, T. (2013). Mesozooplankton community development at elevated CO₂ concentrations: results from a mesocosm experiment in an Arctic fjord. *Biogeosciences* 10, 1391–1406. doi: 10.5194/bg-10-1391-2013
- Ohtsuka, S., Kubo, N., Okada, M., and Gushima, K. (1993). Attachment and feeding of pelagic copepods on larvacean houses. *J. Oceanogr.* 49, 115–120. doi: 10.1007/bf02234012
- Ojeda, A. (1998). *Dinoflagelados de Canarias. Estudio taxonómico y ecológico*. Ph.D. thesis, University of Las Palmas de Gran Canaria, Las Palmas.
- Paul, A. J., Bach, L. T., Schulz, K. G., Boxhammer, T., Czerny, J., Achterberg, E. P., et al. (2015). Effect of elevated CO₂ on organic matter pools and fluxes in a summer Baltic Sea plankton community. *Biogeosciences* 12, 6181–6203. doi: 10.5194/bg-12-6181-2015
- Pedersen, S. A., Hansen, B. H., Altin, D., and Olsen, A. J. (2013). Medium-term exposure of the North Atlantic copepod *Calanus finmarchicus* (Gunnerus, 1770) to CO₂-acidified seawater: effects on survival and development. *Biogeosciences* 10, 7481–7491. doi: 10.5194/bg-10-7481-2013
- Putt, M., and Stoecker, D. K. (1989). An experimentally determined carbon: volume ratio for marine “oligotrichous” ciliates from estuarine and coastal waters. *Limnol. Oceanogr.* 34, 1097–1103. doi: 10.4319/lo.1989.34.6.1097
- Queirós, A. M., Fernandes, J. A., Faulwetter, S., Nunes, J., Rastrick, S. P. S., Mieszkowska, N., et al. (2015). Scaling up experimental ocean acidification and warming research: from individuals to the ecosystem. *Glob. Change Biol.* 21, 130–143. doi: 10.1111/gcb.12675
- Quevedo, M., and Anadón, R. (2001). Protist control of phytoplankton growth in the subtropical north-east Atlantic. *Mar. Ecol. Progr. Ser.* 221, 29–38. doi: 10.3354/meps221029
- Riebesell, U., Aberle-Malzahn, N., Achterberg, E. P., Algueró-Muñiz, M., Alvarez-Fernandez, S., Arístegui, J., et al. (2018). Toxic algal bloom induced by ocean acidification disrupts the pelagic food web. *Nat. Clim. Change* 8, 1082–1086. doi: 10.1038/s41558-018-0344-1
- Riebesell, U., Czerny, J., von Bröckel, K., Boxhammer, T., Büdenbender, J., Deckelnick, M., et al. (2013). Technical Note: a mobile sea-going mesocosm system – new opportunities for ocean change research. *Biogeosciences* 10, 1835–1847. doi: 10.5194/bg-10-1835-2013
- Riebesell, U., and Gattuso, J.-P. (2015). Lessons learned from ocean acidification research. *Nat. Clim. Change* 5, 12–14. doi: 10.1038/nclimate2456
- Rose, J. M., Feng, Y., Gobler, C. J., Gutierrez, R., Hare, C. E., Leblanc, K., et al. (2009). Effects of increased pCO₂ and temperature on the North Atlantic spring bloom. II. Microzooplankton abundance and grazing. *Mar. Ecol. Progr. Ser.* 388, 27–40. doi: 10.3354/meps08134
- Rossoll, D., Bermudez, R., Hauss, H., Schulz, K. G., Riebesell, U., Sommer, U., et al. (2012). Ocean acidification-induced food quality deterioration constrains trophic transfer. *PLoS One* 7:e34737. doi: 10.1371/journal.pone.0034737
- Rossoll, D., Sommer, U., and Winder, M. (2013). Community interactions dampen acidification effects in a coastal plankton system. *Mar. Ecol. Progr. Ser.* 486, 37–46. doi: 10.3354/meps10352
- Sabine, C. L., Feely, R. A., Gruber, N., Key, R. M., Lee, K., Bullister, J. L., et al. (2004). The oceanic sink for anthropogenic CO₂. *Science* 305, 367–371. doi: 10.1126/science.1097403
- Sala, M. M., Aparicio, F. L., Balagué, V., Boras, J. A., Borrell, E., Cardelús, C., et al. (2015). Contrasting effects of ocean acidification on the microbial food web under different trophic conditions. *ICES J. Mar. Sci.* 73, 670–679. doi: 10.1093/icesjms/fsv130
- Sangrà, P., Pascual, A., Rodríguez-Santana, Á., Machín, F., Mason, E., McWilliams, J. C., et al. (2009). The canary eddy corridor: a major pathway for long-lived eddies in the subtropical North Atlantic. *Deep Sea Res. Part I* 56, 2100–2114. doi: 10.1016/j.dsr.2009.08.008
- Schmoker, C., Arístegui, J., and Hernández-León, S. (2012). Planktonic biomass variability during a late winter bloom in the subtropical waters off the Canary Islands. *J. Mar. Syst.* 95, 24–31. doi: 10.1016/j.jmarsys.2012.01.008
- Schmoker, C., Ojeda, A., and Hernández-León, S. (2014). Patterns of plankton communities in subtropical waters off the Canary Islands during the late winter bloom. *J. Sea Res.* 85, 155–161. doi: 10.1016/j.seares.2013.05.002
- Schoo, K. L., Malzahn, A. M., Krause, E., and Boersma, M. (2013). Increased carbon dioxide availability alters phytoplankton stoichiometry and affects carbon cycling and growth of a marine planktonic herbivore. *Mar. Biol.* 160, 2145–2155. doi: 10.1007/s00227-012-2121-4
- Sherr, E. B., and Sherr, B. F. (2007). Heterotrophic dinoflagellates: a significant component of microzooplankton biomass and major grazers of diatoms in the sea. *Mar. Ecol. Progr. Ser.* 352, 187–197. doi: 10.3354/meps07161
- Sieburth, J. M., Smetacek, V., and Lenz, J. (1978). Pelagic ecosystem structure: heterotrophic compartments of the plankton and their relationship to plankton size fractions. *Limnol. Oceanogr.* 23, 1256–1263. doi: 10.4319/lo.1978.23.6.1256
- Silva, N. J., Tang, K. W., and Lopes, R. M. (2013). Effects of microalgal exudates and intact cells on subtropical marine zooplankton. *J. Plankton Res.* 35, 855–865. doi: 10.1093/plankt/ftt026
- Sswat, M., Stiasny, M. H., Taucher, J., Algueró-Muñiz, M., Bach, L. T., Jutfelt, F., et al. (2018). Food web changes under ocean acidification promote herring larvae survival. *Nat. Ecol. Evol.* 2, 836–840. doi: 10.1038/s41559-018-0514-6
- Stange, P., Bach, L. T., Taucher, J., Boxhammer, T., Krebs, L., Algueró-Muñiz, M., et al. (2018). Ocean acidification-induced food web changes slow down degradation of sinking particles in an upwelling-stimulated oligotrophic plankton community. *Front. Mar. Sci.* 5:140. doi: 10.3389/fmars.2018.00140
- Stoecker, D. K., and Capuzzo, J. M. (1990). Predation on Protozoa: its importance to zooplankton. *J. Plankton Res.* 12, 891–908. doi: 10.1093/plankt/12.5.891
- Suffrian, K., Simonelli, P., Nejstgaard, J. C., Putzeys, S., Carotenuto, Y., and Antia, A. N. (2008). Microzooplankton grazing and phytoplankton growth in marine mesocosms with increased CO₂ levels. *Biogeosciences* 5, 1145–1156. doi: 10.5194/bg-5-1145-2008
- Suzuki, K., Nakamura, Y., and Hiromi, J. (1999). Feeding by the small calanoid copepod *Paracalanus* sp. on heterotrophic dinoflagellates and ciliates. *Aquat. Microb. Ecol.* 17, 99–103. doi: 10.3354/ame017099
- Taucher, J., Bach, L. T., Boxhammer, T., Nauendorf, A., Montero, M. F., Achterberg, E. P., et al. (2017a). Impacts of ocean acidification on oligotrophic plankton communities in the subtropical North Atlantic: an *in situ* mesocosm study reveals community-wide responses to elevated CO₂ during a simulated deep-water upwelling event. *Front. Mar. Sci.* 4:85. doi: 10.3389/fmars.2017.00085
- Taucher, J., Haunost, M., Boxhammer, T., Bach, L. T., Algueró-Muñiz, M., and Riebesell, U. (2017b). Influence of ocean acidification on plankton community structure during a winter-to-summer succession: an imaging approach indicates that copepods can benefit from elevated CO₂ via indirect food web effects. *PLoS One* 12:e0169737. doi: 10.1371/journal.pone.0169737
- R Core Team (2012). *R: A Language and Environment for Statistical Computing*. Vienna: R.F.F.S. Computing.
- Thor, P., and Dupont, S. (2015). Transgenerational effects alleviate severe fecundity loss during ocean acidification in a ubiquitous planktonic copepod. *Glob. Change Biol.* 21, 2261–2271. doi: 10.1111/gcb.12815
- Tomas, C. R., and Hasle, G. R. (1997). *Identifying Marine Phytoplankton*. San Diego, CA: Academic Press.
- Troedsson, C., Bouquet, J. M., Lobon, C. M., Novac, A., Nejstgaard, J. C., Dupont, S., et al. (2013). Effects of ocean acidification, temperature and nutrient regimes on the appendicularian *Oikopleura dioica*: a mesocosm study. *Mar. Biol.* 160, 2175–2187. doi: 10.1007/s00227-012-2137-9
- Turner, J. T. (2004). The importance of small planktonic copepods and their roles in pelagic marine food webs. *Zool. Stud.* 43, 255–266.
- Turner, J. T., and Tester, P. A. (1989). “Zooplankton feeding ecology: copepod grazing during an expatriate red tide,” in *Novel Phytoplankton Blooms: Causes and Impacts of Recurrent Brown Tides and Other Unusual Blooms*, eds E. M. Cosper, V. M. Bricelj, and E. J. Carpenter (Berlin: Springer), 359–374. doi: 10.1029/CE035p0359
- Utermöhl, V. H. (1958). Zur Vervollkommenung der quantitativen Phytoplankton-Methodik. *Mitt Int Ver Theor Angew Limnol* 9, 1–38. doi: 10.1080/05384680.1958.11904091
- Wells, M. L., Trainer, V. L., Smayda, T. J., Karlson, B. S. O., Trick, C. G., Kudela, R. M., et al. (2015). Harmful algal blooms and climate change: learning from

- the past and present to forecast the future. *Harmful Algae* 49, 68–93. doi: 10.1016/j.hal.2015.07.009
- Winder, M., Bouquet, J.-M., Rafael Bermúdez, J., Berger, S. A., Hansen, T., Brandes, J., et al. (2017). Increased appendicularian zooplankton alter carbon cycling under warmer more acidified ocean conditions. *Limnol. Oceanogr.* 62, 1541–1551. doi: 10.1002/lno.10516
- Wood, S. N. (2006). *Generalized Additive Models: an Introduction With R*. Boca Raton, FL: CRC Press. doi: 10.1201/9781420010404
- Zuur, A., Ieno, E. N., Walker, N., Saveliev, A. A., and Smith, G. M. (2009). *Mixed Effects Models and Extensions in Ecology with R*. New York, NY: Springer-Verlag. doi: 10.1007/978-0-387-87458-6

Conflict of Interest Statement: The authors declare that the research was conducted in the absence of any commercial or financial relationships that could be construed as a potential conflict of interest.

Copyright © 2019 Algueró-Muñiz, Horn, Alvarez-Fernandez, Spisla, Aberle, Bach, Guan, Achterberg, Riebesell and Boersma. This is an open-access article distributed under the terms of the Creative Commons Attribution License (CC BY). The use, distribution or reproduction in other forums is permitted, provided the original author(s) and the copyright owner(s) are credited and that the original publication in this journal is cited, in accordance with accepted academic practice. No use, distribution or reproduction is permitted which does not comply with these terms.



Effects of Elevated CO₂ on a Natural Diatom Community in the Subtropical NE Atlantic

Lennart T. Bach^{1*}, Nauzet Hernández-Hernández², Jan Taucher¹, Carsten Spisla¹, Claudia Sfora¹, Ulf Riebesell¹ and Javier Aristegui²

¹ Biological Oceanography, GEOMAR Helmholtz Centre of Ocean Research Kiel, Kiel, Germany, ² Instituto de Oceanografía y Cambio Global, Universidad de Las Palmas de Gran Canaria, Las Palmas, Spain

OPEN ACCESS

Edited by:

Laura Anne Bristow,
University of Southern Denmark,
Denmark

Reviewed by:

Koji Suzuki,
Hokkaido University, Japan
Alex J. Poulton,
The Lyell Centre, United Kingdom

*Correspondence:

Lennart T. Bach
lbach@geomar.de

Specialty section:

This article was submitted to
Marine Biogeochemistry,
a section of the journal
Frontiers in Marine Science

Received: 31 October 2018

Accepted: 11 February 2019

Published: 01 March 2019

Citation:

Bach LT, Hernández-Hernández N, Taucher J, Spisla C, Sfora C, Riebesell U and Aristegui J (2019) Effects of Elevated CO₂ on a Natural Diatom Community in the Subtropical NE Atlantic. *Front. Mar. Sci.* 6:75. doi: 10.3389/fmars.2019.00075

Diatoms are silicifying phytoplankton contributing about one quarter to primary production on Earth. Ocean acidification (OA) could alter the competitiveness of diatoms relative to other taxa and/or lead to shifts among diatom species. In spring 2016, we set up a plankton community experiment at the coast of Gran Canaria (Canary Islands, Spain) to investigate the response of subtropical diatom assemblages to elevated seawater *p*CO₂. Therefore, natural plankton communities were enclosed for 32 days in *in situ* mesocosms (~8 m³ volume) with a *p*CO₂ gradient ranging from 380 to 1140 μatm. Halfway through the study we added nutrients to all mesocosms (N, P, Si) to simulate injections through eddy-induced upwelling which frequently occurs in the region. We found that the total diatom biomass remained unaffected during oligotrophic conditions but was significantly positively affected by high CO₂ after nutrient enrichment. The average cell volume and carbon content of the diatom community increased with CO₂. CO₂ effects on diatom biomass and species composition were weak during oligotrophic conditions but became quite strong above ~620 μatm after the nutrient enrichment. We hypothesize that the proliferation of diatoms under high CO₂ may have been caused by a fertilization effect on photosynthesis in combination with reduced grazing pressure. Our results suggest that OA in the subtropics may strengthen the competitiveness of (large) diatoms and cause changes in diatom community composition, mostly under conditions when nutrients are injected into oligotrophic systems.

Keywords: ocean acidification, climate change, mesocosm, food web, phytoplankton, Bacillariophyceae

INTRODUCTION

Diatoms are a group of globally distributed phytoplankton, with an estimated contribution of ~25% to global primary production (Nelson et al., 1995; Field et al., 1998; Tréguer and De La Rocha, 2013). All diatom species share the trait of protecting the organic part of the cell with a shell (frustule) made of amorphous silica (opal), probably to reduce grazing pressure (Hamm and Smetacek, 2007; Pondaven et al., 2007; Friedrichs et al., 2013; Liu et al., 2016). To form the frustule, diatoms require dissolved silicate as an additional nutrient, which is often limiting in seawater and hence limiting their proliferation (Brzezinski and Nelson, 1996). Diatoms are strong competitors

and typically dominate phytoplankton communities early in the succession when nutrients are sufficiently available (Sarhou et al., 2005).

There are at least 30,000 extant diatom species which span a size range from under 3 micro- up to a few millimeters (Mann and Vanormelingen, 2013). They occur as single cells or cell chains in benthic and/or pelagic habitats, and have free-living, surface-associated, symbiotic, or parasitic lifestyles (Armbrust, 2009; Mann and Vanormelingen, 2013).

Changes in diatom community composition can reorganize the flux of elements in oceans and the flow of energy within food webs (Armbrust, 2009; Tréguer et al., 2018). For example, particulate organic carbon sequestration to the deep ocean was shown to be 1.8 times higher in 1989 when the North Atlantic spring bloom was dominated by a larger species compared to the following year when smaller ones dominated (Boyd and Newton, 1995). Likewise, energy transfer to higher trophic levels is likely to be more efficient in assemblages where primary production is dominated by larger diatoms since less trophic intermediates are involved (Sommer et al., 2002). Thus, it is essential to determine how diatom community composition could be affected by different environmental stressors and in different ocean regions due to their enormous relevance for the Earth system.

In the present study we investigated how ocean acidification (OA) – the anthropogenic perturbation of seawater carbonate chemistry – could affect the composition of natural diatom communities in the subtropical NE Atlantic. Therefore, we set up a mesocosm experiment at the coast of Gran Canaria and perturbed the enclosed plankton communities with different CO₂ concentrations. In the study region, diatom blooms often occur in association with meso-/sub-mesoscale structures such as upwelling filaments, zonal fronts, or eddies which inject nutrients into the euphotic zone (Barton et al., 1998; Aristegui et al., 2004; McGillicuddy et al., 2007; Anabalón et al., 2014). To account for this, the mesocosms were enriched with inorganic nutrients (N, P, Si) halfway through the experiment. This allowed us to investigate CO₂ effects on diatoms during oligotrophic conditions (phase I) and during a subsequent nutrient injection to the euphotic zone (phase II).

MATERIALS AND METHODS

Mesocosm Design, Deployment, and Maintenance

On February 23, 2016, we deployed eight *in situ* mesocosms (M1–M8) at the pier of Taliarte harbor, on the eastern coast of Gran Canaria (Canary Islands, 27° 59' 24" N, 15° 22' 8" W). The cylindrical mesocosm bags (Ø 2 m, 2.5 m long) were made of transparent polyurethane foil (PU), which is also used for the larger version of the KOSMOS mesocosm design (Riebesell et al., 2013). The PU bags were installed in a floatation frame made of polyethylene with steel reinforcements and deployed inside the harbor (Figure 1). The floatation

frame was fixed on the pier and on mooring weights on the water side. A pulley system attached to the mooring weights allowed us to move the entire structure ~2 m away from the pier in between samplings. This was necessary to reduce the influence of the pier on the light environment inside the mesocosms.

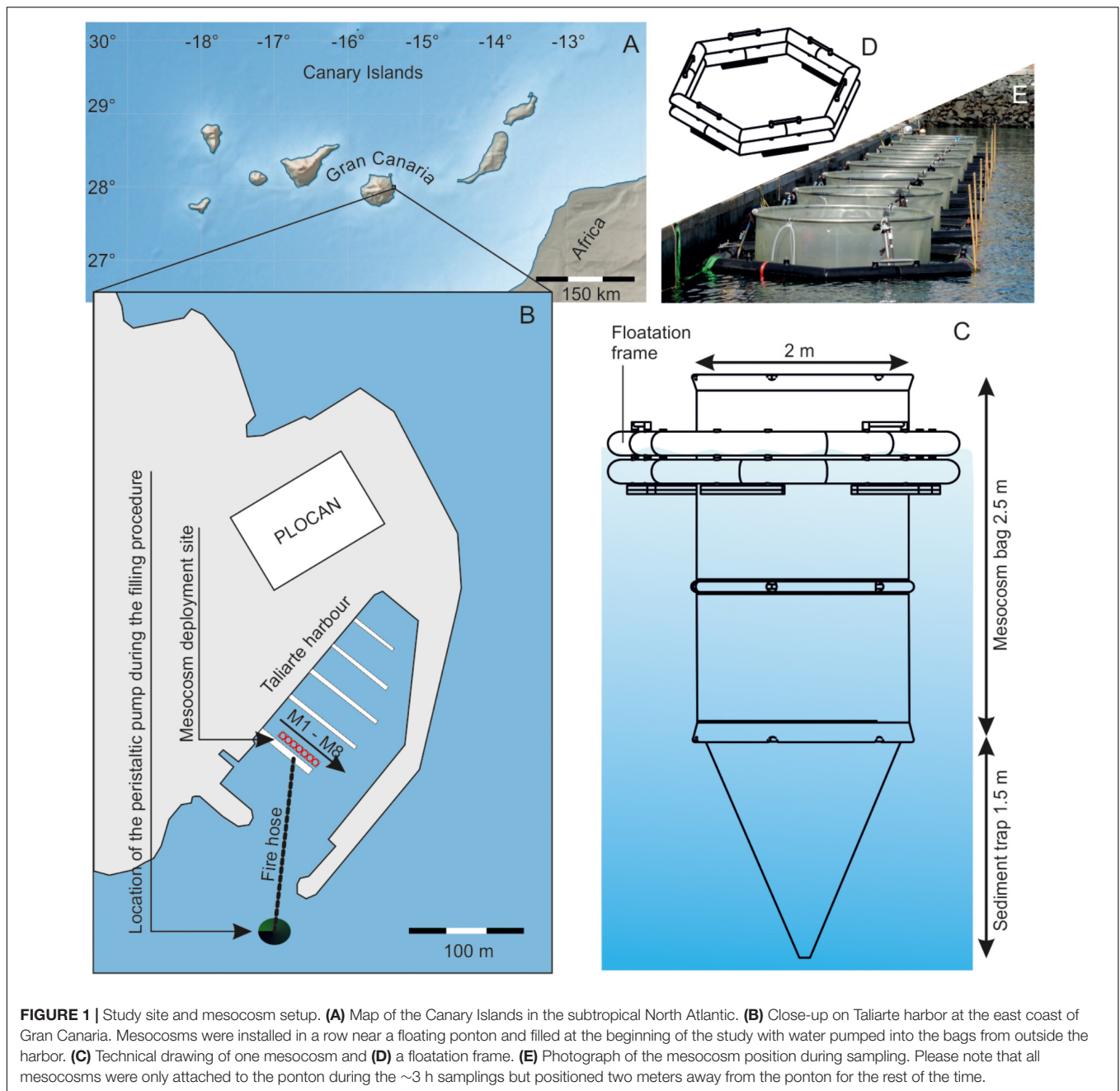
Conical sediment traps were attached to the bottom of the bags, thereby creating 8 isolated volumes (Figure 1). The sediment traps were 1.5 m long and similar to the KOSMOS design (Boxhammer et al., 2016). The mesocosms were initially empty and filled in the morning of March 2 by pumping seawater from ~30 m outside Taliarte harbor into the enclosures (Figure 1). Seawater was pumped with a peristaltic pump from 3 to 5 m depth through a hose (Ø 50 mm with a 3000 µm mesh attached to the inlet) into a central volume on the pier, from where the seawater was simultaneously distributed with separate hoses (Ø 37 mm) into the mesocosms. The entire filling procedure lasted ~4.5 h, and we tried to keep the stress level for pumped organisms low by restricting the speed of the peristaltic pump (3.9 L/s). We cannot fully ensure, however, that particularly sensitive organisms weren't harmed and excluded from the experiment. Each mesocosm contained a volume of ~8 m³ after filling. The filling marks the beginning of the experiment and is hereafter referred to as day -3, while day 0 is the day when the CO₂ manipulation started (see section "Experimental Design").

The mesocosm PU foil must be cleaned on a regular basis to avoid the growth of benthic organisms and to maintain light transmission. The outer sides of the mesocosm bags were cleaned by divers with brushes on days 6, 14, 17, and 25. The inner sides were cleaned on days 6, 14, 18, and 25 with a custom made cleaning ring which has approximately the same diameter as the mesocosm bags and thoroughly wipes the foil while sliding downward (Riebesell et al., 2013). The sediment traps were cleaned from the inside on day 15 with custom made "magnetic brushes" since the cleaning ring could not reach this part of the mesocosms. The magnetic brushes are basically two brushes that connect through the PU foil with a magnet and are operated from the outside by divers.

M1 was damaged early in the experiment (day 4) and therefore excluded from the analysis.

Experimental Design

A gradient of 7 CO₂ concentrations (ambient to on average ~1140 µatm) was established in 3 steps over 3 days (day 0 until day 2) by adding differential amounts [between 35 L (M7) and 70 L (M6)] of CO₂-saturated seawater evenly to the water columns of M2–M8 with a custom-made distribution device (Riebesell et al., 2013). M5 was left unperturbed and served as a control but received non-aerated seawater during CO₂ manipulations. CO₂-saturated seawater had to be added at regular intervals during the experiment (days 6, 8, 10, 14, 18, and 25) to counteract CO₂ outgassing at the surface. On day 18, we added NaNO₃, Na₂HPO₄, and Na₂SiO₃ (3.43 ± 0.32, 0.16 ± 0.01, 1.63 ± 0.12 µmol L⁻¹, mean ± SD between



mesocosms) to each mesocosm to simulate an upwelling event of nutrient rich deep-water.

Sampling

Sinking detritus is collected in the terminal end of the sediment trap and removed from there through a hose connected to a vacuum system (Boxhammer et al., 2016). Sediment traps were emptied every second day to avoid resuspension and anoxic conditions at the bottom of the mesocosms.

Water samples from each mesocosm were collected between 9:00 and 11:00 a.m., either every second day (day –2–17 and 25–29) or daily (day 19–25) to obtain higher temporal

resolution right after nutrient fertilization. Sampling was slightly later on day –3 (1:00–2:30 p.m.) since we wanted to have samples directly after filling the mesocosms with seawater. As sampling gear, we used 2.5 m long polypropylene pipes equipped with a pulley system to close the tube at the upper and the lower end. The pipe was left open on both ends and carefully lowered vertically into the water column until the lower end reached a depth of 2.5 m. The upper and the lower end were then closed from the surface with the pulley system, thereby enclosing a vertically integrated water sample. The integrated sample was gently mixed and transferred from the pipes into different sampling bottles. Between 3 and 5

hauls with the pipes were made to sample enough volume for all measurements.

Samples for dissolved inorganic carbon (DIC), total alkalinity (TA), and dissolved inorganic nutrient concentrations [$\text{NO}_3^- + \text{NO}_2^-$, NH_4^+ , PO_4^{3-} , Si(OH)_4] were transferred directly from the sampling tubes into air-tight 1 L polycarbonate (carbonate chemistry) and 0.25 L polyethylene (PE) bottles (nutrients), respectively. DIC samples were carefully transferred in the 1 L bottles allowing considerable overflow before closing them with negligible headspace (i.e., <1 mL). Both carbonate chemistry and nutrient samples were transported in a cooling box to the land-based laboratories of the Plataforma Oceánica de Canarias (PLOCAN) which is located next to Taliarte harbor and hosted our study (Figure 1). DIC and TA samples were pumped from the 1 L bottles through a syringe filter (0.2 μm , Whatman) into air-tight 50 mL glass bottles (DIC) and 100 mL PE bottles (TA, nutrients), respectively. We allowed considerable overflow before closing the DIC glass bottles to minimize gas exchange. Filtered DIC, TA, and nutrient samples were stored at 4°C until analysis on the same day.

The seawater used to measure chlorophyll *a* (chl_a) and biogenic silica (BSi) concentrations, as well as diatom cell abundance, was carefully transferred from the sampling tubes into 10 L PE carboys and transported into a climate chamber at PLOCAN set to 15°C. Chl_a and BSi samples were tapped from the carboys (0.5–0.2 L depending on concentration), filtered ($\Delta\text{pressure} = 200$ mbar) on glass fiber filters (chl_a, GF/F nominal pore size = 0.7 μm) or cellulose acetate filters (BSi, pore size = 0.65 μm), and stored at –20°C until analysis. Microscopy samples were transferred from the carboys in 200 mL brown glass bottles, fixed with acidic Lugol solution (1% final concentration), and stored for maximally 5 months at room temperature until analysis.

Mesozooplankton (MesoZP) samples were collected every 4 days between 11 a.m. and 1 p.m. with vertical net hauls from 2.5 m to the surface. Sampling was carried out with a 0.6 m long Apstein net (55 μm mesh size), which had a 0.09 m diameter cone-shaped opening. Two consecutive net hauls per mesocosm during every sampling resulted in a sample volume of 32 L for each mesocosm.

Temperature (T) and salinity (S) were measured on every sampling day around noon time with a hand-held self-logging CTD probe (CTD60M, Sea and Sun Technologies). Average T and S were calculated by averaging the vertical profile from the surface (0.3 m) to the bottom of the sediment traps (~3.5 m).

Analytical Procedures

$\text{NO}_3^- + \text{NO}_2^-$ (NO_x^-), PO_4^{3-} (P), and Si(OH)_4 (Si) concentrations were measured photometrically within 10 h after sampling (Hansen and Koroleff, 1999). NH_4^+ concentrations were measured fluorometrically in the same timeframe (Holmes et al., 1999). Precision of nutrient measurements was generally well below $\pm 10\%$ as determined with triplicate measurements of each sample. DIC concentrations were measured within 10 h after sampling with an Autonomous Infra-Red Inorganic Carbon Analyser (AIRICA) system (Marianda, Kiel, Germany). Each sample was measured three times and the precision was in most

cases better than $\pm 3 \mu\text{mol kg}^{-1}$. TA was determined in an open cell titration within 24 h after sampling (Dickson et al., 2003). Each sample was measured twice with a precision that was in most cases better than $\pm 4 \mu\text{mol kg}^{-1}$. Both DIC and TA measurements were accuracy-controlled by measurements of certified reference materials (Dickson et al., 2007). $p\text{CO}_2$ partial pressure was calculated from measured (water-column averaged) temperature and salinity, as well as concentrations of DIC, TA, PO_4^{3-} and Si(OH)_4 using Seacarb (Lavigne et al., 2011). We used the recommended default setting and the carbonate dissociation constants (K_1 and K_2) determined by Lueker et al. (2000). Chl_a was extracted 1–2 days after sampling in acetone (90%) in plastic vials, by homogenization of the filters using glass beads and a cell mill (5 min). After centrifugation (10 min, 800 g, 4°C), the supernatant was analyzed on a fluorometer (TURNER 10-AU) following Welschmeyer (1994). The fluorometer was calibrated with spinach chl_a extract as described by Strickland and Parsons (1972). BSi concentrations were determined by leaching the samples with 0.1 M NaOH for 135 min at 85°C. The leaching process was terminated with 0.05 M H₂SO₄ and dissolved silicate was measured by spectrophotometry following Hansen and Koroleff (1999).

Diatom samples were transferred from the brown glass sampling bottles into 25–100 mL Utermöhl chambers. After at least 24 h of sedimentation, cells were counted with an inverted light microscope (Zeiss Axiovert 100). Cells were classified to the lowest identifiable taxonomical level. Diatom cell volumes were estimated following Olenina et al. (2006). We tried to measure the relevant shape dimensions needed for the geometrical formulas but in cases where this was not possible we used species dimensions provided by Olenina et al. (2006) (see Table 1). Carbon biomasses of individual species ($\mu\text{g C L}^{-1}$) were calculated with the volume to carbon transfer functions provided by Menden-Deuer and Lessard (2000). Diatom diversity was estimated with the Shannon Weaver diversity index (H'):

$$H' = - \sum_i \frac{B_i}{B_{\text{total}}} \cdot \ln \frac{B_i}{B_{\text{total}}} \quad (1)$$

where B_i is the C biomass of diatom species *i* and B_{total} the C biomass of all diatoms. Higher H' is equivalent to a higher diversity.

The average cellular carbon quota (C_q) of the diatom community was calculated as:

$$C_q = \frac{\sum_i C_i N_i}{N_{\text{total}}} \quad (2)$$

where C_i is the carbon content of diatom species *i*, N_i is the abundance of diatom species *i*, and N_{total} is the abundance of all diatoms.

MesoZP was preserved with ethanol (70%) and transferred into a Bogorov counting chamber where it was quantified and classified to the lowest possible taxonomic level using a Leica stereomicroscope (MZ12). Copepodites and adult copepods of each species were counted as separate categories but we pooled them for our analysis. Accordingly, MesoZP abundances shown

in this paper are copepodites + adults for each species. *Nauplii* species were not distinguished and counted as one group.

Data Analyses

To analyze the dataset, we split the experiment into 3 consecutive phases. Phase 0 was the time before the CO₂ manipulation (day –3–day –1). Phase I (day 0–day 17) comprised the oligotrophic conditions that prevailed prior to the nutrient addition on day 18. Phase II (day 19–day 29) comprised the phytoplankton bloom that formed under eutrophic conditions after nutrient fertilization. For the analyses we calculated the phase averages of *p*CO₂ (i.e., the independent variable) and the phase averages

of the various dependent variables (e.g., chl *a* or BSi). Shapiro-Wilk tests revealed non-normal distribution of the datasets so that they were log-transformed. Afterward, we ran regression analyses with the log-transformed data using R¹ as in Schulz et al. (2013) and Paul et al. (2015). CO₂ was considered to influence the abundance of individual diatom species when we detected a significant (*p* < 0.05) correlation between *p*CO₂ and diatom abundance.

Dissimilarities in diatom community composition between CO₂ levels were mapped by means of Principal Coordinate

¹<http://www.r-project.org>

TABLE 1 | List of all diatom species enumerated by means of light microscopy.

Species	Shape	Formula	Dimensions (μm)	Volume (μm ³)	C (pg)	Measured/referenced
<i>Actinocyclus</i> spp.	Sphere	$\pi/6 \cdot d^3$	<i>d</i> = 25	8177	429	Measured
<i>Asterionellopsis glacialis</i>	Cone +half Sphere-40%	$(\pi/12 \cdot d^2 \cdot h) - 40\%$	<i>d</i> = 5; <i>h</i> = 30	118	14	Measured
<i>Bacteriastrum hyalinum</i>	Cylinder	$\pi/4 \cdot d^2 \cdot h$	<i>d</i> = 15; <i>h</i> = 20	3533	217	Measured
<i>Cerataulina</i>	Cylinder	$\pi/4 \cdot d^2 \cdot h$	<i>d</i> = 25; <i>h</i> = 80	39250	1531	Measured
<i>Chaetoceros</i> spp. <10 μm	Oval cylinder	$\pi/4 \cdot d_1 \cdot d_2 \cdot h$	<i>d</i> ₁ = 7; <i>d</i> ₂ = 6; <i>h</i> = 7	229	24	Referenced
<i>Chaetoceros</i> spp. >10 μm	Oval cylinder	$\pi/4 \cdot d_1 \cdot d_2 \cdot h$	<i>d</i> ₁ = 13; <i>d</i> ₂ = 10; <i>h</i> = 20	2041	139	Referenced
<i>Chaetoceros affinis</i>	Oval cylinder	$\pi/4 \cdot d_1 \cdot d_2 \cdot h$	<i>d</i> ₁ = 15; <i>d</i> ₂ = 10; <i>h</i> = 25	2944	187	Referenced
<i>Chaetoceros atlanticus</i>	Oval cylinder	$\pi/4 \cdot d_1 \cdot d_2 \cdot h$	<i>d</i> ₁ = 10; <i>d</i> ₂ = 7; <i>h</i> = 10	550	48	Measured
<i>Chaetoceros curvisetus</i>	Oval cylinder	$\pi/4 \cdot d_1 \cdot d_2 \cdot h$	<i>d</i> ₁ = 15; <i>d</i> ₂ = 8; <i>h</i> = 15	1325	98	Referenced
<i>Chaetoceros decipiens</i>	Oval cylinder	$\pi/4 \cdot d_1 \cdot d_2 \cdot h$	<i>d</i> ₁ = 15; <i>d</i> ₂ = 10; <i>h</i> = 11	1295	96	Referenced
<i>Chaetoceros didymus</i>	Oval cylinder	$\pi/4 \cdot d_1 \cdot d_2 \cdot h$	<i>d</i> ₁ = 20; <i>d</i> ₂ = 10; <i>h</i> = 14	2198	148	Referenced
<i>Chaetoceros lauderi</i>	Oval cylinder	$\pi/4 \cdot d_1 \cdot d_2 \cdot h$	<i>d</i> ₁ = 16; <i>d</i> ₂ = 9; <i>h</i> = 28	3165	199	Referenced
<i>Chaetoceros lorenzianus</i>	Oval cylinder	$\pi/4 \cdot d_1 \cdot d_2 \cdot h$	<i>d</i> ₁ = 12; <i>d</i> ₂ = 9; <i>h</i> = 34	2883	184	Referenced
<i>Corethron</i> spp.	Cylinder	$\pi/4 \cdot d^2 \cdot h$	<i>d</i> = 20; <i>h</i> = 80	25120	1066	Measured
<i>Cylindrotheca</i> spp.	Rotational Ellipsoid	$\pi/6 \cdot d^2 \cdot h$	<i>d</i> = 5; <i>h</i> = 80	1047	81	Measured
<i>Dactyliosolen</i> spp.	Cylinder	$\pi/4 \cdot d^2 \cdot h$	<i>d</i> = 10; <i>h</i> = 55	4318	256	Measured
<i>Eucampia zodiacus</i>	Oval cylinder	$\pi/4 \cdot d_1 \cdot d_2 \cdot h$	<i>d</i> ₁ = 20; <i>d</i> ₂ = 8; <i>h</i> = 10	1256	94	Referenced
<i>Eunotia clevei</i>	Oval cylinder	$\pi/4 \cdot d_1 \cdot d_2 \cdot h$	<i>d</i> ₁ = 10; <i>d</i> ₂ = 5; <i>h</i> = 20	785	64	Measured
<i>Guinardia delicatula</i>	Cylinder	$\pi/4 \cdot d^2 \cdot h$	<i>d</i> = 25; <i>h</i> = 60	29438	1212	Measured
<i>Guinardia</i> spp. <20 μm	Cylinder	$\pi/4 \cdot d^2 \cdot h$	<i>d</i> = 20; <i>h</i> = 170	53380	1965	Measured
<i>Guinardia</i> spp. >20 μm	Cylinder	$\pi/4 \cdot d^2 \cdot h$	<i>d</i> = 25; <i>h</i> = 150	73593	2549	Measured
<i>Helicotheca</i> spp.	Parallelepiped	<i>l</i> * <i>w</i> * <i>h</i>	<i>l</i> = 50; <i>w</i> = 20; <i>h</i> = 5	5000	288	Measured
<i>Hemiaulus hauckii</i>	Oval cylinder	$\pi/4 \cdot d_1 \cdot d_2 \cdot h$	<i>d</i> ₁ = 20; <i>d</i> ₂ = 10; <i>h</i> = 60	9420	481	Measured
<i>Leptocylindrus</i> spp.	Cylinder	$\pi/4 \cdot d^2 \cdot h$	<i>d</i> = 5; <i>h</i> = 28	589	51	Referenced
<i>Leptocylindrus</i> spp. >5 μm	Cylinder	$\pi/4 \cdot d^2 \cdot h$	<i>d</i> = 7; <i>h</i> = 30	1154	88	Measured
<i>Licmophora</i> spp.	Half parallelepiped	<i>l</i> * <i>w</i> * <i>h</i> / 2	<i>l</i> = 35; <i>w</i> = 15; <i>h</i> = 3	788	64	Measured
<i>Navicula</i> spp.	Parallelepiped	<i>l</i> * <i>w</i> * <i>h</i>	<i>l</i> = 25; <i>w</i> = 5; <i>h</i> = 5	375	35	Referenced
<i>Nitzschia</i> spp. <50 μm	Half parallelepiped	<i>l</i> * <i>w</i> * <i>h</i> / 2	<i>l</i> = 40; <i>w</i> = 3; <i>h</i> = 3	180	19	Referenced
<i>Nitzschia</i> spp. >50 μm	Half parallelepiped	<i>l</i> * <i>w</i> * <i>h</i> / 2	<i>l</i> = 80; <i>w</i> = 4; <i>h</i> = 4	640	54	Measured
<i>Pleurosigma</i> spp.	Oval cylinder	$\pi/4 \cdot d_1 \cdot d_2 \cdot h$	<i>l</i> = 110; <i>w</i> = 16; <i>h</i> = 9.6	11827	579	Referenced
<i>Pseudo-nitzschia</i> spp. <60 μm	Parallelepiped	<i>l</i> * <i>w</i> * <i>h</i>	<i>l</i> = 55; <i>w</i> = 2.5; <i>h</i> = 2.5	309	30	Referenced
<i>Pseudo-nitzschia</i> spp. >60 μm	Parallelepiped	<i>l</i> * <i>w</i> * <i>h</i>	<i>l</i> = 110; <i>w</i> = 3; <i>h</i> = 3	792	65	Referenced
<i>Rhizosolenia</i> spp.	Cylinder	$\pi/4 \cdot d^2 \cdot h$	<i>d</i> = 15; <i>h</i> = 250	44156	1685	Measured
<i>Skeletonema costatum</i>	Cylinder	$\pi/4 \cdot d^2 \cdot h$	<i>d</i> = 10; <i>h</i> = 21	1649	117	Referenced
<i>Thalassiosira</i> spp.	Cylinder	$\pi/4 \cdot d^2 \cdot h$	<i>d</i> = 45; <i>h</i> = 22.5	35767	1420	Referenced
<i>Thalassiosira constricta</i>	Cylinder	$\pi/4 \cdot d^2 \cdot h$	<i>d</i> = 15; <i>h</i> = 18	3179	199	Measured
<i>Thalassionema nitzschioides</i>	Parallelepiped	<i>l</i> * <i>w</i> * <i>h</i>	<i>l</i> = 45; <i>w</i> = 5; <i>h</i> = 5	1125	86	Referenced

d, diameter; *h*, height; *l*, length; *w*, width. Measured or referenced indicates whether the dimensions to calculate cell volumes were measured or if they were adopted from Olenina et al. (2006).

Analyses (PCoA) using C biomass data ($\mu\text{mol C L}^{-1}$) from the most important diatom genera: *Guinardia*, *Rhizosolenia*, *Cerataulina*, *Thalassiosira*, *Dactyliosolen*, *Chaetoceros*, *Skeletonema*, *Leptocylindrus*, and *Pseudo-nitzschia*. C biomass data from each species were averaged for phase 0, I, and II to yield one separate dataset for each phase. Two-dimensional PCoA plots ($k = 2$) were generated thereafter with Bray-Curtis dissimilarity matrices using the ‘vegan’ package for R (Oksanen et al., 2018).

RESULTS

Physicochemical Conditions

The average temperature was initially $17.73 \pm 0.01^\circ\text{C}$ (day -3 ; mean of all mesocosms \pm SD) and increased only marginally to $18.86 \pm 0.05^\circ\text{C}$ at the end of the study. Temperature developments were almost identical in all mesocosms and closely followed the temperatures in the surrounding water since the heat transfer between the inside and outside of the mesocosms is extremely fast (Bach et al., 2016). The average salinity inside the mesocosms was initially 36.98 ± 0.04 but increased to 38.48 ± 0.08 at the end of the experiment (day 29) due to evaporation (please note that the initial salinity measurement comes from day 1 because the salinity sensor was malfunctioning from day -3 to day 1). Salinity outside the mesocosms was constant around 37 and the salinity increase must be seen as a mesocosm artifact. However, since the salinity increase was almost identical in all mesocosms, it cannot be responsible for the observed CO₂-dependent differences in the plankton communities presented herein.

The injection of different amounts of CO₂-saturated seawater at the beginning of the experiment resulted in the expected $p\text{CO}_2$ gradient, ranging from 375 (ambient) to 1406 μatm on day 3. The relative $p\text{CO}_2$ gradient between the mesocosms was maintained throughout the experiment, although the absolute $p\text{CO}_2$ values varied. A considerable decline of $p\text{CO}_2$ was observed in all mesocosms after the nutrient fertilization due to the net uptake of CO₂ by phytoplankton (Figure 2A).

At the beginning of the study (day -3), nutrient concentrations were 1.46 ± 0.27 , 0.17 ± 0.02 , 1.29 ± 0.2 , $0.47 \pm 0.15 \mu\text{mol L}^{-1}$ for NO_x[−], P, Si, and NH₄⁺, respectively. These nutrient concentrations were well within the natural range observed in the surface at the nearby European Station for Time Series in the Ocean at the Canary Islands (ESTOC), located in the NE Atlantic subtropical gyre (Cianca et al., 2007). Nutrient concentrations were declining from day -3 onward but at different rates (NO_x[−] > NH₄⁺ > Si > P; Figure 2). All nutrients were exhausted by the end of phase I and hence before nutrient enrichment on day 18 (Figure 2).

NO_x[−], P, and Si concentrations were moderately increased on day 18 and averaged at 3.43 ± 0.32 , 0.16 ± 0.01 , and $1.63 \pm 0.12 \mu\text{mol L}^{-1}$ directly after the nutrient enrichment. These N:P:Si ratios roughly correspond to those of deep water (~ 600 m) around the study area (Taucher et al., 2017). The fertilization induced phytoplankton growth and corresponding nutrient drawdown. NO_x[−] declined fastest reaching values from

before the bloom between days 23–25, and on day 27 in the 619 μatm treatment (Figure 2B). P reached pre-bloom values between days 27 and 29, albeit not in the 1137 μatm treatment (Figure 2C). Si reached pre-bloom values between days 25 and 27 in the three highest CO₂ treatments, whereas Si remained at significantly ($p < 0.05$) higher levels in the two lowest CO₂ mesocosms until the end of the experiment ($> 1 \mu\text{mol L}^{-1}$; Figure 2D). NH₄⁺ was not added during the nutrient enrichment but concentrations showed a higher day to day variability during phase II (Figure 2E).

Bulk Phytoplankton

Chla concentrations were $0.73 \pm 0.07 \mu\text{mol L}^{-1}$ on the first sampling day (day -3) and increased quickly to $2 \pm 0.04 \mu\text{mol L}^{-1}$ on day -1 (Figure 2F), consistent with the decreasing nutrient concentrations (Figures 2B–E). Chla dropped down to the initial values on day 1 and remained quite constant at this level throughout phase I. Chla was slightly, but significantly elevated in the high CO₂ treatments during phase I ($p = 0.043$, Figure 2F). The nutrient enrichment on day 18 led to a rapid chla increase in all mesocosms except for the 619 μatm treatment. Here, the increase was delayed since the chla concentration at the onset of the bloom was considerably lower than in the other mesocosms (check Figure 2F on day 18). CO₂ had no significant influence on chla during phase II.

Biogenic silica concentrations were $0.36 \pm 0.07 \mu\text{mol L}^{-1}$ on the first sampling day (day -3). Concentrations increased thereafter in all mesocosms until peaking at $1.5 \pm 0.1 \mu\text{mol L}^{-1}$ on day 7. BSi declined after the peak to $0.22 \pm 0.11 \mu\text{mol L}^{-1}$ at the end of phase I (Figure 2G). CO₂ had a significant positive influence on the BSi development after the nutrient fertilization ($p = 0.002$). BSi increased to values slightly lower than $2 \mu\text{mol L}^{-1}$ in the three highest CO₂ mesocosms (day 29), while hardly any increase was observed in the two lowest CO₂ mesocosms (day 29; Figure 2G). The BSi development over the course of the study is reflected in the development of dissolved Si (compare Figures 2D,G; please note that the BSi decline at the end of phase I is not leading to increasing concentrations of dissolved Si since the BSi sinks out into the sediment traps and is therefore removed from the water columns).

Diatom Communities

The diatom community was initially diverse (Figure 2H) and dominated by species that are frequently found in the region (Anabalón et al., 2014). The genera with highest C biomass contribution in the mesocosms were: *Guinardia* (Guin), *Rhizosolenia* (Rhiz), *Cerataulina* (Cera), *Thalassiosira* (Thals), *Dactyliosolen* (Dact), *Chaetoceros* (Chae), *Skeletonema* (Skel), *Leptocylindrus* (Lept), and *Pseudo-nitzschia* (Ps-n). These are shown on an individual basis in Figures 3, 4. Subdominant species were pooled and shown as one group (“others,” Figures 3, 4). A full species list with calculated biovolumes and C biomasses is provided in Table 1. The PCoA of phase 0 revealed no treatment-specific dissimilarities between mesocosms before the first CO₂ addition (Figure 5A). The three highest CO₂ treatments were mapped at the extremes of the PCo space. This information is important as it indicates that dissimilarities

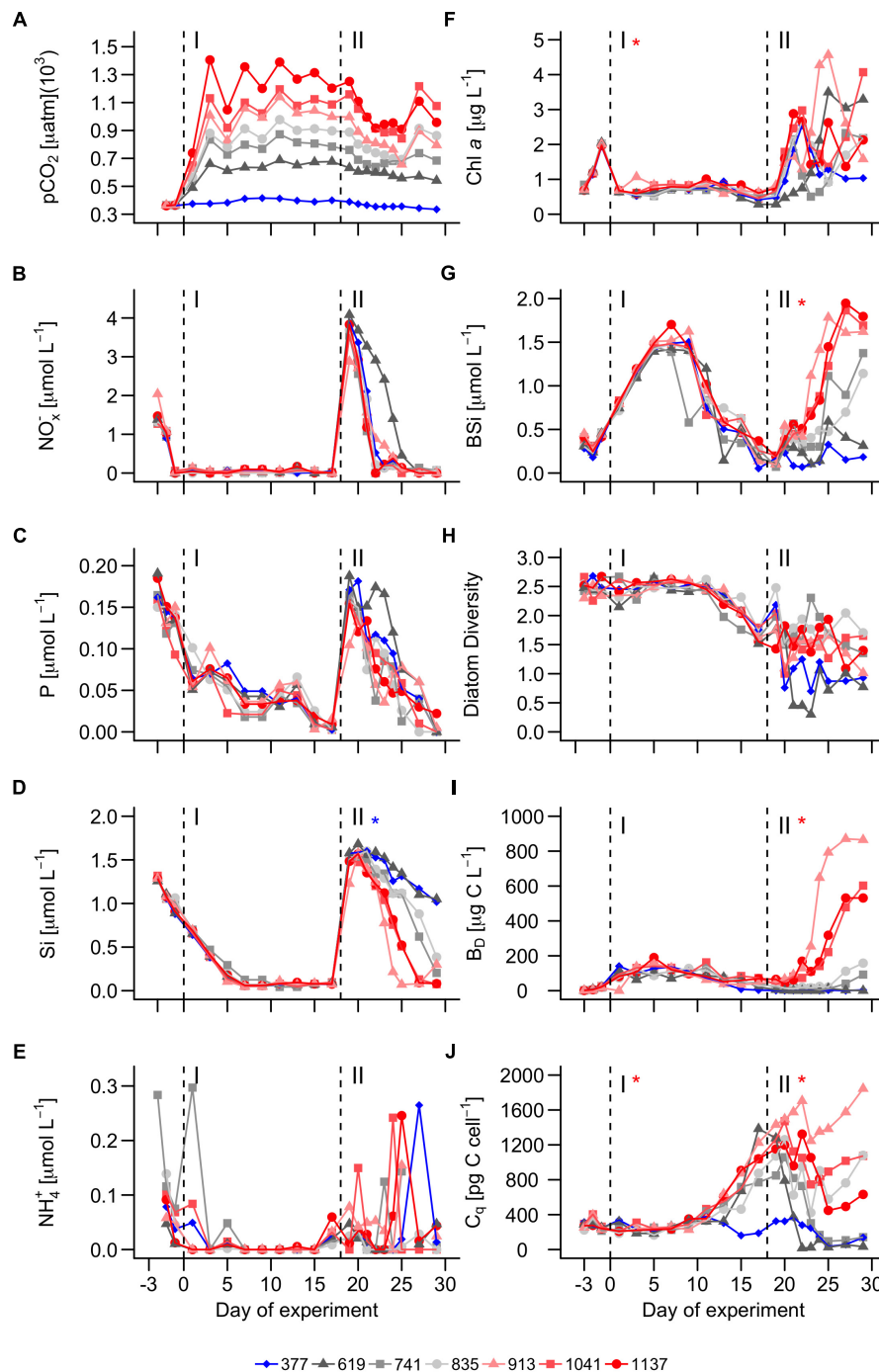


FIGURE 2 | Chemical conditions and bloom formations in the mesocosms. **(A)** pCO₂. **(B)** Nitrate + Nitrite concentrations. **(C)** Phosphate concentration. **(D)** Dissolved silicate concentration. **(E)** Ammonium concentration. **(F)** Chlorophyll *a* concentration. **(G)** Biogenic silica. **(H)** Shannon-Weaver diversity of the diatom community. **(I)** total diatom biomass. **(J)** Cellular C quota averaged over all diatom species (see Eq. 2). Dashed vertical lines separate the three phases of the experiment. Asterisks indicate significantly ($p < 0.05$) positive (red) or negative (blue) CO₂ effects during phases. The legend at the bottom gives mean pCO₂ values (in μatm) of the different treatments.

between treatments later in the experiment are less likely to be predetermined by the initial diatom community structure.

Diatoms started to grow exponentially at the beginning of the study until days 1 to 5, reflected in the BSi build-up and Si

drawdown (**Figures 2D,G**). Abundance and C biomass declined after this initial peak but in some genera (e.g., *Skeletonema*) more than in others (e.g., *Guinardia*; compare **Figures 3A, 4A** with **Figures 3G, 4G**). The decline of some species to almost

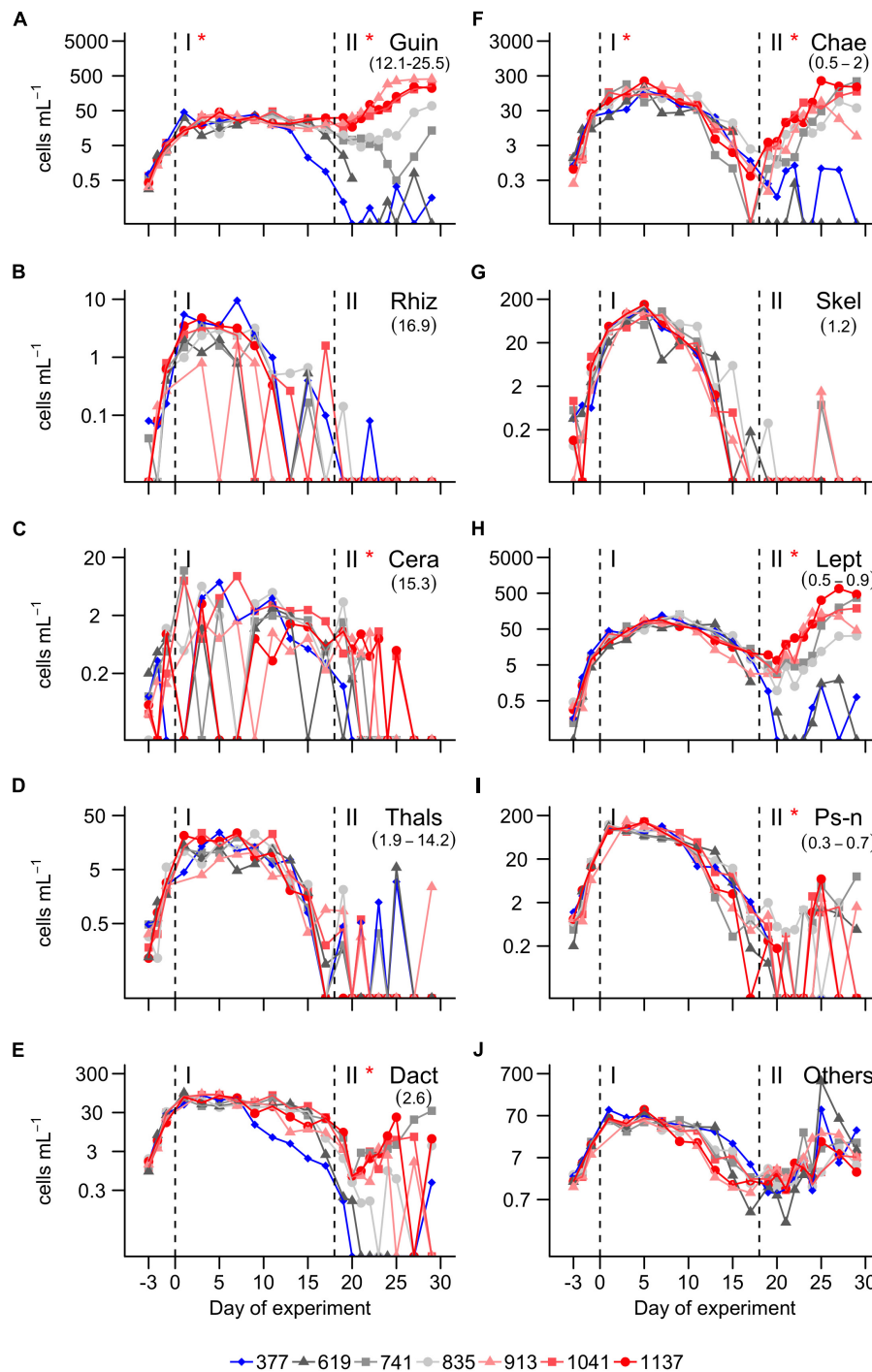


FIGURE 3 | Abundance of the most important diatom genera. **(A)** *Guinardia*. **(B)** *Rhizosolenia*. **(C)** *Cerataulina*. **(D)** *Thalassiosira*. **(E)** *Dactylosolen*. **(F)** *Chaetoceros*. **(G)** *Skeletonema*. **(H)** *Leptocylindrus*. **(I)** *Pseudo-nitzschia*. **(J)** Sum of all other diatom species. A full species list is provided in **Table 1**. Dashed vertical lines separate the three phases of the experiment. Asterisks indicate significantly ($p < 0.05$) positive (red) or negative (blue) CO₂ effects during phases. The legend at the bottom gives mean $p\text{CO}_2$ values (in μatm) of the different treatments.

undetectable abundances toward the end of phase I led to a decrease of diversity from ~ 2 (days -3 – 13) to ~ 1.2 (days 17 – 29 ; **Figure 2H**). Diatoms developed similarly in all treatments during the more oligotrophic conditions in phase I, but we

detected significant CO₂ effects on abundance and C biomass of *Guinardia* and *Chaetoceros* (**Figures 3A,F** and **Table 2**). C_q (Eq. 2) of the diatom community averaged over phase I was positively correlated with $p\text{CO}_2$ (**Figure 2J**). The PCoA of

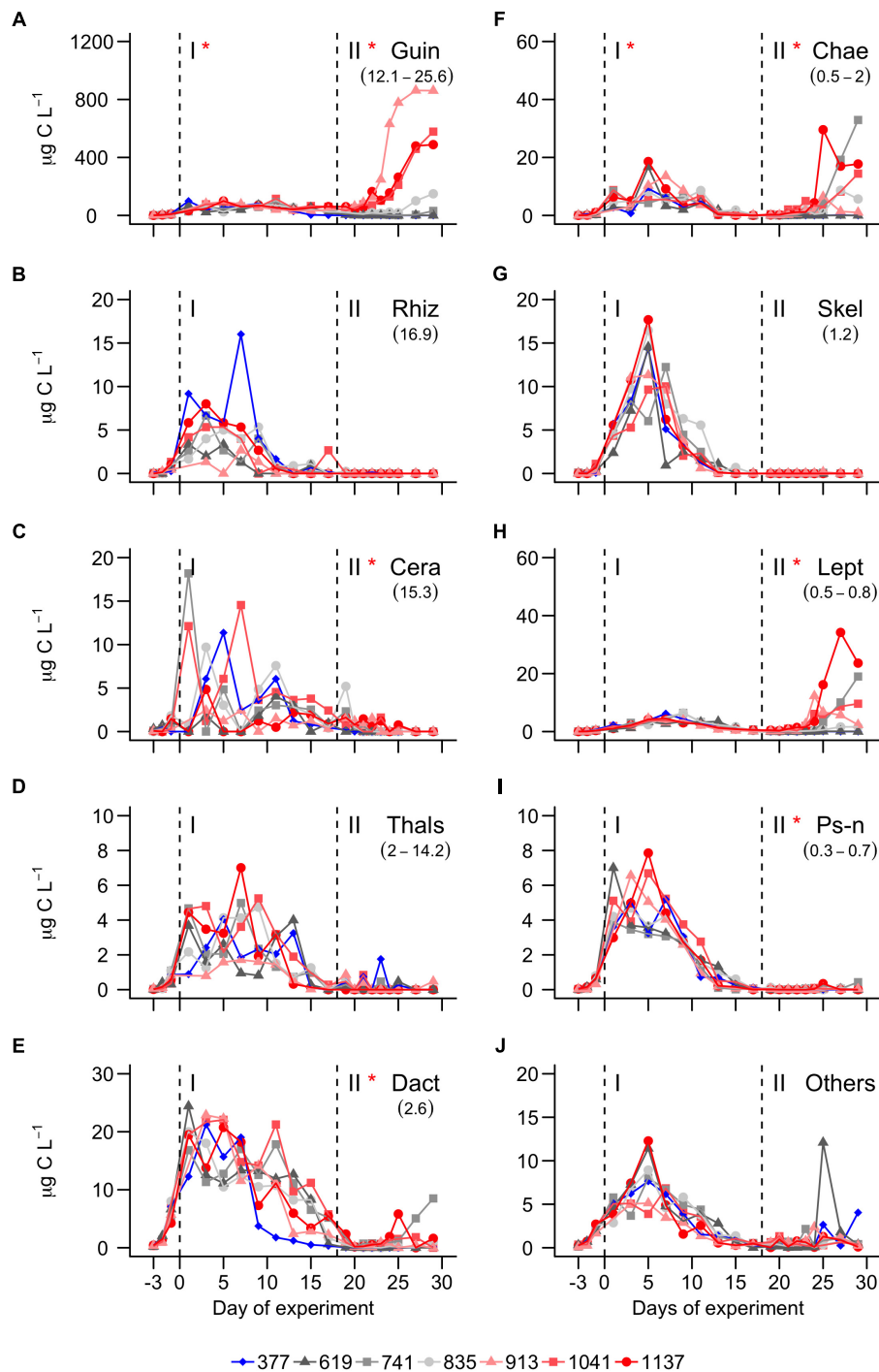


FIGURE 4 | C Biomass of the most important diatom genera. (A) *Guinardia*. (B) *Rhizosolenia*. (C) *Cerataulina*. (D) *Thalassiosira*. (E) *Dactylosolen*. (F) *Chaetoceros*. (G) *Skeletonema*. (H) *Leptocylindrus*. (I) *Pseudo-nitzschia*. (J) Sum of all other diatom species. A full species list is provided in **Table 1**. Dashed vertical lines separate the three phases of the experiment. Asterisks indicate significantly ($p < 0.05$) positive (red) or negative (blue) CO₂ effects during phases. The legend at the bottom gives mean pCO₂ values (in µatm) of the different treatments.

phase I revealed no pronounced CO₂-dependent dissimilarities of the diatom communities, although there is, perhaps, a mild separation between the three highest CO₂ mesocosms and the control along PCo1 (**Figure 5B**).

A pronounced diatom bloom was initiated through the nutrient fertilization at the beginning of phase II. However, the onset of the bloom varied among the different diatom genera. While *Chaetoceros* was responding immediately (day 18), it took

most of the other genera a few days before they started to grow (Figure 3B). Nanoflagellates (0.2–2 μm) were profiting from this delay (Filella et al., 2018) and were largely responsible for the first chl *a* peak on day 22, shortly after nutrient fertilization (Figure 2B). Diatoms became more influential on the bulk chl *a* signal about 1 week after fertilization (compare Figures 2B, 4), although other groups like non-diazotrophic cyanobacteria, dinoflagellates, or nanoflagellates still had a noticeable influence (Filella et al., 2018).

CO₂ had a strong influence on the composition of the diatom assemblage after the nutrient fertilization. Abundance and C biomass of *Cerataulina*, *Chaetoceros*, *Dactyliosolen*, *Guinardia*, *Leptocylindrus*, and *Pseudo-nitzschia* were significantly positively influenced under high CO₂. *Guinardia* was the species with the highest carbon content and profited most strongly from high CO₂ levels (Figures 3D, 4D). C_q of the diatom community was positively correlated with pCO₂ during phase I and II (Figure 2I, phase I, *p* = 0.022; phase II *p* = 0.009). The PCoA for phase II revealed CO₂-dependent dissimilarities of the diatom community where the control and the 619 μatm treatment, the 741 and the 835 μatm treatments, and the three highest CO₂

treatments were mapped in three different regions of the PCo space (Figure 5C).

Mesozooplankton

The MesoZP communities were numerically dominated by copepods (Figure 6). Individuals of the different species were generally small with even the adults hardly ever being larger than 500 μm. The two genera *Clausocalanus* and *Paracalanus* were not distinguishable while counting the sample and were therefore merged into one taxonomic unit, termed *CP-calanus* in the following (please note that both genera were present in the mesocosms as was determined with meta-barcoding). The most abundant copepod genera during phase I were *CP-calanus*, *Oithona*, *Oncaea*, and *Temora* (Figures 6A,C,E,F). *CP-calanus* and *Temora* reached particularly high abundances during phase II but only in the lower CO₂ mesocosms (Figures 6A,E). Copepod nauplii reached abundance peaks on days 13 and 30, although there was a large spread among mesocosms especially during the second peak (Figure 6H). Other MesoZP taxa that occurred in high abundances comprised *Oikopleura dioica* (appendicularia) and foraminifera (most likely *Globigerinidae*

TABLE 2 | Statistics; Regression analyses were performed for time-averaged means for the two experimental phases.

Dependent variable	Phase	<i>p</i> -value	<i>R</i> ²	F statistic	Phase	<i>p</i> -value	<i>R</i> ²	F statistic
NO _x [−]	I	0.728	0.03	0.135	II	0.307	0.21	1.292
PO ₄ ^{3−}	I	0.601	0.06	0.313	II	0.174	0.34	2.514
Si(OH) ₄	I	0.621	0.05	0.276	II	0.024	0.67	10.17
NH ₄	I	0.931	0.01	0.008	II	0.733	0.03	0.13
Chlorophyll <i>a</i>	I	0.043	0.59	7.268	II	0.081	0.49	4.776
BSi	I	0.215	0.21	1.372	II	0.001	0.79	19.1
H'	I	0.932	0.01	0.008	II	0.151	0.36	2.866
B _D	I	0.189	0.32	2.312	II	0.006	0.81	20.96
C _q	I	0.022	0.67	10.62	II	0.009	0.77	16.69
<i>Guinardia</i>	I	0.041	0.60	7.492	II	0.002	0.88	35.2
<i>Rhizosolenia</i>	I	0.451	0.12	0.666	II	0.464	0.11	0.627
<i>Cerataulina</i>	I	0.833	0.01	0.05	II	0.023	0.68	10.46
<i>Thalassiosira</i>	I	0.707	0.03	0.157	II	0.13	0.39	3.283
<i>Dactyliosolen</i>	I	0.161	0.35	2.71	II	0.05	0.57	5.534
<i>Chaetoceros</i>	I	0.006	0.81	21.02	II	0.015	0.81	17.05
<i>Skeletonema</i>	I	0.454	0.12	0.656	II	0.847	0.01	0.041
<i>Leptocylindrus</i>	I	0.218	0.28	1.983	II	0.015	0.73	13.32
<i>Pseudo-nitzschia</i>	I	0.298	0.21	1.346	II	0.044	0.6	7.162
Others	I	0.613	0.11	0.469	II	0.201	0.31	2.162
<i>Clauso-/Paracalanus</i>	I	0.79	0.02	0.079	II	0.022	0.68	10.73
<i>Nannocalanus</i>	I	0.953	0.01	0.004	II	0.212	0.29	2.05
<i>Oncaea</i>	I	0.929	0.01	0.009	II	0.699	0.03	0.167
<i>Oikopleura</i>	I	0.438	0.12	0.71	II	—	—	—
<i>Temora</i>	I	0.295	0.21	1.364	II	0.026	0.66	9.883
<i>Oithona</i>	I	0.641	0.05	0.246	II	0.021	0.69	10.91
Foraminifera	I	0.121	0.41	3.487	II	0.403	0.14	0.833
Copepoda nauplii	I	0.729	0.03	0.134	II	0.934	0.01	0.008

Results were considered to be statistically significant if the correlation between pCO₂ (independent variable) and the dependent variable revealed a significant trend (*p* < 0.05). Please note that results were identical for diatom abundances and C biomasses so that the statistical outcomes apply for both. The bold values indicate statistical significance.

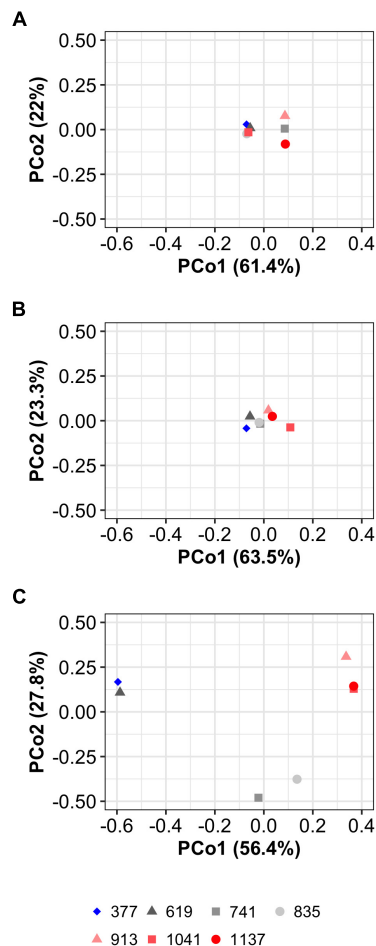


FIGURE 5 | PCoA analyses of the diatom community composition. **(A)** Phase 0 (i.e., before the CO₂ manipulation). **(B)** Phase I. **(C)** Phase II. Explained variance for principal coordinates 1 and 2 (PCo1, PCo2) are given on the axis. The legend at the bottom gives mean PCo2 values (in μatm) of the different treatments.

species). *O. dioica* was initially not detected but occurred suddenly in some mesocosms during phase I (Figure 6D). It disappeared equally quickly after the bloom and remained detectable only in the 619 and 913 μatm treatments (Figure 6D). Foraminifera were detected in low abundances since the first sampling and they thrived in all mesocosms until day 21–25 (Figure 6G).

CO₂ effects on MesoZP were detected only in 3 species and only in phase II. CO₂ had a strong positive influence on the abundance of *CP-calanus* and *Temora* (Figures 6A,E). *Oithona* was negatively affected by CO₂ but the effect was not as pronounced as in the two other genera (Figure 6F).

DISCUSSION

Physiological studies have shown that growth and the metabolism of diatoms can be affected by increasing seawater CO₂

concentrations (Gao and Campbell, 2014). A recent meta-analysis of OA laboratory experiments with diatoms revealed an increase of growth rates under high CO₂, although the response varies widely among different diatom species (Dutkiewicz et al., 2015). This inter-specific variability is an important feature as it suggests that high CO₂ conditions will affect diatom species differentially and therefore, alter the composition of diatom assemblages (Tortell et al., 2008; Hoppe et al., 2013; Endo et al., 2016). Indeed, our experiment revealed a positive effect on the bulk diatom biomass (C_d) that coincided with shifts in the assemblage structure after the nutrient addition.

The exact mechanisms which control diatom responses to high CO₂ are difficult to uncover in mesocosm experiments because the complexity of the food web allows a myriad of explanations (Bach et al., 2017). Therefore, our goal in the discussion is not to mention every imaginable mechanism but to highlight particularly plausible ones while acknowledging that none of them can be proven and none are necessarily exclusive. In fact, several mechanisms could coincide and ultimately explain the observed responses together. After discussing potential mechanisms underlying the observed CO₂ responses (section “Potential Mechanisms Explaining Observed CO₂ Effects on the Diatoms”), we consider our findings in a wider perspective and discuss their value to assess diatom responses to OA in the subtropical NE Atlantic (section “What Can These Results Tell Us About OA Impacts on Diatoms in the Subtropical NE Atlantic?”).

Potential Mechanisms Explaining Observed CO₂ Effects on the Diatoms

CO₂ Fertilization of Photosynthesis

When phytoplankton profits from high CO₂ then this is usually explained with a CO₂ fertilization effect on inorganic carbon acquisition. The idea is that increasing seawater $p\text{CO}_2$ facilitates the diffusive uptake of CO₂, thereby reducing the energy demand for active carbon acquisition (Giordano et al., 2005; Reinfelder, 2011). The energy that is saved by reducing the operation of this so-called “carbon concentrating mechanism (CCM)” can be diverted into the acquisition of other resources, ultimately leading to faster growth. Physiological studies with diatoms generally support this concept, although variability exists between species (Rost et al., 2003; Hopkinson et al., 2011; Trimborn et al., 2013; Gao and Campbell, 2014).

The CCM related explanation may also apply to our results. Elevated $p\text{CO}_2$ may have stimulated resource acquisition in some of the diatom species present in the mesocosms, thereby leading to CO₂-dependent restructuring of the assemblage. Recently, Wu et al. (2014) performed laboratory CO₂ experiments with four different *Thalassiosira* species and *Coscinodiscus wailesii*, and found that the CO₂ fertilization effect on growth rates scales positively with cell volume. Although their concept is derived mainly from one genus, it is physiologically well substantiated and based on the positive correlation between cell size and diffusion gradients, which predicts that high CO₂ is particularly beneficial for carbon acquisition in larger species (Pasciak and Gavis, 1974; Wolf-Gladrow and Riebesell, 1997; Flynn et al., 2012; Shen and Hopkinson, 2015). Applying the cell volume

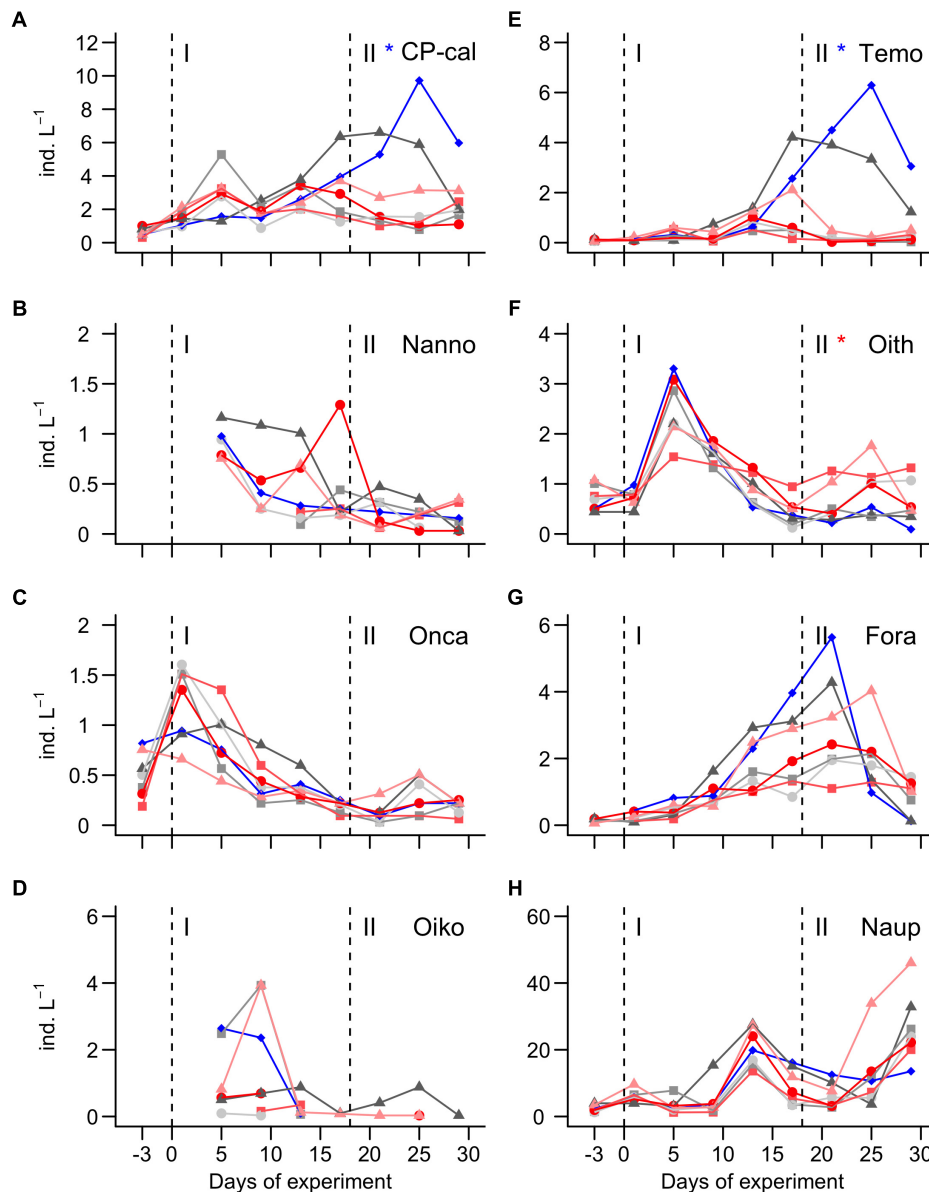


FIGURE 6 | Abundance of the most important mesozooplankton groups **(A)** *CP-calanus*. **(B)** *Nannocalanus*. **(C)** *Oncaea*. **(D)** *Oikopleura dioica*. **(E)** *Temora*. **(F)** *Oithona*. **(G)** *Foraminifera*. **(H)** *Nauplii*. Dashed vertical lines separate the three phases of the experiment. Asterisks indicate significantly ($p < 0.05$) positive (red) or negative (blue) CO₂ effects during phases. The legend at the bottom gives mean $p\text{CO}_2$ values (in μatm) of the different treatments.

dependency determined by Wu et al. (2014) to our dataset partially confirms their concept. As predicted, we observed by far the strongest CO₂ stimulation in *Guinardia*, the largest genus present in the experiment. Apart from *Guinardia*, however, CO₂ effects did not seem to scale with diatom biovolumes. There were small genera (e.g., *Chaetoceros*) that showed clearer CO₂ responses than larger ones (e.g., *Cerataulina*) (Figures 3C,F). Hence, while the Wu et al. (2014) concept provides a great starting point to interpret results observed in field experiments, it still needs to be expanded to account for the ecological complexities occurring outside the laboratory environment and genotype-specific variability. The application of molecular tools

in community studies may help to make significant progress on that matter (Endo et al., 2016).

CO₂ Effect Through Grazer Interactions

Copepods were the most abundant MesoZP group present in the mesocosms and probably had a top-down impact on the diatom community. Three of the five dominant copepod genera were significantly influenced by high CO₂ during phase II. *Oithona* abundance ranged between 100 and 1800 individuals L⁻¹ and was positively affected (Figure 6F). In contrast, *CP-calanus* and *Temora* abundances ranged between 800 to 9700 and 30 to 6900 individuals L⁻¹, respectively, and were both negatively affected

by high CO₂ (Figures 6A,E). The higher abundances of *CP-calanus* and *Temora*, as well as the larger CO₂ effect size relative to *Oithona*, suggests that any CO₂-related top-down control was primarily mediated through these two species. Indeed, abundances of several diatom species and bulk diatom biomass were significantly reduced under high CO₂ during phase II and particularly low in the control and the lowest CO₂ treatment (619 μ atm), where considerably more *CP-calanus* and *Temora* were present (compare Figures 2I, 6A,E). This anti-correlated pattern points toward a causal relationship between diatom and *CP-calanus*/*Temora* abundances that were altered through CO₂ concentrations. The key question is: Through which mechanisms could CO₂ affect the interaction between copepods and diatoms?

The most straight-forward explanation would be a negative CO₂ effect on the physiological performance of *CP-calanus* and *Temora*. High CO₂/low pH conditions may have reduced growth and grazing of these two copepod genera, thereby reducing their abundances and ultimately grazing pressure on diatoms. To the best of our knowledge, there is no published study to date in which direct CO₂ effects on *CP-calanus* were investigated under controlled laboratory conditions. Such experiments exist for *Temora longicornis* but it is unclear whether the *Temora* species in our experiments would show the same insensitivity to high CO₂ as the individuals from the English Channel investigated by McConville et al. (2013). Recent OA experiments with *Calanus glacialis* revealed population-specific CO₂ responses with more robust populations found in naturally CO₂-rich habitats (Thor et al., 2018). These findings suggest that local carbonate chemistry conditions may be a better predictor to assess CO₂ sensitivities of copepods than their taxonomic affiliation (Thor et al., 2018; Zhang et al., 2018). They also suggest that laboratory-based results can only reliably be used to interpret responses observed in experiments with natural assemblages when both experiments were done with individuals from the same population. Thus, with the available data it is not possible to assess the likelihood for such a direct negative CO₂ effect on the metabolism of *CP-calanus* and *Temora*.

Altered interactions between *CP-calanus*/*Temora* and diatoms could also have been provoked through CO₂-induced changes in the nutritional quality of the diatoms. If high CO₂ triggers a physiological response in diatoms, that cause them to be less nutritious, copepod growth would be reduced ultimately leading to lower grazing pressure and higher diatom abundances. A potential explanation for this hypothesis comes from experiments by Rossoll et al. (2012), who found that the diatom *Thalassiosira pseudonana* contained less fatty acids under high CO₂ and the composition of the produced fatty acids had a lower nutritional value. As a consequence, the copepod *Acartia tonsa* fed with these *T. pseudonana* cells grew slower and produced less eggs (Rossoll et al., 2012). Furthermore, carbonate chemistry effects on silicification may have altered the strength of the frustule and therefore the palatability of diatoms (Hamm et al., 2003; Wilken et al., 2011; Friedrichs et al., 2013; Liu et al., 2016). Low seawater pH is considered to be beneficial for the silicification process since opal precipitation does occur in a low pH (pH ~5) compartment of the diatom cell (Vrieling et al., 1999; Martin-Jézéquel et al., 2000). Indeed, Hervé et al. (2012) found

increasing Si incorporation and cellular BSi quota in *T. weissflogii* with decreasing pH from 8 to 7.2. However, other experiments with *T. weissflogii* only found increased Si uptake rates (Milligan et al., 2004) but decreasing BSi quota (Milligan et al., 2004) or BSi/C (Mejía et al., 2013). Thus, with the currently available (and partially controversial) information, it is not possible to assess the relevance of carbonate chemistry dependent silicification changes on grazing but it would be worthwhile to further investigate this important feedback in future studies (Milligan et al., 2004; Mejía et al., 2013; Gao and Campbell, 2014).

What Can These Results Tell Us About OA Impacts on Diatoms in the Subtropical NE Atlantic?

The potential of OA impacts on diatom communities will depend on the degree of future CO₂ increase. In the present experiment, diatom composition was noticeably affected at pCO₂ levels >619 μ atm, during the bloom in phase II (Figure 5C). This should not be regarded as a general threshold for diatom OA sensitivity as it is likely to vary regionally, depending on the prevailing diatom community and regional carbonate chemistry conditions. More productive regions near coasts or estuaries have typically larger natural variations in carbonate chemistry (Hofmann et al., 2011; Wallace et al., 2014) and should harbor generalist species, which are less responsive to increased CO₂. Conversely, CO₂ enrichment studies in more stable oceanic environments should be more likely to induce a response (Duarte et al., 2013). Carbonate chemistry conditions at the coast of Gran Canaria are rather stable with comparatively little seasonal fluctuations (González-Dávila et al., 2010), which may explain why quite pronounced changes in the diatom community composition were observed already above 619 μ atm.

The experiment discussed in the present paper took place in spring 2016 but we did a similar OA experiment at the coast of Gran Canaria with larger mesocosms already in autumn 2014 (Taucher et al., 2017). In this earlier experiment we also observed profound shifts in the diatom community composition, although the CO₂ threshold above which changes occurred could not be determined (Taucher et al., 2018). The diatom genera *Guinardia* and *Leptocylinndrus* were important in both the 2016 and the 2014 study and the comparison of their responses to high CO₂ is valuable because it allows us to assess the “reproducibility” of our findings. *Guinardia* benefitted profoundly from high CO₂ in both experiments which raises confidence that the *Guinardia* species enclosed in the mesocosms (*G. striata* in 2014; *G. delicatula*, *Guinardia* spp. in 2016) could become more competitive in an acidified NE Atlantic. *Leptocylinndrus*, however, responded oppositely which could be due to different *Leptocylinndrus* genotypes being enclosed in the mesocosms (*L. delicatulum* in 2014; *Leptocylinndrus* spp. in 2016). Alternatively, different food web structures could have indirectly caused the opposite responses, for example by altering resource competition or grazing pressure. Such food web related differences could have either developed in the course of the study or were already established at the beginning when the communities were enclosed inside the mesocosms

(Moreno de Castro et al., 2017). In this context it is also important remember that the mesocosm bags were filled with pumps in 2016 (section “Mesocosm Design, Deployment, and Maintenance”) while they were lowered into the water column in 2014 (Taucher et al., 2017). The different filling procedures may have amplified differences in the initial community structure.

The *Guinardia* species enclosed in the mesocosms was a comparatively large diatom and its positive response to high CO₂ drove the significant increase of the average cellular carbon quota (C_q) of the diatom community (Figure 2J). Such a CO₂-induced shift toward larger diatoms was also observed in several earlier OA experiments with natural communities (Tortell et al., 2008; Feng et al., 2009, 2010; Eggers et al., 2014; Bach et al., 2017; Taucher et al., 2018) while the opposite response (i.e., a CO₂-induced shift toward smaller diatoms) was reported only once (Davidson et al., 2016). This suggests that OA will generally favor large diatom species, which is in accordance with the physiological theory described at the beginning of section “Potential Mechanisms Explaining Observed CO₂ Effects on the Diatoms”.

CONCLUSION

In this study we enclosed a natural plankton community from the subtropical NE Atlantic in *in situ* mesocosms to assess their response to simulated future ocean acidification. Our findings suggest that the bulk diatom community in the subtropical NE Atlantic could benefit from high CO₂ conditions projected for the end of this century under nutrient supply (e.g., via seasonal or eddy-induced upwelling). However, the positive CO₂ response of the bulk diatom biomass coincided with pronounced shifts in the diatom species composition because not all diatoms benefitted equally from high CO₂. The largest diatom genus in the mesocosms (*Guinardia*) was particularly CO₂ responsive and its pronounced dominance under high CO₂ caused a significant increase in the average size of the diatom community. The particularly strong CO₂ effect on a large diatom is in accordance with physiological theory and has been observed in earlier studies, which adds confidence to this finding. Nevertheless, the discussed example of the response of *Leptocylindrus* to high CO₂ revealed that many uncertainties are yet to be resolved

before winners and losers within the diatom community can be determined with high confidence.

DATA AVAILABILITY

The datasets generated for this study are available on request to the corresponding author.

AUTHOR CONTRIBUTIONS

LB, JT, UR, and JA designed the experiments. All authors conducted the experiments. LB, NH-H, JT, CaS, and CIS measured the data. LB and NH-H analyzed the data. NH-H performed the statistical analysis and plotted the data. LB drafted the manuscript. LB, NH-H, JT, CaS, UR, and JA revised the manuscript.

FUNDING

This study was financially supported by Cluster of Excellence “The Future Ocean” at the University of Kiel. JA was supported by a Helmholtz International Fellow Award, 2015 (Helmholtz Association, Germany). NH-H and JA benefited also from the FLUXES project (CTM2015-69392-C3-1-R) funded by the Spanish government (Plan Nacional I+D).

ACKNOWLEDGMENTS

We thank Shaomin Chen, Syrmalena Kotronaki, Peter Fritzsche, Andrea Ludwig, Jana Meyer, Alice Nauendorf, and Lena Soumpasis for measuring carbonate chemistry, nutrient, and BSi samples, Andrea Ludwig for logistical support and CTD operations, Michael Krudewig, Michael Sswat, Peter Kohnert, Mario Deckelnick, and Jan Czerny for construction of the mesocosm infrastructure. Furthermore, we also thank the Oceanic Platform of the Canary Islands (PLOCAN) and its staff for the use of their facilities, and for their help with the logistics and organization of this experiment.

REFERENCES

- Anabalón, V., Aristegui, J., Morales, C. E., Andrade, I., Benavides, M., Correa-Ramírez, M. A., et al. (2014). The structure of planktonic communities under variable coastal upwelling conditions off Cape Ghir (31°N) in the Canary Current System (NW Africa). *Prog. Oceanogr.* 120, 320–339. doi: 10.1016/j.pcean.2013.10.015
- Aristegui, J., Barton, E. D., Tett, P., Montero, M. F., García-Muñoz, M., Basterretxea, G., et al. (2004). Variability in plankton community structure, metabolism, and vertical carbon fluxes along an upwelling filament (Cape Juby, NW Africa). *Prog. Oceanogr.* 62, 95–113. doi: 10.1016/j.pcean.2004.07.004
- Armbrust, E. V. (2009). The life of diatoms in the world's oceans. *Nature* 459, 185–192. doi: 10.1038/nature08057
- Bach, L. T., Alvarez-Fernandez, S., Hornick, T., Stühr, A., and Riebesell, U. (2017). Simulated ocean acidification reveals winners and losers in coastal phytoplankton. *PLoS One* 12:e0188198. doi: 10.1371/journal.pone.0188198
- Bach, L. T., Taucher, J., Boxhammer, T., Ludwig, A., Achterberg, E. P., Algueró-Muñiz, M., et al. (2016). Influence of ocean acidification on a natural winter-to-summer plankton succession: first insights from a long-term mesocosm study draw attention to periods of low nutrient concentrations. *PLoS One* 11:e0159068. doi: 10.1371/journal.pone.0159068
- Barton, E. D., Aristegui, J., Tett, P., Canton, M., García-Braun, J., Hernández-León, S., et al. (1998). The transition zone of the Canary Current upwelling region. *Prog. Oceanogr.* 41, 455–504. doi: 10.1016/S0079-6611(98)00023-8
- Boxhammer, T., Bach, L. T., Czerny, J., and Riebesell, U. (2016). Technical note: sampling and processing of mesocosm sediment trap material for quantitative biogeochemical analysis. *Biogeosciences* 13, 2849–2858. doi: 10.5194/bg-13-2849-2016
- Boyd, P., and Newton, P. (1995). Evidence of the potential influence of planktonic community structure on the interannual variability of particulate organic carbon flux. *Deep Sea Res. Part I Oceanogr. Res. Pap.* 42, 619–639. doi: 10.1016/0967-0637(95)00017-Z

- Brzezinski, M. A., and Nelson, D. M. (1996). Chronic substrate limitation of silicic acid uptake rates in the western Sargasso Sea. *Deep Sea Res. Part II Top. Stud. Oceanogr.* 43, 437–453. doi: 10.1016/0967-0645(95)00099-2
- Cianca, A., Helmke, P., Mouriño, B., Rueda, M. J., Llinás, O., and Neuer, S. (2007). Decadal analysis of hydrography and in situ nutrient budgets in the western and eastern North Atlantic subtropical gyre. *J. Geophys. Res. Ocean.* 112:C07025. doi: 10.1029/2006JC003788
- Davidson, A., McKinlay, J., Westwood, K., Thomson, P., van den Enden, R., de Salas, M., et al. (2016). Enhanced CO₂ concentrations change the structure of Antarctic marine microbial communities. *Mar. Ecol. Prog. Ser.* 552, 93–113. doi: 10.3354/meps11742
- Dickson, A. G., Afghan, J. D., and Anderson, G. C. (2003). Reference materials for oceanic CO₂ analysis: a method for the certification of total alkalinity. *Mar. Chem.* 80, 185–197. doi: 10.1016/S0304-4203(02)00133-0
- Dickson, A. G., Sabine, C. L., and Christian, J. R. (2007). *Guide to Best Practices for Ocean CO₂ Measurements*. Sidney: North Pacific Marine Science Organization.
- Duarte, C. M., Hendriks, I. E., Moore, T. S., Olsen, Y. S., Steckbauer, A., Ramajo, L., et al. (2013). Is ocean acidification an open-ocean syndrome? understanding anthropogenic impacts on seawater pH. *Estuaries and Coasts* 36, 221–236. doi: 10.1007/s12237-013-9594-3
- Dutkiewicz, S., Morris, J. J., Follows, M. J., Scott, J., Levitan, O., Dyhrman, S. T., et al. (2015). Impact of ocean acidification on the structure of future phytoplankton communities. *Nat. Clim. Chang.* 5, 1002–1006. doi: 10.1038/nclimate2722
- Eggers, S. L., Lewandowska, A. M., Barcelos E Ramos, J., Blanco-Ameijeiras, S., Gallo, F., and Matthiessen, B. (2014). Community composition has greater impact on the functioning of marine phytoplankton communities than ocean acidification. *Glob. Chang. Biol.* 20, 713–723. doi: 10.1111/gcb.12421
- Endo, H., Sugie, K., Yoshimura, T., and Suzuki, K. (2016). Response of Spring Diatoms to CO₂ Availability in the Western North Pacific as Determined by Next-Generation Sequencing. *PLoS One* 11:e0154291. doi: 10.1371/journal.pone.0154291
- Feng, Y., Hare, C. E., Leblanc, K., Rose, J. M., Zhang, Y., DiTullio, G. R., et al. (2009). Effects of increased pCO₂ and temperature on the north atlantic spring bloom. I. The phytoplankton community and biogeochemical response. *Mar. Ecol. Prog. Ser.* 388, 13–25. doi: 10.3354/meps08133
- Feng, Y., Hare, C. E., Rose, J. M., Handy, S. M., DiTullio, G. R., Lee, P. A., et al. (2010). Interactive effects of iron, irradiance and CO₂ on Ross Sea phytoplankton. *Deep. Res. Part I Oceanogr. Res. Pap.* 57, 368–383. doi: 10.1016/j.dsr.2009.10.013
- Field, C. B., Behrenfeld, M. J., Randerson, J. T., and Falkowski, P. G. (1998). Primary Production of the Biosphere: Integrating Terrestrial and Oceanic Components. *Science* 281, 237–240. doi: 10.1126/science.281.5374.237
- Filella, A., Baños, I., Montero, M. F., Hernández-Hernández, N., Rodríguez-Santos, A., Ludwig, A., et al. (2018). Plankton Community Respiration and ET'S Activity Under Variable CO₂ and Nutrient Fertilization During a Mesocosm Study in the Subtropical North Atlantic. *Front. Mar. Sci.* 5:310. doi: 10.3389/fmars.2018.00310
- Flynn, K. J., Blackford, J. C., Baird, M. E., Raven, J. A., Clark, D. R., Beardall, J., et al. (2012). Changes in pH at the exterior surface of plankton with ocean acidification. *Nat. Clim. Chang.* 2, 510–513. doi: 10.1038/nclimate1489
- Friedrichs, L., Hörnig, M., Schulze, L., Bertram, A., Jansen, S., and Hamm, C. (2013). Size and biomechanic properties of diatom frustules influence food uptake by copepods. *Mar. Ecol. Prog. Ser.* 481, 41–51. doi: 10.3354/meps10227
- Gao, K., and Campbell, D. A. (2014). Photophysiological responses of marine diatoms to elevated CO₂ and decreased pH: A review. *Funct. Plant Biol.* 41, 449–459. doi: 10.1071/FP13247
- Giordano, M., Beardall, J., and Raven, J. A. (2005). CO₂ concentrating mechanisms in algae: mechanisms, environmental modulation, and evolution. *Annu. Rev. Plant Biol.* 56, 99–131. doi: 10.1146/annurev.arplant.56.032604.144052
- González-Dávila, M., Santana-Casiano, J. M., Rueda, M. J., and Llinás, O. (2010). The water column distribution of carbonate system variables at the ESTOC site from 1995 to 2004. *Biogeosciences* 7, 3067–3081. doi: 10.5194/bg-7-3067-2010
- Hamm, C., and Smetacek, V. (2007). “Armor: Why, when, and how,” in *Evolution of Phytoplankton*, eds P. G. Falkowski and A. H. Knoll (Boston, MA: Elsevier), 311–332.
- Hamm, C. E., Merkel, R., Springer, O., Jurkojc, P., Maiert, C., Prechtelt, K., et al. (2003). Architecture and material properties of diatom shells provide effective mechanical protection. *Nature* 421, 841–843. doi: 10.1038/nature01416
- Hansen, H. P., and Koroleff, F. (1999). “Determination of nutrients,” in *Methods of Seawater Analysis*, eds K. Grasshoff, K. Kremling, and M. Ehrhardt (Weinheim: Wiley-VCH), 159–226. doi: 10.1002/9783527613984.ch10
- Hervé, V., Derr, J., Douady, S., Quinet, M., Moisan, L., and Lopez, P. J. (2012). Multiparametric Analyses Reveal the pH-Dependence of Silicon Biomineralization in Diatoms. *PLoS One* 7:e46722. doi: 10.1371/journal.pone.0046722
- Hofmann, G. E., Smith, J. E., Johnson, K. S., Send, U., Levin, L. A., Micheli, F., et al. (2011). High-frequency dynamics of ocean pH: A multi-ecosystem comparison. *PLoS One* 6:e28983. doi: 10.1371/journal.pone.0028983
- Holmes, R. M., Aminot, A., Kérouel, R., Hooker, B. A., and Peterson, B. J. (1999). A simple and precise method for measuring ammonium in marine and freshwater ecosystems. *Can. J. Fish. Aquat. Sci.* 56, 1801–1808. doi: 10.1139/f99-128
- Hopkinson, B. M., Dupont, C. L., Allen, A. E., and Morel, F. M. M. (2011). Efficiency of the CO₂-concentrating mechanism of diatoms. *Proc. Natl. Acad. Sci. U. S. A.* 108, 3830–3837. doi: 10.1073/pnas.1018062108
- Hoppe, C. J. M., Hassler, C. S., Payne, C. D., Tortell, P. D., Rost, B. R., and Trimborn, S. (2013). Iron limitation modulates ocean acidification effects on Southern Ocean phytoplankton communities. *PLoS One* 8:e79890. doi: 10.1371/journal.pone.0079890
- Lavigne, H., Epitalon, J.-M., and Gattuso, J.-P. (2011). *Seacarb: seawater carbonate chemistry with R. R package version 3.0*. Available at: <http://cran.r-project.org/package=seacarb>
- Liu, H., Chen, M., Zhu, F., and Harrison, P. J. (2016). Effect of diatom silica content on copepod grazing, growth and reproduction. *Front. Mar. Sci.* 3:89. doi: 10.3389/fmars.2016.00089
- Lueker, T. J., Dickson, A. G., and Keeling, C. D. (2000). Ocean pCO₂ calculated from dissolved inorganic carbon, alkalinity, and equations for K₁ and K₂: Validation based on laboratory measurements of CO₂ in gas and seawater at equilibrium. *Mar. Chem.* 70, 105–119. doi: 10.1016/S0304-4203(00)00022-0
- Mann, D. G., and Vanormelingen, P. (2013). An Inordinate Fondness? The Number, Distributions, and Origins of Diatom Species. *J. Eukaryot. Microbiol.* 60, 414–420. doi: 10.1111/jeu.12047
- Martin-Jézéquel, V., Hildebrand, M., and Brzezinski, M. A. (2000). Review Silicon Metabolism in Diatoms: Implications for Growth. *J. Phycol.* 36, 821–840. doi: 10.1046/j.1529-8817.2000.00019.x
- McConville, K., Halsband, C., Fileman, E. S., Somerfield, P. J., Findlay, H. S., and Spicer, J. I. (2013). Effects of elevated CO₂ on the reproduction of two calanoid copepods. *Mar. Pollut. Bull.* 73, 428–434. doi: 10.1016/j.marpolbul.2013.02.010
- McGillicuddy, D. J., Anderson, L. A., Bates, N. R., Bibby, T., Buesseler, K. O., Carlson, C. A., et al. (2007). Eddy/Wind Interactions Stimulate Extraordinary Mid-Ocean Plankton Blooms. *Science* 316, 1021–1026. doi: 10.1126/science.1136256
- Mejía, L. M., Isensee, K., Méndez-Vicente, A., Pisonero, J., Shimizu, N., González, C., et al. (2013). B content and Si/C ratios from cultured diatoms (*Thalassiosira pseudonana* and *Thalassiosira weissflogii*): Relationship to seawater pH and diatom carbon acquisition. *Geochim. Cosmochim. Acta* 123, 322–337. doi: 10.1016/j.gca.2013.06.011
- Menden-Deuer, S., and Lessard, E. J. (2000). Carbon to volume relationships for dinoflagellates, diatoms, and other protist plankton. *Limnol. Oceanogr.* 45, 569–579. doi: 10.4319/lo.2000.45.3.0569
- Milligan, A. J., Varela, D. E., Brzezinski, M. A., and Morel, F. M. M. (2004). Dynamics of Silicon Metabolism and Silicon Isotopic Discrimination in a Marine Diatom as a Function of pCO₂. *Limnol. Oceanogr.* 49, 322–329. doi: 10.4319/lo.2004.49.2.0322
- Moreno de Castro, M., Schartau, M., and Wirtz, K. (2017). Potential sources of variability in mesocosm experiments on the response of phytoplankton to ocean acidification. *Biogeosciences* 14, 1883–1901. doi: 10.5194/bg-14-1883-2017
- Nelson, D. M., Tréguer, P., Brzezinski, M. A., Leynaert, A., and Quéguiner, B. (1995). Production and dissolution of biogenic silica in the ocean: Revised global estimates, comparison with regional data and relationship to biogenic sedimentation. *Global Biogeochem. Cycles* 9, 359–372. doi: 10.1029/95GB01070
- Oksanen, A. J., Blanchet, F. G., Friendly, M., Kindt, R., Legendre, P., McGlenn, D., et al. (2018). *Package “vegan.” version 2.5-3*.

- Olenina, I., Hajdu, S., Edler, L., Wasmund, N., Busch, S., Göbel, J., et al. (2006). Biovolumes and size-classes of phytoplankton in the Baltic Sea. *HELCOM Balt. Sea Environ. Proc.* 106, 144.
- Pasciak, W. J., and Gavis, J. (1974). Transport limitation of nutrient uptake in phytoplankton. *Limnol. Oceanogr.* 19, 881–888. doi: 10.1016/j.cub.2014.12.004
- Paul, A. J., Bach, L. T., Schulz, K.-G., Boxhammer, T., Czerny, J., Achterberg, E. P., et al. (2015). Effect of elevated CO₂ on organic matter pools and fluxes in a summer Baltic Sea plankton community. *Biogeosciences* 12, 6181–6203. doi: 10.5194/bg-12-6181-2015
- Pondaven, P., Gallinari, M., Chollet, S., Bucciarelli, E., Sarthou, G., Schultes, S., et al. (2007). Grazing-induced Changes in Cell Wall Silicification in a Marine Diatom. *Protist* 158, 21–28. doi: 10.1016/j.protis.2006.09.002
- Reinfelder, J. R. (2011). Carbon concentrating mechanisms in eukaryotic marine phytoplankton. *Ann. Rev. Mar. Sci.* 3, 291–315. doi: 10.1146/annurev-marine-120709-142720
- Riebesell, U., Czerny, J., von Bröckel, K., Boxhammer, T., Büdenbender, J., Deckelnick, M., et al. (2013). Technical Note: A mobile sea-going mesocosm system – new opportunities for ocean change research. *Biogeosciences* 10, 1835–1847. doi: 10.5194/bg-10-1835-2013
- Rossoll, D., Bermúdez, R., Hauss, H., Schulz, K. G., Riebesell, U., Sommer, U., et al. (2012). Ocean acidification-induced food quality deterioration constrains trophic transfer. *PLoS One* 7:e34737. doi: 10.1371/journal.pone.0034737
- Rost, B., Riebesell, U., Burkhardt, S., and Sültemeyer, D. (2003). Carbon acquisition of bloom-forming marine phytoplankton. *Limnol. Oceanogr.* 48, 55–67. doi: 10.4319/lo.2003.48.1.0055
- Sarthou, G., Timmermans, K. R., Blain, S., and Tréguer, P. (2005). Growth physiology and fate of diatoms in the ocean: A review. *J. Sea Res.* 53, 25–42. doi: 10.1016/j.seares.2004.01.007
- Schulz, K. G., Bellerby, R. G. J., Brussaard, C. P. D., Büdenbender, J., Czerny, J., Engel, A., et al. (2013). Temporal biomass dynamics of an Arctic plankton bloom in response to increasing levels of atmospheric carbon dioxide. *Biogeosciences* 10, 161–180. doi: 10.5194/bg-10-161-2013
- Shen, C., and Hopkinson, B. M. (2015). Size scaling of extracellular carbonic anhydrase activity in centric marine diatoms. *J. Phycol.* 51, 255–263. doi: 10.1111/jpy.12269
- Sommer, U., Stibor, H., Katchikis, A., Sommer, F., and Hansen, T. (2002). Pelagic food web configurations at different levels of nutrient richness and their implications for the ratio fish production:primary production. *Hydrobiologia* 484, 11–20. doi: 10.1023/A:1021340601986
- Strickland, J. D. H., and Parsons, T. R. (1972). in *A practical handbook of seawater analysis*, ed. J. C. Stevenson Ottawa (Ottawa: Fisheries research board of Canada).
- Taucher, J., Aristegui, J., Bach, L. T., Guan, W., Montero, M. F., Nauendorf, A., et al. (2018). Response of Subtropical Phytoplankton Communities to Ocean Acidification Under Oligotrophic Conditions and During Nutrient Fertilization. *Front. Mar. Sci.* 5:330. doi: 10.3389/fmars.2018.00330
- Taucher, J., Bach, L. T., Boxhammer, T., Nauendorf, A., Achterberg, E. P., Alguero-Muñoz, M., et al. (2017). Influence of Ocean Acidification and Deep Water Upwelling on Oligotrophic Plankton Communities in the Subtropical North Atlantic: Insights from an In situ Mesocosm Study. *Front. Mar. Sci.* 4:85. doi: 10.3389/fmars.2017.00085
- Thor, P., Bailey, A., Dupont, S., Calosi, P., Søreide, J. E., De Wit, P., et al. (2018). Contrasting physiological responses to future ocean acidification among Arctic copepod populations. *Glob. Chang. Biol.* 24, e365–e377. doi: 10.1111/gcb.13870
- Tortell, P. D., Payne, C. D., Li, Y., Trimborn, S., Rost, B., Smith, W. O., et al. (2008). CO₂ sensitivity of Southern Ocean phytoplankton. *Geophys. Res. Lett.* 35, L04605. doi: 10.1029/2007GL032583
- Tréguer, P., Bowler, C., Moriceau, B., Dutkiewicz, S., Gehlen, M., Aumont, O., et al. (2018). Influence of diatom diversity on the ocean biological carbon pump. *Nat. Geosci.* 11, 27–37. doi: 10.1038/s41561-017-0028-x
- Tréguer, P. J., and De La Rocha, C. L. (2013). The World Ocean Silica Cycle. *Ann. Rev. Mar. Sci.* 5, 477–501. doi: 10.1146/annurev-marine-121211-172346
- Trimborn, S., Brenneis, T., Sweet, E., and Rost, B. (2013). Sensitivity of Antarctic phytoplankton species to ocean acidification: growth, carbon acquisition, and species interaction. *Limnol. Oceanogr.* 58, 997–1007. doi: 10.4319/lo.2013.58.3.0997
- Vrieling, E. G., Gieskes, W. W. C., and Beelen, T. P. M. (1999). Silicon deposition in diatoms: control by the pH inside the silicon deposition vesicle. *J. Phycol.* 35, 548–559. doi: 10.1046/j.1529-8817.1999.3530548.x
- Wallace, R. B., Baumann, H., Grear, J. S., Aller, R. C., and Gobler, C. J. (2014). Coastal ocean acidification: The other eutrophication problem. *Estuar. Coast. Shelf Sci.* 148, 1–13. doi: 10.1016/j.ecss.2014.05.027
- Welschmeyer, N. (1994). Fluorometric analysis of chlorophyll a in the presence of chlorophyll b and pheopigments. *Limnol. Oceanogr.* 39, 1985–1992. doi: 10.4319/lo.1994.39.8.1985
- Wilken, S., Hoffmann, B., Hersch, N., Kirchgessner, N., Dieluweit, S., Rubner, W., et al. (2011). Diatom frustules show increased mechanical strength and altered valve morphology under iron limitation. *Limnol. Oceanogr.* 56, 1399–1410. doi: 10.4319/lo.2011.56.4.1399
- Wolf-Gladrow, D., and Riebesell, U. (1997). Diffusion and reactions in the vicinity of plankton: A refined model for inorganic carbon transport. *Mar. Chem.* 59, 17–34. doi: 10.1016/S0304-4203(97)00069-8
- Wu, Y., Campbell, D. A., Irwin, A. J., Suggett, D. J., and Finkel, Z. V. (2014). Ocean acidification enhances the growth rate of larger diatoms. *Limnol. Oceanogr.* 59, 1027–1034. doi: 10.4319/lo.2014.59.3.1027
- Zhang, Y., Bach, L. T., Lohbeck, K. T., Schulz, K. G., Listmann, L., Klapper, R., et al. (2018). Population-specific responses in physiological rates of *Emiliania huxleyi* to a broad CO₂ range. *Biogeosciences* 15, 3691–3701. doi: 10.5194/bg-15-3691-2018

Conflict of Interest Statement: The authors declare that the research was conducted in the absence of any commercial or financial relationships that could be construed as a potential conflict of interest.

Copyright © 2019 Bach, Hernández-Hernández, Taucher, Spisla, Sforza, Riebesell and Aristegui. This is an open-access article distributed under the terms of the Creative Commons Attribution License (CC BY). The use, distribution or reproduction in other forums is permitted, provided the original author(s) and the copyright owner(s) are credited and that the original publication in this journal is cited, in accordance with accepted academic practice. No use, distribution or reproduction is permitted which does not comply with these terms.



Application of Stable Carbon Isotopes in a Subtropical North Atlantic Mesocosm Study: A New Approach to Assess CO₂ Effects on the Marine Carbon Cycle

Mario Esposito^{1,2*}, Eric P. Achterberg^{1,2}, Lennart T. Bach^{1,3}, Douglas P. Connelly², Ulf Riebesell¹ and Jan Taucher¹

¹ Marine Biogeochemistry, Biological Oceanography, GEOMAR Helmholtz Centre for Ocean Research Kiel, Kiel, Germany,

² National Oceanography Centre Southampton, Southampton, United Kingdom, ³ Institute for Marine and Antarctic Studies, University of Tasmania, Hobart, TAS, Australia

OPEN ACCESS

Edited by:

Il-Nam Kim,
Incheon National University,
South Korea

Reviewed by:

Sun-Yong Ha,
Korea Polar Research Institute,
South Korea
Frank Dehairs,
Vrije University Brussel, Belgium

*Correspondence:

Mario Esposito
mesposito@geomar.de

Specialty section:

This article was submitted to
Marine Biogeochemistry,
a section of the journal
Frontiers in Marine Science

Received: 16 October 2018

Accepted: 18 September 2019

Published: 02 October 2019

Citation:

Esposito M, Achterberg EP, Bach LT, Connelly DP, Riebesell U and Taucher J (2019) Application of Stable Carbon Isotopes in a Subtropical North Atlantic Mesocosm Study: A New Approach to Assess CO₂ Effects on the Marine Carbon Cycle. *Front. Mar. Sci.* 6:616. doi: 10.3389/fmars.2019.00616

Stable isotope ratio analysis offers a unique opportunity to obtain information on ecosystem processes. The increase in atmospheric CO₂ as a consequence of fossil fuel combustion and land-use change is altering the stable carbon isotope composition ($\delta^{13}\text{C}$) of the atmosphere and ocean. This work investigates the application of using $\delta^{13}\text{C}$ measurements of seawater samples to explore the biogeochemical responses of marine ecosystems to anthropogenic CO₂ perturbations. The combination of isotopic and non-isotopic measurements from a subtropical North-Atlantic mesocosm experiment provided a holistic view of the biogeochemical mechanisms that affect carbon dynamics under a gradient of pCO₂ ranging from ~350 up to ~1,000 μatm during a phytoplankton succession. A clear CO₂ response was detected in the isotopic datasets with ^{13}C shifts of up to ~5‰, but increased CO₂ levels only had a subtle effect on the concentrations of the dissolved and particulate organic carbon pools. Distinctive $\delta^{13}\text{C}$ signatures of the particulate organic carbon pools in the water column and sediment traps were detectable for the different CO₂ treatments after a nutrient stimulated phytoplankton bloom. These signatures were strongly correlated ($p < 0.05$) with the $\delta^{13}\text{C}$ signatures of the inorganic carbon but not with the $\delta^{13}\text{C}$ of the dissolved organic carbon pools ($p > 0.05$). Fractionation of carbon isotopes in phytoplankton was positively affected ($9.6 < \epsilon < 16.5\text{‰}$) by high CO₂ levels either because of the higher CO₂ availability or because of a shift in phytoplankton community composition. Nevertheless, phytoplankton bloom intensity and development was independent of CO₂ concentrations, and higher CO₂ levels had no significant effect on inorganic nutrient uptake. Results from this mesocosm experiment showed that variations in the carbon isotopic signature of the carbon pools depend on both physical (air-sea exchange) and biological (community composition) drivers opening the door to new approaches for investigations of carbon cycling in marine ecosystems.

Keywords: ocean acidification, mesocosm experiment, stable carbon isotopes, marine biogeochemistry, carbon cycle

INTRODUCTION

Since the beginning of the industrial revolution, the concentration of carbon dioxide (CO₂) in the atmosphere has increased by circa 40% from about 280 ppm to values above 400 ppm (<http://www.esrl.noaa.gov>). Atmospheric levels of CO₂ are expected to rise further and if no effective mitigation activities are initiated they could reach levels between 750 and more than 1,300 ppm by the end of this century (IPCC, 2014). The global ocean is attenuating this increase by absorbing about 25% of the CO₂ emitted by human activities (Le Quéré et al., 2016). However, the current rate of CO₂ uptake is leading to perturbations in the carbonate system (ocean acidification, OA) with potentially adverse consequences for marine ecosystems. The flux of CO₂ between the atmosphere and the ocean is mainly controlled by physical processes (Couldrey et al., 2016); however biological processes also affect the air-sea CO₂ transfer: phytoplankton assimilate inorganic carbon dissolved in seawater and convert it into organic forms via photosynthesis. As a consequence, surface water CO₂ concentrations decrease promoting further CO₂ transfer from the atmosphere. In general, it is assumed that primary production and sinking of organic matter to depth (export) contribute to increase ocean CO₂ sequestration from the atmosphere while community respiration tends to decrease it (Volk and Hoffert, 1985).

Over recent years, a wide range of research activities have been conducted to improve our understanding of the effects of rising atmospheric CO₂ levels on carbon fixation and cycling in the marine environment. Mesocosms offer an intermediate scale between laboratory and natural conditions, representing near natural ecosystems in which environmental factors can be manipulated and closely monitored (Riebesell et al., 2013). Over the last few years, several mesocosm studies have been conducted aimed at investigating the effects of elevated CO₂ on marine ecosystems. They have provided comprehensive datasets, although interpretation has been highly complex.

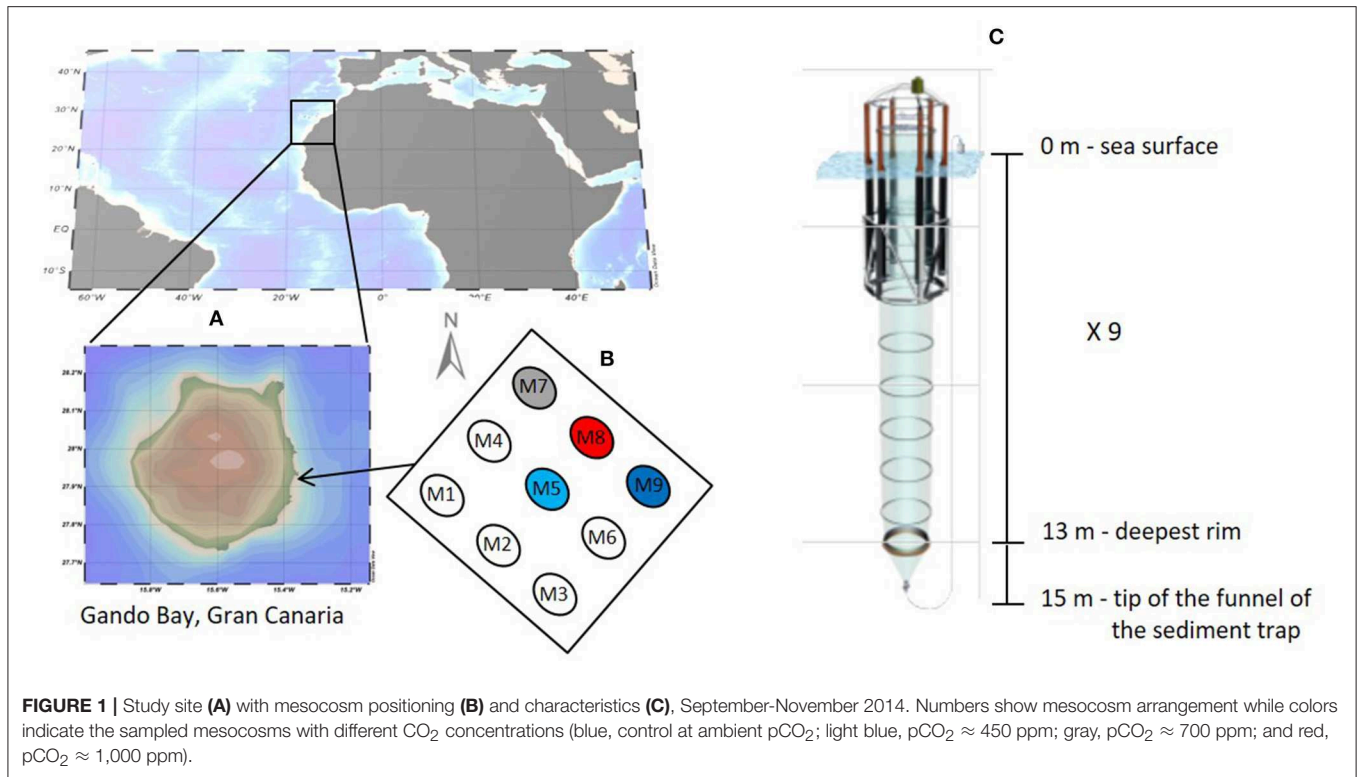
In a mesocosm experiment carried out in the subpolar waters of the Raunefjord, Norway in 2005, high CO₂ levels enhanced inorganic carbon consumption relative to nutrient uptake (Riebesell et al., 2007), however no increased levels of organic material were observed in the water column suggesting a rapid export to the bottom of the mesocosm (Schulz et al., 2008). Interestingly, in the same experiment, labeled ¹³C measurements showed increased biomass of green algae and diatoms under high CO₂ levels, but no indication of enhanced sinking during the bloom phase (De Kluijver et al., 2010). In order to gain further insights into carbon transfer mechanisms, an additional mesocosm study was carried out in the polar region at Ny Ålesund, Svalbard in 2010, and through the use of labeled ¹³C, carbon fluxes were assessed. Elevated CO₂ concentrations had no direct effect on primary production and bacterial activity, however an increase in sedimentation of fresh organic material was observed (De Kluijver et al., 2013). In a recent long-term mesocosm experiment in the Swedish Gullmar Fjord, enhanced CO₂ concentrations had non-detectable effects on plankton community composition (Bach et al., 2016) or on the molecular composition of organic matter (Zark et al., 2017).

The use of a ¹³C labeling technique in past mesocosm experiments has given indications on the direct coupling between phytoplankton and bacteria. However, tracer addition experiments are limited when the product is saturated with the labeled ¹³C as further incorporation of substrate would not change the signature of the product. In the case of phytoplankton and bacteria, the fast turnover rates of 2–6 days (Field et al., 1998) limit the use of the labeled ¹³C incorporation method for a long term assessment of carbon fluxes. Moreover, as carbon cycling in the marine system involves many active exchanges not only between the phytoplankton and bacteria compartments, interactions among all of the carbon pools must be assessed. Here, we explore the feasibility of using stable carbon isotope analysis as a tool for tracing the natural carbon component through the marine system in a long-term mesocosm study. The isotopic signal propagation was “traced” through the various carbon compartments, from the dissolved inorganic pool to the organic pools (dissolved and particulate), as well as the sinking particulate pool collected in sediment traps. The mechanisms driving the partitioning of ¹³C were linked to biogeochemical processes such as photosynthesis, organic matter oxidation and/or export. The main research objective was to investigate how CO₂ additions can be used to trace changes in the isotopic signatures in the various carbon pools. In contrast to previous studies, labeled bicarbonate was not used here. Instead, the processes that control the distribution of stable carbon isotopes within the water column were identified and quantified under different CO₂ levels. To the best of our knowledge, this is the first time that this approach is used to determine the effects and fate of increasing levels of natural carbon in a phytoplankton succession.

MATERIALS AND METHODS

The Study Site and Mesocosm Experiment Description

The study was conducted in the coastal waters of Gran Canaria (Spain) between the 23rd of September and the 27th of November 2014. The Canary Island location represents a transitional zone between the northwest African coastal upwelling region and the open ocean oligotrophic waters of the North Atlantic subtropical gyre (González-Dávila et al., 2003). The islands are characterized by a relatively weak surface current (Canary Current) flowing southwestwards and driven by north-easterly trade winds. The experiment was carried out in Gando Bay (**Figure 1**) in order to ensure wind and wave protection from predominant north easterly wind swells. The experimental setup and mesocosm characteristics are described in detail in Taucher et al. (2017). Briefly, nine Kiel Off-Shore Mesocosms for Future Ocean Simulation (KOSMOS) were deployed and moored in clusters of three at 27° 55'N, 15° 21'W about 4.5 nautical miles (nmi) from Taliarte harbor. A very strong eastward current event (t25–t27) damaged one of the mesocosms (M6) and no more sampling was performed from this unit until the end of experiment. Data from mesocosm M6 were therefore excluded from the analyses. Only four (M5, M7, M8, and M9) of the nine mesocosms were sampled for isotopic analysis and therefore



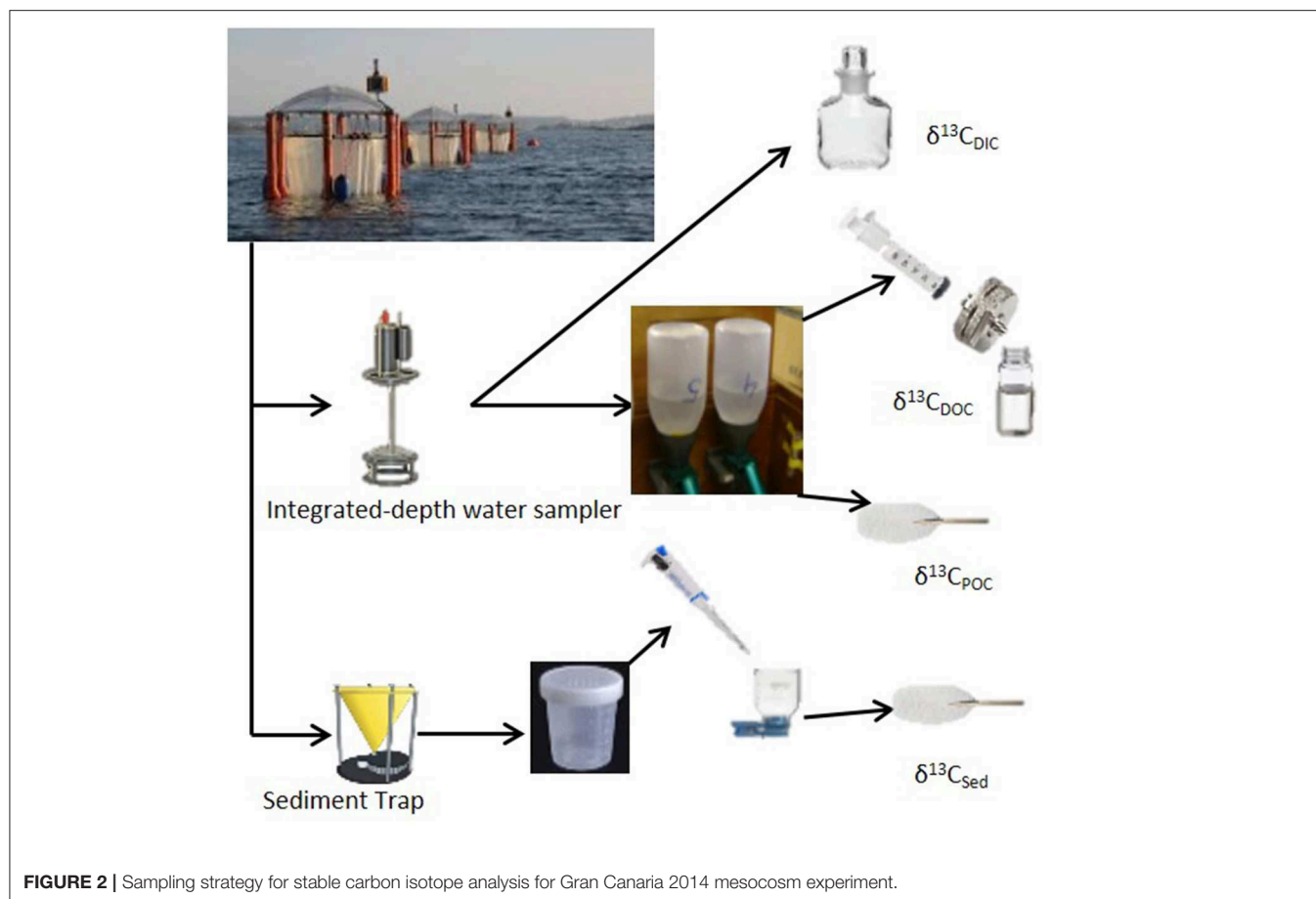
considered herein. The water depth at the deployment site was between 18 and 22 m. The bottom ends of the mesocosm bags were lowered to a depth of 15 m below the surface enclosing a volume of about 35 m³ of seawater. A 3 mm size mesh was attached to the top and bottom of the bags in order to exclude patchily distributed large organisms such as fish larvae or jellyfish from the enclosed water bodies. Free exchange of water and plankton (<3 mm) was allowed for 4 days until divers replaced the bottom mesh with the sediment trap. Attachment of the sediment trap and simultaneous pulling of the upper part of the bags above the sea surface level marked the beginning of the experiment (27th of September 2014) defined as time t-4 with t0 marking the day of the initial CO₂ manipulation. The main CO₂ addition was performed in four steps over 6 days by adding calculated amounts (from 77 L in M5 to 382 L in M8) of CO₂-saturated seawater to each mesocosm as described in Riebesell et al. (2013), in order to yield a pCO₂ gradient from ambient to concentrations corresponding to year 2150 (~1,480 μatm) according to RCP8.5 scenario (IPCC, 2014). The CO₂-saturated seawater was prepared by aerating about 1,500 L of Melenara Bay filtered seawater with pure CO₂ gas for at least one hour to reach pH value of ~4. The water was collected from a depth of 10 m using a pipe and pre-filtration system. Nutrient levels were low with nitrate concentrations equal to 1.8 μM, phosphate 0.1 μM, silicate 2.1 μM, and ammonium 0.1 μM. The CO₂ manipulation was performed by pumping CO₂-saturated seawater directly into the mesocosm bags by using a special distribution device that assured uniform distribution within a radius of ~1 m (Riebesell et al., 2013). No CO₂ addition was performed on mesocosm M9 which was used as a control

(ambient pCO₂). Two further CO₂ additions (t21 and t38) were performed during the course of the experiment to account for CO₂ loss related to outgassing.

At day t24, aliquots of deep water (~8 m³) obtained from a depth of 650 m located about 4 nautical miles north-east from the study site were added to each mesocosm to promote a phytoplankton bloom. The experiment was terminated about 15 days after the decline of the bloom at t55. The whole experiment was divided in three phases (Taucher et al., 2017) based on chlorophyll a (chl *a*) and nutrient dynamics: an oligotrophic phase I (t0–t23), a phytoplankton bloom phase II (t25–t35) and a post bloom phase III (t37–t55).

Sampling Strategy

Sampling was carried out every second day. The particles that settled in the mesocosm sediment traps were removed through a silicon hose connected at one side to the bottom of the sediment trap and at the other side to a vacuum-pump system. Sediment samples were collected before water column sampling directly into a 5 L Schott Duran® glass bottle, following the procedure described in Boxhammer et al. (2016), in order to avoid possible resuspension of the settled material in the mesocosm water column. Subsamples for stable carbon isotope analysis of the sedimented material ($\delta^{13}\text{C}_{\text{Sed}}$) were collected every other sampling day (every 4 days) from the homogenized collected sediment material. Sampling for $\delta^{13}\text{C}_{\text{Sed}}$ was conducted by gentle vacuum (<200 mbar) filtration of 3 ml of homogenized sediment particle suspension on pre-combusted (450°C for 12 h) 25 mm, 0.7 μm pore size glass microfiber Whatman GF/F filters. The



filters were stored frozen (-20°C) immediately after sampling for later analysis.

Water column samples were collected every sampling day using a depth integrating water sampler (IWS, Hydro-Bios) that allows evenly collection of 5 l of seawater over the entire depth (13 m) of the mesocosm. Separate sampling bottles were used to withdraw precise aliquots of seawater from the IWS for specific analysis types. These included samples for inorganic nutrients (nitrate, silicate, phosphate, and ammonium), dissolved inorganic and organic carbon (DIC and DOC, respectively) and pigments. Every other sampling day, the chosen mesocosms were sampled for isotope analysis in the forms of dissolved and particulate inorganic and organic carbon (**Figure 2**). Samples for stable isotopic analyses of dissolved inorganic carbon ($\delta^{13}\text{C}_{\text{DIC}}$) were collected into 100 ml borosilicate glass bottles (Pyrex) with a glass stopper. Sample preservation was performed by spiking the samples with 20 μl of saturated mercuric chloride solution (Dickson et al., 2007). For analyses of stable isotopes of dissolved organic carbon ($\delta^{13}\text{C}_{\text{DOC}}$), samples were collected into 30 ml acid-washed (HCl, 10%) and pre-combusted (at 450°C for 12 h) TOC glass vials after filtration through a pre-combusted 25 mm carbon cleaned glass-fiber filters (GF/F; Whatmann) (Farmer et al., 2007). Samples were acidified to $\text{pH} < 2$ with 100 μl of 4 M hydrochloric acid solution for preservation. Samples for isotopic analysis of particulate organic carbon ($\delta^{13}\text{C}_{\text{POC}}$) were collected

on $0.7\ \mu\text{m}$ pore size pre-combusted (at 450°C for 12 h) GF/F filters by filtration of 1 L of seawater collected into 1 L narrow mouth (Nalgene, HDPE) sampling bottles. The filters were stored frozen (-20°C) immediately after sampling for later analysis.

Every sampling day after sediment and water column sampling, a sensor unit (CTD60M; Sea & Sun Technologies) was used to determine vertical profiles of salinity, temperature, pH, chl *a*, and photosynthetically active radiation (PAR) in every mesocosm and in the surrounding water.

Analytical Methods

In most cases, analysis of the collected samples followed standard procedures. Inorganic nutrients were filtered ($0.45\ \mu\text{m}$ cellulose acetate filters, Whatman) directly after sampling and analyzed on the same day to avoid concentration changes due to biological growth or decay. Measurements were performed using a SEAL Analytical QuAAtro AutoAnalyzer connected to JASCO Model FP-2020 Intelligent Fluorescence Detector and a SEAL Analytical XY2 autosampler. AACE v.6.04 software was used to control the system. The measurement approach is based on spectrophotometric techniques according to Hansen and Koroleff (2007) for the determination of nitrate and silicate, Murphy and Riley (1962) for the determination of phosphate and Holmes et al. (1999) for the determination of ammonium. Carbonate chemistry (DIC and TA) samples were sterile-filtered

(0.2 μm) through a syringe and stored at 4°C in the dark for a maximum of 3 days until infrared absorption and potentiometric titration for the determination of DIC and TA, respectively (Taucher et al., 2017). Phytoplankton pigments were extracted in acetone (90%) to determine chl *a* concentrations using reverse phase high performance liquid chromatography (HPLC) as described by Bach et al. (2016) and Taucher et al. (2017).

Stable Carbon Isotope Analysis

Stable carbon isotope measurements of DIC ($\delta^{13}\text{C}_{\text{DIC}}$) were performed on a GasBench II preparation device connected to a Delta V Advantage isotope ratio mass spectrometer (both Thermo Fisher Scientific). Samples were analyzed in two batches consisting of 88 and 79 measurements each. A total of 27 vials (12 ml Exetainer® Labco Ltd, High Wycombe, UK) per batch were used for calibration and quality control standards, while the rest were used for seawater samples (52 plus 4 CO_2 -saturated seawater). Three in-house calibration standards (Marble-MAB, NaHCO_3 -NA, and Na_2CO_3 -NS) were run at the beginning and at the end of the analytical sequence, while quality control samples (blanks, Na_2CO_3 -NSL and Dickson CRMs) were placed every 12–14 seawater samples. All the samples were run in duplicate.

Measurements of $\delta^{13}\text{C}_{\text{POC}}$ and $\delta^{13}\text{C}_{\text{Sed}}$ were performed on a Flash 2000 Elemental Analyser (EA) connected to a Delta V Advantage IRMS through a ConFlo IV interface device (all Thermo Fisher Scientific). For the determination of $\delta^{13}\text{C}_{\text{POC}}$, one set of samples was acidified for 2 h with 4 M HCl in a dessicator under vacuum to remove calcium carbonate followed by drying overnight at 50°C. The second set was only dried. A total of 104 samples (52 from the water column and 52 from the sediment traps) were analyzed in duplicate over 10 analytical runs. Each run consisted of three initial blank measurements (tin capsule and pre-combusted blank filters), duplicate measurements of calibrated urea, caffeine, and sucrose standards, followed by a set of mesocosm samples. In the case of sediment samples, dilution (78% helium) was activated in order to avoid IRMS signal intensity saturation. It must be noted that during the isotopic analysis of POC in the sediment samples technical problems occurred and only total particulate carbon data could be used. Standard materials were accurately weighed (readability of 0.01 mg) between 0.1 and 1.0 mg in order to bracket the marine particulate carbon concentration range and used both for isotopic calibration and sample concentration determination in terms of POC and TPC. Sediment trap data were converted to daily fluxes normalized by mesocosm volumes determined as described in Taucher et al. (2017).

Measurements of $\delta^{13}\text{C}_{\text{DOC}}$ were carried out using an in-house combined Shimadzu 5000A TOC-IRMS system. A total of 52 samples were analyzed over 5 runs. Each analytical sequence consisted of initial background and ultrapure water blank measurements, followed by calibration standards (phthalate, urea, glutamic acid, and sucrose) and a variable set of seawater samples. Standards were accurately prepared with concentrations ranging between 30 and 600 μM of carbon and used both for isotopic calibration and sample concentration determination, in terms of DOC. Deep seawater consensus reference material (Lot No. 8-08) distributed from the laboratory of D. Hansell

(University of Miami) and additional urea or sucrose standards were analyzed between samples in order to check for accuracy and consistency of the measurements.

Stable Carbon Isotopes Measurement Processing

The three different instrument configurations used to perform stable carbon isotope analysis were calibrated by cross check measurements of the same standard compounds. Raw $\delta^{13}\text{C}$ results were processed following the same procedure: removal of anomalous measurements, linearity correction, blank correction, calibration to V-PDB and average of duplicates. Anomalies were assessed based on peak area height and when the intensity of the signal fell outside of the calibration range, the data point was removed. Only 0.8% of the total number of measurements was eliminated. Linearity correction was performed by quantification of the relationship between the δ values of repeated measurements of standards with increasing concentrations vs. the respective signal intensities. The mean gradient for each standard was calculated and used for linearity correction. Variation among gradients was 0.0083‰. Instrument background, reagent blank intensities and isotopic ratios were stable for all the analytical methods with average total variation of about $2 \pm 1.2\%$. Calibration of the samples to the V-PDB international standards was performed by three-point linear regression fits using standards of known isotopic ratios. Average r^2 was 0.9998 ± 0.00017 . Final $\delta^{13}\text{C}$ values were reported as the average of both analytical replicates and sample duplicates, when available. Calculated uncertainties (2σ) were 0.03, 0.12, and 1.42‰ for $\delta^{13}\text{C}_{\text{DIC}}$, $\delta^{13}\text{C}_{\text{POC}}$, and $\delta^{13}\text{C}_{\text{DOC}}$ measurements, respectively.

Data Analysis

Stable isotope data were expressed in the delta notation ($\delta^{13}\text{C}$) relative to the VPDB standard according to

$$\delta^{13}\text{C} = \frac{R_{\text{sample}} - R_{\text{standard}}}{R_{\text{standard}}} \times 1000 \text{‰} \quad (1)$$

where R represents the ratio of the heavy carbon isotope (^{13}C) to the light isotope (^{12}C). The isotopic incorporation of CO_2 -saturated water into mesocosm systems was calculated as relative changes in the ^{13}C fraction of the samples. Relative changes were calculated as a delta difference ($\Delta\delta^{13}\text{C}$) between the isotopic signature of the samples and the initial carbon isotopic signatures (before CO_2 additions) according to

$$\Delta\delta^{13}\text{C} = \delta^{13}\text{C}_{\text{sample}} - \delta^{13}\text{C}_{\text{initial}} \quad (2)$$

The impact of the different CO_2 additions on the $\delta^{13}\text{C}_{\text{DIC}}$ of the individual mesocosms was quantified with a theoretical mix using the following isotope mixing equation

$$\delta^{13}\text{C}_{\text{DICmix}} = \frac{(\delta^{13}\text{C}_{\text{DICinitial}} \times \text{DIC}_{\text{initial}}) + (\delta^{13}\text{C}_{\text{DICadded}} \times \text{DIC}_{\text{added}})}{(\text{DIC}_{\text{initial}} + \text{DIC}_{\text{added}})} \quad (3)$$

where $\delta^{13}\text{C}_{\text{DICinitial}}$ and $\text{DIC}_{\text{initial}}$ are the average initial carbon isotopic signature and concentration before any CO_2 addition,

respectively, $\delta^{13}\text{C}_{\text{DICadded}}$ is the carbon isotope ratio of the added CO_2 and $\text{DIC}_{\text{added}}$ correspond to the measured DIC differences on each day from the initial DIC concentration. Air-sea gas exchange was calculated both as total flux (F_C) and as outgassing of the ^{13}C fraction ($F_{13\text{C}}$) in $\text{mmol m}^{-2} \text{ s}^{-1}$. The ratio between each mesocosm volume and the mesocosm surface area (3.14 m^2) was used to normalize the air-sea gas exchange rates to units of water and to convert the rates into daily CO_2 fluxes (in $\mu\text{mol l}^{-1} \text{ d}^{-1}$). Fluxes were calculated for phase I and III only, when biological activity was low ($\text{Chl a} < 0.3 \mu\text{g l}^{-1}$). The total flux was determined as

$$F_C = -k(C_{\text{sample}} - C_{\text{sat}}) \quad (4)$$

where C_{sample} is the aqueous CO_2 concentration of the samples, C_{sat} is the saturation concentration corresponding to an atmospheric CO_2 partial pressure of 394 ppm (ftp://aftp.cmdl.noaa.gov/data/trace_gases/co2/flask/surface). The parameter k is the gas transfer velocity in m s^{-1} , which depends on wind speed and sea surface temperature and it was calculated according to Wanninkhof et al. (2009) by using the following equation:

$$k = -0.31u^2 \left(\frac{Sc}{660} \right)^{-0.5} \quad (5)$$

where u is the wind speed, Sc is the sea surface temperature (T) dependent Schmidt number, $Sc = 2073.1 - 125.62 \cdot T + 3.6276 \cdot T^2 - 0.043219 \cdot T^3$ for CO_2 (Schmittner et al., 2013) and 660 is the Schmidt number of CO_2 in seawater at 20°C. Wave motion was able to transfer through the mesocosms bags inducing roughness of the surface layer inside the mesocosms. From here the choice of -0.5 as exponent in Equation 5 which is commonly applied for wavy conditions (Jähne et al., 1984; Nightingale et al., 2000). The median wind speed, recorded a few nautical miles away at 10 m height, was 5.0 m s^{-1} , and because mesocosm surface waters were sheltered by the enclosure bags (about 1.5 m above the water level) a lower wind stress was present. A constant wind speed of 2 m s^{-1} was chosen and used for air-sea exchange calculations. The air-sea flux of $^{13}\text{CO}_2$ ($F_{13\text{C}}$) was calculated according to Zhang et al. (1995) by using the equation:

$$F_{13\text{C}} = -k\alpha_k\alpha_{\text{aq} \leftarrow \text{g}} \left(\frac{R_{\text{DIC}}}{\alpha_{\text{DIC} \leftarrow \text{g}}} C_{\text{sample}} - R_A C_{\text{sat}} \right) \quad (6)$$

where k is the piston velocity in m s^{-1} and α_k is a constant kinetic fractionation factor ($\alpha_k = 0.99915$) adapted from Schmittner et al. (2013). The terms $\alpha_{\text{aq} \leftarrow \text{g}}$ and $\alpha_{\text{DIC} \leftarrow \text{g}}$ are the temperature dependent isotopic fractionation factors from gaseous to aqueous CO_2 and from gaseous CO_2 to DIC, respectively. R_{DIC} and R_A correspond to the heavy to total isotope ratios of DIC and atmospheric CO_2 , respectively, and they were determined from ^{13}C fractions as $R_{\text{DIC}} = {}^{13}\text{C}_{\text{DIC}} / ({}^{12}\text{C}_{\text{DIC}} + {}^{13}\text{C}_{\text{DIC}})$ and $R_A = {}^{13}\text{C}_A / ({}^{12}\text{C}_A + {}^{13}\text{C}_A)$. The R_A was derived from the isotopic signature of the atmospheric CO_2 which was assumed to have a fixed $\delta^{13}\text{C}$ value of -8.2‰ according to the reported monthly average isotopic air measurements for the Canary Islands area (ftp://aftp.cmdl.noaa.gov/data/trace_gases/co2c13/flask/).

The effect of air-sea fluxes on $\delta^{13}\text{C}_{\text{DIC}}$ distributions was calculated as a difference ($\Delta F_{13\text{C}}$) between the $F_{13\text{C}}$ (divided by isotope ratio of the standard, $R_{\text{standard}} = 0.0112$) and the total carbon flux according to Schmittner et al. (2013) by using the following equation:

$$\Delta F_{13\text{C}} = \frac{F_{13\text{C}}}{R_{\text{standard}}} - F_C \quad (7)$$

To estimate carbon uptake by phytoplankton during photosynthesis a mass balance approach was used. The net changes within the various carbon pools were calculated for Phase II and III only as differences relative to initial conditions. The average DOC and POC values measured over the period before deep water addition were used as initial reference conditions. The net community production (NCP) was estimated from the build-up of biogenic carbon as an accumulation (in $\mu\text{mol l}^{-1}$) rather than a rate according to

$$\text{NCP} = \text{DOC}_{\text{diff}} + \text{POC}_{\text{diff}} + \sum \text{TPC}_{\text{Sed}} \quad (8)$$

Photosynthetic isotope fractionation (ε) between CO_2 and phytoplankton during the uptake process was calculated as

$$\varepsilon_{\text{CO}_2\text{-phyto}} = \frac{\delta^{13}\text{C}_{\text{CO}_2} - \delta^{13}\text{C}_{\text{POC}}}{1 + \delta^{13}\text{C}_{\text{POC}}/10^3} \quad (9)$$

where $\delta^{13}\text{C}_{\text{CO}_2}$ is the isotopic signature of aqueous CO_2 calculated from $\delta^{13}\text{C}_{\text{DIC}}$ values using the equilibrium fractionation factors between DIC and $\text{CO}_{2(\text{aq})}$ according to Zhang et al. (1995), and $\delta^{13}\text{C}_{\text{POC}}$ is the isotope ratio of particulate organic carbon assumed to represent the phytoplankton fraction in the water column. Dissolved CO_2 and not bicarbonate was considered as the main form of carbon assimilated by phytoplankton during growth due to its low energy costs associated with passive intracellular transport (Burkhardt et al., 1999; Marty and Planas, 2008) and to its generally high availability ($\text{CO}_{2(\text{aq})} = 10\text{--}14 \mu\text{mol l}^{-1}$) found in geographically proximate areas previously reported for the same time of year (Santana-Casiano et al., 2001; González-Dávila et al., 2003). Comparison with fractionation values calculated vs. total DIC rather than vs. the isotopic composition of dissolved CO_2 are also reported.

The NCP was used to estimate the fraction (f) of inorganic carbon (DIC) converted into organic matter. The latter was used to build an isotope fractionation model to assess the isotopic changes of the POC pool according to the substrate (DIC) uptake during the bloom phase. The model predicts the progress of the accumulated product (δ_P) and the residual substrate (δ_{RS}) according to

$$\delta_P = \delta_{\text{Input}} - \Delta \cdot (1 - f) \quad (10)$$

and

$$\delta_{\text{RS}} = (\delta_{\text{Input}} + 1000) \cdot (f \cdot \alpha + 1 - f) - 1000 \quad (11)$$

where $\alpha = (1,000 + \Delta)/1,000$ and the term δ_{Input} represent the isotopic signatures of DIC of each mesocosm before the onset of the bloom. A fixed fractionation factor (Δ) of 20‰ was used.

Statistical Analysis

The isotopic data reported are average values between duplicate samples (when available) with standard deviations (1σ) within the analytical error. The dataset was tested for normality distribution using the online Grubbs test (<http://graphpad.com/quickcalcs/grubbs1/>) and eventual outliers were removed and/or mathematically interpolated. Linear regression analyses were used to determine the relationship between $p\text{CO}_2$ and average response of the variables to each CO_2 addition phase. Significance was accepted for p -values < 0.05 . The potential effect of the added CO_2 on the various parameters was also calculated by subtracting observations of the control mesocosm from the treated mesocosms for the specific sampling day.

RESULTS

Mesocosm Performance and Mesocosm Phases

A total of 9 mesocosms were deployed in Gando Bay, but only four of them (M5, M7, M8, and M9) were sampled for stable carbon isotope analysis. The water inside the mesocosms was allowed to exchange with the surrounding water for a total of 4 days before isolation of the mesocosms water body from the surrounding water. Initial salinity, temperature, density, chl a and nutrient concentrations between the mesocosms were comparable. Average initial salinity in the mesocosms was 37.08 ± 0.01 and gradually increased throughout the experiment to reach final values of 38.03 ± 0.02 . The reason for the change was mostly due to evaporation although the addition of less saline deep water halfway through the experiment tempered the increase. Temperatures decreased gradually from $24.31 \pm 0.02^\circ\text{C}$ to $22.22 \pm 0.01^\circ\text{C}$ during the course of the experiment. According to CTD profiles, no halocline or thermocline developed during the experiment and all mesocosm parameters were relatively homogeneous through the water column. Injections of CO_2 -saturated seawater into the designated mesocosms formed a concentration gradient with average $p\text{CO}_2$ values of $473.9 \pm 22.6 \mu\text{atm}$ (M5), $776.8 \pm 42.8 \mu\text{atm}$ (M7), and $1311.7 \pm 105.3 \mu\text{atm}$ (M8) determined after each CO_2 addition (t5, t23, and t39). Mesocosm M9 was not treated (control) and exhibited average $p\text{CO}_2$ concentrations of $364.4 \pm 64.0 \mu\text{atm}$ measured over the same periods. Additions of CO_2 -saturated seawater increased mesocosm DIC concentrations proportionally and linear regression analysis confirmed the significant differences ($p < 0.05$) among treatments. However, no significant differences among mesocosms were observed overall for other physical parameters or nutrient data when CO_2 treatments were compared (Table 1).

Nutrient concentrations as well as chl a variations and CO_2 manipulation were used to define the different experimental phases (Figure 3). Initial concentrations of inorganic nitrate plus nitrite ($\text{NO}_3^- + \text{NO}_2^-$) were between 0.06 and $0.15 \mu\text{M}$, inorganic phosphate (PO_4^{3-}) ranged between 0.01 and $0.07 \mu\text{M}$, silicic acid (SiO_4^{4-}) was on average $0.23 \pm 0.054 \mu\text{M}$ and ammonium was variable between 0.04 and $0.34 \mu\text{M}$ for all mesocosms until the day of deep water addition. On day t24

about 8 m^3 of deep seawater were added per mesocosm bringing nutrient concentrations to 3.19 ± 0.02 , 0.17 ± 0.01 , and $1.61 \pm 0.11 \mu\text{M}$ for $\text{NO}_3^- + \text{NO}_2^-$, PO_4^{3-} , and SiO_4^{4-} , respectively. Ammonium levels were not affected by the addition of deep seawater and exhibited concentrations around $0.07 \pm 0.03 \mu\text{M}$ for all mesocosms. The simulated upwelling event triggered a phytoplankton bloom that lasted circa 10 days after which inorganic nutrients stabilized back to initial levels (Figure 3). Measurements of chl a confirmed the progression of the three phases (Figure 3). During the initial oligotrophic phase, chl a values ranged between 0.18 and $0.24 \mu\text{g l}^{-1}$. With the development of the bloom phase chl a values increased and on t31 the average concentration was $2.95 \pm 0.67 \mu\text{g l}^{-1}$. The maximum value ($5.62 \mu\text{g l}^{-1}$) was recorded for mesocosm M9 on t28. In the post bloom phase chl a concentrations dropped although they were on average higher ($0.57 < \text{chl } a < 1.10 \mu\text{g l}^{-1}$) than the initial concentrations. No statistically significant differences in chl a concentrations were observed between $p\text{CO}_2$ treatments (Table 1).

During the oligotrophic phase, the mesocosm communities were mainly consisting of pico- and nano-phytoplankton with cyanobacteria constituting the predominant group. The phytoplankton bloom in phase II, fuelled by deep water addition, was dominated by diatoms which accounted for more than 70% of the total chl a . Following the bloom, the microphytoplankton communities in the mesocosms were mainly dominated by large dinoflagellates (Taucher et al., 2017). The mesozooplankton community was dominated by copepods ($\sim 90\%$ of the total mesozooplankton abundance) throughout the whole experiment. During the oligotrophic phase zooplankton abundances were comparable among the different mesocosms, however after deep water addition, generally higher zooplankton abundances were observed in the high CO_2 treatments. However, a surprising temporal delay in zooplankton abundance was observed in the high $p\text{CO}_2$ mesocosms compared to the low and medium $p\text{CO}_2$ conditions (Algueró-Muñoz et al., 2019).

Mesocosm Carbon Dynamics: Concentrations and Stable Isotopes

In most of the cases, carbon trends agreed well with the phases defined by nutrients and chl a dynamics: oligotrophic phase I, phytoplankton bloom phase II and post bloom phase III. Before any CO_2 addition, on t-1, the $\delta^{13}\text{C}_{\text{DIC}}$ of the water was 1.06‰ . Analysis of aliquots of CO_2 -saturated seawater showed that the isotopic signature ($\delta^{13}\text{C}_{\text{DIC}}$) of the added seawater was $-35.64 \pm 0.43\text{‰}$ ($n = 10$) for the first batch and $-36.28 \pm 0.06\text{‰}$ ($n = 12$) for the second batch. Samples from the third batch were not taken therefore no measurements are available. The effects of the added CO_2 on mesocosm carbon species are summarized in Table 2 where statistical significance of $p\text{CO}_2$ treatments on each of the carbon system parameters for each experimental phase is reported.

Oligotrophic Phase I

Following the first CO_2 addition, the $\delta^{13}\text{C}_{\text{DIC}}$ of the mesocosms decreased significantly (Table 2 and Figure 4) in proportion to the added amount with average ^{13}C depletion of 1.4, 2.9, and

TABLE 1 | Results of linear regression analyses testing for statistical significance of pCO₂ effect on mesocosm nutrients and chlorophyll *a* for each experimental phase.

	Parameter	P-value	Multiple R ²	F statistic	Parameter	P-value	Multiple R ²	F statistic
Phase I	NO ₃ ⁻ + NO ₂ ⁻	0.183	0.816	3.997	PO ₄ ³⁻	0.899	0.100	0.020
Phase II		0.972	0.027	0.002		0.224	0.753	3.015
Phase III		0.772	0.228	0.110		0.125	0.874	6.507
Phase I	SiO ₄ ⁴⁻	0.089	0.910	9.733	Chl <i>a</i>	0.291	0.708	2.017
Phase II		0.015	0.984	63.446		0.911	0.088	0.015
Phase III		0.795	0.204	0.081		0.079	0.920	11.126

The statistically significant ($p < 0.05$) effects of CO₂ are reported in bold.

4.8‰ for mesocosm M5, M7, and M8, respectively, throughout the whole oligotrophic phase. A slight isotopic enrichment (0.2‰) combined with a decrease in DIC concentrations over time was observed in the treated mesocosms M7 and M8. The tendency to isotopic enrichment (greater amount of heavy isotope ¹³C) of surface water DIC for the higher CO₂ level mesocosms was confirmed by the positive values of ΔF_{13C} in mesocosm M7 and M8 (Table 3). This trend was mostly driven by outgassing indicated by the negative values of F_c and F_{13C} calculated for these mesocosms (Table 3). Average CO₂ efflux was 0.9 and 2.6 μmol l⁻¹ d⁻¹ for mesocosm M7 and M8, respectively, while an average daily CO₂ influx of 0.4 ± 0.04 μmol l⁻¹ was observed for the ambient pCO₂ control mesocosm M9. Mesocosm M5 exhibited variable daily fluxes with an overall CO₂ influx of 0.07 ± 0.05 μmol l⁻¹ d⁻¹ throughout the oligotrophic phase I. The average isotopic signature of the particulate carbon in the water column and in the sediment traps was -22.8 ± 0.72‰ and -21.1 ± 1.71‰ from t-1 to t13 for all mesocosms. A small decrease in δ¹³C_{POC} was observed at t19 in the treated mesocosms. An explanation for this small drop could be related to the Saharan dust event which occurred between t16 and t22. The dust event induced an increase of diatom biomass (Taucher et al., 2017), mainly composed of nanophytoplankton (Hernández-Hernández et al., 2018) that could have contributed to decrease the isotopic signature of POC in the water column at t19 due to an initial uptake of the added lighter carbon. Dissolved organic carbon concentrations gradually increased in all mesocosms from an average initial value of 98 ± 2.4 μmol l⁻¹ on t5 to a mean value of 108 ± 0.4 μmol l⁻¹ on t19. Ammonium concentrations, although highly variable, corroborate the DOC trend showing a general increase from 0.04 ± 0.02 μM at t1 to 0.13 ± 0.01 μM on t19 (Figure 3). The δ¹³C of the DOC pool was highly variable with observed ratios between -25.8 and -21.1‰. At first glance the CO₂ treatments appeared to lower ¹³C of the DOC component, however isotopic ratios of DOC in mesocosm M9 (control) were similar to the high treatment mesocosm with an average δ¹³C_{DOC} value of -23.9 ± 1.06‰. Linear regression analysis confirmed there was no significant effect of pCO₂ treatment on δ¹³C_{DOC} dynamics (Table 2).

Phytoplankton Bloom Phase II

The second CO₂ addition (t21) in general tended to stabilize DIC concentrations to target levels without causing any major

effect on the isotopic signature of the inorganic carbon pool. The addition of deep water stimulated a phytoplankton bloom which characterized the second phase (t25–t35). With the development of the bloom, the DIC concentrations decreased on average by 5% with a corresponding isotopic enrichment of about 2‰ for all mesocosms. The DOC concentrations decreased soon after the addition (average DOC = 98 ± 4.2 μmol/l at t26) possibly due to dilution with deepwater of lower DOC concentration. An increase in DOC of about 25% (mean value of 131 ± 4.9 μmol l⁻¹) followed and was noticed in all mesocosms. Measurements of δ¹³C_{DOC} samples showed reduced variation among mesocosms during the bloom period with an average value of -23.4 ± 0.49‰. Particulate organic carbon in general mirrored chl *a* dynamics showing a rapid increase in all mesocosms to concentrations up to 53.9 μmol l⁻¹ (M5 at t31). The sediment counterpart showed a slight delay with TPC_{Sed} fluxes starting to increase at the end of phase II. The particulate carbon in the water column showed a rapid isotopic enrichment (about 4‰) following deep water addition, however with the development of the phytoplankton bloom, the isotopic ratios of POC in individual mesocosms tended to significantly diverge (Table 2 and Figure 4) according to the added CO₂ levels (lower ratios for higher pCO₂ treatments). A similar trend was observed for δ¹³C_{Sed} samples although the corresponding isotopic response was detected on the successive sampling day (temporal shift).

Post Bloom Phase III

The last CO₂ addition on t38 brought concentrations and isotopic ratios of DIC close to pre-bloom levels. Over the entire post bloom phase, DIC concentrations in mesocosm M8 and M7 decreased by 1.5 and 0.5%, respectively, while an increase of 0.9 and 1.5% was observed in mesocosms M5 and M9, respectively. This trend suggested that air-sea gas exchange was driving seawater pCO₂ toward the equilibrium with the overlaying atmosphere. Similarly to Phase I the gas exchange had little effect on the δ¹³C_{DIC} distribution with isotopic variations within mesocosms lower than 0.2‰ for the duration of the entire phase III. The tendency to isotopic enrichment of surface water DIC for the higher CO₂ level mesocosms was confirmed by the positive values of ΔF_{13C} in mesocosms M7 and M8 while isotopic DIC depletion was suggested for M5 and M9 according to the calculated negative ΔF_{13C} values (Table 3). Compared to phase I

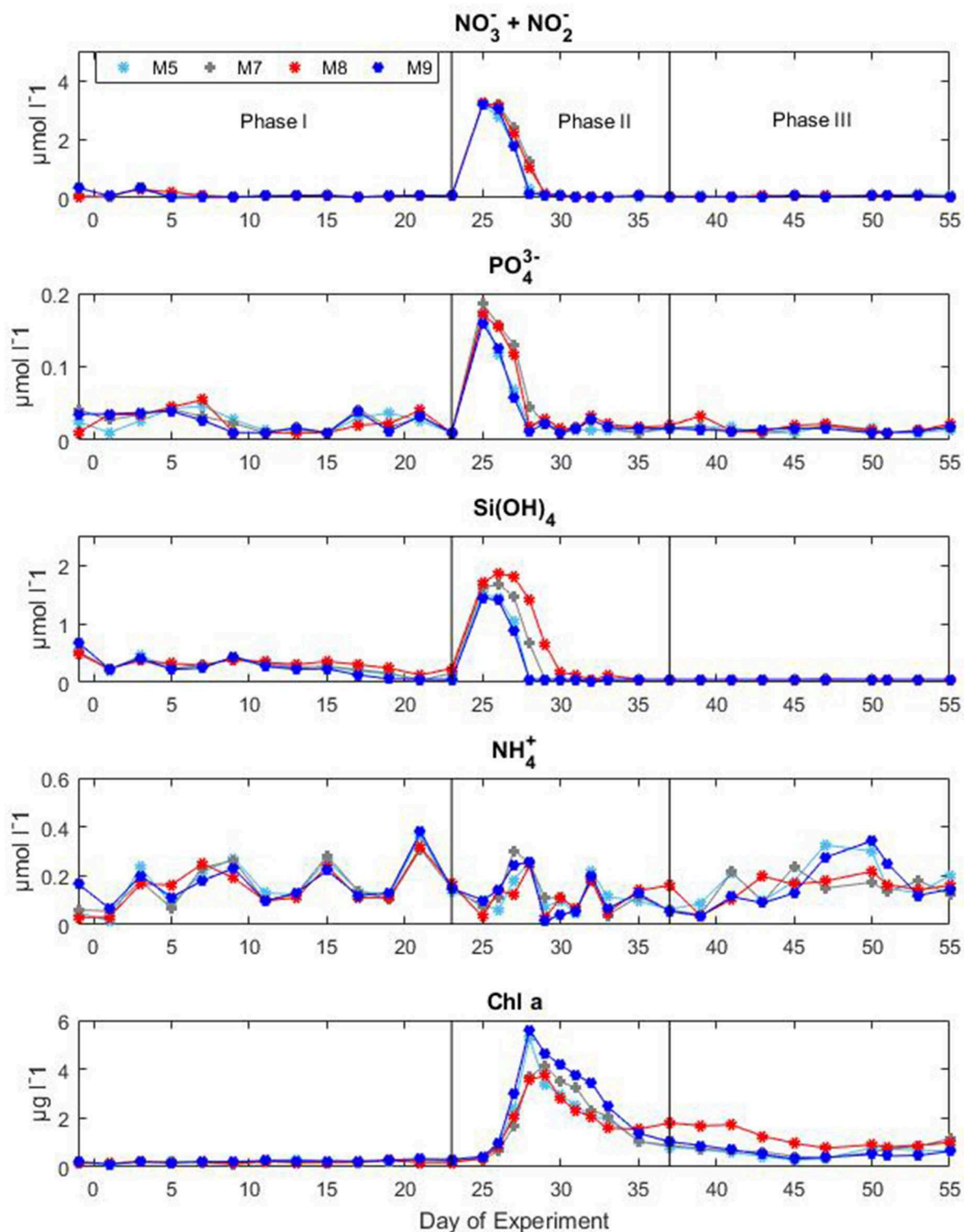


FIGURE 3 | Concentrations of inorganic nutrients and chlorophyll a during the Gran Canaria mesocosm experiment (2014). Sampling days (t-days) and main experimental manipulations are shown on the x-axis. Vertical lines define the experimental phases.

there was a general tendency to hold more CO_2 in the mesocosm waters and this was possibly due to the lower temperatures ($\Delta T = 2^\circ\text{C}$) observed during phase III. The DOC levels remained

stable with average concentrations of $123.8 \pm 5.02 \mu\text{mol l}^{-1}$ and the $\delta^{13}\text{C}_{\text{DOC}}$ showed no significant differences (**Table 2**) among treatments. The measured $\delta^{13}\text{C}$ of the DOC pool was reasonably

TABLE 2 | Results of linear regression analyses testing for statistical significance of pCO₂ effect on mesocosm carbon system parameters for each experimental phase.

	Parameter	P-value	Multiple R ²	F statistic	Parameter	P-value	Multiple R ²	F statistic
Phase I	DIC	0.021	0.987	43.718	$\delta^{13}\text{C}_{\text{DIC}}$	0.019	0.981	51.213
Phase II		0.016	0.983	59.050		0.038	0.962	24.796
Phase III		0.026	0.974	36.902		0.009	0.990	101.072
Phase I	DOC	0.711	0.286	0.711	$\delta^{13}\text{C}_{\text{DOC}}$	0.329	0.670	1.632
Phase II		0.224	0.775	3.021		0.930	0.068	0.001
Phase III		0.190	0.809	3.808		0.456	0.543	0.838
Phase I	POC	0.558	0.441	0.484	$\delta^{13}\text{C}_{\text{POC}}$	0.126	0.873	6.431
Phase II		0.083	0.916	10.528		0.002	0.998	509.683
Phase III		0.133	0.866	6.023		0.008	0.991	112.841
Phase I	TPC _{Sed}	0.242	0.757	2.698	$\delta^{13}\text{C}_{\text{Sed}}$	0.112	0.888	7.439
Phase II		0.131	0.868	6.141		0.037	0.962	24.950
Phase III		0.228	0.771	2.945		0.008	0.992	120.018

The statistically significant ($p < 0.05$) effects of CO₂ are reported in bold. DIC, dissolved inorganic carbon; DOC, dissolved organic carbon; POC, particulate organic carbon; and TPC_{Sed}, total particulate carbon in sediment traps.

similar for all the mesocosms with a slight increase over time from an average of $-23.6 \pm 0.82\%$ at t39 to $-21.9 \pm 0.57\%$ at t55 (excluding M5). In mesocosm M5, the last sample (at t55) had a $\delta^{13}\text{C}_{\text{DOC}}$ value of -24.6% . In the water column, concentrations of particulate carbon decreased by more than a half compared to the bloom period for all mesocosms. In the sediment traps, maximum fluxes ($2.83 \pm 0.30 \mu\text{mol l}^{-1} \text{d}^{-1}$) were recorded at the beginning of phase III on t43 as a consequence of the phytoplankton bloom decline and subsequent settling, until they stabilized to final TPC values of $1.32 \pm 0.59 \mu\text{mol l}^{-1} \text{d}^{-1}$. A second sedimentation event occurred on the last sampling day at t55 when divers scraped off the benthic microalgae layer that had grown on the side walls of the sediment trap funnel in order to collect all the material, clean the mesocosm bags, and conclude the experiment. Compared to the other mesocosms, at the end of the experiment, M8 had higher POC concentrations ($18.6 \mu\text{mol l}^{-1}$) in the water column and consequently lower TPC flux ($0.73 \mu\text{mol l}^{-1}$ per day) in the sediment trap. Isotopic signatures of the particulate carbon reflected the isotopic trend of $\delta^{13}\text{C}_{\text{DIC}}$ both in the water column and in the sediment traps showing significant correlations (Table 2) with the pCO₂ treatments. The measured isotopic values of POC were on average -19.8 ± 1.17 , -22.5 ± 0.97 , -27.2 ± 0.55 , and $-18.4 \pm 1.02\%$, for mesocosm M5, M7, M8, and M9, respectively, from t39 to t55 (Figure 4). Average $\delta^{13}\text{C}_{\text{Sed}}$ values over the same period were -20.2 ± 0.35 , -22.9 ± 0.32 , -24.9 ± 0.60 , and $-18.7 \pm 0.65\%$, for mesocosm M5, M7, M8, and M9, respectively (Figure 4).

DISCUSSION

Impacts of CO₂ Addition on the Stable Carbon Isotope Composition of Mesocosm Waters

The increasing anthropogenic CO₂ emissions and the consequent oceanic uptake are altering the marine environment.

One line of evidence of this CO₂-induced change is a reduction of the isotopic ratio of surface ocean waters known as the ¹³C Suess effect (Keeling, 1979). In this study, the addition of isotopically light CO₂ to the mesocosm systems simulated the oceanic CO₂ accumulation and therefore the evaluation of any CO₂ derived effect could improve our understanding of future ecosystem responses. The CO₂ manipulation formed a DIC concentration gradient among the considered mesocosms which was indicative of the potential atmospheric CO₂ increases expected over the next few decades without substantial emission reductions. The CO₂ treatment gradient was reflected in the isotopic signature of DIC (Figure 4) indicating the added lighter carbon ($\delta^{13}\text{C}_{\text{DIC}} = -35.96 \pm 0.45\%$) mixed homogeneously in the water columns of the mesocosms. Comparison of the measured $\delta^{13}\text{C}_{\text{DIC}}$ with theoretical mixing values gave an indication of the true isotopic variability within each mesocosm (Figure 5). The theoretical $\delta^{13}\text{C}_{\text{DIC}}$ values vs. the inverse of the DIC concentrations defined the true isotopic response to CO₂ additions for each mesocosm. The binary mixing line confirmed the establishment of a linear correlation with the various CO₂ additions although a slight underestimation of the theoretical isotopic response compared to the measured values was observed (Figure 5). Higher deviations from the theoretical values were observed mainly in the higher treatment mesocosms M8 and M7, probably because of the higher degassing rate of the samples during analysis. The mixing model allowed also for the extrapolation of the isotopic composition of the added CO₂ defined by the y-intercept. The extrapolated value of -36% agrees well with the measured $\delta^{13}\text{C}_{\text{DIC}}$ of the added CO₂ rich water.

The small isotopic effect (about 0.2‰ enrichment) due to air-sea gas exchange was discernible both during Phase I and Phase III where a slight increase in $\delta^{13}\text{C}_{\text{DIC}}$ was observed (Figure 5). Compared to DIC variations $\delta^{13}\text{C}_{\text{DIC}}$ variations were substantially smaller with rather constant isotopic composition of DIC observed in the treated mesocosms.

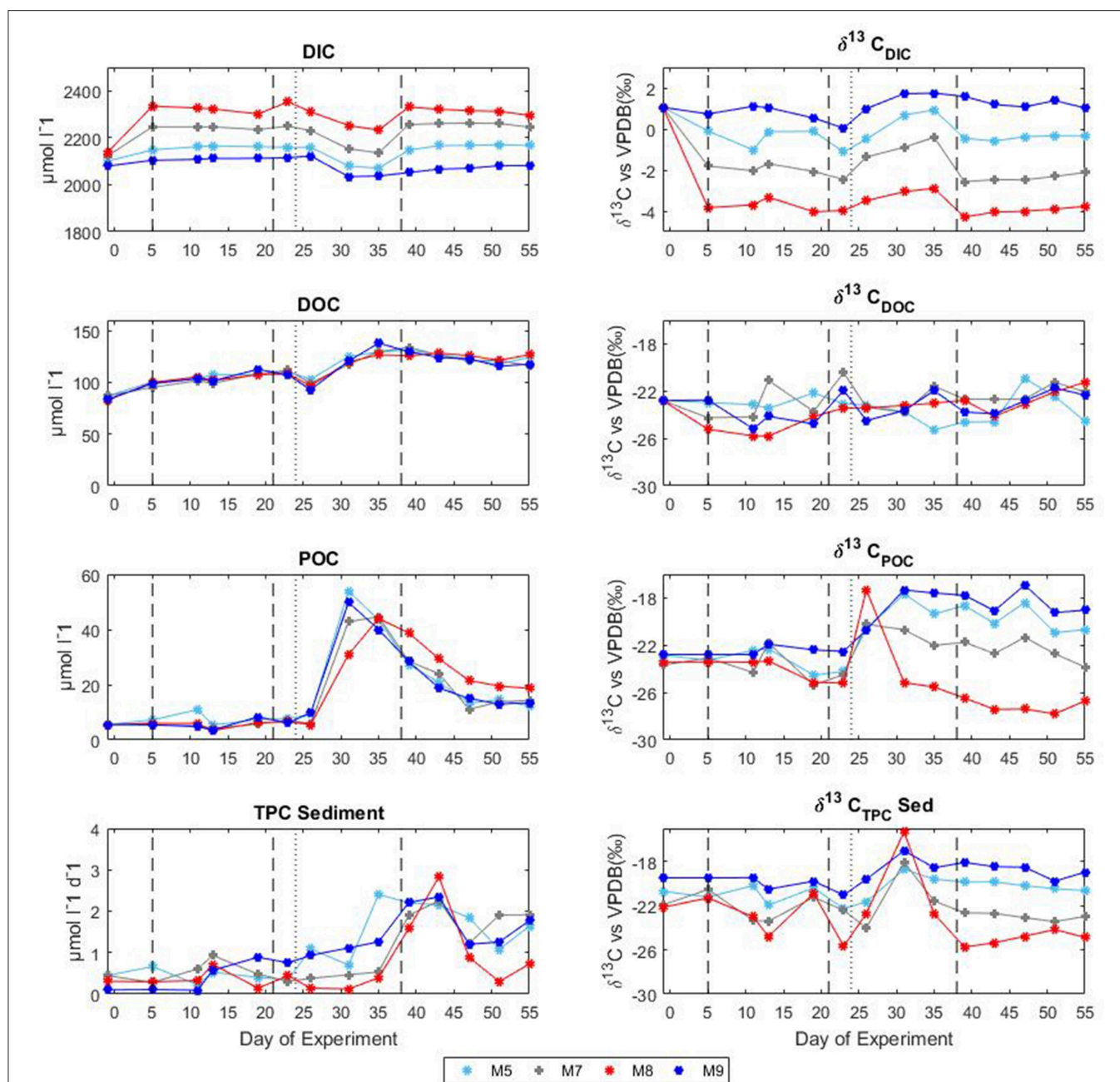


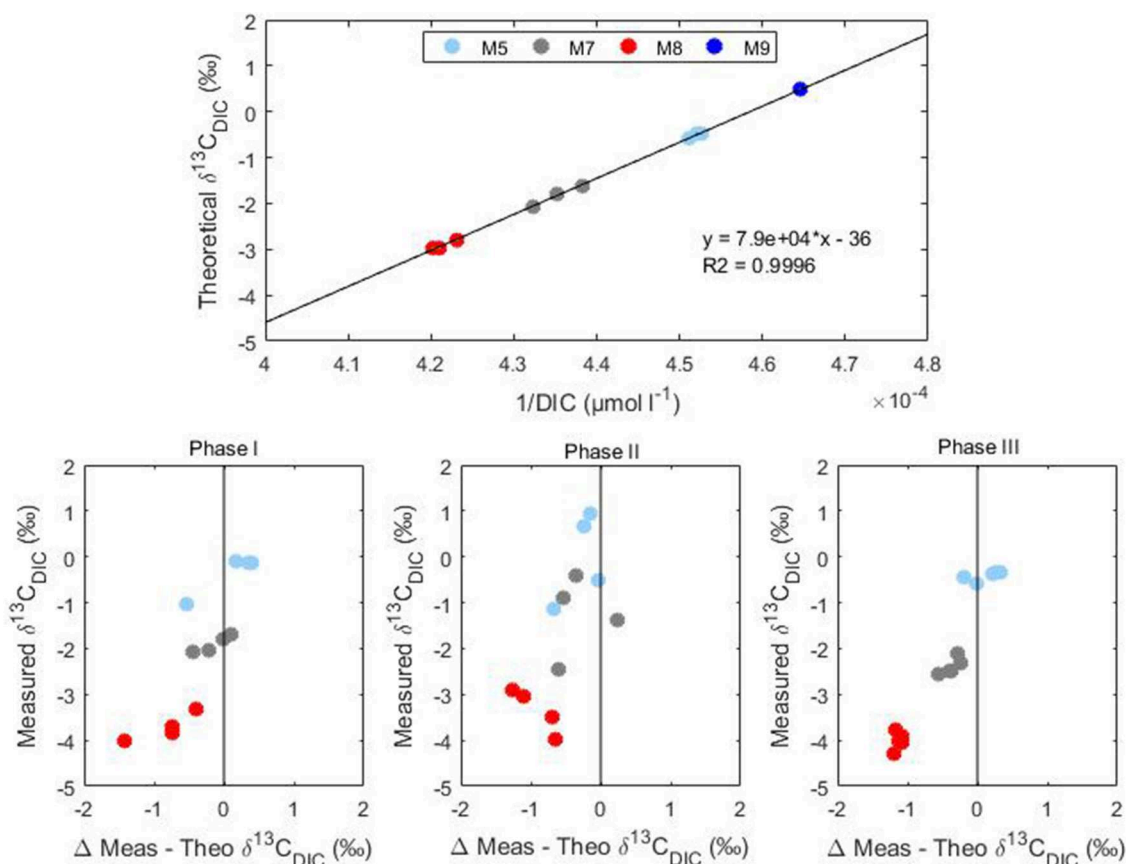
FIGURE 4 | Temporal development of concentrations and stable isotopes of carbon during the mesocosm experiment in Gran Canaria 2014. The vertical dashed lines denote the timing of CO₂ additions, the vertical dotted lines indicate deep water addition. DIC, dissolved inorganic carbon; DOC, dissolved organic carbon; POC, particulate organic carbon; and TPC, total particulate carbon.

This trend was most likely due to the longer times required by carbon isotopes compared to concentrations to reach the equilibrium with the atmosphere. Equilibration times for $\delta^{13}\text{C}_{\text{CO}_2}$ are estimated to be 10–20 times longer compared to the total CO₂ (Lynch-Stieglitz et al., 1995). This effect is confirmed by the substantially smaller values observed for $F_{13\text{C}}$ compared to F_{C} in all mesocosms during Phase I and III (Table 3).

The influence of isotopic equilibration on $\delta^{13}\text{C}_{\text{DIC}}$ depends not only on physical gas exchange, but also on biological processes. During the bloom phase, the gas exchange effect was “masked” by the biological uptake which sharply raised the isotopic composition of DIC in the mesocosm waters. The transfer from DIC to phytoplankton during phase II was rapid with an average phytoplankton carbon uptake of $52.9 \pm 8.83 \mu\text{mol l}^{-1}$ per day, between t26 and t35. Comparable rates of

TABLE 3 | Air-sea CO₂ fluxes for the mesocosm M5, M7, M8, and M9 during Phase I and Phase III.

	Phase I				Phase III			
	F _C (mmol m ⁻² s ⁻¹)	F _{13C} (mmol m ⁻² s ⁻¹)	ΔF _{13C} (mmol m ⁻² s ⁻¹)	CO ₂ flux (μmol l ⁻¹ d ⁻¹)	F _C (mmol m ⁻² s ⁻¹)	F _{13C} (mmol m ⁻² s ⁻¹)	ΔF _{13C} (mmol m ⁻² s ⁻¹)	CO ₂ flux (μmol l ⁻¹ d ⁻¹)
M5	0.78 ± 0.57	0.01 ± 0.01	-0.003 ± 0.01	0.07 ± 0.05	2.57 ± 0.27	0.03 ± 0.003	-0.02 ± 0.004	0.24 ± 0.02
M7	-9.65 ± 1.50	-0.11 ± 0.02	0.15 ± 0.02	-0.86 ± 0.13	-6.92 ± 1.68	-0.08 ± 0.02	0.13 ± 0.02	-0.62 ± 0.15
M8	-28.99 ± 4.99	-0.32 ± 0.06	0.47 ± 0.07	-2.59 ± 0.45	-16.81 ± 3.25	-0.18 ± 0.04	0.31 ± 0.05	-1.50 ± 0.29
M9	4.87 ± 0.46	0.05 ± 0.01	-0.07 ± 0.01	0.44 ± 0.04	8.40 ± 0.30	0.09 ± 0.003	-0.10 ± 0.005	0.75 ± 0.03

**FIGURE 5** | Conservative binary mixing plot of theoretical $\delta^{13}\text{C}_{\text{DIC}}$ vs. the inverse of DIC concentrations and measured stable carbon isotopic signatures ($\delta^{13}\text{C}_{\text{DIC}}$) vs. differences between theoretical and measured values during Phase I, II, and III of Gran Canaria mesocosm experiment (2014).

primary production were reported by Hernández-Hernández et al. (2018) for this study. With the development of the bloom, the $\delta^{13}\text{C}_{\text{POC}}$ values rapidly decreased with consequent associated increase of $\delta^{13}\text{C}_{\text{DIC}}$ in the residual seawater according to uptake.

Effects of CO₂ Addition on the Dissolved Organic Carbon Pool

No significant differences in DOC concentrations and isotopic composition (Table 2) were observed among the mesocosms during the course of the experiment. In agreement with our results, in the same study, Zark et al. (2017) could not find a detectable imprint in the molecular composition of organic

matter suggesting a universal microbial transformation of freshly produced dissolved organic matter despite the presence of different phytoplankton species and CO₂ concentrations. Unlike the study by De Kluijver et al. (2010), in this study, direct phytoplankton to bacteria transfer dynamics could not be revealed as group specific labeled biomarkers were not used. However, the combination of DOC measurements with $\delta^{13}\text{C}_{\text{DOC}}$, could give indirect indication of bacterial behavior. The rapid increase in DOC concentrations following the phytoplankton bloom, and the successive slow DOC build-up following the collapse, could be partly associated with bacterial biomass dynamics. Bulk $\delta^{13}\text{C}_{\text{DOC}}$ measurements, could instead be used to

define phytoplankton-bacteria interactions. Bacterial production is significantly correlated with planktonic primary production as phytoplankton derived organic matter forms an important food source for heterotrophic bacteria (Cole et al., 1988). The weak response observed in the $\delta^{13}\text{C}_{\text{DOC}}$ signal might indicate that bacteria utilized the freshly produced DOC and transferred it back into the DIC pool before it could accumulate into a more refractory DOC pool. On the other hand, the increase in DOC concentration could be explained by intensive exudation of DOC by phytoplankton. The absence of a strong DOC isotopic signal could also have originated from organic matter such as dying zooplankton which were present before any isotopically light CO_2 addition. Similar results were obtained in incubation (Norrman et al., 1995) and past mesocosm experiments (De Kluijver et al., 2010, 2013) where bacterial $\delta^{13}\text{C}$ never fully reached the signature of the labeled ^{13}C value of the corresponding algal POC, although a stronger isotopic signal was measured in these studies. It must be noted that the uncertainties associated with $\delta^{13}\text{C}_{\text{DOC}}$ measurements in the present study were relatively high ($\sigma = 0.71\text{‰}$) and this might have masked some underlying signal. Moreover, contrary to previous studies in which the isotopic signal was intensified through the use of labeled ^{13}C , here the small difference in the isotopic signature of the two organic carbon pools, might have constrained further the quantification of potential isotopic incorporation into the DOC pool.

Net Community Production and Settled Biomass

Mesocosm water columns were homogeneously mixed without formation of any thermo- or halocline that could cause stratification. This situation facilitated particle mixing throughout the full water column. Prior to the phytoplankton bloom, autotrophic activity, and sedimentation rates were generally low reflecting the low biomass in the water column (Figures 4, 6). During the bloom phase autotrophic activity was contributing for more than 60% to the total NCP. From t35 until the end of the experiment, the contribution of heterotrophic activity was about 40% for all mesocosms (Figure 6). It must be mentioned that neither bacterial nor zooplankton biomass were taken into account for the calculation of the NCP so that uncertainties in the total transfer and storage of carbon might be present. Sedimentation of particulate matter and build-up of dissolved carbon started to increase toward the end of the bloom phase. Highest sedimentation rates were observed at the end of the bloom peak, implying a temporal delay between primary production and sinking particle flux. During the post bloom phase, the mesocosm (M8) with highest CO_2 level showed higher build-up of particulate matter in the water column compared to the other treatments even though Chl *a* levels were relatively low. Interestingly, slower sedimentation rates were observed in the sediment trap of M8 and this was also reflected in a more pronounced isotopic enrichment of the particulate carbon compared to the low CO_2 level mesocosms (Figures 4, 6). This situation suggests a highly efficient transfer of autotrophic into non-sinking phytodetritus accumulating in the water column. In

shallow sediment traps zooplankton can largely contribute to the settling material either by production of sinking detrital carbon (feeding products and fecal pellets) or by actively swimming into the trap (Buesseler et al., 2007). In a previous mesocosm experiment (De Kluijver et al., 2013), high mesozooplankton biomass was observed and zooplankton products were estimated to have contributed for 82% to the carbon isotopic signature of the sediment material. According to their findings, the observed decreased export in mesocosm M8 compared to the other mesocosms could be related to the fact that the high CO_2 level mesocosm showed a temporal delay in zooplankton development (Algueró-Muñiz et al., 2019) resulting in less degradation and consequent sinking of organic material. This was confirmed by Stange et al. (2018) where in the same study, based on changes in the C:N ratio of sediment trap material, they attributed the increased retention of water column POM under elevated levels of CO_2 to the lower abundance of micro- and mesozooplankton. In terms of isotopic composition of the exported material, in general, during and after the phytoplankton bloom, a good agreement between the carbon isotopic signature in the mesocosm sediment traps and the isotopic signature of POC in the water column was observed. The match confirmed the sinking material was formed of freshly produced aggregates although a temporal decoupling was observed.

Phytoplankton Fractionation Response to CO_2 Additions

During photosynthesis, the lighter isotope of carbon, ^{12}C , is preferentially taken up relative to the heavier isotope, ^{13}C (O'Leary, 1981; Gruber et al., 1999). The inorganic carbon source utilized by phytoplankton either diffuses or is actively transported across the membrane into the cell. Once in the cell, carbon is fixed by an enzymatic reaction mainly driven by the enzyme ribulose-1,5-bisphosphate Carboxylase/Oxygenase (RubisCO) to produce phytoplankton biomass or diffuses back into the environment (Farquhar et al., 1982). Overall, the carbon isotopic composition of phytoplankton is determined by the isotopic composition of the source of inorganic carbon (CO_2 or HCO_3^-), isotope fractionation during transport into the cell, leakage of CO_2 out of the cell and isotopic discrimination during enzymatic carboxylation (Hayes, 1993). In our experiment, the isotopic signature of the particulate organic carbon in the water column of all mesocosms sharply increased (on t26) following deep water addition (Figure 4). Stable carbon isotopic measurements of the collected deep water were not performed however it is possible that the added deep water had a more positive $\delta^{13}\text{C}_{\text{POC}}$ value compared to the one inside the mesocosms that contributed to increase the $\delta^{13}\text{C}_{\text{POC}}$ signatures of the mesocosm waters. The breakdown of large isotopically heavy particles originating in or above the pycnocline and the transformation of DOC into POC have been considered to be responsible for reported isotopically heavier signatures of particulate carbon at depths compared to the surface for several study areas including the equatorial Atlantic Ocean (Jeffrey et al., 1983).

Over the past decades, many studies have shown that carbon isotope fractionation in marine phytoplankton varies according

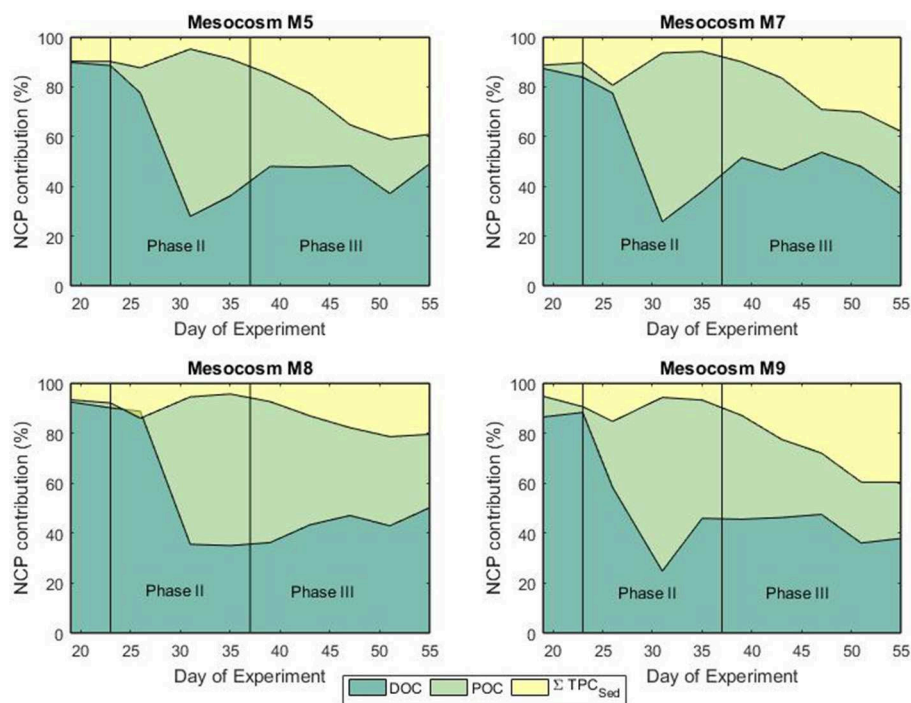


FIGURE 6 | Fractional contribution (%) of DOC, POC, and sedimentation to the net community production during the bloom (phase II) and post-bloom (phase III) phases.

to the CO_2 concentrations of surface water (Hinga et al., 1994; Rau et al., 1996; Burkhardt et al., 1999) with a general increase in ^{13}C fractionation under higher CO_2 levels. One of the major factors controlling the fractionation of carbon into phytoplankton is the availability of aqueous CO_2 . In this study the calculated phytoplankton fractionation (ϵ) ranged between 9.6 and 16.5‰ with higher values observed in the high CO_2 treatment mesocosm (mean $\epsilon = 15.6\text{‰}$ in mesocosm M8). Average fractionation values of 11.9, 12.8 and 12.0‰ were calculated for mesocosms M5, M7, and M9, respectively (Figure 7). In agreement with previous laboratory based work (Hinga et al., 1994; Laws et al., 1997; Kukert and Riebesell, 1998; Burkhardt et al., 1999), in our study, isotope fractionation between CO_2 and phytoplankton was higher in the communities grown under higher CO_2 , however, the response did not follow a linear concentration gradient but was mainly detected in the highest CO_2 treatment mesocosm M8 suggesting the possible presence of a threshold level. Interestingly, all the calculated ϵ for the high CO_2 treatment mesocosm M8 showed also a narrower range compared to the control and the other treatments.

In this study the net community production was used to estimate the fraction of DIC consumed by the phytoplankton hence fixed as biomass during the development of the bloom. In this case, the fraction could serve as an indication of growth and be used to simulate the theoretical progress of the bloom in terms of isotopic change in the DIC and POC. The use of a fixed fractionation factor value allowed for the assessment of the relationship between the signature of the substrate and the

POC pool. In our model, the substrate pool (DIC) splits into a product (POC) according to the fractionation value of 20‰ and into a residual substrate (DIC left in the pool). According to the model, the resulting isotopic variations in the formed product and residual substrate agreed well with the measured values of both $\delta^{13}\text{C}_{\text{POC}}$ and $\delta^{13}\text{C}_{\text{DIC}}$, respectively (Figure 8). No significant differences between modeled and measured values could be observed in mesocosm M5, M7 and M9. On the contrary the isotopic signatures of POC in mesocosm M8 diverged from the model suggesting again a higher fractionation value for this mesocosm. A plausible explanation for the smaller range and higher fractionation values found in mesocosm M8 could be linked to a shift in phytoplankton community composition. It has been shown that isotopic fractionation by autotrophic phytoplankton can be taxon-specific (Pagani et al., 2002; Vuorio et al., 2006). According to Chemtax analyses, the mesocosms were dominated by diatoms with high abundance of bacillariophyta (diatoms) and almost complete absence of chlorophyte (green alga) (Taucher et al., 2017). Mesocosms M8 developed a bloom of a Dictyocha-like toxic microscopic alga (*Vicicitus globosus*) which affected the phytoplankton community structure (Riebesell et al., 2013). Autotrophic dinoflagellates did not develop in the high CO_2 treatment mesocosm M8 until the post bloom phase (t43) when *v. globosus* abundance decreased. Whether it was the high CO_2 availability, the dominance of a specific planktonic group or a combination of both, in this mesocosm experiment elevated CO_2 concentrations positively affected the stable carbon isotope fractionation in phytoplankton.

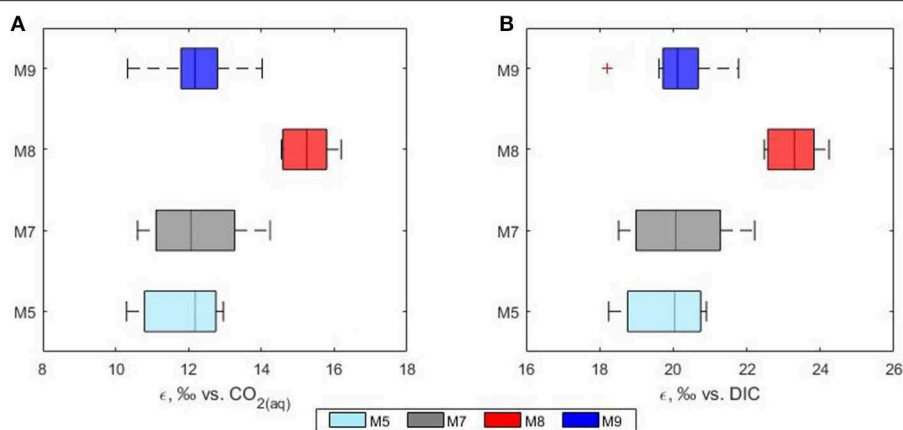


FIGURE 7 | Phytoplankton discrimination values (ϵ) calculated relative to the isotopic composition of (A) $\text{CO}_2(\text{aq})$ and (B) total DIC. Mesocosms. M5 (light blue), 450 ppm; M7 (gray), 700 ppm; and M8 (red), 1,000 ppm; M9 (blue), control mesocosm at ambient pCO_2 concentrations.

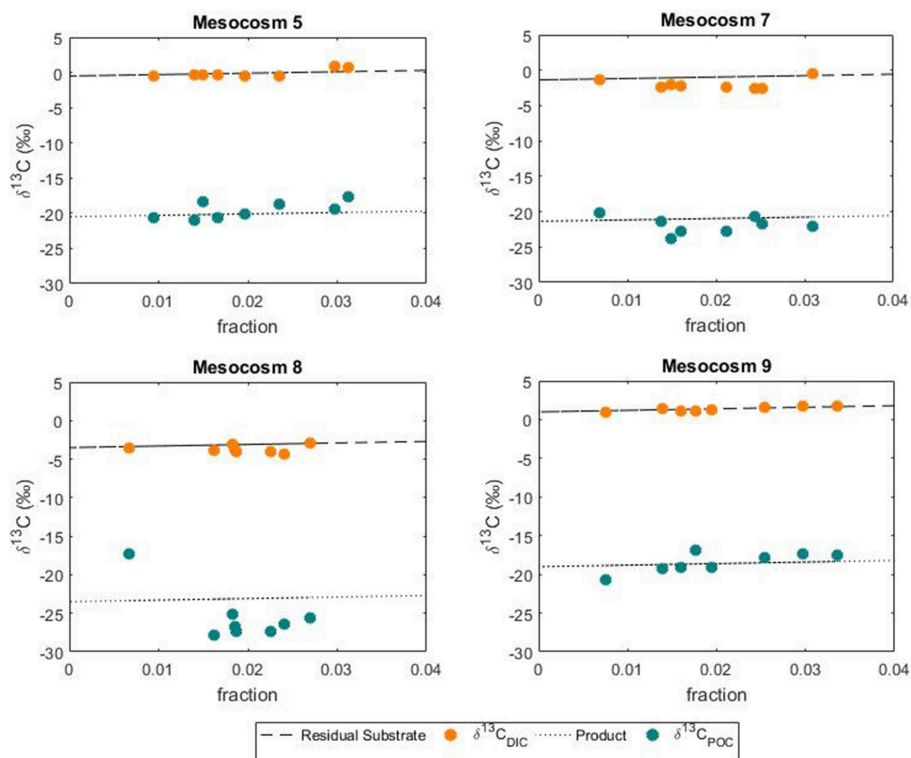


FIGURE 8 | Variations in the POC pool according to substrate uptake. Comparison between modeled changes and measured isotopic signatures of DIC and POC during the phytoplankton bloom.

CONCLUSION

The close-to-natural conditions in mesocosm compared to laboratory experiments, make mesocosms ideal platforms to investigate carbon dynamics whilst allowing the study of the effects of CO_2 on phytoplankton species and composition. This study was the first to employ stable isotope analysis of unlabelled

natural carbon in order to examine carbon transfer mechanisms and dynamics during a phytoplankton succession. Additions of isotopically light CO_2 from the CO_2 manipulation, established an isotopic gradient in the DIC pool which, following the nutrient-induced phytoplankton bloom, mirrored the isotopic signature of the organic carbon pools in both the water column

and sediment traps. No significant CO₂ effects were observed in the either particulate or dissolved organic carbon stocks. High CO₂ conditions decreased the export of material to the deeper layer during the post bloom phase, however the response was not gradual but was only found for the highest CO₂ treatment (~1,000 ppm) mesocosm. A CO₂ effect on phytoplankton fractionation was observed and similarly, the response was predominantly noticed in the highest CO₂ treatment mesocosm. High CO₂ concentrations affected fractionation values either directly as a consequence of the higher CO₂ availability or indirectly as a consequence of the phytoplankton community composition change observed in the highest CO₂ treatment mesocosm.

In general, results from this mesocosm experiment showed that stable isotope analysis of each of the individual carbon system pools within the marine environment is aiding the assessment of carbon dynamics in an oceanic system. However, when stable carbon isotopes are applied to estimate future oceanic interactions that are relevant for our climate, careful evaluation of the underlying processes is needed. Stable isotopic analysis confirmed that the material accumulating in the sediment trap was similar to that in the water column, an observation that is widely assumed when estimations of past natural changes in oceanic and atmospheric CO₂ are performed. However, in this study we found that other factors (allochthonous carbon, phytoplankton fractionation, and community composition) rather than CO₂ alone can influence the isotopic signature of the water column and the sediment material, therefore it is important to identify and understand the processes driving these changes in order to hindcast past and forecasts future oceanic CO₂-driven effects.

REFERENCES

- Algueró-Muñoz, M., Horn, H. G., Alvarez-Fernandez, S., Spisla, C., Aberle, N., Bach, L. T., et al. (2019). Analyzing the impacts of elevated-CO₂ levels on the development of a subtropical zooplankton community during oligotrophic conditions and simulated upwelling. *Front. Mar. Sci.* 6, 1–18. doi: 10.3389/fmars.2019.00061
- Bach, L. T., Taucher, J., Boxhammer, T., Ludwig, A., Aberle-Malzahn, N., Achterberg E. P. et al. (2016). Influence of ocean acidification on a natural winter-to-summer plankton succession: first insights from a long-term mesocosm study draw attention to periods of low nutrient concentrations. *PLoS ONE* 11:e0159068. doi: 10.1371/journal.pone.0159068
- Boxhammer, T., Bach, L. T., Czerny, J., and Riebesell, U. (2016). Technical note: sampling and processing of mesocosm sediment trap material for quantitative biogeochemical analysis. *Biogeosciences* 13, 2849–2858. doi: 10.5194/bg-13-2849-2016
- Buesseler, K. O., Antia, A. N., Chen, M., Fowler, S. W., Gardner, W. D., Gustafsson, O., et al. (2007). An assessment of the use of sediment traps for estimating upper ocean particle fluxes. *J. Mar. Res.* 65, 345–416. doi: 10.1357/002224007781567621
- Burkhardt, S., Riebesell, U., and Zondervan, I. (1999). Stable carbon isotope fractionation by marine phytoplankton in response to daylength, growth rate, and CO₂ availability. *Mar. Ecol. Prog. Ser.* 184, 31–41. doi: 10.3354/meps184031
- Cole, J., Findlay, S., and Pace, M. (1988). Bacterial production in fresh and saltwater ecosystems: a cross-system overview. *Mar. Ecol. Prog. Ser.* 43, 1–10. doi: 10.3354/meps043001

AUTHOR CONTRIBUTIONS

UR conceived, initiated, and organized the mesocosm study. JT and LB were involved in conceiving and performing the mesocosm experiment. ME performed the carbon isotope experiment, analyzed the data, and wrote the paper with comments and inputs from all co-authors.

FUNDING

The mesocosm project was funded by the German Federal Ministry of Education and Research (BMBF) in the framework of the coordinated project BIOACID—Biological Impacts of Ocean Acidification, phase 2 (FKZ 03F06550). UR received additional funding from the Leibniz Award 2012 by the German Research Foundation (DFG). Financial support for the stable carbon isotope study was provided by the Natural Environment Research Council as part of the UK Ocean Acidification Programme (NE/H017348/1).

ACKNOWLEDGMENTS

We would like to thank the KOSMOS team and all of the participants for their contribution during the Gran Canaria mesocosm campaign. In particular we would like to thank UR for giving us the opportunity to join the mesocosm projects and A. Ludwig for the magnificent coordination of the campaign logistics. We thank M. Martinez Cabanas for the help with data processing. We also thank the team of the Plataforma Oceanica de Canarias (PLOCAN) for their hospitality, research facilities and technical support. The authors would like to thank the reviewers of this work who provided insightful and constructive comments that improved the paper.

- Couldrey, M. P., Oliver, K. I. C., Yool, A., Halloran, P. R., and Achterberg, E. P. (2016). On which timescales do gas transfer velocities control North Atlantic CO₂ flux variability? *Glob. Biogeochem. Cycles* 30, 787–802. doi: 10.1002/2015GB005267
- De Kluijver, A., Soetaert, K., Czerny, J., Schulz, K. G., Boxhammer, T., Riebesell, U., et al. (2013). A 13C labelling study on carbon fluxes in Arctic plankton communities under elevated CO₂ levels. *Biogeosciences* 10, 1425–1440. doi: 10.5194/bg-10-1425-2013
- De Kluijver, A., Soetaert, K., Schulz, K. G., Riebesell, U., Bellerby, R. G. J. J., and Middelburg, J. J. (2010). Phytoplankton-bacteria coupling under elevated CO₂ levels: a stable isotope labelling study. *Biogeosciences* 7, 3783–3797. doi: 10.5194/bg-7-3783-2010
- Dickson, A. G., Sabine, C. L., and Christian, J. R. (eds.). (2007). *Guide to Best Practice for Ocean CO₂ Measurements. PICES Special Publication*, Vol. 3. Sidney, BC: North Pacific Marine Science Organization. Retrieved from: https://www.nodc.noaa.gov/ocads/oceans/Handbook_2007.html
- Farmer, C., Hansell, D. A., Dickson, A. G., Savine, C. L., and Christian, J. R. (2007). “Determination of dissolved organic carbon and total dissolved nitrogen in sea water,” in *Guide to Best Practices for Ocean CO₂ Measurements, Vol. 3 PICES Special Publication*, eds A. G. Dickson, C. L. Sabine, and J. R. Christian, 191. Retrieved from: http://cdiac.ornl.gov/ftp/oceans/Handbook_2007/sop07.pdf
- Farquhar, G., O’Leary, M., and Berry, J. (1982). On the relationship between carbon isotope discrimination and the intercellular carbon dioxide concentration in leaves. *Funct. Plant Biol.* 9:121. doi: 10.1071/PP9820121

- Field, C. B., Behrenfeld, M. J., Randerson, J. T., and Falkowski, P. (1998). Primary production of the biosphere: integrating terrestrial and oceanic components. *Science* 281, 237–240. doi: 10.1126/science.281.5374.237
- González-Dávila, M., Santana-Casiano, J. M., Rueda, M.-J., Llinás, O., and González-Dávila, E.-F. (2003). Seasonal and interannual variability of sea-surface carbon dioxide species at the European Station for Time Series in the Ocean at the Canary Islands (ESTOC) between 1996 and 2000. *Global Biogeochem. Cycles* 17, 2–1. doi: 10.1029/2002GB001993
- Gruber, N., Keeling, D., Bacastow, R. B., Guenther, P. R., Lueker, T. J., Wahlen, M., et al. (1999). Spatiotemporal patterns of carbon-13 in the global surface oceans and the oceanic Suess effect. *Global Biogeochem. Cycles* 13, 307–335. doi: 10.1029/1999GB900019
- Hansen, H. P., and Koroleff, F. (2007). “Determination of nutrients,” in *Methods of Seawater Analysis* (Weinheim: Wiley-VCH Verlag GmbH), 159–228. doi: 10.1002/9783527613984.ch10
- Hayes, J. M. (1993). Factors controlling ^{13}C contents of sedimentary organic compounds: principles and evidence. *Mar. Geol.* 113, 111–125. doi: 10.1016/0025-3227(93)90153-M
- Hernández-Hernández, N., Bach, L. T., Montero, M. F., Taucher, J., Baños, I., Guan, W., et al. (2018). High CO_2 under nutrient fertilization increases primary production and biomass in subtropical phytoplankton communities: a mesocosm approach. *Front. Mar. Sci.* 5:213. doi: 10.3389/fmars.2018.00213
- Hinga, K. R., Arthur, M. A., Pilson, M. E. Q., and Whitaker, D. (1994). Carbon isotope fractionation by marine phytoplankton in culture: the effects of CO_2 concentration, pH, temperature, and species. *Glob. Biogeochem. Cycles* 8, 91–102. doi: 10.1029/93GB03393
- Holmes, R. M., Aminot, A., Kérouel, R., Hooker, B. A., and Peterson, B. J. (1999). A simple and precise method for measuring ammonium in marine and freshwater ecosystems. *Can. J. Fish. Aquatic Sci.* 56, 1801–1808. doi: 10.1139/f99-128
- IPCC (2014). “Climate change 2014: impacts, adaption, and vulnerability. Part A: global and sectoral aspects,” in *Contribution of Working Group II to the Fifth Assessment Report of the Intergovernmental Panel on Climate Change* (Cambridge; New York, NY: Cambridge University Press).
- Jähne, B., Huber, W., Dutzi, A., Wais, T., and Ilmberger, J. (1984). “Wind/wave-tunnel experiment on the schmidt number-and wave field dependence of air/water gas exchange,” in *Gas Transfer at Water Surfaces*, eds W. Brutsaert and G. Jirka (Dordrecht: Springer), 303–309. doi: 10.1007/978-94-017-1660-4_28
- Jeffrey, A. W. A., Pflaum, R. C., Brooks, J. M., and Sackett, W. M. (1983). Vertical trends in particulate organic carbon ^{13}C : ^{12}C ratios in the upper water column. *Deep Sea Res. Part A Oceanogr. Res. Pap.* 30, 971–983. doi: 10.1016/0198-0149(83)90052-3
- Keeling, C. D. (1979). The suess effect: ^{13}C Carbon- ^{14}C Carbon interrelations. *Environ. Int.* 2, 229–300. doi: 10.1016/0160-4120(79)90005-9
- Kukert, H., and Riebesell, U. (1998). Phytoplankton carbon isotope fractionation during a diatom spring bloom in a Norwegian fjord. *Mar. Ecol. Prog. Ser.* 173, 127–138. doi: 10.3354/meps173127
- Laws, E. A., Bidigare, R. R., and Popp, B. N. (1997). Effect of growth rate and CO_2 concentration on carbon isotopic fractionation by the marine diatom *Phaeodactylum tricornutum*. *Limnol. Oceanogr.* 42, 1552–1560. doi: 10.4319/lo.1997.42.7.1552
- Le Quéré, C., Andrew, R. M., Canadell, J. G., Sitch, S., Ivar Korsbakken, J., Peters, G. P., et al. (2016). Global carbon budget 2016. *Earth Syst. Sci. Data* 8, 605–649. doi: 10.5194/essd-8-605-2016
- Lynch-Stieglitz, J., Stocker, T. F., Broecker, W. S., and Fairbanks, R. G. (1995). The influence of air-sea exchange on the isotopic composition of oceanic carbon: observations and modeling. *Global Biogeochem. Cycles* 9, 653–665. doi: 10.1029/95GB02574
- Marty, J., and Planas, D. (2008). Comparison of methods to determine algal $\delta^{13}\text{C}$ in freshwater. *Limnol. Oceanogr. Methods* 6, 51–63. doi: 10.4319/lom.2008.6.51
- Murphy, J., and Riley, J. P. (1962). A modified single solution method for the determination of phosphate in natural waters. *Anal. Chim. Acta* 27, 31–36. doi: 10.1016/S0003-2670(00)88444-5
- Nightingale, P. D., Malin, G., Law, C. S., Watson, A. J., Liss, P. S., Liddicoat, M. I., et al. (2000). *In situ* evaluation of air-sea gas exchange parameterizations using novel conservative and volatile tracers. *Glob. Biogeochem. Cycles* 14, 373–387. doi: 10.1029/1999GB900091
- Norrmann, B., Zwelfel, U. L., Hopkinson, C. S., and Fry, B. (1995). Production and utilization of dissolved organic carbon during an experimental diatom bloom. *Limnol. Oceanogr.* 40, 898–907. doi: 10.4319/lo.1995.40.5.0898
- O’Leary, M. H. (1981). Carbon isotope fractionation in plants. *Phytochemistry* 20, 553–567. doi: 10.1016/0031-9422(81)85134-5
- Pagani, M., Freeman, K. H., Ohkouchi, N., and Caldeira, K. (2002). Comparison of water column $[\text{CO}_2\text{aq}]$ with sedimentary alkenone-based estimates: a test of the alkenone- CO_2 proxy. *Paleoceanography* 17, 21–1–21–12. doi: 10.1029/2002PA000756
- Rau, G., Riebesell, U., and Wolf-Gladrow, D. (1996). A model of photosynthetic ^{13}C fractionation by marine phytoplankton based on diffusive molecular CO_2 uptake. *Mar. Ecol. Progress Ser.* 133, 275–285. doi: 10.3354/meps133275
- Riebesell, U., Czerny, J., von Bröckel, K., Boxhammer, T., Büdenbender, J., Deckelnick, M., et al. (2013). Technical Note: a mobile sea-going mesocosm system - new opportunities for ocean change research. *Biogeosciences* 10, 1835–1847. doi: 10.5194/bg-10-1835-2013
- Riebesell, U., Czerny, J., Von Bröckel, K., Boxhammer, T., Büdenbender, J., Deckelnick, M., et al. (2013). Technical note: a mobile sea-going mesocosm system - new opportunities for ocean change research. *Biogeosciences*. doi: 10.5194/bg-10-1835-2013
- Riebesell, U., Schulz, K. G., Bellerby, R. G., Botros, M., Fritsche, P., Meyerhöfer, M., et al. (2007). Enhanced biological carbon consumption in a high CO_2 ocean. *Nature* 450, 545–548. doi: 10.1038/nature06267
- Santana-Casiano, J. M., González-Dávila, M., Laglera Baquer, L. M., and Rodríguez Somoza, M. J. (2001). Carbon dioxide system in the Canary region during October 1995. *Sci. Mar.* 65, 41–50. doi: 10.3989/scimar.2001.65s141
- Schmittner, A., Gruber, N., Mix, A. C., Key, R. M., Tagliabue, A., and Westberry, T. K. (2013). Biology and air-sea gas exchange controls on the distribution of carbon isotope ratios ($\delta^{13}\text{C}$) in the ocean. *Biogeosciences* 10, 5793–5816. doi: 10.5194/bg-10-5793-2013
- Schulz, K. G., Riebesell, U., Bellerby, R. G. J., Biswas, H., Meyerhöfer, M., Uller, M. N., et al. (2008). Build-up and decline of organic matter during PeECE III. *Biogeosciences* 5, 707–718. doi: 10.5194/bg-5-707-2008
- Stange, P., Taucher, J., Bach, L. T., Algueró-Muñoz, M., Horn, H. G., Krebs, L., et al. (2018). Ocean acidification-induced restructuring of the plankton food web can influence the degradation of sinking particles. *Front. Mar. Sci.* 5:140. doi: 10.3389/fmars.2018.00140
- Taucher, J., Bach, L. T., Boxhammer, T., Nauendorf, A., Achterberg, E. P., Algueró-Muñoz, M., et al. (2017). Influence of ocean acidification and deep water upwelling on oligotrophic plankton communities in the subtropical north atlantic: insights from an *in situ* mesocosm study. *Front. Mar. Sci.* 4:85. doi: 10.3389/fmars.2017.00085
- Volk, T., and Hoffert, M. I. (1985). Ocean carbon pumps: analysis of relative strengths and efficiencies in ocean-driven atmospheric CO_2 changes. 99–110.
- Vuorio, K., Meili, M., and Sarvala, J. (2006). Taxon-specific variation in the stable isotopic signatures ($\delta^{13}\text{C}$ and $\delta^{15}\text{N}$) of lake phytoplankton. *Freshw. Biol.* 51, 807–822. doi: 10.1111/j.1365-2427.2006.01529.x
- Wanninkhof, R., Asher, W. E., Ho, D. T., Sweeney, C., and McGillis, W. R. (2009). Advances in quantifying air-sea gas exchange and environmental forcing. *Ann. Rev. Mar. Sci.* 1, 213–244. doi: 10.1146/annurev.marine.010908.163742
- Zark, M., Broda, N. K., Hornick, T., Grossart, H.-P., Riebesell, U., and Dittmar, T. (2017). Ocean acidification experiments in large-scale mesocosms reveal similar dynamics of dissolved organic matter production and biotransformation. *Front. Mar. Sci.* 4, 1–11. doi: 10.3389/fmars.2017.00271
- Zhang, J., Quay, P. D., and Wilbur, D. O. (1995). Carbon isotope fractionation during gas-water exchange and dissolution of CO_2 . *Geochim. Cosmochim. Acta* 59, 107–114. doi: 10.1016/0016-7037(95)91550-D

Conflict of Interest: The authors declare that the research was conducted in the absence of any commercial or financial relationships that could be construed as a potential conflict of interest.

Copyright © 2019 Esposito, Achterberg, Bach, Connelly, Riebesell and Taucher. This is an open-access article distributed under the terms of the Creative Commons Attribution License (CC BY). The use, distribution or reproduction in other forums is permitted, provided the original author(s) and the copyright owner(s) are credited and that the original publication in this journal is cited, in accordance with accepted academic practice. No use, distribution or reproduction is permitted which does not comply with these terms.

Advantages of publishing in Frontiers



OPEN ACCESS

Articles are free to read
for greatest visibility
and readership



FAST PUBLICATION

Around 90 days
from submission
to decision



HIGH QUALITY PEER-REVIEW

Rigorous, collaborative,
and constructive
peer-review



TRANSPARENT PEER-REVIEW

Editors and reviewers
acknowledged by name
on published articles

Frontiers

Avenue du Tribunal-Fédéral 34
1005 Lausanne | Switzerland

Visit us: www.frontiersin.org

Contact us: info@frontiersin.org | +41 21 510 17 00



REPRODUCIBILITY OF RESEARCH

Support open data
and methods to enhance
research reproducibility



DIGITAL PUBLISHING

Articles designed
for optimal readership
across devices



FOLLOW US

@frontiersin



IMPACT METRICS

Advanced article metrics
track visibility across
digital media



EXTENSIVE PROMOTION

Marketing
and promotion
of impactful research



LOOP RESEARCH NETWORK

Our network
increases your
article's readership